



## Durham E-Theses

---

### *Far-infrared studies on molecular motions and interactions in liquids*

James, Peter L.

#### How to cite:

---

James, Peter L. (1982) *Far-infrared studies on molecular motions and interactions in liquids*, Durham theses, Durham University. Available at Durham E-Theses Online: <http://etheses.dur.ac.uk/7895/>

#### Use policy

---

The full-text may be used and/or reproduced, and given to third parties in any format or medium, without prior permission or charge, for personal research or study, educational, or not-for-profit purposes provided that:

- a full bibliographic reference is made to the original source
- a [link](#) is made to the metadata record in Durham E-Theses
- the full-text is not changed in any way

The full-text must not be sold in any format or medium without the formal permission of the copyright holders.

Please consult the [full Durham E-Theses policy](#) for further details.

**UNIVERSITY OF DURHAM**

**A Thesis Entitled**

**FAR-INFRARED STUDIES ON MOLECULAR  
MOTIONS AND INTERACTIONS IN LIQUIDS**

**Submitted by**

**Peter L. James B.Sc. M. Sc.  
(Graduate Society)**

**A candidate for the degree of  
Doctor of Philosophy 1982**

The copyright of this thesis rests with the author.  
No quotation from it should be published without  
his prior written consent and information derived  
from it should be acknowledged.



**FOR MY PARENTS**

## DECLARATION

The research described in this Thesis was carried out by the author in the Department of Chemistry, University of Durham, and the National Physical Laboratory, Teddington, between October 1976 and December 1978. It has not been submitted for any other degree. The work is original except where acknowledged by reference.

### **ACKNOWLEDGEMENTS**

**I would like to thank the academic and technical staff and my fellow research workers at Durham University and The National Physical Laboratory. In particular I am grateful to Dr. J. Yarwood for his encouragement and guidance. For financial support my thanks are due to The Science Research Council and Beckman-RIIC Ltd. Lastly I wish to thank Mrs. R. Bennett for preparing the final manuscript.**

## ABSTRACT

Far-infrared spectroscopy has been applied to the study of liquid phase molecular dynamics and interactions.

The absorption and dispersion spectra of solutions of acetonitrile in carbon tetrachloride, across a range of temperatures and concentrations, have been obtained. These spectra have been interpreted with the parameters obtained from a model developed from a generalised Langevin equation of motion which includes intermolecular torque terms.

The results obtained from the model analysis have been applied in an investigation of the non-reorientational contributions to the Raman and infrared bands arising from the  $\nu_1$  and  $\nu_3$  modes. This study has shown that contrary to the assumptions commonly made, these contributions are not equal and some possible explanations for the discrepancies are given.

A number of internal field theories are discussed and have been applied to the acetonitrile systems. The interpretation of the results of this analysis in terms of a simple model suggest that there is a preferred i.e. non-random orientation of the acetonitrile molecules in solution.

A study of some tertiary alkyl ammonium halide solutions has revealed that there is a series of systems which separate into two liquid phases.

Further investigation has highlighted the role of small amounts of water in these systems.

## CONTENTS

### CHAPTER 1

MOLECULAR MOTIONS AND INTERACTIONS	p1
INTRODUCTION	p2
THEORETICAL BACKGROUND	p3

### CHAPTER 2

DIELECTRIC THEORY AND THE MOLECULAR DYNAMICS OF LIQUIDS	p9
A. DIELECTRIC DISPERSION IN LIQUIDS - PHENOMENOLOGICAL DEFINITIONS AND RELATIONS	p10
B. THE APPLICATION OF MICROWAVE AND FAR-INFRARED SPECTROSCOPY TO THE ELUCIDATION OF THE MOLECULAR DYNAMICS OF LIQUIDS	p12
Internal Field	p12
Dielectric Friction	p15
C. DETAILS OF SOME OF THE MODELS USED TO DESCRIBE THE MOLECULAR DYNAMICS OF LIQUIDS	p23
(i) Rotational Diffusion	p23
(ii) Inertia Corrected Debye Models	p24
(iii) The Far-Infrared 'Poley' Absorption	p26
(iv) The Extended Diffusion Models of Gordon	p28
(v) The Memory Function Formalism	p29

### CHAPTER 3

FAR-INFRARED SPECTROSCOPY USING A MICHELSON INTERFEROMETER	p35
INTRODUCTION	p36
A. GENERAL THEORY OF A MICHELSON INTERFEROMETER	p36
(i) The Fellgett Advantage	p38
(ii) The Jacquinot Advantage	p38
(iii) Spectral Resolution	p38
(iv) Apodisation	p39
(v) Sampling of the Interferogram	p39
(vi) Beam Splitters and Optical Filtering	p40
B. THE DURHAM INTERFEROMETER	p42
(i) General	p42
(ii) The Cooled Detector	p42
(iii) The Polarising Optical Configuration	p42
(iv) Operational Configuration of the Interferometer	p43
(v) Further Modifications	p45

## CHAPTER 4

THE DETERMINATION OF REFRACTIVE INDEX SPECTRA BY DISPERSIVE FOURIER TRANSFORM SPECTROSCOPY (DFTS)	p46
A. INTRODUCTION	p47
(i) An Outline of the Basic Principles and Theory of DFTS	p47
(ii) A Brief Description of Some Practical Methods of Applying DFTS	p50
B. THE APPLICATION OF THE DFTS TECHNIQUE IN THIS WORK	p51
(i) Refractive Index Measurement Using the Durham Cell	p51
Results and Analysis	p51
(ii) Refractive Index Measurement by the Free Layer Technique	p55
Computation of Results	p55
(iii) Refractive Index Determinations of CH <sub>3</sub> CN/CCl <sub>4</sub> Solutions Using the Leiden Cell	p62
A Summary of the Advantages and Disadvantages of the Leiden Cell Compared to the Durham Cell	p65
A Brief Description of Operation of the Leiden Cell	p65
(iv) Errors in the Refractive Indices Determined	p66

## CHAPTER 5

A STUDY OF THE FAR-INFRARED SPECTRA OF ACETONITRILE (CH <sub>3</sub> CN) IN SOLUTION WITH CARBON TETRACHLORIDE (CCl <sub>4</sub> ) [BENZENE (C <sub>6</sub> H <sub>6</sub> ) AND N. HEPTANE (C <sub>7</sub> H <sub>16</sub> )]	p73
INTRODUCTION	p74
A. EXPERIMENTAL PROCEDURES AND ERRORS	p75
(i) Solution Preparation	p75
(ii) Sample Cell Preparation	p75
(iii) Temperature Control	p77
(iv) Recording of Interferograms and Calculation of Spectra	p77
Absorbance Spectra	p77
Refractive Index Spectra	p83
(v) The Determination of the Static and Infinite Frequency Permittivity, $\epsilon_0$ and $\epsilon^\infty$ , of the Solutions Studied	p83
B. TREATMENT OF RAW DATA AND INITIAL ANALYSIS OF SPECTRA	p86
(i) Averaging of Spectra	p86
(ii) Matching of Data Sets and Editing Procedures	p86
(iii) Initial Analysis of Spectra	p86
(iv) The Variation in the Observed Spectral Features with Temperature	p91
(v) The Variation in the Observed Spectral Features with Concentration	p96
(vi) The Calculation of Loss Spectra ( $\epsilon''$ vs $\bar{\nu}$ ) for the Solutions at 288K and 318K	p96

C.	A DESCRIPTION OF THE PROCEDURE APPLIED TO THE MODEL ANALYSIS	p101
(i)	The Definitions Applied in the Model Analysis	p101
(ii)	A General Description of the Least Squares Fitting Routine	p103
	Convergence and Determination of Solution	p103
(iii)	Fitting to Different Data Sets	p106
D.	THE CALCULATION OF MOLECULAR AND MICROSCOPIC CORRELATION TIMES	p110
(i)	Internal Field Factors	p110
(ii)	A General Discussion of the Results of the Internal Field Calculations	p110

## CHAPTER 6

	THE MOLECULAR DYNAMICS OF ACETONITRILE IN SOLUTION: MODEL ANALYSIS AND DISCUSSION OF RESULTS	p115
A.	MODEL ANALYSIS	
	INTRODUCTION	p116
(i)	A Brief Evaluation of Some Models Applied to $\text{CH}_3\text{CN}/\text{CCl}_4$ Solutions	p116
(ii)	Analysis of the Model Developed by the Solution of a Generalised Rotational Langevin Equation	p118
a.	Direct Calculation of the Model Parameters	p118
b.	The Application of the Model Fitting Procedure with Two Variable Parameters $K_1(0)$ and $\gamma$	p119
	Variation in the Fitted Parameters $K_1(0)$ and $1/\gamma$	p138
	Rotational Correlation Times Obtained from the Model	p142
	Further Discussion of the Variations in Intensity of the Observed Spectra	p150
	A Brief Comparison of the Spectral 4th Moments, $M_{4R}$ of the Solutions Studied	p151
c.	Fitting With Three Variables: $\gamma$ , $K_1(0)$ , $K_0(0)$	p154
B.	THE COMPARISON OF VIBRATIONAL CONTRIBUTIONS TO BAND WIDTH	p160
a.	Energy Relaxation Processes	p161
b.	Phase Relaxation Processes	p161
C.	A FURTHER DISCUSSION OF THE INTERNAL FIELD CORRECTION FACTORS APPLIED IN CHAPTER 5	p163

## CHAPTER 7

ION-ION AND ION-SOLVENT INTERACTION IN NON-POLAR SOLVENTS	p165
INTRODUCTION	p166
(i) Extended studies of the concentration effect	p166
(ii) Attempts to study solvent and/or ion penetration effects	p174
(iii) The role of water in these systems	p182
APPENDIX 1: REFERENCES	p184
APPENDIX 2: Comparison of Infrared and Raman Vibrational Relaxation Functions of the $\nu_1$ and $\nu_3$ Modes of Acetonitrile	p193
APPENDIX 3: Studies of Molecular Motions and Vibrational Relaxation in Acetonitrile iv. Far-Infrared and Molecular Dynamics in Carbon Tetrachloride Solution	p209
APPENDIX 4: The Far-Infrared Dispersion of Acetonitrile in Dilute Solution in Carbon Tetrachloride	p228
APPENDIX 5: A New Cell for Liquid Phase Refractive Index Determinations in the Submillimetre Spectral Region	p236
APPENDIX 6: Studies of Ion-Ion and Ion-Solvent Interactions Using Far-Infrared Spectroscopy	p242
APPENDIX 7: Far-Infrared Spectroscopic Studies of Motions and Interactions in Solutions of Tetra-n-alkylammonium Halides	p260
APPENDIX 8: a. Research Colloquia	p274
b. Research Conferences and Papers Presented	p278

## TABLES

1.1	INFORMATION YIELDED BY VARIOUS SOECTROSCOPIC TECHNIQUES	p2
5.1	SOLUTION CONCENTRATIONS, PATH LENGTHS AND PATH LENGTH ERRORS	p76
5.2	ERRORS RESULTING FROM THE SUBTRACTION OF A SOLVENT BACKGROUND	p78
5.3	THE ERRORS CALCULATED FOR THE SUBTRACTION OF THE SOLVENT SPECTRUM SHOWN IN FIGURE 5.2a FROM A SOLUTION SPECTRUM OF 0.018mf CH <sub>3</sub> CN/CCl <sub>4</sub> RECORDED AT 318K	p82
5.4	PERMITTIVITY VALUES OF VARIOUS SOLVENTS AND SOLUTIONS OF ACETONITRILE	p85
5.5	A SUMMARY OF THE OBSERVED SPECTRAL FEATURES OF THE ACETONITRILE SOLUTIONS STUDIED	p90
5.6	A SUMMARY OF THE OBSERVED SPECTRAL FEATURES OF A RANGE OF SOLUTION OF ACETONITRILE AT 298K	p92
5.7	TESTS FOR FUNCTION MINIMA IN A LEAST SQUARES FIT	p106
5.8	PARAMETERS OBTAINED FROM A LOW FREQUENCY DATA FIT	p108
5.9	A SUMMARY OF INTERNAL FIELD CORRECTION EQUATIONS	p111
5.10	OBSERVED MICROWAVE CORRELATION TIMES $\tau_D$ FOR CH <sub>3</sub> CN/CCl <sub>4</sub> SOLUTIONS ADJUSTED BY VARIOUS INTERNAL FIELD FACTORS TO OBTAIN $\tau^{mic}$ AND $\tau^s$	p112
6.1	MODEL PARAMETERS OBTAINED BY DIRECT CALCULATION USING EQUATIONS 5.14 AND 5.15	p119
6.2	RESULTS OF MODEL FITTING WITH 2 VARIABLE PARAMETERS TO CH <sub>3</sub> CN/CCl <sub>4</sub> SOLUTIONS AT VARIOUS TEMPERATURES	p123
6.3	RESULTS OF MODEL FITTING WITH 2 VARIABLE PARAMETERS TO VARIOUS CH <sub>3</sub> CN SOLUTIONS AT 298K	p124
6.4	VARIATION IN FITTED PARAMETERS WITH TEMPERATURE AND CONCENTRATION	p138
6.5a	CORRELATION TIMES CALCULATED FROM MODEL PARAMETERS OBTAINED BY A TWO PARAMETER FIT (TEMPERATURE AND CONCENTRATION DEPENDENCE)	p143
6.5b	CORRELATION TIMES CALCULATED FROM MODEL PARAMETERS OBTAINED BY A TWO PARAMETER FIT (CONCENTRATION AND SOLVENT DEPENDENCE) AT 298K	p144
6.6	SPECTRAL 4th MOMENTS CALCULATED FROM MODEL PARAMETERS (2 PARAMETER FIT) COMPARED WITH VALUES OBTAINED BY INTEGRATION	p152

6.7	SPECTRAL 4th MOMENTS CALCULATED FROM THE MODEL PARAMETERS (TEMPERATURE AND CONCENTRATION DEPENDENCE)	p153
6.8	THE RESULTS OF A MODEL FITTING WITH 3 VARIABLE PARAMETERS $\gamma$ , $K_1(0)$ AND $K_0(0)$	p156
6.9	CALCULATED AND OBSERVED VIBRATIONAL HALF WIDTHS FOR ACETONITRILE IN CARBON TETRACHLORIDE	p160
7.1	BAND CENTRE OF B WITH RESPECT TO CATION AND ANION	p169
7.2	A SUMMARY OF THE SOLUTE/SOLVENT SYSTEMS OBSERVED	p175
7.3	WATER CONTENT OF SOLUTIONS	p177

## FIGURES

2.1	SCHEMATIC LOSS AND PERMITTIVITY SPECTRA	p11
3.1	SCHEMATIC DIAGRAM OF A MICHELSON INTERFEROMETER	p37
3.2	THEORETICAL EFFICIENCY OF SOME TYPICAL BEAM SPLITTERS	p41
3.3	TRANSMISSION CHARACTERISTICS OF SOME RULED POLYETHYLENE FILTERS	p41
3.4a	SPECTRUM RECORDED WITH COOLED DETECTOR AND 100 $\mu$ m BEAMSPLITTER	p44
3.4b	SPECTRUM RECORDED WITH COOLED DETECTOR AND POLARISING OPTICS	p44
4.1	SCHEMATIC DIAGRAM OF A MICHELSON INTERFEROMETER IN THE DISPERSIVE CONFIGURATION	p48
4.2	SCHEMATIC INTERFEROGRAMS	p48
4.3	INTERFEROGRAMS RECORDED WITH THE DURHAM CELL	p52
4.4a	REFRACTIVE INDEX SPECTRA OF P. DIFLUOROBENZENE	p53
4.4.b	REFRACTIVE INDEX SPECTRA OF TETRABROMOETHANE	p53
4.5	INTERFEROGRAMS RECORDED BY THE 'FREE LAYER' METHOD	p56
4.6	SCHEMATIC FREE LAYER INTERFEROGRAMS	p57
4.7.a	P. DIFLUOROBENZENE 0.5mm FREE LAYER	p58
4.7b	P. DIFLUOROBENZENE 0.5mm FREE LAYER (BRANCHING CORRECTED)	p58
4.8a	P. DIFLUOROBENZENE 1.0mm FREE LAYER	p59
4.8b	P. DIFLUOROBENZENE 1.0mm FREE LAYER (BRANCHING CORRECTED)	p59
4.9a	P. DIFLUOROBENZENE 2.5mm FREE LAYER	p60
4.9b	P. DIFLUOROBENZENE 2.5mm FREE LAYER (BRANCHING CORRECTED)	p60
4.10	REFRACTIVE INDEX OF P. DIFLUOROBENZENE AT 298K	p61
4.11	REFRACTIVE INDEX OF CH <sub>3</sub> CN/CCI <sub>4</sub> 0.018mf AT 45°C	p63
4.12	A SCHEMATIC DIAGRAM OF THE LEIDEN CELL	p64
4.13	INTERFEROGRAMS RECORDED WITH THE LEIDEN CELL	p67
4.14	REFRACTIVE INDEX SPECTRA MEASURED USING THE LEIDEN CELL CH <sub>3</sub> CN/CCI <sub>4</sub> 0.018mf AT 288K	p68
	CH <sub>3</sub> CN/CCI <sub>4</sub> 0.061 mf AT 288K	p68
4.15	REFRACTIVE INDEX SPECTRA MEASURED USING THE LEIDEN CELL CH <sub>3</sub> CN/CCI <sub>4</sub> 0.018mf AT 318K	p69
	CH <sub>3</sub> CN/CCI <sub>4</sub> 0.061 mf AT 318K	p69

4.16a	ABSORPTION SPECTRUM OF CH <sub>3</sub> CN/CCl <sub>4</sub> 0.018 mf AT 288K	p70
4.16b	ABSORPTION SPECTRUM OF CH <sub>3</sub> CN/CCl <sub>4</sub> 0.061 mf AT 288K	p70
4.17a	ABSORPTION SPECTRUM OF CH <sub>3</sub> CN/CCl <sub>4</sub> 0.018 mf AT 318K	p71
4.17b	ABSORPTION SPECTRUM OF CH <sub>3</sub> CN/CCl <sub>4</sub> 0.061 mf AT 318K	p71
5.1a	REPRODUCIBILITY OF ABSORPTION SPECTRA (HIGH FREQUENCY)	p79
5.1b	REPRODUCIBILITY OF ABSORPTION SPECTRA (LOW FREQUENCY)	p79
5.2a	ABSORPTION SPECTRA OF CARBON TETRACHLORIDE	p81
5.2b	SOLUTION SUBTRACTION ERROR vs FREQUENCY	p81
5.3	TYPICAL AVERAGING OF LOW FREQUENCY DATA SETS	p87
5.4a	AN EDITED ABSORPTION SPECTRUM	p88
5.4b	AN EDITED ABSORPTION SPECTRUM	p88
5.5	TYPICAL ABSORPTION SPECTRA EDITING	p89
5.6a	OBSERVED SPECTRA $\bar{\nu}_{\max}$ vs TEMPERATURE	p93
5.6b	OBSERVED SPECTRA INTEGRATED INTENSITY PER MOLECULE vs TEMPERATURE (INTENSITY ERROR $\pm 5\%$ )	p93
5.7a	OBSERVED SPECTRA $\alpha_{\max}$ vs TEMPERATURE	p95
5.7b	OBSERVED SPECTRA $\Delta\bar{\nu}_{1/2}$ vs TEMPERATURE ( $\Delta\bar{\nu}_{1/2}$ ERROR $\pm 2\text{cm}^{-1}$ )	p95
5.8a	OBSERVED SPECTRA $\bar{\nu}_{\max}$ vs CONCENTRATION	p97
5.8b	OBSERVED SPECTRA $\bar{\nu}_{\max}$ vs CONCENTRATION	p97
5.9a	OBSERVED SPECTRA $\Delta\bar{\nu}_{1/2}$ vs CONCENTRATION ( $\Delta\bar{\nu}_{1/2}$ ERROR $\pm 2\text{cm}^{-1}$ )	p98
5.9b	OBSERVED SPECTRA $\alpha_{\max}$ vs CONCENTRATION	p98
5.10a	LOSS SPECTRUM OF CH <sub>3</sub> CN/CCl <sub>4</sub> 0.061 mf AT 288K	p99
5.10b	LOSS SPECTRUM OF CH <sub>3</sub> CN/CCl <sub>4</sub> 0.018 mf AT 288K	p99
5.11a	LOSS SPECTRUM OF CH <sub>3</sub> CN/CCl <sub>4</sub> 0.061 mf AT 318K	p100
5.11b	LOSS SPECTRUM OF CH <sub>3</sub> CN/CCl <sub>4</sub> 0.018 mf AT 318K	p100
5.12a	A WIDE FLAT-BOTTOMED MINIMUM IN WHICH LARGE VARIATIONS IN X (RELATIVE TO V(I)) ONLY PRODUCE SMALL VARIATIONS IN Y (XPS = +1.0)	p104
5.12b	A STEEP-SIDED MINIMUM IN WHICH SMALL VARIATIONS IN X LEAD TO LARGE FUNCTION VARIATIONS (XPS = -1.0)	p104
5.13	AN ILLUSTRATION OF THE DIFFERENT FUNCTION MINIMA PRESENT IN A LEAST SQUARES FITTING ROUTINE	p105

5.14	SPECTRA RECALCULATED FROM TWO DIFFERENT LEAST SQUARES FIT SOLUTIONS FOR THE MODEL	p107
5.15	SPECTRA RECALCULATED FROM A MODEL FIT TO LOW FREQUENCY DATA	p109
5.16	CH <sub>3</sub> CN/CCl <sub>4</sub> CORRELATION TIMES ( $\tau$ ) vs CONCENTRATION	p113
6.1	EXAMPLES OF MODEL SPECTRA CALCULATED FOR 0.018 mf CH <sub>3</sub> CN/CCl <sub>4</sub> AT 45°C	p117
6.2	SPECTRA RECALCULATED FROM THE MODEL PARAMETERS OBTAINED BY DIRECT CALCULATION (EQUATIONS 5.14 AND 5.15)	p120
6.3	SPECTRA RECALCULATED FROM THE MODEL PARAMETERS OBTAINED BY DIRECT CALCULATION (EQUATIONS 5.14 AND 5.15)	p121
6.4 - 6.13	RECALCULATED SPECTRA FROM A TWO PARAMETER MODEL FIT	
6.4	CH <sub>3</sub> CN/CCl <sub>4</sub> 0.018 mf AT -21°C	p125
6.5	CH <sub>3</sub> CN/CCl <sub>4</sub> 0.018 mf AT 15°C	p126
6.6	CH <sub>3</sub> CN/CCl <sub>4</sub> 0.018 mf AT 45°C	p127
6.7	CH <sub>3</sub> CN/CCl <sub>4</sub> 0.018 mf AT 70°C	p128
6.8	CH <sub>3</sub> CN/CCl <sub>4</sub> 0.06 mf AT 25°C	p129
6.9	CH <sub>3</sub> CN/CCl <sub>4</sub> 0.3 mf AT 25°C	p130
6.10	CH <sub>3</sub> CN/CCl <sub>4</sub> 0.7 mf AT 25°C	p131
6.11	LIQUID CH <sub>3</sub> CN AT 25°C	p132
6.12	CH <sub>3</sub> CN/BENZENE 0.06 mf AT 25°C	p133
6.13	CH <sub>3</sub> CN/N.HEPTANE 0.027 mf AT 25°C	p134
6.14a -	OBSERVED AND MODEL RECALCULATED LOSS SPECTRA	
6.15b	6.14a CH <sub>3</sub> CN/CCl <sub>4</sub> 0.018 mf AT 288K	p136
	6.14b CH <sub>3</sub> CN/CCl <sub>4</sub> 0.061 mf AT 15°C	p136
	6.15a CH <sub>3</sub> CN/CCl <sub>4</sub> 0.018 mf AT 318K	p137
	6.15b CH <sub>3</sub> CN/CCl <sub>4</sub> 0.061 mf AT 318K	p137
6.16a	MODEL PARAMETER $\gamma$ vs TEMPERATURE	p139
6.16b	MODEL PARAMETER K <sub>1</sub> (0) vs TEMPERATURE	p139
6.17	MODEL PARAMETER K <sub>1</sub> (0) vs CONCENTRATION	p140
6.18	MODEL PARAMETER 1/ $\gamma$ vs CONCENTRATION	p141
6.19	LOSS AND PERMITTIVITY CALCULATED FROM MODEL PARAMETERS FOR 0.018 mf CH <sub>3</sub> CN IN CCl <sub>4</sub> SOLUTION	p146
6.20	MODEL CALCULATED $\tau_{MORI}$ vs TEMPERATURE	p147
6.21	MODEL CALCULATED $\tau_{MORI}$ vs CONCENTRATION	p149
6.22-6.23	SPECTRA RECALCULATED FROM A THREE PARAMETER MODEL FIT	
6.22	CH <sub>3</sub> CN/CCl <sub>4</sub> 0.018 mf AT -21°C	p157
6.23	CH <sub>3</sub> CN/CCl <sub>4</sub> 0.018 mf AT 45°C	p158

7.1	ABSORPTION SPECTRA OF $\text{Bu}_4\text{N}^+\text{Cl}^-$ IN BENZENE SOLUTION (0.0133 mol $\text{cm}^{-1}$ ) RECORDED WITH THE GOLAY DETECTOR (PATH LENGTH 7.5mm)	p167
7.2	ABSORPTION SPECTRUM OF $\text{Bu}_4\text{N}^+\text{Cl}^-$ IN BENZENE SOLUTION (0.0133 mol $\text{cm}^{-1}$ ) RECORDED WITH THE COOLED DETECTOR (PATH LENGTH 7.5mm)	p168
7.3	LOW FREQUENCY SPECTRUM OF $\text{Bu}_4\text{N}^+\text{Cl}^-$ IN BENZENE SOLUTION (0.0133 mol $\text{cm}^{-1}$ ) RECORDED WITH COOLED DETECTOR AND POLARISING OPTICS	p170
7.4	COMPUTED BAND FIT OF 3 GAUSSIAN BANDS TO THE SPECTRUM OF $\text{Bu}_4\text{N}^+\text{Cl}^-$ IN BENZENE SOLUTION (0.4980 mol $\text{cm}^{-1}$ )	p171
7.5	ABSORPTION SPECTRA OF A RANGE OF CONCENTRATIONS OF $\text{Bu}_4\text{N}^+\text{Cl}^-$ IN BENZENE	p173
7.6	NEAR-INFRARED SPECTRA OF $\text{Bu}_4\text{N}^+\text{Cl}^-$ (SOLID), P.XYLENE AND SOLUTION LAYERS	p176
7.7	FAR-INFRARED SPECTRA OF $\text{Bu}_4\text{N}^+\text{Cl}^-$ /P.XYLENE (BOTTOM LAYER)	p178
7.8	FAR-INFRARED SPECTRA OF $\text{Bu}_4\text{N}^+\text{Cl}^-$ /P.XYLENE (TOP LAYER)	p178
7.9	ABSORPTION SPECTRUM OF DRIED $\text{Bu}_4\text{N}^+\text{Cl}^-$ IN P.XYLENE (SATURATED SOLUTIONS)	p179
7.10	NEAR-INFRARED SPECTRA OF $\text{Bu}_4\text{N}^+\text{Cl}^-$ (SOLID), P.XYLENE AND SOLUTION $\text{H}_2\text{O}$ (BOTTOM LAYER)	p180
7.11	ABSORPTION SPECTRUM OF DRIED $\text{Bu}_4\text{N}^+\text{Cl}^-$ IN BENZENE (SATURATED SOLUTION)	p183

**CHAPTER 1**  
**MOLECULAR MOTIONS AND INTERACTIONS**



**CHAPTER 1**  
**MOLECULAR MOTIONS AND INTERACTIONS**

**INTRODUCTION**

The studies of molecular motions and interactions in liquids can be carried out with a number of different spectroscopic techniques. It is because these techniques yield information of the different modes of molecular relaxation that they are often used together to provide an overall picture of the phenomena occurring and giving rise to the spectral profiles. Table 1.1 summarises the molecular motions which can be observed by some common spectroscopic techniques.

SPECTROSCOPIC TECHNIQUE	RELAXATION PROCESS
Far-Infrared	Rotation, Translation (including pair correlations)
Infrared	Vibration, Rotation
Raman isotropic	Vibrational relaxation
Raman anisotropic	Vibration, Rotation
Depolarised Rayleigh	Rotation, Translation (including pair correlations)
Microwave	Rotation (including pair correlations)
Nuclear Magnetic Resonance	Rotation, Translation
Neutron scattering	Vibration, Rotation, Translation (including pair correlations)

NB. The term rotation is used here to describe rotations and librations i.e. hindered rotations.

**TABLE 1.1**  
**INFORMATION YIELDED BY VARIOUS SPECTROSCOPIC TECHNIQUES**

In this work<sup>1,2</sup> a study has been made of the far-infrared spectra of acetonitrile ( $\text{CH}_3\text{CN}$ ) in carbon tetrachloride ( $\text{CCl}_4$ ) to complement and elucidate data obtained from the application of Raman<sup>3,4,5</sup> and Infrared<sup>6,7</sup> techniques. In particular we have tried to determine the contribution of different relaxation processes to the spectral profiles in order to check some of the assumptions made previously<sup>7,8,9,10,11</sup> (see next section).

**THEORETICAL BACKGROUND**

The analysis of infrared and Raman bandshapes have usually been made using two major assumptions.

For a given mode:

- i. The reorientational and vibrational motions of the molecules are statistically uncorrelated.
- ii. The vibrational contribution to a band profile is the same in the isotropic Raman, anisotropic Raman and infrared spectrum, i.e.:

$$I_{VV}(\omega) \equiv I_{VH}(\omega) \equiv I_{IR}(\omega) \quad \dots\dots\dots 1.1$$

where I indicates the intensity of a band as a function of frequency  $\omega$  and the subscripts VV and VH refer to the parallel and perpendicular components of the scattered light respectively.

In the case of Raman spectroscopy for symmetric top molecules we can derive the reorientational correlation function  $\phi_{2R}^s(t)$  from the equation:

$$\phi_{2R}^s(t) = \langle P_2 [\bar{u}^z(0) \cdot \bar{u}^z(t)] \rangle \quad \dots\dots\dots 1.2$$

where  $\langle \rangle$  brackets indicate an ensemble average of the molecules.

$\bar{u}^z(t)$  is the unit vector indicating the direction of the molecular symmetry axis at time t. and  $P_l$  indicates a Legendre polynomial of order l.

For Raman spectroscopy the tensor rank is 2 and the value of  $P_2$  is given by:

$$P_2 = \frac{1}{2} [3\cos^2 \Theta_{ij}(t) - 1] \quad \dots\dots\dots 1.3$$

where  $\Theta$  is the angle of rotation and the use of subscripts i j in this and subsequent expressions indicate that the equation embodies intermolecular cross correlations between molecules i and j as shown (for example) in equations 1.21 and 1.23. These cross correlations have often, but not always been assumed to be unimportant for vibrational-rotational, infrared and Raman, spectra. (See further discussion in this chapter and reference 12).

For the vibrational correlation function the equivalent equation is:

$$\phi_v^R(t) = \langle [Q_{vi}(0) \cdot Q_{vj}(t)] \rangle \quad \dots\dots\dots 1.4$$

where  $Q_{vi}$  is the normal coordinate of the  $v^{th}$  mode of the  $i^{th}$  molecule.

Thus assumption (i) can be expressed as:

$$\begin{aligned} \langle [Q_{vi}(0) \cdot Q_{vj}(t)] \cdot P_2 [u_i(0) \cdot u_j(t)] \rangle &\equiv \langle [Q_{vi}(0) \cdot Q_{vj}(t)] \rangle \langle P_2 [u_i(0) \cdot u_j(t)] \rangle \quad \dots\dots 1.5 \\ &\text{correlated} \qquad \qquad \qquad \text{uncorrelated} \\ &= \phi_v^R(t) \phi_{2R}^s(t) \quad \dots\dots\dots 1.6 \end{aligned}$$

The anisotropic Raman spectrum arises from vibrational and reorientational relaxation whereas the isotropic part of the scattered light depends only on the vibrational relaxation. For

plane polarised light where the observed bands  $I_{iso}(\omega)$  and  $I_{aniso}(\omega)$  have been corrected for finite resolution we can write: <sup>7-10,12-14</sup>

$$I_{aniso}(\omega) = I_{VH}(\omega) \quad \dots\dots\dots 1.7$$

and

$$I_{iso}(\omega) = I_{VV}(\omega) - 4/3 I_{VH}(\omega) \quad \dots\dots\dots 1.8$$

The correlation functions are then given by:

$$\phi_v^{iso}(t) \phi_{2R}^s(t) \propto \int_{band} I_{aniso}(\omega) \exp(-i\omega t) d\omega \quad \dots\dots\dots 1.9$$

$$\phi_v^{iso}(t) \propto \int_{band} I_{iso}(\omega) \exp(-i\omega t) d\omega \quad \dots\dots\dots 1.10$$

From equation 1.1 and assumption (ii) we can derive a similar expression for the vibrational correlation functions:

$$\phi_v^{iso} \equiv \phi_v^{aniso} \equiv \phi_v^{IR} \quad \dots\dots\dots 1.11$$

Hence, using assumptions (i) and (ii) (and therefore equations 1.9, 1.10 and 1.11) the reorientational correlation function can be calculated from:

$$\phi_{2R}^s(t) = \frac{\phi_{total}^{aniso}}{\phi_v^{iso}} = \frac{\int I_{aniso}(\omega) \exp(-i\omega t) d\omega}{\int I_{iso}(\omega) \exp(-i\omega t) d\omega} \quad \dots\dots\dots 1.12$$

For the infrared band profile <sup>7-10</sup>, which also arises from vibrational and rotational motions, we can write the equations equivalent to 1.5 and 1.6:

$$\langle [Q_{ui}(0) \cdot Q_{uj}(t)] \cdot P_1 [\bar{u}_i(0) \cdot \bar{u}_j(t)] \rangle \equiv \langle [Q_{ui}(0) \cdot Q_{uj}(t)] \rangle \langle P_1 [\bar{u}_i(0) \cdot \bar{u}_j(t)] \rangle \quad \dots\dots\dots 1.13$$

$$= \phi_v^{IR}(t) \phi_{1R}^s(t) \quad \dots\dots\dots 1.14$$

Where  $\phi_{1R}^s$  = pure rotational correlation function, and  $\bar{u}$  is a unit vector along the direction of the transition moment  $d\mu/dQ_v$  ( $\mu$  = the molecular dipole moment).

For an infrared band the tensor rank is 1 and

$$P_1 = \cos\Theta_{ij}(t) \quad \dots\dots\dots 1.15$$

The total infrared correlation function  $\Phi_{tot}^{IR}$  is given by:

$$\Phi_{tot}^{IR} = \phi_v^{IR}(t) \phi_{1R}^s \propto \int_{band} I_{IR}(\omega) \exp(-i\omega t) d\omega \quad \dots\dots\dots 1.16$$

Applying assumptions (i) and (ii) with equations 1.10, 1.11 and 1.12 we can write an expression for the correlation function of the pure rotational part of the infrared spectrum if we have the isotropic Raman spectrum of the same mode, i.e.

$$\phi_{1R}^s(t) = \frac{\int I_{IR}(\omega) \exp(i\omega t) d\omega}{\int I_{iso}(\omega) \exp(i\omega t) d\omega} \quad \dots\dots\dots 1.17$$

It has been useful to determine  $\phi_{1R}^s$  and  $\phi_{2R}^s$  because the difference between the reorientational correlation functions can be used as a means of testing the validity of and distinguishing between models describing reorientational motions of molecules. For example, one of the simplest models for describing the reorientational motion of molecules is the small step angular (rotational) diffusion, (Debye model)<sup>15</sup> in which it is assumed that only hard collisions affect the rotational angular momentum. It has been shown<sup>16</sup> that if this model is obeyed then the reorientational correlation times for the Raman,  $\tau_{2R}^s$  and the infrared,  $\tau_{1R}^s$  will be related by:

$$\tau_{1R}^s / \tau_{2R}^s = 3 \quad \dots\dots\dots 1.18$$

Where  $\tau_{iR} = \int_{t=0}^{t=\infty} \phi_{iR}(t) dt \quad \dots\dots\dots 1.19$

This method of distinguishing between models describing molecular motions has been used extensively.<sup>7,8,10,17-27</sup> However it has been shown recently by Yarwood and Arndt<sup>7</sup> that the assumptions made (i, ii) in determining  $\phi_{1R}^s$  and  $\phi_{2R}^s$  are invalid for at least one (or possibly two) of the normal modes for acetonitrile. In particular it has been shown that equation 1.1 does not hold. This was discovered from measurements of the half widths of the isotropic Raman spectrum and the infrared spectrum of the  $\nu_1$  (stretching mode) and  $\nu_3$  (symmetric bending mode) bands of acetonitrile (pure liquid and in solution with carbon tetrachloride) (see discussion Chapter 6). Subtraction of the isotropic Raman (vibrational) half width from the infrared half width (vibrational and rotational) in accordance with assumptions i and ii, to give the rotational contribution to the band has been shown to give different values for the  $\nu_1$  and  $\nu_3$  bands. As these bands both arise from  $A_1$  modes, (i.e. they measure rotation about the principal axis) the rotational contributions should be equal. Therefore it has been concluded that the assumption:

$$\phi_v^{iso} = \phi_v^{IR} \quad \dots\dots\dots 1.20$$

is invalid in this case.

The reasons for the invalidity of equation 1.20 have been suggested previously. It is known<sup>7</sup> that it is unlikely that molecular motions will be statistically uncorrelated unless their relaxation rates are very different. Until recently it was thought that energy relaxation was always much slower than phase relaxation however, it is now thought that this is not always the case for liquid phase vibrational/reorientational bands such as these<sup>7</sup>. The vibrational relaxations are often controlled by hard collisions<sup>14,28</sup> and therefore the translational - rotational motions must be correlated with vibrational dephasing and vibrational energy level (population) relaxation. Döge<sup>29</sup> has shown that the vibrational contribution to the same bands in the isotropic and anisotropic Raman spectra are expected to be different. This difference is thought to arise because of the

existence of an exchange term between different molecules due to strong mode-mode coupling via the resonant transfer of vibrational energy. Such energy transfer is usually caused by strong intermolecular interactions and is associated with a non-random distribution of molecules in the solution. Isotopic dilution<sup>2,9</sup> is expected to eliminate the effects of resonant energy transfer and has been used as a test for the presence of an exchange term between molecules *i* and *j*.

Recently Lynden-Bell<sup>3,10,31</sup> has firmly established some theoretical reasons underlying the invalidities of equation 1.11. She has pointed out that the vibrational (phase) relaxation function ( $\phi_{pp}$ ), of the  $\nu^{\text{th}}$  normal mode, can be written:

$$\begin{aligned} \phi_{pp}(t) &= \sum_{i,j} \langle Q_{\nu i}(0) \cdot Q_{\nu i}(t) \rangle \\ &= \sum_i \underbrace{\langle Q_{\nu i}(0) \cdot Q_{\nu i}(t) \rangle}_{\text{self term}} + \sum_{i \neq j} \underbrace{\langle Q_{\nu i}(0) \cdot Q_{\nu j}(t) \rangle}_{\text{exchange term}} \end{aligned} \quad \dots\dots\dots 1.21$$

$$\text{Where } \phi_{\nu}(t) = \phi_{pp}(t) \phi_E(t) \quad \dots\dots\dots 1.22$$

(If  $\phi_E(t)$ , the function measuring the rate of energy (population) relaxation is relatively slow).

She has shown (via the solution of a Langevin equation for the diffusion of angular velocity) that for an effective potential of dipolar or dispersive forces there is a cross term between the 'self' and 'exchange' parts in equation 1.21. This cross term contributes strongly to the vibrational dephasing in the isotropic Raman ( $\iota=0$ ), negligibly to the anisotropic Raman ( $\iota=2$ ) and not at all to the infrared ( $\iota=1$ ). Therefore if there is an exchange term in equation 1.21 one would not expect equation 1.11 or the basic assumptions to be valid. However, isotopic dilution studies<sup>4</sup> have indicated that there is little evidence for an 'exchange' via resonant energy transfer in the  $\nu_1$  or  $\nu_3$  bands of acetonitrile. It is therefore interesting that there is evidence for differences between  $\tau_{\nu}^{\text{iso}}$  and  $\tau_{\nu}^{\text{IR}}$  particularly as the spectra recorded were of dilute solutions for which it is believed that 'exchange' effects are eliminated<sup>1</sup>.

Because of these discrepancies it has become apparent that different and independent methods of determining the vibrational correlation functions (which yield  $\tau_{\nu}$ ) are necessary in order to elucidate the nature of the effective intermolecular potential. Several methods of either, obtaining directly or separating, the vibrational correlation functions (or correlation times) have been used.

Rakov<sup>3,2</sup> assumed that the rotational motion of molecules would be completely damped at low temperatures and so the spectral band width would be due to vibrational motion alone. Therefore the 'pure' vibrational correlation function could be obtained from such an experiment. This method has been used<sup>11,33</sup> but it is not completely successful because it assumes that the vibrational relaxation of a molecule is independent of temperature which has been shown to be untrue<sup>1,3,34-36</sup>. However, the method may still be the best in some cases, especially for E bands since for these depolarised bands  $I_{\text{VH}}/I_{\text{VV}} = 3/4$  and therefore the calculation of  $I_{\text{iso}}$  via equations 1.7 and 1.8 and the separation of the reorientational and vibrational parts, is not possible.<sup>7,11</sup>



$$\tau_D = \tau_{1R}^s \frac{(1 + Nf)}{(1 + N\dot{f})} \quad \text{..... 1.24}$$

Where  $Nf$  = the static orientation correlation factor.  
and  $N\dot{f}$  = the dynamic orientation correlation factor.

In very dilute solution however, pair correlations may usually be assumed to be negligible<sup>10,49</sup> and therefore only single molecule correlations will be observed, hence equation 1.24 becomes:

$$\tau_D \equiv \tau_{1R}^s \quad \text{..... 1.25}$$

In this work the far-infrared spectrum of acetonitrile ( $\text{CH}_3\text{CN}$ ) has been recorded in very dilute solutions of a non-polar non-interacting<sup>1,10</sup> solvent, carbon tetrachloride ( $\text{CCl}_4$ ). Solvent spectra backgrounds were subtracted from the solution spectra in order to remove the contribution of the solvent dipole-induced dipole absorption (see Chapter 5), the solvent-solute induced dipole absorption remains however. (See Chapter 6). These dilute solutions were studied at 4 temperatures and in addition the spectra of some more concentrated solutions have been included in the analysis.

An attempt to clarify the molecular dynamics of these solutions has been made by the use of a model based on an extended Langevin equation of motion<sup>23</sup> developed by the memory function approach and the Mori formalism<sup>51</sup> described in Chapter 2. The results of this analysis are presented in Chapter 6.

Finally, in Chapter 7 a study of some solutions of tertiary alkyl ammonium salts is described.

**CHAPTER 2**  
**DIELECTRIC THEORY AND THE MOLECULAR DYNAMICS OF LIQUIDS**

## CHAPTER 2

### DIELECTRIC THEORY AND THE MOLECULAR DYNAMICS OF LIQUIDS

#### A. DIELECTRIC DISPERSION IN LIQUIDS - PHENOMENOLOGICAL DEFINITIONS AND RELATIONS

When an electric field  $E$ , is applied to a dielectric material the material becomes electrically polarised. This electrical polarisation is the total response of the system to the applied field and is the result of the alignment of dipoles, permanent and induced, within the medium. The permanent dipoles are those associated with the charge distribution on the molecules in the medium while the induced dipoles are considered to be due to electron cloud deformation and atomic nuclei displacement by the applied field. When the system is allowed to reach a steady state i.e. the field is static, the total polarisation of the dielectric medium contributes to the capacitance of the system by an amount proportional to the extra charge per unit area which results from that polarisation. From this, the static permittivity ( $\epsilon_0$ ) is defined as

$$\epsilon_0 = C/C_0 \quad \dots\dots\dots 2.1$$

where  $C$  = capacitance of system in presence of dielectric  
 $C_0$  = capacitance of system in vacuo

Where the applied field is removed, the dielectric material returns to its unpolarised state and dielectric relaxation is said to have taken place. The time which this relaxation takes is dependent upon which type of dipole is involved and the physical environment in which it exists. The parameter  $\tau$  is used to describe the time which the total polarisation takes to fall to a certain value, usually  $1/e$ , of its value in the presence of the electric field, by this relaxation process.

If the applied field is now allowed to alternate, i.e. is reversed, the dipole moments will attempt to remain aligned and in phase. While the frequency of the alternating field is low the value of the permittivity will be the same as the static permittivity  $\epsilon_0$ . As the frequency is increased the dipoles begin to lag behind the applied field and can no longer contribute to the polarisation of the medium. At a frequency of about  $10^{10}, 10^{12}$  Hz, the microwave region, the permanent molecular dipoles, which have to undergo orientational motion to remain in phase, begin to lag behind the applied field. The fall in polarisation which results from this reduces the capacitance of the system and leads to a decrease in the permittivity from its static value and a loss of energy from the applied field. This fall in permittivity and absorption of energy, known as the dielectric loss  $\epsilon''$ , constitutes the phenomenon known as dielectric dispersion. The maximum loss occurs when the dipoles are  $\pi/2$  out of phase with the applied field which in dipolar liquids corresponds to a frequency of about  $2\text{cm}^{-1}$ . At higher frequencies which correspond to the infrared and ultraviolet region, the other dipoles which contribute to the total polarisability of the dielectric also begin to lag behind the applied field and give rise to <sup>absorption</sup> features.<sup>58</sup>

The total complex permittivity is given by Debye<sup>15</sup>

$$\hat{\epsilon}(\omega) = \epsilon'(\omega) - i\epsilon''(\omega) \quad \dots\dots\dots 2.2$$

where  $\epsilon'(\omega)$  = the dielectric permittivity, which is the in phase dispersive component  
and  $\epsilon''(\omega)$  = dielectric loss, which arises from the out of phase, dissipative component

and 
$$\hat{\epsilon}(\omega) = \epsilon_{\infty} + \frac{\epsilon_0 - \epsilon_{\infty}}{1 + i\omega\tau} \quad \dots\dots\dots 2.3$$

where  $\epsilon_{\infty}$  = the dielectric permittivity at infinite frequency

$\omega$  = angular frequency of applied field

$\epsilon_0 - \epsilon_{\infty}$  = dispersion - corresponds to in phase resonance

By assuming that the relaxation process is exponential the familiar Debye<sup>15</sup> equations are derived

$$\epsilon'(\omega) = \epsilon_{\infty} + \frac{\epsilon_0 - \epsilon_{\infty}}{1 + \omega^2 \tau^2} \quad \dots\dots\dots 2.4$$

and 
$$\epsilon''(\omega) = \frac{(\epsilon_0 - \epsilon_{\infty}) \omega\tau}{1 + \omega^2 \tau^2} \quad \dots\dots\dots 2.5$$

Finally, referring to Figure 2.1 we have:

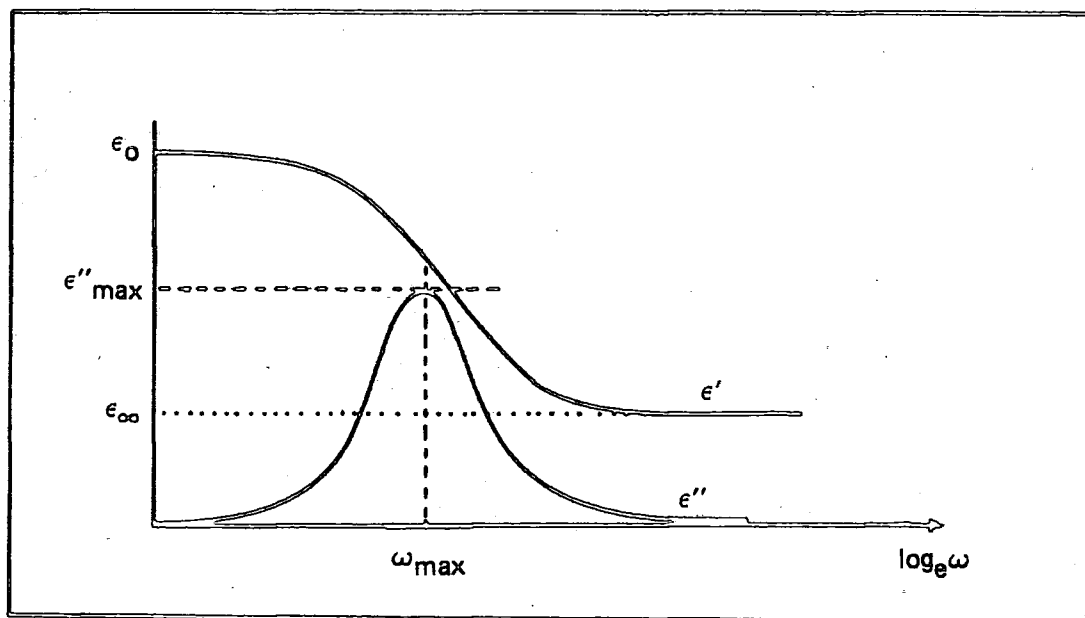


FIGURE 2.1  
SCHEMATIC LOSS AND PERMITTIVITY SPECTRA

$$\epsilon'' \text{ max} = \frac{\epsilon_0 - \epsilon_{\infty}}{2} \quad \dots\dots\dots 2.6$$

$$\tau = 1/\omega \text{ max} \quad \dots\dots\dots 2.7$$

## B. THE APPLICATION OF MICROWAVE AND FAR INFRARED SPECTROSCOPY TO THE ELUCIDATION OF THE MOLECULAR DYNAMICS OF LIQUIDS

It can be considered that there are two problems concerned with the understanding of the molecular dynamics of liquids in the frequency region of  $10^{10} - 10^{12}$  Hz. The first is due to the fact that the parameters obtained by microwave and far infrared methods  $\epsilon'(\omega), \epsilon''(\omega), \alpha(\omega), \eta(\omega)$ , all arise from the bulk macroscopic or multi-molecular behaviour of the dielectric in the alternating field. Ideally, the information required is of the dynamics on a microscopic or preferably a molecular, single particle scale and so it is necessary to derive a relationship between the measured parameters such as  $\tau$  macro ( $\tau_D$ ) and the unknown parameter  $\tau$  molecular ( $\tau^S$ ) on the basis of some reasonable theory. Throughout this thesis  $\tau^{\text{mic}}$  will be taken to be a microscopic approximation of  $\tau^S$ .

The second problem is that the molecular dynamics behaviour established by such a study must be explained in terms of the molecular properties and interactions in the system. This is discussed in Part C of this Chapter.

### Internal Fields

Many attempts at solving the first of these problems have been made by developing theories which lead to expressions for the relationship between the external applied field  $E$  and the internal field  $F$  which can then be used to convert measured parameters to molecular quantities or by remodelling the system with an internal field correction to achieve the 'same' result. The reason for the interest in this approach is understandable when we consider the environment of a dipolar molecular liquid such as acetonitrile ( $\text{CH}_3\text{CN}$ ) which has been the subject of this work. This strongly dipolar molecule (dipole moment 3.9D) will exhibit a field of its own which will influence its close neighbours and vice versa. It is unlikely therefore that the molecule in the centre of such a dielectric medium will be responding only to the fluctuations in the applied field  $E$ . Attempts to reduce this effect can be made by making the dielectric measurements on dilute solutions in non-polar solvents such as carbon tetrachloride  $\text{CCl}_4$  but the effects of the dipolar fields are known to be long range and in addition there is the possibility of induced dipole effects which make it difficult to dismiss the internal field problem.

Initially considering the static or low frequency limit case, Debye<sup>15</sup> pioneered the development or more precisely in this case, the application, of internal field theories. First he derived an expression for the polarisability of the dipole  $\alpha_0$  and hence its contribution to the total polarisability  $P$  in terms of the dipole moment  $\mu$ . To do this he applied a method originally developed by Langevin<sup>82</sup> to find the mean magnetic moment parallel to an applied field for a system containing gas molecules with a permanent magnetic moment. The polarisation due to the permanent electric dipoles is given by:

$$P_{\text{dipole}} = N, \mu^2 E / 3kT$$

$N$	=	number density of dipoles
$\mu$	=	dipole moment
$E$	=	applied field
$k$	=	Boltzmanns constant
$T$	=	temperature



arising from the dipole orientation will decay exponentially. Applying the Lorentz field (equation 2.9) after replacing the static permittivity  $\epsilon_0$  with the complex permittivity  $\hat{\epsilon}(\omega)$  because we now consider an alternating, frequency dependent field yields the following expressions for the polarisability and permittivity.

$$\text{Polarisability} \quad P = N, \left[ a + \frac{\mu^2}{3kT (1 + i\omega\tau^{\text{mic}})} \right] \frac{\hat{\epsilon}(\omega) + 2}{3} E \quad \dots\dots\dots 2.11$$

$$\text{Permittivity} \quad \frac{\hat{\epsilon}(\omega) - 1}{\hat{\epsilon}(\omega) + 2} = \frac{4\pi N, a}{3\epsilon} \left( a + \frac{1}{1 + i\omega\tau^{\text{mic}}} \frac{\mu^2}{3kT} \right) \quad \dots\dots\dots 2.12$$

Neglect of the fields (F3) due to the neighbouring dipoles dictates that this is a microscopic approximation, hence the relaxation time is denoted  $\tau^{\text{mic}}$ . The expression for permittivity reduces to the expression for static permittivity at  $\omega\tau^{\text{mic}} \ll 1$  as would be expected. In the high frequency limit the permittivity becomes  $\epsilon^\infty$  where there is no longer a contribution from dipolar orientation polarisation and only distortion polarisation remains, in which case:

$$\frac{\epsilon^\infty - 1}{\epsilon^\infty + 2} = \frac{4\pi N, a}{3\epsilon} \quad \dots\dots\dots 2.13$$

By this method Debye also obtained an expression for the relationship between the macroscopic relaxation time  $\tau_D$  and the molecular relaxation time  $\tau^{\text{mic}}$

$$\tau_D = \left[ \frac{\epsilon_0 + 2}{\epsilon^\infty + 2} \right] \tau^{\text{mic}} \quad \dots\dots\dots 2.14$$

Recognising that the Lorentz field was inadequate, only being valid for low density gases or dilute solutions and predicting ferroelectricity<sup>58</sup> for many dielectrics such as water (which does not exhibit this phenomenon), Onsager<sup>85</sup> established a relationship between the permittivity and the dipole moment with a different model for the determination of the internal field. This model is similar to that of Lorentz except that the sphere is now considered to be of molecular dimensions in the homogeneous medium. The molecule is assumed to have the properties of a point dipole at the centre of the sphere and the total volume of the spheres is equal to the total volume of the system.

The internal field then comprises two parts:

1. The cavity field (G) i.e. that which would be produced in the empty sphere by the applied field E, given by

$$G = \frac{3\epsilon_0}{2\epsilon_0 + 1} E \quad \dots\dots\dots 2.15$$

2. The reaction field (R) which results from the polarisation caused by the dipole in the cavity, given by

$$R = \frac{2(\epsilon_0 - 1)}{2\epsilon_0 + 1} \frac{m}{a^3} \frac{1}{\epsilon} \quad \dots\dots\dots 2.16$$

where  $a$  = sphere radius  
 $m$  = total moment of molecule  
 $m = \mu + aF$

The internal field according to Onsager is then given by  $F = G + R$ ; in full

$$F = \frac{[3\epsilon_0 / (2\epsilon_0 + 1)] E + [2(\epsilon_0 - 1) / (2\epsilon_0 + 1)\epsilon] \mu / a^3}{1 - [2(\epsilon_0 - 1) / (2\epsilon_0 + 1)\epsilon] a / a^3} \dots\dots\dots 2.17$$

Onsager then derived his expression for the static permittivity

$$\frac{(\epsilon_0 - \epsilon^\infty) (2\epsilon_0 + \epsilon^\infty)}{\epsilon_0 (\epsilon^\infty + 2)^2} = \frac{4\pi N_p \mu^2}{9kT\epsilon} \dots\dots\dots 2.18$$

where  $\eta_\infty^2$  has been rewritten  $\epsilon^\infty$  (according to Maxwell).

The main differences between Onsager's model and Lorentz's are that Onsager's equation does not predict ferroelectricity and that he has not had to make the assumption that the field  $F_3$  is zero. However, the assumption that a molecular sized cavity can be treated as a sphere can only be valid in special cases (spherical, molecules) where there are no strong local fields. In fact, it is unlikely that the cavity would be spherical in the case of  $\text{CH}_3\text{CN}$  which has an ellipsoid ratio of 1:1.7.

For the dynamic case, Collie et al<sup>86</sup> have applied the Onsager field to Debye's diffusive theory of relaxation (described previously). The result shown below:

$$\frac{(\hat{\epsilon}(\omega) - \epsilon^\infty) (2\hat{\epsilon}(\omega) + 1) (2\epsilon_0 + \epsilon^\infty)}{\hat{\epsilon}(\omega) (\epsilon^\infty + 2)^2 (2\epsilon_0 + 1)} = \frac{4\pi N_p \mu^2}{9kT\epsilon} \frac{1}{1+i\omega\tau^{\text{mic}}} \dots\dots\dots 2.19$$

(where  $\epsilon^\infty = \eta_\infty^2$ )

can be solved for  $\hat{\epsilon}(\omega)$  as a function of  $\omega\tau^{\text{mic}}$  by successive approximation.

Nee and Zwanzig<sup>43</sup> have also solved the Onsager for the dynamic case and rederived the results of Klug et al<sup>96</sup>, Fatuzzo Mason<sup>97</sup> and Scaife.<sup>98</sup> The general expression for the frequency dependent case based on the Onsager cavity model is

$$\frac{(\hat{\epsilon}(\omega) - \epsilon^\infty) (2\hat{\epsilon}(\omega) + \epsilon^\infty)}{3\hat{\epsilon}(\omega)} = \frac{4\pi N_p \mu^2}{3kT} Z \left( \frac{-d\phi}{dt} \right) \dots\dots\dots 2.20$$

where  $\phi(t) = \langle \mu(0) \cdot \mu(t) \rangle / \langle \mu(0) \cdot \mu(0) \rangle$  (the normalised dipole correlation function).

Z denotes a Laplace transform.

To solve this expression the concept of dielectric friction is used.

### Dielectric Friction

The field associated with the dipole induces polarisation in the surrounding medium, but the response of this medium is not instantaneous (determined by  $\epsilon(\omega)$ ). Therefore the dynamic polarisation field is no longer identical to the static polarisation field for a given dipole orientation. The net effect is the creation of an electric field in the cavity which exerts a torque opposing reorientation of the dipole, and its rotational kinetic energy is degraded into random molecular motion in the surrounding fluid.

(Dielectric friction is in addition to Stokes friction which pertains to viscosity).

The expression for the dielectric friction ( $\xi_D$ ) derived for rotational Brownian motion is

$$\xi_D(\omega) = \frac{2kT}{i\omega} \frac{(\epsilon_0 - \epsilon^\infty) (\hat{\epsilon}(\omega) - \epsilon_0)}{\epsilon_0 (2\hat{\epsilon}(\omega) + \epsilon^\infty)} \dots\dots\dots 2.21$$

Then considering the case of the unhindered rotation of a spherical isotropic molecule and assuming Debye type low frequency behaviour yields the useful relation

$$\tau_D = \left[ \frac{(2\epsilon_0 + \epsilon^\infty)}{(\epsilon_0 + 2\epsilon^\infty)} \right] \tau^{\text{mic}} \quad \dots\dots\dots 2.22$$

Lobo's<sup>102</sup> expression for dynamic dielectric behaviour is a Nee and Zwanzig<sup>43</sup> - Onsager model which is generalised for the high frequency region by the inclusion of the inertial terms and incorporates single particle and collective behaviour. They have criticised Fatuzzo and Mason's<sup>97</sup> dielectric function because the polarisability used was of a freely-rotating dipole, i.e. no allowance was made for the dipole renormalization energy due to the reaction field which contributes to the viscous torque (see Hubbard and Wolynes<sup>103</sup>).

The following relations have been defined

$$\tau^{\text{mic}} = \tau_D (\epsilon_0 + 2\epsilon^\infty) / (2\epsilon_0 + \epsilon^\infty) \quad \left[ \begin{array}{l} \text{as for Nee \&} \\ \text{Zwanzig} \\ \text{equation 2.22} \end{array} \right]$$

$$\tau^{\text{sp}} = \tau^{\text{mic}} (2\epsilon_0^2 + \epsilon^\infty^2) / (\epsilon_0 (\epsilon_0 + 2\epsilon^\infty)) \quad \dots\dots\dots 2.23$$

Kirkwood<sup>87</sup> and Fröhlich<sup>88</sup> derived expressions for the static permittivity of a dielectric without making the assumptions which lead to the limited applicability of Debye's and Onsager's equations by modelling the system with the sphere (or non-spherical in Fröhlich's case) in a dielectric medium and solving by statistical techniques. They arrived at similar results to each other for the case of non-polarisable dipoles but when the effect of polarisable dipoles was included their expressions appeared to be different. Brown<sup>89</sup> has shown that this difference was due to Kirkwood's use of the cavity field when calculating the distortion polarisation where in fact application of the total field expression and rewriting some of the terms yields a result identical with that of Fröhlich.

$$\frac{(\epsilon_0 - \epsilon^\infty) (2\epsilon_0 + \epsilon^\infty)}{\epsilon_0 (\epsilon^\infty + 2)^2} = \frac{4\pi N_g \mu_g^2}{9kT\epsilon} \quad \dots\dots\dots 2.24$$

where  $g$  is Kirkwood's correlation parameter, a measure of local order, and  $\mu_g$  refers to the dipole moment in the gaseous state and  $\mu$  is related to  $\mu_g$  (using Onsager's definition of internal refractive index) by

$$\mu = \frac{(2\epsilon_0 + 1) (n^2 + 2)}{3 (2\epsilon_0 + n^2)} \mu_g \quad \dots\dots\dots 2.25$$

In 1957, Cole derived a similar expression to Kirkwood and Fröhlich by a method based on Van Fleck's calculation for non-polar liquids and later<sup>92</sup> developed an expression for the dynamic case using a method first applied by Glarum<sup>93</sup> employing linear response theory,<sup>52</sup> which relates the behaviour of a weakly coupled system under the influence of a stimulus to its behaviour in the absence of a stimulus.

By this method the following expression for the relationship between  $\tau_D$  and  $\tau^{\text{mic}}$  has been derived.

$$\tau_D = \frac{3\epsilon_0\tau^{\text{mic}}}{2\epsilon_0 + \epsilon^\infty} \quad \dots\dots\dots 2.26$$

When the value for the relaxation time of the inner sphere used by Cole in this derivation was applied to Powles<sup>94</sup> result it was shown that the relationship of  $\tau_D$  to  $\tau^{\text{mic}}$  from the separate derivations is identical.

Fatuzzo and Mason<sup>97b</sup> applied the Glarum-Cole approach using linear response theory and arrived at a different result for the relationship between  $\phi(t)$  and  $\epsilon(\omega)$

i.e. (Fatuzzo and Mason) 
$$Z (-d\phi/dt) = \frac{(\epsilon(\omega) - 1) (2\epsilon(\omega) + 1) \epsilon_0}{(\epsilon_0 - 1) (2\epsilon_0 + 1) \epsilon(\omega)} \quad \dots\dots\dots 2.27$$

(Glarum and Cole) 
$$Z (-d\phi/dt) = \frac{(\epsilon(\omega) - 1) 3\epsilon_0}{(\epsilon_0 - 1) (\epsilon(\omega) + 2\epsilon_0)} \quad \dots\dots\dots 2.28$$

where  $Z$  denotes a Laplace transform

$\epsilon(\omega)$  denotes the frequency dependent dielectric permittivity

$\phi$  is the normalised autocorrelation function for the net dipole moment of an embedded sphere

Fatuzzo and Mason also derived their equation by direct application of linear response theory to the sphere in a medium which was the method employed by Klug<sup>96</sup>, Zwanzig<sup>43</sup> and Hill<sup>99</sup>, who generalized the theory to include induced dipoles. Titular and Deutch<sup>100</sup> have suggested that the reason for the discrepancy between Fatuzzo-Mason and Glarum-Cole is that Glarum-Cole assumed that the medium in which the sphere is immersed has frequency independent permittivity, where Fatuzzo-Mason have assumed that the surrounding medium has the same frequency dependence as the sphere. In the case of a strongly polar molecule in dilute solution of a non-polar solvent, the Fatuzzo-Mason assumption is unlikely to hold, but Titular and Deutch have favoured their approach and indicated that it is a convenient point to start for molecular modelling.

More recently, Williams<sup>95</sup> has examined the Kirkwood-Fröhlich expression and extended it to include the frequency dependent case. His solution introduces a dynamic factor  $g(t)$  which is the time dependent Kirkwood  $g$  factor. (Brot<sup>42</sup> has reviewed this approach.)

However, Kivelson and Madden<sup>101</sup> have pointed out that most of the theories discussed model the system with sample cavities which are reduced to molecular dimensions but then assume that macroscopic dielectric theory can be applied. They have criticised expressions relating macroscopic to molecular parameters (such as equations 2.22 and 2.23) on the grounds that a molecular property cannot be related to a macroscopic property by an expression which only has macroscopic parameters. The theory which they have developed relates the frequency dependent permittivity to a true single particle correlation function without the use of local field theories. Initially, the relationship between the macroscopic correlation function  $\Phi_m(t)$  and the complex dielectric constant is found with the use of Kubo<sup>80</sup> linear response theory. The relationship

between the macroscopic correlation function  $\Phi_m(t)$  and the corresponding molecular correlation function  $\phi^S(t)$  is then sought by application of the 'corresponding micro - macro correlation theorem' (cmmc). This theorem states 'that if the molecular correlation function can be expanded as a sum of exponentials, then the macroscopic correlation function has the same form with appropriately scaled parameters'.

Assuming that the molecular and macroscopic relaxation decays exponentially, Keyes and Kivelson<sup>44</sup> have given the expression:

$$\tau_D^S = \tau^S \frac{(1 + Nf)}{(1 + N\dot{f})} \quad \dots\dots\dots 2.29$$

where  $f$  is a structure factor which measures the orientational correlation of the dipoles  
 $\dot{f}$  is the dynamic  $f$   
 and  $(1 + Nf)$  is equivalent to the Kirkwood 'g' factor .

The theorem has been applied by Kivelson and Madden<sup>101</sup> to derive the expression for spherical samples in a vacuum

$$\tau^S = \tau_D \frac{(\epsilon_{\infty} + 2)(\epsilon_0 + 2)}{(\epsilon_0 - \epsilon_{\infty})} \frac{N, \langle \mu \rangle^2}{3kT} \frac{4\pi}{3} \quad \dots\dots\dots 2.30$$

A similar expression for an embedded sphere of Kirkwood-Fröhlich is

$$\tau^S = \tau_D \frac{\epsilon_0 (\epsilon_{\infty} + 2)^2}{(\epsilon_0 - \epsilon_{\infty})(2\epsilon_0 + \epsilon_{\infty})} \frac{4\pi N, \langle \mu \rangle^2}{9kT} \quad \dots\dots\dots 2.31$$

where the mean squared dipole moment  $\langle \mu \rangle^2$  is given by the approximation

$$N, \langle \mu \rangle^2 / 3kt = 4.85 \mu_g^2 p / M(T/300)$$

$p$  = density

$M$  = molecular weight

Note with reference to criticisms of other results that these expressions include both macroscopic and molecular terms. ( $\langle \mu \rangle^2$ ).

Brot et al<sup>104, 105, 106</sup> have developed a molecular dynamics simulation approach to the problem which is based on an electrostatic two-dimensional disc of approximately 13 molecules in diameter, representing an isolated dipolar system of Stockmayer molecules. Comparison of the autocorrelation functions of the inner microscopic disc and the outer disc gives the response function which is in agreement with Fatuzzo and Mason. By this method, Brot has shown that a good simulation can be made by the statistical modelling of a few hundred (313) molecules. For distances greater than 3-5 molecule diameters, macroscopic laws of electrostatics apply. The results obtained

$$\tau_D / \tau^{\text{mic}} = \frac{\epsilon_0 [(d-1)\epsilon_0 + 1]}{(d-1)\epsilon_0^2 + 1} \quad \dots\dots\dots 2.32$$

$d$  = No. of dimensions

can, with appropriate assumptions, be shown to be in agreement with Fatuzzo and Mason.<sup>97b</sup>

Kluk et al<sup>108a</sup> have given a complete breakdown of the long and short range effects as follows. The macroscopic measured parameter  $\tau_D$  is related to a microscopic multiparticle correlation time  $\tau^{\text{mic}}$  by the use of Frölich's model and the application of linear response theory. This accounts for the long range effects. The relationship obtained is given by

$$\tau^{\text{mic}} = \left[ \frac{1 + (\epsilon^\infty / 2\epsilon_0)}{1 + (1 / 2\epsilon_0)} \right] \tau_D \equiv f[\epsilon_0, \epsilon^\infty] \tau_D \quad \dots\dots\dots 2.33$$

This expression can be shown to be identical to that derived by Brot for the three dimensional case (equation 2.32). It should be noted that taking typical values of  $\epsilon_0 = 5$  and  $\epsilon^\infty = 2.25$  reveals that the ratio of  $\tau^{\text{mic}}/\tau_D$  is 0.95 which is in agreement with Hill's<sup>58</sup> suggestion that taking  $\tau^{\text{mic}} = \tau_D$  was a reasonable approximation.

A rigorous method using the Mori formalism<sup>51</sup> based on Kivelson and Maddens<sup>101</sup> approach with variables taken from Gierke's paper<sup>109</sup> has been applied to calculate the short range effects. This yields an expression relating  $\tau^{\text{mic}}$  to  $\tau^s$ , the single particle dipole moment correlation time.

$$\tau_{\text{mic}}^{-1} = K^{-1} \left[ (\tau^s)^{-1} + (1 - K^{-1}) \int_0^\infty (\omega_\perp^{(2)}(t), \omega_\perp^{(1)}(0)) dt \right] \quad \dots\dots\dots 2.34$$

where  $K = 1 + (N - 1) (Y_0^l(2,0), l)$

and  $Y_0^l$  describes the coordinates of the molecular tensors of rank =  $l$

$\omega_\perp$  denotes the angular velocity coordinate which is perpendicular to the Z axis of the molecule.

An approximation of this expression is made by neglecting the 2nd term and assuming that:

- i. the molecule has at least  $C_{2V}$  symmetry ( $\text{CH}_3\text{CN}$  has  $C_{3V}$ ) symmetry
- ii. the dipole is at the centre of the molecule
- iii. the effective dipole depends only on instant polarisation

The Kirkwood coefficient  $K$  is then given by the expression for an ellipsoid cavity which is appropriate for  $\text{CH}_3\text{CN}$ .

$$K = \frac{9kT}{4\pi N \mu_g^2} \frac{(\epsilon_0 - \epsilon^\infty)(2\epsilon_0 + \epsilon^\infty)}{[1 + D(\epsilon^\infty - 1)]^2 \epsilon_0} \quad \dots\dots\dots 2.35$$

where  $D =$  depolarisation coefficient<sup>122</sup> along the principle axis (for  $\text{CH}_3\text{CN}$ ,  $D = 0.21$ )

The relationship of  $\tau^s$  to  $\tau^{\text{mic}}$  is then given by

$$\tau^s = \tau^{\text{mic}} K^{-1} \quad \dots\dots\dots 2.36a$$

and for  $\tau^s$  to  $\tau_D$

$$\tau^s = f[\epsilon_0, \epsilon^\infty] K^{-1} \tau_D \quad \dots\dots\dots 2.36b$$

Equation 2.36b in full becomes

$$\tau^s = \tau_D \frac{\left[ \frac{1 + (\epsilon^\infty / 2\epsilon_0)}{1 + (1/2\epsilon_0)} \right] \left[ 4\pi N \mu_g^2 (1 + D(\epsilon^\infty - 1))^2 \epsilon_0 \right]}{\left[ 9kT (\epsilon_0 - \epsilon^\infty) (2\epsilon_0 + \epsilon^\infty) \right]} \quad \dots\dots\dots 2.37$$

In a study of the dielectric relaxation of liquid methyl iodide, Kluk<sup>108b</sup> has neglected the correction of long range effects and applied equation 2.36b with  $\tau_D$  for  $\tau$  micro. The results from this have been adjusted by the Hubbard relation.<sup>16</sup>

$$\tau_{1R} = 3\tau_{2R}$$

microwave                  Raman

and have been found to be in good agreement, within experimental error, with the results obtained from Raman Scattering experiments.

Bordewijk<sup>107</sup> has also taken account of the long and short range effects without recourse to the sphere in a continuum model. By his statistical method he has rederived the Kirkwood-Fröhlich expression for the static case, and found agreement with Titulear-Deutch<sup>100</sup> and Fatuzzo-Mason<sup>97</sup> for the frequency dependent case when  $\epsilon^\infty$  is taken as unity i.e. for non-polarisable dipoles. Further reduction of his expression

$$\frac{1}{g\mu^2} Z i\omega \left\langle \mu_1(0) \cdot \sum \mu_i(t) \right\rangle_0^\infty = \frac{(\hat{\epsilon}(\omega) - \epsilon^\infty) (2\hat{\epsilon}(\omega) + \epsilon^\infty) \epsilon_0}{\hat{\epsilon}(\omega) (\epsilon_0 - \epsilon^\infty) (2\epsilon_0 + \epsilon^\infty)} \quad \dots\dots\dots 2.38$$

where  $\mu = \mu_g$  for spherical molecules with isotropic polarisability.

by removing the cross correlation terms yields Klug's<sup>96</sup> result and Rivail's if  $g = 1$ .

Hubbard and Wolynes<sup>103a</sup> have developed a theory of dielectric friction, which has been criticised by Brito and Bordewijk,<sup>110</sup> based on a rotational Smoluchowski equation derived from Einstein's equation for Brownian motion<sup>84</sup> with the inclusion of terms to account for interacting particles and external fields. This is a macroscopic theory originally developed by Smoluchowski to explain coagulation in colloidal dispersions. The model allows for fluctuating torques caused by variations in the polarisation which arise in the dynamic system and therefore permits the external (long range) medium to have a different decay time to that of the cavity. An expression for  $\tau^S$  is given

$$1/\tau^S = \frac{2\epsilon_0 + 1}{3\tau_D} + 6D_0 \quad \dots\dots\dots 2.39$$

$D_0$  = 'bare' rotational diffusion coefficient

The limitations to the model are that a diffusional system has been assumed to apply the Smoluchowski equation and this breaks down for smooth molecules. In addition, local structure has not been accounted for in the calculation of the electric field fluctuations.

The full equation for the total friction on the molecule which comprises a dielectric part  $\rho_D$  and a viscous part  $\rho_{vis}$  is given by<sup>103b</sup>

$$\rho_D + \rho_{vis} = (8\pi\eta a^3 a) + \frac{3k T \tau_D (\epsilon_0 - \epsilon^\infty)^2}{\epsilon_0 (2\epsilon_0 + \epsilon^\infty)} \left[ \frac{2}{3} - \frac{4a}{3} + \frac{61a^2}{60} \right] \quad \dots\dots\dots 2.40$$

where  $a$  is a friction coefficient which is equal to zero for perfect slip and unity for stick conditions.

The method used by Schurr<sup>111</sup> involves the rigorous determination of the relationship between the self rotational diffusion coefficient,  $D_R$ , and the initial (short time) part of the orientational correlation function. An approximate expression for the relation between the auto-correlation function of the net permanent dipole moment and the total dipole moment of a sphere as described by Onsager with time dependent dipole moment in the cavity is then derived by application of linear response theory. A simple expression has been given for an assembly of permanent dipoles with a single relaxation time.

$$(2D_R)^{-1} = \tau_D \left( 4\pi \frac{\langle N \rangle \mu^2}{V 3kT} \right) / (\epsilon_0 - 1) \quad \left[ \text{where } (2D_R)^{-1} = \tau^{\text{mic}} \right] \dots\dots\dots 2.41$$

However, as Schurr has indicated, this is not a realistic physical situation and so the equation is of little value. Instead we must make use of equation 2.42 and its derivatives 2.43 and 2.44.

For dielectric relaxation

$$(2D_R)^{-1} = \tau_D \left( \frac{4\pi\rho N_A}{M} \frac{\mu^2}{3kT} \right) \frac{1}{81(\epsilon_0 - \epsilon_\infty)} \left( \frac{(2\epsilon_\infty + 1)(\epsilon_\infty + 2)}{\epsilon_\infty} \right)^2 \dots\dots\dots 2.42$$

- $\rho$  = density
- $N_A$  = Avogadro's constant
- $M$  = molecular weight

For dilute solution in non-polar solvent

$$(2D_R)^{-1} = \tau_D \left( \frac{4\pi\langle N \rangle}{V} \frac{\mu^2}{3kT} \right) \frac{1}{81(\epsilon_0^s - \epsilon_1)} \left[ \frac{(2\epsilon_1 + 1)(\epsilon_1 + 2)}{\epsilon_1} \right]^2 \dots\dots\dots 2.43$$

For very dilute solution in non-polar solvent

$$(2D_R)^{-1} = \tau_D \left( \frac{2\epsilon_1 + 1}{3\epsilon_1} \right)^2 \dots\dots\dots 2.44$$

- $\langle N \rangle / V$  =  $\rho N_A / M$
- $\epsilon_1$  = dielectric permittivity of solvent
- $\epsilon_0^s$  = static permittivity of solution

By applying this method and comparing results for a wide range of solutes and solvents, Schurr has found that in general the correlation times have fallen approximately 30% below the results obtained by the Rayleigh scattering and NMR techniques.

Rosenthal and Strauss<sup>41</sup> have made use of the theories developed in recent years to relate the measured parameters obtained from the Raman and Far-Infrared spectra of chloroform and chlorobenzene. Corrections to the far infrared correlation times were made using Klug's internal field. This was then compared to the Kirkwood-Fröhlich model as a check by back calculation of the g factors. The agreement was found to be very good for  $\text{CHCl}_3$  but unsatisfactory for chlorobenzene. This is thought to be because of the use of spherical fields where in fact an elliptical field is probably more likely to be a true physical representation.

It was also found that the intensities of the depolarised Rayleigh spectrum did not match up with theoretical levels which was again attributed to the need for cavity corrections to the polarisability anisotropy. Combination of the correlation functions found in the experiment yield the 'distinct' correlation function given by

$$\phi_d^{(1)} = \frac{1}{N} \left\langle \sum_{i \neq j} \vec{\mu}_i(0) \cdot \vec{\mu}_j(t) \right\rangle$$

The distinct functions were found to decay much more slowly than those for the FIR, IR, Rayleigh and Raman, which is in agreement with Keyes and Kivelson.<sup>44</sup>

### C. DETAILS OF SOME OF THE MODELS USED TO DESCRIBE THE MOLECULAR DYNAMICS OF LIQUIDS

The models used to describe liquid molecular dynamics are all based on a knowledge of the behaviour of macroscopic objects according to the fundamental laws of motion. The simplest model which might be used to describe molecular rotation is that of the free rotor. As this condition could only be expected to apply in the very dilute gas phase it is of no use for describing condensed liquid phases in which the molecules are undergoing multiple interruptions to their motion by their 'collisions' with each other.

The expression for free rotation of a symmetric top molecule is given by<sup>113</sup>

$$\phi_{FR}(t) = \langle \bar{\mu}(0) \cdot \bar{\mu}(t) \rangle \propto \int_0^\infty \sum_{K=-J}^J \left[ S(I,K) \left( \frac{\bar{\nu}^3}{2B} - 2B\bar{\nu}K^2 \right) \exp\left(\frac{-[(A-B)K^2hc]}{kT}\right) \right] \exp\left(-\frac{Bhc}{kT} \left(\frac{\bar{\nu}}{2B} - 1\right) \frac{\bar{\nu}}{2B}\right) \cos(2\pi\bar{\nu}ct) d\bar{\nu} \quad \dots\dots\dots 2.45$$

where  $J = \bar{\nu}/2B - 1$

$S(I,K)$  is the nuclear spin weighting factor<sup>114</sup>

$A$  and  $B$  are rotational constants

$K$  is the quantum number for the component of angular momentum along the  $C_3$  axis.

#### i) Rotational Diffusion

For the condensed phases Debye<sup>15</sup> considered the rotational motion of a spherical molecule in an applied field to be constantly interrupted by collisions with its neighbours. The collisions are assumed to be completely elastic i.e. they are instantaneous and therefore the acceleration is infinite. This condition for the collisions implicitly assumes that the rotating, interacting molecules have no inertia which if they had would modify the acceleration characteristics to something other than a delta function. The second of Debye's assumptions is that the time between collision is infinitesimally small: the molecules are literally undergoing continuous collisions which limits the change in angle of the molecules to small values. This allows the application of the diffusional theory and equations of motion originally derived by Langevin<sup>82</sup> for the Brownian motion of macroscopic particles under the influence of collisions by molecules undergoing thermal motion i.e.

$$m\dot{\nu}(t) = mc\nu + K(t) \quad \dots\dots\dots 2.46$$

$-mc\nu$  friction retardation

$K(t)$  randomly fluctuating force arising from molecular impact

Debye considered the effect of the applied field on a molecule and exerting a torque, to be resisted by the microscopic friction introduced by collision with its neighbours.

The torque on a dipole is given by

$$M = F\mu \sin\theta \quad \dots\dots\dots 2.47$$

if it is assumed that  $F$  is the field experienced by a dipole of moment  $\mu$  at an angle of  $\theta$  to the field.

This torque exists because of the resistance arising from local coefficient of frequency independent friction  $\beta$

$$M = \beta d\theta/dt \quad \dots\dots\dots 2.48$$

This situation is usually expressed as

$$\text{Sin } \theta \mu F = -\beta d\theta/dt \quad \dots\dots\dots 2.49$$

The Langevin equation for rotational motion per unit moment of inertia is then

$$d\dot{\theta}/dt = -\beta d\theta/dt + \Gamma(t) \quad \dots\dots\dots 2.50$$

where  $\Gamma(t)$  is the random torque on the molecule due to the motion of its neighbours.

The neglect of inertia in the Debye equations was known to limit their range of application to relatively low frequencies (i.e. longer time motions). Debye predicted that his expressions were valid up to field frequencies of approximately  $10^{12}$  Hz. In terms of the dielectric response which Debye obtained by application of the Lorentz field as described previously in this Chapter, the expression below was given

$$(\hat{\epsilon}(\omega) - \epsilon_{\infty}) / (\epsilon_0 - \epsilon_{\infty}) = (1 - i\omega\tau_D)^{-1} \quad \dots\dots\dots 2.51$$

It was predicted that equation 2.51 was valid for frequencies  $\bar{\nu}$  of less than  $(2\pi\tau_D)^{-1}$  which in terms of the Debye relaxation time  $\tau_D$  is approximately  $10^{11}$  S. The breakdown of the Debye theory is shown most dramatically by the power absorption coefficient  $a(\omega)$  which is related to the loss  $\epsilon''(\omega)$  by

$$a(\omega) = \omega\epsilon''(\omega) / \eta(\omega)c \quad \dots\dots\dots 2.52$$

It can be shown<sup>115</sup> by integration of equation 2.50 that

$$a(\omega) \propto \omega^2 (1 + \omega^2)^{-1} \text{ (approx)} \quad \dots\dots\dots 2.53$$

This relation of  $a(\omega)$  and  $\omega$  accounts for the familiar 'plateau' in the  $a(\omega)$  spectrum at frequencies above the microwave as illustrated by Figure 6.1. This opacity, which would extend to the visible region, is obviously not observed in practice.

Despite the failure of the Debye theory, it has been used extensively, particularly by early workers who were unable to observe the far-infrared region where the deviation from the model becomes pronounced. The apparent lack of importance of the breakdown of the Debye theory at very high frequencies did not, of course, deter the theorists from attempting to formulate a theory which was valid over the wider range. At the time of the early Debye modifications<sup>77,78</sup> the presence of any additional absorption features as later predicted by Poley<sup>61,63</sup> had not been suspected and so the models proposed were the Debye type, corrected by including inertial terms, which would predict a return to transparency of the absorption spectrum at some frequency below the visible region.

ii) **Inertia Corrected Debye Models**

Rocard<sup>77</sup> and later Powles<sup>78</sup> gave expressions for the Debye theory with the additional inertial terms. The expression for the torque on the dipole is then given by

$$M = \underbrace{\beta d\theta/dt}_{\text{friction term}} + \underbrace{I_b d\dot{\theta}/dt}_{\text{inertial term}} \quad \dots\dots\dots 2.54$$

where  $I_b$  = moment of inertial perpendicular to  $C_3$  axis.

This introduces a friction time  $\tau_F$  into the equation for the dielectric permittivity and the equivalent of equation 2.51 is then given by

$$\text{(Rocard)} \quad (\hat{\epsilon}(\omega) - \epsilon_{\infty}) / (\epsilon_0 - \epsilon_{\infty}) = \left[ (1+i\omega\tau_D) (1+i\omega\tau_F) \right]^{-1} \quad \dots\dots\dots 2.55$$

$$\text{where } \tau_F = l/(2kT\tau_D) \quad \dots\dots\dots 2.56$$

$$\text{(Powles)} \quad (\hat{\epsilon}(\omega) - \epsilon_{\infty}) / (\epsilon_0 - \epsilon_{\infty}) = \left[ 1+i\omega\tau_D + (1-\lambda)i\omega\tau_F - \tau_F\tau_D\omega^2 \right]^{-1} \quad \dots\dots\dots 2.57$$

where  $\lambda$  is an arbitrary parameter  $0 \leq \lambda \leq 1$

This expression is identical to the Rocard result for  $\lambda = 0$  and for  $\lambda = 1$  reduces to equation 2.58 which is itself identical to the relation derived by Sack.<sup>79</sup>

$$(\hat{\epsilon}(\omega) - \epsilon_{\infty}) / (\epsilon_0 - \epsilon_{\infty}) = \left[ 1 + i\omega\tau_D - \omega^2\tau_D\tau_F \right]^{-1} \quad \dots\dots\dots 2.58$$

Kubo<sup>80</sup> has pointed out that this equivalent to the use of the Debye equation 2.51 with  $\tau_D$  substituted with the frequency dependent relaxation time  $\tau$  (Sack) where

$$\tau \text{ (Sack)} = \tau_D (1 + i\omega\tau_F) \quad \dots\dots\dots 2.59$$

McConnell<sup>120</sup> has recently criticised the result of Rocard on the grounds that the derivation was based on a non-existent differential equation of Brownian motion. He has carried out a rigorous derivation of the equations of motion for liquid molecules and shown that the Rocard result for spherical molecules (equation 2.55) is more accurately given by

$$(\hat{\epsilon}(\omega) - \epsilon_{\infty}) / (\epsilon_0 - \epsilon_{\infty}) = \left[ (1 + i\omega(\tau_D - \frac{1}{4}\tau_F)) (1 + i\omega\tau_F) \right]^{-1} \quad \dots\dots\dots 2.60$$

McConnell has also given the expression for other model shapes, the one of interest in the case of acetonitrile being for the symmetric top rotator

$$(\hat{\epsilon}(\omega) - \epsilon_{\infty}) / (\epsilon_0 - \epsilon_{\infty}) = \left[ \left( 1 + i\omega\tau_D \left[ 1 - \frac{D_1^{(2)}}{D_1^{(1)}} \right] \right) (1 + i\omega\tau_F) \right]^{-1} \quad \dots\dots\dots 2.61$$

where  $D_1^{(2)}$  and  $D_1^{(1)}$  are the rotational diffusion constants<sup>116,117</sup>

$$D_1^{(1)} + D_1^{(2)} = D_1 \quad \dots\dots\dots 2.62$$

$$D_1^{(1)} = \frac{kT}{I_1 B_1} \quad \dots\dots\dots 2.63$$

$$D_1^{(2)} = \frac{(kT)^2}{I_1^2 I_3} \left[ I_1 \frac{2B_1 - B_3}{B_1^2 B_3 (B_1 + B_3)} + I_3 \frac{-3B_1^2 + B_1 B_3 + B_3^2}{B_1^3 B_3 (B_1 + B_3)} - \frac{(I_1 - I_2)^2}{I_1 B_1^2 (B_1 + B_3)} \right] \quad \dots\dots\dots 2.64$$

where  $I$  and  $B$  denote the moment of inertia and frictional constants appropriate to the axis of rotation.

### iii) The Far Infrared 'Poley' Absorption

Microwave studies of the dielectric properties of liquids have most frequently been analysed from the form of the dielectric loss spectra ( $\epsilon''(\omega)$ ). These analyses, often made with the Cole-Cole plot representation<sup>123</sup>, expose the deviation of the system behaviour from the Debye model at high frequencies<sup>68</sup> where previously experimental limitations became apparent.<sup>54</sup> However, the presence of very large features in the  $\epsilon(\omega)$  spectrum in the far-infrared result is only a small feature on the shoulder of the loss curve. The converse of this is also true in that observations in  $\alpha(\omega)$  do not clearly reveal evidence of large features in the  $\epsilon''(\omega)$  spectrum.

The presence of an additional absorption region was first suggested by Poley<sup>61</sup> in 1955, following a study of the spectroscopic parameters of a series of halobenzenes, which had been recorded elsewhere. Initially Poley observed that the values recorded for  $\epsilon^\infty$  (the value of dielectric permittivity  $\epsilon'$  at infinite frequency) were not equal to the value of  $n_D^2$  ( $n_D$  the refractive index in the optical region) as they should be according to Maxwell's equations if the difference due to the IR vibrational bands is neglected. This led him to speculate that there was a region of absorption between the microwave and the infrared which must be fairly large to account for the discrepancy and since the difference was proportional to the square of the dipole moment then it must be of dipolar origin.<sup>63</sup> Further support for his theory was published the same year when he noted the deviation from Debye behaviour in the Cole-Cole plots ( $\epsilon'$  vs  $\epsilon''$ ) of these liquids. Poley's explanation of the additional feature, which has since become known as the 'Poley' absorption, was that it arose from the oscillation of polar molecules about a locally temporarily defined position in the liquid.

In 1963, Hill<sup>56</sup> formulated a theory which predicted the presence of a feature in the far-infrared in order to account for the  $\epsilon^\infty, n_D^2$  differences which remained after the IR resonance modes had been accounted for. The model proposed was one in which the absorbing molecule is librating in a flexible molecular cage which by damping of the resonances will result in the broadening of the feature. This band was predicted to occur at approximately  $30\text{cm}^{-1}$ , well out of the microwave range and below the frequencies studied with extended infrared instruments. This was the first version of the 'itinerant oscillator' model also known as the 'quasi crystalline' model.

Finally, in 1964, evidence of the Poley feature was observed for the first time at the National Physical Laboratories<sup>59</sup> (NPL) with the newly-developed HCN Maser operating at  $29.712\text{cm}^{-1}$ . This initial observation showed that the value of  $\alpha$  for chlorobenzene at this frequency was more than twice the hypothetical value  $\alpha^\infty$  obtained from the extended Debye models accounting for the microwave feature. In the same year interferometer experiments by Chantry and Gebbie<sup>55</sup> revealed the full far infrared spectrum and confirmed the presence of the Poley feature in Chlorobenzene. It is worth noting that also in 1964 working down from the low infrared  $250\text{cm}^{-1} - 50\text{cm}^{-1}$  using a double beam Perkin Elmer 301 grating spectrophotometer, Günthard<sup>70</sup> et al had observed the edge of the Poley feature for a number of liquids both polar and non-polar including chlorobenzene but did not discuss it in their assignment of the features.

Chantry and Gebbie<sup>55</sup> noted that the integrated intensity of the Poley absorption remained constant with temperature but the frequency shifted to slightly higher frequency and became sharper on cooling. This behaviour is similar to that observed for lattice bands and was assigned to a pseudo lattice mode with the supportive evidence that the crystal structure of chlorobenzene recorded at 130K showed some sharp lattice band absorption in this region. It was speculated that these features could partially collapse to give the broadened feature of the liquid spectrum.

In 1966 Bradley<sup>60</sup> et al performed some experiments on liquids in order to examine the effects of pressure on the Poley band. It was shown that the intensity of the feature increases rapidly with pressure which led them to the conclusion that they must have been observing the result of a multipole interaction which would be expected to depend on molecular separation to a high inverse power.

In 1967 Kroon and van der Elksen<sup>71</sup> first suggested that the far infrared Poley absorption was predominantly the result of a rotational motion but there was a residual component which was accounted for by a translation mode. The evidence for the presence of a resonance absorption in the Poley region was presented by Chamberlain<sup>72</sup> in 1968 when he obtained the far infrared refractive index spectrum of chlorobenzene by dispersive fourier transform spectrometry at NPL. The refractive index spectrum showed the type oscillatory features which are associated<sup>54,124</sup> with resonance phenomena at the centre of the Poley band. At the same time Hill<sup>73</sup> calculated the profiles of  $\alpha(\omega)$  and  $\epsilon''(\omega)$  for a model of 3 overlapping resonance features which was in good agreement with the spectra recorded to date.<sup>55,64,67,71</sup> In fact, it was suggested that the Poley band was composed of a continuously distributed number of overlapping damped resonances.

Brot and Lassiers<sup>74</sup> explanation (1969) of the observed features allowed for the presence of relaxation and resonance phenomena. They envisaged a situation where the absorbing molecules are librating in a shallow potential well which accounts for the resonance contribution. The relaxation contribution is then accounted for by the molecules periodically 'flipping' into other configurations. Adjustment of the parameters in this theory, known as the 'multisite' or libration in a two well potential model, enabled them to reproduce the correct form for both the absorption and refractive index (dispersion) spectrum in the far infrared region.

Also in France during 1971-2 Brot<sup>75,76</sup> carried out some high pressure gas far-infrared measurements on carbonyl sulphide, chloroform and some halobenzenes. These spectra were recorded at pressures up to the critical point and it was concluded from the appearance of the Poley band that most of it results from a hindered rotational type of molecular motion.

Further extensions to Hill's<sup>56</sup> 'itinerant oscillator' model have been made by Coffey<sup>121</sup> and Wyllie.<sup>47</sup> In this model the molecule of interest is considered to be librating within a cage of neighbouring molecules which is itself performing a rotational diffusion motion. The libration frequency is fixed in the 'Poley' region and the cage rotational diffusion gives rise to a feature in the Debye relaxation domain. The result of this model is that a clear distinction is seen between the microwave and far infrared region absorptions. (See Figure 6.1.)

Recently Chantry et al<sup>118</sup> have examined the two component hypotheses by a novel technique which they have attributed in the first instance to Darmon, Gerschel and Brot.<sup>75</sup> The assumption has been made that if the 'Poley' absorption arises from some kind of liquid 'lattice' vibration then it will be evident in the spectrum of a non-polar liquid while the reorientational Debye type absorption will be absent. Thus it has been assumed that the comparison of two physically (inertially) similar molecules, polar and non-polar, can be used to reveal the 'non-resonant' contribution to the polar spectrum by subtracting the non-polar spectrum after suitable scaling. (This scaling is required because of the much lower absorption found in non-polar liquids). In the case of methyl chloroform (CH<sub>3</sub>CCl<sub>3</sub>) the subtraction of a carbon tetrachloride spectrum (X 10.8) has produced a low frequency feature of approximately the same intensity and a similar shape to that predicted by an inertia-corrected Debye model developed by McConnell. At present the agreement is not completely satisfactory but the result does offer some support to the argument for the two component hypotheses. However, it must be noted that Hildebrand has indicated by thermodynamic argument<sup>125</sup> that structure, such as lattices, cells, etc. cannot exist in simple liquids (see Chapter 6).

iv) The Extended Diffusion Models of Gordon<sup>81</sup>

Gordon recognised that the Debye model (in which the molecules undergo rotation in infinitesimally small steps) was not realistic for small molecules. Accordingly, his theory developed two models in which the steps between collisions are of an arbitrary large size. The probability of a molecule undergoing *n* collisions from *t*(0)<sup>+</sup> (*t*) is described by a Poisson distribution

$$P(n,t) = \frac{1}{n!} \left( \frac{t}{\tau_c} \right)^n \exp(-t/\tau_c) \quad \dots\dots\dots 2.65$$

where  $\tau_c$  is the mean time between collisions. Both of Gordon's models are basically inertia-corrected Debye models. In the 'm' diffusion model the instantaneous collisions result in the randomising of the direction of the angular momentum of the molecule.

The J diffusion model describes a system in which the instantaneous collisions results in both the magnitude and direction of the angular momentum being randomised.

Gordon's general expression (for linear molecules) for the correlation function  $\phi(t)$  is given by

$$\phi(t) = \exp(t/\tau) \sum_{n=0}^{\infty} \frac{1}{\tau_c^n} \left[ \int_0^t dt_n \cos \omega_{n+1} (t-t_n) \int_0^{t_n} dt_{n-1} \cos \omega_n (t_n-t_{n-1}) \dots \dots \int_0^{t_2} dt_1 \cos \omega_2 (t_2-t_1) \cos \omega_1 t_1 \right] \quad \dots\dots\dots 2.66$$

where  $t_n$  denotes the instants of collision and  $\omega_n$  are the angular velocities.

For the m-diffusion case,  $\omega_n$  are all equal and are taken to be

$$\omega_0 = \sqrt{2kT/I} \quad \dots\dots\dots 2.67$$

Brot<sup>119</sup> has solved this expression for three cases  $\omega_0 > 1/(2\tau_c)$ ;  $\omega_0 = 1/(2\tau_c)$  and  $\omega_0 < 1/(2\tau_c)$ . However for the case of CH<sub>3</sub>CN the solution for a symmetric top is required. This has been given by McClung<sup>17a</sup> for the J diffusion case as

$$K_{(m)}^{(j)}(J, \omega_0) \sum_{n=0}^{\infty} \frac{\tau_J}{(2j+1)^n} \sum_r (-1)^r \frac{n!}{(n-2r)!(2r)!} \left\{ \left(\frac{2}{\pi}\right)^{1/2} \bar{\omega}^{-3} \sum_{a=j}^j \int_0^{\infty} d\omega \frac{\omega^2 \exp(-\omega^2/2\bar{\omega}^2)}{1+(a\omega+\omega_0)^2 \tau_J^2} \right\}^{n-2r} \\ \times \left\{ (2/\pi)^{1/2} \bar{\omega}^{-3} \sum_{b=j}^j \int_0^{\infty} d\omega \omega^2 \exp(-\omega^2/2\bar{\omega}^2) \left[ \frac{(b\omega + \omega_0) \tau_J}{1 + (b\omega + \omega_0)^2 \tau_J^2} \right] \right\}^{2r} \dots\dots\dots 2.68$$

where  $\bar{\omega} = (kT/I)^{1/2}$  and  $K_m^{(j)}(J, \omega_0)$  is the Fourier Transform of the correlation function  $G_m^{(j)}(J, t)$ . Figure 6.1 illustrates the result of applying this model to CH<sub>3</sub>CN with some results obtained from other models.

The models described so far in this section are inadequate because they are all based on the simple rotational Langevin equation (2.50). This equation contains a friction term  $\beta$  which is constant with respect to time and therefore cannot represent the contribution to the intermolecular torques which arise from the dynamic interactions in the liquid phase. The solution of the simple Langevin equation yields an auto-correlation function of the form given by equation 2.69 which is a pure exponential

$$C_{\omega}^{(j)}(t) = \frac{\langle \omega(0) \cdot \omega(t) \rangle}{\langle \omega(0) \cdot \omega(0) \rangle} = \exp(-\beta t) \dots\dots\dots 2.69$$

where  $\omega =$  the angular frequency  $d\theta/dt$

In practice the correlation functions of molecules in a liquid are far from exponential.<sup>2,126,7,4</sup> In order that a model be valid for, and describe, the Poley feature of a liquid it is necessary that it includes the correlated motions of the molecules since it is these dynamic interactions (rotational hinderance)<sup>127</sup> which account for the Poley feature lying to the high frequency side of the gas phase rotational envelope.

v) The Memory Function Formalism

The method which has been applied in this work is the development and solution of a more complex equation of motion by the memory function approach.<sup>50,75</sup> This formalism does not require an underlying model but is a scheme which allows the introduction of memory functions, denoted by  $K(t)$  that can be developed to describe the observed phenomena. The method adopted here is that which has been applied by Evans et al<sup>2,17,23,25,26</sup> to the solution of a more general Langevin equation attributed to Kubo<sup>128</sup>

$$\dot{\omega}(t) + \int_0^t K_{\omega}(t-\tau') \omega(\tau') d\tau' = \Gamma(t) \dots\dots\dots 2.70$$

where  $K_{\omega}(t)$  is a memory function, the correlation function of the random torque on the molecule (the time dependent friction tensor).

Then from equation 2.70 we can write<sup>22,50</sup>

$$\frac{d\langle \omega(0) \cdot \omega(t) \rangle}{dt} = - \int_0^t K_{\omega}(t-\tau') \langle \omega(0) \cdot \omega(\tau') \rangle + \langle \omega(0) \cdot \Gamma(t) \rangle \dots\dots\dots 2.71$$

We know that for a stochastic process  $\langle \Gamma(t) \rangle = 0$  and  $\langle \omega(0) \cdot \Gamma(t) \rangle = 0$

The rotational autocorrelation function  $C_m(t)$  of a microwave/far-infrared band is given by<sup>81</sup>

$$C_m(t) = \langle \bar{\mu}(0) \cdot \bar{\mu}(t) \rangle = \int_{-\infty}^{+\infty} \exp(i\omega t) \frac{3hc}{4\pi^2} \frac{\sigma(\omega)d\omega}{\omega [1 - \exp(-h\omega/kT)]} \dots\dots\dots 2.72$$

where  $\sigma(\omega)$  = absorption cross section per unit area:

Using  $C_m(t)$  in the classical limit ( $\hbar \rightarrow 0$ ) equation 2.71 yields.<sup>22</sup>

$$\dot{C}_m(t) = - \int_0^t K_0(t-\tau') C_m(\tau') d\tau' \dots\dots\dots 2.73$$

where the Fourier transform of  $K_0(t-\tau')$  is the frequency dependent friction coefficient ( $\beta(\omega)$ ).

The set of memory functions  $K_0(t) \dots \dots K_n(t)$  obey a set of coupled Volterra equations such that<sup>50</sup>

$$\frac{\partial K_{n-1}(t)}{\partial t} = - \int_0^t K_n(t-\tau') K_{n-1}(\tau') d\tau' \dots\dots\dots 2.74$$

Hence we can write the expressions

$$\frac{\partial K_0(t)}{\partial t} = - \int_0^t K_1(t-\tau') K_0(\tau') d\tau' \dots\dots\dots 2.75$$

and

$$\frac{\partial K_1(t)}{\partial t} = - \int_0^t K_2(t-\tau') K_1(\tau') d\tau' \dots\dots\dots 2.76$$

**Definitions**

**Laplace transformation<sup>129</sup>**

$Z \{ f(x) \}$  denotes a Laplace transform of  $f(x)$

$$Z \{ f(x) \} = \hat{f}(p) = \int_0^{\infty} e^{-px} f(x) dx$$

If  $f(x) = e^{ax}$

then  $Z \{ e^{ax} \} = \hat{f}(p) = \int_0^{\infty} e^{-px} e^{ax} dx = \frac{1}{p-a}$

**Laplace transform of a derivative<sup>130</sup>**

$$Z \{ \dot{f}(t) \} = p Z \{ f(t) \} - f(0) = p\hat{f}(p) - f(0)$$

**Convolution Theorem<sup>129</sup>**

$$Z \left\{ \int_0^x f(x-y) g(y) dy \right\} = \hat{f}(p) \hat{g}(p)$$

Taking Laplace transforms of equation 2.73 and applying convolution theorem.

$$Z \left\{ \dot{C}_m(t) \right\} = Z \left\{ - \int_0^t K_0(t-r') C_m(r') dr' \right\} \quad \dots\dots\dots 2.77$$

$$p \hat{C}_m(p) - C_m(0) = Z \left\{ K_0(t) \right\} Z \left\{ C_m(t) \right\} = -\hat{K}_0(p) \hat{C}_m(p) \quad \dots\dots\dots 2.78$$

Using the approximation for Gordons M diffusion model<sup>81</sup> i.e. K has no memory, then the correlation function is a simple exponential<sup>22</sup>

$$K_0(t) = K_0(0) \exp(-\gamma_0 t) \quad \dots\dots\dots 2.79$$

this leads to  $Z \left\{ K_0(t) \right\} = \hat{K}_0(p) = \int_0^\infty \exp(-pt) K_0(t) dt$

substitution for  $K_0(t) = \int_0^\infty \exp(-pt) \exp(-\gamma_0 t) K_0(0) dt$

$$= K_0(0) \int_0^\infty \exp(-pt) \exp(-\gamma_0 t) dt$$

rearranging  $= K_0(0) \int_0^\infty \exp(-[p + \gamma_0] t) dt$

$$\hat{K}_0(p) = K_0(0) \left[ \frac{\exp(-[P + \gamma_0] t)}{-[P + \gamma_0]} \right]_0^\infty$$

solution  $\hat{K}_0(p) = \frac{K_0(0)}{p + \gamma_0} \quad \dots\dots\dots 2.80$

rewriting equation 2.78 gives  $\hat{C}_m(p) [P + \hat{K}_0(p)] = \hat{C}_m(0)$

substituting for  $\hat{K}_0(p)$  and rewriting yields

$$\hat{C}_m(p) = \frac{C_m(0)}{P + \left( \frac{K_0(0)}{P + \gamma_0} \right)} \quad \dots\dots\dots 2.81$$

[ which is Moris<sup>51</sup> continued fraction representation of the correlation function truncated at 1st order ]

$$\hat{C}_m(p) = \frac{C_m(0) (P + \gamma_0)}{p^2 + p\gamma_0 + K_0(0)} \quad \dots\dots\dots 2.82$$

now  $p = -i\omega$

therefore  $\hat{C}_m(-i\omega) = \frac{C_m(0) (-i\omega + \gamma_0)}{-\omega^2 - i\omega\gamma_0 + K_0(0)} \quad \dots\dots\dots 2.83$

The spectral density  $a(\omega)$  is related by<sup>92</sup>

$$a(\omega) \propto \omega^2 \text{Real} \left[ \hat{C}_m(-i\omega) \right]$$

rearranging 2.83 gives 
$$\hat{C}_m(i\omega) = \frac{\gamma_0 C_m(0) - i\omega C_m(0)}{(K_0(0) - \omega^2) - i\omega\gamma_0}$$

multiplying by denominator/denominator and taking<sup>50</sup>  $C_m(0) = 1$

leads to 
$$\hat{C}_m(-i\omega) = \frac{(\gamma_0 - i\omega) [(K_0(0) - \omega^2) + i\omega\gamma_0]}{[K_0(0) - \omega^2]^2 + \omega^2\gamma_0^2}$$

expand and separate

$$\hat{C}_m(-i\omega) = \frac{\gamma_0 K_0(0)}{[K_0(0) - \omega^2]^2 + \omega^2\gamma_0^2} - i \frac{[\omega K_0(0) + \omega^3 + \omega\gamma_0^2]}{[K_0(0) - \omega^2]^2 + \omega^2\gamma_0^2}$$

$$\therefore a(\omega) = \frac{A\omega^2 \gamma_0 K_0(0)}{[K_0(0) - \omega^2]^2 + \omega^2\gamma_0^2} \dots\dots\dots 2.84$$

where A is a constant.

Now applying the same approach to equation 2.75

$$Z \{ K_0(t) \} = Z \left\{ - \int_0^t K_1(t-\tau') K_0(\tau') d\tau' \right\} \dots\dots\dots 2.85$$

$$p\hat{K}_0(p) - K_0(0) = -\hat{K}_1(p) \hat{K}_0(p) \dots\dots\dots 2.86$$

Using the approximation

$$K_1(t) = K_1(0) \exp(-\gamma_1 t) \dots\dots\dots 2.87$$

$$Z \{ K_1(t) \} = \hat{K}_1(p) = \int_0^\infty \exp(-pt) K_1(t) dt \dots\dots\dots 2.88$$

substituting for  $K_1(t)$

$$\hat{K}_1(p) = \int_0^\infty \exp(-pt) K_1(0) \exp(-\gamma_1 t) dt \dots\dots\dots 2.89$$

$$= K_1(0) \int_0^\infty \exp(-pt) \exp(-\gamma_1 t) dt \dots\dots\dots 2.90$$

rearranging

$$= K_1(0) \int_0^\infty \exp[-(p + \gamma_1) t] dt \dots\dots\dots 2.91$$

solved as previously

$$\hat{K}_1(p) = K_1(0) \left[ \frac{\exp[-(p + \gamma_1) t]}{-(p + \gamma_1)} \right]_0^\infty$$

$$\hat{K}_1(p) = \frac{K_1(0)}{p + \gamma_1} \dots\dots\dots 2.92$$

Using equations 2.78 and 2.86 leads to the construction of the continued fraction in full (to 2nd order).

$$\begin{aligned}\hat{C}_m(p) &= \frac{C_m(0)}{p + \hat{K}_0(p)} = \frac{C_m(0)}{P + K_0(0)} \\ &\quad \frac{1}{P + \hat{K}_1(p)} \\ &= \frac{C_m(0)}{P + K_0(0)} \frac{1}{\frac{P + K_1(0)}{P + \gamma_1}}\end{aligned}\quad \dots\dots\dots 2.93$$

$$\begin{aligned}\hat{C}_m(p) &= \frac{C_m(0)}{\frac{P(P + K_1(0)) + K_0(0)}{P + \gamma_1}} \\ &= \frac{C_m(0) \left[ \frac{P + K_1(0)}{P + \gamma_1} \right]}{\frac{P(P^2 + p\gamma_1 + K_1(0)) + K_0(0)(P + \gamma_1)}{P + \gamma_1}} \\ &= \frac{C_m(0) [P^2 + P\gamma_1 + K_1(0)]}{\frac{P^3 + P^2\gamma_1 + K_1(0)P + K_0(0)(P + \gamma_1)}{(P + \gamma_1)}}\end{aligned}$$

$$C_m(0) = 1 \quad \hat{C}_m(p) = \frac{P^2 + P\gamma_1 + K_1(0)}{P^3 + P^2\gamma_1 + pK_1(0) + K_0(0)p + K_0(0)\gamma_1} \quad \dots\dots\dots 2.94$$

$$p = -i\omega$$

$$\therefore \hat{C}_m(p) = \frac{K_1(0) - \omega^2 - i\omega\gamma_1}{K_0(0)\gamma_1 - \omega^2\gamma_1 - i\omega K_1(0) - i\omega K_0(0) + i\omega^3}$$

Separating variables

$$\text{Now let } R = K_0(0)\gamma_1 - \omega^2\gamma_1 = \gamma_1 [K_0(0) - \omega^2]$$

$$\text{and } I = \omega^3 - \omega K_1(0) - \omega K_0(0) = \omega^3 - \omega [K_1(0) + K_0(0)]$$

$$\text{then } \hat{C}_m(-i\omega) = \frac{K_1(0) - \omega^2 - i\omega\gamma_1}{R + iI} \times \frac{R - iI}{R - iI}$$

$$= \frac{RK_1(0) - R\omega^2 - Ri\omega\gamma_1 - iIK_1(0) + iI\omega^2 - I\omega\gamma_1}{R^2 + I^2}$$

$$= \frac{RK_1(0) - R\omega^2 - I\omega\gamma_1}{R^2 + I^2} - i \frac{[R\omega\gamma_1 + IK_1(0) + I\omega^2]}{R^2 + I^2}$$

taking real part substituting for R and I

$$= \frac{K_1(0)K_0(0)\gamma_1 - \omega^2\gamma_1K_1(0) - \cancel{K_0(0)\gamma_1\omega^2} + \omega^4\gamma_1}{R^2 + I^2}$$

$$\frac{-\omega^4\gamma_1 + \omega^2\gamma_1K_1(0) + \omega^2\gamma_1K_0(0)}{R^2 + I^2}$$

$$\therefore \text{Re} [\hat{C}_m(-i\omega)] = \frac{K_1(0)K_0(0)\gamma_1}{R^2 + I^2}$$

$$a(\omega) = A \omega^2 \text{Re} [\hat{C}_m(-i\omega)]$$

Result of the 2nd order truncation of the Mori continued fraction

$$a(\omega) = \frac{A \omega^2 K_1(0) K_0 \gamma_1}{\gamma_1^2 [K_0(0) - \omega^2]^2 + [\omega^3 - \omega (K_1(0) + K_0(0))]^2} \dots\dots\dots 2.95$$

where  $K_0(0) = 2kT/I_B$  for a symmetric top or linear molecule

$K_1(0)$  is related to the intermolecular mean square torque  $\langle O(V)^2 \rangle$  (Chapter 5)

$\gamma_1^{-1}$  is a torque relaxation time

The model described by equation 2.95 has been applied in this work with the proportionality constant A determined by the relation.<sup>22</sup>

$$A = \frac{4\pi N\mu^2}{3kTV} = \frac{\epsilon_0 - \epsilon_\infty}{\eta(\omega)} \dots\dots\dots 2.96$$

**CHAPTER 3**  
**FAR—INFRARED SPECTROSCOPY USING A MICHELSON INTERFEROMETER**

## CHAPTER 3

### FAR-INFRARED SPECTROSCOPY USING A MICHELSON INTERFEROMETER

#### INTRODUCTION

A detailed account of the theory of a Michelson interferometer is not included in this thesis. For such information the reader is referred to two of the many excellent books on this subject, those by Bell<sup>131a</sup> and Chamberlain<sup>131b</sup>. A fully detailed description of the operational procedures and theory applicable to the particular instrument and peripherals used in this work has been given previously.<sup>132</sup> Therefore in this chapter only a brief description is given, highlighting where necessary the features pertinent to the study of the systems described in Chapters 5, 6 and 7.

#### A. GENERAL THEORY OF A MICHELSON INTERFEROMETER

This type of interferometer can be represented as shown in Figure 3.1. The source, a mercury vapour lamp emits polychromatic radiation with frequencies from the far-infrared into the ultraviolet. This broadband radiation is collimated at C and directed onto the 'Mylar' (polyethylene terephthalate) beam splitter B. This thin dielectric sheet partially reflects and partially transmits the incident radiation onto the two mirrors M<sub>1</sub> and M<sub>2</sub>. The two beams are then reflected back to the beam splitter where interference occurs due to the phase lag of one relative to the other. The radiation is again partially transmitted and reflected, the beam which returns to the source is lost while the other beam is focused at C', then passes through the sample and is detected usually by its heating effect at the detector D. The movement of the mirror M<sub>2</sub> allows the introduction of a variable phase difference between the two beams. This phase difference results in an interference which can be plotted from the intensity of the radiation incident at the detector D against the optical path difference x. This plot known as the interferogram has the form

$$I(x) = \int_{-\infty}^{+\infty} G(\bar{\nu}) \cos(2\pi\bar{\nu}x) d\bar{\nu} + \int_{-\infty}^{+\infty} \sqrt{-1} G(\bar{\nu}) \sin(2\pi\bar{\nu}x) d\bar{\nu} \quad \dots\dots\dots 3.1$$

where  $G(\bar{\nu})$  is the spectral intensity  
 $\bar{\nu}$  = frequency (cm<sup>-1</sup> when x is in cm)

For a perfectly symmetrical interferogram the sine term of equation 3.1 is zero and can be neglected therefore Fourier transformation of equation 3.1 yields the desired expression for the spectral intensity given by

$$G(\bar{\nu}) = \int_{-\infty}^{+\infty} I(x) \cos(2\pi\bar{\nu}x) dx \quad \dots\dots\dots 3.2$$

Now, since the interferogram is symmetrical about the point of zero path difference (i.e. where  $x_1 = x_2$ ) then equation 3.2 can be rewritten;

$$G(\bar{\nu}) = 2 \int_0^{x \text{ max}} I(x) \cos(2\pi\bar{\nu}x) dx \quad \dots\dots\dots 3.3$$

Thus the spectrum can be recovered from the interferogram recorded from the point of zero path difference to x max (half the total interferogram).

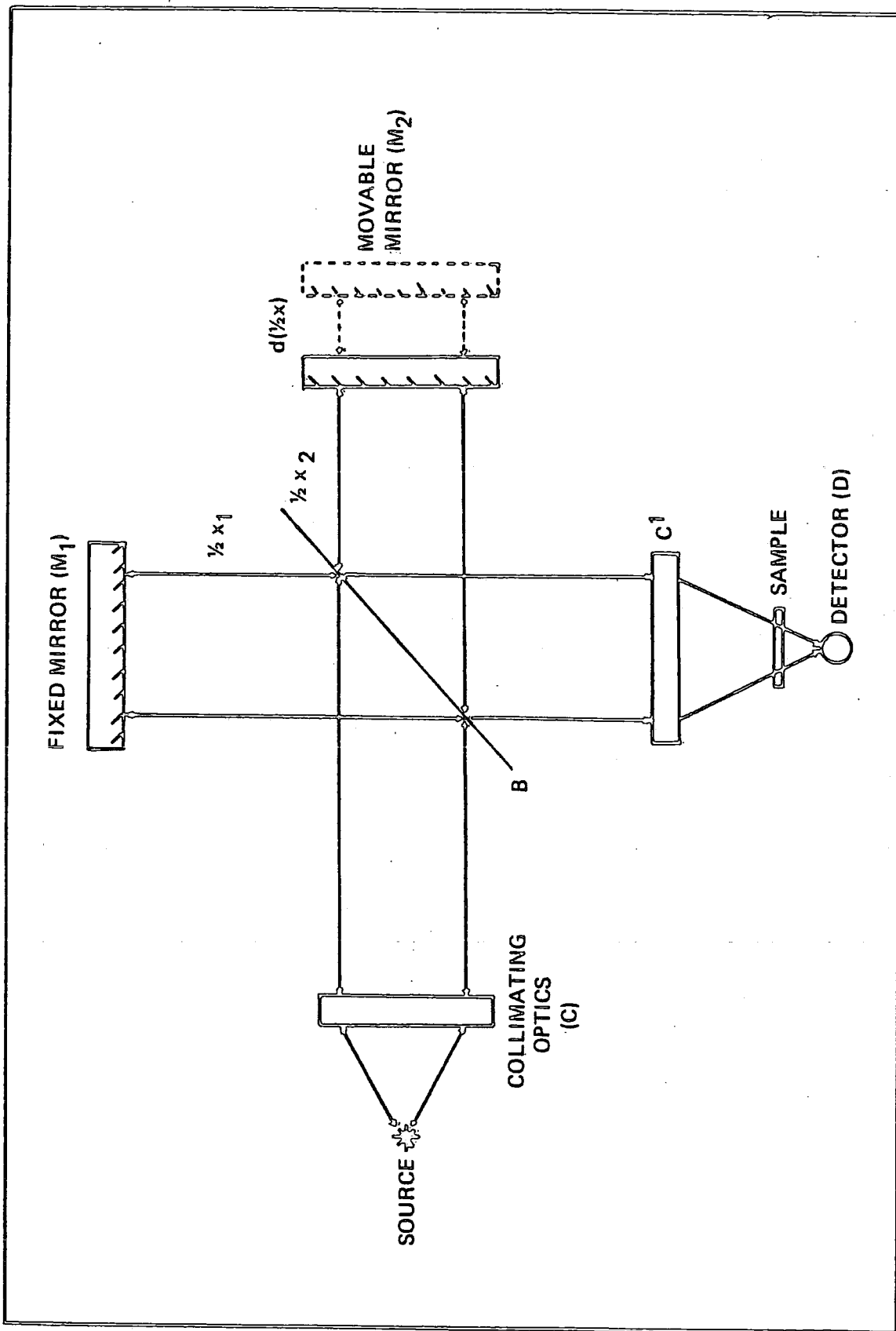


FIGURE 3.1  
 SCHEMATIC DIAGRAM OF A MICHELSON INTERFEROMETER

There are two main advantages which the interferometer enjoys over the conventional grating spectrometer for the study of the far-infrared spectrum.

**i) The Fellgett Advantage<sup>133</sup>**

In a grating instrument the particular frequencies are scanned and analysed separately for short periods and therefore very little energy of interest reaches the detector compared to any background energy (noise). For far-infrared radiation this becomes more of a problem because in the first instance the radiation is very difficult to diffract and secondly the commonly available sources are very weak in this region. However, the interferometer is a multiplex instrument which samples all of the 'scanned' frequencies for the duration of the measurement. Therefore provided that the system is detector noise dominated<sup>134</sup> there is an improvement in signal to noise ratio with this type of system of  $\sqrt{N}$  where  $N$  is the number of spectral elements equal to the resolution.<sup>130</sup> This is known as the Fellgett or multiplex advantage.

**ii) The Jacquinot Advantage<sup>135</sup>**

The second advantage arises from the high energy throughput of the interferometer because it does not have the radiation limiting slit of the grating instrument. In the case of the Beckman-RIIC FS720 interferometer used in this work the optical configuration allows the propagation of a beam approximately 7cm in diameter. This feature which leads to the Jacquinot or throughput advantage enables a higher signal to noise ratio to be achieved by ensuring that the signal energy dominates the detector.

The one major disadvantage which the interferometer suffers from is that a computer analysis is required to extract the frequency spectrum from the interferogram. Therefore it has often been necessary (as in the case of this work) to record the interferograms onto punched paper tape prior to transfer onto large multiple access computers for this calculation. This procedure has often led to delays of up to 36 hours between recording the interferogram and obtaining the required spectrum. The advent of inexpensive microcomputers which can be connected on line to the instrument such as the dedicated system now operating in Durham<sup>136</sup> have obviously reduced this problem to a minimum. One further problem remains however, due to the fact that the interferometer is a single beam instrument. This requires that sample and background spectra (interferograms) are measured separately and ratio'd numerically afterwards if the experiment requires a background subtraction.

**iii) Spectral Resolution**

The spectral resolution obtainable by this method is determined in the ideal case by the maximum magnitude of the path difference ( $x_{\max}$ ) over which the interferogram is recorded. The expression for the calculation of the resolution  $\Delta\bar{\nu}$  is given by<sup>53</sup>

$$\Delta\bar{\nu} = 1.2 / x_{\max} \approx (x_{\max})^{-1} \quad \text{..... 3.4}$$

In practice the resolving power of an interferometer is limited by the solid angle  $\Omega$  of the limiting stop of the collimating optics due to the phase difference which exists between the axial and meridional rays.

For a uniformly radiating disc Jacquinot has given expression 3.5 for the path difference  $x_{\max}$  (and hence the maximum resolution by equation 3.4) over which the intensity interferogram can be recorded.

$$\Omega = 2\pi (\bar{\nu} x_{\max})^{-1} \dots\dots\dots 3.5$$

where  $\Omega$  is given by  $\Omega = \pi a^2 / f^2$

$a$  = radius of the aperture (limiting stop)

$f$  = focal length of collimating system.

Therefore, in the case of the FS 720 interferometer  $a^2 / f^2 = 2.5 \times 10^{-3}$  (for example) and thus for a frequency  $\bar{\nu} = 50\text{cm}^{-1}$  the limiting resolution is approximately  $0.06\text{cm}^{-1}$ . However the total mirror travel is only 10cm, or  $\pm 5\text{cm}$  about the Zero Path Difference (ZPD) position, which limits the theoretical resolution to  $0.1\text{cm}^{-1}$  by equation 3.4. Higher resolution ( $0.05\text{cm}^{-1}$ ) could be achieved if the fixed mirror was adjusted (displaced by 5cm along the optical axis) such that the point of ZPD was at one extreme of the moving mirror range and a single sided interferogram was recorded ( $x_{\max} = 20\text{cm}$ ).

iv) Apodisation

The interferogram produced in an experiment can only be recorded over a finite path difference  $x_{\max}$ . The truncation of the interferogram at this point results in a sharp 'step' which if transformed may lead to the generation of undesirable (and unreal) features in the frequency spectrum.<sup>53</sup> This is easily overcome by applying a weighting function to the interferogram which smoothes the intensity to zero at  $x_{\max}$  thus eliminating the sharp transition. This procedure, known as apodisation results in a reduction in spectral resolution by a factor of approximately 2. The function employed for apodising the interferograms in this work (FTRAN series of programs) is given by

$$f(x) = \cos^2(\pi x / 2x_{\max}) \dots\dots\dots 3.6$$

v) Sampling of the interferogram

The interferogram generated by the movement of the mirror  $M_2$  is sampled at discrete intervals of path length known as the sampling intervals  $\Delta x$ . Sampling theory requires that in order for a wave to be correctly recovered it must be sampled at least once every half cycle. This imposes an upper frequency limit  $\bar{\nu}_{\max}$  on the spectral range of the instrument in terms of  $\Delta x$  given by the expression

$$\bar{\nu}_{\max} = \frac{1}{2\Delta x} \dots\dots\dots 3.7$$

The replacement of the continuous function by a sampled one requires that equation 3.3 is now rewritten as the summation:-

$$G(\bar{\nu}) = 2\Delta x \sum_0^n I(x) \cos(2\pi\bar{\nu}n\Delta x) \dots\dots\dots 3.8$$

$n$  = number of points

This gives rise to a further complication as follows

If waves of a higher frequency than  $\bar{\nu}_{\max}$  are present in the system they will also contribute to the energy of the sampled interferogram but they will not be explicitly resolved. Their effect is to distort the recovered spectrum and generate a pattern which repeats itself at regular intervals,<sup>53</sup>

a phenomenon known as aliasing. To prevent this it is essential that frequencies higher than  $\nu_{\max}$  be excluded from the detector by some suitable optical filtering. Sampling at discrete intervals also results in the recovery of an asymmetric interferogram due to the fact that the exact centre, i.e. the ZPD is unlikely to be sampled. Other asymmetry may also be present because of misalignment in the instrument itself. These effects can be substantially reduced by the application of an autocorrelation procedure<sup>126,137</sup> or alternatively by a phase correction process.<sup>138</sup> The autocorrelation method which has been employed throughout this work requires that double sided interferograms are recorded. In contrast the phase correction procedure requires only a single sided interferogram and a few points over the ZPD from which the phase function of the spectrum can be calculated. The results obtained by the two different methods have been shown<sup>126</sup> to be virtually indistinguishable.

vi) **Beam Splitters and Optical Filtering**

The thin dielectric beam splitters which are most commonly employed in a Michelson interferometer exhibit a regular variation (in the ideal case) in efficiency through the frequency spectral which arises from the interference within the film itself. This interference pattern is a function of the thickness of the film such that

$$d = (2\iota + 1) / (4\eta\bar{\nu} \cos \theta) \quad \dots\dots\dots 3.9$$

- where  $d$  = the thickness of the film
- $\eta$  = the refractive index
- $\bar{\nu}$  = frequencies of maximum efficiency
- $\theta$  = refraction angles in the film
- $\iota$  = 0, 1, 2, 3, etc.

Figure 3.2 shows the theoretical efficiencies of some typical beam splitters used with the instrument in Durham. This phenomenon requires that several interferograms are recorded with different beam splitters and separately computed in order to obtain a spectrum over a wide frequency range. The resulting spectra are then matched up to obtain the full spectrum.

An alternative beam splitter which has been used in part of this work is a free standing wire grid which is employed with the instrument converted to the polarising mode.<sup>132,139</sup> (See Part B). The important feature of these grids is that they are almost 100% efficient (for the appropriate plane of polarisation) up to the frequency limit given by

$$\bar{\nu}_{\max} = 1/2d \quad \dots\dots\dots 3.10$$

- where  $d$  = the spacing between the grid wires

Modified coil winding techniques have been employed, for example, at the National Physical Laboratories to manufacture such grids with approximately uniform (high) efficiency over a several hundred wave number ( $\text{cm}^{-1}$ ) range. The tungsten wire grids (manufactured by Queen Mary College, London) used in this work have a useful, efficient high frequency limit of  $120\text{cm}^{-1}$  and have employed mainly to take advantage of their high throughput when used with the polarising interferometer<sup>132,139</sup> which allows the study of highly absorbing samples at low frequencies.

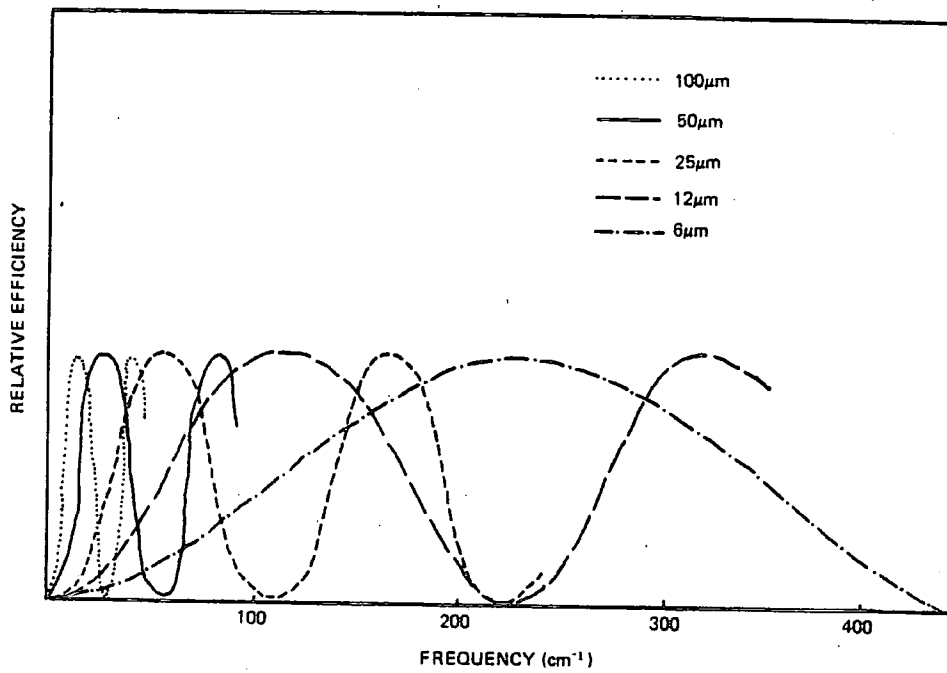


**FIGURE 3.2**  
**THEORETICAL EFFICIENCY OF SOME TYPICAL BEAM SPLITTERS**

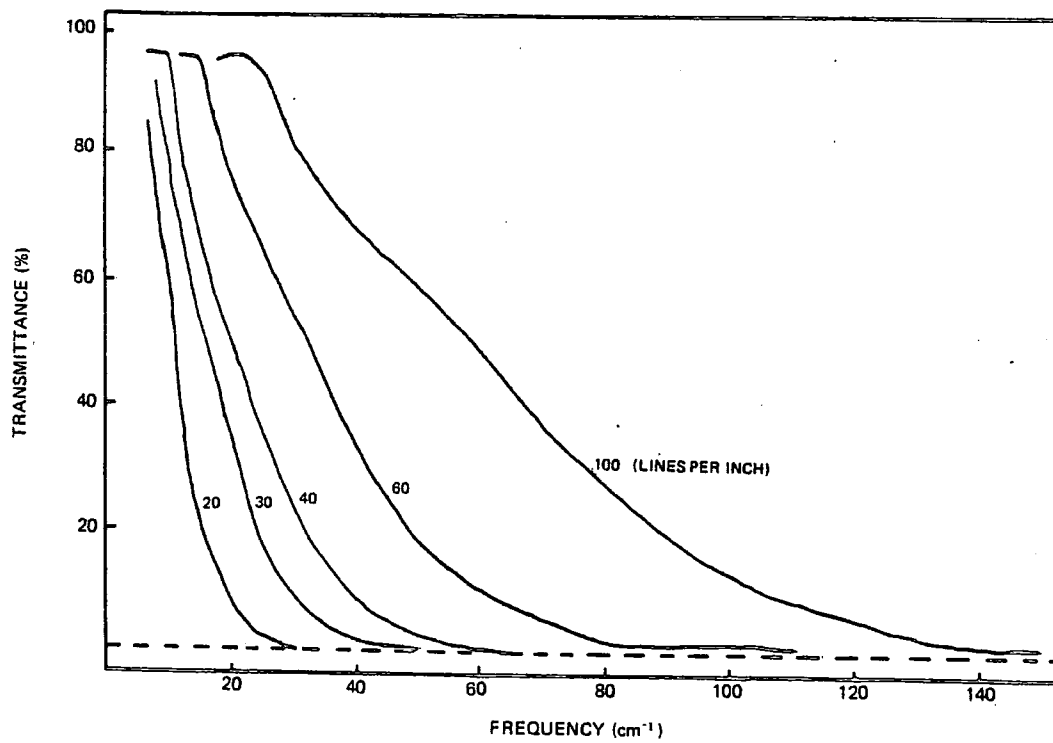


**FIGURE 3.3**  
**TRANSMISSION CHARACTERISTICS OF SOME RULED POLYETHYLENE FILTERS**

It was indicated in section v that optical filtering is essential to prevent the distortion of the recovered spectrum due to a phenomena known as aliasing. However it is also advantageous to filter the radiation from the source so that the dynamic range of the instrument detector and electronics are filled with the information from the frequency region of interest. This is a particularly valuable technique for low frequency studies since the intensity of the source decreases rapidly at longer wave lengths. A wide range of filters are available for this purpose, for example, ruled polyethylene filters which attenuate by interference effects, have sometimes been employed.<sup>132</sup> Figure 3.3 shows the absorption characteristics of a range of this type of filter.

## **B. THE DURHAM INTERFEROMETER**

### **i) General**

The Beckman-RIIC FS720 interferometer and its general mode of operation has been described previously.<sup>132</sup> The important features are as follows.

The radiation from the source is amplitude modulated at 12.5Hz by a rotating sectorised disc of approximately 7cm diameter. A reference signal from this disc is used to synchronise the signal from the detector in a phase sensitive electronic circuit in the FS200 electronics. The recovered signal is amplified, digitised and outputted onto punched paper tape. Double sided interferograms were recorded so that the symmeterising autocorrelation procedure in the FTRAN series of programs could be applied. After subtraction of the mean level the symmetrical interferograms were then Fourier transformed with a Cooley-Tukey<sup>140</sup> algorithm on a main frame IBM 370/168 computer. The sampling intervals available on this instrument were 4, 8, 16, 32 and 64 microns. Most of the interferograms recorded in this work were sampled at 16 or 8 micron intervals. When recording the interferograms the instrument was usually evacuated to eliminate water vapour which absorb strongly in the far-infrared region. When evacuation of the entire instrument was not possible, for example, if the temperature control module was fitted, the open compartments were flushed with dry nitrogen gas.

### **ii) The Cooled Detector**

In addition to the standard Golay detector which has an effective low frequency limit of approximately  $15\text{cm}^{-1}$  the interferometer can be fitted with a low noise liquid helium cooled detector for lower frequency studies. This detector, which has been described in detail previously,<sup>132,137</sup> is a thermal device operating at 1.5K. Essentially the device detects the impinging radiation by its heating effect and subsequent change in resistance of the detector element, an antimony doped germanium crystal. With the standard thin film beam splitters and suitable filtering this detector extends the range of the interferometer down to below  $5\text{cm}^{-1}$ .

### **iii) The Polarising Optical Configuration**

The Durham interferometer can be configured to operate in the Martin-Puplett<sup>139</sup> polarising mode as described in references 132 and 137. The principle features of this configuration are as follows. A rotating wire grid chopper modulates the polarisation of the source radiation which is then collimated as in the conventional instrument and directed onto a wire grid beam splitter (described in section A (vi)). The beam splitter transmits or reflects (according to the direction of

polarisation) the radiation onto the mirrors. In this case the mirrors are  $90^\circ$  roof mirrors or retro-reflectors and therefore the polarisation of the reflected wave is orthogonal to the incident wave. This ensures that no radiation is transmitted or reflected back to the source when the recombination occurs at the beam splitter and thus a high throughput is achieved. In the focusing optics a plane polarising 'analyzer' allows the transmission of one of the polarisation planes and therefore the detector receives an amplitude modulated signal.

There are several advantages of operating the interferometer in the polarising mode. Firstly, the method effectively eliminates the interferogram mean level with its associated noise and allows the dynamic range of the digitising electronics to be filled more easily without using large offset bias voltages. The higher throughput allows the study of highly absorbing samples and/or studies in the region where the source intensity is weak i.e. long wave lengths.

The overall advantage of these effects combined with the high efficiency and relatively feature less transmission characteristics of the free standing wire grid beam splitters are that the frequency range of the instrument can be extended to cover approximately  $3\text{cm}^{-1}$  to  $100\text{cm}^{-1}$  in a single experiment (using the cooled detector).

Figure 3.4a shows the low frequency spectra of a highly absorbing system recorded with the conventional optical system (beam splitter  $400\mu$ ). For comparison Figure 3.4b shows a similar spectrum recorded with the polarising interferometer. In both cases heavy optical filtering has been used to attenuate the frequencies above  $70\text{cm}^{-1}$  and thus optimise for the low frequency region. The low frequency limit in each case is below  $5\text{cm}^{-1}$  (possibly slightly less noise on 3.4b) however 3.4a clearly shows at  $30\text{cm}^{-1}$  evidence of the beam splitter efficiency characteristic which has not been accurately subtracted with the spectral background.

#### iv) Operational Configuration of the Interferometer

These can be summarised as follows:

##### a) Low Frequency Studies

These can be achieved with the instrument in the polarising or non polarising mode with the cooled detector. Either of these systems will cover the range  $5\text{cm}^{-1}$  to  $60\text{cm}^{-1}$  which provides good overlap with the high frequency spectrum. The need for conversion to the polarising system will be determined by the exact nature of the experiment, (for example absorption or dispersive study, see Part iv, c) the problems arising from beam splitter effects and possibly the time required for instrument conversion.

##### b) Higher Frequency Studies

In general the Golay detector has been employed for studies of the frequency range above  $15\text{cm}^{-1}$  although the cooled detector is also sensitive in this region however it has a high frequency limit of  $200\text{cm}^{-1}$  due to the internal low frequency optimisation filtering.<sup>132</sup> The polarising wire grid efficiency decreases rapidly above<sup>132</sup>  $120\text{cm}^{-1}$  therefore the conventional beam splitter configuration has usually been adopted. The actual beam splitter and filtering selected are determined by the feature to be observed and reference to Figures 3.2 and 3.3.

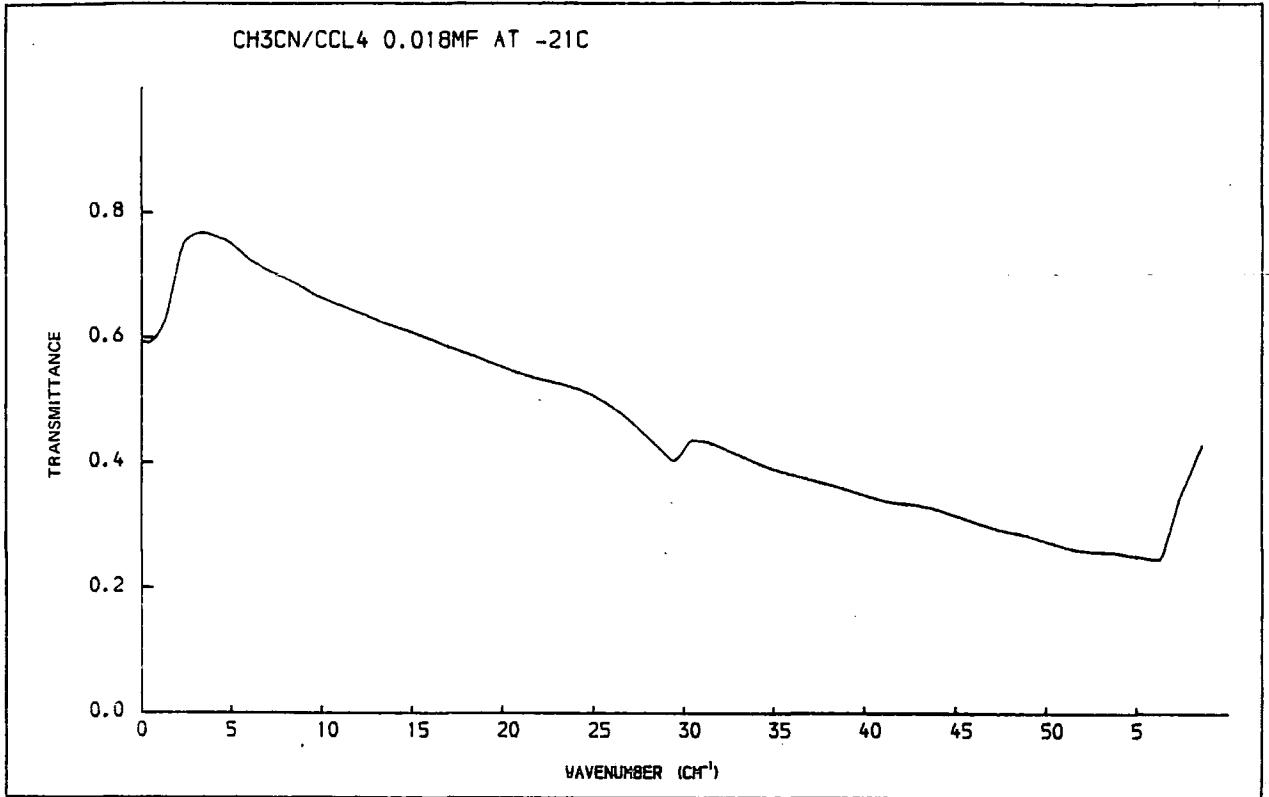


**FIGURE 3.4a**  
**SPECTRUM RECORDED WITH COOLED DETECTOR AND 100 $\mu$ m BEAMSPLITTER**

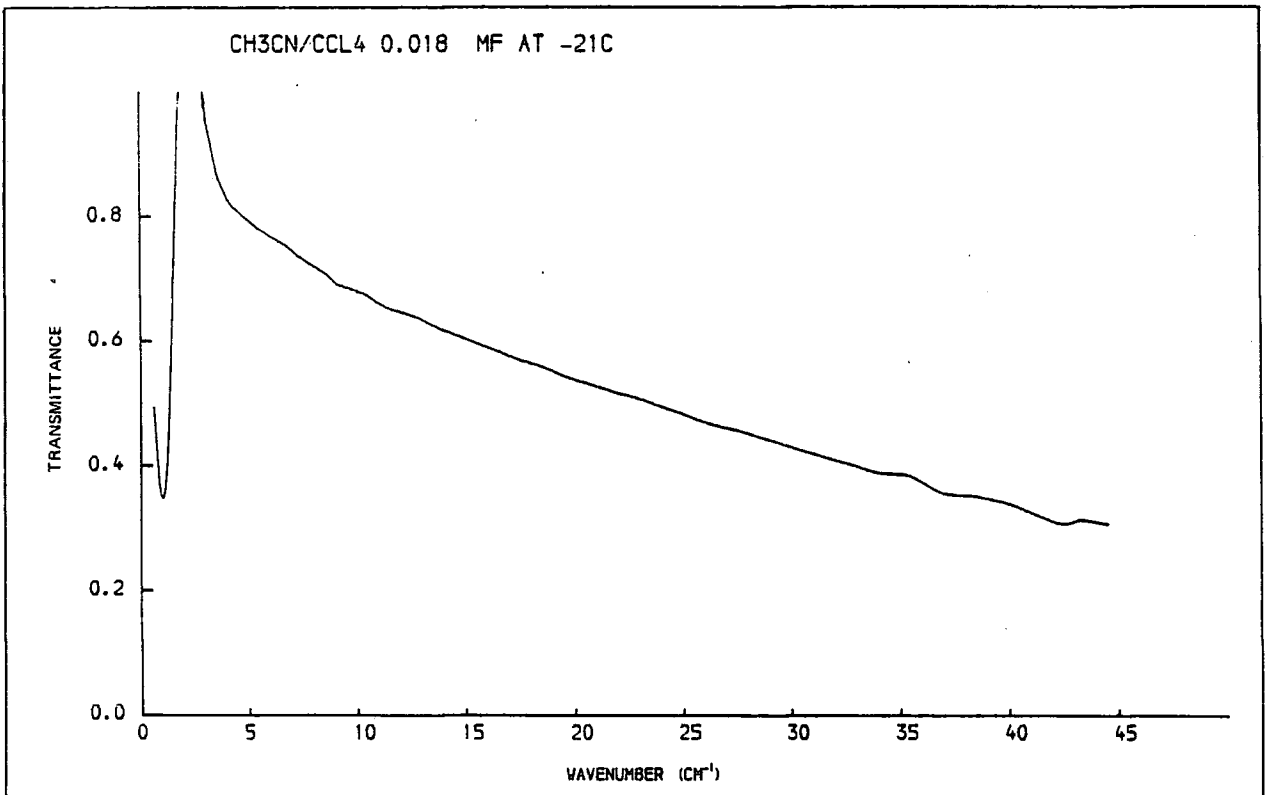


**FIGURE 3.4b**  
**SPECTRUM RECORDED WITH COOLED DETECTOR AND POLARISING OPTICS**

**c) Refractive Index Determinations**

In this work the refractive index spectra of some liquids have been determined by the dispersive technique described in Chapter 4. These experiments require that the liquid specimen is held against one of the mirrors in a special cell and therefore forbids the use of the polarising system which requires retroreflectors in both arms of the interferometer.

Either the cooled detector or the Golay detector can be used.

**v) Further Modifications**

In the final stages of this work some further instrument modifications were introduced but not tested. They are included here for completeness.

a) Modifications were made to the RIIC FS200 amplifier to incorporate the later model's increased range of time constants of 0.08, 0.16, 0.4, 0.8, 2, 4, 8, and 16 seconds.

b) The digitising electronics were expanded from 12-bit to 16-bit resolution.

c) A faster tape punch (Data Dynamics 1183) capable of operating at a theoretical 120-bits per second.

The combined effects of these modifications was to reduce the data collection time by a factor of 2 – 5 depending upon the range and resolution of the spectrum required.

**CHAPTER 4**  
**THE DETERMINATION OF REFRACTIVE INDEX SPECTRA BY**  
**DISPERSIVE FOURIER TRANSFORM SPECTROSCOPY (DFTS)**

**CHAPTER 4**  
**THE DETERMINATION OF REFRACTIVE INDEX SPECTRA BY**  
**DISPERSIVE FOURIER TRANSFORM SPECTROSCOPY (DFTS)**

**A. INTRODUCTION**

In this work the refractive indices of some  $\text{CH}_3\text{CN}/\text{CCl}_4$  solutions have been determined by the Transmission Dispersive Fourier Transform Spectroscopy (TDFTS) technique.<sup>141-149</sup> These experiments<sup>150</sup> were carried out at the National Physical Laboratory (NPL) using a cell developed jointly between the NPL, Division of Electrical Science and The Gorlaeus Laboratoria, Rijksuniversiteit, Leiden, The Netherlands (henceforth referred to as The Leiden cell).<sup>151-154</sup> In addition some measurements of the refractive index spectra of two pure liquids were made using the free layer technique.<sup>155,156</sup> These results are compared to the measurements made in this laboratory<sup>157</sup> using vertically mounted sealed cell (referred to as The Durham cell).<sup>132,157</sup>

Dispersive Fourier Transform Spectroscopy has been the topic of many research papers<sup>141-159</sup> since 1963. More recently the subject has been covered by a series of papers<sup>160,151,155</sup> an excellent review<sup>161</sup> and a bibliography<sup>162</sup>.

In this work the details of the theory of DFTS and the design of liquid cells are not repeated however references and experimental procedures specifically relevant to the systems studied are given where appropriate.

**i) An Outline of the Basic Principles and Theory of DFTS**

During a 'normal' non-dispersive experiment (as described in Chapter 3) a phase lag is introduced into one of the interferometer beams by the displacement of the moving mirror. This produces an interference pattern which is a function of the frequencies present and the displacement

$$I(x) = \int_{-\infty}^{+\infty} G(\bar{\nu}) \cos(2\pi\bar{\nu}x) d\bar{\nu} \quad \dots\dots\dots 4.1$$

Fourier inversion of this function yields an expression for the intensity as a function of frequency:-

$$G(\bar{\nu}) = \int_{-\infty}^{+\infty} I(x) \cos(2\pi\bar{\nu}x) dx \quad \dots\dots\dots 4.2$$

(as for 3.2)

For the symmetrical interferogram this can then be written

$$G(\bar{\nu}) = 2 \int_0^X I(x) \cos(2\pi\bar{\nu}x) dx \quad \dots\dots\dots 4.3$$

(as for 3.3)

where  $X$  = total path difference.

The introduction of a dielectric material into one of the beams in the interferometer as illustrated in Figure 4.1 causes an additional phase lag  $(2\pi(\bar{\eta}-1)d)$  which effectively displaces the interference maximum from the original position of zero path difference (Figure 4.2) by  $\bar{x}$  given by

$$\bar{x} = 2(\bar{\eta} - 1)d \quad \dots\dots\dots 4.4$$

where  $\bar{\eta}$  = the mean refractive index of the sample in the frequency range observed  
 $d$  = sample thickness

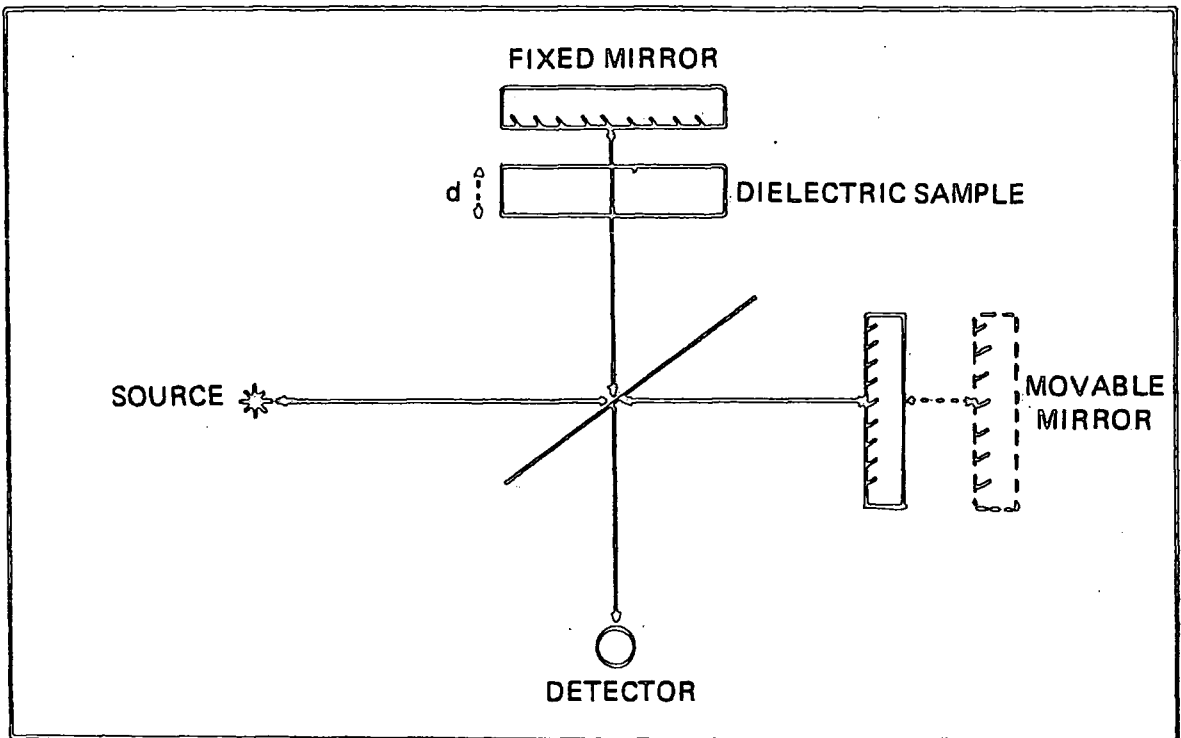


**FIGURE 4.1**  
**SCHEMATIC DIAGRAM OF A MICHELSON INTERFEROMETER**  
**IN THE DISPERSIVE CONFIGURATION**

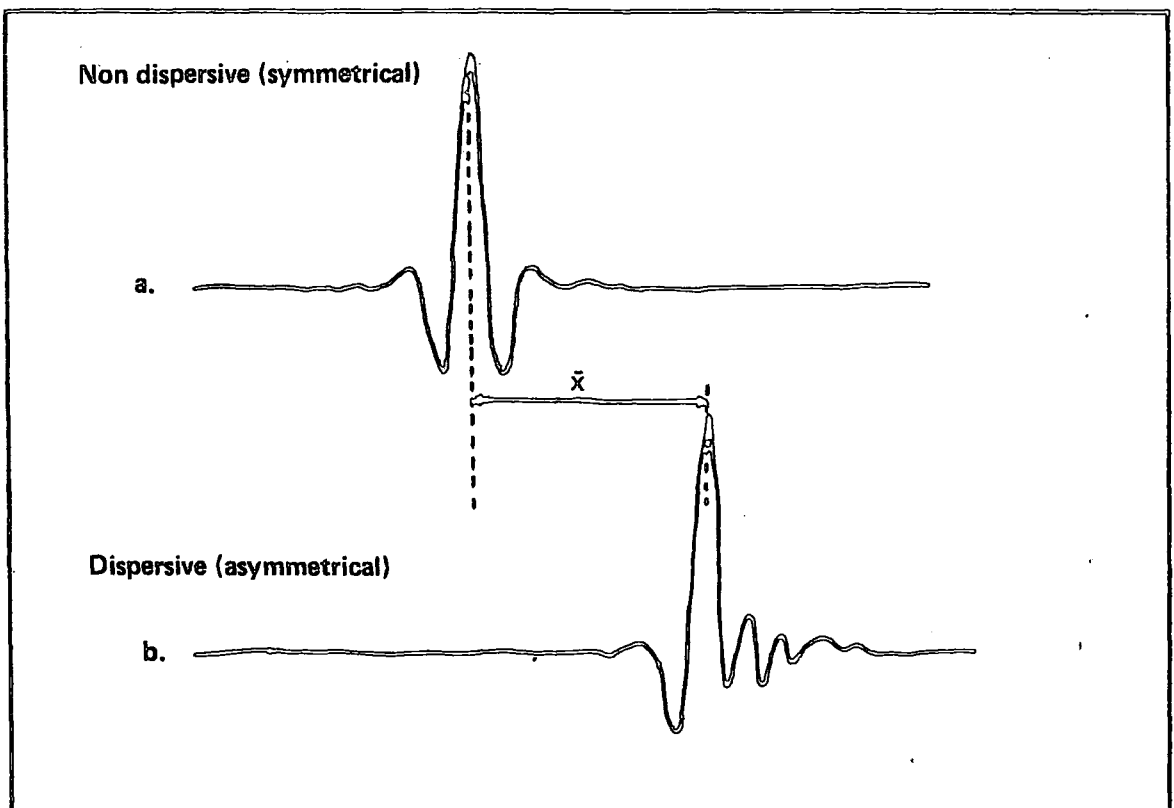


**FIGURE 4.2**  
**SCHEMATIC INTERFEROGRAMS**

When the dielectric material exhibits some dispersion, its refractive index is not constant in the frequency region observed. In this case the displacement  $\bar{x}$  is frequency dependent ( $\bar{x}(\bar{\nu})$ ) and therefore the resulting interferogram is asymmetrical as indicated in Figure 4.2. The path difference due to the sample at a frequency  $\bar{\nu}$  is given by

$$\bar{x}(\bar{\nu}) = 2(\eta(\bar{\nu}) - 1) d \quad \dots\dots\dots 4.5$$

Whereas in the case of a symmetrical interferogram the sine terms in equation 4.1 are zero (see Chapter 3) this is not so for the asymmetrical interferogram. This interferogram has the form

$$I(x) = \int_{-\infty}^{+\infty} G(\bar{\nu}) \cos \phi(\bar{\nu}) \cos (2\pi\bar{\nu}x) d\bar{\nu} + \int_{-\infty}^{+\infty} G(\bar{\nu}) \sin \phi(\bar{\nu}) \sin (2\pi\bar{\nu}x) d\bar{\nu} \quad \dots\dots\dots 4.6$$

where  $\phi(\bar{\nu})$  is the total phase difference arising from the introduction of the sample + the residual phase shift due to other asymmetry.

Fourier transformation as previously yields the terms:

$$P(\bar{\nu}) = \int_{-\infty}^{+\infty} I(x) \cos (2\pi\bar{\nu}x) dx = G(\bar{\nu}) \cos \phi(\bar{\nu}) \quad \dots\dots\dots 4.7a$$

and

$$Q(\bar{\nu}) = \int_{-\infty}^{+\infty} I(x) \sin (2\pi\bar{\nu}x) dx = G(\bar{\nu}) \sin \phi(\bar{\nu}) \quad \dots\dots\dots 4.7b$$

The energy spectrum is then given by

$$G(\bar{\nu}) = \left( P^2(\bar{\nu}) + Q^2(\bar{\nu}) \right)^{1/2} \quad \dots\dots\dots 4.8$$

and the phase by

$$\phi(\bar{\nu}) = \arctan \left[ Q(\bar{\nu}) / P(\bar{\nu}) \right] \quad \dots\dots\dots 4.9$$

The recovery of the frequency dependent refractive index  $\eta(\bar{\nu})$  from this interferogram is then completed with a knowledge of the sample thickness  $d$  the optical displacement  $\bar{x}$  and the expression

$$\eta(\bar{\nu}) = 1 + \frac{\bar{x}}{2d} + \frac{1}{4\pi d \bar{\nu}} \left( \arctan \frac{Q(\bar{\nu})}{P(\bar{\nu})} + m\pi \right) \quad \dots\dots\dots 4.10$$

Where  $m$  is an integer which is zero except for regions of high absorption where<sup>132</sup> the optical thickness  $\eta(\bar{\nu})d$  deviates by more than  $1/4\bar{\nu}$  from the mean optical thickness  $\eta d$ , a situation which results in the branching of the recovered phase spectrum which can be corrected by inspection. Some examples of this phenomenon are shown in Section B of this Chapter.

In an attempt to eliminate systematic errors due to instrument imperfections and phase errors resulting from surface reflections a background subtraction can be made and equation 4.10 is then rewritten:-

$$\eta(\bar{\nu}) = 1 + \frac{\bar{x}}{2d} + \frac{1}{4\pi d \bar{\nu}} \left[ \left( \arctan \frac{Q(\bar{\nu})}{P(\bar{\nu})} \right) - \left( \arctan \frac{Q^1(\bar{\nu})}{P^1(\bar{\nu})} \right) + m\pi \right] \quad \dots\dots\dots 4.11$$

where sample  $Q(\bar{\nu}) / P(\bar{\nu})$  includes cell and instrument residual phase errors.  
background  $Q^1(\bar{\nu}) / P^1(\bar{\nu})$  is solvent or empty cell and includes residual phase.

ii) **A Brief Description of Some Practical Methods of Applying DFTS**

The study of solids by the dispersive technique described is a relatively simple task providing that the samples are not too highly absorbing and are available in thin uniform sheets (where the exact thickness depends on the absorption properties). This type of sample can easily be mounted in front of one beam of the interferometer without elaborate equipment modifications and much of the early work by researchers in this field has been carried out on solid samples.<sup>141</sup> The study of liquid specimens requires that the sample is contained in some way.<sup>157, 158, 160</sup> However for certain non volatile non-toxic liquids which do not absorb too strongly ( $a(\nu) < 150 \text{ nepers cm}^{-1}$ ) this can be a fairly simple arrangement with the liquid held by gravity against the reflecting mirror (referred to as the free layer method). For liquids which do not meet these criterion or for instruments which do not readily allow the horizontal mirror configuration (eg. the Beckmann—RICC FS720 used in this work) a more sophisticated cell is required in which the liquid can be totally sealed (temperature controlled) and studied at thinner path lengths than surface tension effects will allow in the free layer method.

Associated with the sample and the cell components in the beam are a number of reflections. These occur at the window and sample interfaces as well as at the mirror. These cause a number of problems, all of which can be overcome with a knowledge of the full theory<sup>160</sup> and sophisticated computation. In some cases certain reflection effects can be reduced by background subtraction techniques but in the simplest experiments the close proximity of an unwanted reflection fringe, such as that from a sample surface may result in the length of available interferogram being severely limited in which case the resolution of the recovered spectrum will be low. A third method, which has not been applied in this work is Reflection DFTS<sup>161</sup> (RDFTS). This technique can be applied to liquids or solids and is particularly useful for studying highly absorbing samples. The method requires that the interferogram from one of the sample interface reflections is recorded. This interferogram contains all of the necessary phase information required to recover the spectrum. A combination of this with the DFTS method is also possible and is sometimes known as the full interferogram method<sup>136, 151, 152</sup> i.e. the spectral information is recovered from the total interferogram arising from all of the sample interface reflections.

## B. THE APPLICATION OF THE DFTS TECHNIQUE IN THIS WORK

### i) Refractive Index Measurement Using the Durham Cell

A full description of the Durham cell and details of its operation have been given previously.<sup>132</sup> In addition an outline of its operation and some results obtained prior to and during this work are presented in reference 157 a copy of which is included in Appendix 5.

This sealed cell is designed to mount vertically on the fixed arm of an FS720 interferometer separated from the evacuated instrument by a thin 'mylar' membrane which is supported by a wire grid. The space between the cell window which is also mylar and the vacuum window, is flushed with dry nitrogen during the course of an experiment.

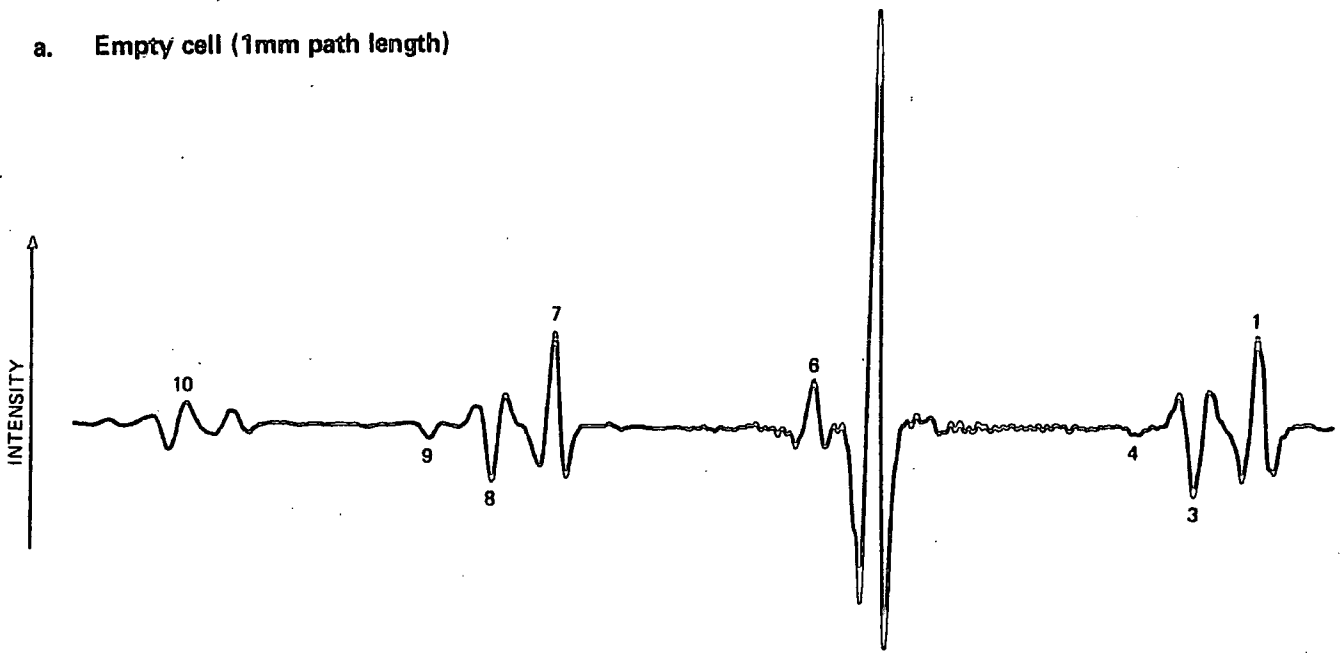
The cell depth ( $d$ ) is varied by the use of teflon spacers which are sealed with rubber 'O' rings. The assembled cell can be filled and drained via teflon tubes located through the back of the gold plated glass mirror. The main feature of this cell which distinguishes it from several other designs is the incorporation of a reference mirror in the same plane as the main mirror. This can be used to calculate the cell optical thickness when a sample has been introduced and hence facilitates the direct calculation of  $\bar{n}$  if  $d$  is known. (Note that this also requires a knowledge of the displacement due to the cell window).

This cell does not have any means of temperature control therefore all of the spectra were recorded at room temperature  $20^{\circ}\text{C} \pm 2^{\circ}\text{C}$  ( $293 \pm 2\text{K}$ ). The frequency dependent refractive indices of pure liquid p.difluorobenzene ( $\text{C}_6\text{H}_4\text{F}_2$ ) and 1.1.2.2 tetrabromoethane ( $\text{C}_2\text{H}_2\text{Br}_4$ ) have been recorded. In both cases a background empty cell phase spectrum was subtracted from the sample phase spectrum. The resolution of the recovered spectra (limited by the length of interferogram available between window reflections in the background cell) is approximately  $10\text{cm}^{-1}$ . The use of this cell considerably reduces the intensity of the radiation incident on the detector therefore the more sensitive helium cooled detector was employed for the study of these liquids.

### Results and Analysis

A typical set of interferograms recorded with the Durham cell are shown in Figure 4.3. A full assignment of the reflection fringes can be found in Appendix 5 of this thesis. The spectra obtained for the two liquids measured are shown in Figure 4.4 compared with results obtained by the free layer technique which is described in the next section. The dispersion curves obtained with this cell have been found to be consistently higher than those obtained at The National Physical Laboratories although the profiles show good agreement. It can be shown<sup>157</sup> that the differences in level are within the random error of the two experimental methods but the systematic nature of the deviation suggests a more fundamental problem. The cell window of the Durham cell is a thin mylar film which by a single internal reflection gives rise to a fringe (6) very close to the main reflection fringe (5) from the mirror. This fringe and its effects on the phase changes observed have been completely neglected in the computation procedures applied to the interferogram recorded. This will obviously introduce additional phase errors of an undefined nature. In addition there are the phase changes at the liquid/window boundaries which differ in a complex way from the air/window boundary effects of the empty background cell. Moreover these phase terms (see Section ii) ) become

a. Empty cell (1mm path length)



b. p.difluorobenzene sample



c. tetrabromoethane sample

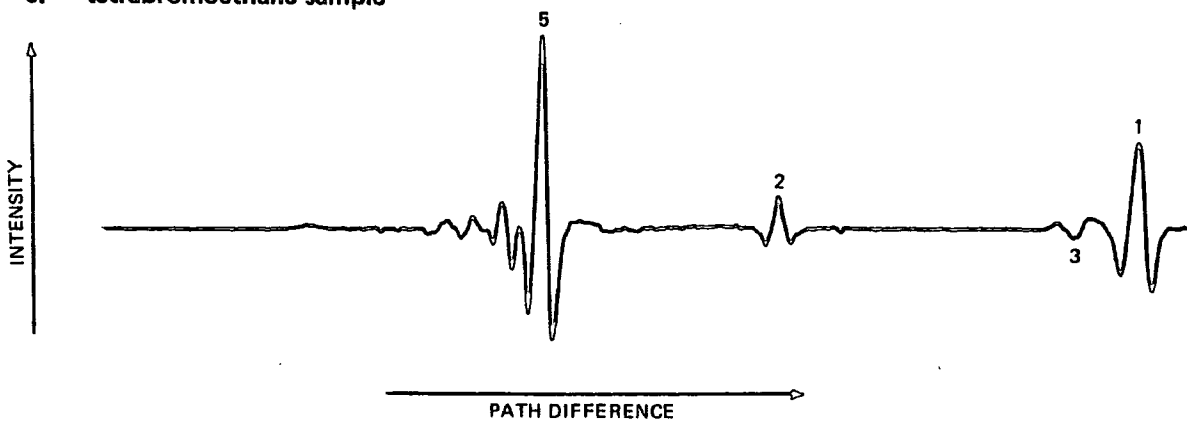


FIGURE 4.3  
INTERFEROGRAMS RECORDED WITH THE DURHAM CELL

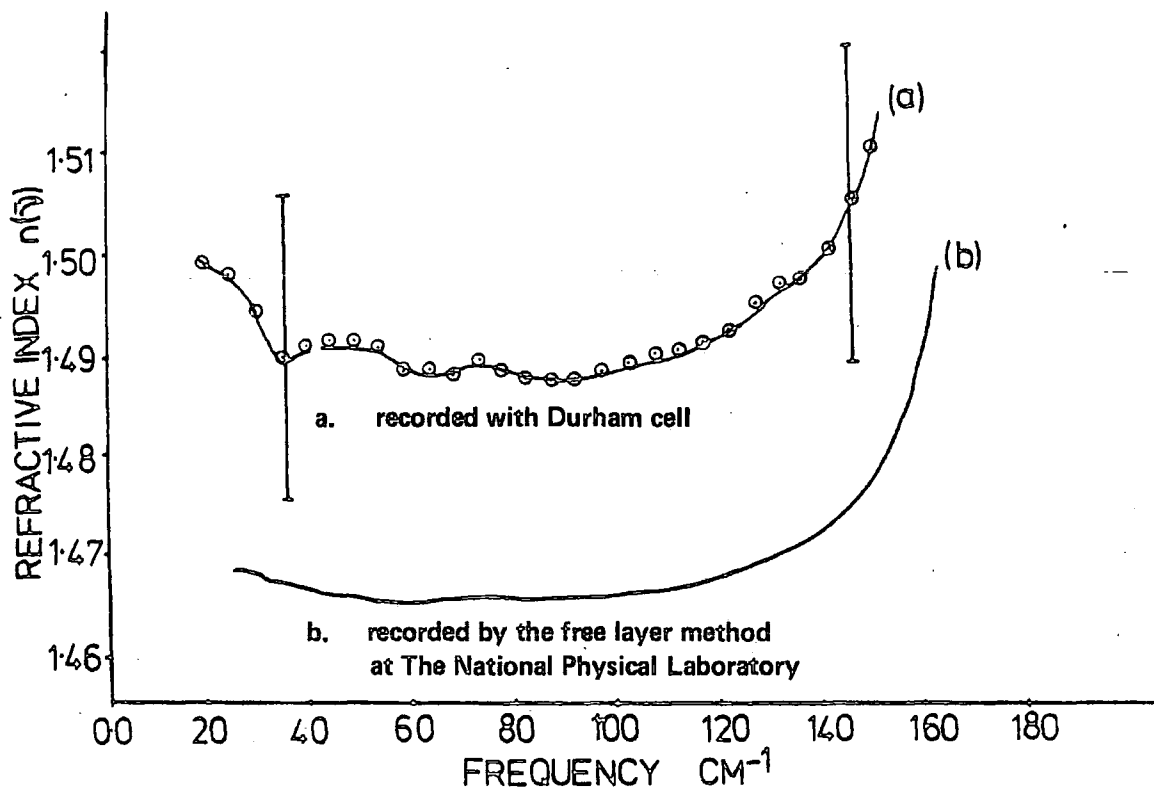


FIGURE 4.4a REFRACTIVE INDEX SPECTRA OF P-DIFLUOROBENZENE

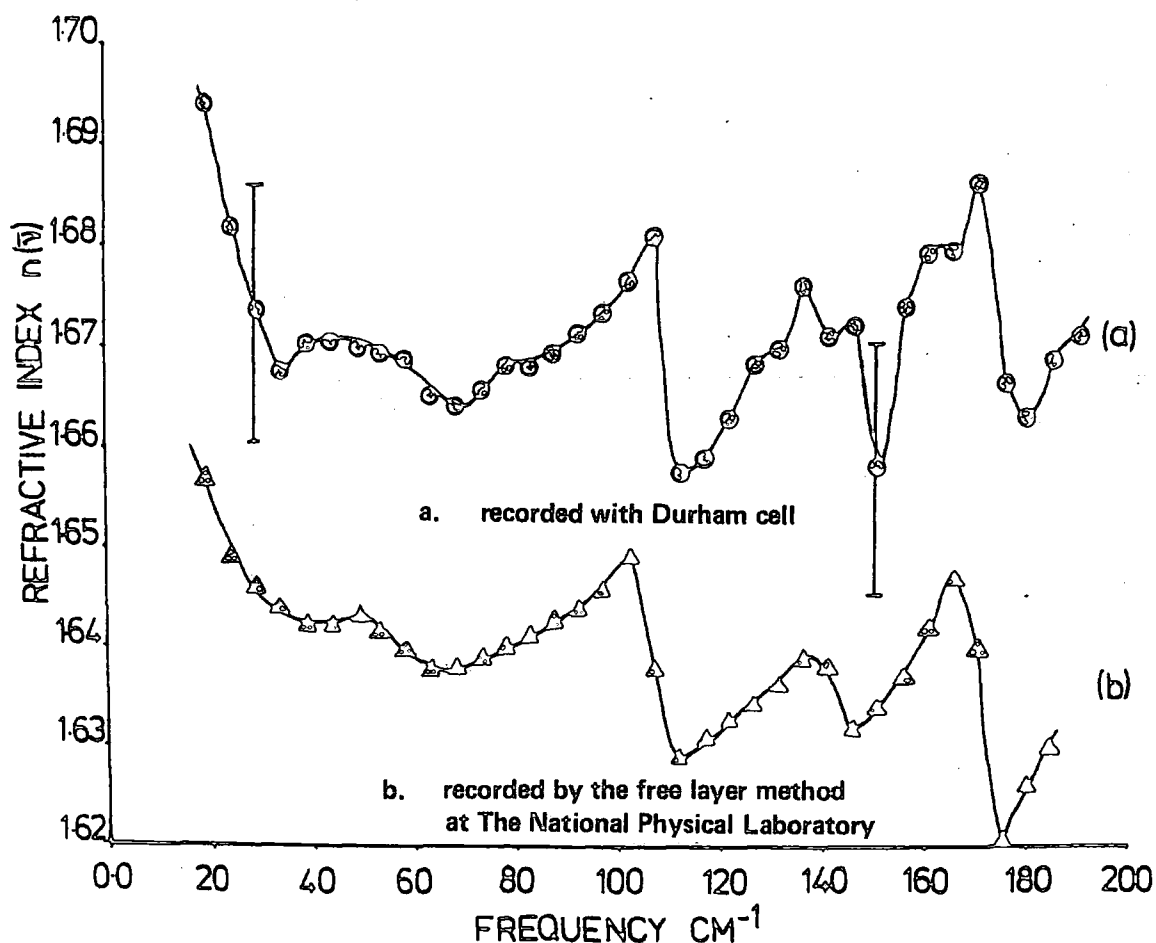


FIGURE 4.4b REFRACTIVE INDEX SPECTRA OF TETRABROMOETHANE

more significant as the cell depth ( $d$ ) is decreased to study more absorbing samples (such as acetonitrile solutions). Therefore the subtraction of an empty cell phase spectrum background from the sample cell phase spectrum without accounting for these characteristics may lead to a large phase error. However in the frequency range of interest ( $5 - 100\text{cm}^{-1}$ ) in this work the spectral profiles are in good agreement with those observed by other workers<sup>155,163</sup> therefore the cell may be put to good use if a maser measurement is available to 'fix' the level of the spectrum. This method has been applied by early workers<sup>155</sup> in this field who found similar 'level' problems which were probably also due to the neglect of interface effects when applying the free layer method. Unfortunately such maser determined refractive index values are not available for the range of acetonitrile/carbon tetrachloride solutions studied in this work. Further there are other problems associated with the Durham cell as follows:

a) **Pathlength.**

This is difficult to vary precisely since the spacers are only available in standard thicknesses and distortion occurs when under compression in the cell. Changing the path length is time consuming because it requires that the cell is emptied and cleaned before dismantling particularly if toxic chemicals are studied. The path length of the assembled cell can be measured from the internal window reflection however this is subject to relatively large errors due to the small size of this reflection. Larger reflections are observed from the silicon window used in the Leiden cell (described in this Chapter) due to the high refractive index of silicon with respect to air.

b) **Window Properties.**

In addition to the problem arising from the close proximity of the internal reflection fringe (6) to the main fringe (5) there is also a problem due to the window distortion which occurs in this non rigid 'mylar' when dense liquids are studied. This leads to a loss of intensity due to the defocusing effect and also results in an uncertainty in the path length determination. These problems could be resolved by the modification of the cell to accept a thicker rigid window such as silicon, as used in the Leiden cell<sup>160</sup>, germanium which has been employed in a similar cell<sup>159</sup> developed by workers at the University of Nancy, France or possibly crystal quartz if a relatively narrow transmission window could be tolerated (absorption feature at  $120\text{cm}^{-1}$ ).

c) **Temperature Control.**

This is not a feature of this cell, thus rendering it unsuitable for the study of the solutions over the full range of conditions desired. Incorporating temperature control would be a relatively simple task requiring the bonding or clamping of some thin walled copper tubes to the cell body. These would then be circulated with water or other suitable fluid from a thermostated bath. In conjunction with this it may be necessary to thermally insulate the interferometer from the cell as large temperature variations will result in interferometer distortion. (Some recent modifications<sup>136</sup> to the Durham interferometer include independent temperature stabilisation).

d) **Vacuum Window.**

It is necessary to separate the cell from the main body of the interferometer by a vacuum window supported by a wire grid. Although the intensity losses due to the presence of this window are of little significance compared to those arising from window bowing of the cell window they are none the less undesirable. The two alternatives which eliminate the need for this window are either to flush the entire instrument with dry nitrogen rather than evacuating (to remove water vapour) or to seal the cell window against the instrument body, which requires that the window be rigid and strong. The second method employed by the Leiden group has also been adopted more recently for the cell which has been developed jointly between The National Physical Laboratories and this Laboratory.<sup>136,158</sup>

ii) **Refractive Index Measurement By The Free Layer Technique**

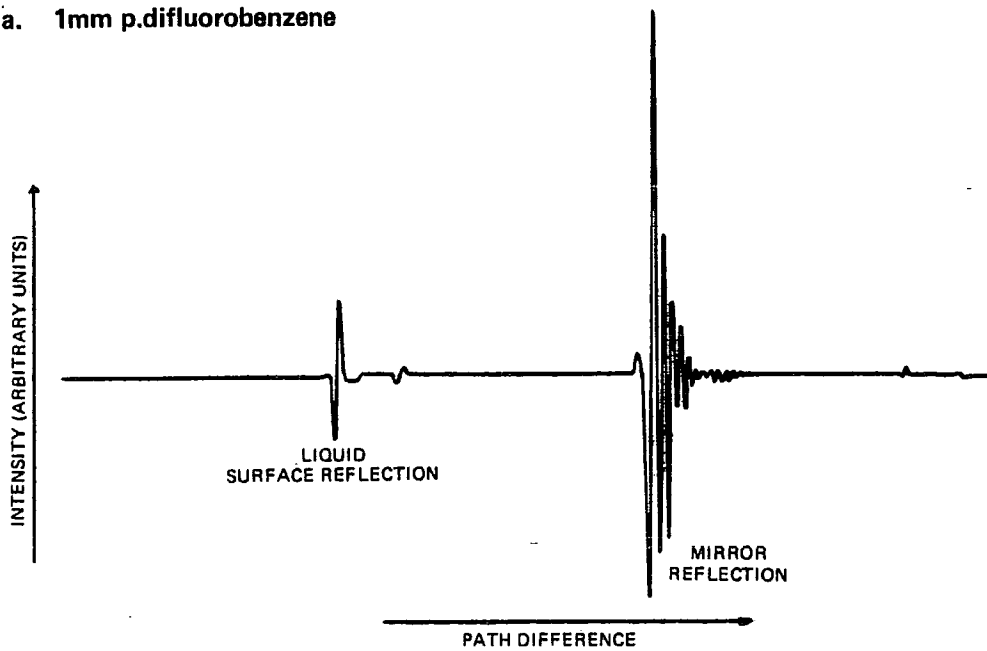
These measurements were made at the National Physical Laboratory, Teddington. Initially the free layer technique was employed to establish the refractive index spectrum of para difluorobenzene for comparison with the results obtained from the Durham cell. This method does not require the liquid to be contained by a window and hence does not suffer from the phase errors thought to arise from the computation of fringe 6 as outlined previously. Using a Golay detector the interference patterns of three different thicknesses of sample were recorded in addition to several empty cell interferograms. Some examples of the interferograms recorded are shown in Figure 4.5, where the separation of the main fringe from the surface reflection can clearly be seen to increase with sample thickness. (Note the different form of these interferograms due to the fact that this is a phase modulated instrument<sup>54</sup>). The interferograms were recorded on paper tape in ASCII code (ISO-6). A copy was also made in binary code which could be easily read to determine the sample optical thickness  $\bar{x}$ . These tapes were also used to determine the exact centre of the interferogram maximum (which is not necessarily sampled) so that a correction could be made to the computation origin in the manner described by Chamberlain.<sup>145</sup> However it has recently been shown<sup>161</sup> that these corrections were not necessary and may actually lead to greater errors in the final spectrum.

**Computation of results**

The relatively long path lengths employed ensured a wide separation of the reflection fringes and thus enabled a simple editing procedure to be carried out to remove the unwanted signatures. The phase spectra calculated from the edited sample interferograms are shown in Figures 4.7a, 4.8a and 4.9a. In these examples the phase branching (see Section A) can clearly be seen to increase with the optically thicker, more absorbing samples. Conversion of these spectra to binary code on paper tape facilitated the accurate location of the branch points and their subsequent correction with the appropriate phase terms. The corrected spectra are shown in Figures 4.7b, 4.8b and 4.9b.

For the free layer method the interferograms with and without a sample present can be represented by Figure 4.6.

a. 1mm p.difluorobenzene



b. 2.5mm p.difluorobenzene

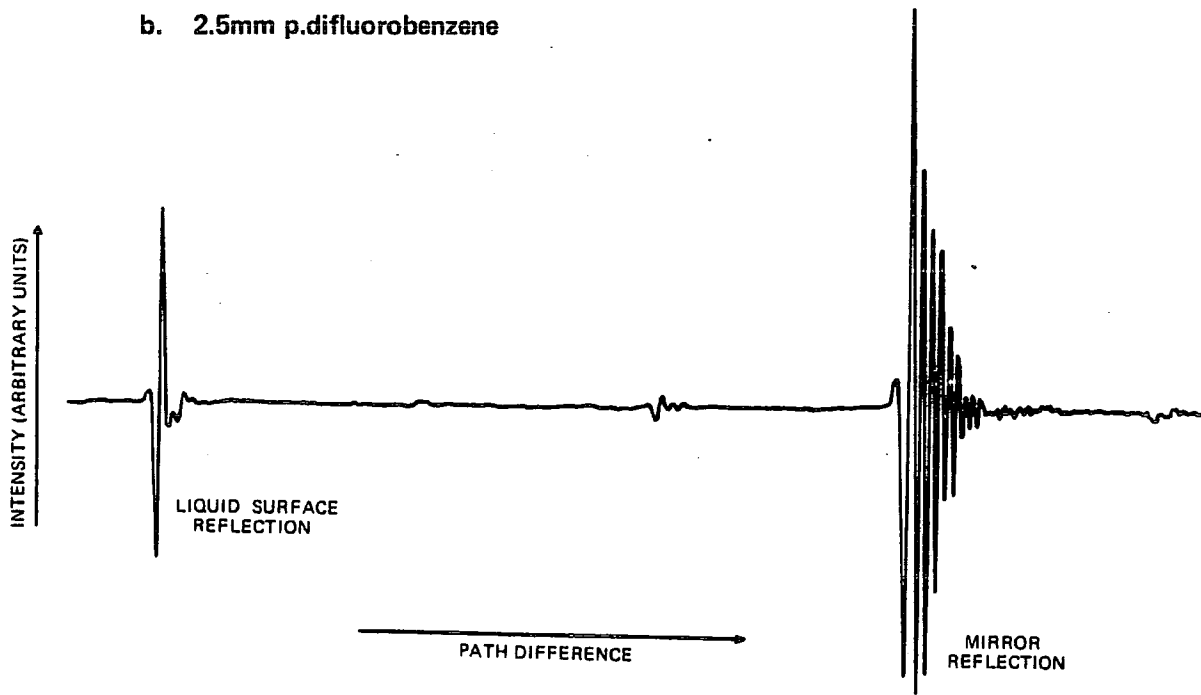


FIGURE 4.5  
INTERFEROGRAMS RECORDED BY THE 'FREE LAYER' METHOD

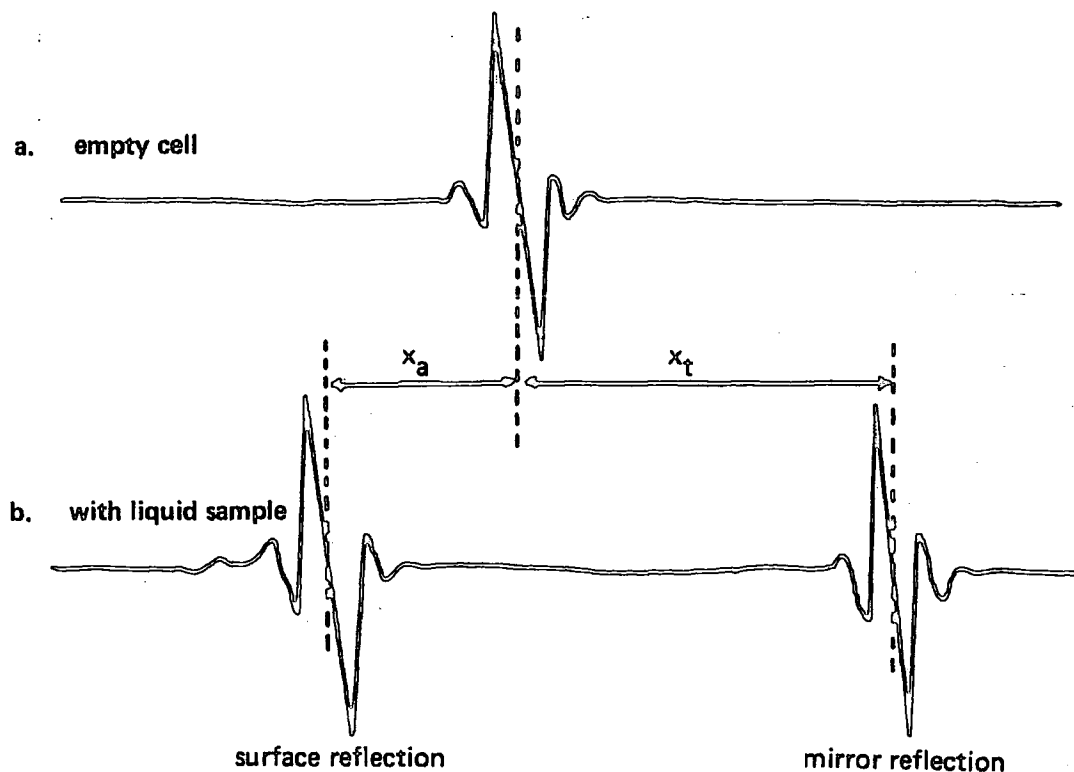


FIGURE 4.6  
SCHEMATIC FREE LAYER INTERFEROGRAMS

The optical shifts  $x_a$  and  $x_t$  including boundary phase change effects are then given by:

$$x_a = -2d + \left[ \frac{1}{2\pi\bar{\nu}} \right] (\phi_a^r - \pi) \quad \dots\dots\dots 4.12$$

$$\text{and } x_t = 2(\bar{n} - 1) d + \left[ \frac{1}{2\pi\bar{\nu}} \right] (\phi_{OL}^t + \phi_{LO}^t + \phi_{LM}^r - \pi) \quad \dots\dots\dots 4.13$$

Where the subscripts O, L and M refer to air, liquid and mirror respectively.

superscripts t = transmitted

r = reflected

therefore  $\phi_{OL}^t$  is the phase change of a transmitted wave at the air/liquid boundary and the  $-\pi$  term is due to the phase shift which occurs at the moving mirror.

The final refractive index spectra shown in Figure 4.10 have then been obtained by two different methods. The slightly higher values have been calculated by subtracting an empty cell 'background' spectrum and neglecting the interface phase terms of equations 4.12 and 4.13. These are expected to be directly comparable with the results obtained with the Durham cell and have been reproduced with those results for comparison in Figure 4.4.

Also included in Figure 4.4 is the spectrum of tetrabromoethane obtained previously<sup>132</sup> with the Durham cell compared with Chamberlain's spectrum<sup>155</sup> recorded by the free layer method.

P.DIFLUOROBENZENE 0.5mm FREE LAYER.

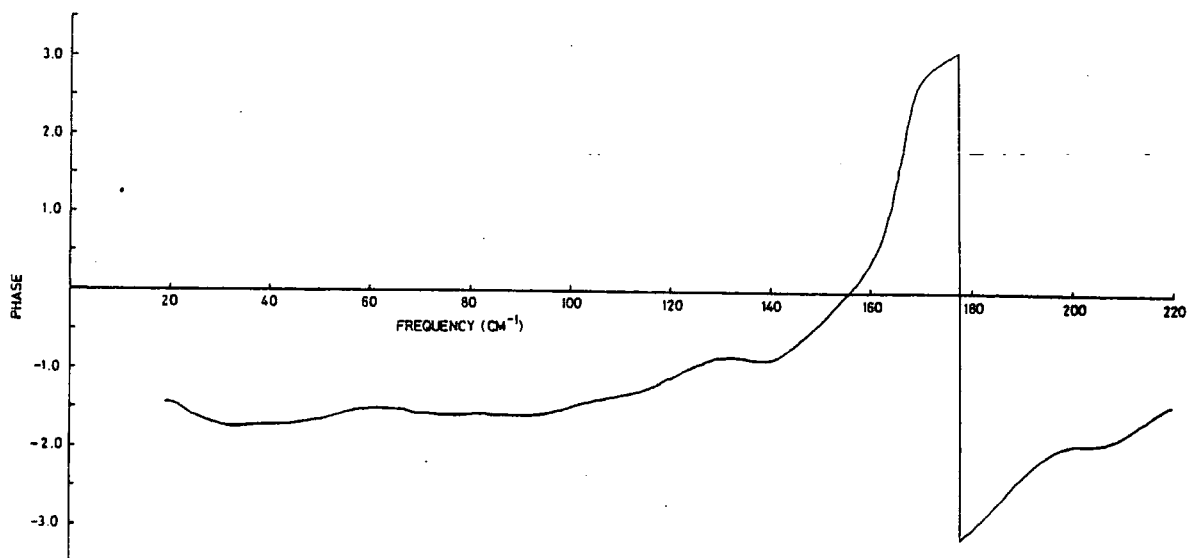


FIGURE 4.7a

P.DIFLUOROBENZENE 0.5mm FREE LAYER  
(BRANCHING CORRECTED)

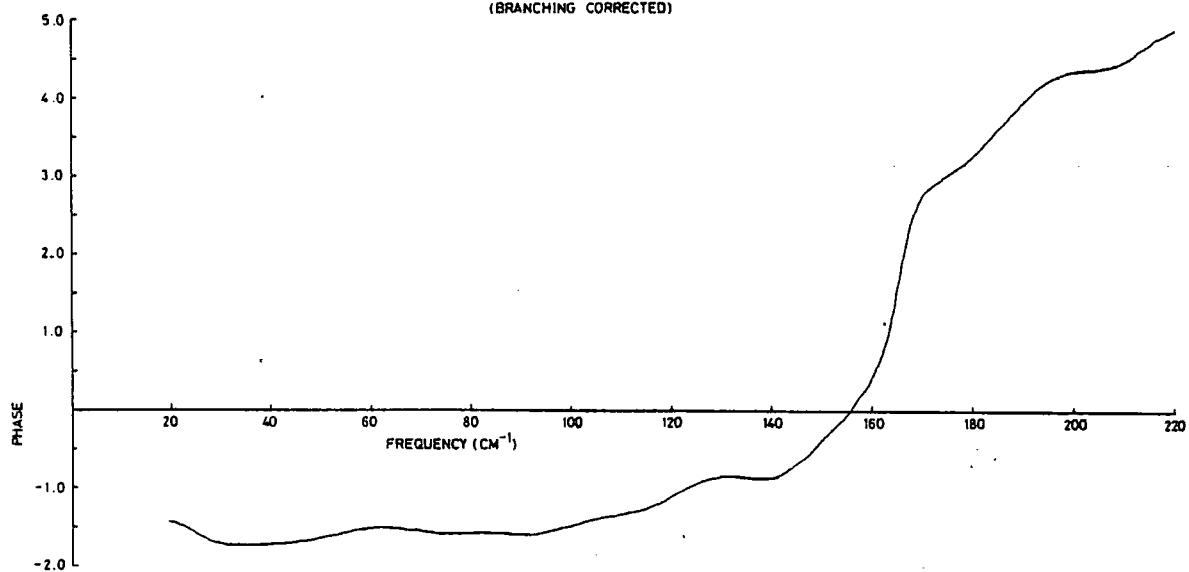


FIGURE 4.7b

P-DIFLUOROBENZENE 1.0mm FREE LAYER

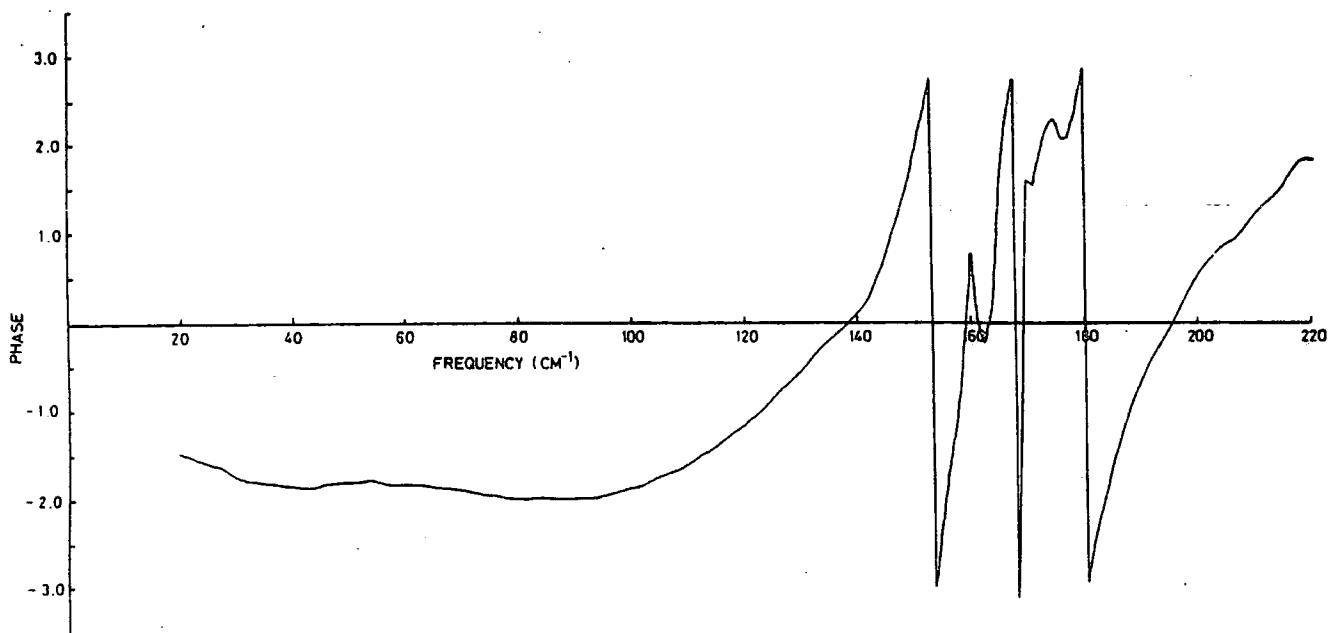


FIGURE 4.8a

P-DIFLUOROBENZENE 1.0mm FREE LAYER  
(BRANCHING CORRECTED)

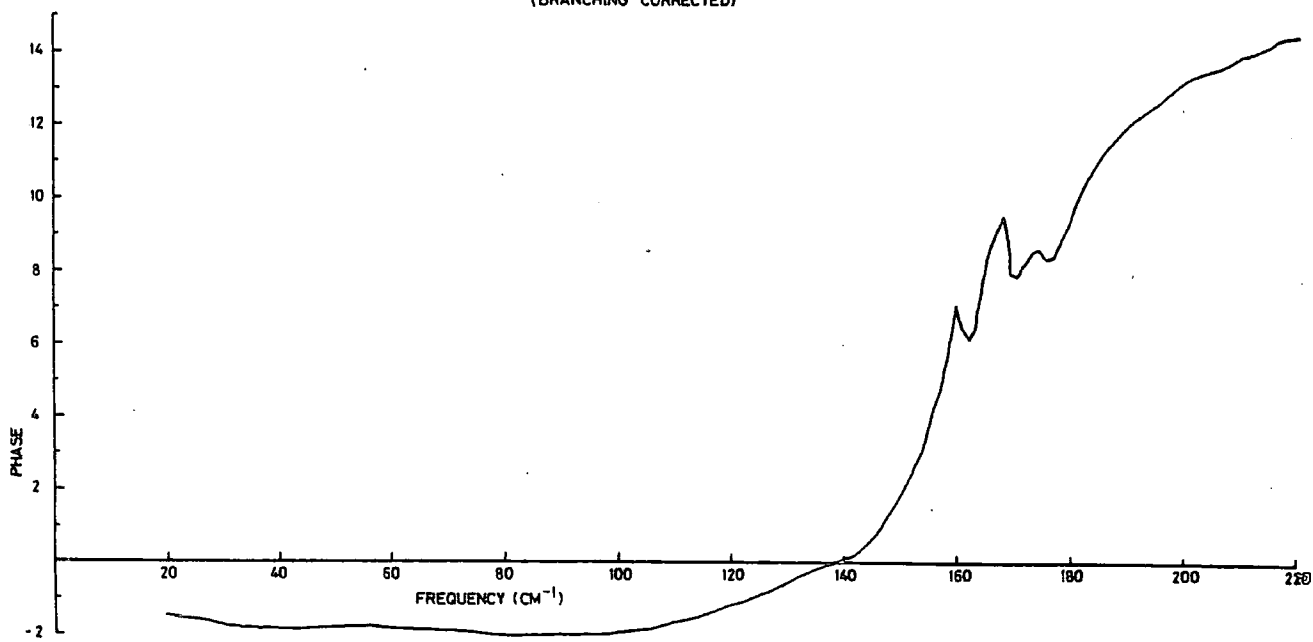


FIGURE 4.8b

P-DIFLUOROBENZENE 2.5mm FREE LAYER

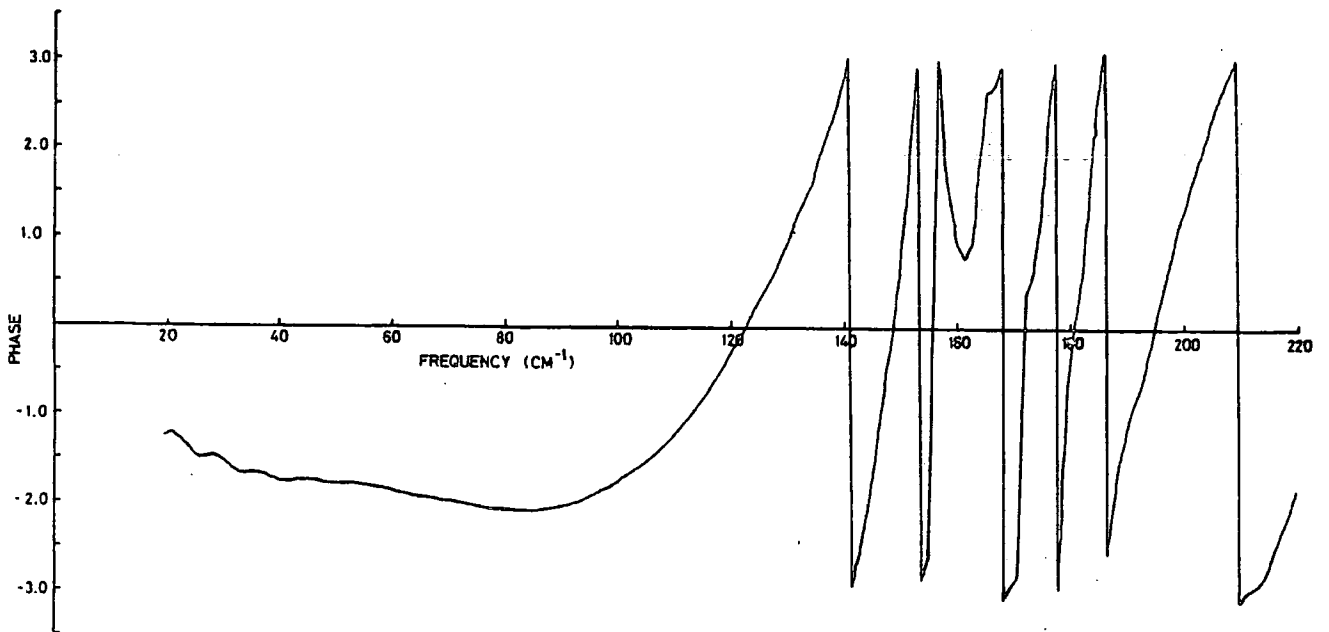


FIGURE 4.9a

P-DIFLUOROBENZENE 2.5mm FREE LAYER  
(BRANCHING CORRECTED)

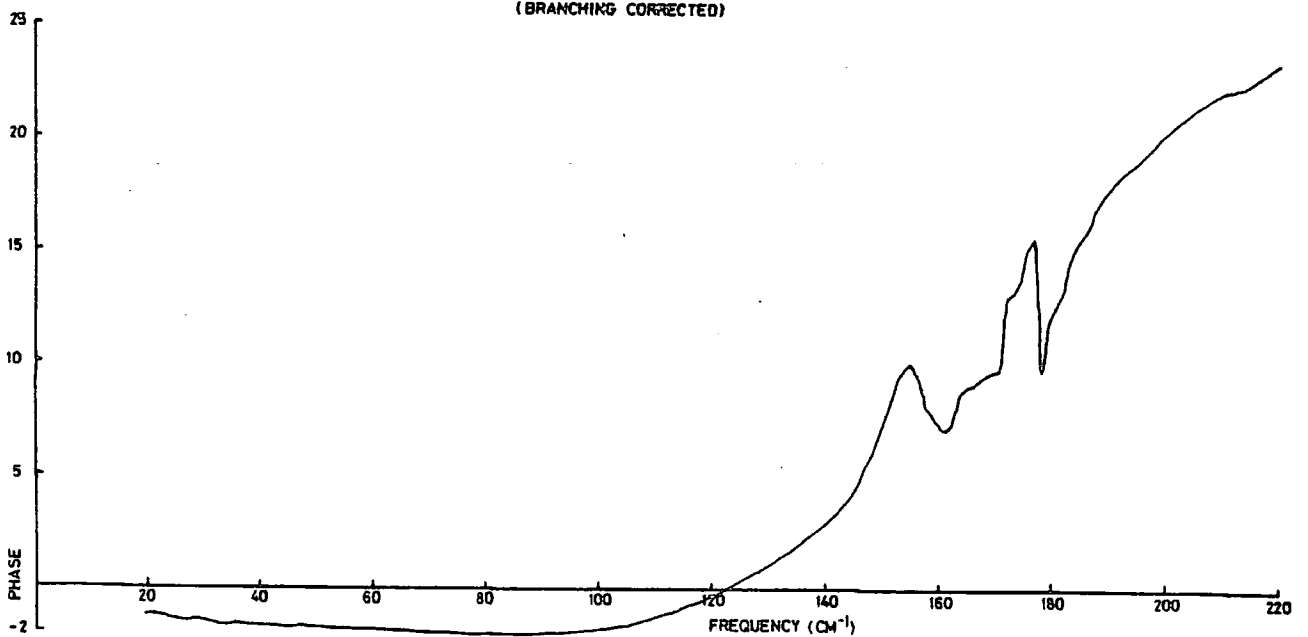
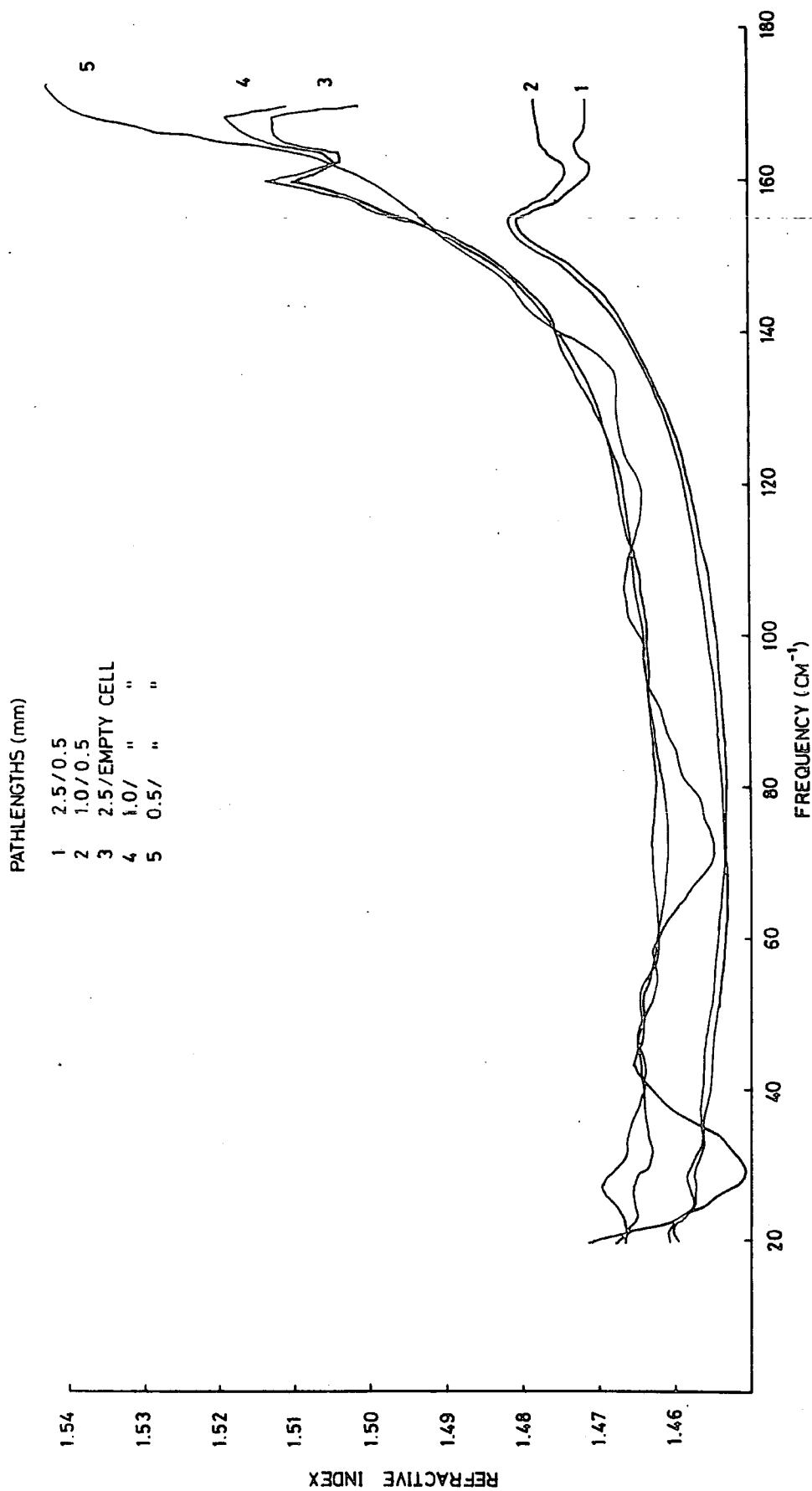


FIGURE 4.9b

FIGURE 4.10

REFRACTIVE INDEX OF P. DIFLUOROBENZENE AT 298K.



It is apparent from the comparison of these sets of results that the level problem encountered with the Durham cell is not simply due to the neglect of the phase changes at the reflecting boundaries unless these are considerably greater for the mylar window used. This is possible but it is thought that such a large systematic error probably arises from the difficulties of using the cell in its present form. Cell window distortion for example must be eliminated before this problem can be approached with confidence.

The second method which has been applied to the computation of the refractive index from these results is the two thickness method described by Afsar.<sup>164</sup> Quite simply this method requires the subtraction of one phase spectra of a thin sample from another of a thicker sample in a similar method to that employed in transmission spectroscopy. Because the phase changes on reflection will be constant for each spectra these are removed by the subtraction procedure and thus a phase corrected spectrum can be calculated. The results of the two possible subtraction for the data recorded are also shown in Figure 4.10, (the lower spectra). The difference in level between these and the uncorrected sets serve to illustrate the error that arises from the neglect of surface phase change effects i.e. the liquid thickness is underestimated and therefore the refractive index curve obtained is too high.

An attempt was made to obtain the spectra of the  $\text{CH}_3\text{CN}/\text{CCl}_4$  solutions by the free layer method. As anticipated this proved difficult because of the highly volatile nature of these solutions. The one result obtained, for 0.018 mf  $\text{CH}_3\text{CN}/\text{CCl}_4$  at  $45^\circ\text{C}$  is presented in Figure 4.11. Further measurements of these solutions were made using the Leiden cell described in the next Section.

### iii) Refractive Index Determinations of $\text{CH}_3\text{CN}/\text{CCl}_4$ Solutions Using the Leiden Cell

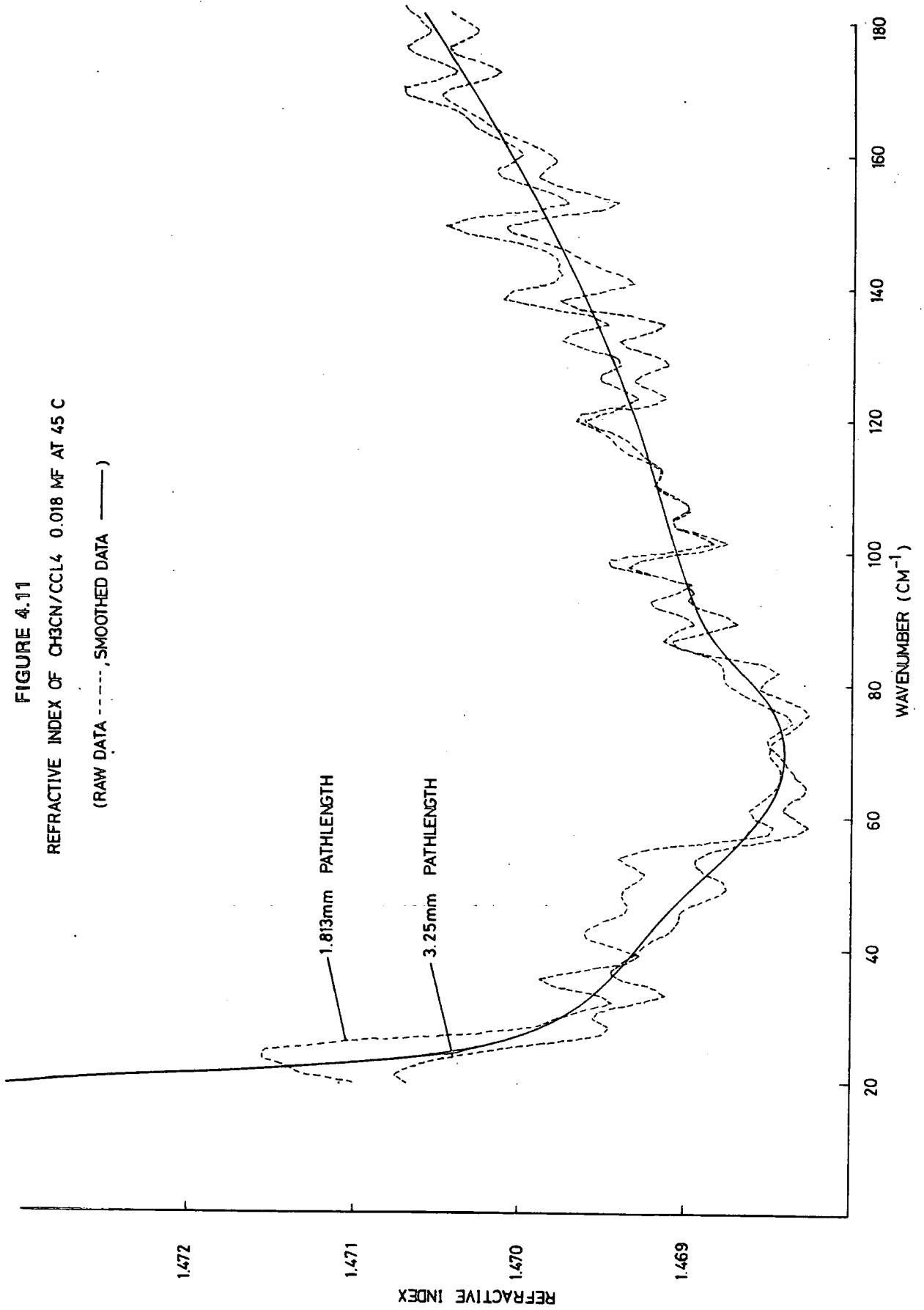
These solutions are particularly volatile and toxic and therefore it was not possible to study them using the free layer technique. To prevent excessive loss of vapour, which would lead to concentration variation and exposure to harmful vapour these studies were made at The National Physical Laboratory using the sealed Leiden cell mounted on an NPL cube interferometer. This cell has been described in detail previously<sup>154,160</sup> and therefore in this work only the salient features are outlined.

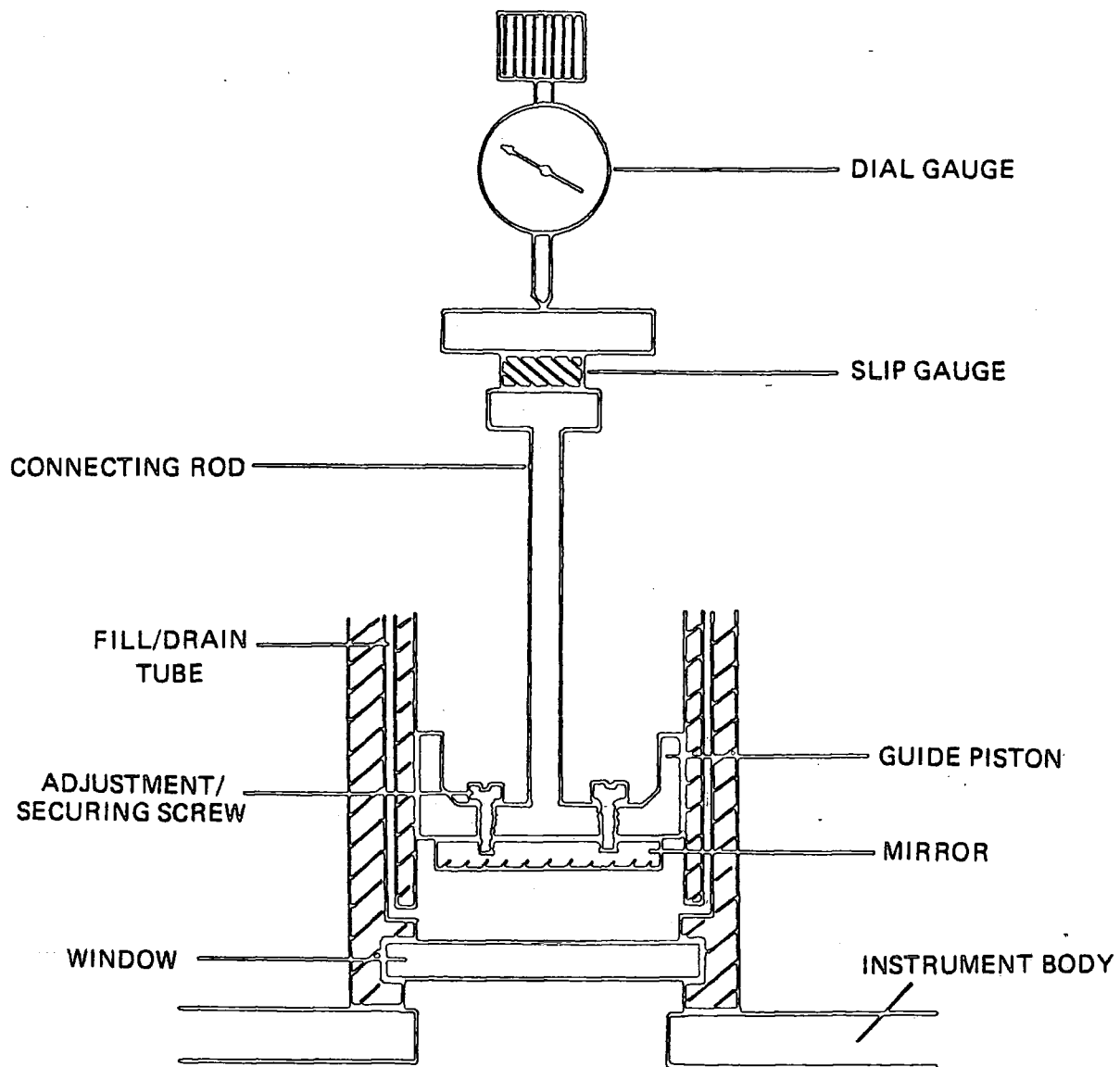
The Leiden cell, which is shown schematically in Figure 4.12 is constructed as follows. The window, exposed to the interferometer vacuum, is a piece of optically flat silicon approximately 40mm in diameter and 2.5mm in thickness. Behind this in a parallel plane is situated the gold plated stainless steel cell mirror, mounted on a piston which can be moved relative to the window thus varying the cell path length. The movement of the piston is controlled by air pressure and accurately monitored by the slip gauges and a dial gauge shown. Thermal stability of the cell is ensured by recirculating fluid from a thermostated bath whilst the actual temperature is monitored by a thermocouple attached to the window mounting. The entire unit is encased in an air tight jacket which is exposed to the evacuated instrument. The liquid samples are introduced into the cell by two thin walled tubes passing through the evacuated jacket. The complete assembly is mounted on top of the interferometer as shown in the diagram.

FIGURE 4.11

REFRACTIVE INDEX OF CH<sub>3</sub>CN/CCL<sub>4</sub> 0.018 MF AT 45 C

(RAW DATA -----, SMOOTHED DATA -----)





**FIGURE 4.12**  
**A SCHEMATIC DIAGRAM OF THE LEIDEN CELL**

The interferometer was a heavily modified NPL cube incorporating phase modulation, wire grid beam splitter, stepping motor mirror drive and in this case employing a Helium cooled Putley-Rollin detector capable of low noise operation at low frequency. This instrument is fully temperature stabilised with a recirculating water system (25°C) and thermally insulated from the Leiden cell with a perspex spacer.

#### **A Summary of the Advantages and Disadvantages of the Leiden Cell Compared to the Durham Cell**

##### **Advantages**

**a) Temperature Control**

Precise temperature control is possible while in addition the thermal stability of the interferometer is ensured.

**b) Cell Pathlength**

This is accurately determined from the slip gauges and can be varied conveniently without dismantling. A knowledge of the exact pathlength also facilitates the calculation of transmission spectra.

**c) Window Reflections**

The single internal window reflection gives rise to a fringe as in the Durham cell. In this case the fringe is conveniently displaced away from the central fringe by the thicker window (2.5mm). Thus the computation of this fringe and the associated uncertainties are avoided.

##### **Disadvantages**

**a) Window Reflections**

The size of the reflection fringes from the window surfaces serve to indicate the loss of energy in the system. These losses are greater than those found in the free layer method or the Durham cell because of the high refractive index of silicon ( $\approx 3$ ). The top window reflection cannot be used to recover spectral information of the liquid however the internal reflection can be used in the full interferogram method described by Honijk and Passchier.

**b) Operation**

This highly sophisticated cell is complicated to operate and difficult to adjust if it becomes misaligned. In addition the piston and sleeve arrangement by which the cell mirror is moved, seems to be prone to jamming when used with the solutions studied in this work.

#### **A Brief Description of Operation of the Leiden Cell**

The cell pathlength is set by the use of the slip and dial gauges whilst the mirror is held in position by air pressure. Dry air is flushed through the cell to ensure that all vapour has been eliminated. The cell is then sealed and allowed to reach thermal equilibrium (approximately 10 minutes). The interferograms of different pathlengths were then recorded consecutively. Each run was started at the same point, (read from the stepping motor drive) just before the window reflection, for the convenience of analysis and computing.

The freshly prepared solutions (for details of preparation of all solutions refer to Chapter 5) were flushed through the cell to eliminate air bubbles, the cell was then sealed and again allowed to

reach thermal equilibrium. It has been found to be good practice to work through the sample runs recording the longest pathlength interferogram first. In this way the problem of air bubble trapping need only be considered when filling the cell initially.

The sizes of the two main peaks corresponding to the front window reflection and the cell mirror reflection were checked prior to recording the interferogram. Gain adjustments were made as appropriate to achieve good modulation depth and thus fill the dynamic range of the digitizing electronics. A typical set of interferograms recorded with the Leiden cell in this work are shown in Figure 4.13. The ASCII coded tapes were converted to binary for point counting and estimation of the true zero path position as in the free layer method. The phase spectra were calculated from the main fringe as previously using a fast Fourier transform program and then examined for the effects of phase branching. After correcting for branching the final refractive index spectra were derived from the ratio of the solution phase spectra against the empty cell phase spectra. For comparison interferograms were recorded for two different pathlengths at each temperature. The pathlengths used were 2.6mm and 3.1mm for the 0.018mf solutions and 1.1mm and 1.6mm for the 0.061mf solutions.

#### Results

The results obtained for the four solutions studied, 0.018mf and 0.061mf at 15°C and 45°C are shown in Figures 4.14 and 4.15. In these figures the broken lines are the refractive index curves obtained from the ratios of the various cell thicknesses against empty cell backgrounds as described. The continuous line smooth curves are the estimated averages used in the model analysis described in Chapters 5 and 6.

The absorption spectra have also been calculated from the dispersive interferograms and are shown in Figures 4.16 and 4.17. These spectra clearly show a higher absorption level than the results given in Chapter 5 which were recorded with the non-dispersive technique. This difference is due to the solution background subtraction which has been made in the latter case which yields solute in solvent spectra whereas the dispersive experiment described yields the solute + solvent spectra.

Some of the spectra (both  $\eta(\nu)$  and  $\alpha(\nu)$ ) recorded in this experiment exhibit noise which appears to be oscillatory. Afsar<sup>165</sup> has observed similar features (though of greater magnitude) in the recovered spectrum when the surface reflection fringe is transformed with the main fringe at the dispersion interferogram of liquid chlorobenzene (free layer method). Therefore it seems likely that the small oscillation observed are due to the transformation of a superfluous feature in the interferogram which may be present because of inaccurate editing of the window/solution reflection.

#### iv) Errors in the Refractive Indices Determined

It is apparent from the previous discussion that the Durham cell suffers from a large systematic error due at least in part to the neglect the liquid/window boundary phase effects. This leads to a discrepancy between these results and those obtained by the free layer measurements at NPL of +2%. An error of this magnitude is expected to dominate the random errors completely.

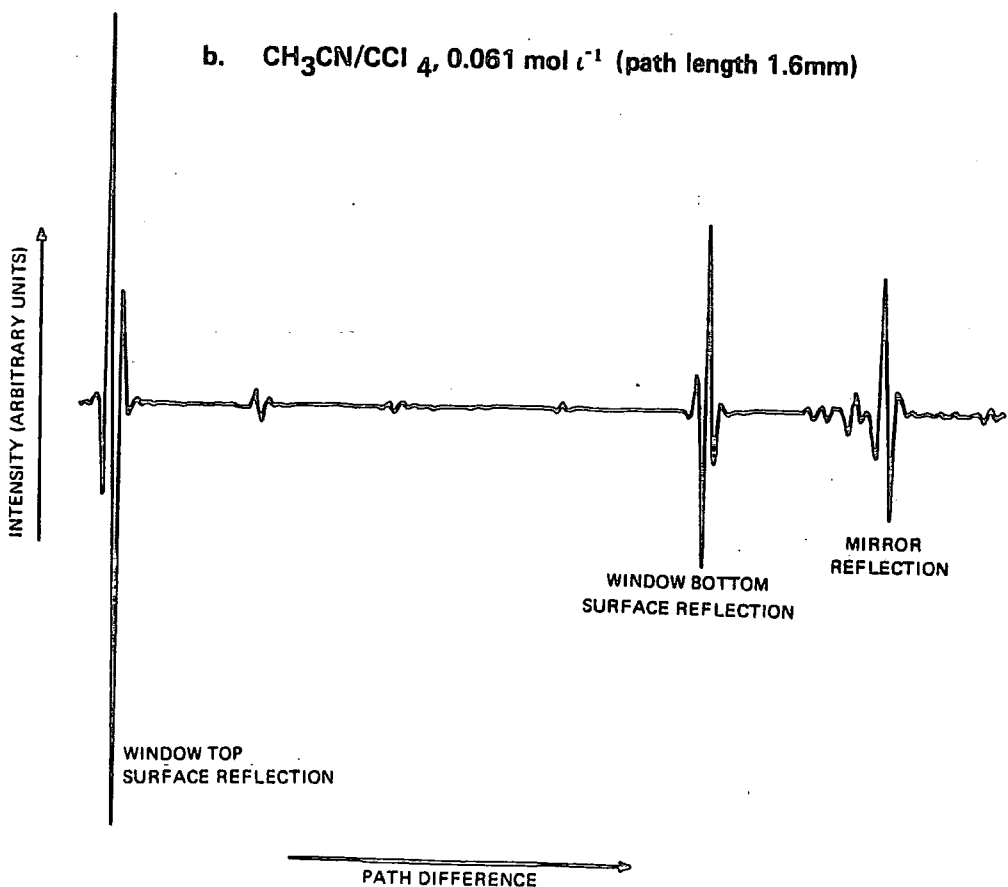
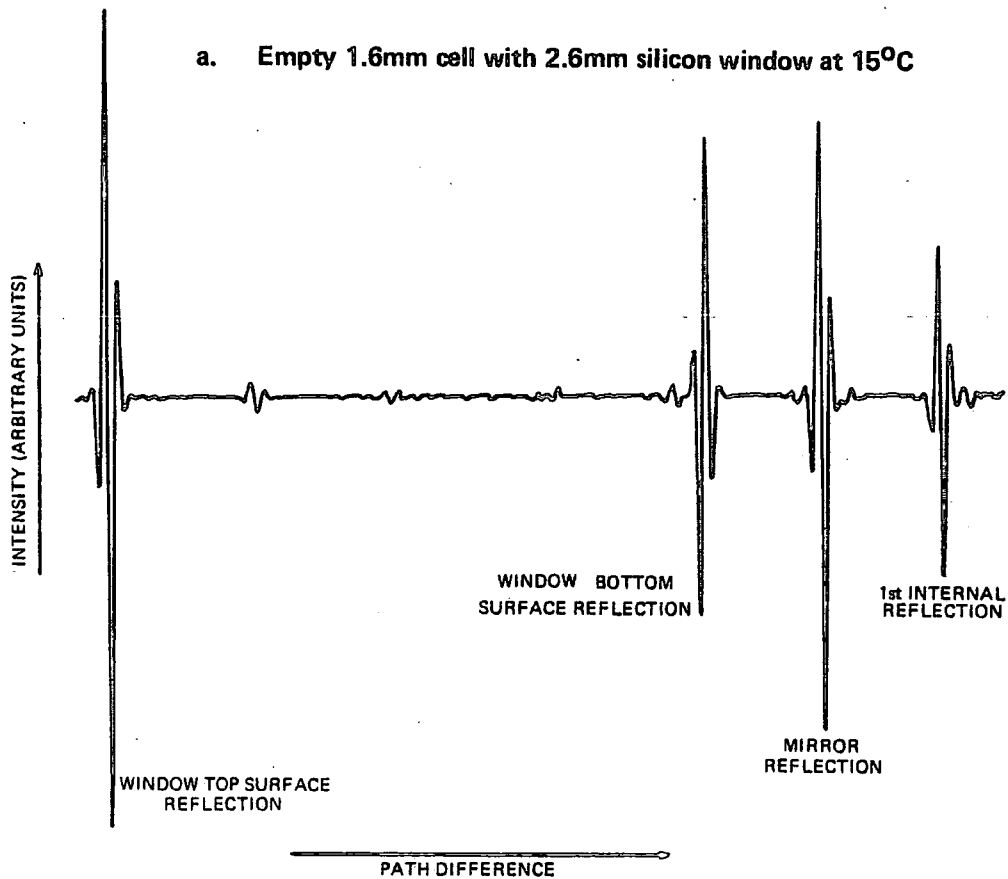
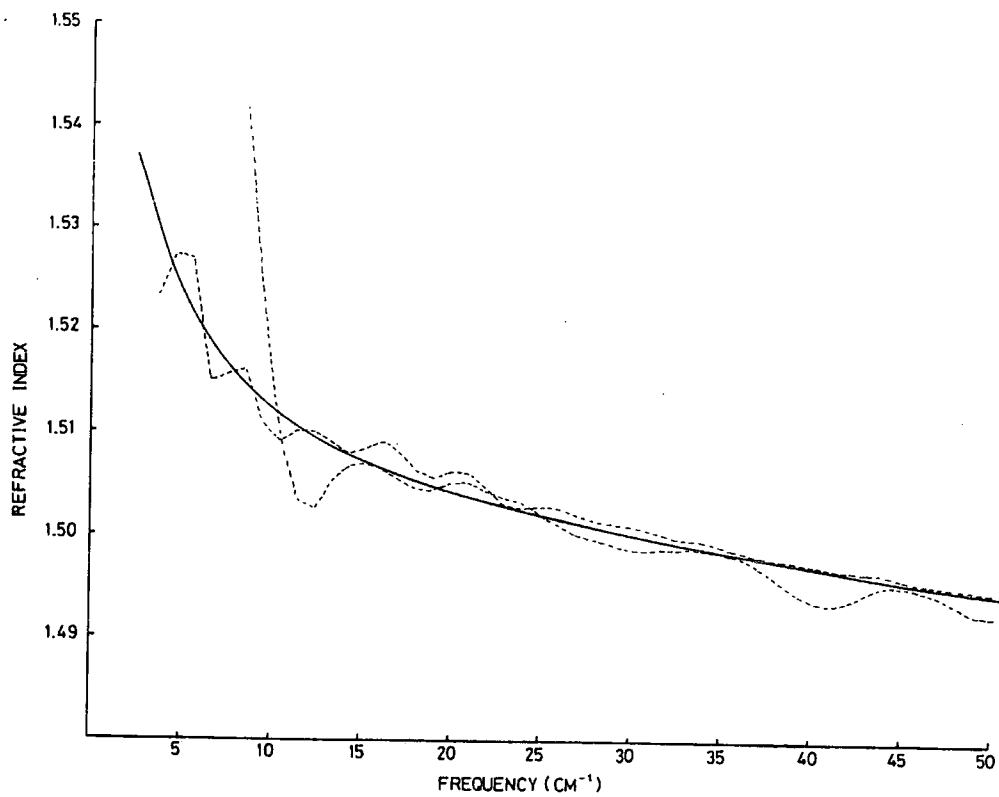


FIGURE 4.13  
INTERFEROGRAMS RECORDED WITH THE LEIDEN CELL

CH<sub>3</sub>CN/CCL<sub>4</sub> 0.018MF AT 288K



CH<sub>3</sub>CN/CCL<sub>4</sub> 0.061MF AT 288K

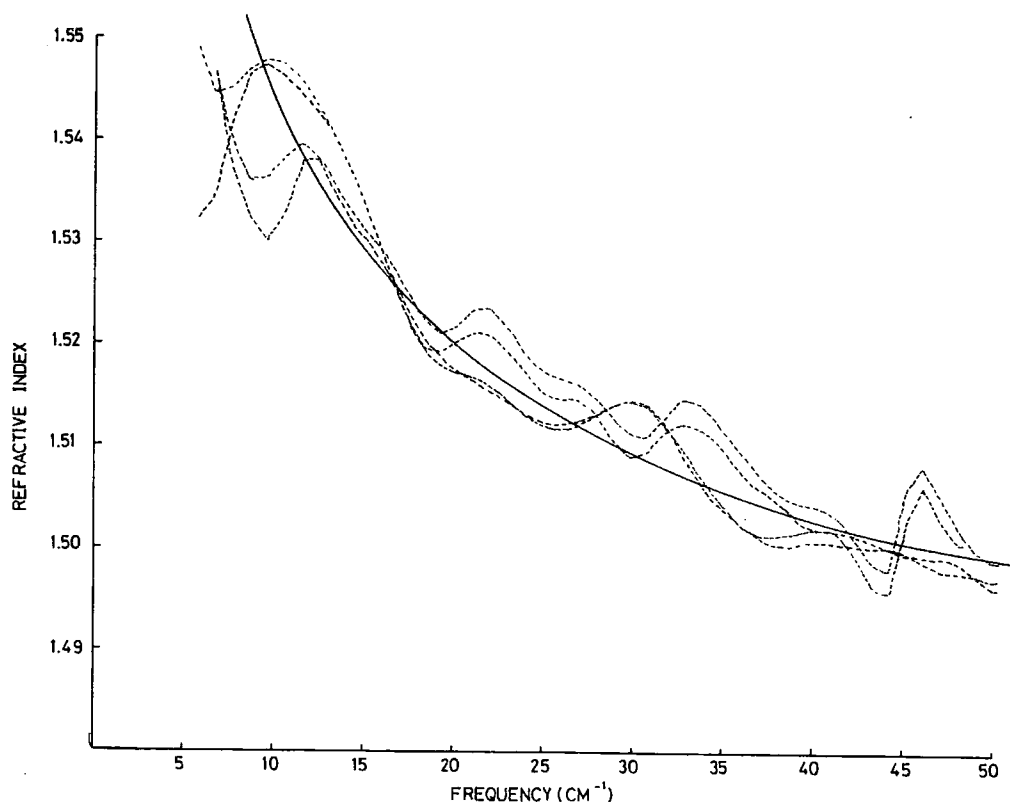
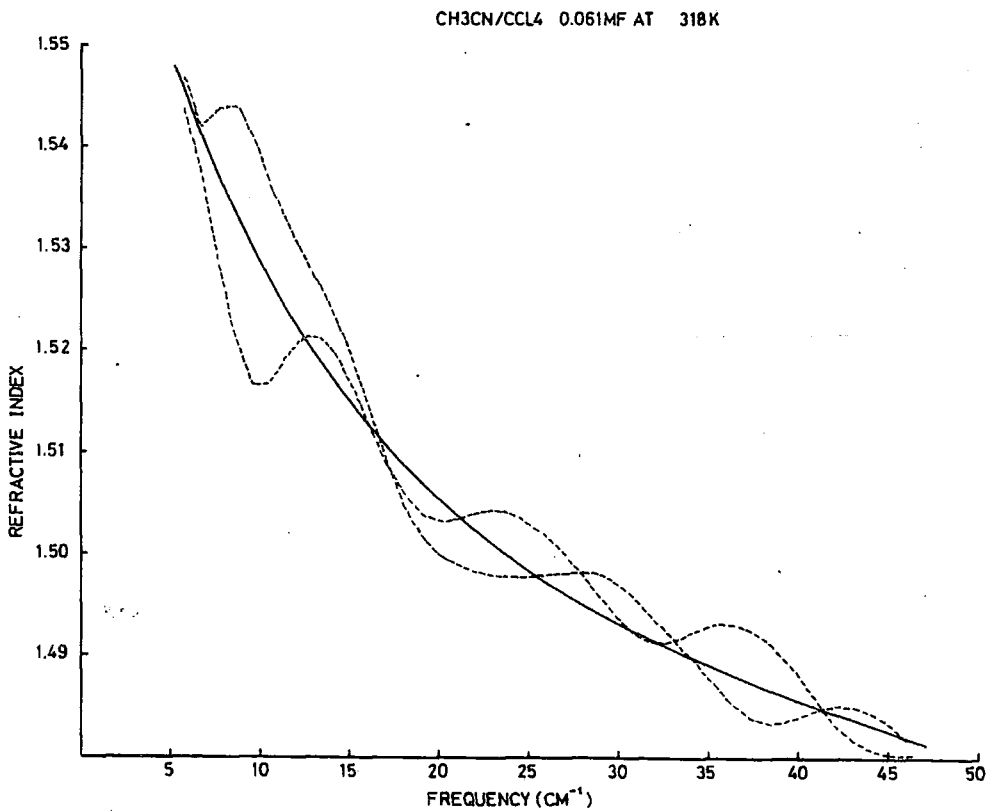
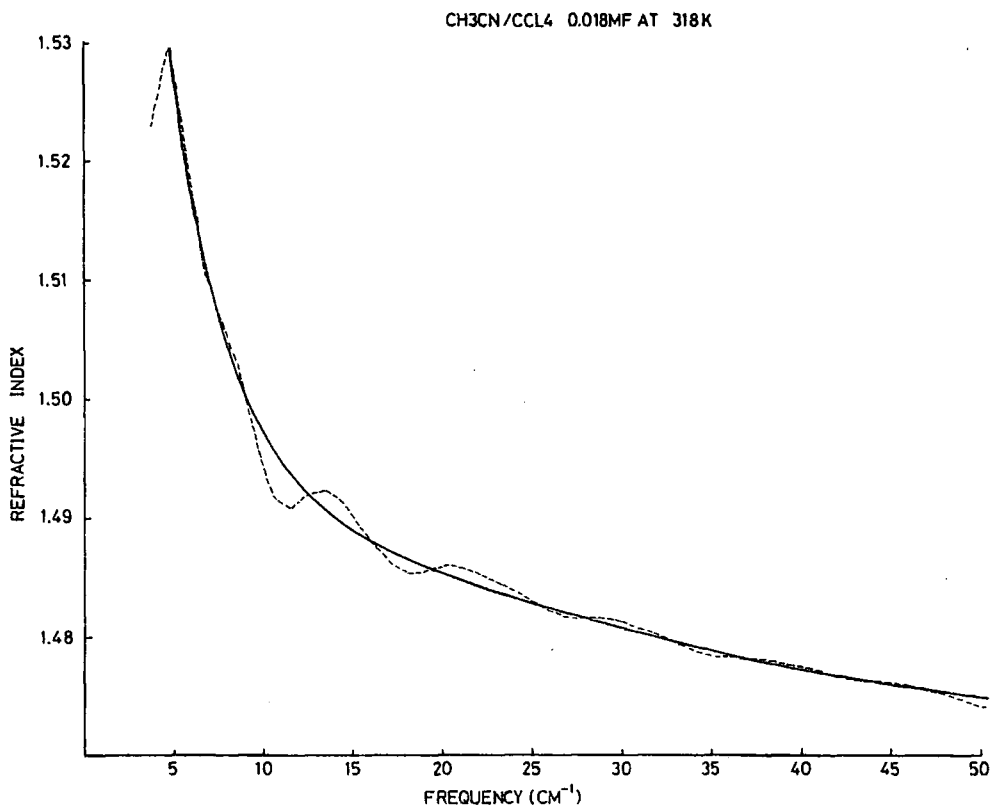
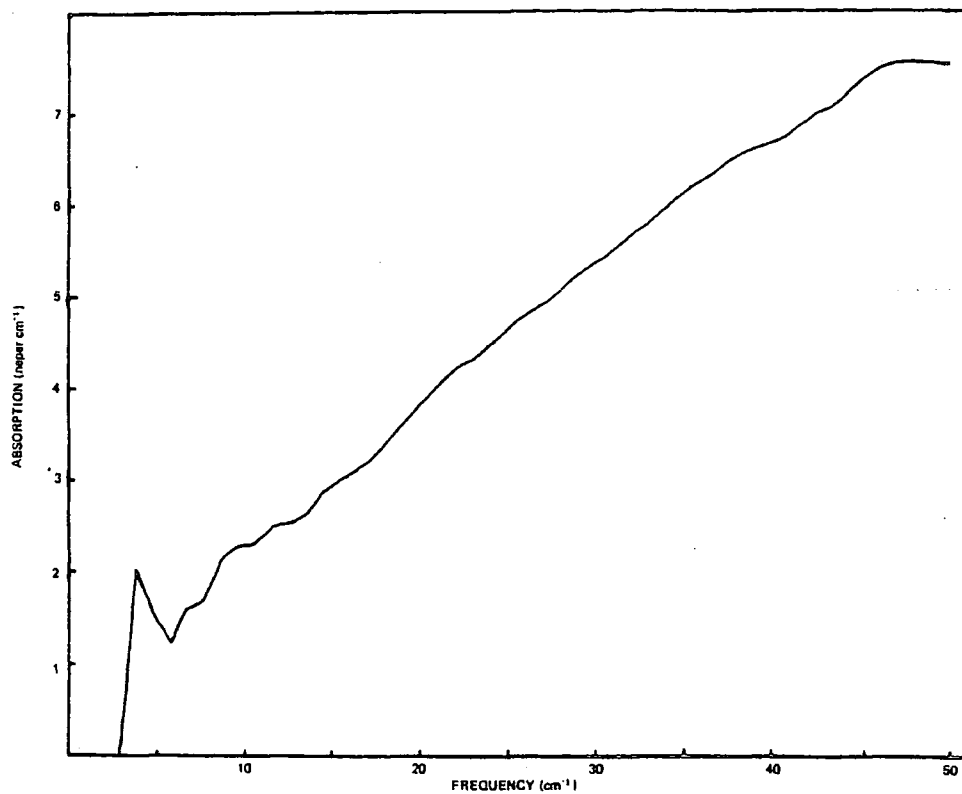


FIGURE 4.14

REFRACTIVE INDEX SPECTRA MEASURED USING THE LEIDEN CELL



**FIGURE 4.15**  
REFRACTIVE INDEX SPECTRA MEASURED USING THE LEIDEN CELL



**FIGURE 4.16a**  
**ABSORPTION SPECTRUM OF CH<sub>3</sub>CN/CCl<sub>4</sub>, 0.018mf AT 288K**

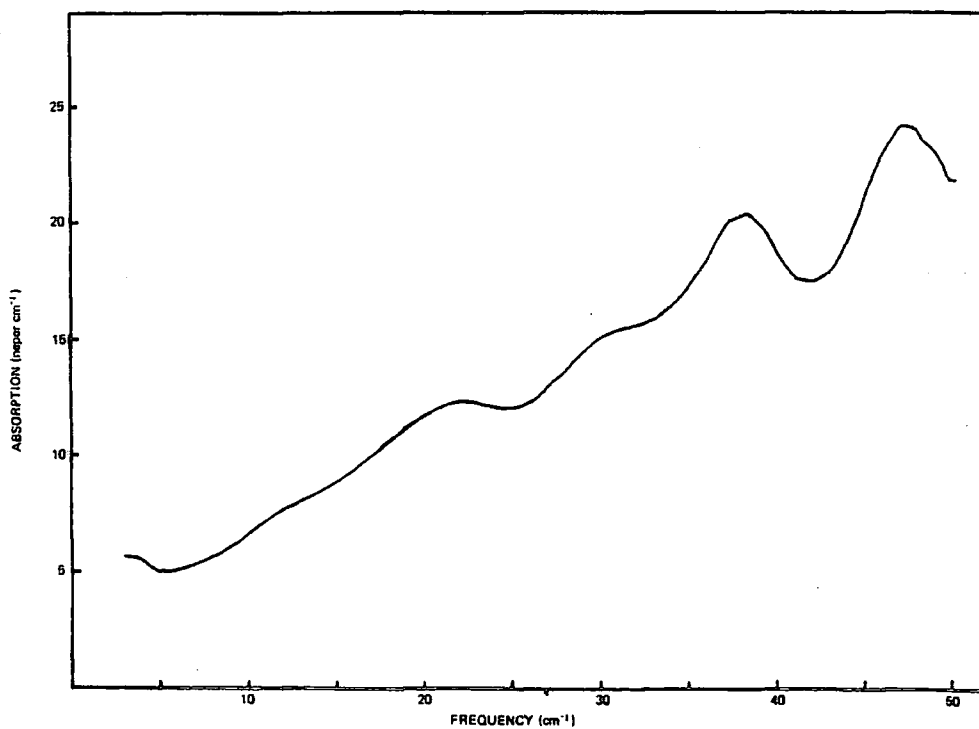


**FIGURE 4.16b**  
**ABSORPTION SPECTRUM OF CH<sub>3</sub>CN/CCl<sub>4</sub>, 0.061mf AT 288K**

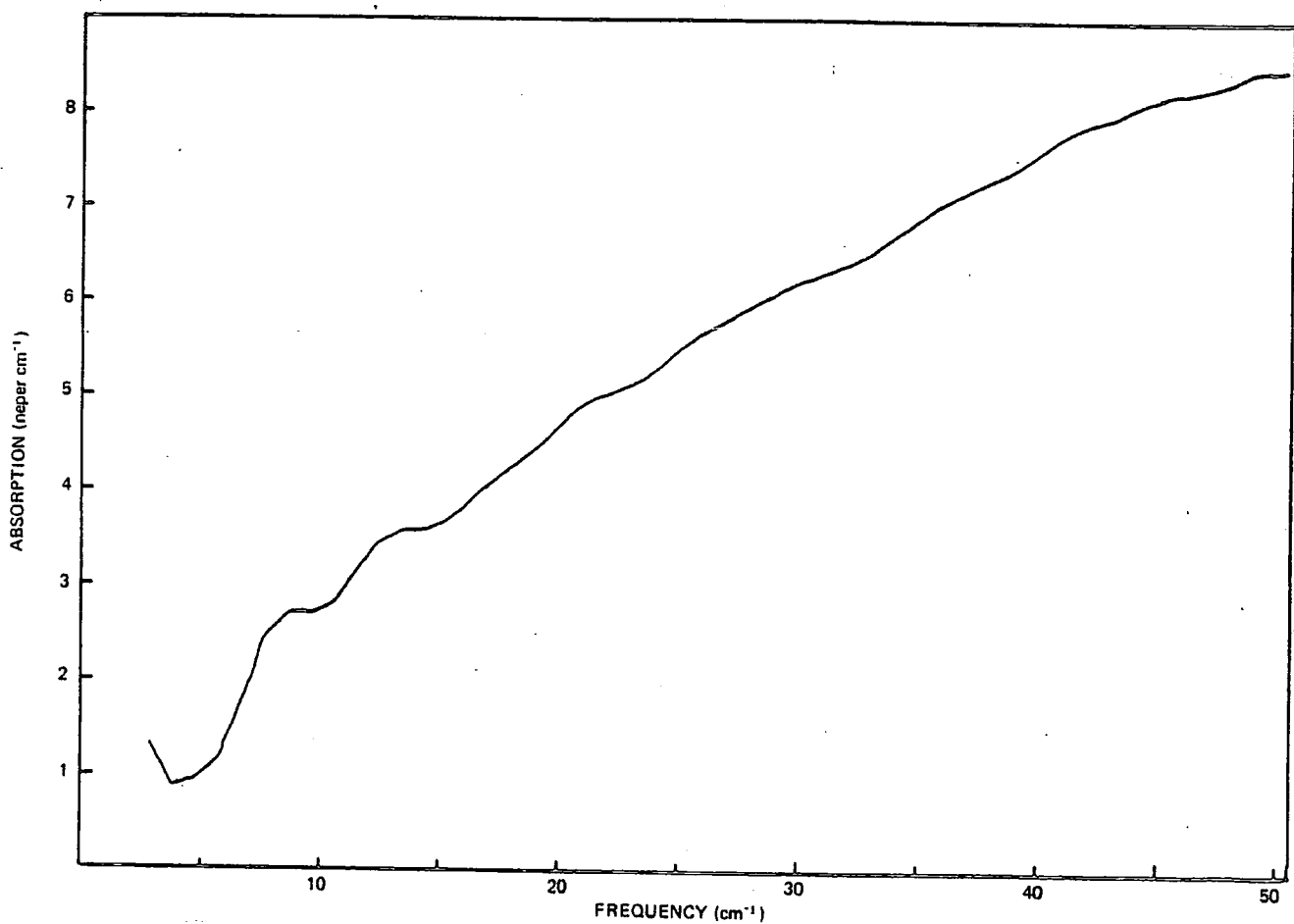


FIGURE 4.17a ABSORPTION SPECTRUM OF  $\text{CH}_3\text{CN}/\text{CCl}_4$ , 0.018mf AT 318K

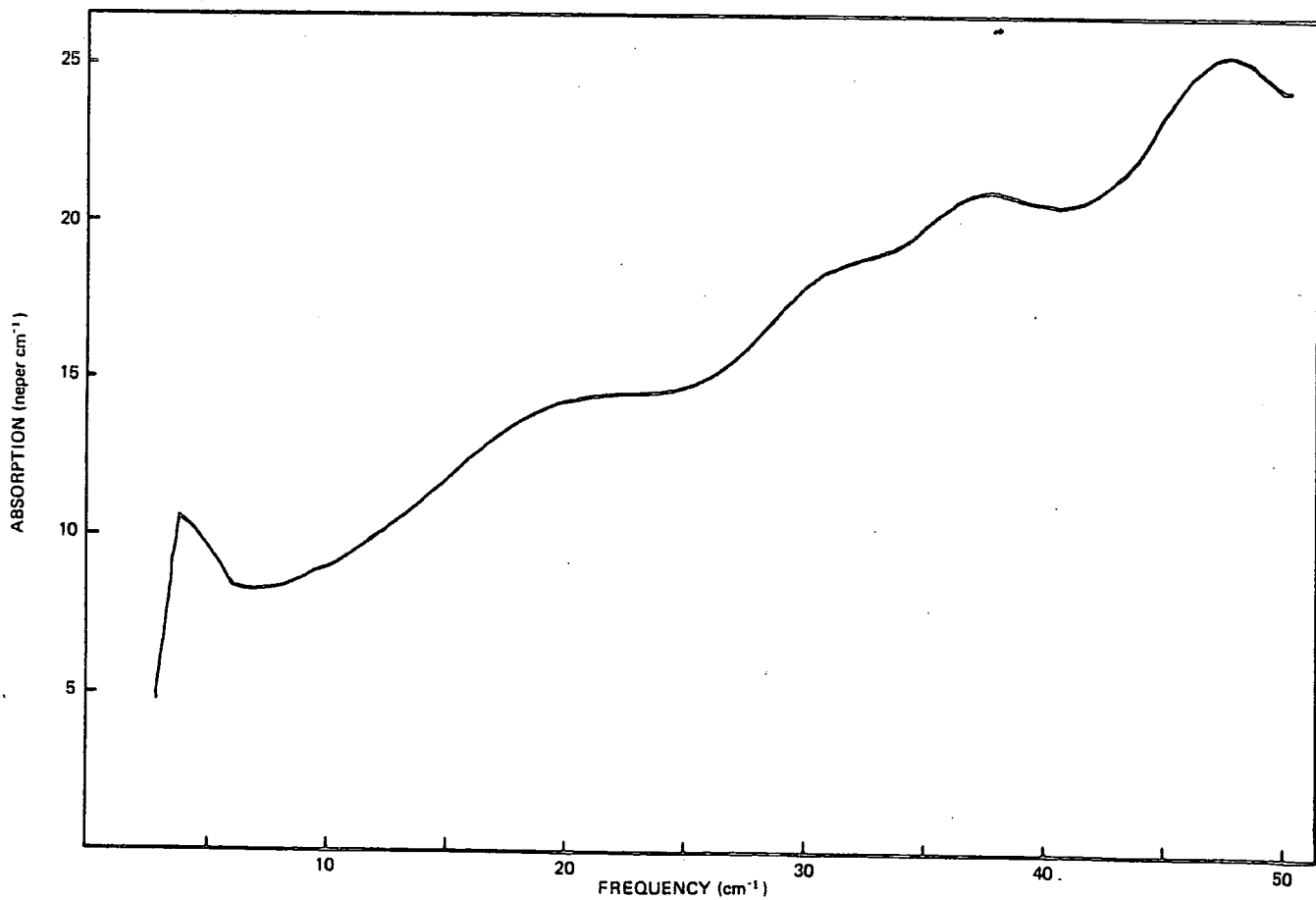


FIGURE 4.17b ABSORPTION SPECTRUM OF  $\text{CH}_3\text{CN}/\text{CCl}_4$ , 0.061mf AT 318K

For the Leiden cell, used in the manner described in this thesis, Passchier<sup>154</sup> has estimated that the refractive index determinations are subject to an error of  $\pm 0.001$  maximum and the absorption values calculated to be accurate within a few per cent. Comparison between the results obtained with the Leiden cell and the one solution measured by the free layer method show agreement within 0.8%. However the solution studied by the free layer method is subject to some additional uncertainty due to the presence of vapour and the variation in concentration resulting from evaporation. Afsar<sup>159</sup> has made similar comparisons for chlorobenzene ( $C_6H_5Cl$ ) at 25°C and found agreement to within 0.2% in refractive index values and 1-2% in absorption. For the liquid para. difluorobenzene measured by the free layer method in this work the scatter in refractive index curves recorded for different sample thicknesses is approximately 0.07% and 0.1% maximum over the frequency range 20-150 $cm^{-1}$  for the two thicknesses and the empty cell subtraction methods respectively. (This neglects the results of the 0.5mm sample which shows considerably more deviation in the region of low absorption around 20-40 $cm^{-1}$ ). The deviation in the values obtained for the  $CH_3CN/CCl_4$  solution by this method is 0.5% maximum which is too small to account for the difference between them and the Leiden cell results. However these also exhibit a scatter of approximately 0.5% (for the 0.061mf at 45°C 1.3%) but as these are maximum deviations (i.e.  $\pm 0.25\%$  of the mean) the results cannot be said to be in agreement.

From these observations it is clear that the scatter in the results obtained from the Leiden cell are considerably greater than the error estimates made by Passchier. These larger figures are assumed to be the relevant ones for the assessment of these results.

**CHAPTER 5**  
**A STUDY OF THE FAR INFRARED SPECTRA OF ACETONITRILE ( $\text{CH}_3\text{CN}$ )**  
**IN SOLUTION WITH CARBON TETRACHLORIDE ( $\text{CCl}_4$ )**  
**[ BENZENE ( $\text{C}_6\text{H}_6$ ) AND n. HEPTANE ( $\text{C}_7\text{H}_{16}$ ) ]**

CHAPTER 5  
 A STUDY OF THE FAR INFRARED SPECTRA OF ACETONITRILE (CH<sub>3</sub>CN)  
 IN SOLUTION WITH CARBON TETRACHLORIDE (CCl<sub>4</sub>)  
 [BENZENE (C<sub>6</sub>H<sub>6</sub>) AND n. HEPTANE (C<sub>7</sub>H<sub>16</sub>)]

INTRODUCTION

This Chapter describes the results obtained from the study of the far-infrared spectra of solutions of acetonitrile (CH<sub>3</sub>CN) across a range of temperatures and concentrations. The feature of interest here is the 'Poley' absorption,<sup>61,63</sup> which for these solutions is found between 5cm<sup>-1</sup> and 100cm<sup>-1</sup>. (See Chapter 2.)

The absorption spectra were measured in this laboratory with the instrument described in Chapter 3, a modified Beckman-R11C FS720 interferometer. The higher frequency part of the features were observed using a Golay IR50 detector, whilst the low frequency (5cm<sup>-1</sup> – 60cm<sup>-1</sup>) were recorded separately using a helium cooled germanium bolometer. In all cases the instrument was also modified to operate in the polarising mode<sup>132,139</sup> for the low frequency studies in order to eliminate the intensity variations which occur with conventional beam splitters (which decrease the signal-to-noise ratio) and to obtain data to the low frequency possible with this method.

The solutions were contained in Beckman FH01 cells between high density polyethylene windows and teflon spacers. The temperature was maintained (monitored by a thermocouple inserted in the cell) by recirculating water from a thermostated bath through a jacket surrounding the cell and by heating coils. When operating in this configuration, the cell compartment was separated from the main instrument (evacuated) by an additional polyethylene window and flushed with dry nitrogen for the duration of the experiment. A detailed description of the instrument and its method of operation, data recording and data handling can be found in Chapter 3.

Four of the solutions described have also been studied at the National Physical Laboratory using the dispersive technique<sup>132</sup>. This method enables calculation of the refractive index spectra which have been combined with the absorption spectra for analysis. A description of the instrument used and its operation to obtain these spectra is given in Chapter 4.

The following chapter also includes the analysis of some far-infrared and microwave data obtained by Arnold<sup>126</sup> for a range of concentrations of acetonitrile in carbon tetrachloride, benzene and n. heptane. The far-infrared spectra were recorded in this laboratory with the instrument described previously with further modifications.<sup>136</sup> The microwave data were recorded at the University College of Wales, Edward Davies Chemical Laboratories, Aberystwyth. The frequency range 4-18GHz was measured using the swept frequency technique on an instrument manufactured by the Systron and Donner Company. Measurements were also taken at two higher 'spot' frequencies of 33.9775GHz and 69.66GHz. The combined span of these microwave measurements is approximately 0.13cm<sup>-1</sup> to 2.337cm<sup>-1</sup>. The Kramer relation<sup>166</sup>

$$E_o/E_i = K_{exp}(ad) = t \quad \dots\dots\dots 5.1$$

where E<sub>o</sub> and E<sub>i</sub> are the output and input wave amplitudes

d	=	sample depth
K	=	a reflection coefficient
$\alpha$	=	attenuation coefficient ( $\text{cm}^{-1}$ )

has been used to derive the absorption coefficient. This data has been extrapolated into the far infrared to join with the spectra recorded by the interferometry techniques. A full account of the experimental details of this work can be found in the thesis of Arnold.<sup>126</sup>

## A. EXPERIMENTAL PROCEDURES AND ERRORS

### (i) Solution Preparation

The solutions were prepared from spectroscopic grade reagents purchased from Kodak Eastman and the B.D.H. Chemical Companies. Before use the reagents were thoroughly dried, and subsequently stored, over molecular sieves. The water content of the samples is estimated to be less than 0.001%. Before a period of runs with the instrument a batch of the required solutions was prepared. These batches were used over a period of 5-7 days. The prepared samples were not stored over molecular sieves so as to preclude the possibility of concentration variations which might occur if the solute and solvent molecules bound unequally to the sieve. As these solutions were not stored for long periods, fresh samples had to be prepared when the instrument was converted from the polarising mode to the normal mode or vice versa. The variation which occurs between the concentrations of samples prepared separately is estimated to be less than  $\pm 1\%$ .

### (ii) Sample Cell Preparation

The cells used in this temperature and concentration study were Beckman FH01 type, compatible with the temperature control equipment described in section (iii). The cells were also drilled to receive a thermocouple so that the local temperature, in addition to the water bath and water jacket temperature, could be monitored. The cells required for the concentrations studied varied in path length from 3mm to 160 $\mu\text{m}$ . These were prepared with new polythene windows, sealing washers and teflon spacers. The spacers were measured by micrometer before assembly; the thickness, and therefore the nominal path lengths of the cells were known to within 0.25 $\mu\text{m}$ . As it was not possible to measure the path length of the assembled cells, great care was taken to ensure that the minimum distortion of the cell components occurred when the bolts were tightened. The same cells were then used for all runs of a particular concentration so that any path length errors would be constant. In some cases, particularly the highest and lowest temperatures (70°C and -21°C), it was necessary to tighten the cells to prevent leakage. It is anticipated that this may have caused some additional cell distortion and hence led to path length inconsistencies between runs recorded at different times. O'Neill<sup>167</sup> has recorded distortion of up to 0.052mm in the 3mm cell windows of a cell which has been dismantled after tightening down hard for a short time. If both of the cell windows suffered the same distortion on compression of the cell components, the total reduction in path length would be approximately 0.1mm. In the study of the more dilute solutions, which are recorded with long path lengths (3mm in the case of a 0.018mf solution) the error resulting from this problem would be 3%. (Note that this distortion only results in a reduction of path length.)

The solutions studies would have a maximum error where the path length was shortest i.e. with the most concentrated solutions. In the case of the 0.370mf solution, which was studied in a 160 $\mu$ m path length cell, the error would be -62%. Arnold<sup>126</sup> has carried out similar measurements on these cells and concludes that a window distortion of 5 $\mu$ m is a realistic figure for a cell which has not been tightened down abnormally hard.

Arnold has also checked for compression of the cell spacers (teflon) by clamping them between rigid silicon windows and scanning them through the mid-infrared region with a Perkin-Elmer 580B spectrometer. By measurement of the interference fringes arising from the internal reflections between the cell windows, it is possible to calculate the path length and it was found that no spacer compression was evident. Table 5.1 shows the range of concentrations studied and the cell path length indicating the percentage errors which may result from cell window distortion.

Concentration (Mole Fraction)	Path Length ( $\mu$ m)	Error Resulting From a Total Distortion of 100 $\mu$ m	Error Resulting From a Total Distortion of 10 $\mu$ m
0.018	3000	-3.3%	-0.33%
0.061	1000	-10%	-1.0%
0.162	330	-30%	-3.0%
0.370	160	-62%	-6.2%

TABLE 5.1  
SOLUTION CONCENTRATIONS, PATH LENGTHS AND PATH LENGTH ERRORS

The observed spectra (Section B) do not appear to show the deviations in intensity which would be expected if the path length errors were as large as 100 $\mu$ m, therefore I consider that the actual error lies somewhere between the upper and lower estimates. For the three longer path lengths an error of 10% is estimated, while for the 160 $\mu$ m cell a figure of 15% is more realistic. It should be noted that this error is the maximum difference which might be observed between two cells or runs i.e. it represents the upper and lower limits 0% - 10% or 0% - 15% and may be expressed in the more familiar form showing the deviation from the mean i.e.  $\pm 5\%$  and  $\pm 7.5\%$ .

The error which occurs as a result of the thermal expansion of the cell components over the temperature range 252K to 343K is 0.12%. This very small change in path length is not considered to be significant.

Before filling, the cells were flushed several times with the prepared solutions and finally stoppered and dried prior to mounting in the temperature control jacket. Flushing the cells in this way ensured that there were no air bubbles trapped inside, which would cause intensity errors, and that any traces of contaminating solvent or solution from a previous run were removed.

### (iii) Temperature Control

The filled cells were mounted in a Beckman VLT-2 variable temperature control jacket which was connected to a Eurotherm TEM1C controller unit. The higher temperatures, 318K and 343K(338K), were achieved by pumping water from a thermostated bath through the central core of the jacket. The water bath temperature was maintained  $\pm 0.5\text{K}$  by the combined heater and pump (TECAM TU-14). The cell temperature and jacket temperature were monitored by separate thermocouples embedded into the drilled metal bodies. The cell temperature was observed to approach jacket temperature and therefore equilibrium before the spectra were recorded. This generally took about 5 minutes. The lower temperature ranges 288K and 252K were achieved as follows. For 288K, the central body of the temperature jacket was filled with iced water. The cell jacket heaters were then used to maintain a constant temperature,  $\pm 1\text{K}$ . A similar method was employed to obtain a cell temperature of  $252\text{K} \pm 1\text{K}$  by filling the central reservoir with acetone and solid carbon dioxide. During the recording of the low temperature runs it was particularly important to ensure that the cell compartment was completely dry in order to prevent 'frosting' of the external cell windows. This was achieved by passing the already 'dry' laboratory nitrogen through a silica gel drying tube before flushing through the instrument cell compartment.

### (iv) Recording of Interferograms and Calculation of Spectra

Full details of the instruments and computation used to measure the absorbance spectra and refractive index spectra have been given in Chapters 3 and 4 respectively. In this section a short description is given of the experimental details which are pertinent in these particular experiments. Examples of the spectra are shown in Sections B and D of this Chapter.

#### Absorbance Spectra

The absorbance spectra were recorded in two parts, these being dictated by the frequency range of the FS720 interferometer in its two modes of operation. The low frequency data,  $5\text{cm}^{-1}$  to  $60\text{cm}^{-1}$ , was recorded with the instrument in the polarising mode with the helium cooled germanium bolometer detector. The interferograms in this case were recorded over a total mirror displacement of 1.6cm and sampled at path differences of  $16\mu\text{m}$ . Double sided interferograms were recorded so that phase errors arising from the instrument imperfections (alignment and collimation) and sampling effects could be corrected by the autocorrelation procedure described previously. The resolution of the low frequency range spectra, calculated from equation 3.4 was  $0.61\text{cm}^{-1}$  ( $1.22\text{cm}^{-1}$  after apodisation). The aliasing frequency given by equation 3.7 was  $310\text{cm}^{-1}$  and all frequencies above this were effectively eliminated by the rapid decrease in efficiency of the polarising wire grid beam splitter above  $100\text{cm}^{-1}$ . In addition, 3mm of black polythene was used to limit the range of detection to below  $70\text{cm}^{-1}$  and thus concentrate the full dynamic range of the instrumentation on the region of interest.

The higher frequency range part of the spectra,  $20\text{cm}^{-1}$  to  $250\text{cm}^{-1}$ , were recorded with the instrument configured in its 'normal' mode i.e. with conventional 'Mylar' beam splitter and IR50 Golay type detector. The beam splitter used was  $12\mu\text{m}$  thick (50 gauge) which due to internal

interference effects has a theoretical efficient frequency range of  $0 - 230\text{cm}^{-1}$  in the first transmission window. (For further explanations of beam splitter efficiency and 'hooping', see Chapter 3). The interferograms were recorded over a mirror displacement of  $0.8\text{cm}$ , which yields a spectral resolution of  $1.22\text{cm}^{-1}$  ( $2.44\text{cm}^{-1}$  after apodisation). The interferograms were sampled at  $8\mu\text{m}$  intervals (path difference) and a thin piece of black polythene was used to ensure that frequencies above the aliasing limit ( $625\text{cm}^{-1}$ ) did not impinge on the detector.

In both cases, background interferograms were recorded with the cells filled with pure solvent. Several runs of sample and background were recorded to ensure that the results were reproducible. The background transmission spectra were subtracted from the solution spectra before calculation of the absorbance spectra which are analysed in this thesis. Examples of the spectra showing the typical reproducibility are shown in Figures 5.1a and 5.1b.

It is apparent that a background subtraction performed in this way in fact amounts to an over-subtraction because the sample cell does not contain the same number of solvent molecules as a full background cell of the same path length (the same cell in this case). The error which arises from this technique will vary according to the solvent absorption intensity in the region studied. In the ideal case the solvent will not have any absorption features in this region i.e. the background will be flat and 100% transparent so there would be no shape change resulting from the subtraction. In the second case to be considered, assuming that there is some solvent absorption the error arising will vary according to the concentration of the system studied, because the over-subtraction will become more pronounced at high concentrations when the number of solvent molecules is least. The magnitude of this error at the band peak for each of the concentrations studied is shown in Table 5.2.

Concentration (Mole Fraction)	Solvent Subtraction Factor *	Error in $a_{\text{max}}$ † %
0.018	1.018	-0.4
0.061	1.065	-0.4
0.162	1.193	-0.5
0.370	1.587	-0.6

\* Given by  $N_s/N's$  where  $N_s$  = number of solvent molecules in background cell  
and  $N's$  = actual number of solvent molecules in the solution.

† Calculated from equation 5.2.

**TABLE 5.2**  
**ERRORS RESULTING FROM THE SUBTRACTION OF A SOLVENT**  
**BACKGROUND**

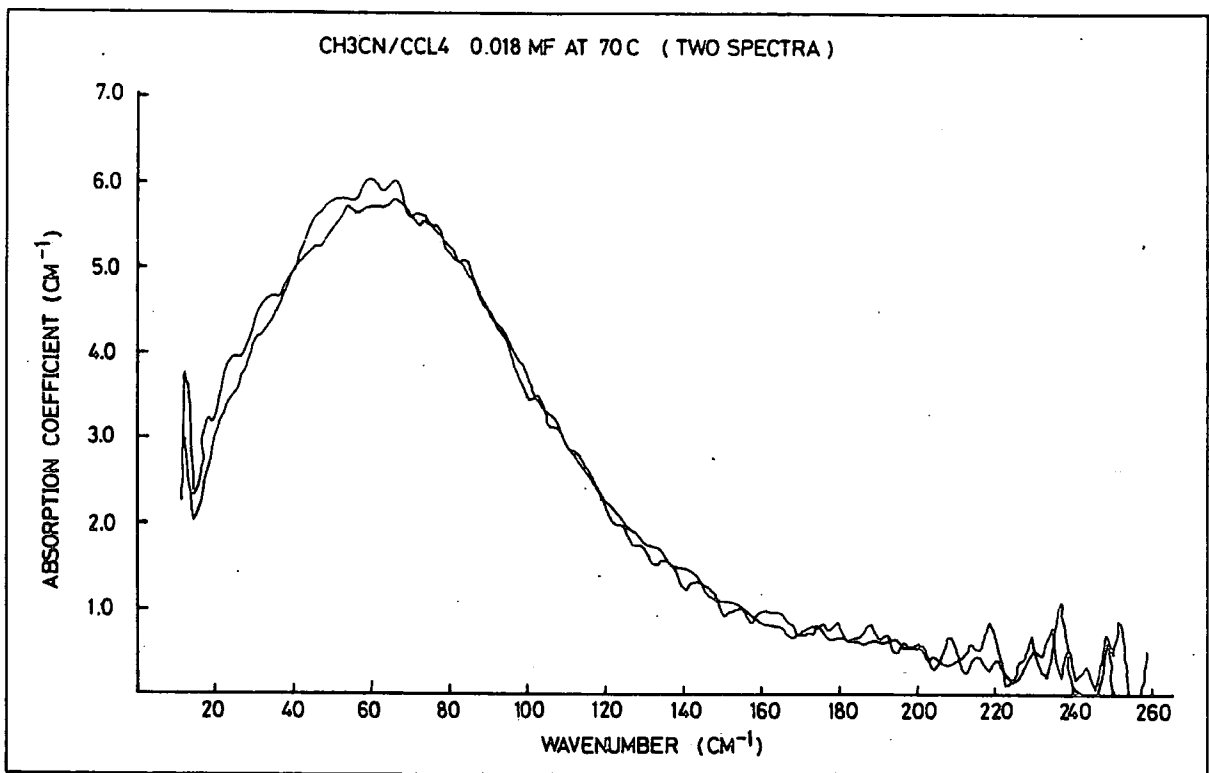


FIGURE 5.1a

REPRODUCIBILITY OF ABSORPTION SPECTRA (HIGH FREQUENCY)

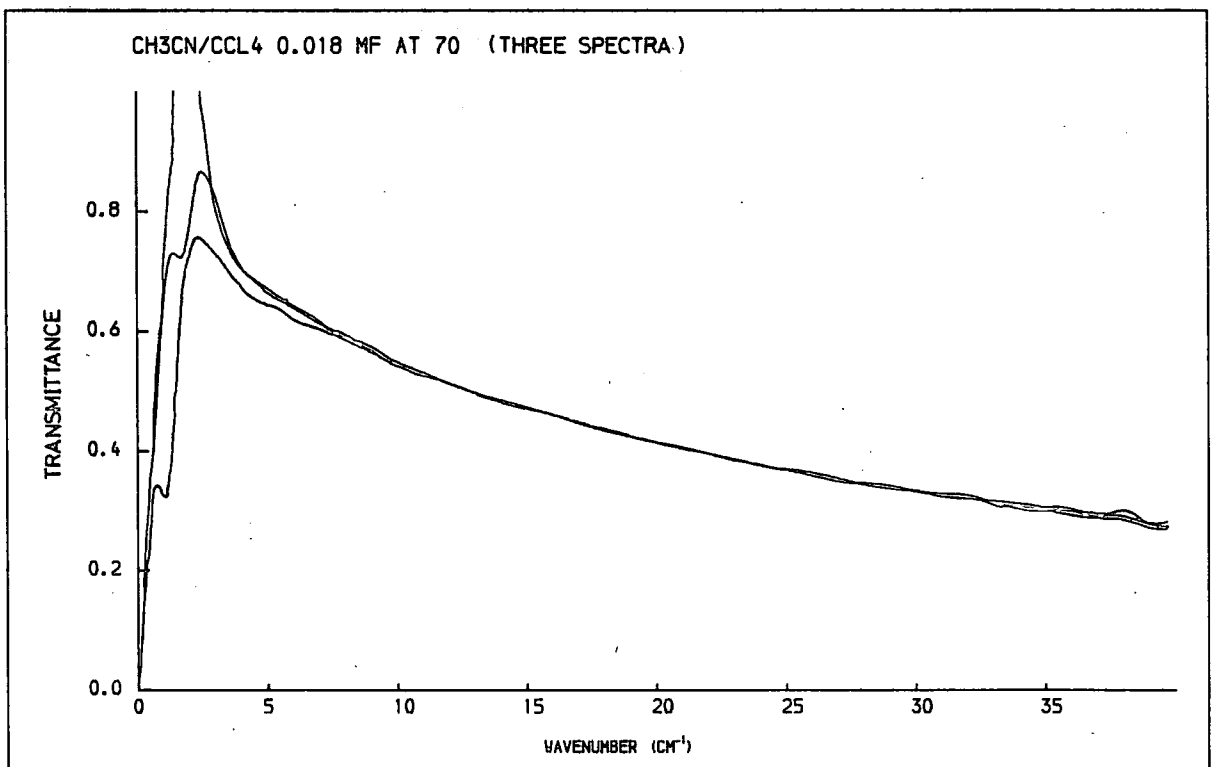


FIGURE 5.1b

REPRODUCIBILITY OF ABSORPTION SPECTRA (LOW FREQUENCY)

The error in  $a_{\max}$  (Table 5.2) is given by

$$\text{Error} = \left[ (N_s/N'_s) a_s(\bar{\nu}) - a_s(\bar{\nu}) \right] / a_{\text{obs}}(\bar{\nu}) \quad \dots\dots\dots 5.2$$

where  $a_s(\bar{\nu}) =$  average solvent absorption<sup>167</sup> (Figure 5.2a)

$a_{\text{obs}}(\bar{\nu}) =$  average observed absorption after subtraction (Table 5.5)

It is clearly seen from Table 5.2 that as the solvent over-subtraction factor increases in magnitude this is off-set almost completely by the overall increase in absorption of the system, so that the errors remain approximately constant for this range of concentration. The actual percentage error which results, approximately 0.5%, is well within the other experimental uncertainties such as those arising from the measurement of the peak height and total intensities described in Part B of this Chapter. However, the error resulting from this problem is systematic and will always result in an observed spectral intensity being lower than the 'true' value.

In addition to the intensity errors, which occur due to the subtraction of a solvent background by this procedure, there will also be a change of band shape unless the solvent spectrum is exactly the same shape and centred at the same frequency as the solute system spectrum recovered. This change of shape is a direct result of the intensity error described previously, which varies according to the relative spectral intensities of the solvent and sample at different frequencies. The selection of a solvent, such as carbon tetrachloride which has relatively small absorption features in the region of observation, has contained these errors to low magnitude: approximately 2.4% for the worst case in the region of the 'Poley' absorption at  $120\text{cm}^{-1}$  where the relative intensity of the solvent is greatest.

The calculated errors for a 0.018mf solution at 318K are given in Table 5.3 and expressed graphically in Figure 5.2b. This plotted error can be thought of as the bandshape distortion curve. Above  $120\text{cm}^{-1}$  the error continues to rise as the solution absorption decreases and the solvent absorption begins to increase again. However, in this region other workers<sup>168</sup> have not found such a high absorption level, and the plateau observed extends to  $170\text{cm}^{-1}$  where the solution band approaches zero intensity, therefore the error calculated in this region may itself be erroneous.

The intensity of radiation reaching the detector is also reduced by reflections which occur at the boundaries between regions of varying refractive index. These are present at the external and internal surfaces of the cell windows, but as the external reflections are constant for sample and background interferograms we need only to consider the effect of the reflections from the internal cell surfaces. The ratio of the reflected radiation intensity ( $I_R$ ) to the incident radiation intensity ( $I_0$ ) is given by Fresnel<sup>169</sup>

$$I_R / I_0 = \left[ (n_2 - n_1) / (n_2 + n_1) \right]^2 \quad \dots\dots\dots 5.3$$

where  $n_2 =$  refractive index of medium met by the incident ray.

$n_1 =$  refractive index of propagating medium.

CARBON TETRACHLORIDE AT 47°C

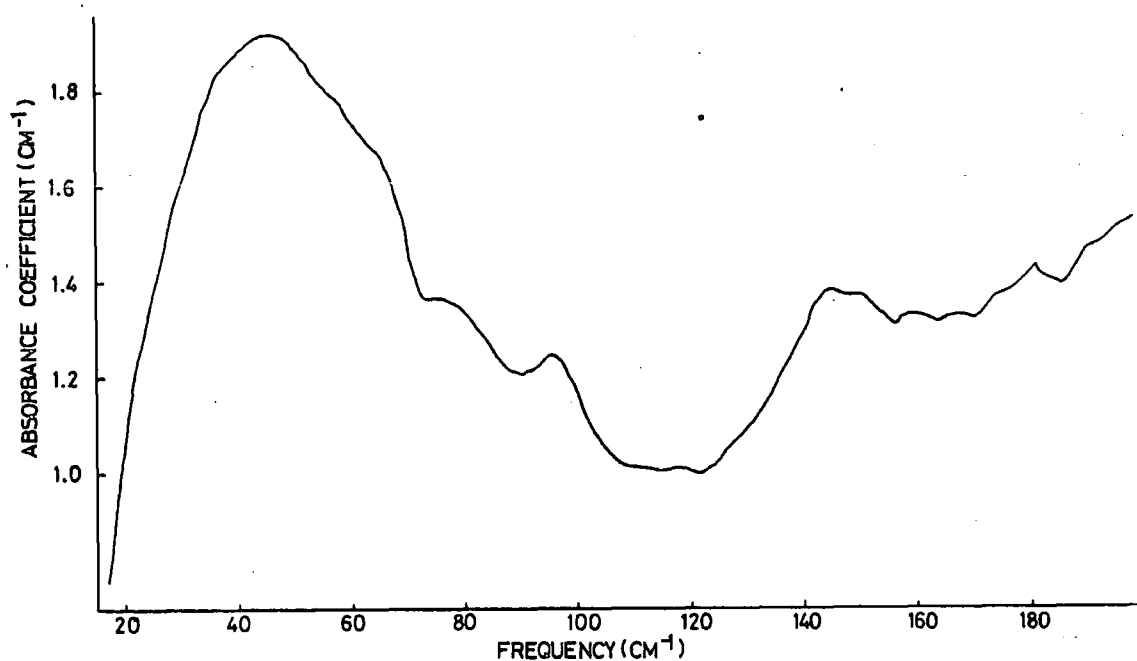


FIGURE 5.2a

ABSORPTION SPECTRA OF CARBON TETRACHLORIDE

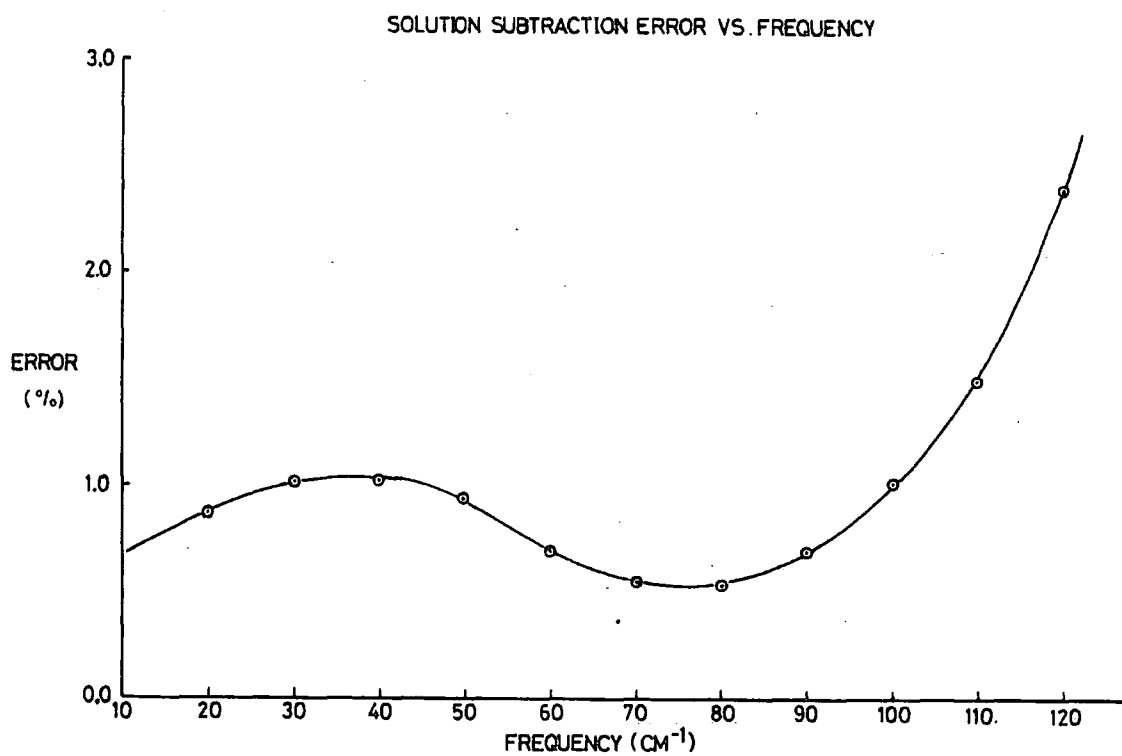


FIGURE 5.2b

Frequency ( $\text{cm}^{-1}$ )	Solvent Absorption ( $\text{neper cm}^{-1}$ )	Solution Absorption ( $\text{neper cm}^{-1}$ )	Oversubtraction ( $\text{neper cm}^{-1}$ )	Error With Respect To Solution Absorption
20	1.05	2.22	0.019	$8.7 \times 10^{-3}$
30	1.55	2.55	0.028	$1.1 \times 10^{-2}$
40	1.9	3.02	0.035	$1.2 \times 10^{-2}$
50	1.9	3.70	0.035	$9.4 \times 10^{-3}$
60	1.7	4.50	0.031	$6.9 \times 10^{-3}$
70	1.5	5.02	0.028	$5.5 \times 10^{-3}$
80	1.3	4.46	0.024	$5.3 \times 10^{-3}$
90	1.2	3.19	0.022	$6.9 \times 10^{-3}$
100	1.15	2.05	0.021	$1.02 \times 10^{-2}$
110	1.05	1.30	0.019	$1.5 \times 10^{-2}$
120	1.05	0.80	0.019	$2.4 \times 10^{-2}$
130	1.1	0.54	0.020	$3.7 \times 10^{-2}$
140	1.3	0.37	0.024	$6.4 \times 10^{-2}$
150	1.35	0.27	0.025	$9.17 \times 10^{-2}$
160	1.3	0.20	0.024	$11.9 \times 10^{-2}$

Note:  $N/N_s$  1.0184

**TABLE 5.3**  
**THE ERRORS CALCULATED FOR THE SUBTRACTION OF THE SOLVENT SPECTRUM**  
**SHOWN IN FIGURE 5.2a FROM A SOLUTION SPECTRUM OF 0.018mf  $\text{CH}_3\text{CN}/\text{CCl}_4$**   
**RECORDED AT 318K**

In the region from  $20\text{cm}^{-1}$  upwards, this does not cause very large errors because the refractive index of the solutions becomes very similar to that of the window. For example, where the solution refractive index is 1.5 and the window refractive index is 1.4 the ratio given by equation 5.3 is  $10^{-3}$  (i.e. 0.1% of the radiation incident on the cell window liquid face is reflected back). However, in the lower frequency region  $5 - 25\text{cm}^{-1}$  the refractive index of the solutions studied rises dramatically and therefore the reflection losses become more significant. The losses due to this phenomenon will also become more apparent in the spectra of the pure  $\text{CH}_3\text{CN}$  which is also analysed in this Chapter. For example, where the liquid has a refractive index of 2.0 the factor  $I_R/I_0$  increases to  $3 \times 10^{-2}$  i.e. 3% of the radiation is reflected at the liquid surface.

In the case of samples which are studied with path lengths of the order of millimetres it is possible to eliminate the reflection errors by subtracting a background of the same solution measured at a different path length. However this yields a spectrum of the solute + solvent rather than the

spectrum of the solute in solution which is required. To achieve this, a separate calculation of a solvent spectrum from a similar 'two path length' experiment, is necessary. It is then possible to subtract the solvent spectrum, suitably scaled for path length (to avoid the over-subtraction problem discussed previously), from the solute + solvent spectrum to obtain the desired result.

Obviously this method is more rigorous than the one adopted, but it must be appreciated that there may be additional path length errors introduced which will in part negate the advantages to be gained. Furthermore, the errors remaining in the system, such as path length errors, are dominant. Also, the method has the disadvantage of time, in that twice the number of interferograms have to be recorded and the computation task is more than doubled.

Finally, it should be noted that the spectral features observed in this region may well be due, in part, to solute induced solvent effects such as dipole-induced dipole absorptions. If this is the case then even the most rigorous solvent subtraction method, such as that described, will be inadequate due to the different environments of the solvent molecules in solution and in pure liquid.

#### **Refractive Index Spectra**

These experiments were carried out at the National Physical Laboratory using the Dispersive Fourier Transform Spectroscopy (DFTS) technique described in Chapter 4. The cell used for these measurements, developed at the Leiden University, Netherlands, was maintained at the constant temperatures required by a recirculating water supply from a thermostated bath.

The observed solute + solvent spectra exhibit a scatter of  $\pm 0.25\%$  which dominates the theoretical errors.<sup>154</sup>

#### **(v) The Determination of the Static and Infinite Frequency Permittivity, $\epsilon_0$ and $\epsilon_\infty$ , of the Solutions Studied**

The static permittivity ( $\epsilon_0$ ) values of the solutions studied in this work were measured in this laboratory with a WTW Dipolemeter Type DM01, manufactured by Weilheim of Germany. This instrument operates by the superposition principle by which the oscillations of two high frequency (2.0MHz) oscillators are mixed so that beating can occur which is measured on an oscilloscope. The sample is placed in a cell which combined with a tuning condenser contributes to the capacitance of one of the oscillator circuits and therefore controls the frequency of its output. The variation in the tuning condenser required to return to the 'zero beat' condition provides a measure of the capacitance of the sample which is directly related to the permittivity. Calibration of the instrument with samples of known permittivity then facilitated the calculation of the solution permittivities.

The instrument is fully temperature stabilised and capable of measurement to 5 decimal places on all ranges (manufacturers' specification). The measurements taken were recorded after temperature stabilisation for one hour and calibration checks were made before and after the experiment. No variation in the values of  $\epsilon_0$  for the calibrating samples (cyclohexane and Toluene) were recorded.

The range of the instrument was not sufficient to cover the high concentration solutions studied, and therefore extra points were recorded within the range for extrapolation purposes in order to carry out the initial data analysis since the value of  $\epsilon_0$  is expected to have a linear relationship with concentration for low concentrations. The data recorded elsewhere<sup>126</sup> at 25°C shows this approximation to be true. However, in the final analysis this uncertainty was avoided by utilising the results obtained by direct measurement on a Wayne Kerr bridge instrument at The University College of Wales, Aberystwyth. The values used for the lower temperature solutions (288K and 252K) were also taken from this data.

The refractive index measurements carried out at The National Physical Laboratory and described in Chapter 4 enabled the calculation of the permittivity at infinite frequency by the familiar Maxwell relation (see Chapter 2).

$$\eta_{\infty}^2 = \epsilon_{\infty}$$

(Note: A similar relation can be used to obtain  $\epsilon_0$  if  $\eta(\nu)$  is known for very low frequency).

The  $\epsilon_{\infty}$  values for the solutions 0.018mf, 0.061mf at 252K and 343/338K were approximated to the values calculated for 288K and 318K respectively. The  $\epsilon_{\infty}$  values for the two higher concentration solutions 0.162mf and 0.370mf at 318K were calculated from the  $\eta_{\infty}$  values obtained from the Kramers Kronig analysis carried out by Arnold<sup>126</sup> for solutions at 298K. The results obtained and used in the analysis are summarised in Table 5.4.

Solution	Concentration (mole fraction)	$\epsilon_0 (\pm 0.1)$				$\epsilon_{\infty} (\pm 0.1)$			
		252K	288K	318K	343/388K	252K	288K	318K	343/388K
Cyclohexane	1.0	-	-	1.98	-	-	-	-	-
Toluene	1.0	-	-	2.33	-	-	-	-	-
Carbon Tetrachloride	1.0	-	-	2.19 <sup>a</sup>	-	-	-	-	-
CH <sub>3</sub> CN / CCl <sub>4</sub>	0.018	2.38	2.38	2.38	2.38	2.22	2.17	2.22	2.17
CH <sub>3</sub> CN / CCl <sub>4</sub>	0.036	-	-	2.55	-	-	-	-	-
CH <sub>3</sub> CN / CCl <sub>4</sub>	0.061	3.05	3.05	2.79	2.79	2.28	2.19	2.28	2.19
CH <sub>3</sub> CN / CCl <sub>4</sub>	0.071	-	-	2.89	-	-	-	-	-
CH <sub>3</sub> CN / CCl <sub>4</sub>	0.162	-	-	4.67	-	-	2.52	-	-
CH <sub>3</sub> CN / CCl <sub>4</sub>	0.370	-	-	8.80	-	-	2.30	-	-

a. In agreement with Hills,<sup>58</sup> result  $\epsilon_0 = 2.234$  at 20°C.

(Note:  $\epsilon_0$  decreases as increasing thermal motion reduces polarisation of dielectric.)

TABLE 5.4

PERMITTIVITY VALUES OF VARIOUS SOLVENTS AND SOLUTIONS OF ACETONITRILE

## B. TREATMENT OF RAW DATA AND INITIAL ANALYSIS OF SPECTRA

### (i) Averaging of Spectra

The model which is analysed with the spectra recorded in this work is essentially a Debye type with modifications, described in Chapter 2, to extend its applicability to include the 'Poley' feature observed in the  $5\text{cm}^{-1}$  to  $100\text{cm}^{-1}$  frequency region. The method of obtaining the model parameters, related to the intermolecular torques, which have been included in this extended model, is mainly by a routine of fitting the equations derived in Chapter 2 (part C (v)) to the observed spectra. The model is intrinsically a low frequency, microwave model and is therefore expected to be particularly sensitive to the lower frequency region of the spectrum when fitted in this way. The spectra recorded in this region are highly reproducible and show very little noise from  $7\text{cm}^{-1}$  to  $40\text{cm}^{-1}$ , but exhibit considerably more deviation (noise) below  $7\text{cm}^{-1}$ . Therefore, in order to obtain smoother spectra in this range, the data sets used in the analysis were averaged from two or three runs recorded consecutively. A typical set of three low frequency spectra and the average set derived from them is shown in Figure 5.3. For the higher frequency region the raw spectra were analysed except where indicated in the next section.

### (ii) Matching of Data Sets and Editing Procedures

Attempts to match the high frequency and low frequency data sets have revealed a considerable absorption level 'step' between these regions in several of the spectra. The discrepancy between the absorption coefficients in the region of  $40\text{cm}^{-1}$  where the matching was carried out was in the worst case 15%. The errors described in Section A of this Chapter can account for this difference (when applied to both spectra) i.e. it is within the estimated random error - however, it appears to be mainly a systematic error arising from path length uncertainties. This is likely because the high and low frequency spectra were often recorded with a considerable time lapse in between. During this period cells were used for different temperature runs, which may have necessitated them being tightened to prevent leaking (see Section A) and thus the path length may have changed due to window distortion. In addition, there is the possibility (although this is merely conjecture) that a cell left assembled for a long period may be subject to a path length change due to the gradual deformation of the polyethylene cell windows which would be under compression. In some cases record book notes have enabled the error to be corrected with reasonable certainty. In the cases where this was not possible, an editing procedure has been carried out as shown in Figure 5.4a.

Also shown in Figure 5.4b is the editing of a spurious feature which was recorded in the spectrum of the 0.018 mole fraction solution at  $70^\circ\text{C}$ . Figure 5.5 shows evidence at  $70\text{cm}^{-1}$  of a polyethylene absorption band which has not been fully subtracted with the background. Where this is apparent, the smoothed curve has been taken for the purposes of peak height  $a_{\text{max}}$ , peak position  $\bar{\nu}_{\text{max}}$  measurement, and total intensity calculations.

### (iii) Initial Analysis of Spectra

Table 5.5 summarises the parameters measured from the absorption spectra of each of the solutions studied. The integrated intensity values were calculated from the smoothed curves as

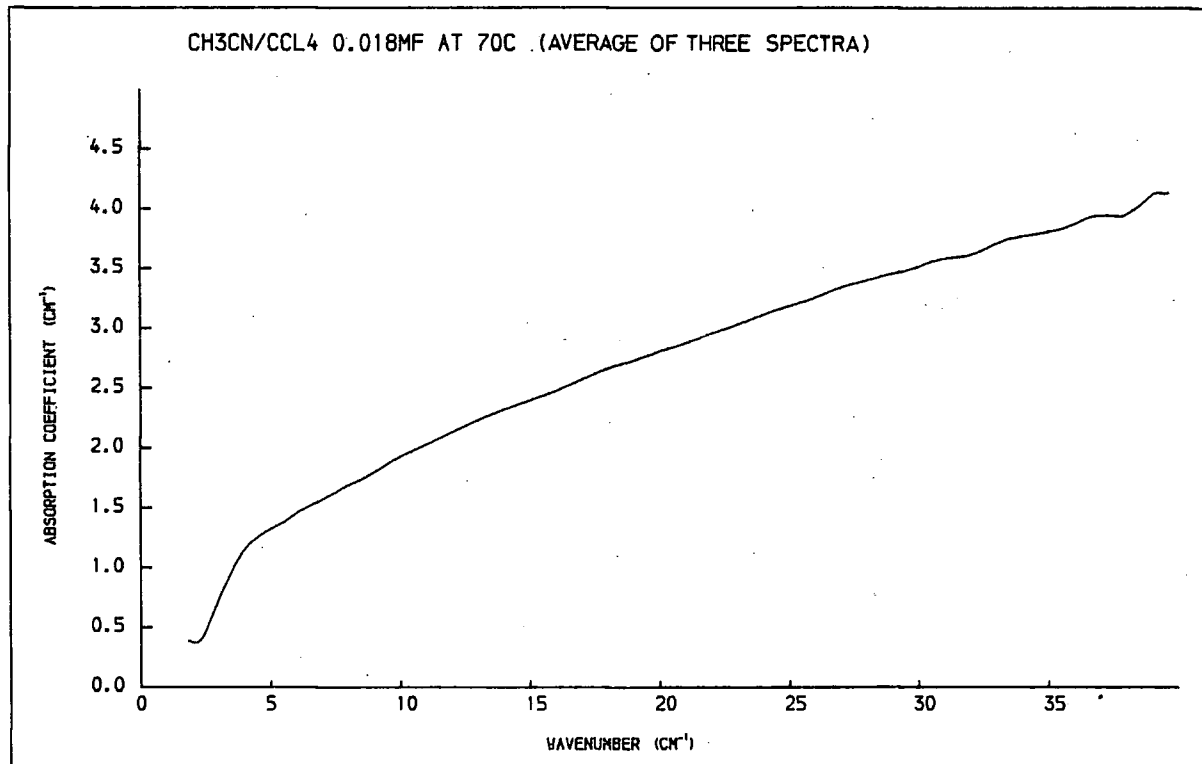
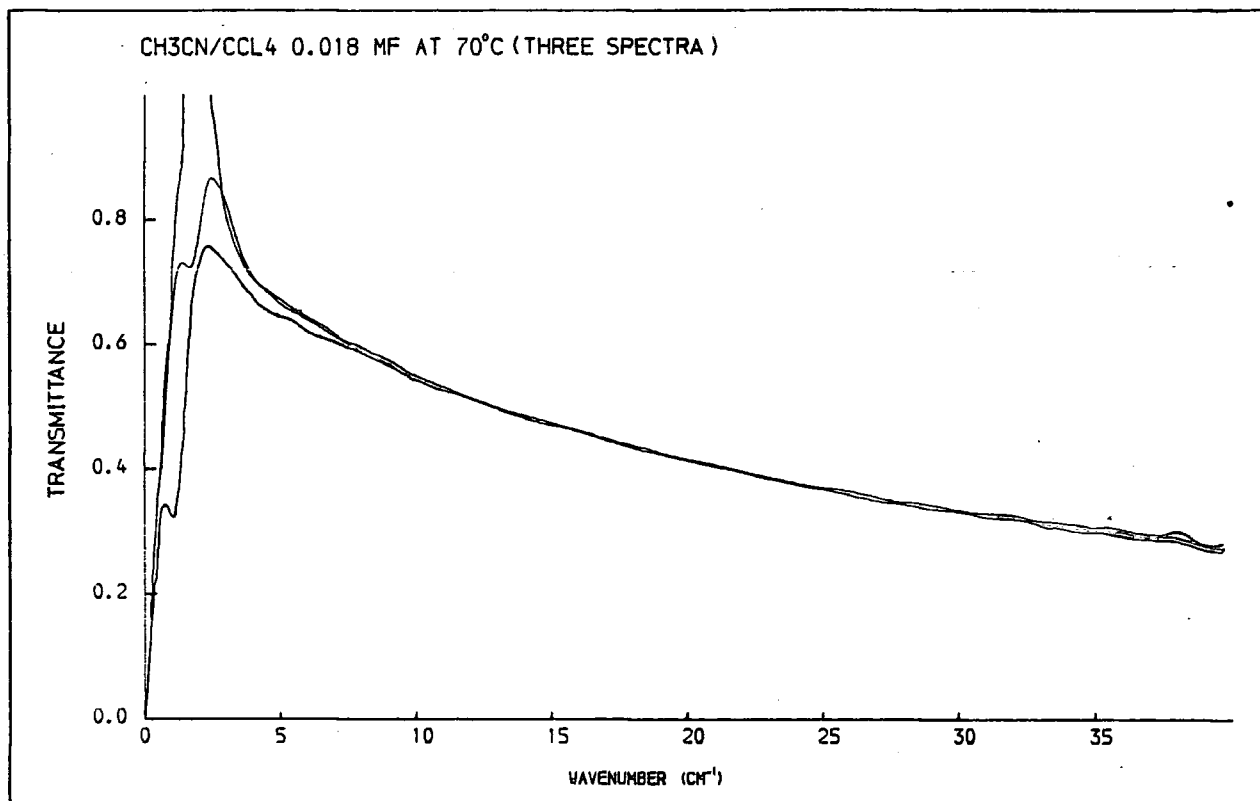


**FIGURE 5.3**  
**TYPICAL AVERAGING OF LOW FREQUENCY DATA SETS**

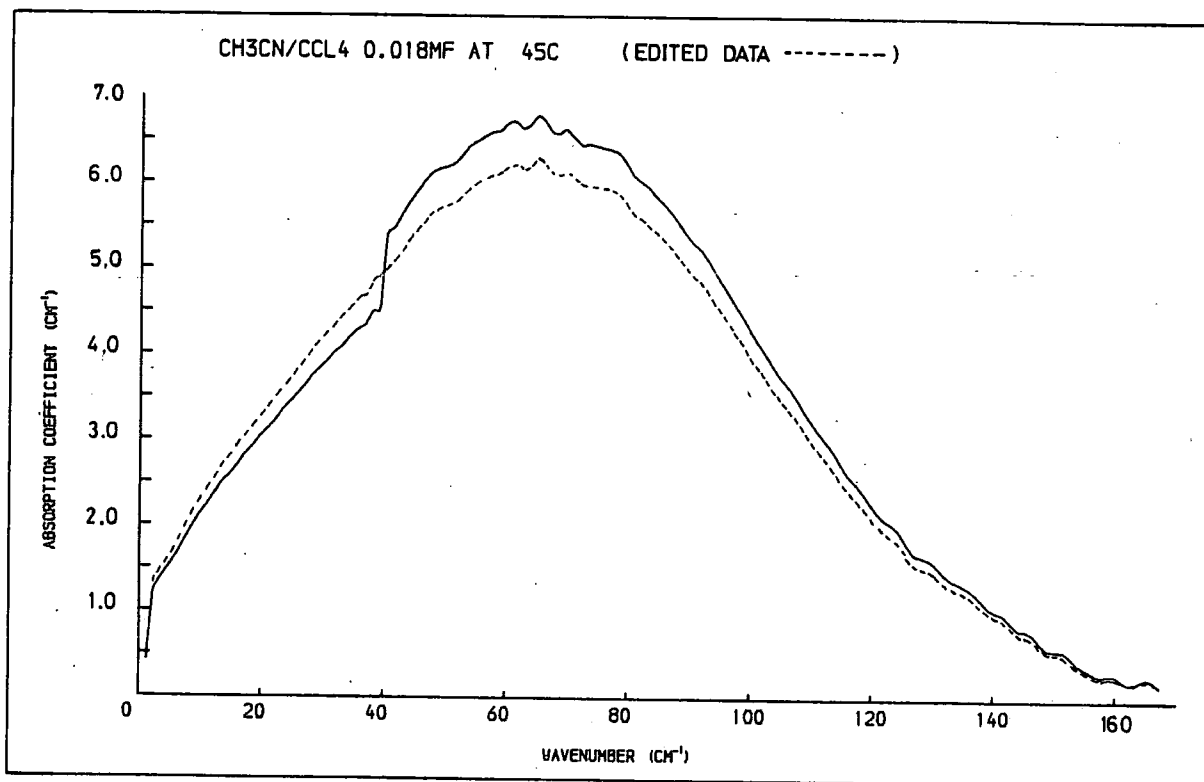


FIGURE 5.4a  
AN EDITED ABSORPTION SPECTRUM

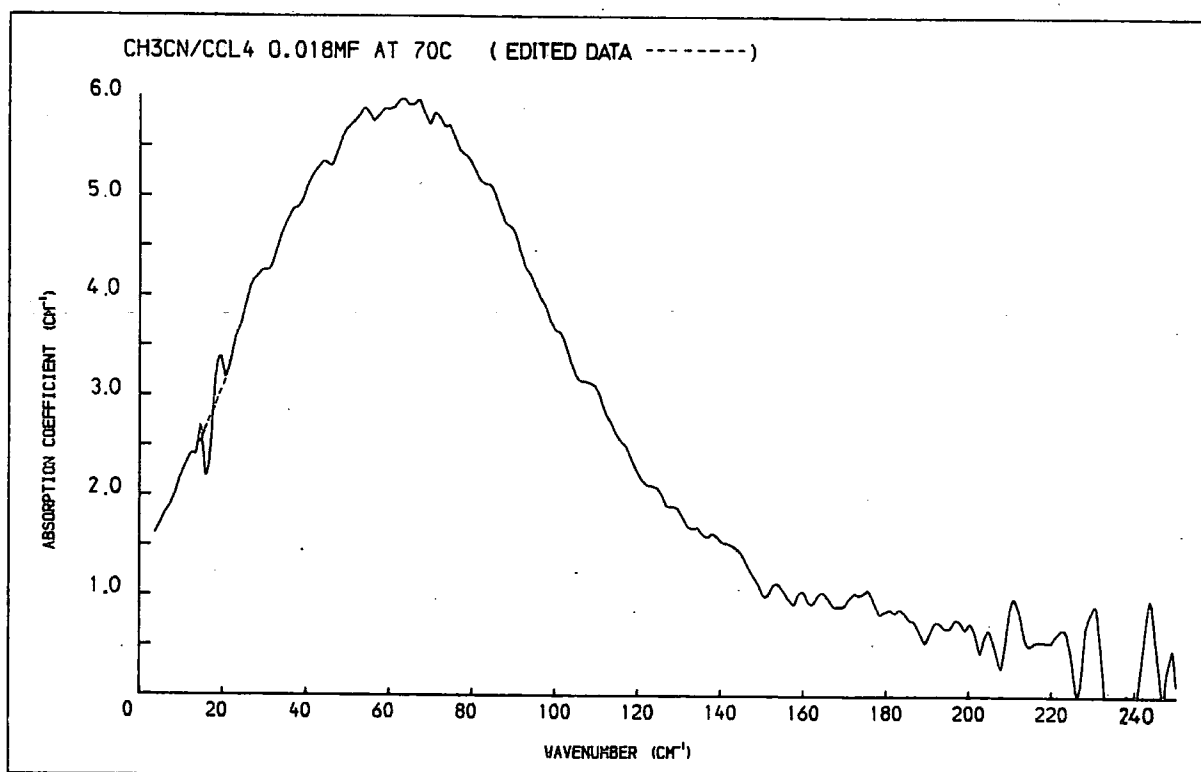


FIGURE 5.4b  
AN EDITED ABSORPTION SPECTRUM

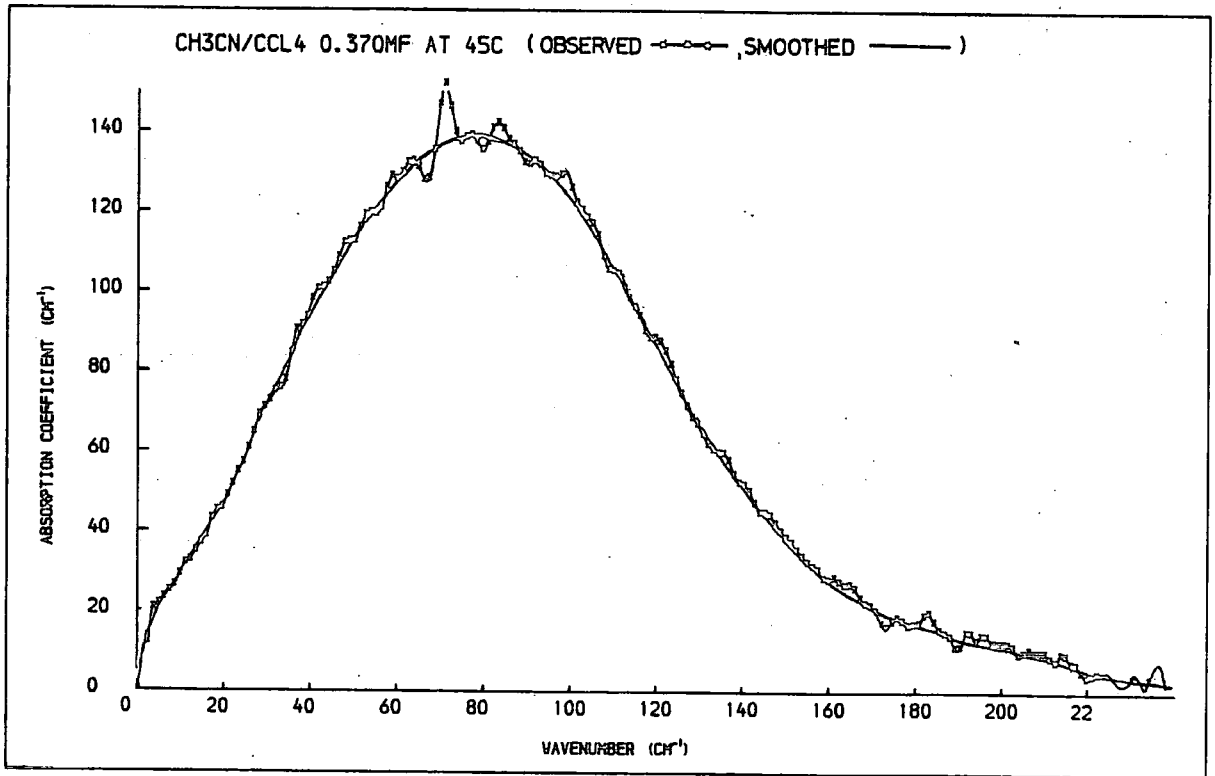
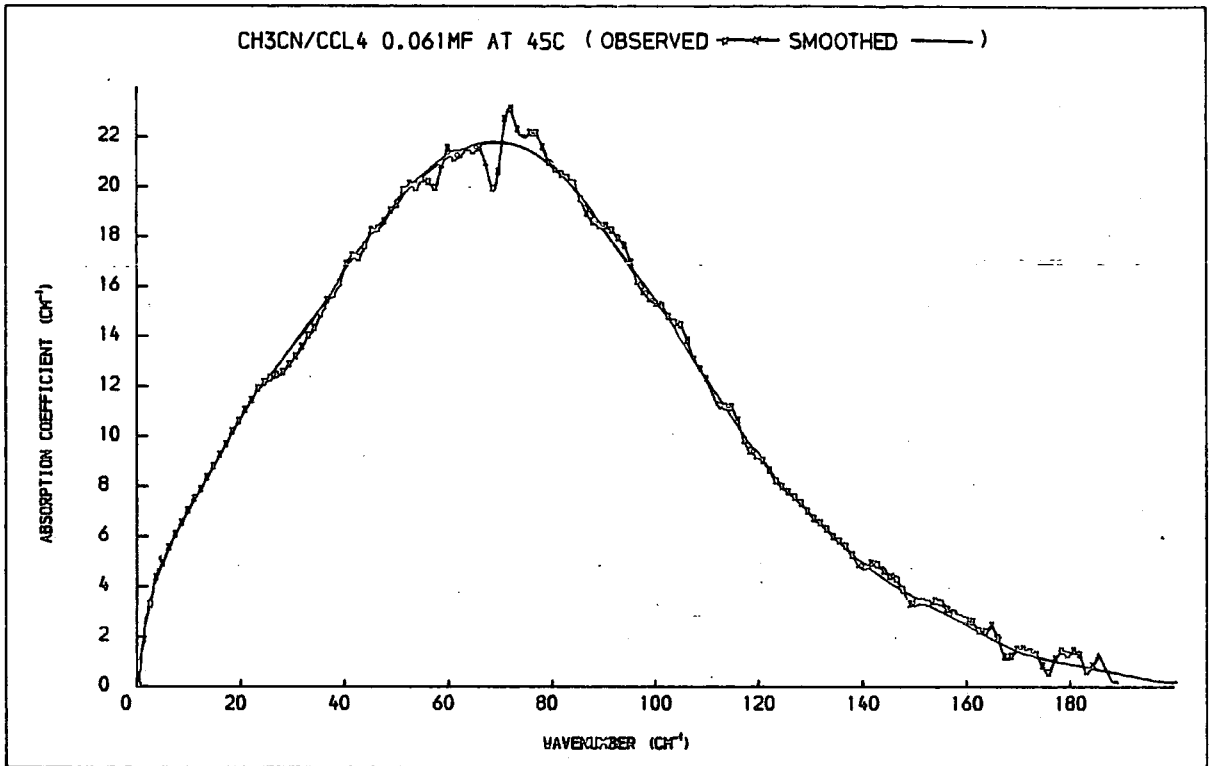


FIGURE 5.5  
TYPICAL ABSORPTION SPECTRA EDITING

Temperature (K)	Concentration (Mole Fraction) ±1%	$\bar{\nu}_{\max}$ ( $\text{cm}^{-1}$ ) ±2 $\text{cm}^{-1}$	$a_{\max}$ (neper $\text{cm}^{-1}$ ) <sup>d</sup> ±2%	$\Delta\bar{\nu}_{1/2}$ ( $\text{cm}^{-1}$ ) ±2 $\text{cm}^{-1}$	Integrated Intensity (neper $\text{cm}^2$ ) ±5%	Integrated Intensity per Molecule (neper $\text{cm mol}^{-1}$ ) ±5%
252±1	0.018	77	6.9 (36.3)	87	640	3369
252	0.061	82	23.5 (35.8)	89	2192	3337
288	0.018	72	6.7 (35.3)	88	602	3168
288	0.061	76	22.2 (33.8)	92	2159	3286
318±0.5	0.018	64	6.2 (32.6)	91 96 <sup>a</sup>	568 613 <sup>a</sup>	2991 3230 <sup>a</sup>
318	0.061	70	21.2 (32.3)	93	2077	3162
318	0.162	77	57.0 (30.8)	94	5686	3074
318	0.370	80	138.0 (29.7)	99	14862	3196
343	0.018	62	6.0 (31.5)	91 93 <sup>c</sup>	617 555 <sup>b</sup> 600 <sup>c</sup>	3248 2919 <sup>b</sup> 3158 <sup>c</sup>
338	0.061	66	19.9 (30.4)	94	2012	3063

- a. Parameters recorded for a spectrum with wider half width ( $\Delta\bar{\nu}_{1/2}$ ) i.e. outside of estimated errors.
- b. Spectral intensity did not reach zero values obtained with artificial base line.
- c. Parameters measured for a spectrum with slightly wider  $\Delta\bar{\nu}_{1/2}$  not requiring baseline correction.
- d. Values in parentheses are neper  $\text{cm}^{-1}$  mole<sup>-1</sup>.

**TABLE 5.5**  
**A SUMMARY OF THE OBSERVED SPECTRAL FEATURES OF**  
**THE ACETONITRILE SOLUTIONS STUDIED**

described above, using an Apple II microcomputer with an electrostatic graphics tablet. The intensities are recorded in both absorption and absorption per molecule i.e. absorption divided by concentration. The band heights ( $\alpha_{\max}$ ) are also given in absorption ( $\text{neper cm}^{-1}$ ) and in absorption per molecule (figures in parentheses) measured from the base ( $\alpha = 0$ ). The half width values,  $\Delta\bar{\nu}_{1/2}$ , quoted are the width of the absorption features at half their height.

The results obtained by Arnold<sup>126</sup> in this laboratory are also analysed here and discussed in Chapter 6. The parameters measured from these spectra recorded at 298K are shown in Table 5.6. In this case the intensities were calculated by computer and include the noise in the spectra. This may account for the difference observed between the average intensities per molecule of the two sets of data. The average intensity per molecule values differ by approximately 12% from the values recorded by Arnold for the same concentration range which are higher at 3660  $\text{neper cm mole}^{-1}$ . A recalculation of some of the intensities using the graphics tablet method and tracing a smoothed curve accounted for 2% of the observed difference. Arnold has estimated errors of  $\pm 10\%$  on the values recorded, which means they fall well within the values ( $\pm 5\%$  error) recorded in this work.

The direct comparison of the  $\alpha_{\max}$  values cannot be made with any certainty, as the spectral bandshapes are expected to vary with temperature (although the total integrated intensities may remain constant), becoming lower and broader as the temperature is increased. However the values recorded at 298K would reasonably be expected to lie between the average values obtained at 288K and 318K in this work, whereas in fact they are larger than either of these figures (7% greater than the mean). Again this discrepancy falls well within the random errors estimated for the two data sets. However, the systematic nature of the deviation is probably accounted for by the differences between the lines assumed when approximating the peak height and shape when there is noise on the spectra (such as that arising from the  $70\text{cm}^{-1}$  polyethylene band described previously).

For similar reasons, a direct comparison between the  $\bar{\nu}_{\max}$  values cannot be made, except for a reasonable approximation in the case of the 0.06 mole fraction solution. The  $\bar{\nu}_{\max}$  value for this concentration at 298K recorded by Arnold is  $73.5 \pm 3\text{cm}^{-1}$ , which falls between the values recorded in this work for the 0.061 mole fraction solutions at 288K,  $76 \pm 2\text{cm}^{-1}$  and 318K,  $70 \pm 2\text{cm}^{-1}$ .

From these comparisons, it is concluded that the independently recorded data sets are in good agreement, within the experimental errors.

In the  $5-50\text{cm}^{-1}$  the refractive indices of the solutions studied decrease asymptotically (Figures 4.14 and 4.15). In addition the spectra of the  $20-180\text{cm}^{-1}$  region (Figure 4.11) exhibits a shallow dip at  $70\text{cm}^{-1}$  which may be associated with a resonance process<sup>54, 124</sup> in the absorption as described in Chapter 2.

#### (iv) The Variation in the Observed Spectral Features with Temperature

The  $\bar{\nu}_{\max}$  values from Table 5.5 are plotted against temperature in Figure 5.6a. This plot clearly shows the trend of decreasing frequency of the peak in the Poley feature as the temperature

Concentration		$\bar{\nu}_{\max}$ ( $\text{cm}^{-1}$ )	$a_{\max}$ (neper $\text{cm}^{-1} \text{mol}^{-1}$ )	$\Delta\bar{\nu}_{1/2}$ ( $\text{cm}^{-1}$ )	Integrated intensity <sup>a</sup> (neper $\text{cm}^{-1} \text{mol}^{-1}$ )
(mole fraction)	( $\text{mole dm}^{-3}$ )				
<b>CH<sub>3</sub>CN/CCl<sub>4</sub></b>					
0.01	0.099	71.8 ±3.0	37.1 ±10%	87.72 ±10%	3413.77 ±10%
0.016	0.170	72.4	37.5	95.39	3962.48
0.06	0.652	73.5	36.6	93.20	3662.26
0.10	1.085	74.6	36.5	91.01	3413.92
0.16	1.825	80.0	36.0	93.2	3558.5
0.20	2.294	80.0	36.6	93.20	3610.17
0.30	3.608	82.2	35.7	93.20	3723.5
0.40	5.072	85.5	36.8	96.49	3939.6
0.50	6.718	86.6	36.4 ±20%	99.78 ±20%	3929.6 ±20%
0.70	10.682	88.8	37.3	107.46	4363.37
1.00	19.137	93.3	35.1	100.88	3712.7
<b>CH<sub>3</sub>CN/Benzene</b>					
0.016	0.182	72.4 ±3.0	35.7 ±10%	95.4 ±10%	3727.9 ±10%
0.06	0.704	74.6	35.0	100.88	3725.8
0.16	1.955	80.0	35.1	97.58	3597.6
<b>CH<sub>3</sub>CN/n-Heptane</b>					
0.027	0.189	44.76 ±3.0	33.0 ±10%	81.88 ±10%	2691.48 ±10%

a Measured from 0 - 250 $\text{cm}^{-1}$

TABLE 5.6  
A SUMMARY OF THE OBSERVED SPECTRAL FEATURES OF A RANGE OF  
SOLUTION OF ACETONITRILE AT 298K

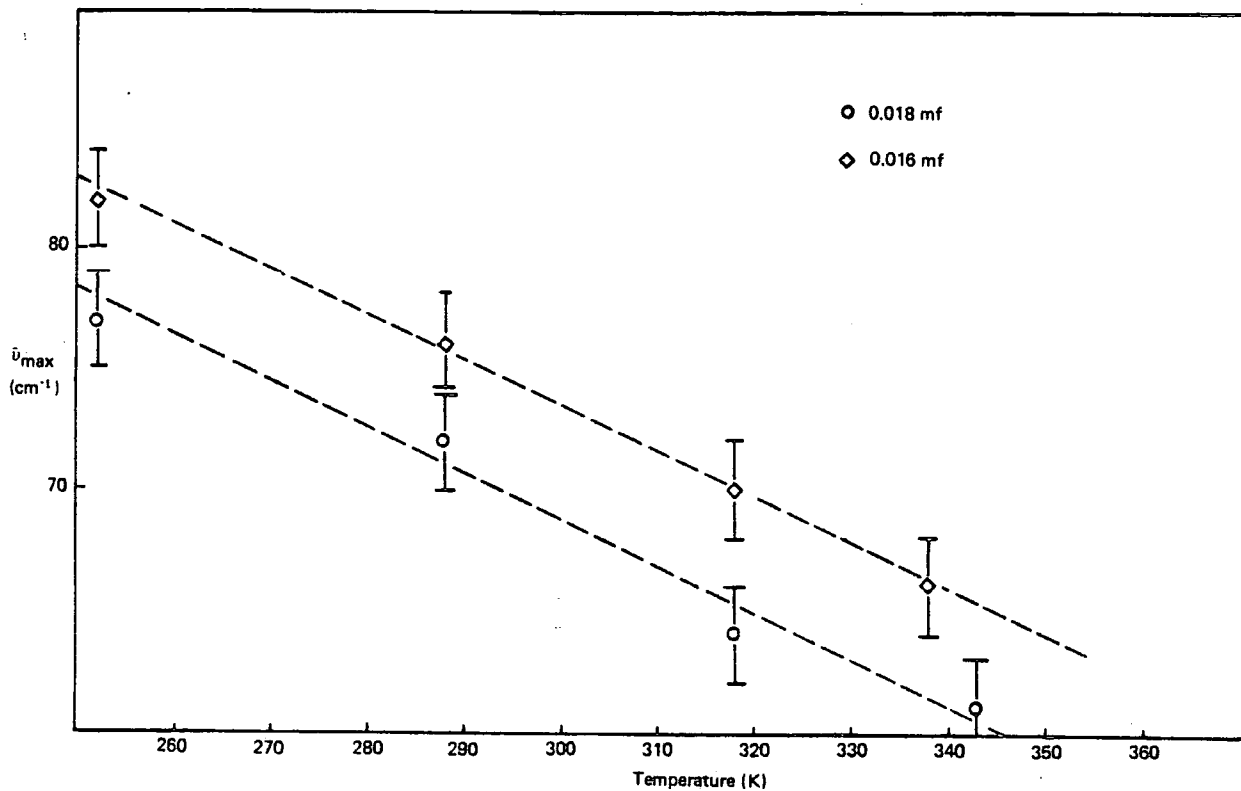


FIGURE 5.6.a  
OBSERVED SPECTRA  $\bar{\nu}_{\max}$  vs TEMPERATURE

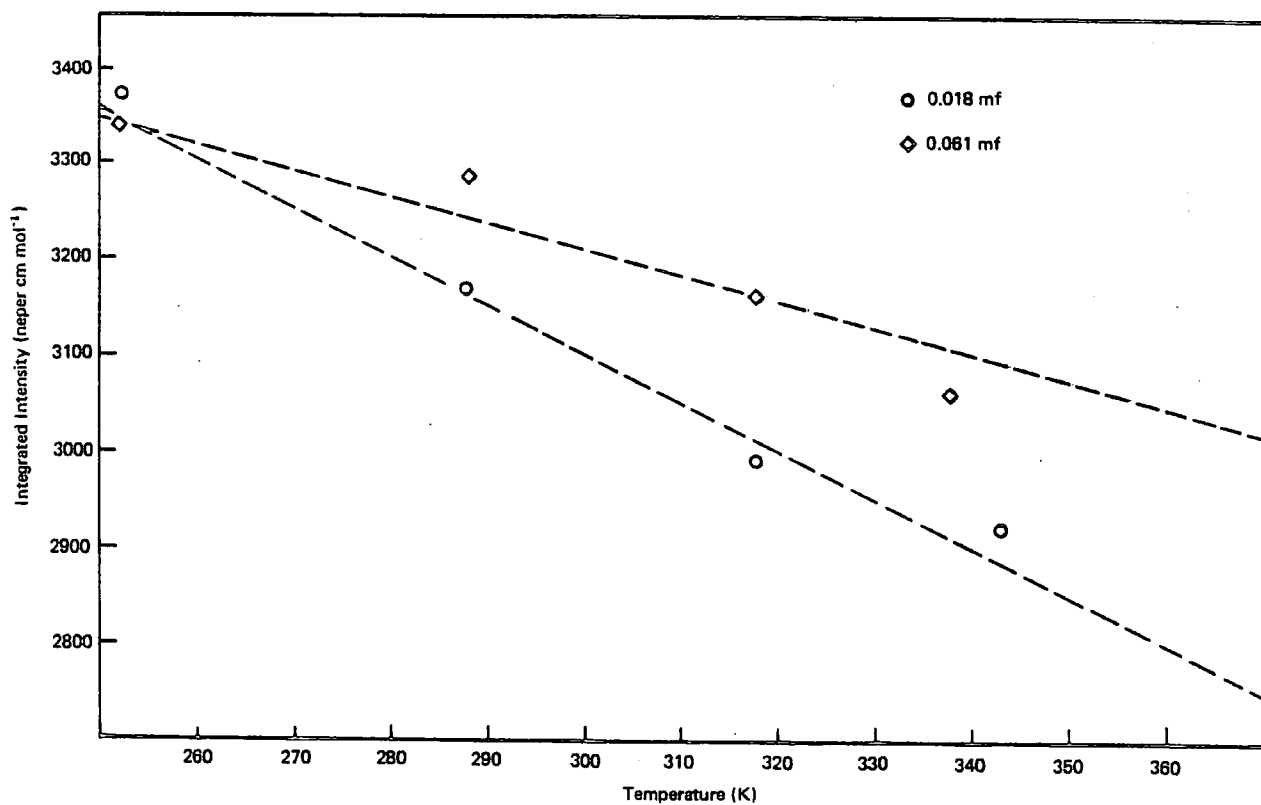


FIGURE 5.6.b  
OBSERVED SPECTRA INTEGRATED INTENSITY PER MOLECULE vs TEMPERATURE  
(INTENSITY ERROR  $\pm 5\%$ )

is increased. This type of behaviour, normally seen in Poley features of dipolar liquids, is the opposite of that observed in non-polar fluids<sup>170</sup> and the rotational relaxation behaviour observed in the microwave loss curves of liquids. The reason for this apparent trend and its different temperature dependence compared to Debye type behaviour is taken to be an indication that the processes giving rise to the features are, at least in part, different. If the breakdown of the Debye model at high frequencies can be accounted for by its lack of intermolecular torque terms then the extended model described previously in Chapter 2 and applied in Chapter 6 should elucidate this process by exposing an associated trend in the magnitude of the model parameter  $K_1(0)$  which is directly related to the intermolecular mean torques  $\langle O(V)^2 \rangle$ . (This relationship is described in Section C of this Chapter.)

Figure 5.6b shows the change in integrated intensity with temperature. Although it appears that there is a decrease in intensity with temperature, the total variation is very close to the error of  $\pm 5\%$  and with only 4 temperatures for comparison it is difficult to justify any detailed analysis of this. Furthermore, the intensities of two additional spectra recorded for the 0.018mf solutions at 318K and 343K lie well outside this trend. However, if the existence of such a trend is to be considered, it would possibly be explained in terms of a breakdown of clusters of molecules which are contributing to the overall absorption. This hypothesis draws some support from the theory of Leutloff and Knozinger,<sup>171</sup> who have found evidence for the presence of  $\text{CH}_3\text{CN}$  dimers in the gas phase which lead to a weak band in this region ( $78\text{cm}^{-1}$ ) due to the intermolecular vibrational modes. The presence of dimers in the gas phase indicates the tendency for the molecules to group, and the underlying strong attractive forces may well be exerting considerable influence in the liquid/solution phase particularly at short range. The molecular clusters which form in such a system would not necessarily be permanent of course - they would quite likely be breaking down and reforming continuously and would be less likely to reform as the temperature of the solution rises due to the increase in thermal motion. It should also be noted that the study of non-dipolar liquids<sup>170</sup> (carbon disulphide) over a range of temperatures has revealed evidence of an increase in integrated intensity with temperature, and that this has been explained in terms of an increase in the collisionally induced dipole moment with increasing collisional energy at higher temperatures. The absorption observed for dipolar liquids may be composed of a permanent dipole part and an induced dipole part and therefore this opposing mechanism would be masking, to some degree, the evidence of dimer/cluster type behaviour.

The plots of  $a_{\text{max}}$  and  $\Delta\bar{\nu}_{1/2}$  against temperature (Figures 5.7a and 5.7b) show the steady decrease in band height accompanied by a broadening of the 'Poley' feature which accounts for the almost constant values of total intensity discussed. The exception to this is the point recorded for 318K 0.018 mole fraction (Footnote a, Table 5.5) which has a much wider half width and resulted in a greater total intensity as seen in the previous figure. The second value recorded at 343K (Footnote c, Table 5.5) for the 0.018 mole fraction solution falls on a line drawn through the other data points recorded and is therefore, if judged by this criterion, a reliable

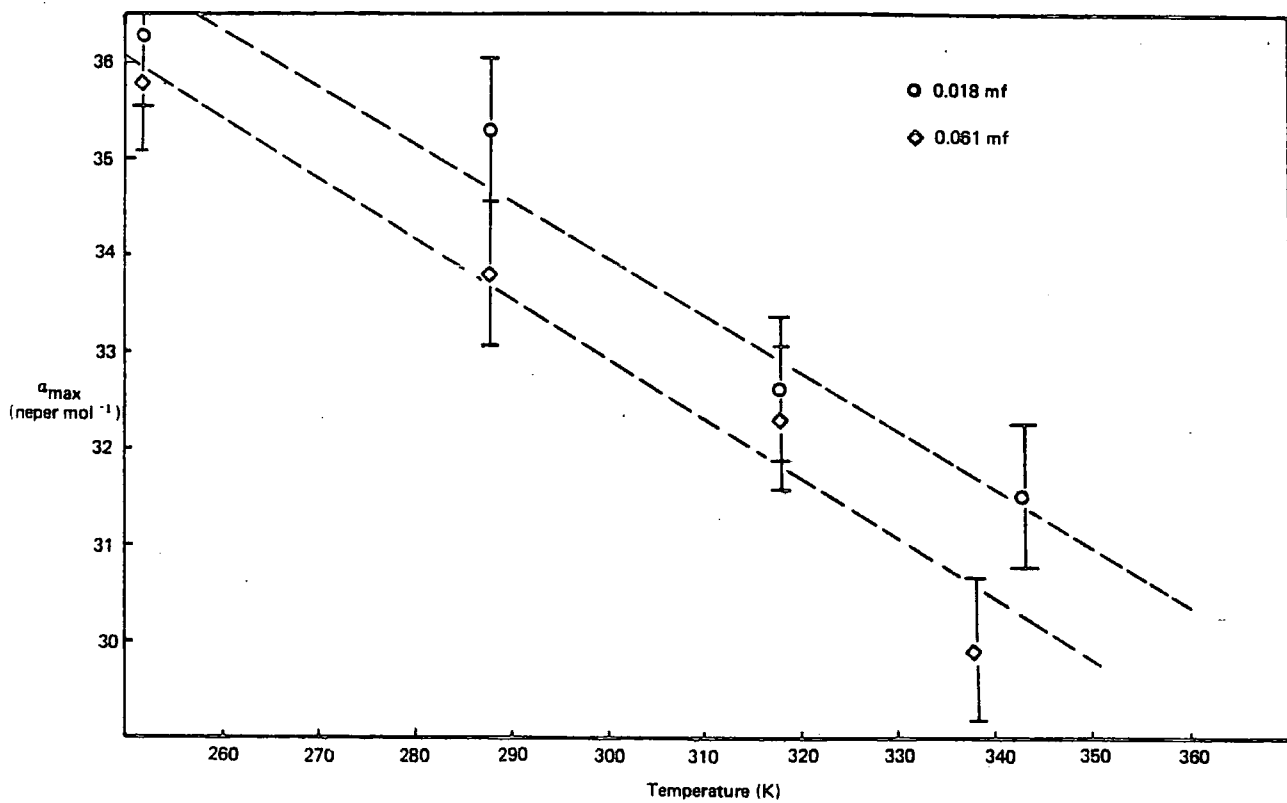


FIGURE 5.7a  
OBSERVED SPECTRA  $a_{\max}$  vs Temperature

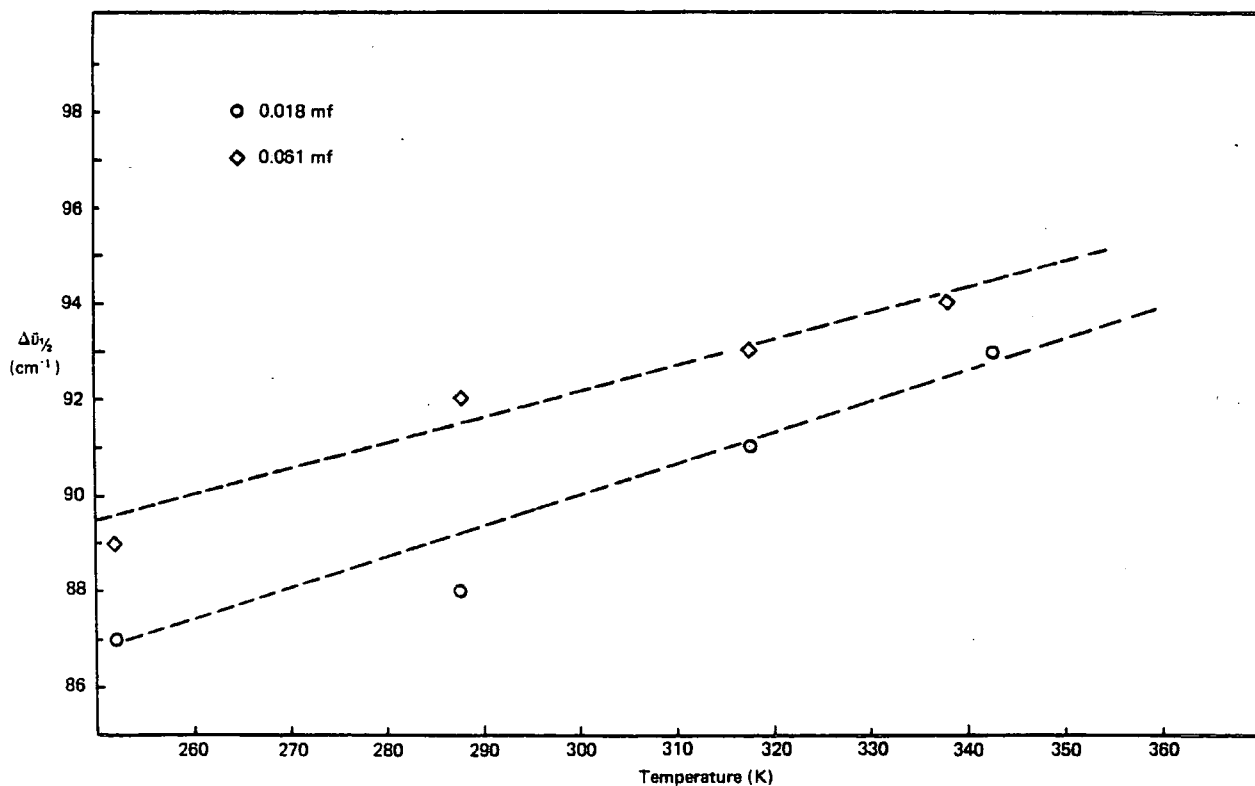


FIGURE 5.7b  
OBSERVED SPECTRA  $\Delta\bar{\nu}_{1/2}$  vs TEMPERATURE ( $\Delta\bar{\nu}_{1/2}$  ERROR  $\pm 2\text{cm}^{-1}$ )

point. However, the total intensity calculated from this spectrum clearly does not add weight to the argument for the existence of a trend with temperature related to the formation of clusters as discussed in the previous paragraph. The broadening of the band with temperature is due to the increase in the thermal energy which leads to an increase of the relaxation rates in the system. The model parameter  $\gamma$  (Section C) provides a measure of the relaxation rate of the intermolecular mean squared torques  $\langle 0(v)^2 \rangle$  and is expected to reflect the increase in energy, becoming faster as the temperature is increased.

(v) **The Variation in the Observed Spectral Features with Concentration**

The band peak frequencies  $\bar{\nu}_{\max}$  show an increase which tends to level off at higher concentrations (Figure 5.8a). A similar pattern is exhibited by Arnold's data (Figure 5.8b) for the  $\text{CH}_3\text{CN}/\text{CCl}_4$  solutions and also for the  $\text{CH}_3\text{CN}/\text{Benzene}$  solutions, which have very similar values. The shift in the peak frequency is probably due to the closer packing of the molecules in the more concentrated solutions and is discussed in Chapter 6 in terms of the variation in the model parameter  $K_1(0)$  which is related to the mean squared torque  $\langle 0(V)^2 \rangle$  between the molecules.

The changes in  $\alpha_{\max}$  and  $\Delta\bar{\nu}_{1/2}$  with concentration at 318K are shown in Figure 5.9. It can be seen that the decrease in band maximum is offset by an increase in half band width which accounts for the constant values of the integrated intensity of the features i.e. Beer's law is obeyed. In contrast, the data recorded by Arnold does seem to exhibit a steady increase in band width over the concentration range from 0.1 to 0.7 mole fraction which is not offset by a decrease in  $\alpha_{\max}$  and hence gives rise to a similar increase in the total integrated intensity. However, the errors estimated are  $\pm 10\%$ , which almost completely 'swamps' the change in the  $\Delta\bar{\nu}_{1/2}$  values and leaves little clear evidence of any deviation from Beer's law.

(vi) **The Calculation of Loss Spectra ( $\epsilon''$  vs  $\bar{\nu}$ ) for the Solutions at 288K and 318K**

The loss spectra have been calculated using the relation (Chapter 2)

$$\epsilon''(\nu) = \frac{\alpha(\bar{\nu}) \eta(\bar{\nu})}{2\pi\bar{\nu}} \quad \dots\dots\dots 5.4$$

The results are shown in Figures 5.10 and 5.11. The loss spectrum of the 0.018 mole fraction solution at 318K exhibits a maximum at a frequency of  $2.44\text{cm}^{-1}$ . This peak frequency of the loss spectrum has been used to calculate the rotational correlation time  $\tau_{\text{loss}}$  via the relation

$$\tau_{\text{loss}} = 1 / 2\pi c \bar{\nu}_{\max}^{\text{loss}} \quad \dots\dots\dots 5.5$$

This yields a value of  $\tau_{\text{loss}} = 2.2 \pm 0.3$  p secs (error derived from spectral resolution of  $0.61\text{cm}^{-1}$ ), which is considerably shorter than the values obtained by the integration of the total correlation function<sup>172</sup> (microwave and far-infrared). In the work cited, the nearest experimental conditions for comparison would be the value recorded for a 0.016 mole fraction solution at 298K for which a  $\tau$  of 4.41 p secs was obtained. The peak in the loss spectra of the remaining three solutions was not observed.

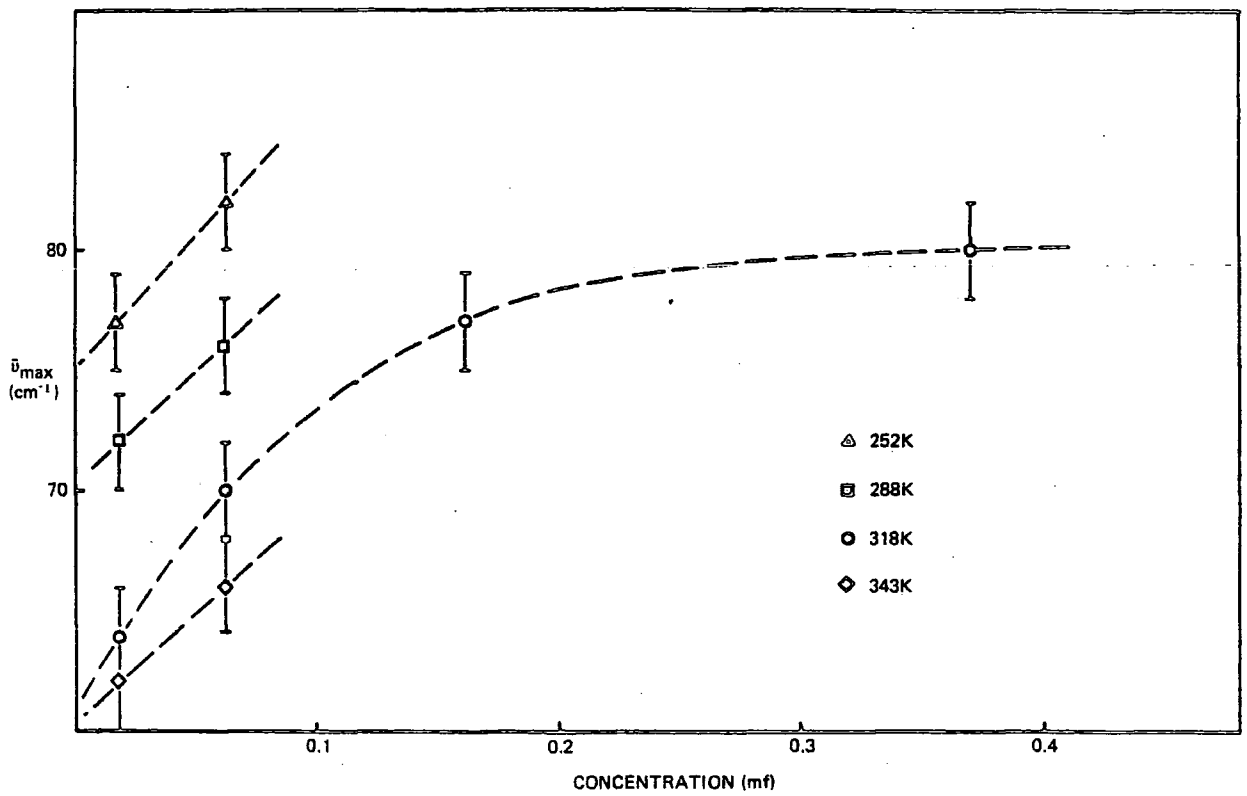


FIGURE 5.8a  
OBSERVED SPECTRA  $\bar{\nu}_{\max}$  vs CONCENTRATION

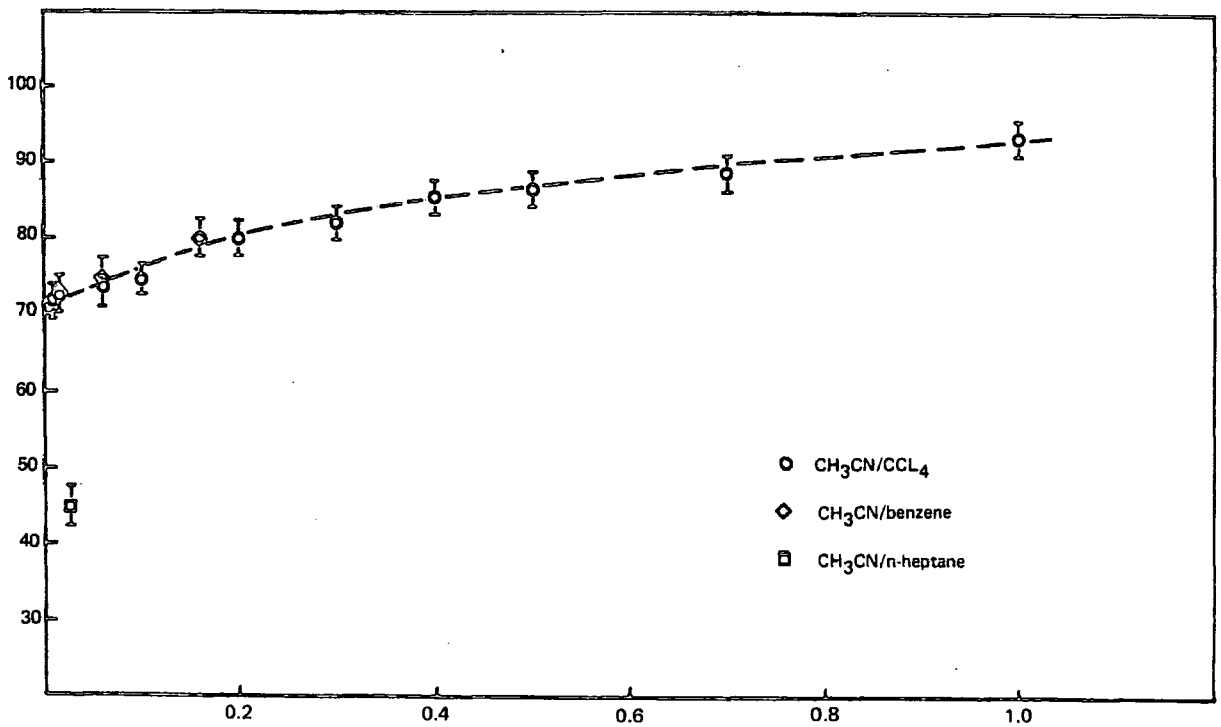


FIGURE 5.8b  
OBSERVED SPECTRA  $\bar{\nu}_{\max}$  vs CONCENTRATION

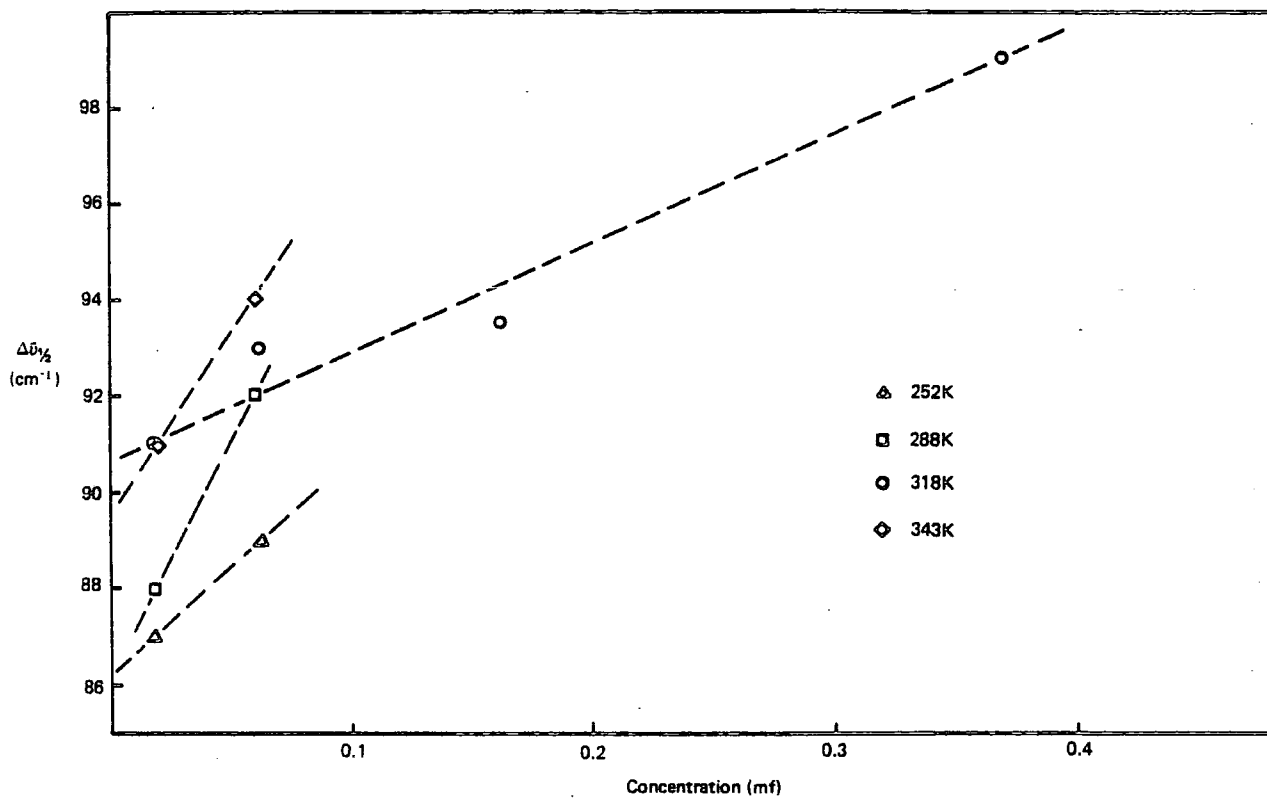


FIGURE 5.9a  
OBSERVED SPECTRA  $\Delta\bar{\nu}_{1/2}$  vs CONCENTRATION ( $\Delta\bar{\nu}_{1/2}$  ERROR  $\pm 2\text{cm}^{-1}$ )

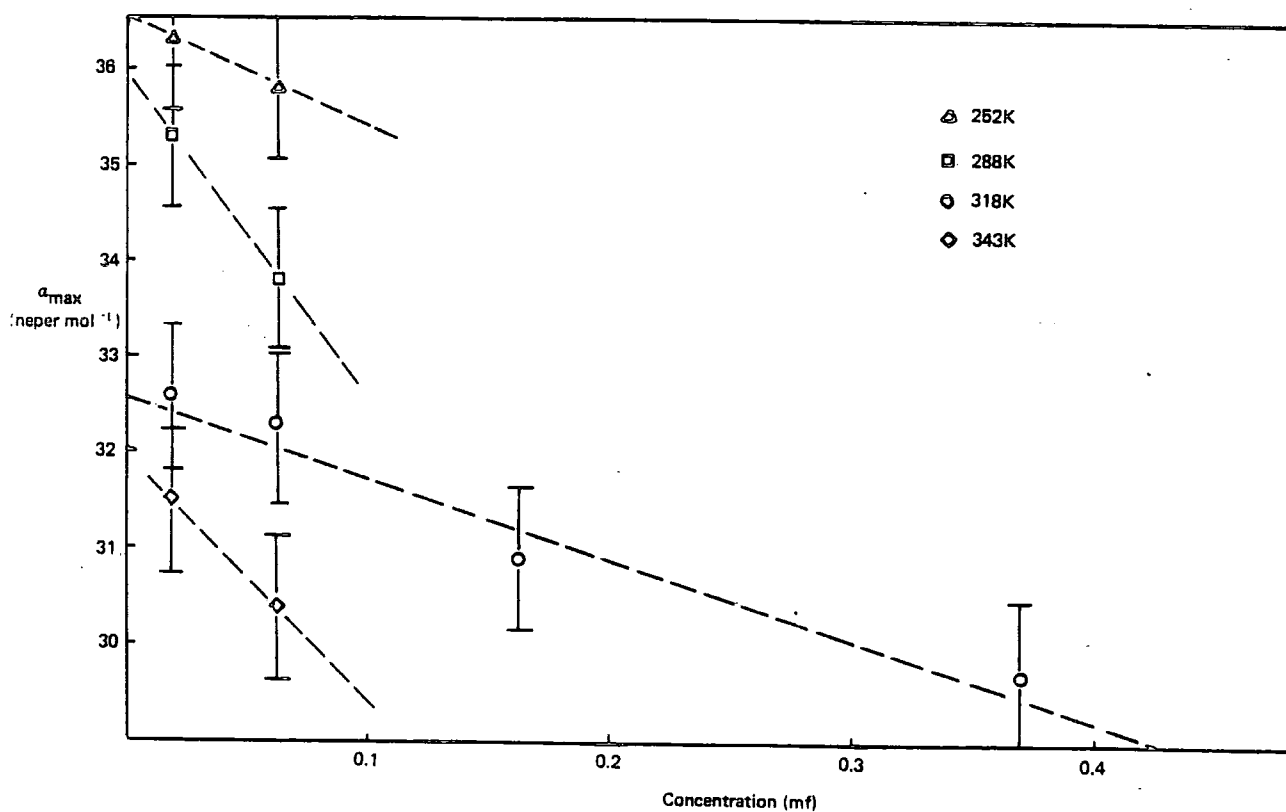


FIGURE 5.9b  
OBSERVED SPECTRA  $a_{\text{max}}$  vs CONCENTRATION

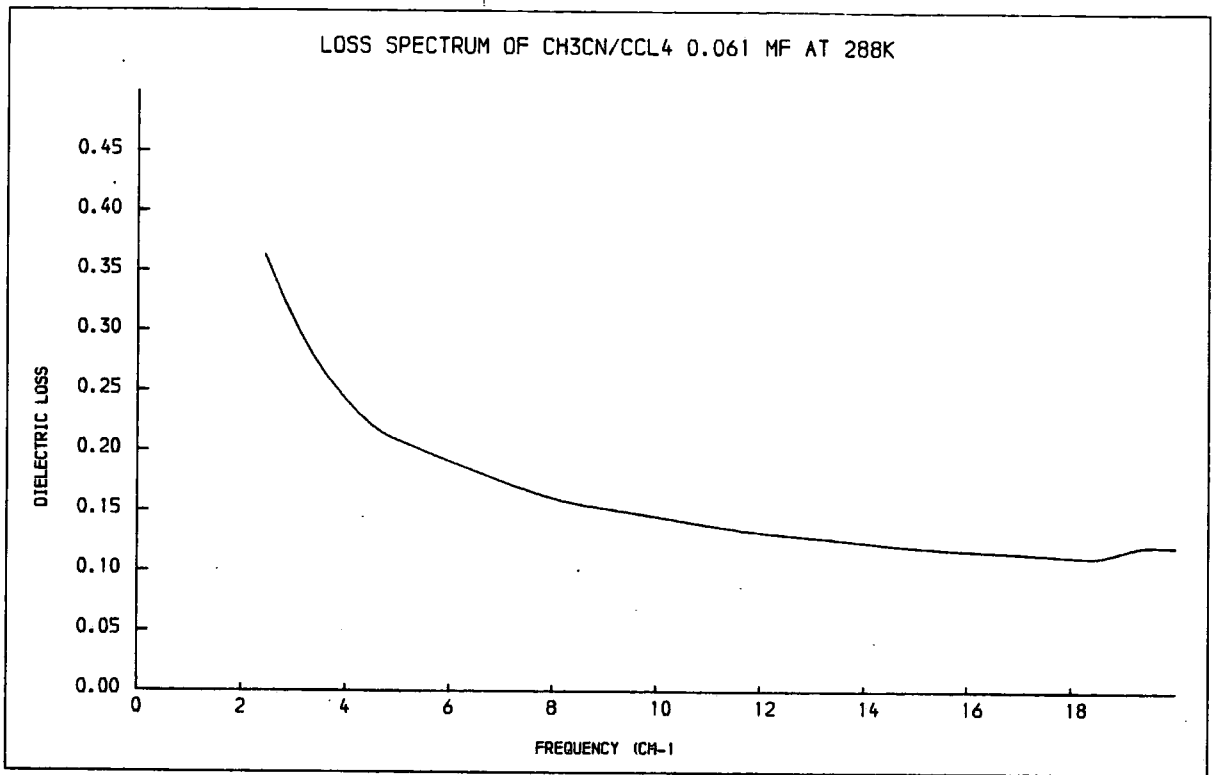


FIGURE 5.10a

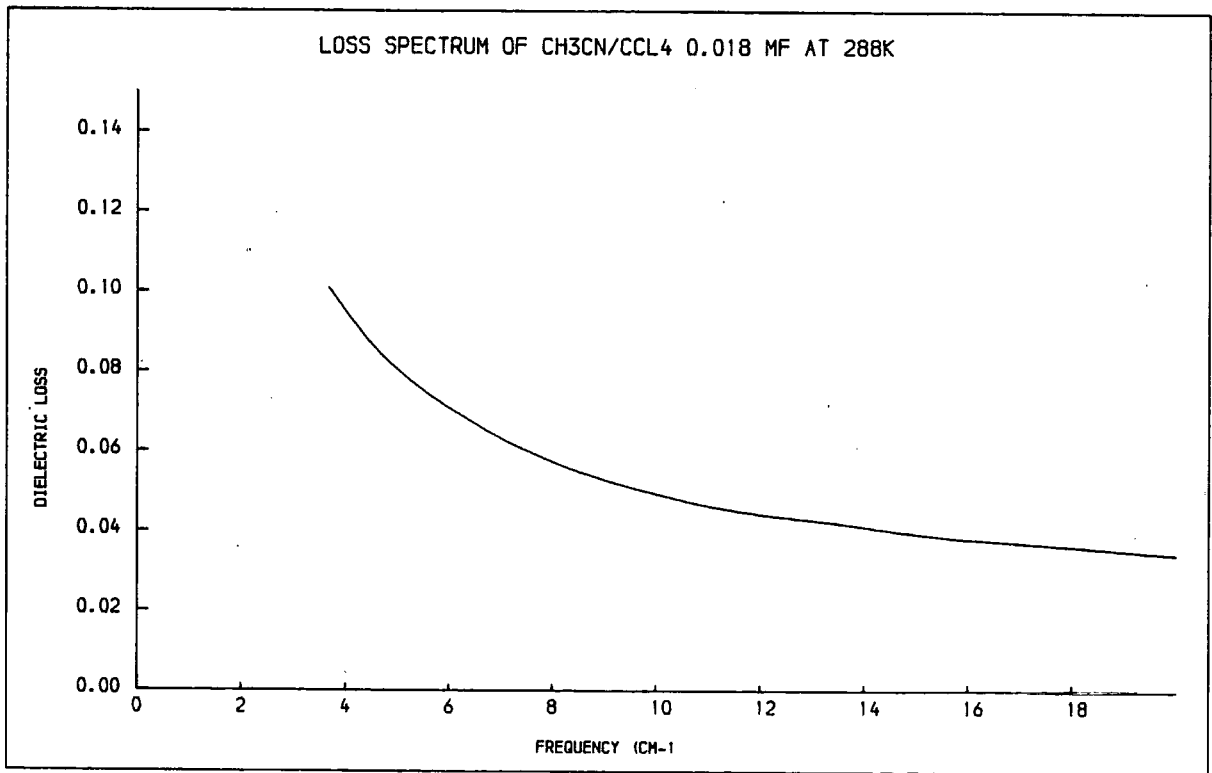


FIGURE 5.10b

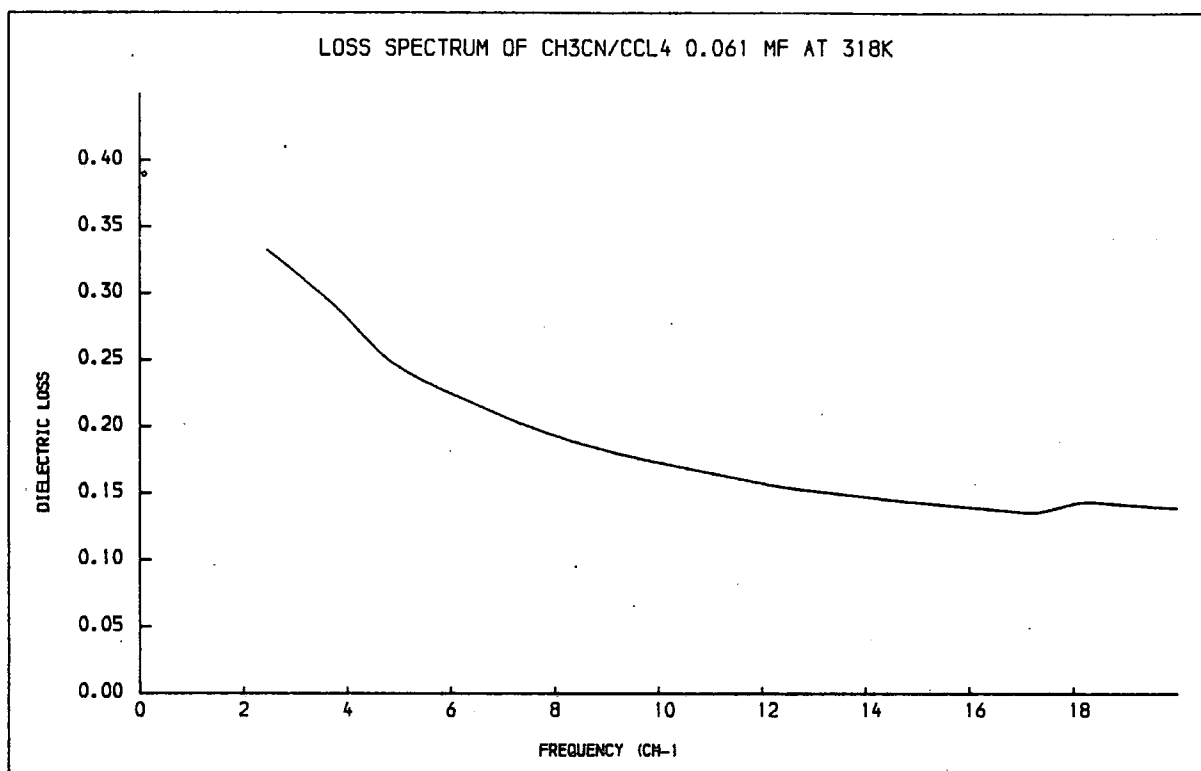


FIGURE 5.11a

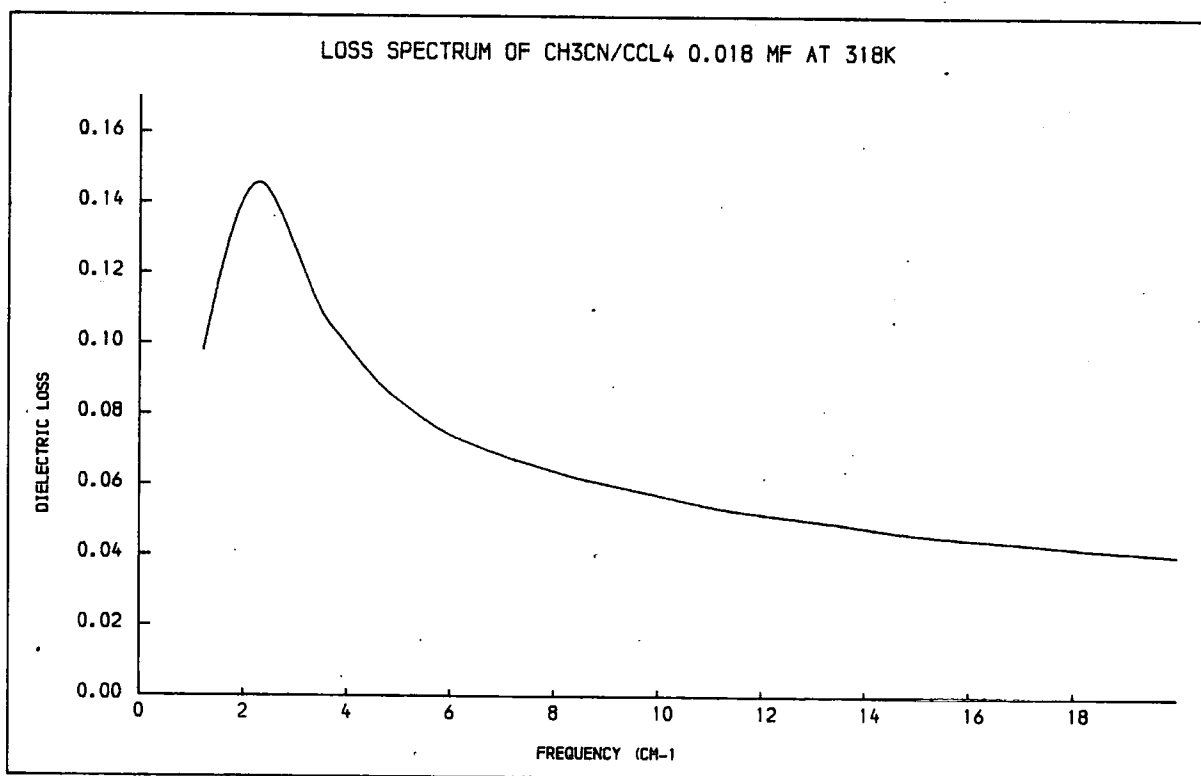


FIGURE 5.11b

### C. A DESCRIPTION OF THE PROCEDURE APPLIED TO THE MODEL ANALYSIS

The model developed by the memory function approach and described in Chapter 2C Part V has been applied in this work by a procedure of computer fitting to the observed spectra and by a numerical calculation. With these methods, some values have been obtained for the model parameters. These parameters are related to the torques (magnitude and correlation time) acting between the molecules in the solutions and are intended to elucidate the mechanism from which the spectral feature arise.

In this section the methods of application of the model are described with the results of some tests which have been performed on the fitting routine. The results obtained from the application of the model to the spectra are given in Chapter 6.

#### (i) The Definitions Applied in the Model Analysis

The basic equation, derived in Chapter 2C, which encompasses the model is given by:

$$a(\omega) = \frac{(\epsilon_0 - \epsilon_\infty) \gamma \cdot K_0(0) \cdot K_1(0) \omega^2}{\eta(\omega) \left[ \gamma^2 (K_0(0) - \omega^2)^2 + \omega^2 [\omega^2 - (K_0(0) + K_1(0))]^2 \right]^2} \dots\dots\dots 5.6$$

- where  $K_0(0) = 2KT/l_B$  (rotational 2nd moment)  
 $K_1(0)$  is related<sup>173</sup> to the intermolecular mean square torques  $\langle 0(V)^2 \rangle$  via the rotational 4th moment,  $M_{4R}$  (equations 5.7 and 5.9)  
 $1/\gamma$  is the torque correlation time  
 $\epsilon_0$  = static permittivity  
 $\epsilon_\infty$  = permittivity between far-infrared (Poley absorption) and mid-infrared (vibrational features)  
 $\omega$  = angular frequency given by  $\omega = 2\pi c\bar{\nu}$  where  $\bar{\nu}$  = wavenumber ( $\text{cm}^{-1}$ )

$$M_{4R} = 8 \left( \frac{kT}{l_B} \right)^2 \left( 1 + \frac{l_A}{4l_B} + \frac{\langle 0(v)^2 \rangle}{k^2 T^2} \right) \dots\dots\dots 5.7$$

Since the short time part of the orientational correlation function has been given:<sup>174</sup>

$$\phi(t) = 1 - a_1 t^2 / 2! + a_2 t^4 / 4! \dots\dots\dots 5.8a$$

$$= 1 - M_{2R} t^2 / 2! + M_{4R} t^4 / 4! \dots\dots\dots 5.8b$$

where  $K_0(0) = 2kT/l_B = -a_1$  and  $K_1(0) = a_1 - a_2/a_1$

$$\text{then } M_{4R} = K_0(0) K_1(0) + K_0^2(0) \dots\dots\dots 5.9$$

In addition expressions have been given<sup>175, 176</sup> for the permittivity and loss in terms of the model parameters, i.e.

$$\epsilon''(\omega) = \frac{(\epsilon_0 - \epsilon_\infty) K_0(0) K_1(0) \gamma \omega}{\gamma^2 \left[ K_0(0) - \omega^2 \right]^2 + \omega^2 \left[ \omega^2 - \left[ K_0(0) + K_1(0) \right] \right]^2} \dots\dots\dots 5.10$$



$$\epsilon'(\omega) = \frac{\epsilon_0 - (\epsilon_0 - \epsilon_\infty) \omega^2 \left[ \left[ \omega^2 - K_0(0) \right] \left[ \omega^2 - [K_0(0) + K_1(0)] \right] + \gamma^2 \left[ \omega^2 - K_0(0) \right] \right]}{\gamma^2 [K_0(0) - \omega^2]^2 + \omega^2 \left[ \omega^2 - [K_0(0) + K_1(0)] \right]^2} \quad 5.11$$

Through the definition of the dielectric loss given by equation 5.4 and the relation

$$\eta(\omega) = \left[ \frac{[(\epsilon''(\omega) + \epsilon'(\omega)^2)^{1/2} + \epsilon'(\omega)]}{2} \right]^{1/2} \quad \dots\dots\dots 5.12$$

an expression has been developed for the determination of the model values of  $a(\omega)$  in the absence of a knowledge of  $\eta(\omega)$  viz

$$a(\omega) = \frac{\sqrt{2} \epsilon''(\omega) \omega}{c \left[ (\epsilon'(\omega)^2 + \epsilon''(\omega)^2)^{1/2} + \epsilon'(\omega) \right]^{1/2}} \quad \dots\dots\dots 5.13$$

Expressions which enable the calculation of the parameters  $K_1(0)$  and  $\gamma$  without recourse to the fitting procedure have also been applied in this work. The relation derived by the differentiation of equation 5.6 is<sup>177</sup>

$$K_1(0) = \frac{4\omega_m^2 [\omega_m^2 - K_0(0)]}{\pi [K_0(0) - \omega_m^2] [K_0(0) + \omega_m^2] + 4\omega_m^4} \quad \dots\dots\dots 5.14$$

which only requires a knowledge of the peak frequency,  $\omega_m$ , and the second moment,  $K_0(0)$  to obtain  $K_1(0)$ . This value can then be used to calculate the torque correlation time parameter via the expression given by Drawid and Halley<sup>178</sup>

$$\gamma = \left[ \frac{K_1(0)\pi}{2} \right]^{1/2} \quad \dots\dots\dots 5.15$$

The parameters obtained, by either method, are used to recalculate the various spectra of the solutions, i.e.  $a(\omega)$ ,  $\epsilon''(\omega)$ ,  $\epsilon'(\omega)$  and  $\eta(\omega)$  from equations 5.4, 5.10, 5.11 and 5.12 respectively. The relaxation time  $\tau^{\text{model}}$  can be obtained directly from the peak frequency of the loss spectrum (see previous section) or by the relation

$$\tau^{\text{model}} = \left( \frac{[K_0(0) + K_1(0)]^2 - 2K_0(0) \gamma^2}{K_0(0)^2 \gamma^2} \right)^{1/2} \quad \dots\dots\dots 5.16$$

These models produce very similar values but the calculation from the loss peak has the disadvantage of a finite resolution limit which is imposed by the recalculation frequency interval. The results of both methods of calculation are given in Chapter 6. Another expression for the calculation of the relaxation time has been derived<sup>178</sup> by the differentiation of the expression for the dielectric loss. This approximation is given by the equation

$$K_1(0) \approx \frac{\pi}{2} \left[ \frac{2k T \tau}{I_B} \right]^2 \quad \dots\dots\dots 5.17$$

(ii) **A General Description of the Least Squares Fitting Routine**

A Numerical Algorithms Group (NAG) computer routine E04FAF has been employed to calculate the best fit of the model to the observed spectra. The routine is based on a procedure described by Peckham which calculates the minimum sum of squares of the deviation between observed and calculated solutions, without calculating the gradients (an alternative method using spline functions). This technique enjoys the advantage over other methods (see, for example, Powell)<sup>179</sup> that it requires less function evaluations to achieve a solution and is therefore economical in computing time: an important consideration when fitting typically 200 plus data points in this work. The routine is called by a program NEWFITF.S3/4 which is based on a series of programs originally translated from Evans' Algol version to FORTRAN by Arnold and O'Neill and subsequently modified to its present form in this work. For the purposes of a more rapid calculation and the minimizing of rounding errors which would result from the manipulation of very large and very small numbers, the equations and the input parameters to the routine are weighted by the factor  $2KT/I_B$ . This weighting factor is removed before the spectral parameters are recalculated. Double precision (approximately 15 significant figures) logic is used throughout the fitting routine. The equations applied are 5.6 and 5.13 rewritten in the general form

$$\text{Residual } a(\bar{\nu}) = \text{FUNCTION (PARAMETERS FITTED)} \\ - \text{OBSERVED VALUE } a(\bar{\nu})$$

for manipulation by the NAG routine.

The program can be configured to allow up to four parameters in the function applied to vary in order to obtain a fit to the observed spectrum. The four possible variables are  $\gamma$ ,  $K_1(0)$ ,  $K_0(0)$  and  $(\epsilon_0 - \epsilon_\infty)$ . In this work mainly two parameter fits  $\gamma$  and  $K_1(0)$  have been applied although the analysis in Chapter 6 includes some three parameter fitting ( $\gamma$ ,  $K_1(0)$ ,  $K_0(0)$ ) and in Appendix 3 an example of a four parameter fit can be found.

**Convergence and Determination of Solution**

The first calculation made by the routine determines the values of  $a(\bar{\nu})$  for each of the observed points using the starting values of  $\gamma$ ,  $K_1(0)$ ,  $K_0(0)$  and  $(\epsilon_0 - \epsilon_\infty)$ . The starting values are the routine users guesses of the possible solution values in the weighted form referred to in the program as Theta (I) where I is equal to the number of function variables. The observed value of  $a$  at each point is subtracted from the recalculated value and the residual is squared. The sum of the squares of the residuals is a measure of the degree of fit obtained and must be minimized for the best fit, hence the name 'least squares fit'. A perfect fit would yield a value of zero sum of squares. Assuming that the parameters have not led to a zero-sum of squares, successive iterations will take place. For these iterations theta (I) or theta (I)'s will take up new values which will depend on the values of the sum of squares (SQS) from the previous fit/fits and a user selected parameter V(I). These values are user estimates of the relative magnitude of the variables and the range of values over which a function minimum might be found. A third condition applies if the point set becomes degenerate i.e. it does not span the whole space. In that case a new point is generated by an internal random number generator.

The 'flag' IFAIL indicates the success or failure of the routine: the conditions are

- IFAIL 0 successful exit from program
- IFAIL 1 parameters out of range (SQS not converging)
- IFAIL 2 maximum number of iterations (user determined)  
completed – SQS converging

If the iterations are successful i.e. the values have been set such the function minimum has been found, the sum of squares will reduce in successive iterations as the values approach the lowest point in the minimum. Exit from the program with this solution can then occur in several ways. The conditions which were satisfied by the parameters are indicated by the flag XPS, which on exit from the program will be set to +1.0, -1.0 or 0.0. XPS = +1.0 indicates that the condition satisfied was the test on the relative values of the SQS over successive iterations. This is determined by an input parameter (XPS (in)). XPS = -1.0 indicates that the relative condition on the position of the minimum was satisfied. This condition is given by

$$\left| Y_I - Z_I \right| < ALF \times V(I)$$

$$I = 1, 2, \dots, N$$

where Y is the best point obtained for one iteration, Z is the best point obtained for a successive iteration and ALF is directly related to the input value of XPS.

These two conditions can be illustrated by Figures 5.12a and 5.12b.

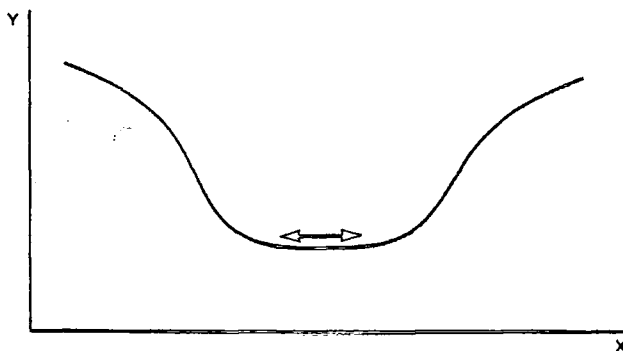


FIGURE 5.12a

A WIDE FLAT-BOTTOMED MINIMUM IN WHICH LARGE VARIATIONS IN X (RELATIVE TO V(I)) ONLY PRODUCE SMALL VARIATIONS IN Y (XPS = +1.0)

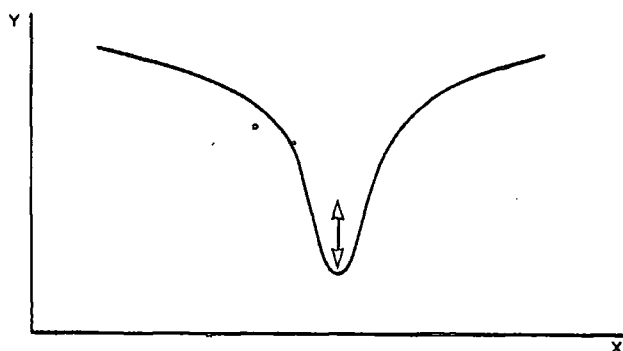


FIGURE 5.12b

A STEEP-SIDED MINIMUM IN WHICH SMALL VARIATIONS IN X LEAD TO LARGE FUNCTION VARIATIONS. (XPS = -1.0)

The flag  $XPS = 0.0$  indicates that the absolute condition was satisfied i.e.  $SQS < \text{input } XPS$ .

If the condition  $IFAIL 1$  is flagged the starting values assigned are out of range of the routine and new values must be assigned. Following an  $IFAIL 2$  message, inspection of the  $SQS$  values over a few iterations may indicate that more iterations are required. If the failure is a result of a restriction of the range of the parameters by the value  $V(I)$ , this is indicated by the monitor flag 'LIMITED' after each iteration. In this case the value of  $V(I)$  may be increased or the starting values of theta (i) may be adjusted (to bring them into range). However, the effects of these variables on the routine are closely related and it has been found that their manipulation can result in exit from the routine with alternative solutions which correspond to different function minima as illustrated in Figure 5.13.

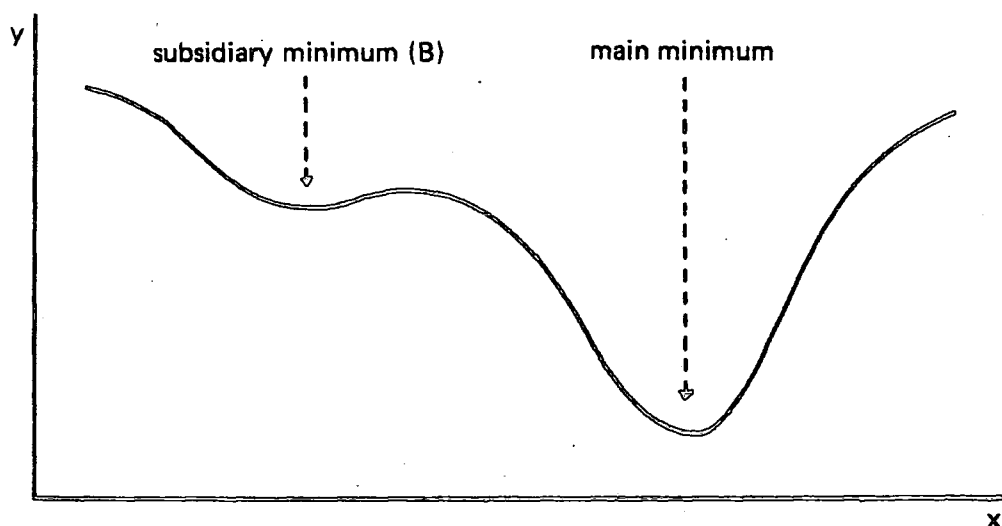


FIGURE 5.13

A SCHEMATIC REPRESENTATION OF THE DIFFERENT FUNCTION MINIMA FOUND BY A LEAST SQUARES FITTING ROUTINE

Table 5.7 summarises some input parameters which result in solutions at different minima. The spectra recalculated from these two function solutions are shown in Figure 5.14.

Starting values (Weighted)				Exit values (Weighted)						
theta (1)	V(1)	theta (2)	V(2)	theta (1)	theta (2)	SQS	iterations			
								minimum		
										comments
0.01	1.0	0.01	10.0	3.0282	22.1494	637	40	A		jumped over B
0.1	1.0	0.1	10.0	0.0817	0.7107	4418	23	B		note SQS
0.1	1.0	10.0	10.0	3.0282	22.1494	637	34	A		note iterations
5.0	1.0	20.0	10.0	3.0282	22.1494	637	29	A		note iterations
100.0	10.0	100.0	10.0	3.0282	22.1493	637	54	A		note iterations

TABLE 5.7  
TESTS FOR FUNCTION MINIMA IN A LEAST SQUARES FIT

In this work trial runs have been made using XPS(in) values of  $10^{-7}$ ,  $10^{-10}$  and  $10^{-15}$ . It has been found that setting XPS(in) to a value of  $10^{-7}$  only leads to very small differences (5th significant figure) in the values of Theta (1) between that and the XPS(in) =  $10^{-15}$  case. In addition, when XPS(in) =  $10^{-15}$  the routine usually fails to reach a solution at 999 iterations. Further tests have shown that the Theta (1) values after 200, 500 and 999 iterations, with XPS(in) equal to  $10^{-15}$ , vary only in the 7th significant figure. These differences are of course undetectable in the recalculated spectra which are only plotted from single precision arrays (7 figures).

The results of these tests have indicated that a value of  $10^{-10}$  is suitable for XPS(in), giving more than adequate precision and yet still allowing for a programmed exit in all cases. However, the exit condition on XPS does vary (+1.0 or -1.0). No absolute solutions (i.e. perfect fits) have been found.

### (iii) Fitting to Different Data Sets

Tests have been carried out fitting to different numbers of points of the same spectrum. The results of this test have shown that there is a small advantage in computing time to be gained in fitting smaller numbers of points (28 – 200). However, the difference in the final solution values (3rd or 4th significant figure) for a factor of 7 in the number of points fitted, and the uncertainties involved with different data sets, dictated that all of the observed points were fitted (points fitted marked 'x' in the figures throughout this thesis). The fitting routine was also tested on truncated low frequency data sets. However, the results of these fits did not produce satisfactory recalculated

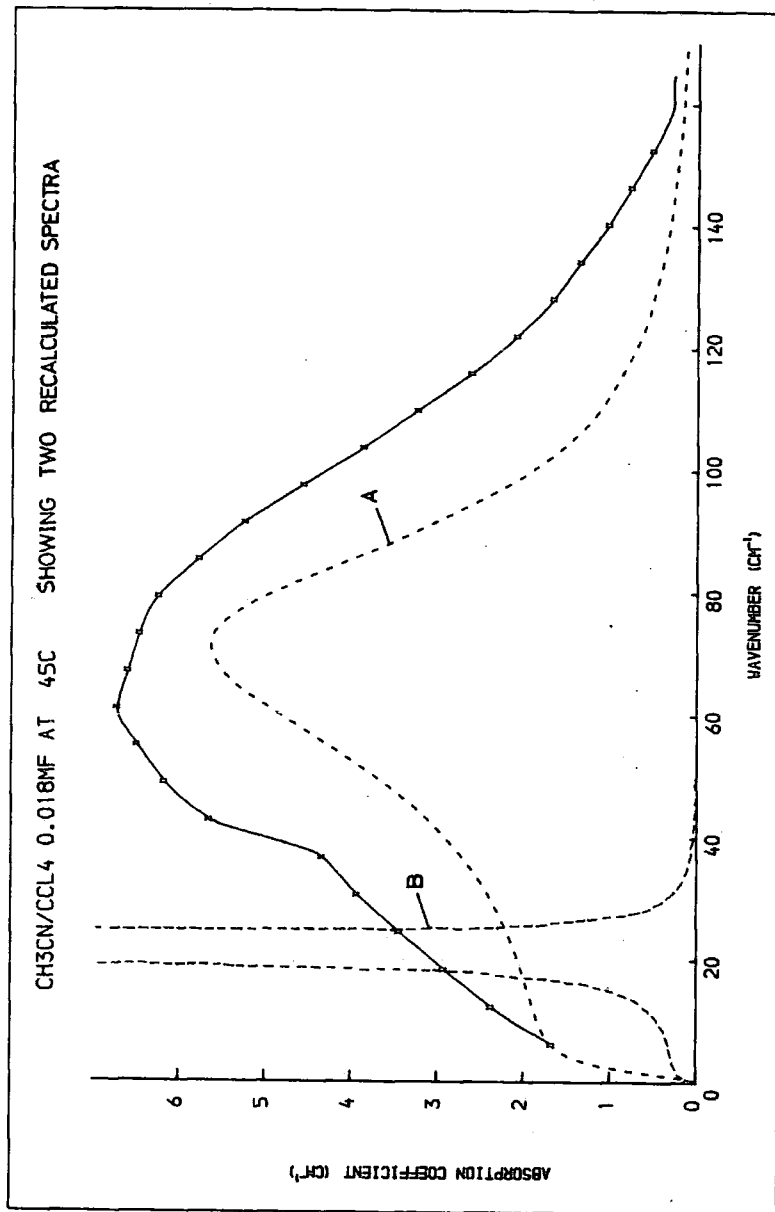


**FIGURE 5.14**  
**SPECTRA RECALCULATED FROM TWO DIFFERENT LEAST SQUARES**  
**FIT SOLUTIONS FOR THE MODEL (A AND B REFER TO TEXT)**

spectra. A spectra recalculated from the parameters given in Table 5.8 obtained from a low frequency data fit is shown in Figure 5.15.

frequency range - cm <sup>-1</sup>	$\gamma x^{1/2}$	$xK_{\eta}(0)$	$\tau_A$ (ps)	$\tau_B$ (ps)	SQS	iterations
2 - 40	2.3270	13.8353	1.93	1.88	42	19

$$x = I_B/2kT$$

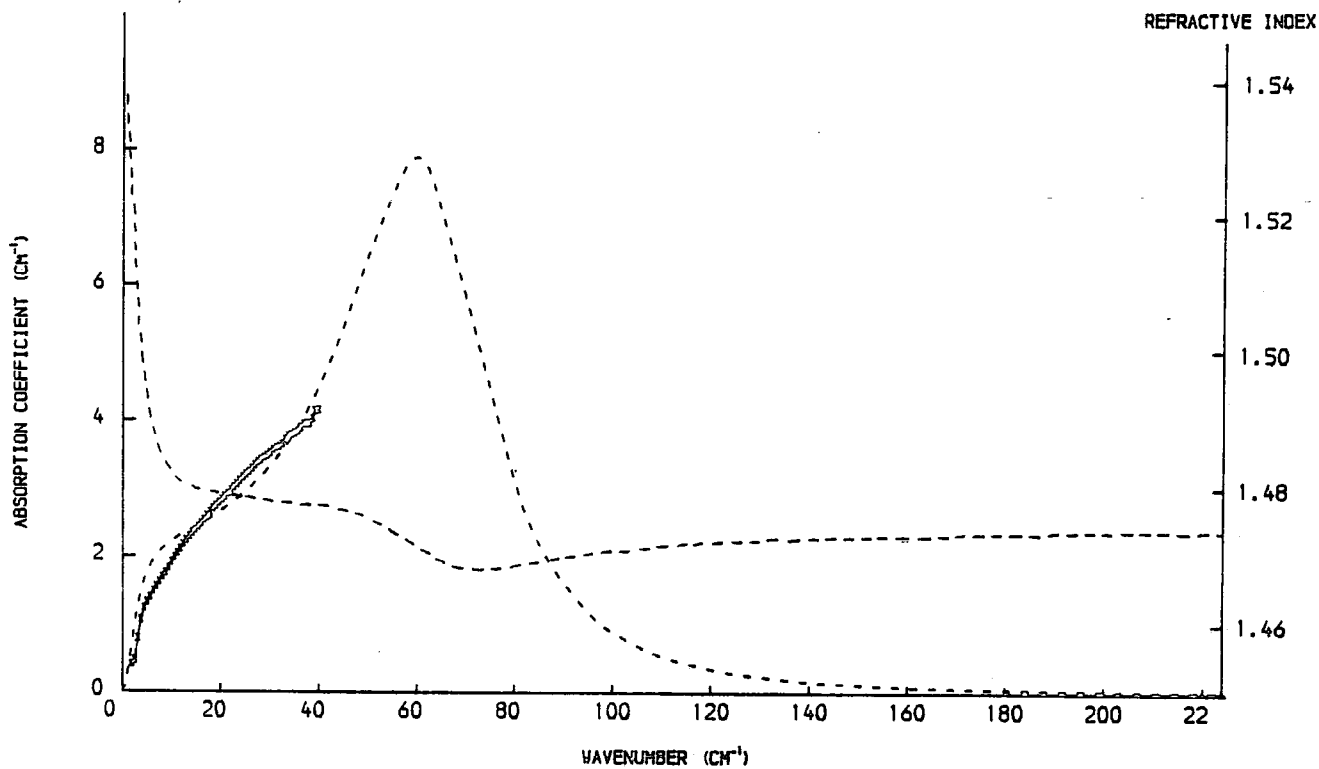
$\tau_A$  from Equation 5.16

$\tau_B$  from loss peak frequency via Equation 5.5.

TABLE 5.8  
PARAMETERS OBTAINED FROM A LOW FREQUENCY DATA FIT

CH3CN/CCL4 0.018MF AT 70C

(FIT TO LOW FREQ)



CH3CN/CCL4 0.018MF AT 70C

(FIT TO LOW FREQ)

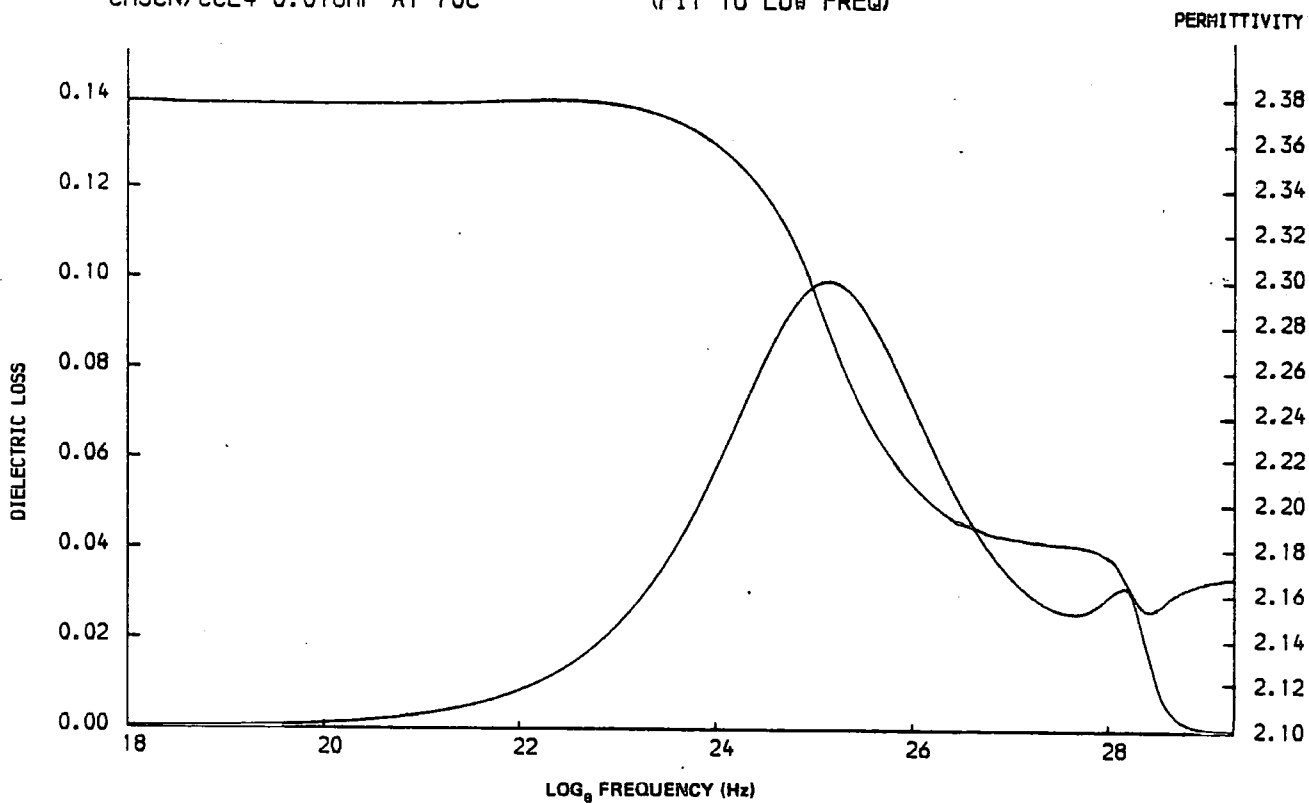


FIGURE 5.15  
SPECTRA RECALCULATED FROM A MODEL FIT TO LOW FREQUENCY DATA

## D. THE CALCULATION OF MOLECULAR AND MICROSCOPIC CORRELATION TIMES

### (i) Internal Field Factors

The microwave data for the range of concentrations of acetonitrile in carbon tetrachloride studied by Arnold<sup>126</sup> have been analysed using a modified Fuoss-Kirkwood equation<sup>180</sup> to obtain the microwave correlation times  $\tau_D$ . The equations are

$$v_{\max} = \left[ (3\epsilon_0 + \epsilon_\infty) / (\epsilon_0 + 3\epsilon_\infty) \right]^{1/2} / 2\pi\tau_D \quad \dots\dots\dots 5.18$$

where  $v_{\max}$  is obtained from the function

$$\cosh^{-1} \frac{(a(v) / v_{\max})}{(a(v) / v)} = \beta \log_e (v_{\max}/v) \quad \dots\dots\dots 5.19$$

- where  $a$  = an absorption coefficient
- $v$  = frequency (Hz)
- $\beta$  = an empirical parameter ( $0 < \beta < 1$ )

In this section the microwave correlation times  $\tau_D$  derived from this analysis are 'corrected' to obtain the microscopic/molecular correlation times, denoted by  $\tau_{\text{mic}}$  and  $\tau^S$  respectively. These 'corrections' are made using the equations derived from the internal field theories described in Chapter 2. A summary of the internal field factors applied, in their appropriate form, is given in Table 5.9.

### (ii) A General Discussion of the Results of the Internal Field Calculations

The results of the application of the internal field theories cited are shown in Table 5.10. These results have been divided into two main groups according to the type of field approximation inherent in the model. The first group comprises the  $\tau$  values which cannot be true single particle (molecular) correlation times because they are calculated from theories which approximate the internal field to the field experienced by a cavity of microscopic proportions in the dielectric medium. Figure 5.16 compares the  $\tau_D$  and  $\tau_{\text{mic}}$  values across the concentration range. In all cases, these  $\tau_{\text{mic}}$  values are shorter than the observed  $\tau_D$  times. In general, the  $\tau_{\text{mic}}$  values follow the trend in the  $\tau_D$  values, i.e. they reach a maximum value for a concentration of approximately 0.5 or 0.6 mole fraction.

The results from the Brot and the Kluk (long range) equations are only slightly shorter than the observed  $\tau_D$  values, which is in agreement with Hill's approximation<sup>58</sup> that  $\tau_{\text{mic}} = \tau_D$ . The main exceptions are in the values obtained from the Debye, Lorentz(DL) theory and the Nee, Zwanzig, Onsager (NZO) expression. Both of these field corrections predict a maximum of  $\tau_{\text{mic}}$  occurring for the 0.2 mole fraction solution. In addition, the results of the Debye, Lorentz equation show a rapid decrease at higher concentrations, yielding a microscopic correlation time  $\tau_{\text{mic}}$  for the pure liquid acetonitrile of less than 1 ps ( $7 \times 10^{-13}$  s).

(Refer to Chapter 2 for explanation of notation)

References	Abbreviations	Equation	Comments
Debye, <sup>15</sup> Lorentz <sup>83</sup>	DL	$r^{\text{mic}} = \frac{\epsilon_{\infty} + 2}{\epsilon_0 + 2} \tau D$	
Cole, <sup>92</sup> Glarum, <sup>93</sup> Powles <sup>94</sup>	CGP	$r^{\text{mic}} = \frac{2\epsilon_0 + \epsilon_{\infty}}{3\epsilon_0} \tau D$	
Nee, Zwanzig, <sup>43</sup> Onsager <sup>85</sup> (Klug, <sup>96</sup> Fatuzzo, Mason, <sup>97</sup> Scaife <sup>98</sup> )	NZO	$r^{\text{mic}} = \frac{2\epsilon_0 + \epsilon_{\infty}}{2\epsilon_{\infty} + \epsilon_0} \tau D$	Spherical isotropic molecules.
Kluk, <sup>108</sup> Brot <sup>104-106</sup>	BK(L)	$r^{\text{mic}} = \left( \frac{1 + (\epsilon_{\infty} / (2\epsilon_0^2))}{1 + (1/2\epsilon_0)} \right) \tau D$	Long range interactions. (L)
Kluk <sup>108</sup>	K(S)	$r^{\text{S}} = \frac{(N_1 \mu g^2 [1 + D(\epsilon_{\infty} - 1)]^2 \epsilon_0) r^{\text{mic}}}{kT (\epsilon_0 - \epsilon_{\infty}) (2\epsilon_0 + \epsilon_{\infty})}$	Short range interactions. (S) (Shape dependent)
Lobo <sup>102</sup> (Nee, Zwanzig, Onsager)	LO	$r^{\text{S}} = \frac{2\epsilon_0^2 + \epsilon_{\infty}^2}{\epsilon_0 (\epsilon_0 + 2\epsilon_{\infty})} r^{\text{mic}}$	Extended NZO to $r^{\text{S}}$
Kivelson, Madden <sup>101</sup>	KM(V)	$r^{\text{S}} = \tau D \left[ \frac{(\epsilon_{\infty} + 2)(\epsilon_0 + 2)}{(\epsilon_0 - \epsilon_{\infty})} \right] \frac{N_1 \langle \mu \rangle^2}{3kT} \frac{4\pi}{9}$	Equation for reaction sphere in a vacuum.
Kivelson, Madden <sup>101</sup>	KM(D)	$r^{\text{S}} = \tau D \left[ \frac{\epsilon_0 (\epsilon_{\infty} + 2)^2}{(\epsilon_0 - \epsilon_{\infty})(2\epsilon_0 + \epsilon_{\infty})} \right] \frac{4\pi N_1 \langle \mu \rangle^2}{9kT}$	Equation for sphere embedded in a dielectric material.

TABLE 5.9

A SUMMARY OF INTERNAL FIELD CORRECTION EQUATIONS

Observed Parameters			$\tau^{\text{mic}}$ (ps)					$\tau^{\text{s}}$ (ps)					
Concentration (mole fraction)	$\epsilon_0$	$\epsilon_\infty$	$\tau_D$ (ps)	DL	CGP	NZO	BK(L)	K(S) <sup>b</sup>	LO <sup>d</sup>	KM(V)	KM(D)	K factor from Kluk <sup>108</sup>	Molecular factor from KM C
0.01	2.388	2.26	3.26	3.16	3.20	3.20	3.23	3.82	3.20	5.02	4.93	0.846	0.0076
0.016	2.450	2.22	2.91	2.76	2.82	2.82	2.86	3.23	2.84	4.30	4.18	0.885	0.0130
0.06	3.050	2.28	3.88	3.29	3.55	3.52	3.74	5.23	3.60	7.56	6.95	0.716	0.0500
0.10	3.652	2.10	4.55	3.30	3.91	3.80	4.32	5.01	4.21	7.85	6.59	0.863	0.0830
0.16	4.670	2.52	4.35	2.95	3.68	3.56	4.16	6.82	2.92	11.85	9.42	0.610	0.1390
0.20	5.188	2.47	5.90	3.66	4.87	4.65	5.63	9.26	5.17	17.04	12.74	0.608	0.1750
0.30	7.382	2.32	6.14	2.82	4.74	4.32	5.87	8.31	5.52	18.89	11.19	0.707	0.2750
0.40	9.576	2.46	6.23	2.40	4.69	4.17	6.00	9.11	5.60	24.42	12.41	0.659	0.3870
0.50	12.412	3.25	6.47	2.35	4.88	4.35	6.29	12.45	5.48	38.24	18.33	0.505	0.5120
0.60	15.753	2.25 <sup>a</sup>	6.60	1.58	4.71	3.96	6.43	8.58	6.22	33.78	11.24	0.749	0.6560
0.70	19.636	2.28	5.50	1.09	3.88	3.20	5.38	7.10	5.22	33.39	9.29	0.758	0.8150
1.00	36.500	2.49	6.00	0.70	4.14	3.30	5.92	7.82	5.76	62.17	10.44	0.757	1.4600

a estimated value

b taken from BK(L) result

c to calculate the molecular  $\langle \mu \rangle^2$  Kivelson and Madden<sup>101</sup>

make the approximation  $N \langle \mu \rangle^2 / 3kTV = 4.85\mu_0^2 \rho / m(T/300)$   
where  $\rho$  = mass density,

$m$  = molecular weight,

$\mu_0$  = dilute gas value of dipole moment.

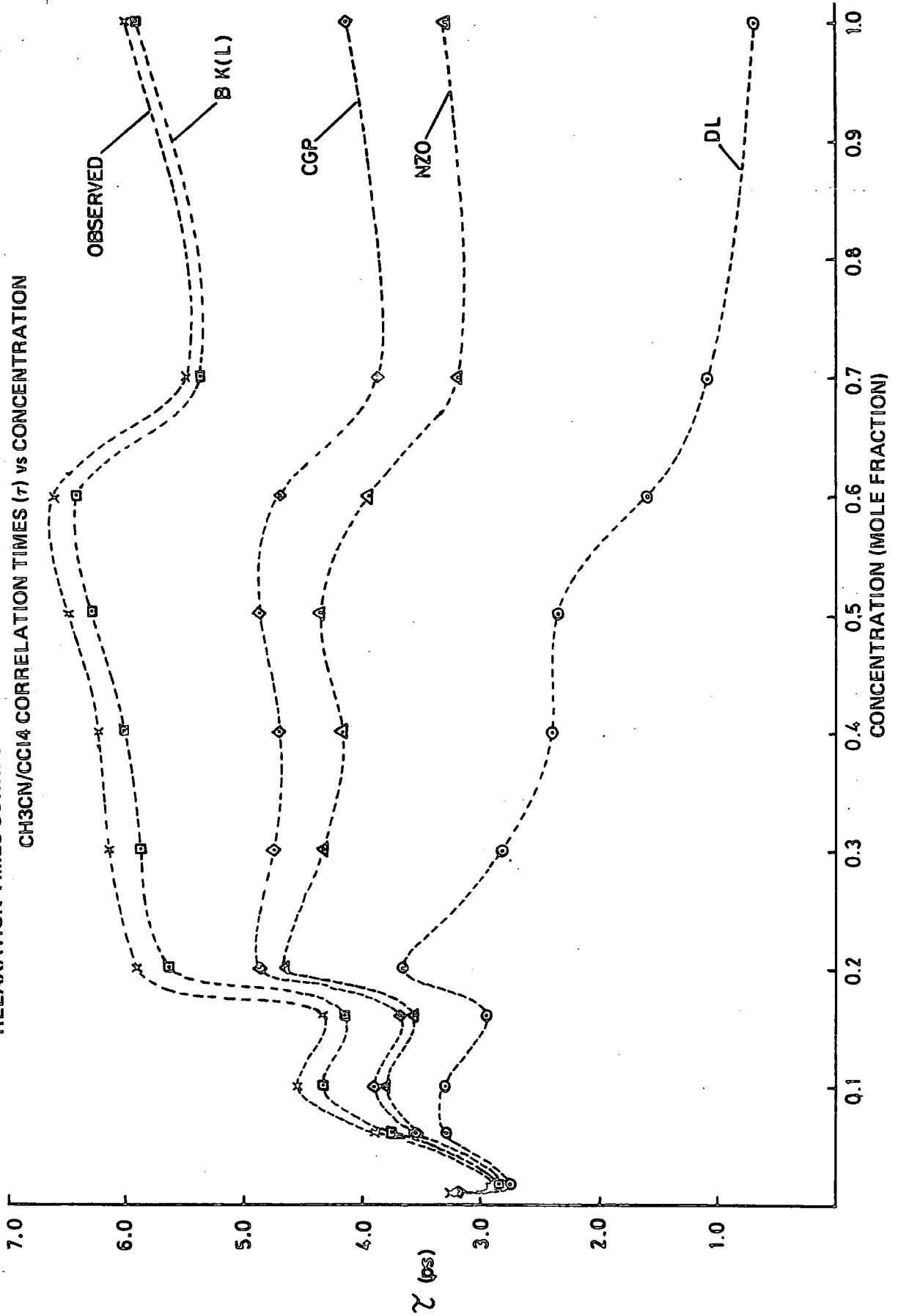
(See Chapter 2 for further details).

d applied to NZO

result.

TABLE 5.10  
OBSERVED MICROWAVE CORRELATION TIMES  $\tau_D$  FOR  $\text{CH}_3\text{CN}/\text{CCl}_4$  SOLUTIONS  
ADJUSTED BY VARIOUS INTERNAL FIELD FACTORS TO OBTAIN  $\tau^{\text{mic}}$  AND  $\tau^{\text{s}}$

FIGURE 5.16  
 RELAXATION TIMES CORRECTED BY VARIOUS INTERNAL FIELD FACTORS (--- FOR CLARITY ONLY)  
 CH<sub>3</sub>CN/CCl<sub>4</sub> CORRELATION TIMES ( $\tau$ ) vs CONCENTRATION



The theories which pertain to the molecular correlation times,  $\tau^S$ , fall into two groups. The first group comprises the Kluk<sup>108a</sup> (short range) and the Lobo<sup>102</sup> theories. Both of these theories relate the  $\tau^{\text{mic}}$  values, obtained by one of the previous methods, to the  $\tau^S$  time by accounting for the short range interactions which are effective within the microscopic cavity. The application of these methods yields  $\tau^S$  times which are longer than the  $\tau^{\text{mic}}$  times from which they are calculated. For most of the concentrations studied the values obtained by Kluk's equation are also longer than the observed  $\tau_D$  times. A similar trend has been observed by Kluk et al<sup>108b</sup> for Methyl Iodide across a range of temperatures.

The results yielded from the equations derived by Kivelson and Madden's<sup>101</sup> 'corresponding micro-macro correlation theorem' are in all cases longer than the observed  $\tau_D$  values. It is not surprising that the relation derived for a sphere in a vacuum is particularly badly behaved as this neglects all effects (long range) of the surrounding medium. The results of the calculations for the model of a sphere embedded in a dielectric also exhibit correlation times in general greater than  $\tau_D$ . In this case the explanation may be due to the neglect of the dynamic factor  $1 + Nf$  (see Chapter 2).

The dynamic correlations in the system are presumed to be effective at close range i.e. within the reaction sphere. By neglecting this contribution, the theory can only at best account for the long range interactions which may not be the dominant factors. These comments are not intended to be exhaustive, as a further discussion is included in Chapter 6.

**CHAPTER 6**  
**THE MOLECULAR DYNAMICS OF ACETONITRILE IN SOLUTION:**  
**MODEL ANALYSIS AND DISCUSSION OF RESULTS**

**CHAPTER 6**  
**THE MOLECULAR DYNAMICS OF ACETONITRILE IN SOLUTION :**  
**MODEL ANALYSIS AND DISCUSSION OF RESULTS**

**A. MODEL ANALYSIS**

**INTRODUCTION**

In this Chapter some results from the application of various models described in Chapter 2 are presented. These include the models of Debye,<sup>15</sup> Rocard<sup>77</sup> and Powles,<sup>78</sup> Gordon<sup>81</sup> (J. diffusion) and Hill<sup>56</sup> (itinerant oscillator). Comparisons are made between these early inertia-corrected Debye type models and the model developed by the memory function formalism approach described in Chapter 2. This model, which is distinguished from the alternatives by the inclusion of the torque related parameters  $K_1(0)$  (directly related to the intermolecular mean squared torque  $\langle 0(V)^2 \rangle$  and  $\gamma$  (torque relaxation rate), has been applied by three different methods to the data recorded for a range of concentrations of carbon tetrachloride solutions of acetonitrile across a range of temperatures.

These results have been complemented by those obtained from a 2 parameter model fit to the spectra of a wide range of acetonitrile solutions in carbon tetrachloride, benzene and n-heptane recorded<sup>126</sup> at 298K.

**(i) A Brief Evaluation of Some Models Applied to  $\text{CH}_3\text{CN}/\text{CCl}_4$  Solutions**

Firstly, it must be appreciated that all of the models described fit the very low frequency region equally well. In the region of the Debye feature they predict an exponential decay in the orientational correlation function and cannot be distinguished from each other. Therefore it is necessary to consider the behaviour of the models in the short time region, where the decay is distinctly non-exponential and they can more clearly be discriminated, i.e. it is essential to examine the short time characteristics of the models in order to evaluate their validity for the entire frequency range where re-orientational motion gives rise to absorption.

Figure 6.1 shows a comparison of observed spectra of a 0.018mf solution of  $\text{CH}_3\text{CN}$  in  $\text{CCl}_4$  compared to the spectra predicted by the three models mentioned previously.

The Debye model, on which the others are based, predicts no spectral features above the microwave region and in fact does not even account for the return to transparency which must occur, as these liquids are not opaque in the visible region. Debye was well aware of the limitations imposed by the neglect of inertia in his model, and indicated that it was valid up to frequencies of approximately  $10^{12}$  Hz only.

The addition of inertial effects to the Debye type model as described by Rocard and Powles results in the 'roll off' of the Debye absorption through the far-infrared and beyond the observed Poley feature. This obviously eliminates the paradoxical absorption in the visible region but does not predict the increase in absorption seen in the far-infrared spectrum.

The next model to be considered is that of Gordon, the J. diffusion model. As described previously (Chapter 2), this model is basically an inertia corrected Debye type, where the instantaneous molecular collisions lead to a randomisation of both the direction and magnitude of the

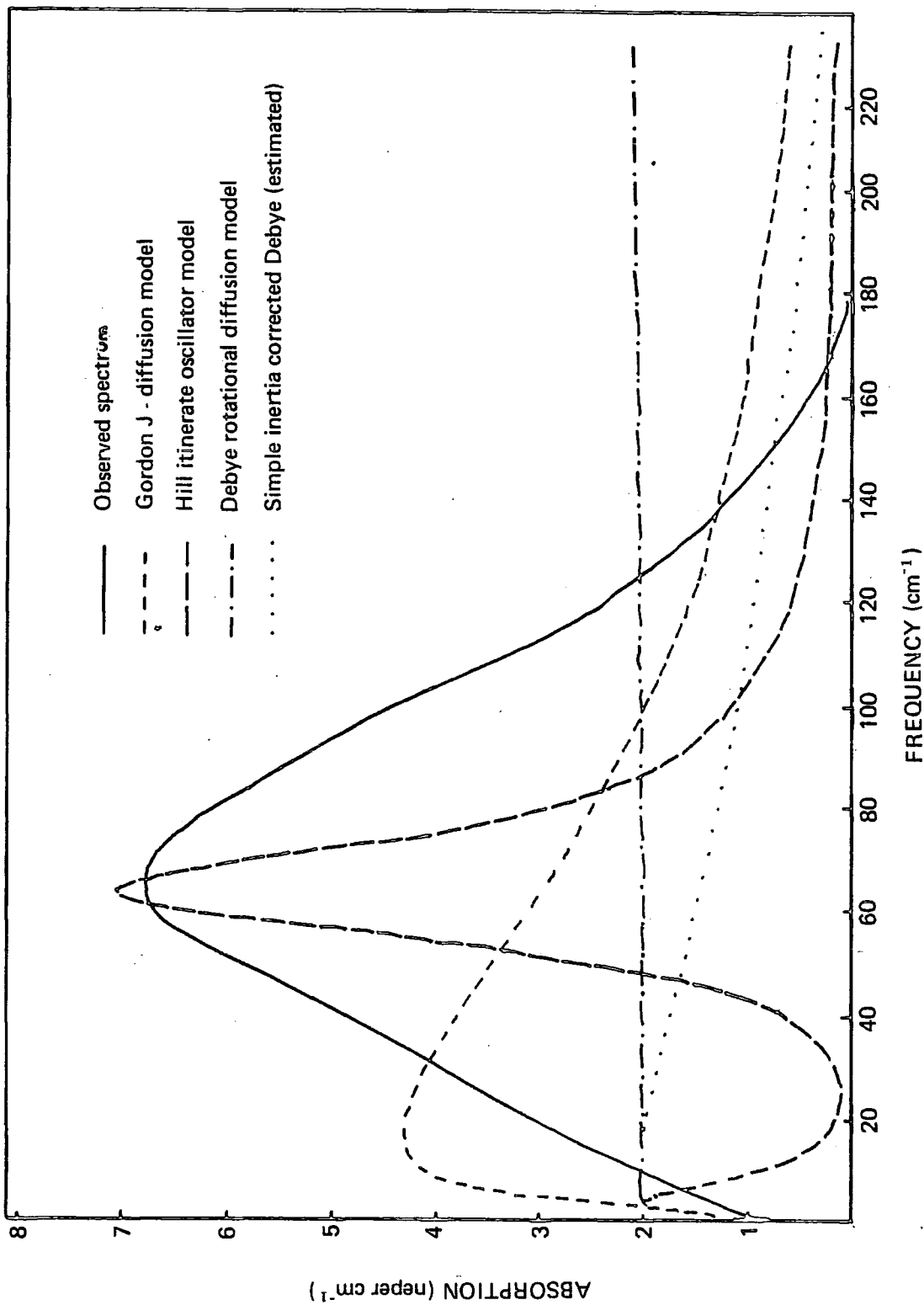


FIGURE 6.1  
 EXAMPLES OF MODEL SPECTRA CALCULATED FOR 0.018mf CH<sub>3</sub>CN/CCl<sub>4</sub> AT 45°C

angular momentum. At very low frequencies this provides a reasonable fit to the observed spectrum (as all of these models do), but moving out into the far-infrared it becomes apparent that the peak of the absorption spectrum is at too low a frequency. In fact, this model predicts a peak frequency centred on the gas phase rotational envelope, and it has been shown<sup>181,182</sup> that it cannot reproduce the absorption in the 'Poley' region unless the collisions are correlated. No allowance is made for the intermolecular torques, which shift the peak frequency to approximately  $70\text{cm}^{-1}$  in this case. The result of the J diffusion model can be summarised as a broadened pure rotational contour ( $J \rightarrow J + 1$ ). This model is also unsatisfactory at shorter times, corresponding to frequencies of  $140\text{cm}^{-1}$  to  $200\text{cm}^{-1}$ . In this region the observed spectral density has decreased almost to zero, whereas the J diffusion model predicts a much slower return to transparency, similar to that seen for the Rocard/Powles model. O'Dell and Berne<sup>183</sup> have established that Gordon's models are unsatisfactory even when applied to the dynamics of rough spheres which meet almost all of the criteria dictated by the hypothesis.

The spectrum calculated from the itinerant oscillator model indicates quite clearly the distinction which this theory makes between the two regions of absorption, microwave and far-infrared (Poley feature). These regions correspond to the model environments directly; the far-infrared part arising from the librational motion of the dipole engaged by its neighbours, and the microwave absorption which results from the rotational diffusion of the entire cage complete with the 'trapped' dipole. It can be seen here, as it has been found in previous studies on highly polar molecules,<sup>24,184,185</sup> that this model produces a far-infrared spectral feature which is much narrower than the observed absorption. It has further been shown,<sup>2</sup> with a model of this type described by Coffey,<sup>24</sup> that even drastic variation of the model parameters does little to improve its far-infrared behaviour.

(ii) **Analysis of the Model Developed by the Solution of a Generalised Rotational Langevin Equation**

a) **Direct Calculation of the Model Parameters**

Initially equations 5.14 and 5.15 have been applied to obtain the model parameters  $K_1(0)$  and  $\gamma$ . This method requires only a knowledge of the position of the peak in the absorption spectrum  $\bar{\nu}_{\text{max}}$ , which are included in Table 5.5, and a value for the rotational 2nd moment  $K_0(0)$  which has been given by

$$K_0(0) = 2kT/I_B$$

The relaxation time  $\tau^{\text{model}}$  has then been calculated from the  $K_1(0)$  value by the approximation given by equation 5.17 rewritten

$$\tau^{\text{model}} = \left( \frac{2K_1(0)}{\pi} \right)^{1/2} / \left( \frac{2kT}{I_B} \right) \quad \dots\dots\dots 6.1$$

The results of this analysis are given in Table 6.1 following.

Temperature (K)	Concentration (mole fraction)	$K_1(0) \times 10^{-25}$ (s <sup>-2</sup> )	$1/\gamma \times 10^{+14}$ (s)	$\tau_{\text{model}}$ (ps)
252	0.018	91.49	2.64	3.2
252	0.061	107.29	2.43	3.4
288	0.018	80.99	2.80	2.6
288	0.061	83.46	2.76	2.7
318	0.018	66.60	3.10	2.1
318	0.061	75.74	2.90	2.3
318	0.162	92.90	2.62	2.5
318	0.370	100.74	2.51	2.6
343	0.018	55.44	3.39	1.8
338	0.061	64.05	3.15	2.0

**TABLE 6.1**  
**MODEL PARAMETERS OBTAINED BY DIRECT CALCULATION**  
**USING EQUATIONS 5.14 AND 5.15**

The parameters obtained by this calculation have then been used as described in Chapter 5 to recalculate the spectral profiles. Two examples of the spectra obtained compared to the observed features are shown in Figures 6.2 and 6.3. The Poley region is not very well described by the model at all when operated in this way. There is a slight increase in absorption level corresponding in frequency to the centre of the Poley band, but overall the result does not describe the far-infrared region much better than an inertially corrected Debye model, merely ensuring a return to transparency at high frequency. However the high frequency 'roll off' is more rapid than that seen with some models (Rocard for example) which is in line with the observed feature and reflects the fact that the models are describing a different underlying mechanism.

The calculated parameters  $K_1(0)$ ,  $\gamma$  and  $\tau$  all increase with concentration and decrease with temperature which is similar (except for  $1/\gamma$  with temperature) to the trends observed in the fitted model results which are discussed in the next section.

**b) The Application of the Model Fitting Procedure with Two Variable Parameters  $K_1(0)$  and  $\gamma$**

The least squares fitting routine described in Chapter 5 has been employed here to fit the model embodied in equations 5.6 and 5.13 to the observed spectra. The variable parameters  $K_1(0)$  and  $\gamma$  are related to the intermolecular mean squared torque, magnitude (via equations 5.7 - 5.9) and relaxation rate respectively. The number of points fitted in each case varied from 170-210. In all cases the initial values of  $\gamma$  and  $K_1(0)$  were set to 5.00 and 20.00 (weighted by  $2kT/l_B$ ).

The other parameters required for the fitting procedure were as follows

- (i) The dispersion ( $\epsilon_0 - \epsilon_\infty$ ). This value was obtained from the observed parameters given in Table 5.4.

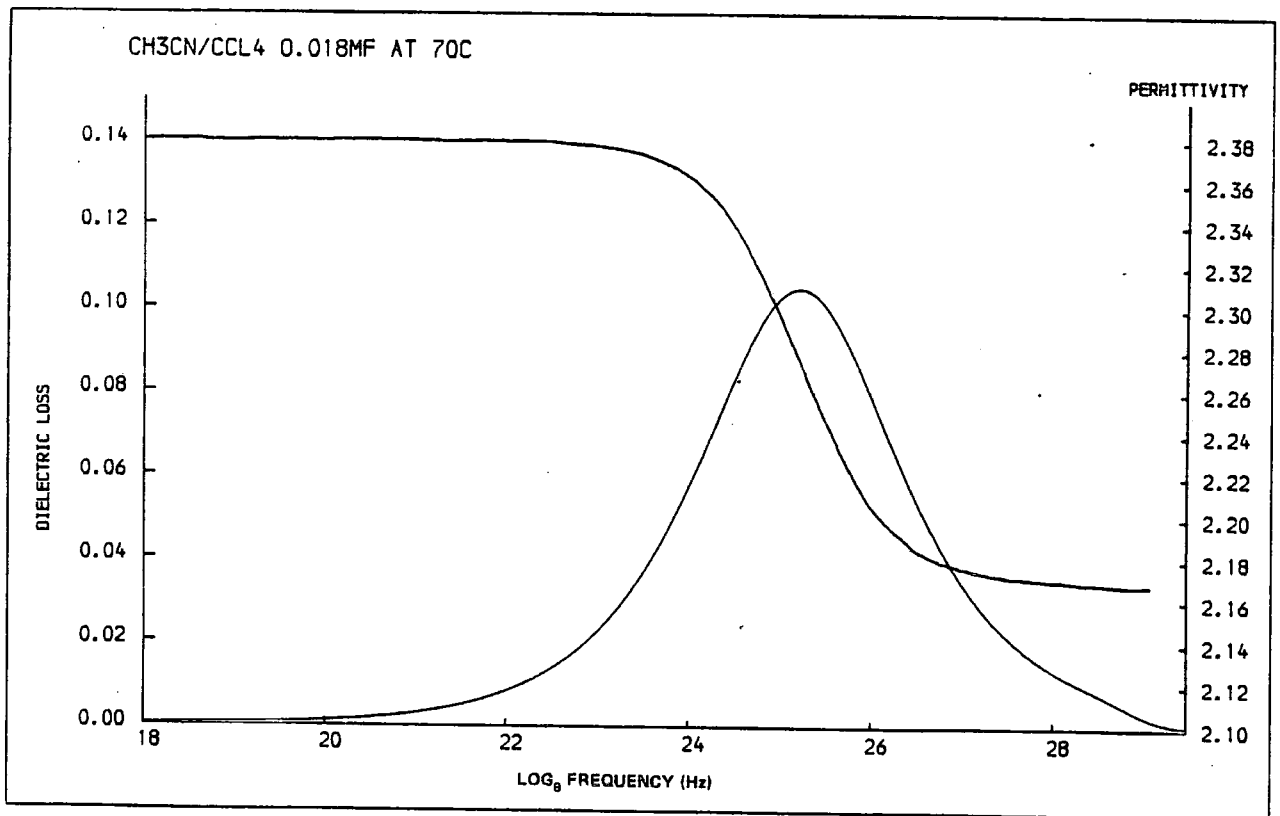
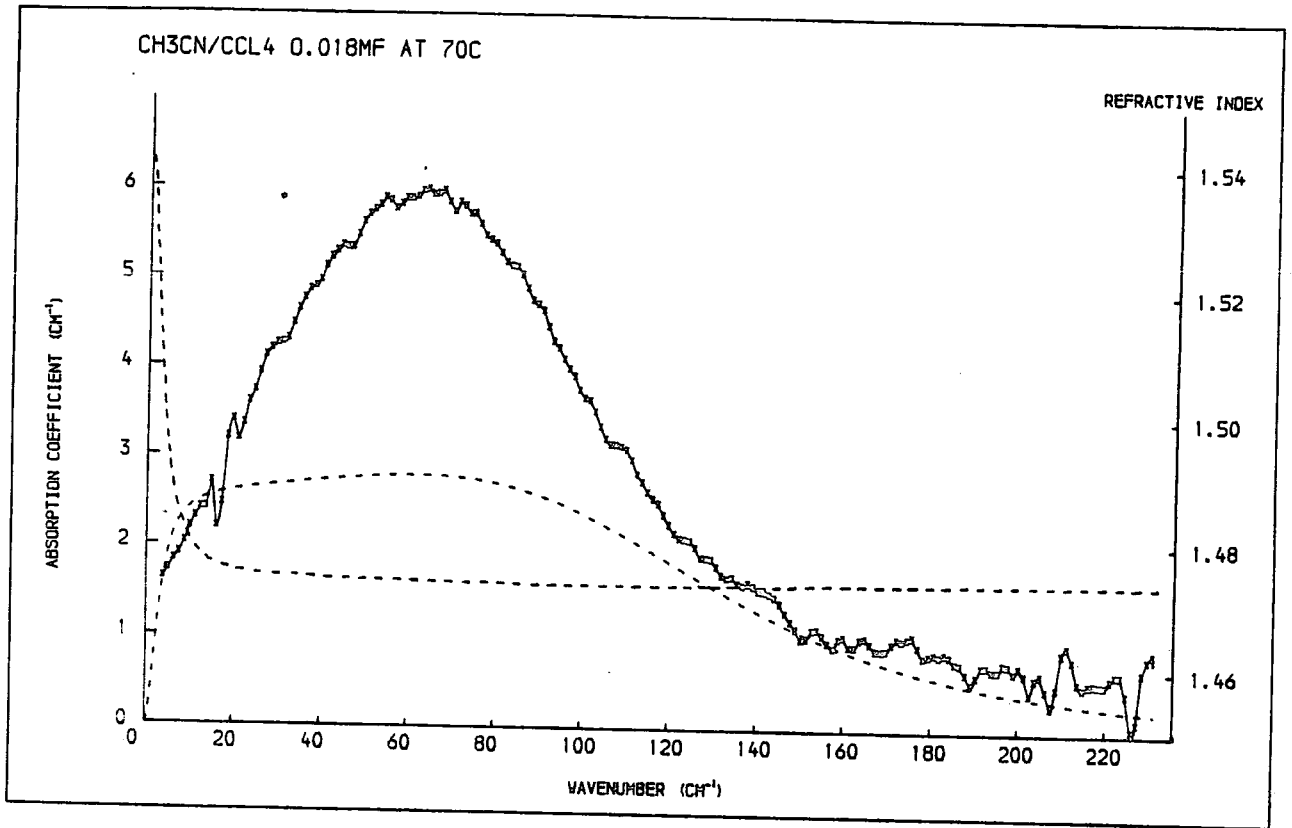


**FIGURE 6.2**  
**SPECTRA RECALCULATED FROM THE MODEL PARAMETERS OBTAINED BY**  
**DIRECT CALCULATION (EQUATIONS 5.14 AND 5.15)**

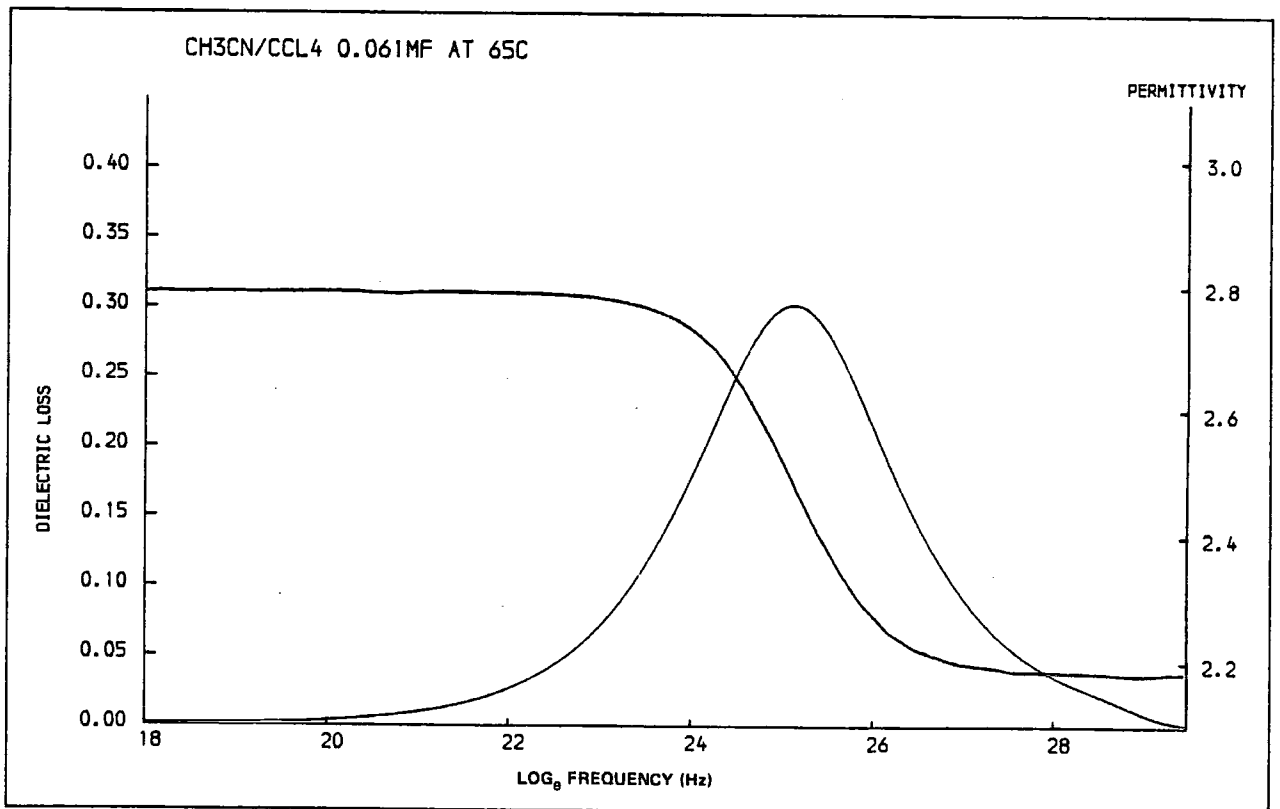
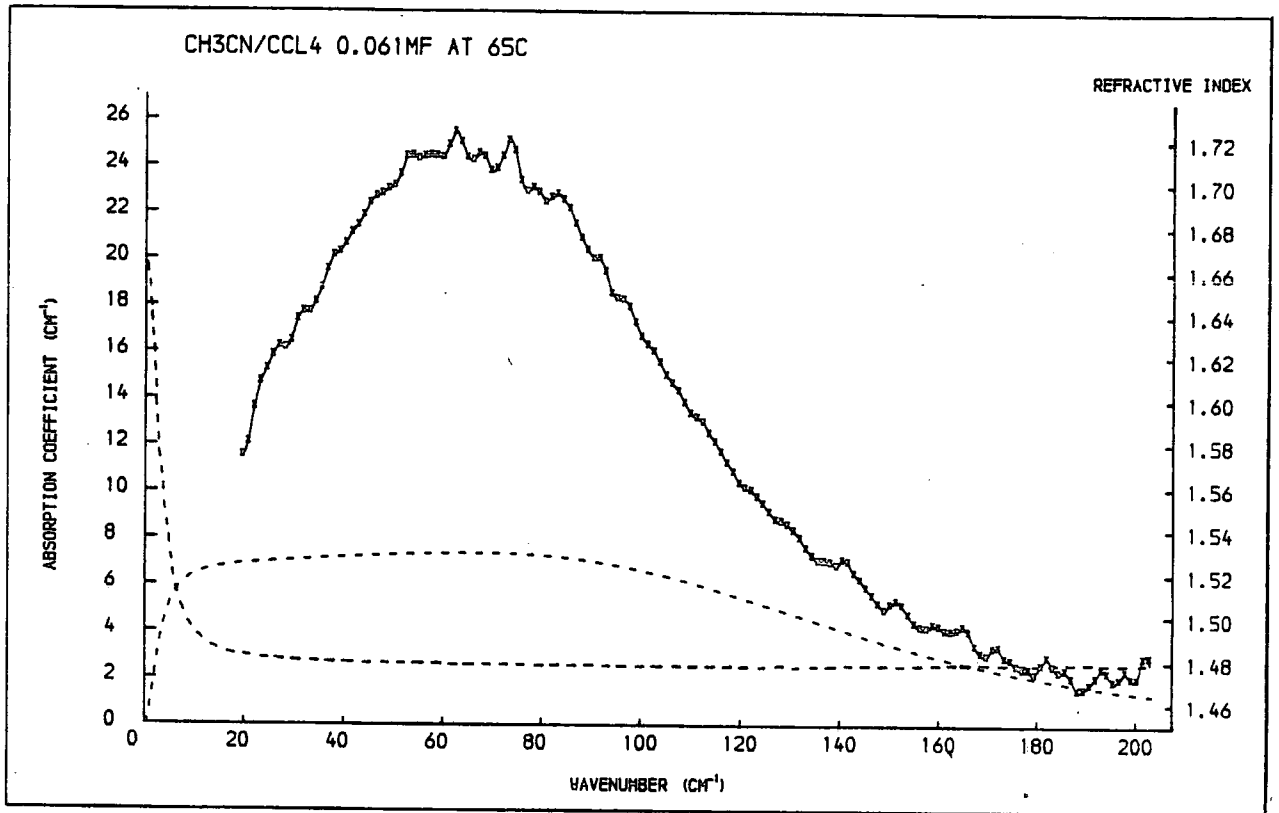


**FIGURE 6.3**  
**SPECTRA RECALCULATED FROM THE MODEL PARAMETERS OBTAINED**  
**BY DIRECT CALCULATION (EQUATIONS 5.14 AND 5.15)**

(ii) The rotational second moment ( $K_0(0)$ ). This value was calculated from the usual relation  $2kT/I_B = K_0(0)$

where  $I_B$  = the moment of inertia about the principle axis

$k$  = Boltzmann's constant

$T$  = temperature (K)

The solutions studied by the dispersive technique (Chapter 4) have been characterised with their refractive index spectra in addition to their absorption spectra. The fitting routine has been applied to these by two methods. Initially the fit has been performed with a refractive index calculated by a Kramers-Kronig relation in a similar manner to the earlier work in this field<sup>1</sup> and with the other solutions. Secondly, the spectra have been fitted to equation 5.6 which includes the variable (observed) refractive index. Comparisons between fitting by the two different methods show very little difference, but the quality of the fit obtained can also be judged against the observed refractive index and the calculated (observed) loss curve in addition to the absorption spectra.

The parameters obtained from the best fit to the equations describing the model are given in Table 6.2 and 6.3 which also include the recalculated spectra details. Some examples of the spectra which have been recalculated from these parameters covering a range of temperatures, concentrations and solvents are shown in Figures 6.4 - 6.13. In these examples the full lines are the observed spectra, the x's denote the points fitted and the broken lines are the recalculated spectra.

The results have been analysed in terms of the quality of model fit as this assessment is required before comments on the values of  $K_1(0)$  and  $1/\gamma$  can be made. Inspection and comparison of the recalculated absorption spectra with the observed spectra indicate quite clearly the improvement that this model exhibits over some of the alternatives described previously. The agreement in the low frequency region is good while at higher frequencies the predicted intensity falls lower than the observed value in all cases, and the absorption peak  $\bar{\nu}_{\max}$  lies to a slightly higher frequency. The integrated intensities of the recalculated spectra of the 0.061mf solution remain fairly constant with temperature, although the 0.018mf solutions do show a slight increase in intensity over the entire temperature range which is not seen in the observed spectra. In the case of the 0.018mf solutions the recalculated half band widths  $\Delta\bar{\nu}_{1/2}$  ( $\text{cm}^{-1}$ ) exhibit a trend similar to that seen in the observed spectra with temperature (i.e. an increase). This is not clear in the more concentrated solutions although the overall change is a similar increase in  $\Delta\bar{\nu}_{1/2}$ .

The slight decrease in  $a_{\max}$  values of the 0.018mf solutions with temperature which occurs in the observed spectra is not reflected in the recalculated  $a_{\max}$  values, which accounts for the slight increase in total intensity for these spectra. The 0.061mf recalculated spectra do exhibit the observed pattern overall, which when considered with the overall trend in  $\Delta\bar{\nu}_{1/2}$  accounts for the reasonably constant total intensities with temperature.

Over the small concentration range at 318K the recalculated  $\Delta\bar{\nu}_{1/2}$  show an increase overall which is in line with the observed data. This is accompanied by a slight overall increase in total intensity per molecule which is not apparent in the observed data. This is a result of the  $a_{\max}$

Temperature (K)	Concentration (mf)	Equation <sup>a</sup>	Fitted Parameters			Recalculated Spectra Details			
			$1/\gamma \times 10^{14}$ (s)	$K_{\eta}(0) \times 10^{-25}$ (s <sup>-2</sup> )	$\delta_{\max}$ (cm <sup>-1</sup> ) ±1cm <sup>-1</sup>	$\Delta\bar{\nu}/2$ (cm <sup>-1</sup> ) ±1cm <sup>-1</sup>	Intensity (cm mol <sup>-1</sup> ) ±5%	$\alpha_{\max}$ (neper cm <sup>-1</sup> mol <sup>-1</sup> ) ±1%	
252	0.018	1	13.38	24.92	81	41	1537	27.9	
252	0.061	1	12.89	27.56	85	43	1620	28.0	
288	0.018	1	11.47	22.84	76	49	1794	28.5	
288	0.018	2	11.58	22.76	—	—	—	—	
288	0.061	1	10.99	25.04	78	52	1880	28.9	
288	0.061	2	12.02	24.20	—	—	—	—	
318	0.018	1	9.70	21.54	70	62	1932	27.9 *	
318	0.018	2	9.26	22.60	71	57	1961	26.6 *	
318	0.061	1	11.17	22.11	—	—	—	—	
318	0.061	2	11.23	22.15	74	50	1595	25.9	
318	0.162	1	9.44	26.84	—	—	—	—	
318	0.370	1	7.79	32.77	80	63	1902	25.9	
343	0.018	1	8.38	23.17	86	77	2396	27.9	
338	0.061	1	9.66	22.50	70	78	2079	26.9	
					67	79	2060	27.4 *	
					72	62	1739		

\* As for Table 5.5.

<sup>a</sup>

1 Refers to Equation 5.13 with observed  $\alpha(\bar{\nu})$  and calculated  $\eta(\bar{\nu})$ .

2 Refers to Equation 5.6 with observed  $\alpha(\bar{\nu})$  and  $\eta(\bar{\nu})$ .

TABLE 6.2

RESULTS OF MODEL FITTING WITH 2 VARIABLE PARAMETERS TO CH<sub>3</sub>CN/CCL<sub>4</sub> SOLUTIONS AT VARIOUS TEMPERATURES

Concentration (mf)	Solvent	Fitted Parameters			Recalculated Spectra Details			
		$1/\gamma \times 10^{14}$ (s)	$K_1(0) \times 10^{-25}$ (s <sup>-2</sup> )	$\bar{\nu}_{\max}$ (cm <sup>-1</sup> ) ±1cm <sup>-1</sup>	$\frac{1}{2} \Delta \bar{\nu}$ (cm <sup>-1</sup> ) ±1cm <sup>-1</sup>	Intensity (cm mol <sup>-1</sup> ) ±5%	$\alpha_{\max}$ (neper cm <sup>-1</sup> mol <sup>-1</sup> ) ±1%	
0.01	CCl <sub>4</sub>	10.68	23.47	75	52	2080	31.3	
0.016	CCl <sub>4</sub>	10.16	24.03	76	56	2226	32.3	
0.06	CCl <sub>4</sub>	11.11	24.78	77	51	1896	29.1	
0.10	CCl <sub>4</sub>	9.61	24.69	76	60	2379	33.2	
0.16	CCl <sub>4</sub>	11.46	26.81	82	49	1780	28.5	
0.20	CCl <sub>4</sub>	11.53	27.05	83	48	1839	29.2	
0.30	CCl <sub>4</sub>	9.63	30.20	86	58	2240	30.5	
0.40	CCl <sub>4</sub>	9.98	30.79	87	50	2145	30.4	
0.50	CCl <sub>4</sub>	11.01	30.84	89	50	1824	27.7	
0.70	CCl <sub>4</sub>	8.18	35.80	94	68	2578	31.8	
1.0	—	7.64	36.15	95	72	2730	31.9	
0.016	Benzene	8.97	27.00	78	68	2257	29.1	
0.06	Benzene	9.40	26.65	78	63	2029	27.3	
0.16	Benzene	9.81	27.69	82	59	2019	27.6	
0.027	n.Heptane	8.22	16.16	52	74	2057	28.6	

TABLE 6.3  
RESULTS OF MODEL FITTING WITH 2 VARIABLE PARAMETERS TO VARIOUS CH<sub>3</sub>CN SOLUTIONS AT 298K

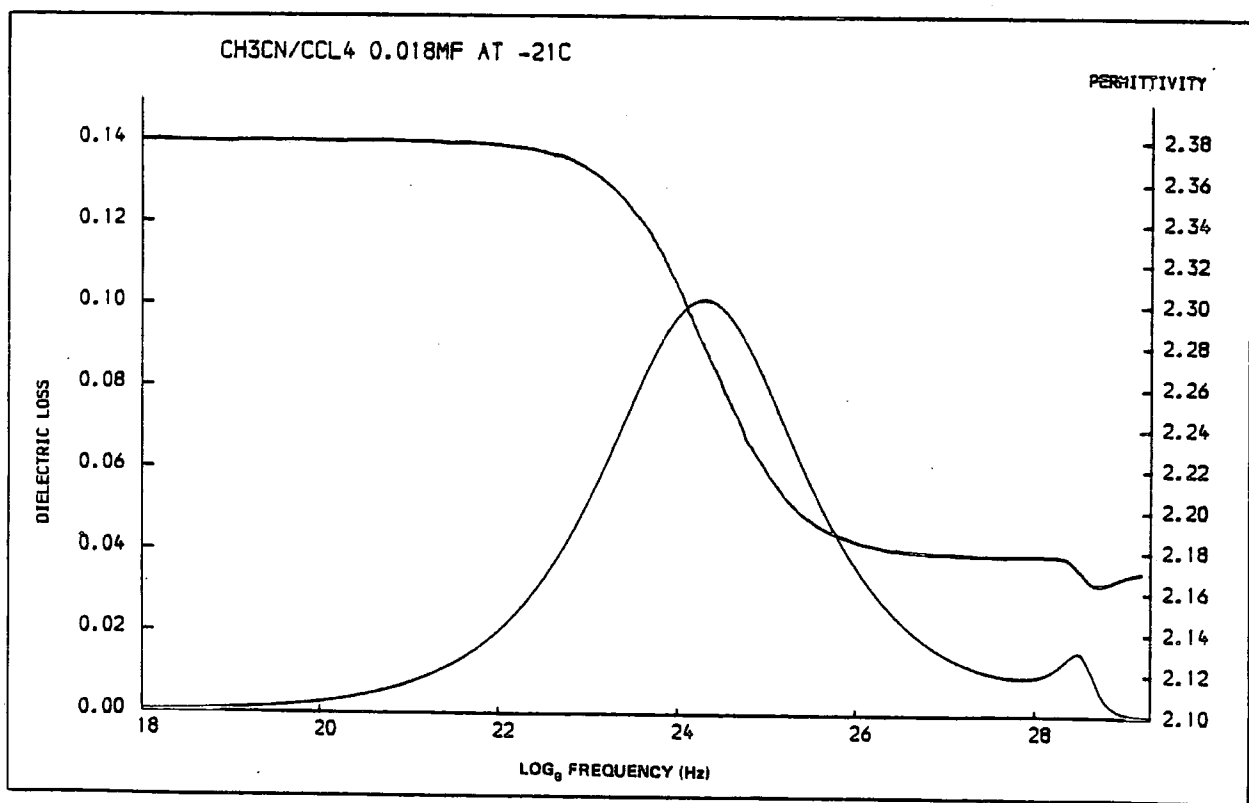
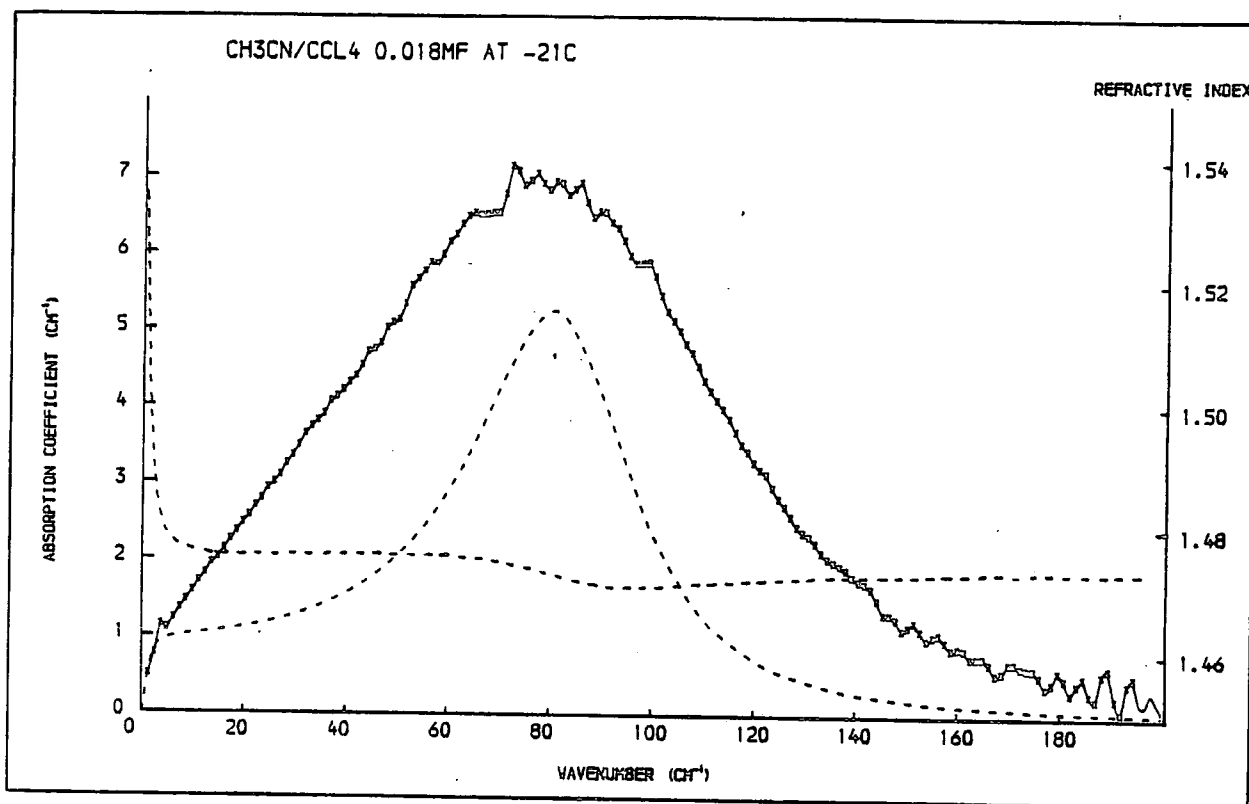


FIGURE 6.4  
 RECALCULATED SPECTRA FROM A TWO PARAMETER MODEL FIT

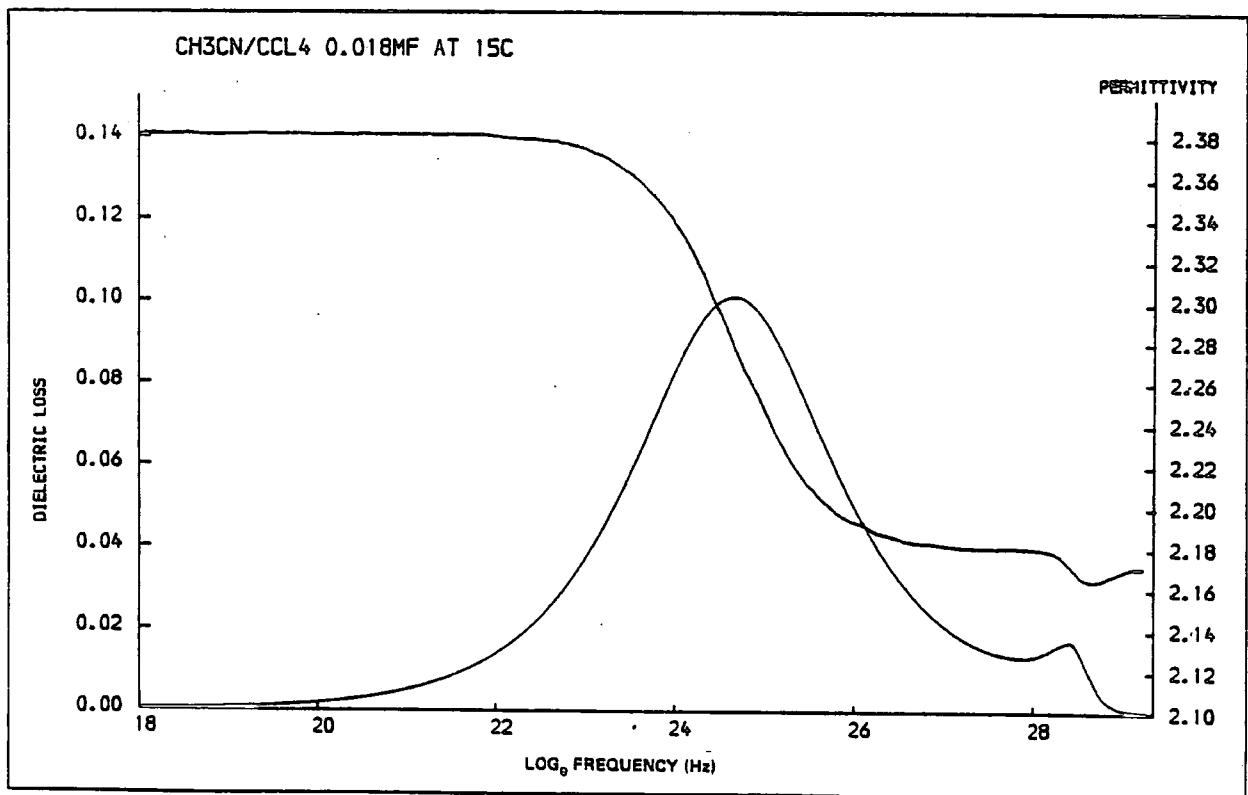
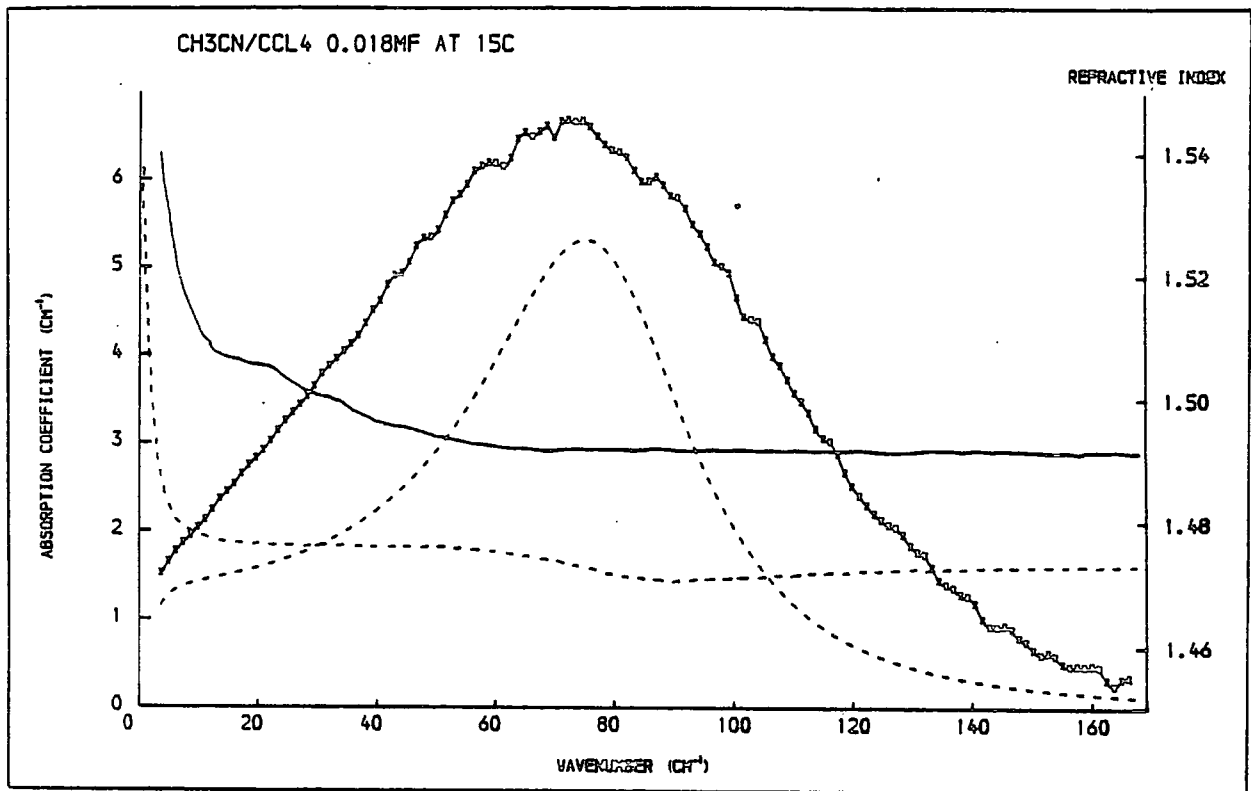


FIGURE 6.5  
SPECTRA RECALCULATED FROM A TWO PARAMETER MODEL FIT

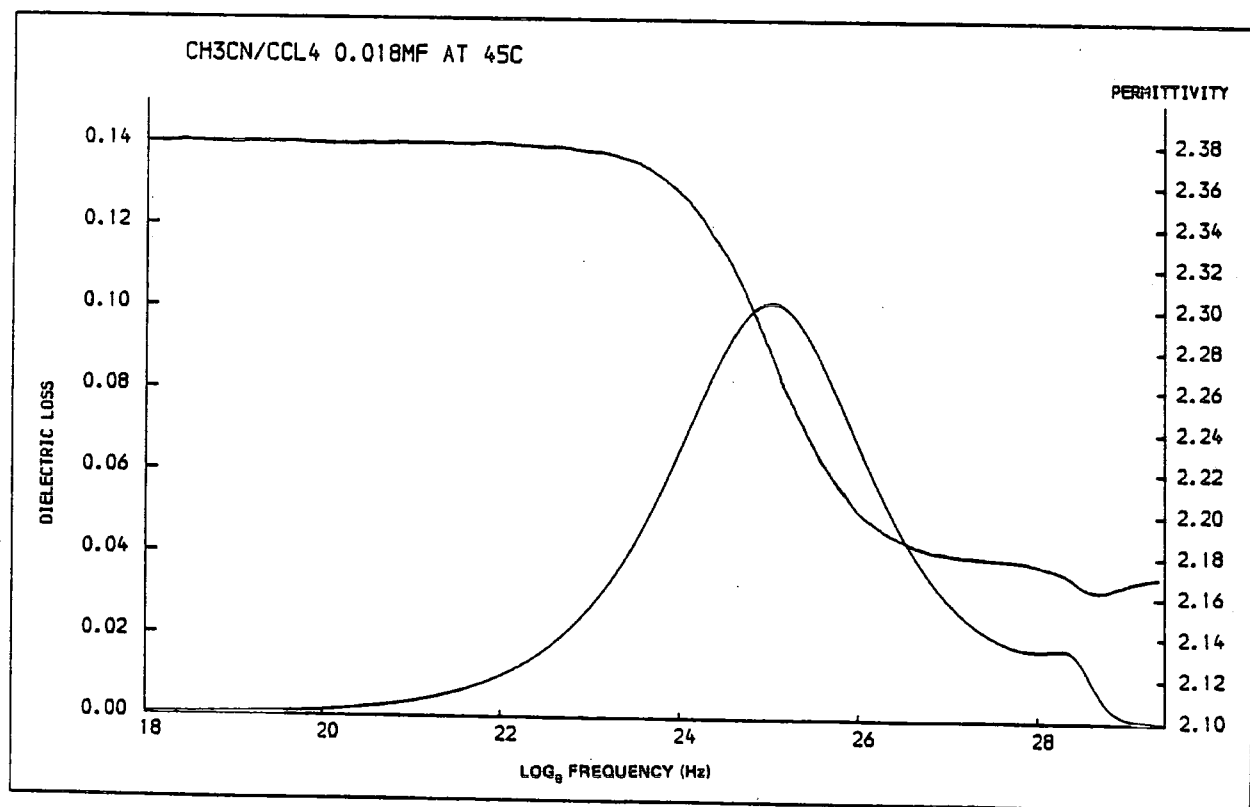
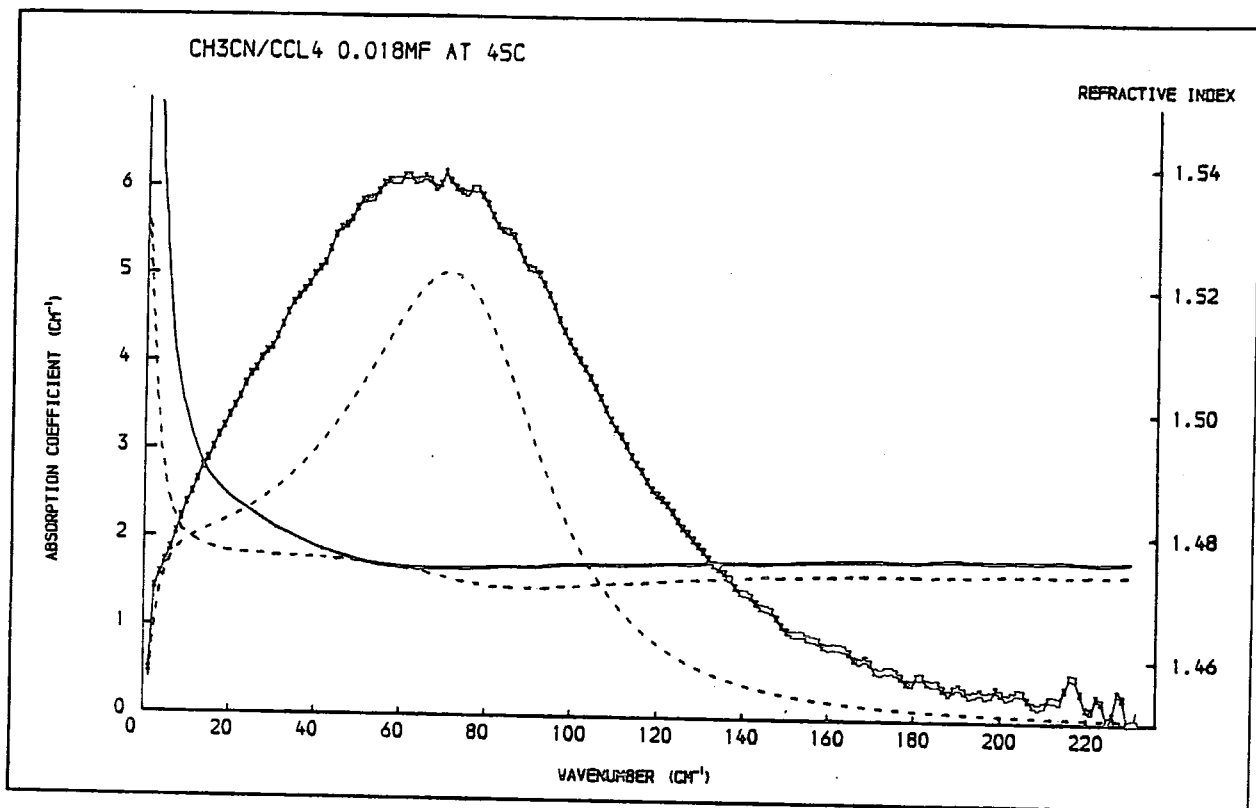
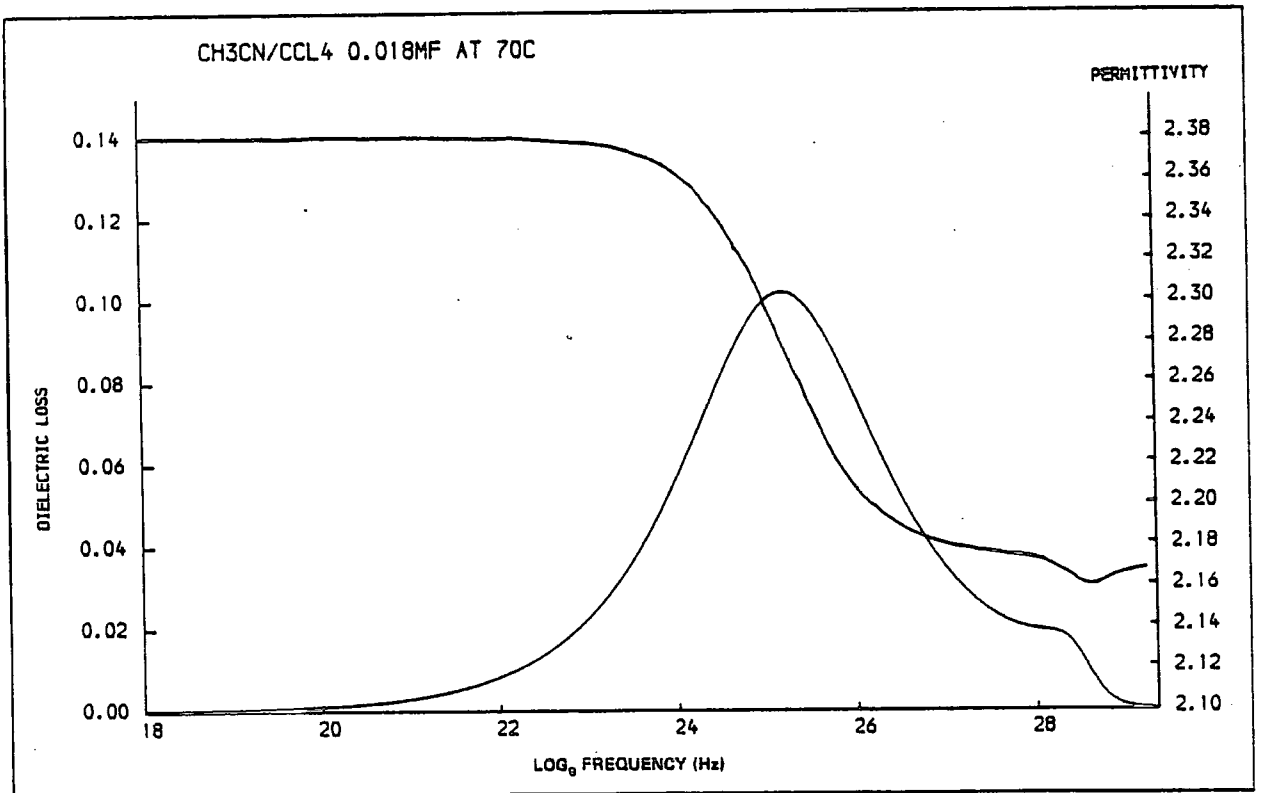
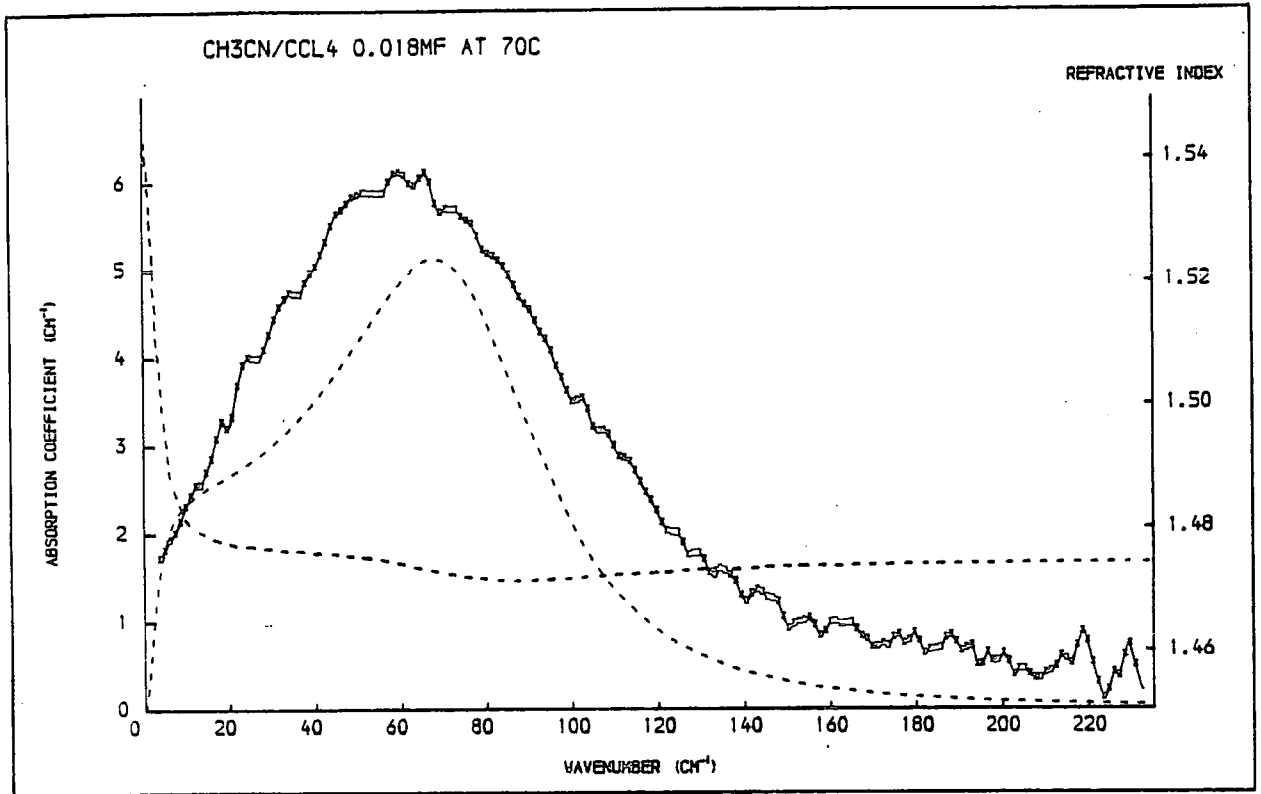


FIGURE 6.6  
 RECALCULATED SPECTRA FROM A TWO PARAMETER MODEL FIT



**FIGURE 6.7**  
**SPECTRA RECALCULATED FROM A TWO PARAMETER MODEL FIT**

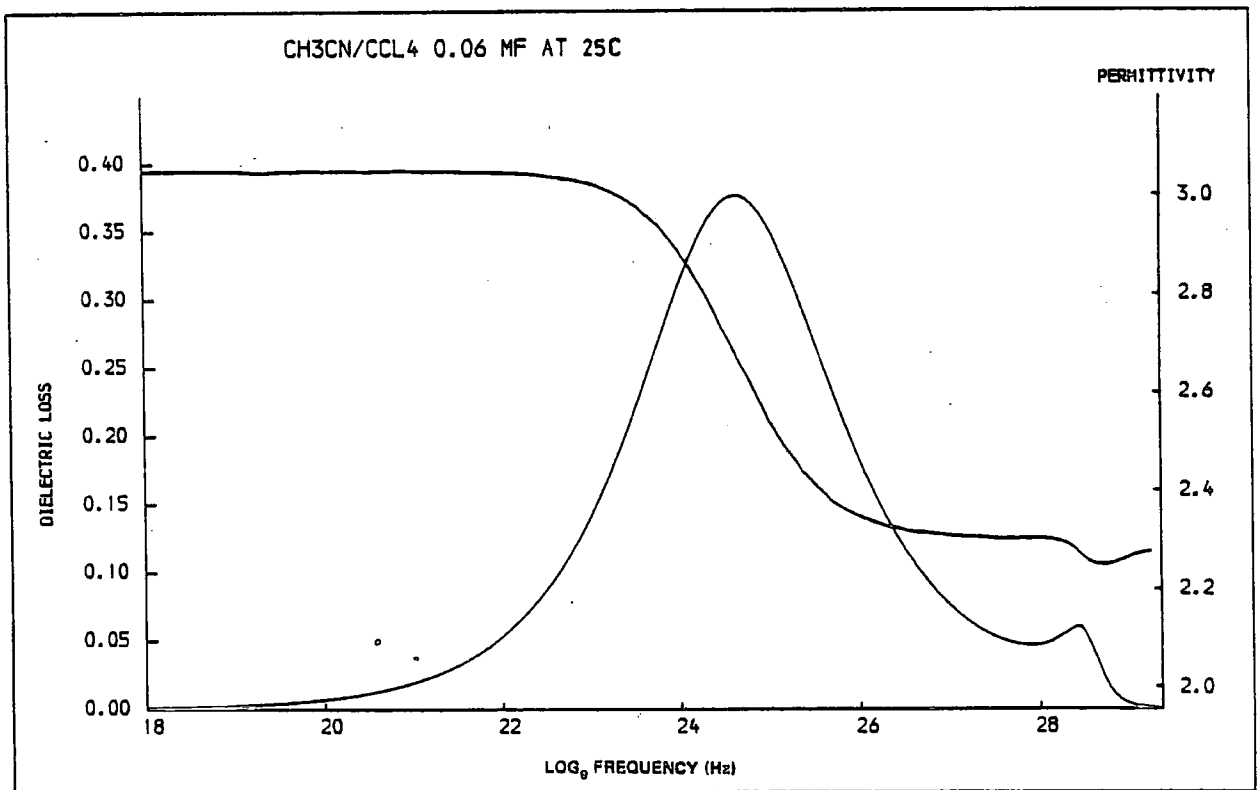
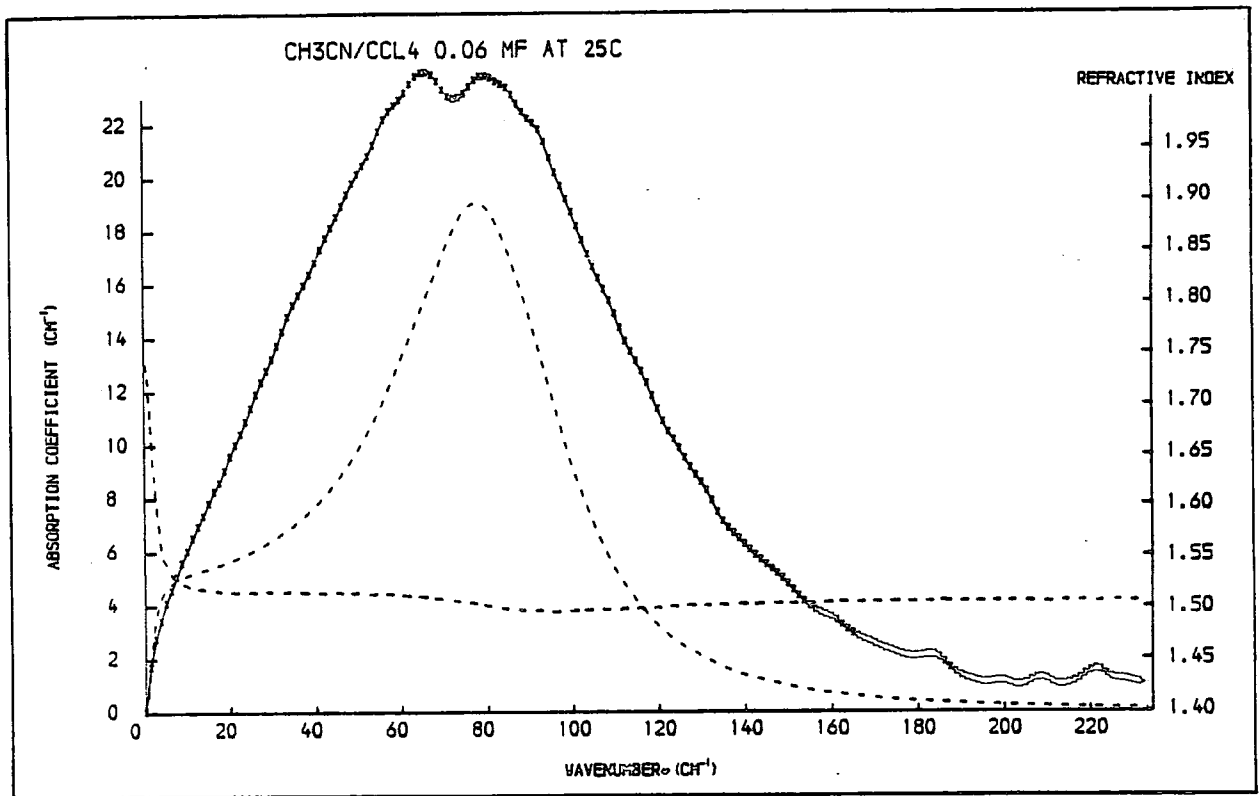
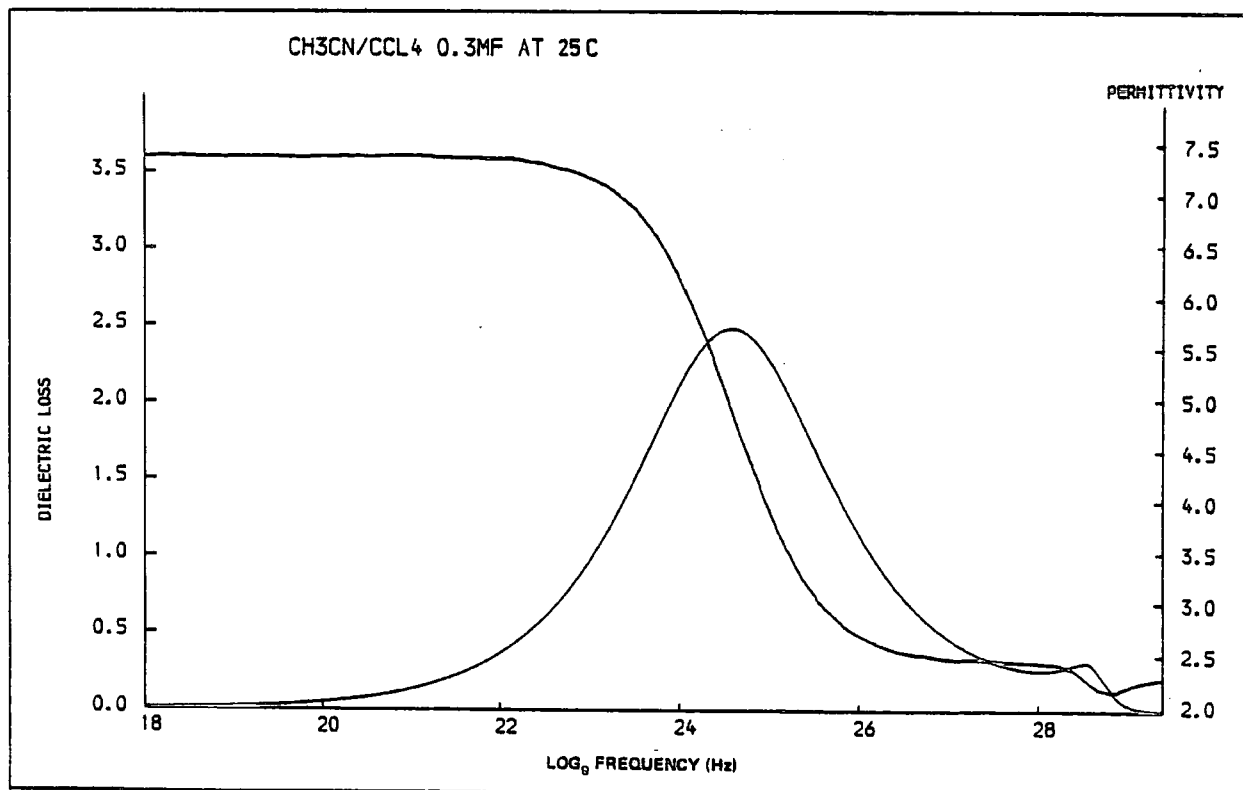
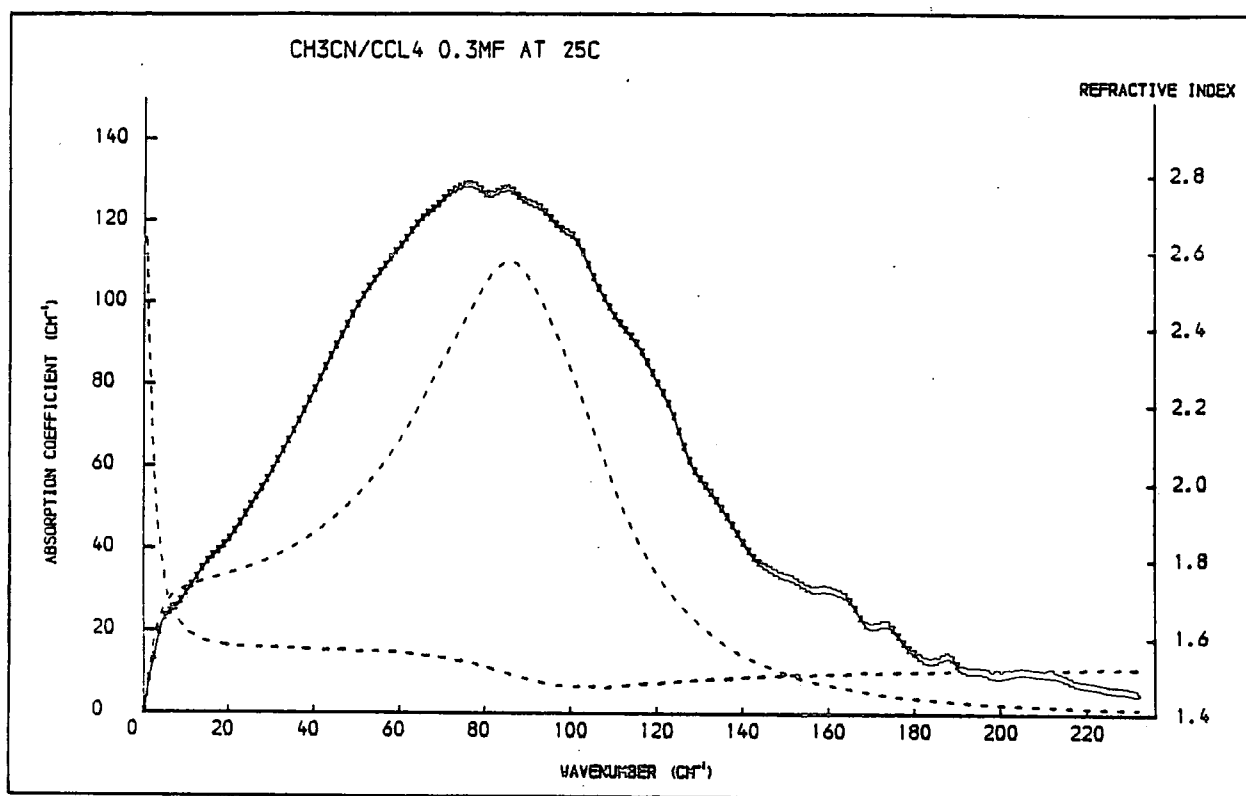
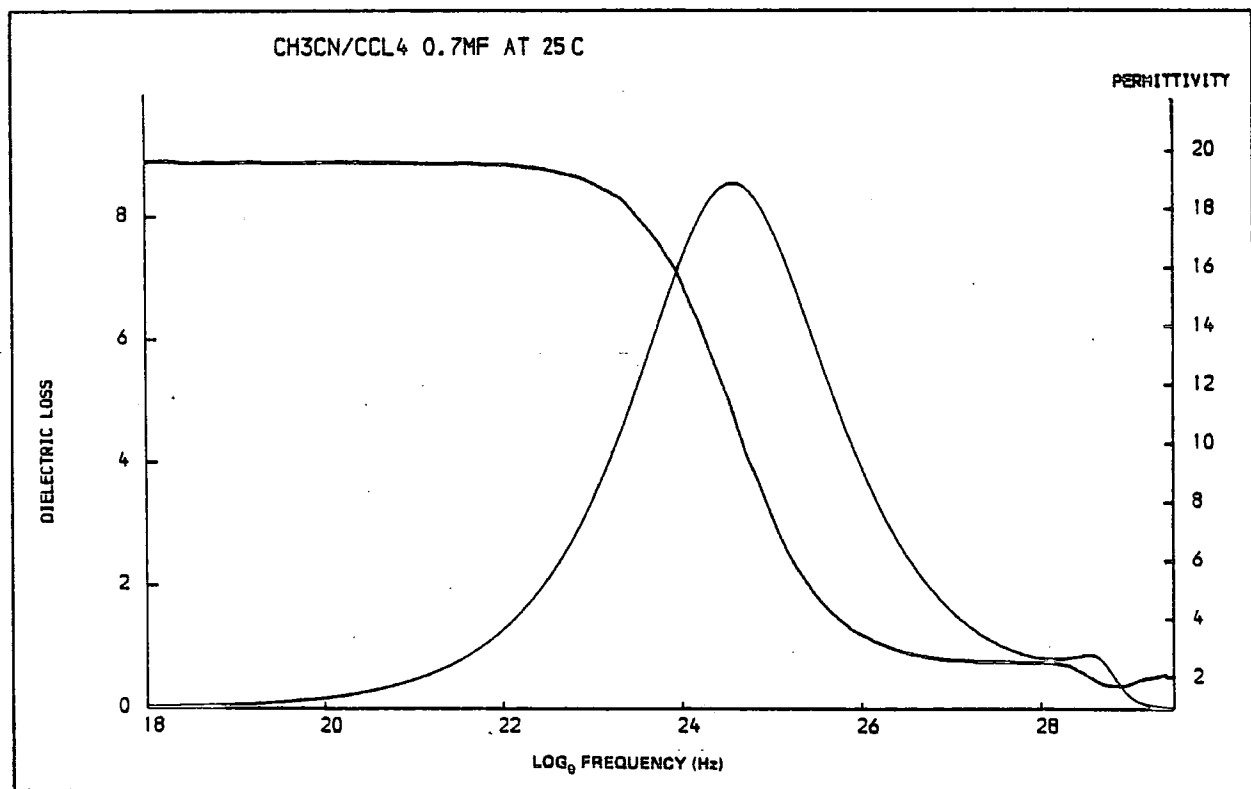
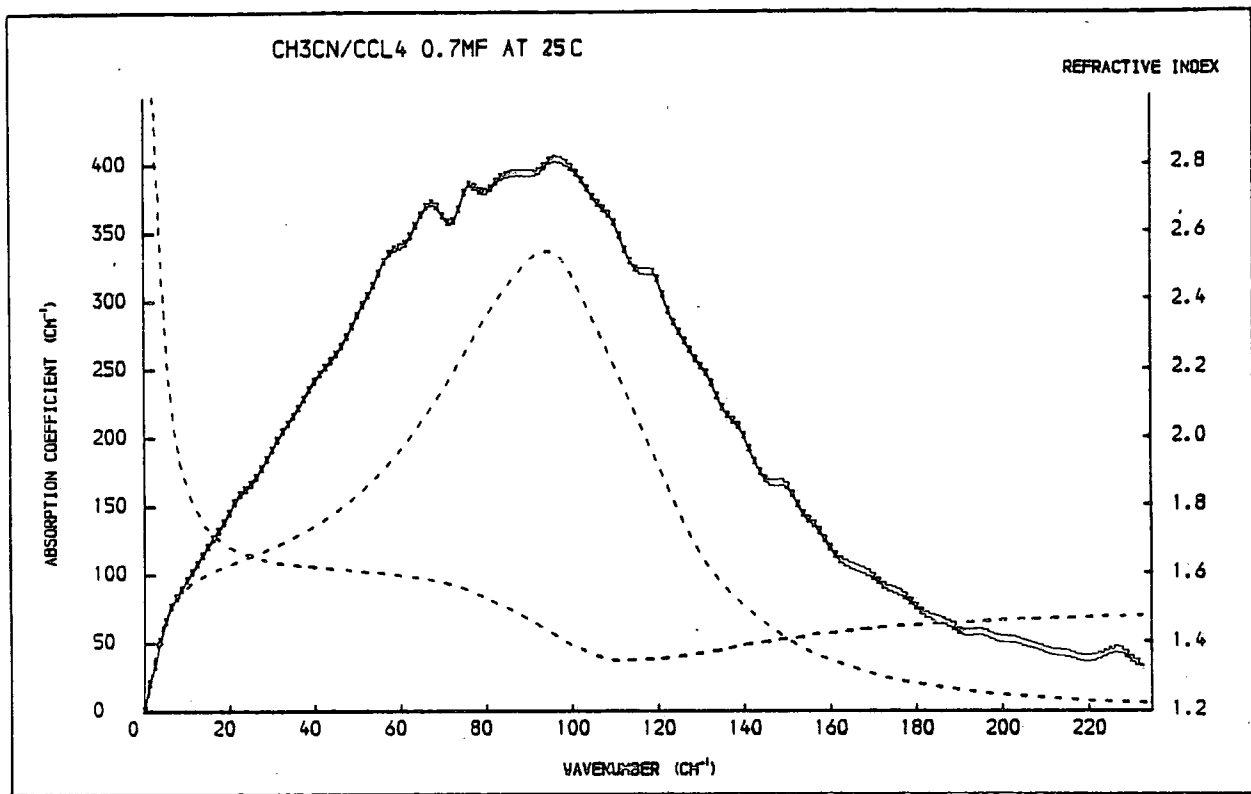


FIGURE 6.8  
SPECTRA RECALCULATED FROM A TWO PARAMETER MODEL FIT



**FIGURE 6.9**  
SPECTRA RECALCULATED FROM A TWO PARAMETER MODEL FIT



**FIGURE 6.10**  
**SPECTRA RECALCULATED FROM A TWO PARAMETER MODEL FIT**

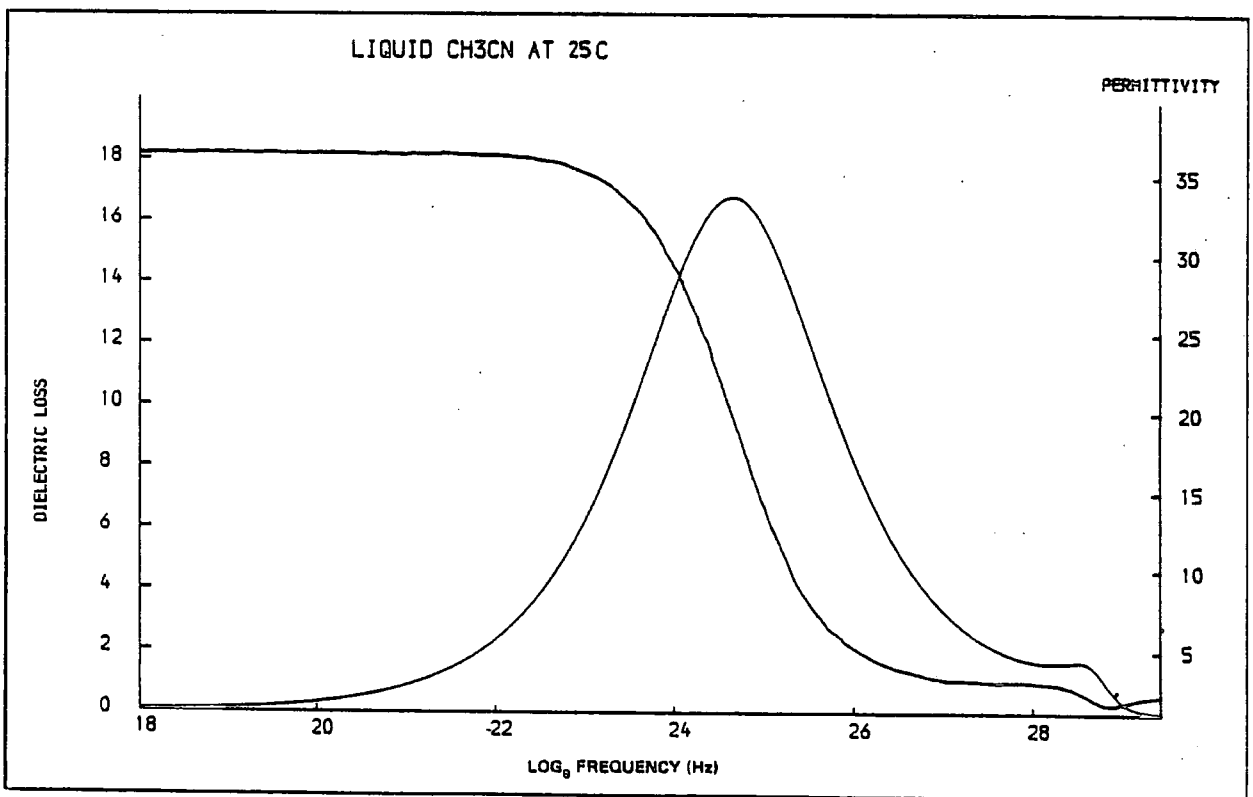
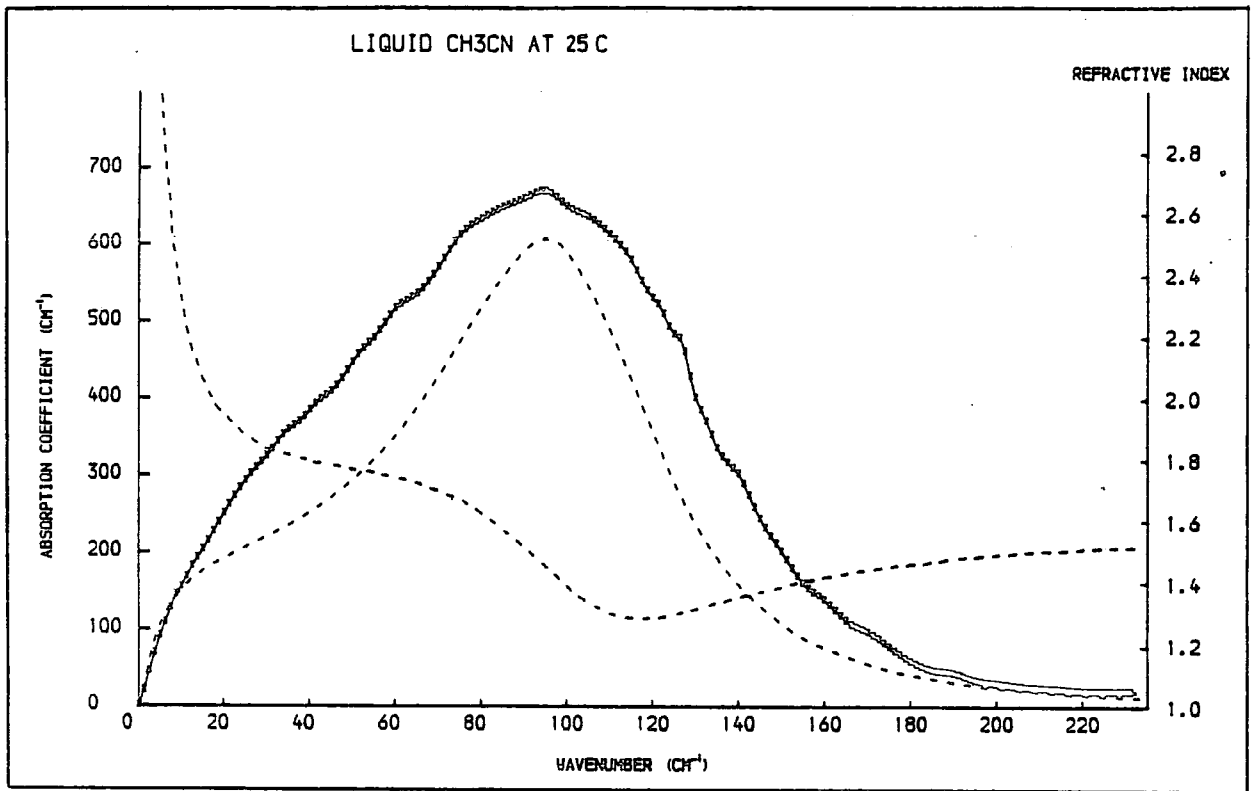


**FIGURE 6.11**  
**SPECTRA RECALCULATED FROM A TWO PARAMETER MODEL FIT**

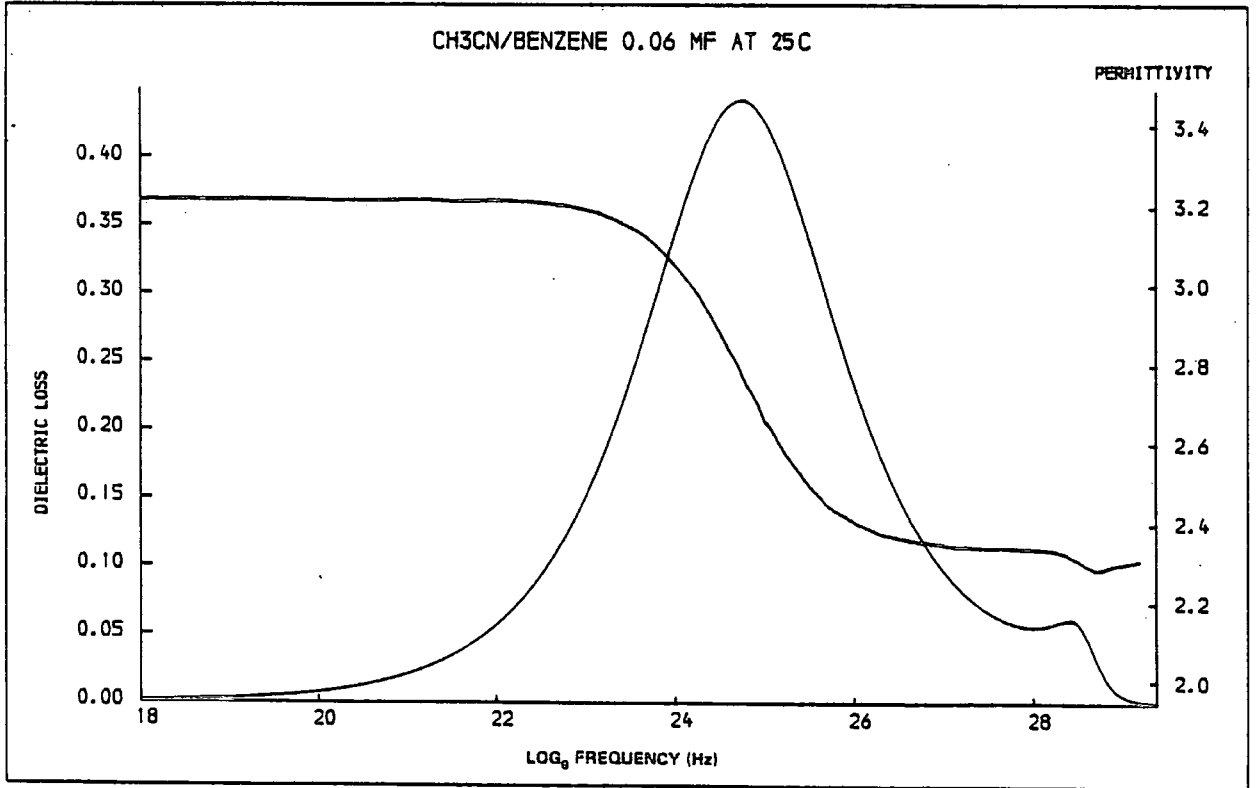
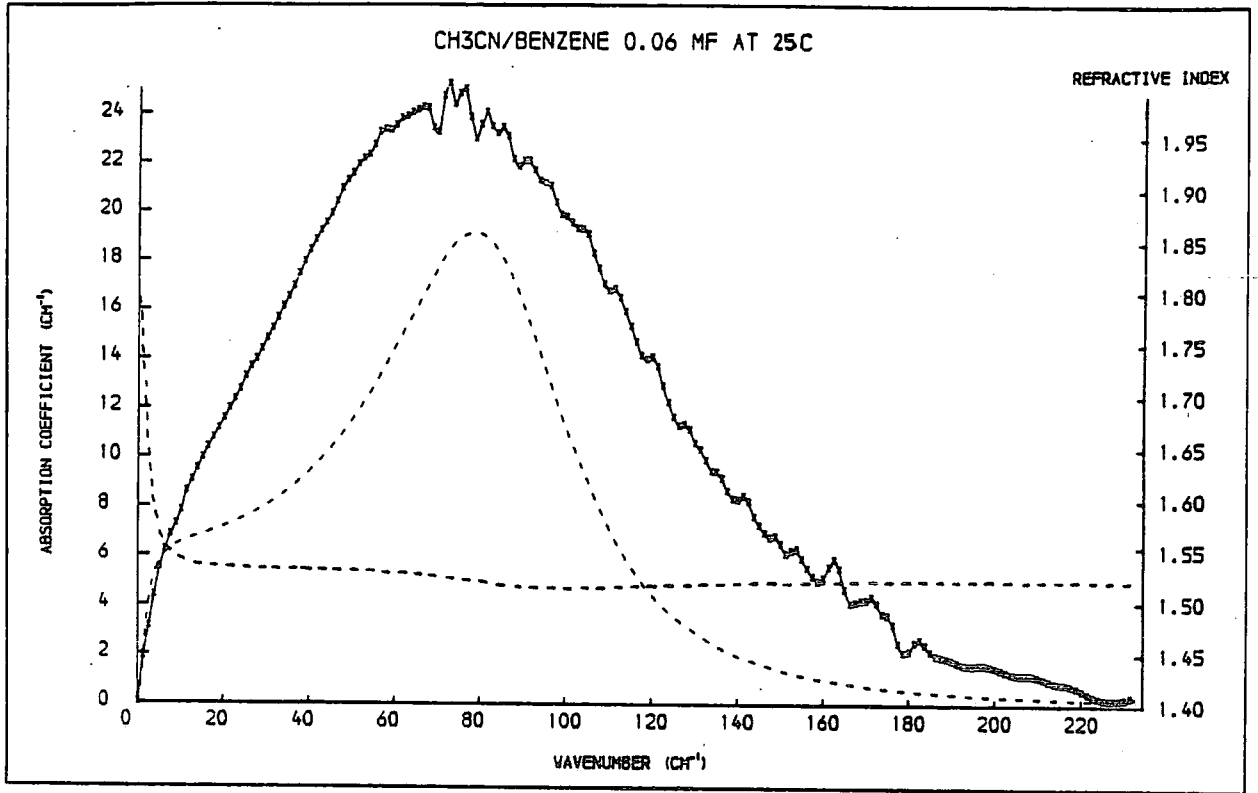


**FIGURE 6.12**  
SPECTRA RECALCULATED FROM A TWO PARAMETER MODEL FIT

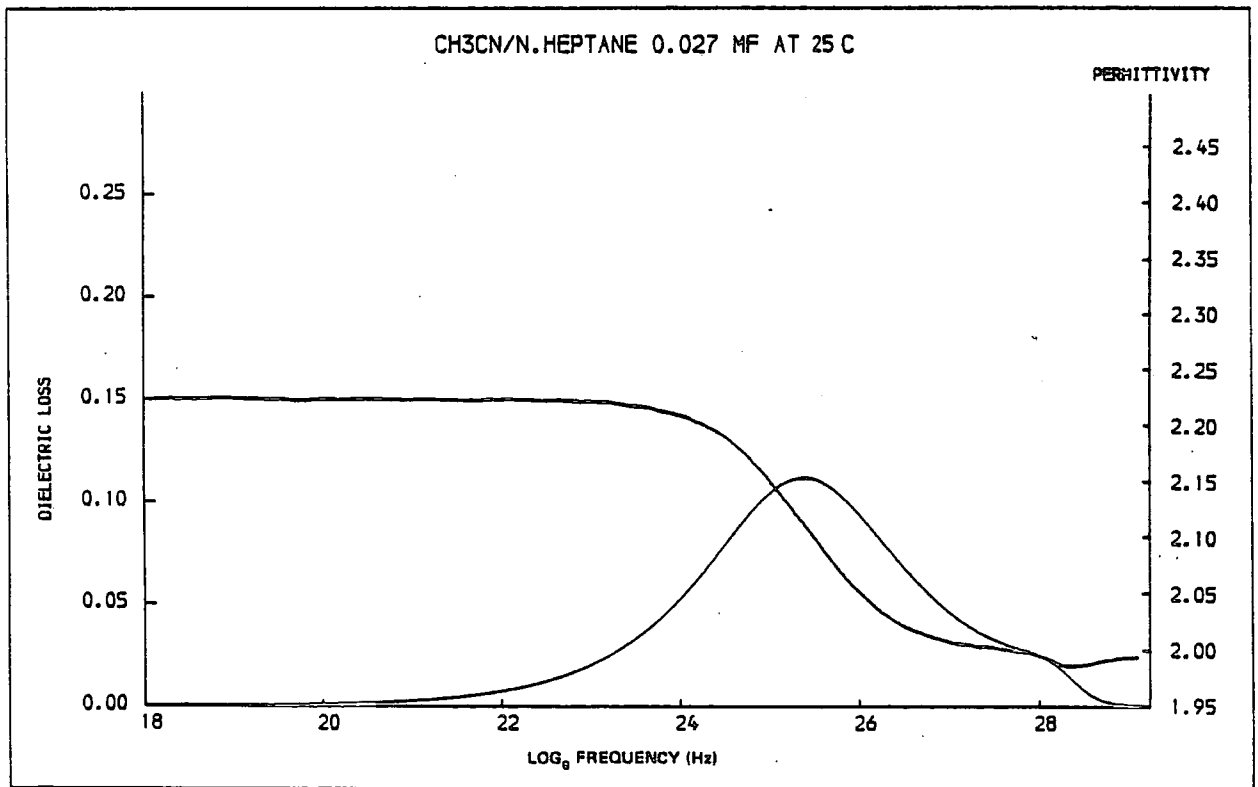
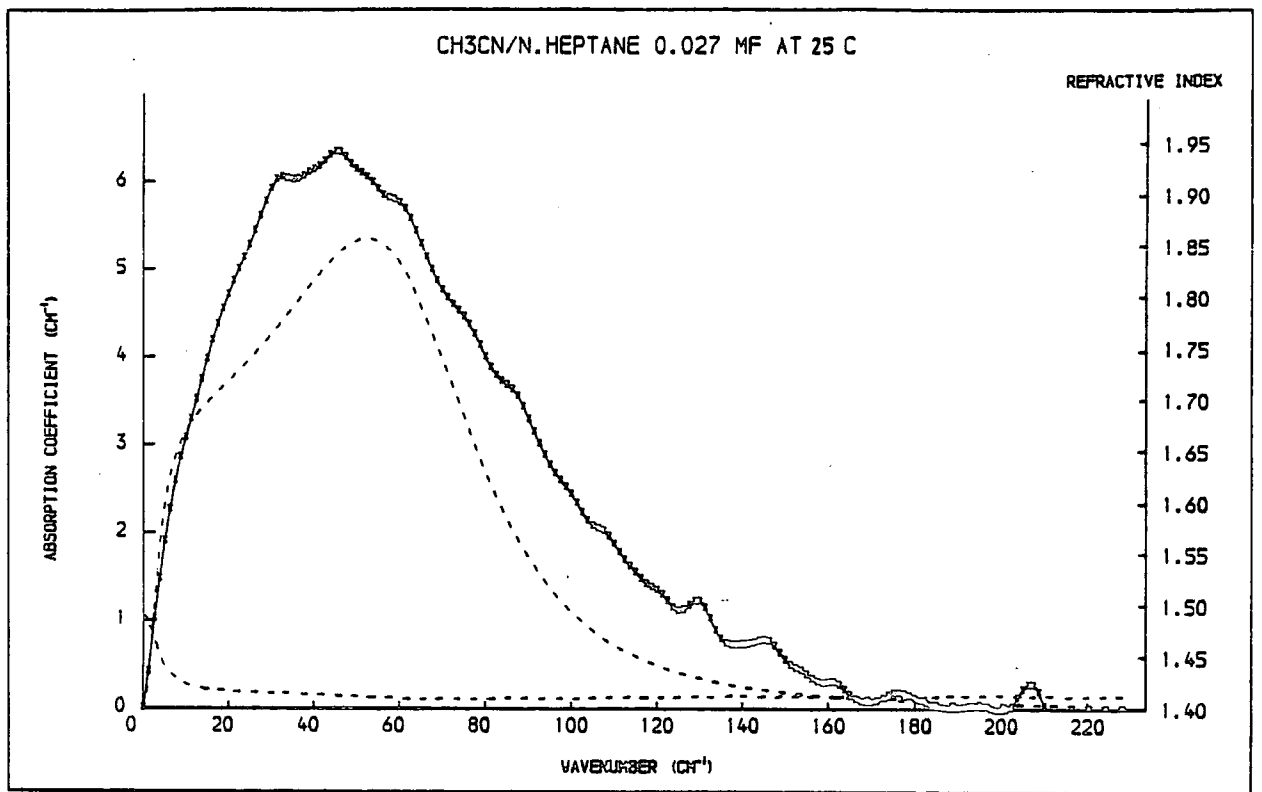


**FIGURE 6.13**  
**SPECTRA RECALCULATED FROM A TWO PARAMETER MODEL FIT**

values which remain fairly constant (increasing slightly) as the recalculated  $\Delta\bar{\nu}_{1/2}$  widths increase, whereas in the observed spectra the increase in  $\Delta\bar{\nu}_{1/2}$  is less pronounced and is offset by the slight decrease in  $a_{\text{max}}$  (neper per molecule).

The recalculated spectra recorded over the wider concentration range at 298K exhibit a steady increase in  $\bar{\nu}_{\text{max}}$  with concentration as seen in the observed data. The half-band widths of the recalculated spectra are disappointing in that they do not closely follow the observed values. However the only trend in the observed data, an increase at high concentrations, is reproduced. This is accompanied by a reasonably constant  $a_{\text{max}}$  value (also as in the observed spectra) which together with the  $\Delta\bar{\nu}_{1/2}$  trend leads to a reflection of the observed spectra in the total intensity data, although on average the recalculated values for both sets of data (Tables 6.2 and 6.3) are 41% lower. It has been suggested<sup>27</sup> that this discrepancy in absorption intensities is partly due to the difference between the dynamic internal field and the Maxwell field. There is some evidence to suggest that this may be the case in the work of Arnold<sup>126</sup> who has fitted this model to the spectra of pure acetonitrile with a Polo-Wilson internal field factor<sup>186</sup> and accounted for almost 100% of the observed absorption.

The fits to the benzene solution spectra are not noticeably different from those to the  $\text{CH}_3\text{CN}/\text{CCl}_4$  solution spectra which reflects the similarity of the observed spectra. However, the spectrum of  $\text{CH}_3\text{CN}$  in n.heptane is considerably different. The match on  $\Delta\bar{\nu}_{1/2}$  is within the experimental error for this solution which leads to an increase (relatively) in the total intensity bringing the recalculated value within 24% of the observed. The predicted  $\bar{\nu}_{\text{max}}$  is at a considerably higher frequency, 16% greater than the observed as compared to an average of 5% in the other solutions.

In general for all of the spectra recalculated the bulge in the absorption spectrum corresponding to the microwave region is more pronounced than in the observed spectra. This is the effect of the model which does not completely merge the two absorption regions. Evans accounts for this in terms of the translational rotation coupling and the 'cog wheel' effect of large angled motions.<sup>127</sup>

The recalculated refractive index spectra all exhibit a small minimum to the high frequency side of the recalculated absorption peak which is evidence of a resonance phenomenon as described in Chapter 2. These spectra are almost within the experimental error of the observed data but at all frequencies lower. The one exception to this is the 0.061mf solution at 288K which exhibits an observed refractive index spectrum 13% higher than the recalculated data. It is considered that this is probably due to an error in the observed data rather than an exceptional deviation in the model behaviour.

The loss spectra for four of the solutions have also been compared with the recalculated data (Figures 6.14 and 6.15). At low frequency there is very good agreement and in the case of the 0.018mf solution studied at 318K the loss peak observed and the loss peak recalculated are coincident (in frequency). However the recalculated loss spectrum and the observed loss spectrum are only calculated to a resolution limit of  $0.125\text{cm}^{-1}$  and  $0.61\text{cm}^{-1}$  respectively in this region.

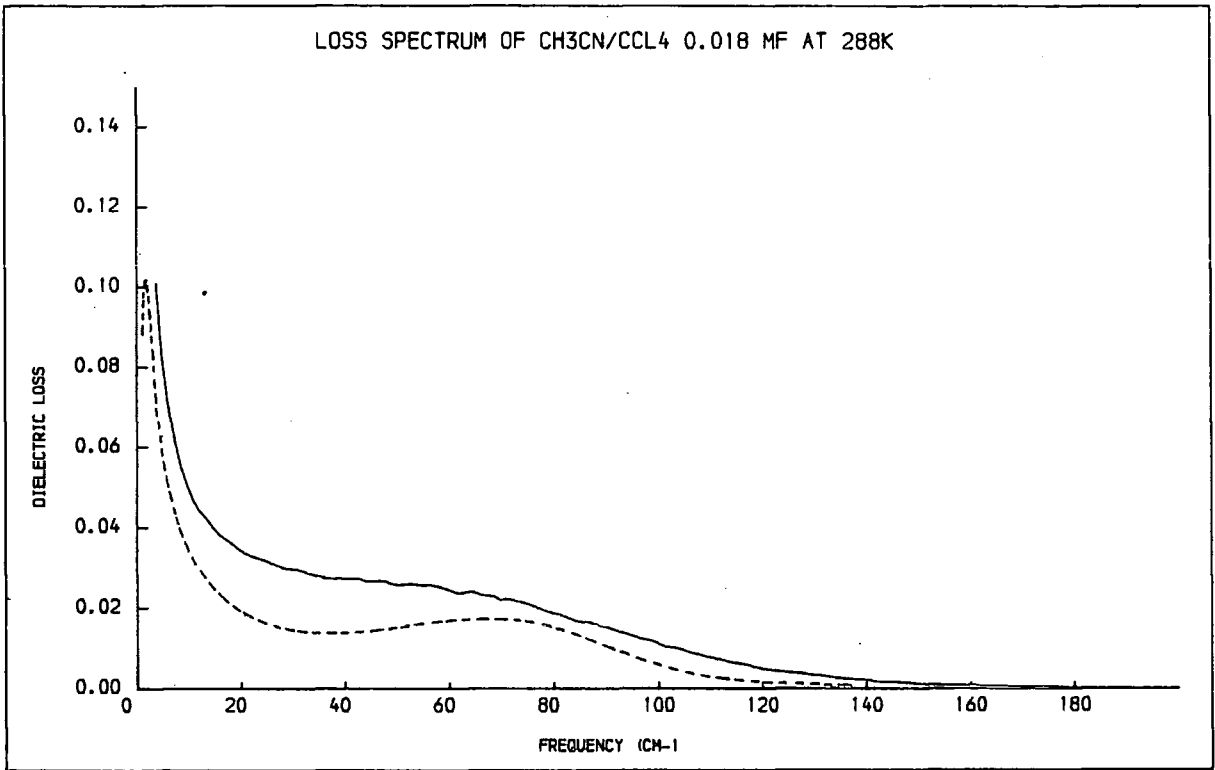


**FIGURE 6.14a**  
**OBSERVED AND MODEL RECALCULATED LOSS SPECTRA**

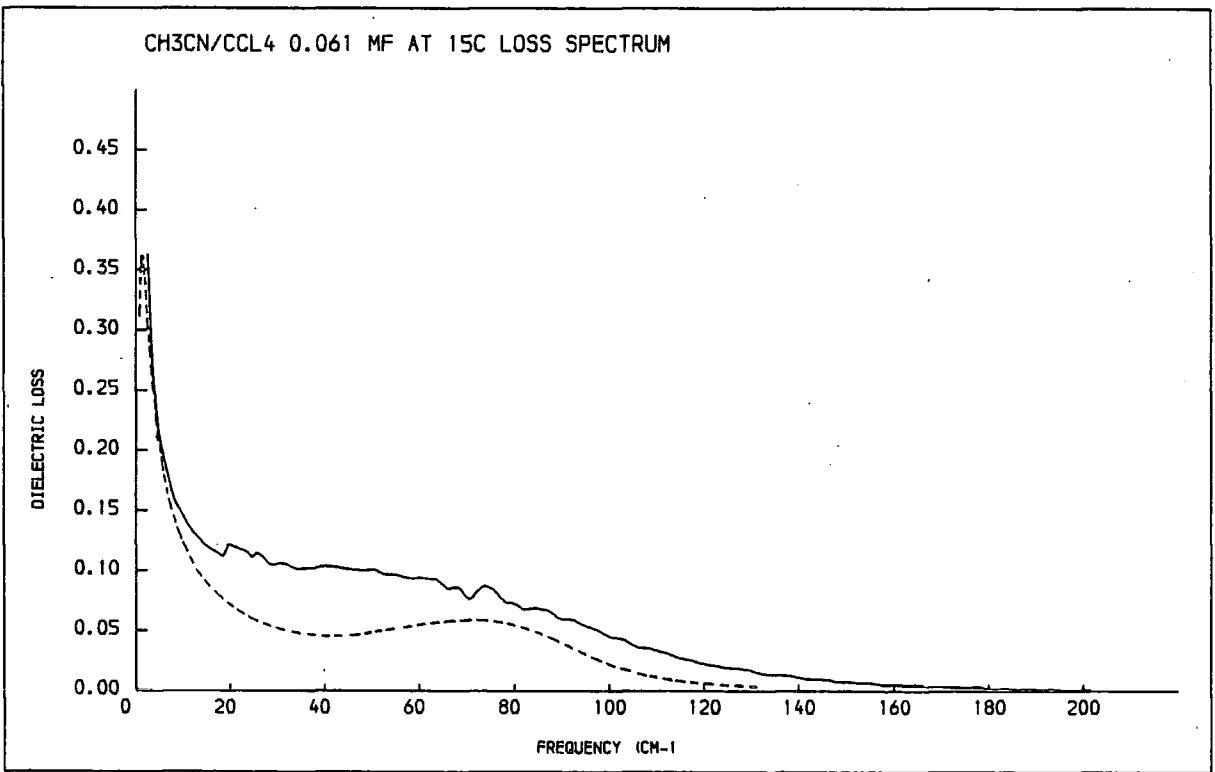


**FIGURE 6.14b**

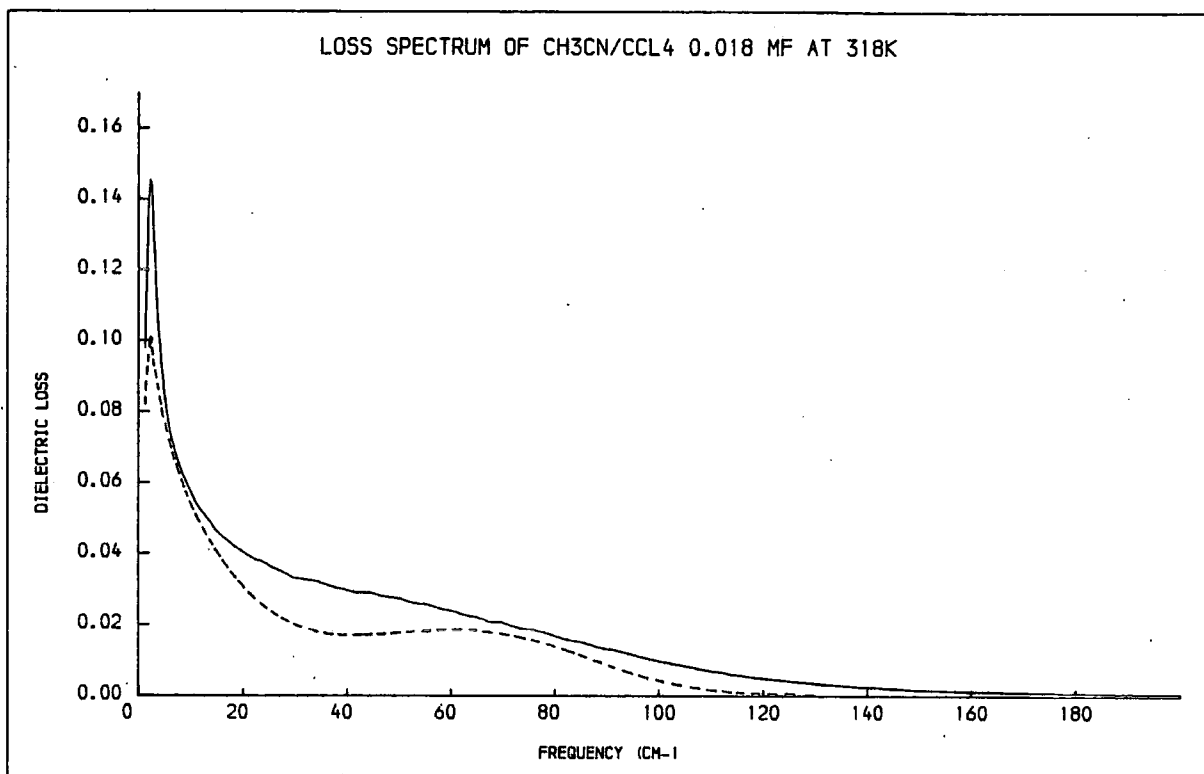


**FIGURE 6.15a**  
**OBSERVED AND MODEL RECALCULATED LOSS SPECTRA**

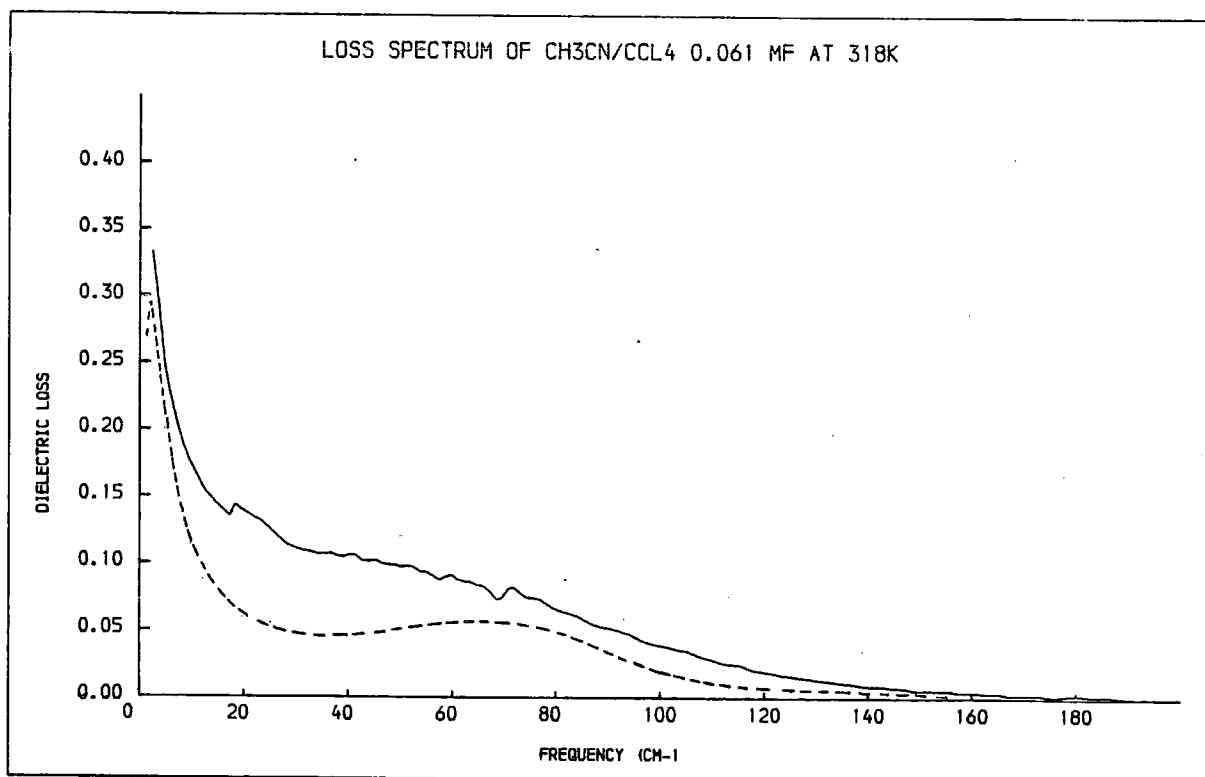


**FIGURE 6.15b**

The recalculated loss spectra (for all the fits) also show the small bulge in the region of the peak in the absorption spectra. This feature can also be seen in the observed loss spectra, although much less pronounced, in the same region. (This may not be clear because the  $\eta(\nu)$  above  $50\text{cm}^{-1}$  are extrapolated values.)

#### Variation in the Fitted Parameters $K_1(0)$ and $1/\gamma$

A table summarising these results is shown below:

	$\bar{\nu}_{\max}$	$\Delta\bar{\nu}_{1/2}$	$1/\gamma$	$K_1(0)$
↑ Temperature	↓	↑	↓ <sup>a</sup>	↓
↑ Concentration	↑	↑	↓	↑

a = the results obtained by direct calculation. (iia)

TABLE 6.4

#### VARIATION IN FITTED PARAMETERS WITH TEMPERATURE AND CONCENTRATION

In addition  $1/\gamma \downarrow \text{CCL}_4 \rightarrow \text{Bz} \rightarrow \text{n.Heptane}$

and  $K_1(0) \text{CCL}_4 \leq K_1(0) \text{Bz} \geq K_1(0) \text{n.heptane}$

Figure 6.16a shows the torque correlation time parameter  $\gamma$  plotted against temperature. It is clearly evident, particularly in the case of the 0.018mf solutions, that the  $\gamma$  values increase with temperature. At a molecular level this can be interpreted as a decrease in the torque relaxation time  $1/\gamma$  at higher temperatures, due to viscosity effects. The width of the band then becomes broader as the relaxation rate  $\gamma$  gets faster, which is in line with the observed half widths. The torque magnitude, which is related directly to  $K_1(0)$ , goes down with the temperature increase as shown in Figure 6.16b (although there is a slight increase in the value of  $K_1(0)$  at 343K). This results in the  $\bar{\nu}_{\max}$  frequency decreasing as seen in the observed spectra.

The torque magnitude parameter  $K_1(0)$  clearly increases with concentration (see Figure 6.17) which indicates a greater hinderance to rotation in the system. However this cannot be due to simple viscosity effects since the viscosity of pure acetonitrile is less than that in carbon tetrachloride solution<sup>187,188</sup> and therefore the opposite trend would be observed if these effects were dominant. Overall the torque relaxation rate is faster with concentration although the trend is not clear (Figure 6.18). The values obtained from the spectra recorded at 298K for a wide concentration range seem to show signs of reading a maximum value (in  $1/\gamma$  the torque relaxation time) at a concentration around 0.2 mole fraction. This adds further weight to the argument that a simple viscosity effect is not dominant in these systems.

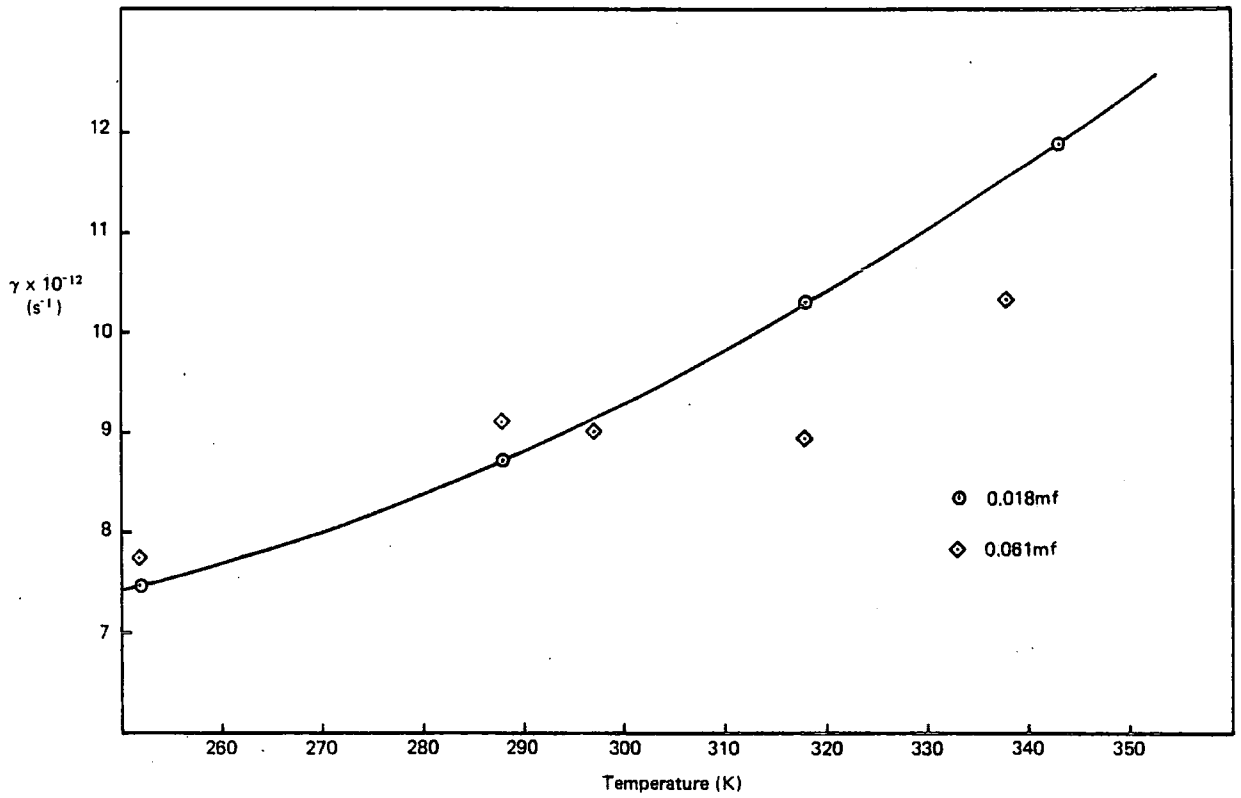


FIGURE 6.16a

MODEL PARAMETER  $\gamma$  vs TEMPERATURE

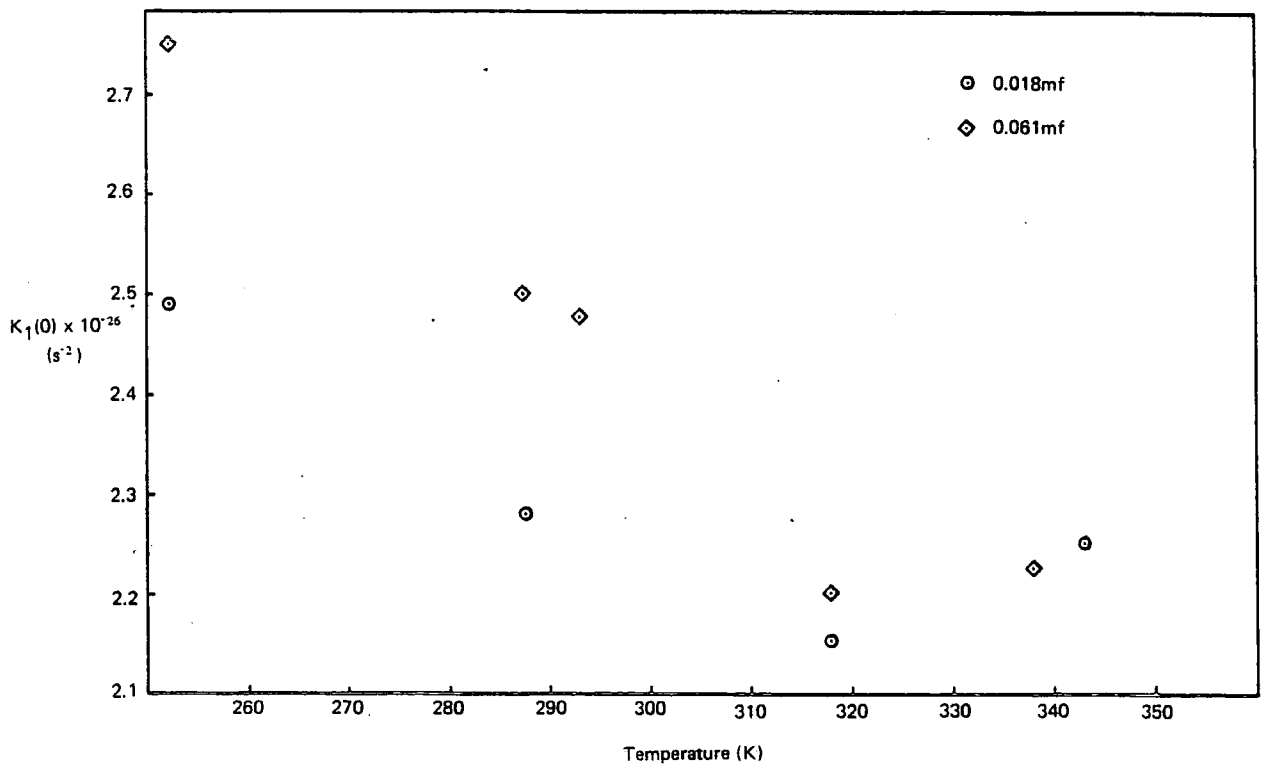


FIGURE 6.16b

MODEL PARAMETER  $K_1(0)$  vs TEMPERATURE

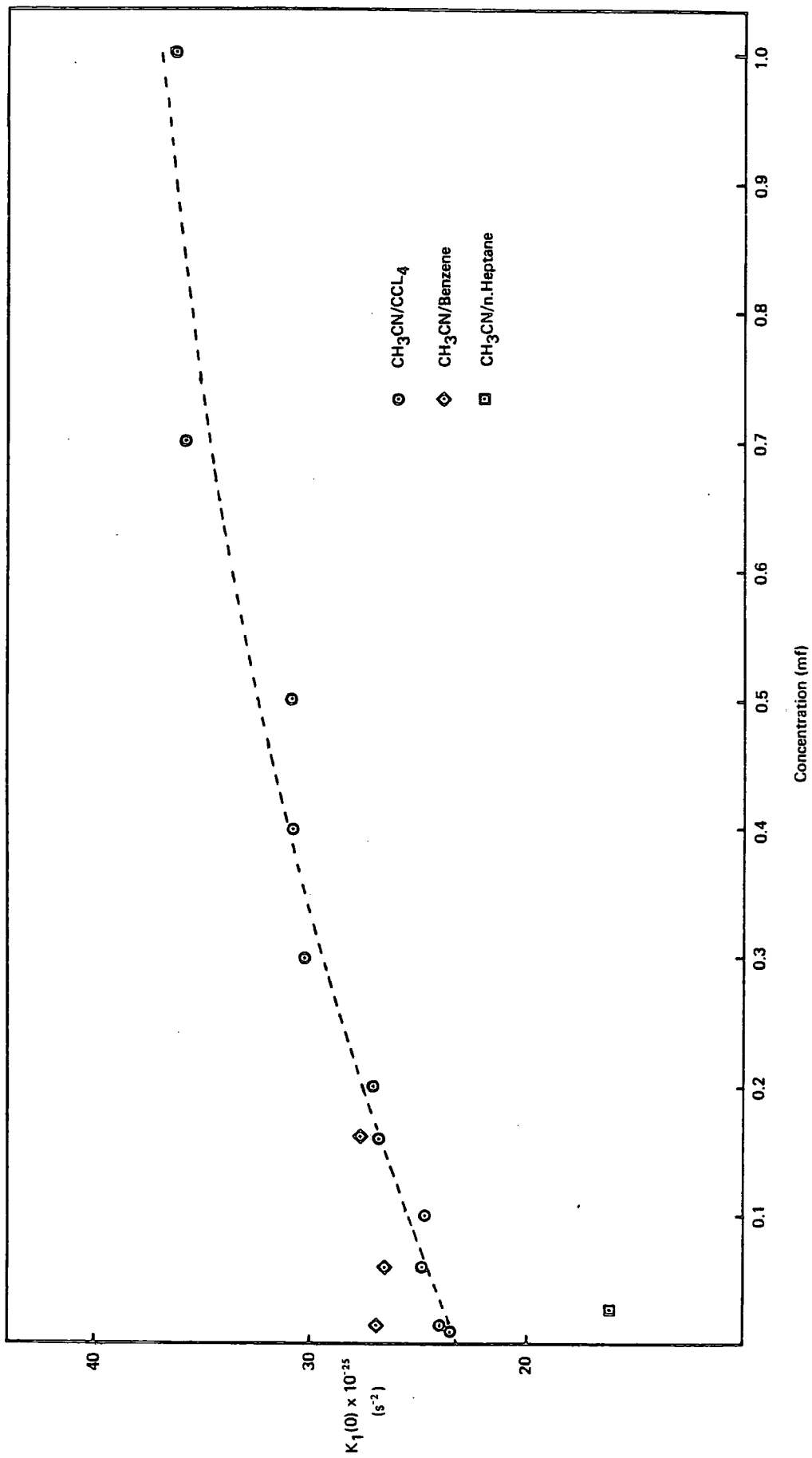


FIGURE 6.17  
 MODEL PARAMETER  $K_1(0)$  vs CONCENTRATION

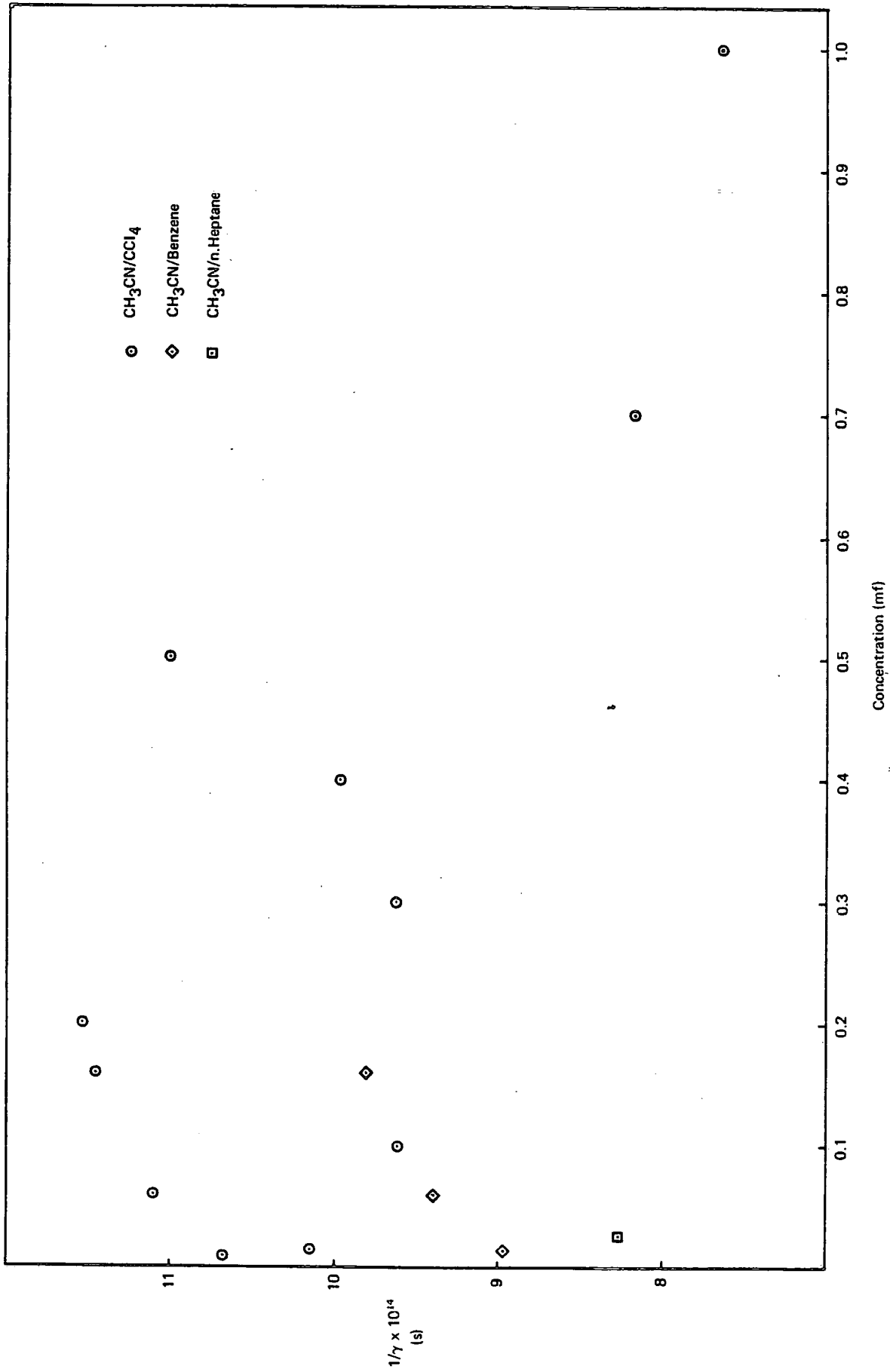


FIGURE 6.18  
MODEL PARAMETER 1/γ vs CONCENTRATION

Meanwhile comparison with the results for the two remaining solvents, benzene and n. heptane, reveal an interesting phenomenon. The torque magnitude is considerably smaller for the n. heptane solution which has a lower  $\nu_{\max}$  frequency. However the observed  $\Delta\bar{\nu}_{1/2}$  is also much smaller than for the other solutions and therefore, we would expect the  $\gamma$  values from the model to be less i.e. the relaxation rate to be slower. However, the fitted value of  $\Delta\bar{\nu}_{1/2}$  is much greater than for the other solutions i.e.  $1/\gamma$  is very much shorter. The most likely explanation of this anomaly is probably in terms of the quality or closeness of fit which has been achieved. This arises because, in common with the other models, this model describes the long time, low frequency region very well. Therefore it might reasonably be expected that the fit obtained would be better if the observed spectra was centred at a lower frequency (closer to the low frequency 'bulge' seen in all of the recalculated results). For the n-heptane solution this is the case with the band peak  $\bar{\nu}_{\max}$  occurring at  $45\text{cm}^{-1}$  considerably lower than for the other solutions.

However this improvement in fit quality is not reflected in the recalculated value of  $\bar{\nu}_{\max}$  which at  $52\text{cm}^{-1}$  is 16% higher than the observed value. This illustrates the care which must be taken in judging the quality of a model fit from a routine which only seeks to minimise the sum of the squares of the residuals to achieve a solution.

The model's affinity for a low frequency fit might also account for the scatter seen in the  $1/\gamma$  values over increasing concentration (apart from the very highest concentrations, which in terms of  $\Delta\bar{\nu}_{1/2}$  fit better than the others): It seems likely that the fit is being further distorted as the band centre moves to higher frequency which compromises the  $\gamma$  values obtained. By a related argument it could be suggested that the trend of decreasing  $1/\gamma$  with temperature could be partly if not completely due to the improvement in the fit obtained as the band moves to lower frequency.

It has been considered that the model might describe the high frequency region more accurately if the Mori formalism was truncated at higher order. In Appendix 3 the results of a 3rd order truncation using the approximation

$$K_2(t) = K_2(0) \exp(-\gamma_2 t)$$

are presented. It can be seen that the fit obtained from this solution is in fact considerably poorer than for the 2nd order truncation. A similar conclusion was reached by Evans<sup>27</sup> in the study of pure liquid chlorobenzene with a third order truncated solution.

#### Rotational Correlation Times Obtained from the Model

The rotational correlation times quoted in Table 6.5 have been obtained by two slightly different procedures which are mathematically related. The values marked  $\tau_A$  have been obtained from the fitted parameters via the equation

$$(\tau_A)^2 = \frac{[K_0(0) + K_1(0)]^2 - 2K_0(0)\gamma^2}{K_0(0)^2 \gamma^2}$$

The set of values  $\tau_C$  have been calculated from the peak in the recalculated loss curve. It has been pointed out earlier that these values have an uncertainty due to the finite recalculation resolution.

Temp (K)	Concentration (mole fraction)	Freq Range of Fit (cm <sup>-1</sup> )	Equation <sup>a</sup>	$\tau_A$ (ps)	$\tau_C$ (ps)	Comments
252	0.018	0-210	1	4.5	4.7 ± .3	
252	0.061	0-210	1	4.8	4.7	
288	0.018	0-180	1	3.1	3.0	
288	0.018	0-180	2	3.1	3.0	$\eta(\bar{\nu})$ data 0-60cm <sup>-1</sup>
288	0.061	0-200	1	3.2	3.4	
288	0.061	0-200	2	3.4	3.4	$\eta(\bar{\nu})$ data 0-60cm <sup>-1</sup> (levels of $\eta(\bar{\nu})$ may be incorrect)
318	0.018	0-170 0-250	1	2.2 2.2	2.1 2.1	$\tau_D^{\text{loss}}$ (observed) * = 2.2 ± 0.3ps
318	0.018	0-170 0-250	2	2.2 2.2	2.1 2.1	$\eta(\bar{\nu})$ data 0-180cm <sup>-1</sup> *
318	0.061	0-200	1	2.6	2.7	$\tau_D^{\text{loss}}$ (observed) > 2.6 ± 0.3 ps
318	0.061	0-200	2	2.7	2.7	$\eta(\bar{\nu})$ data 0-60cm <sup>-1</sup>
318	0.162	0-230	1	2.7	2.7	
318	0.370	0-240	1	2.7	2.7	
343	0.018	0-250	1	1.9 1.9	1.9 1.9	*
338	0.061	20-220	1	2.2	2.1	Note lack of low frequency data

\* Alternative data set. Refer to footnotes of Table 5.5.

- a. 1. Refers to Equation 5.13 with observed  $\alpha(\nu)$  and calculated  $\eta(\nu)$ .  
2. Refers to Equation 5.6 with observed  $\alpha(\nu)$  and  $\eta(\nu)$ .

TABLE 6.5a  
CORRELATION TIMES CALCULATED FROM MODEL PARAMETERS OBTAINED BY A TWO  
PARAMETER FIT.  
(TEMPERATURE AND CONCENTRATION DEPENDENCE)

Concentration (mole fraction)	Solvent	$\tau_A$ (ps)	$\tau_C$ (ps)	$\tau_D$ (observed <sup>126</sup> ) (ps) <sup>a</sup>
0.01	CCl <sub>4</sub>	2.9	3.0	3.26
0.016	CCl <sub>4</sub>	2.8	2.7	2.91
0.06	CCl <sub>4</sub>	3.2	3.4	3.88
0.10	CCl <sub>4</sub>	2.7	2.7	4.55
0.16	CCl <sub>4</sub>	3.6	3.8	4.35
0.20	CCl <sub>4</sub>	3.6	3.8	5.90
0.30	CCl <sub>4</sub>	3.3	3.4	6.14
0.40	CCl <sub>4</sub>	3.5	3.4	6.23
0.50	CCl <sub>4</sub>	3.9	3.8	6.47
0.70	CCl <sub>4</sub>	3.4	3.4	5.50
1.0	CCl <sub>4</sub>	3.2	3.0	6.00
0.016	Benzene	2.8	2.7	3.23
0.06	Benzene	2.9	3.0	3.55
0.16	Benzene	3.1	3.0	3.91
0.027	n-Heptane	1.5	1.5	2.04

All fitted over frequency range 0-250cm<sup>-1</sup>.

All fits to Equation 5.13 (observed  $\alpha(\bar{\nu})$  and calculated  $\eta(\bar{\nu})$ ).

<sup>a</sup> Obtained by Fuoss-Kirkwood analysis of combined microwave and far-infrared data, see Chapter 5.

**TABLE 6.5b**  
**CORRELATION TIMES CALCULATED FROM MODEL PARAMETERS OBTAINED BY A**  
**TWO PARAMETER FIT.**  
**(CONCENTRATION AND SOLVENT DEPENDENCE) AT 298K**

The results are separated into two groups, comprising the data recorded in this thesis which is mainly useful for temperature comparison (6.5a) and the data recorded by Arnold<sup>126</sup> which has been analysed here for the assessment of concentration and solvent molecule dependence (6.5b).

The shift in the recalculated loss peak towards high frequency with temperature is clearly shown in Figure 6.19. This trend, which is reflected in the relaxation times obtained from the model (see Figure 6.20), is the behaviour expected for a dipolar system which obeys the Debye theory of rotational diffusion. The decrease in rotational relaxation time  $\tau^{\text{rot}}$  arises from the increase in rate of relaxation which occurs as a result of the decrease in density, viscosity effects and the increase in thermal motion, which is proportional to R.T where R = the gas constant and T = the temperature (Arrhenius behaviour). It is also known that at higher frequencies there will be further contributions to the absorption: in particular there is almost certainly a contribution from induced dipoles in the solvent. This is accounted for by a theory which was originally proposed by Whiffen<sup>189</sup> to explain the far-infrared absorptions observed in non-polar liquids. Of particular interest in this case are the induced effects which can occur in the solvent molecule. Basically there are two mechanisms which can induce dipoles in a non-polar molecule. There is the purely inductive effect which results in the formation of a dipole due to the distortion of the electronic distribution on the molecule caused by the close proximity ( $r^{-3}$  effect) of another dipole. Secondly there is the dipole which results from a mechanical distortion of the molecule when undergoing collisions. In the case of carbon tetrachloride, which is a highly polarisable molecule on account of its bulky chlorine groups, Whiffen has calculated that the energy available in a bimolecular collision (proportional to RT) occurring at 293K is 2.5KJ mole<sup>-1</sup>. The mechanical distortion of the molecule by 6° would require an energy of half that figure and result in an induced dipole of 0.1 Debye. The relaxation of the induced dipole would be able to occur in two ways, by reorientation or by configuration changes in the surrounding environment, both of which would be on the same timescale and have the same temperature dependence as the relaxation of the permanent dipoles and would therefore be indistinguishable in this experiment.

Comparison of the relaxation times obtained from the model ( $\tau^{\text{MORI}}$ ) with those obtained by a Fuoss-Kirkwood analysis of observed microwave and far-infrared data (see Chapter 5) indicate that  $\tau^{\text{MORI}}$  is not simply a rotational relaxation time since  $\tau^{\text{MORI}} \ll \tau_{\text{D}}$  (observed) particularly at high concentrations.

Madden<sup>190</sup> has studied the spectrum of CS<sub>2</sub> (liquid) by Raman spectroscopy and concluded that the contribution of the induced effects to allowed bands is in the region of 50%, this figure being based on the observation of non-allowed bands which are mainly accounted for by induced effects. He has further suggested that the collision induced dipole contribution to the far-infrared features of acetonitrile solutions is considerably more than 50%. If this is the case then the relaxation time  $\tau^{\text{MORI}}$  gives some measure of the time between molecular collisions.

It is interesting to investigate the effect of temperature on the collision time in the light of the trends observed in the model values. As the temperature is raised the velocity of the molecule

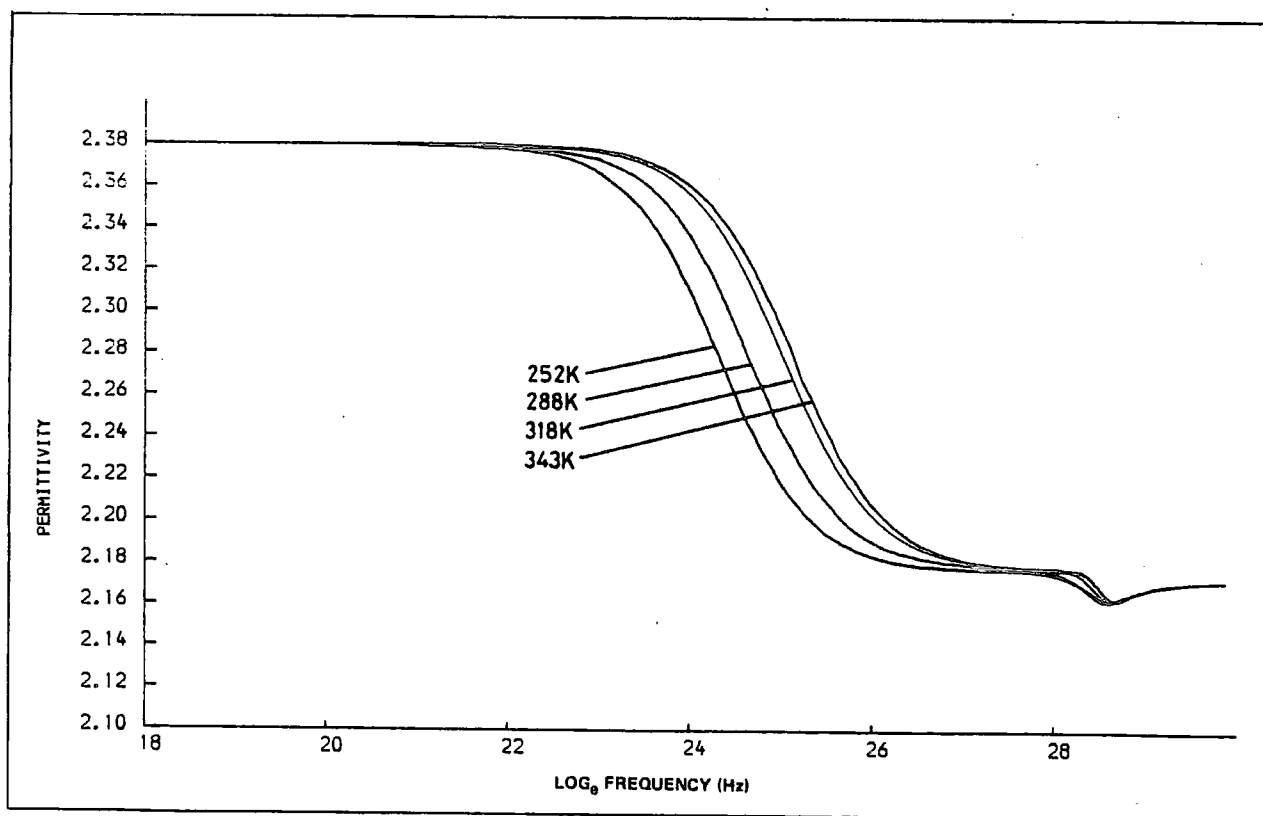
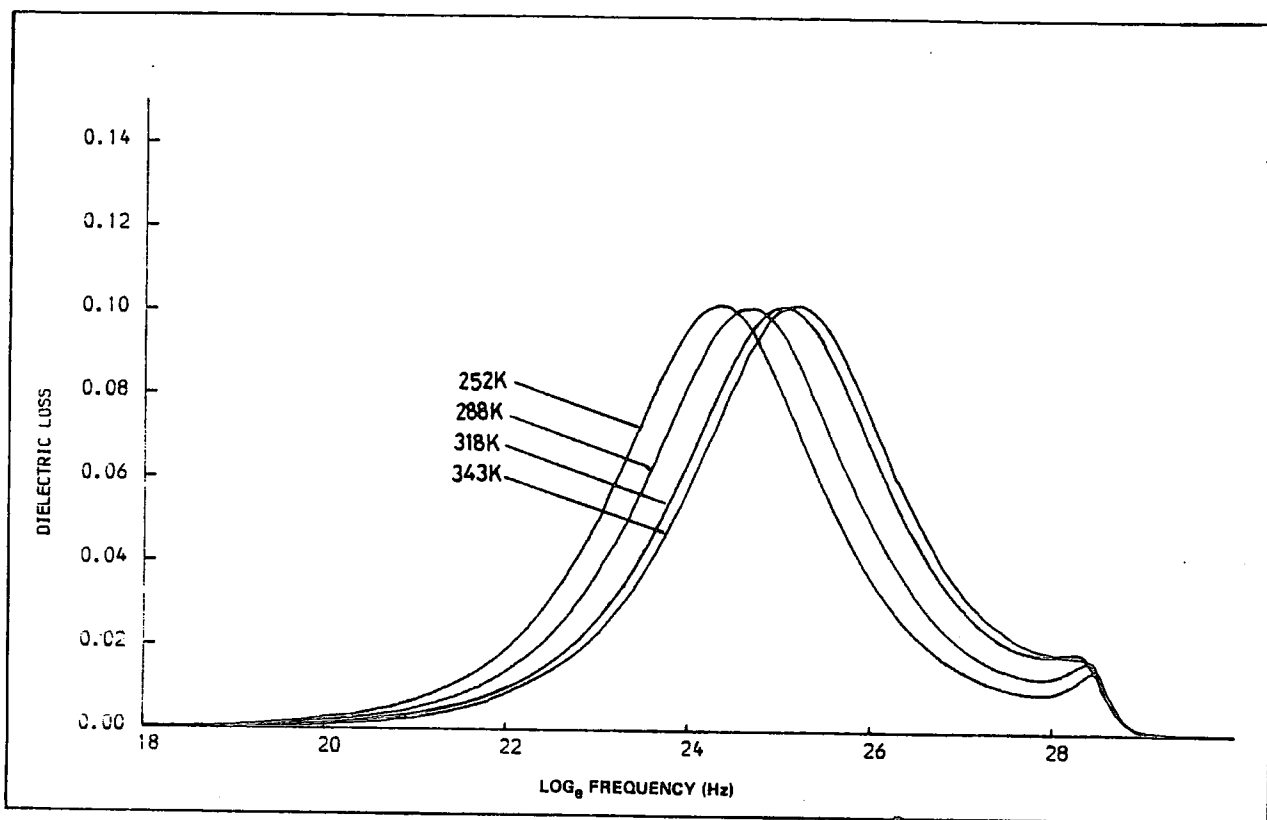


**FIGURE 6.19**  
**LOSS AND PERMITTIVITY CALCULATED FROM MODEL PARAMETERS**  
**FOR 0.018 mf  $\text{CH}_3\text{CN}$  IN  $\text{CCl}_4$  SOLUTION**

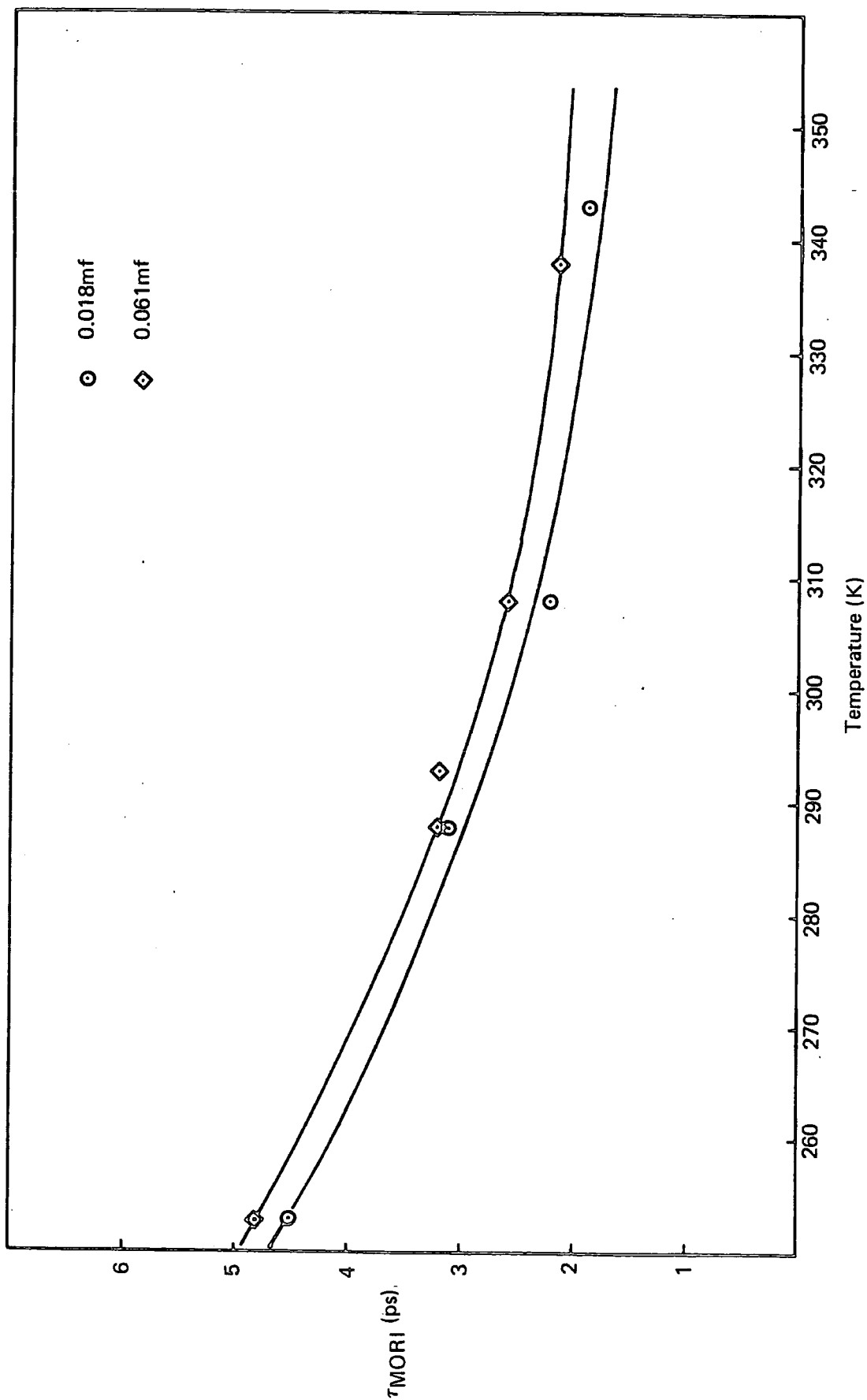


FIGURE 6.20  
MODEL CALCULATED  $\tau_{MORI}$  vs TEMPERATURE

increases. If this were the only effect then there would be a decrease in  $\tau^{\text{MORI}}$  in line with the observed results. However, there is an opposing effect: the decrease in density which increases the average distance between the molecules. It has been shown<sup>13</sup> that for  $\text{CH}_3\text{CN}$ , in line with many other liquids, the increase in velocity of the molecules is completely 'swamped' by the increase in the mean free path caused by the density change. The net effect is that the time between collisions should increase with temperature. As this is not the case, it may be concluded that the collision induced effect is not the predominant mechanism of absorption. Further support to this conclusion can be taken from the results of a Gordon<sup>192</sup> Sum Rule analysis. This procedure seeks to calculate the molecular dipole moment  $\mu_{\text{CALC}}$  from the observed integrated absorption intensity  $A_i$  via the relation<sup>42, 192</sup>

$$A_i = 2\pi\mu^2_{\text{CALC}} \left(1/I_B\right) / 3c^2 \quad \dots\dots\dots 6.2$$

The calculated dipole moment, which includes all of the effective dipoles which exist in the timescale of the experiment, is then compared with gas dipole moment  $\mu_{\text{gas}}$  which is corrected ( $\mu^*$ ) for internal (Onsager) field effects by

$$\mu^* = (2\epsilon_0 + 1) (\epsilon_\infty + 2) \mu_{\text{gas}} / 3 (\epsilon_0 + \epsilon_\infty) \quad \dots\dots\dots 6.3$$

For these solutions it has been found<sup>126, 193</sup> that  $\mu^*$  agrees very well with  $\mu_{\text{CALC}}$  and therefore any induced dipole contribution to the absorption intensity is small compared to the permanent dipole contribution.

The relationship between the relaxation times and concentration is rather less apparent than the temperature dependence. Initially, referring to Table 6.5a and looking across the temperature ranges we can see that in all cases  $\tau^{\text{MORI}}_{(0.018)} < \tau^{\text{MORI}}_{(0.061)}$  which is in agreement with the observed values obtained in this work, i.e. we have an observed value of  $2.2 \pm 0.3$  ps for  $\tau^{\text{LOSS}}_{\text{D}}$  for the 0.018mf solution at 318K measured directly from the loss curve. The corresponding plot for the 0.061mf solution does not peak in the range of measurement but we have recorded to a frequency which enables the prediction (with reasonable certainty) that  $\tau^{\text{LOSS}}_{\text{D}}(0.061) > 2.6 \pm 0.3$  ps. The results obtained from the analysis of the data recorded at 298K show, in general an increase in  $\tau^{\text{MORI}}$  with increasing concentration, at least for the lower concentration range (Figure 6.21). However, as mentioned previously the actual values calculated by the microwave analysis described in Chapter 5 are somewhat longer.

Moving to the higher concentrations, the calculated relaxation times appear to reach a maximum value at about 0.5mf and then decrease with the addition of further solute molecules. This behaviour is also reminiscent of that observed for the Fouss-Kirkwood results, although the trend is largely obscured by the scatter in the values. The results appear to be even more similar to those recorded for the internal field corrected  $\tau_{\text{D}}$  values. For example the Nee Zwanzig-Onsager field corrected  $\tau_{\text{D}}$  values calculated in Chapter 5 show a similar trend and magnitude to the recalculated model values. The scatter in the recalculated values could be due to the fitting problem described earlier

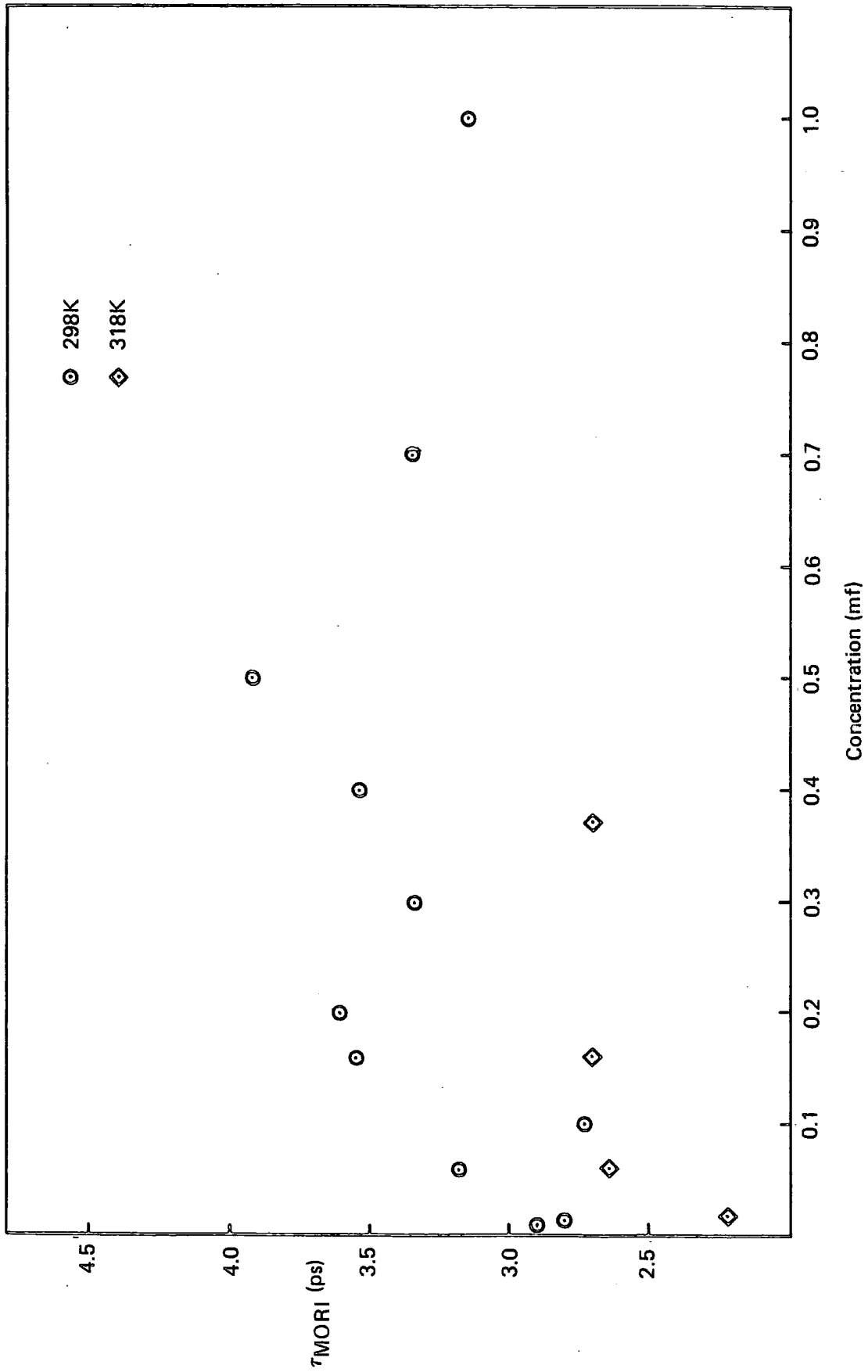


FIGURE 6.21  
 MODEL CALCULATED  $\tau_{MORI}$  vs CONCENTRATION

i.e. as the concentration increases the  $\bar{\nu}_{\max}$  value moves to a higher frequency, and there is some evidence from temperature shifts studied that the model does not fit as well to a band centred at a higher frequency.

Although in general at higher concentrations the agreement between the model recalculated and Fuoss-Kirkwood analysis, relaxation times is poor the  $\tau^{\text{MORI}}$  value obtained for the pure liquid 3.2 ps (298K) is in very good agreement with that recorded by Eloranta,<sup>188</sup> 3.3 ps at 308K determined by microwave measurement.

The increase in  $\tau^{\text{MORI}}$  when moving from the pure liquid acetonitrile to the solution may be accounted for by the sharp increase in viscosity on addition of  $\text{CCl}_4$  since the viscosity<sup>187</sup> of  $\text{CH}_3\text{CN}$  is  $325 \times 10^5$  cp and that of  $\text{CCl}_4$   $912 \times 10^5$  cp at 298K. This effect may then be countered to successively greater extents by the decrease in cross correlation contributions to Equation 1.21 as the solutions are diluted; thus the  $\tau^{\text{MORI}}$  values decrease again in very dilute solution.

#### Further Discussion of the Variations in Intensity of the Observed Spectra

There is a slight decrease in the absorption intensity per molecules of the solutions as the temperature is increased (Figure 5.6b) which may be accounted for by the theory of clustering outlined in Chapter 5 or in terms of a collision induced dipole contribution to the overall absorption. By a similar argument to that applied previously, the opposing effects of density change and increased velocity of the molecules with temperature would lead to a decrease in the rate of collisions between molecules. Hence the number of collision induced dipoles decreases, which leads to a decrease in the intensity. However, there is a complication to this effect in that although there are fewer dipoles the increase in velocity of the colliding molecules will result in a greater mechanical distortion of the bonds which in turn might increase in magnitude the induced dipole moment. To some extent this countering effect could be masking the trend which would be expected based simply on the decrease in collision rate. Davies et al<sup>170</sup> believe this is the case for liquid carbon disulphide which exhibits a positive intensity, temperature dependence.

The study of the total integrated intensity per molecule with concentration shows that there is little evidence of any pronounced deviations from Beer's law, although as pointed out previously there is the possibility of a slight increase in intensity over the 0.1mf to 0.7mf concentration range, followed by a decrease to the pure liquid. If induced effects were significant we might expect to see some saturation i.e. a limit to the contribution at high concentrations when all of the available solvent molecules were highly polarised. Such an effect would be expected to occur at a lower concentration, where the numbers of solvent and solute molecules were almost equal. At concentrations above that, the contribution from the solvent induced dipoles would decrease rapidly due to their diminishing numbers although this effect may well be totally masked by the increase in solute dipole contribution, particularly when the permanent dipole moment of  $\text{CH}_3\text{CN}$  is so large. Further complications to the elucidation of these contributions arise if collision dipoles are included. These contributions would be affected by the dipole number density, which would control the collision rate, and by their total numbers and magnitude. In order to clarify this

further it would be necessary to record the solution spectra at constant concentration and temperature whilst varying the density (a high pressure experiment such as that made by Bradley<sup>60</sup> and described in Chapter 2C).

It may be more informative to analyse the spectral intensities of the acetonitrile in solvents of different polarisabilities. The polarisabilities of carbon tetrachloride and benzene are very similar. An indication of this is given by the 0.016mf solution  $\epsilon_{\infty}$  values which are 2.22 and 2.34 respectively. This is reflected in the intensities of these systems which are also very similar at approximately 3700 nepers mole<sup>-1</sup> cm. Calculation of the energy required to distort these molecules and the dipole moment which would result may shed some light on the collision induced contribution to the absorption i.e. if one type of solvent molecule requires more energy to form collision induced dipoles whilst the total induced contribution is the same then it could be concluded that the electronic induced effect is predominant. The error on these intensity measurements is  $\pm 10\%$  which renders such a detailed analysis futile in this case. The intensity of the acetonitrile/n-heptane solution is only 2700 neper cm mole<sup>-1</sup>, some 30% less than for the CCl<sub>4</sub> and benzene solutions and well outside the experimental error. The polarisability of n-heptane is also considerably less than that of the other solvents ( $\epsilon_{\infty} = 2.00$ , 0.027mf) which indicates that the solvent induced contribution to the absorption in this region is significant.

Further experiments with a wider range of solvents are required to confirm these theories. In addition the solute could be varied, selecting molecules with weaker permanent dipoles which should cause less electronic distortion of the solvent molecules. O'Neill's<sup>136</sup> work on methyl iodide solutions may provide some useful information for such an analysis. Initial results<sup>191</sup> indicate that the Mori model describes these solution spectra more accurately than it does the solutions studied in this work and that the induced dipole absorption contributions are not of major importance for the CH<sub>3</sub>I/CS<sub>2</sub> system.

Finally the collision induced effects might be separated by measuring the intensities of mixed systems of non-polar molecules of different polarisability, although it must be appreciated that collision induced solvent dipoles can in turn induce electronic distortion effects in neighbouring molecules.

#### A Brief Comparison of the Spectral 4th Moments, $M_{4R}$ Of the Solutions Studied

The spectral 4th moments given in Tables 6.6 and 6.7 have been calculated from the model parameters via the relation given previously (Equation 5.9). For comparison Table 6.6 includes the values obtained<sup>126</sup> from the relation

$$M_{(n)} = \int_0^{\infty} I(\omega) \omega^n d\omega \quad \dots\dots\dots 6.4$$

where  $I(\omega)$  is the spectral intensity with different internal field corrections applied. Since the model applied in this work does not explicitly include induced dipole effects the difference between these values of  $M_{4R}$  and those obtained directly from the observed intensity is taken as some indication of the presence of induced dipole contributions in these systems. Further evidence for

Concentration (mf)	Solvent	Spectral 4th moments, $M_{4R}$		
		Calculated from Model $\times 10^{-50} (s^{-4})$	Obtained by Integration <sup>a</sup> $\times 10^{-50} (s^{-4})$	Obtained by Integration <sup>b</sup> $\times 10^{-50} (s^{-4})$
0.01	CCl <sub>4</sub>	21.8	23.95 ± 10%	36.06 ± 10%
0.016	CCl <sub>4</sub>	22.3	31.42	46.45
0.06	CCl <sub>4</sub>	23.0	32.12	48.68
0.10	CCl <sub>4</sub>	22.9	24.99	34.56
0.16	CCl <sub>4</sub>	24.8	29.47	49.68
0.20	CCl <sub>4</sub>	25.0	27.46	44.97
0.30	CCl <sub>4</sub>	27.8	36.53	56.06
0.40	CCl <sub>4</sub>	28.4	39.48	64.51
0.50	CCl <sub>4</sub>	28.4	33.88 ± 20%	76.39 ± 20%
0.70	CCl <sub>4</sub>	32.8	51.04	76.73
1.0	—	33.2	34.31	55.01
0.016	Benzene	25.0	34.18 ± 10%	53.39 ± 10%
0.06	Benzene	24.7	31.85	49.26
0.16	Benzene	25.6	30.61	52.53
0.027	n-Heptane	15.3	9.22	13.04

$$K_o(0) = 2kT/\mu_B = 8.95 \times 10^{24} \text{ sec}^{-2} \text{ at } 293\text{K}$$

a Corrected with Klug<sup>96</sup> internal field (as for Nee-Zwanzig,<sup>43</sup> see Chapters 2 and 5).

b Corrected with Polo-Wilson<sup>186</sup> internal field (based on Onsager<sup>85</sup> model) =  $9\eta_{\infty} / (\eta_{\infty}^2 + 2)^2$

TABLE 6.6  
SPECTRAL 4th MOMENTS CALCULATED FROM MODEL PARAMETERS  
(2 PARAMETER FIT) COMPARED WITH VALUES OBTAINED BY INTEGRATION<sup>126</sup>

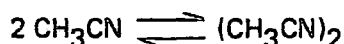
Temperature (K)	Concentration (mf)	$M_{2R} \times 10^{-24}$ (s <sup>-2</sup> )	Obtained by a 2 variable parameter fit		By direct calculation
			$K_1(0) \times 10^{-25}$ (s <sup>-2</sup> )	$M_{4R} \times 10^{-50}$ (s <sup>-4</sup> )	$M_{4R} \times 10^{-50}$ (s <sup>-4</sup> )
252	0.018	7.6196	24.92	19.57	70.3
252	0.061	7.6196	27.56	21.58	82.3
288	0.018	8.7081	22.84	20.65	71.3
288	0.018	8.7081	22.76	20.58	—
288	0.061	8.7081	25.04	22.56	73.4
288	0.061	8.7081	24.20	21.83	—
318	0.018	9.6152	21.54	21.64	65.0
318	0.018	9.6152	22.60	22.65	—
318	0.061	9.6152	22.11	22.18	73.8
318	0.061	9.6152	22.15	22.22	—
318	0.162	9.6152	26.84	26.73	90.3
318	0.370	9.6152	32.77	32.43	97.8
343	0.018	10.3711	23.17	25.11	58.6
343	0.018	10.3711	22.50	24.41	—
338	0.061	10.3711	22.39	23.93	64.4

**TABLE 6.7**  
**SPECTRAL 4th MOMENTS CALCULATED FROM THE MODEL PARAMETERS**  
**(TEMPERATURE AND CONCENTRATION DEPENDENCE)**

this can be seen in the values calculated by the two methods for the n-heptane solution. In this case the induced effects are expected to be less due to the lower polarisability of this solvent and therefore the model calculated  $M_{4R}$  values would be similar to the observed values. In fact this is so for the results corrected with the Polo-Wilson internal field factor (b in Table 6.6). The difference is also positive in this example but it is thought that this is probably due to model and internal field correction inadequacies rather than a direct consequence of the different solvent polarisabilities and relative induced dipole effects.

c) Fitting With Three Variables:  $\gamma$ ,  $K_1(0)$ ,  $K_0(0)$

The presence of a plateau in the values of  $\tau_D$  obtained from the Fuoss-Kirkwood analysis of the range of concentrations of  $\text{CH}_3\text{CN}/\text{CCl}_4$  solutions described (Figure 5.16) has been interpreted<sup>126</sup> as evidence for the possibility of the formation of clusters in these systems. It is speculated that these clusters could reorient together, giving rise to the increase in rotational correlation times observed at higher solute concentrations. It has already been mentioned in this thesis (Chapter 5) that there is some evidence for the presence of dimer formation in an acetonitrile system studied by Lentloff and Knözinger<sup>171</sup>. (It has already been established that dimers can be observed in gas matrix isolated systems).<sup>194</sup> This study, which was initially made of the vapour phase acetonitrile at low pressures, revealed a high intensity feature at  $20\text{cm}^{-1}$  which corresponds to the peak in the gas phase rotational envelope, and a weak band at  $78\text{cm}^{-1}$  with a half width  $\Delta\tilde{\nu}_{1/2}$  of  $40\text{cm}^{-1}$  and no structure. This weak band at  $78\text{cm}^{-1}$  was studied at different pressures whilst maintaining the  $\text{CH}_3\text{CN}$  number density by varying the path length (i.e. path length x pressure = constant). The band intensity was observed to increase with pressure and thus it was concluded that it must be related to an association of  $\text{CH}_3\text{CN}$  molecules. Simply on the grounds of the low pressures involved the association factor was speculated to be 2 (i.e. dimer) and the equilibrium constant was calculated for its formation. A value of  $42 \pm 26 \text{ } \mu\text{mole}^{-1}$  was obtained for the equilibrium



Isotopic dilution experiments revealed a shift on deuteration of approximately  $5\text{cm}^{-1}$  which is reasonable for librations about the axes perpendicular to the molecular axis of molecules arranged in an anti-parallel configuration.

In the light of these results it is surprising that the Gordon sum rule analysis described earlier does not indicate the presence of any significant absorption in the far infrared other than that due to the monomeric dipole reorientation. However it has been indicated<sup>195</sup> that the sum rule may not be accurate due to the fact that at short time the random orientations caused by librational motion of the molecules will not be averaged out. This error is proportional to the size of the angle swept by the molecule and for example in the case of a  $6^\circ$  libration amounts to an error of 4% in the value of  $\mu_{\text{calc}}$ , the effective dipole moment calculated.

If there are dimers present in the liquid and solution phase acetonitrile and contributing to the far infrared 'Poley' absorption, then the rotational moment,  $K_0(0)$  in this model set to the value

given by  $2KT/I_B$  will be inaccurate because the reduced mass will not have been correctly defined. An experiment in which the parameter  $K_0(0)$  is allowed to vary might elucidate the dimer theory. Such an experiment has been carried out by fitting the model equations described previously with three variable parameters:  $\gamma$ ,  $K_1(0)$  and  $K_0(0)$ . The fitting was carried out using the same parameter values as previously with the 2nd moment set initially to its calculated value (weighted). At each iteration  $K_0(0)$  was changed by a maximum of 0.1 since the new value was expected to be close to the original if any significance was to be attached to it.

Two examples of the absorption spectra recalculated from the values given in Table 6.8 are shown in Figures 6.22 and 6.23. A casual inspection of these reveals that the fit is better than for the two parameter model. This is not surprising since it has been established previously<sup>2</sup> that the greater the number of variables in a model the better able it is to fit the data. A four parameter fit is a good example of this (see Figure 5, Reference 2).

The most obvious features of the three parameter recalculated spectra is the increase in intensity the improvement of the fit at high frequency and poor fit to the low frequency region. The failure of the three parameter fitted model in the microwave region is illustrated by the relaxation times  $\tau^{\text{MORI}}$  which are now considerably shorter than the observed values.

Unfortunately, the more variable parameters available in a model the more difficult the interpretation becomes. Referring to Table 6.8 we can see that the trend with temperature of the torque correlation time parameter  $1/\gamma$  is still evident although the actual magnitude has changed by a factor of approximately two, which is the result of the better match of the  $\Delta\bar{\nu}_{1/2}$  values. The evidence of any pattern in the  $1/\gamma$  values with concentration is difficult to discern; however this trend was not strongly evident in this small concentration range for the two parameter fits. The  $K_1(0)$  values have remained within about 30% greater than the magnitude of the two parameter fit values which is a result of a slightly poorer fit on the  $\bar{\nu}_{\text{max}}$  frequency.

The trends exhibited by the three parameter  $K_1(0)$  values with both temperature and concentration are similar to those seen for the two parameter fits. It should be borne in mind that the actual physical significance of the magnitudes of  $K_1(0)$  and  $1/\gamma$  are not clearly defined and therefore accepting that the salient trends (which are more easily understood) with concentration and temperature still exist in these results attention can be turned to the new values of  $K_0(0)$ , the rotational 2nd moment.

If dimers were present and reorienting together (i.e. as one) then the moment of inertial  $I_B$ , which is calculated for a simple diatomic rigid rotor by the relation

$$I_B = \frac{m_1 m_2}{m_2 + m_1} r_0$$

where  $r_0$  is the separation of centres of mass of the bodies and  $m_1$  and  $m_2$  are the masses of the bodies

would be greater than the calculated  $I_B$  and hence the rotational second moment

$$M_{2R} = 2KT/I_B = K_0(0)$$

would be smaller than calculated. In all cases this has taken up a new value of approximately twice

Temperature (K)	Concentration (mole fraction)	Equation	Model Parameters				Recalculated Spectra Details				$\tau_A$ (ps)	$\tau_C$ (ps)
			$1/\gamma \times 10^{14}$ (sec)	$K_1(0) \times 10^{25}$ ( $s^{-2}$ )	$K_0(0) \times 10^{-24}$ ( $s^{-2}$ )	$\bar{\nu}_{max}$ ( $cm^{-1}$ )	$\Delta\bar{\nu}_{1/2}$ ( $cm^{-1}$ )	Total Intensity ( $cm \text{ mol}^{-1}$ )				
252	0.018	1	7.11	32.77	16.96	84	90	3384	1.41	1.33		
252	0.061	1	7.17	35.19	16.14	88	86	3340	1.60	1.68		
288	0.018	1	7.10	29.50	15.76	78	92	3149	1.35	1.33		
288	0.018	2	7.07	29.54	16.01	—	—	—	1.33	1.33		
288	0.061	1	6.77	32.56	15.65	82	98	3304	1.43	1.50		
288	0.061	2	6.67	32.64	17.92	—	—	—	1.24	1.19		
318	0.018	1	5.85	32.00	15.97	73	97	2991	1.17	1.19 *		
318	0.018	2	6.58	28.01	15.12	—	104	3239	1.17	1.19 *		
318	0.018	2	5.88	32.02	16.10	—	—	—	1.17	1.19 *		
318	0.061	1	6.56	28.11	15.19	—	—	—	1.23	1.19 *		
318	0.061	1	6.18	31.44	19.11	77	101	3170	1.03	1.06		
318	0.061	2	6.19	31.50	19.19	—	—	—	1.03	1.06		
318	0.162	1	6.22	34.90	15.40	82	97	3063	1.43	1.50		
318	0.370	1	5.99	38.91	12.81	88	110	3239	1.84	1.88		
343	0.018	1	5.59	31.30	15.30	71	105	3147	1.14	1.18 *		
338	0.061	1	5.50	32.49	15.45	72	103	3113	1.16	1.18 *		
338	0.061	1	5.22	34.18	18.54	72	106	3401	0.96	0.94		

\* As for Table 5.5.

a As for Table 6.2

$K_0(0)$  values calculated from  $K_0(0) = 2kT/\beta$

252K =  $7.6196 \times 10^{24}$   
 288K =  $8.7081 \times 10^{24}$   
 318K =  $9.6152 \times 10^{24}$   
 343K =  $10.3711 \times 10^{24}$   
 338K =  $10.2199 \times 10^{24}$

TABLE 6.8  
 THE RESULTS OF A MODEL FITTING WITH  
 3 VARIABLE PARAMETERS  $\gamma$ ,  $K_1(0)$  AND  $K_0(0)$

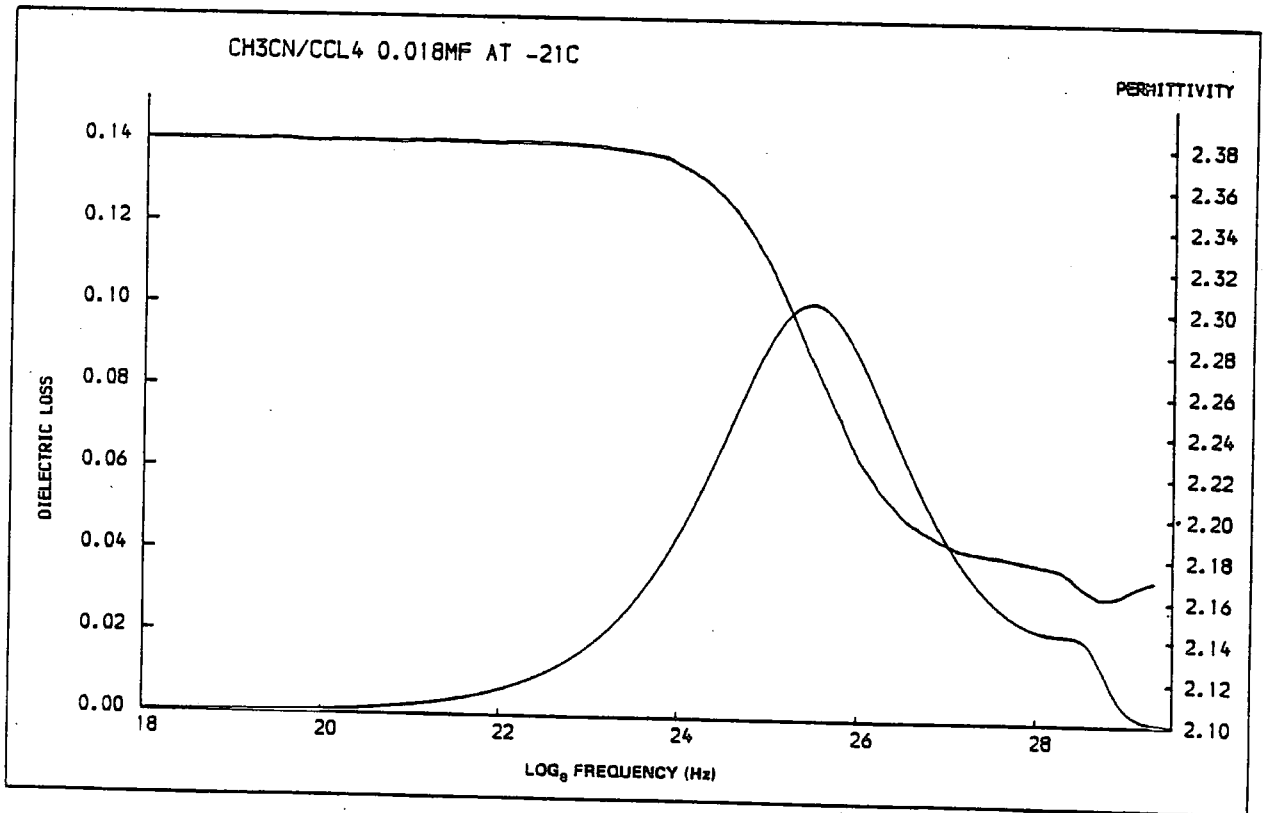
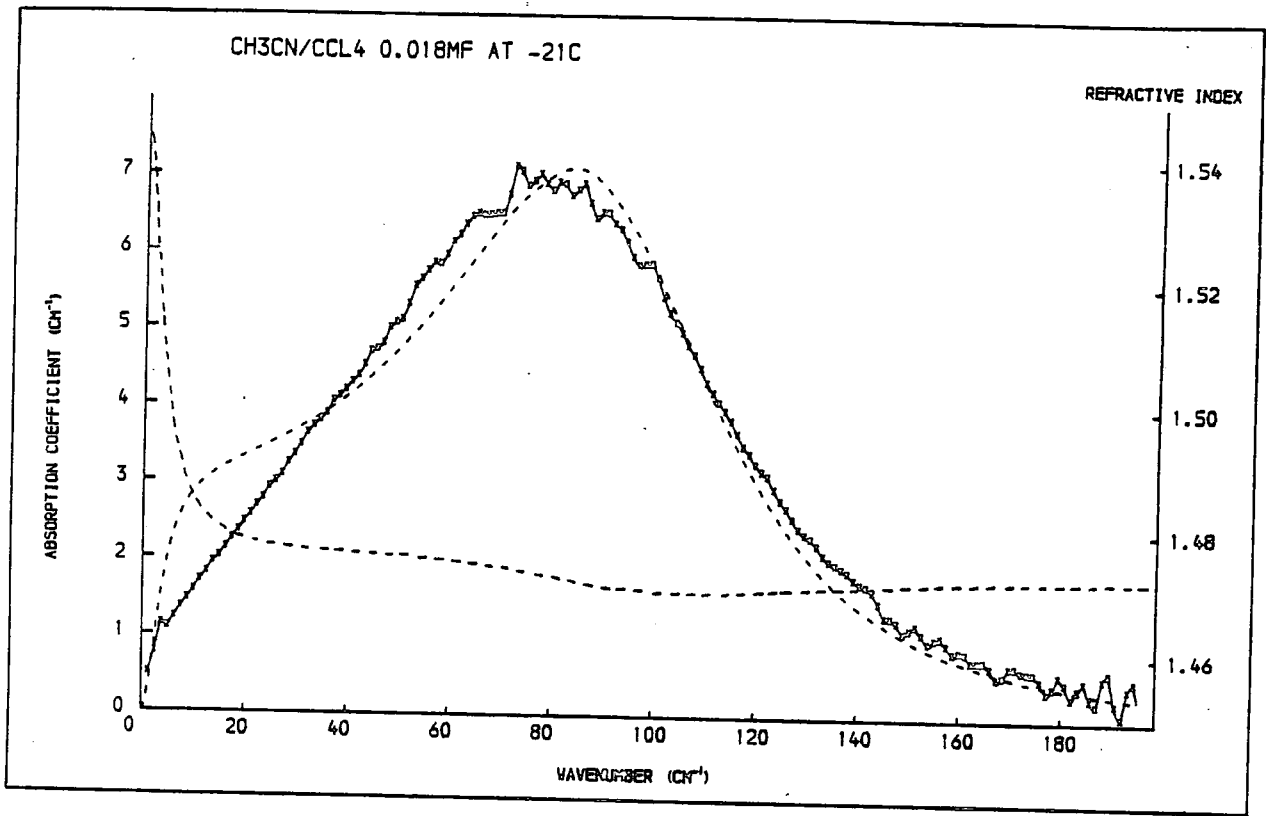


FIGURE 6.22  
SPECTRA RECALCULATED FROM A THREE PARAMETER MODEL FIT

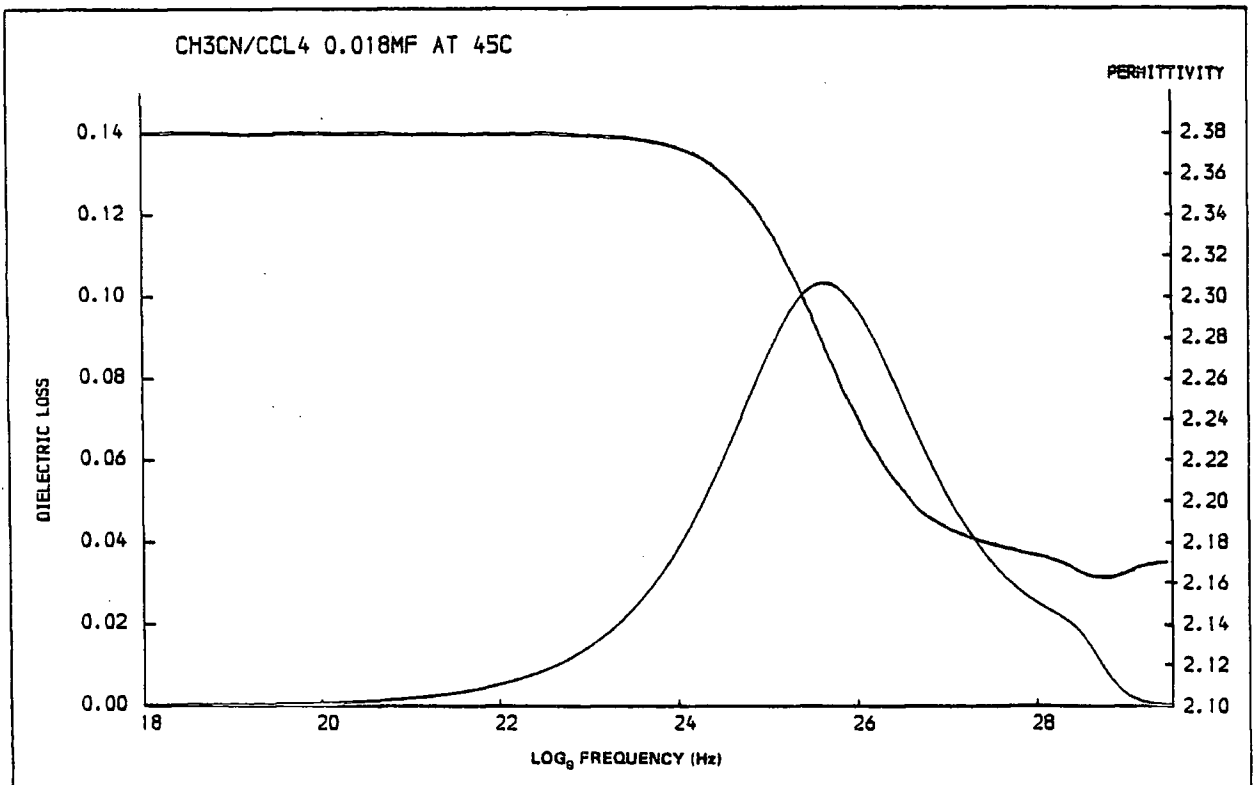
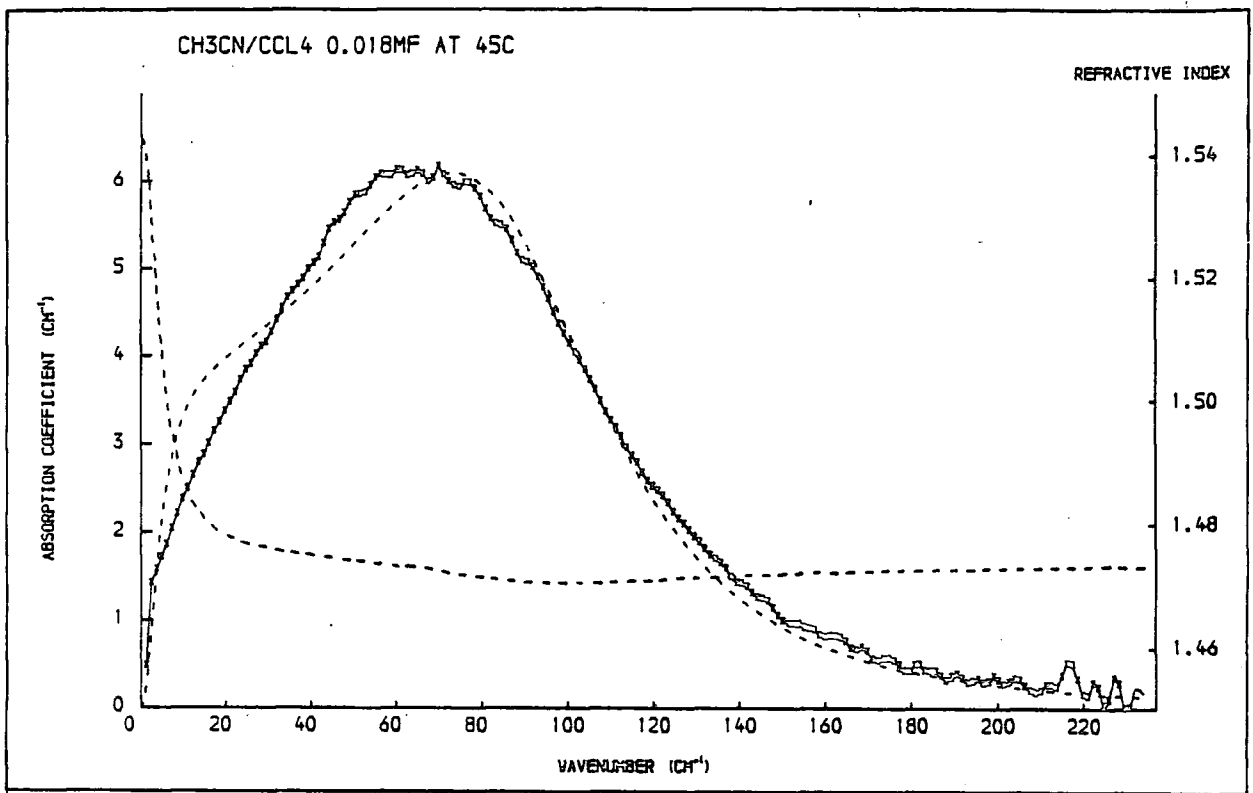


FIGURE 6.23  
SPECTRA RECALCULATED FROM A THREE PARAMETER MODEL FIT

that calculated by the conventional formula. In itself this immediately contradicts the possibility of dimers being present in quantity and accounting for absorption to any significant degree.

## B. THE COMPARISON OF VIBRATIONAL CONTRIBUTIONS TO BAND WIDTH

In Chapter 1 the basic theory for the separation of contributions of the  $\nu_1$  stretching mode and the  $\nu_3$  symmetric bending mode to the band width was outlined. This was based on the assumption that the vibrational contribution obtained from the isotropic Raman spectrum is the same as that in the anisotropic Raman and the infrared spectrum for a given mode. Hence the relation

$$\phi_{\text{V}}^{\text{IR}} = \phi_{\text{V}}^{\text{ISO}} = \phi_{\text{V}}^{\text{aniso}}$$

is often assumed.

Since the infrared spectrum comprises a vibrational and a reorientational part and the far-infrared spectrum does not include a vibrational contribution it is possible to obtain the vibrational part of the infrared (total) spectrum by a simple subtraction of the rotational part assuming that this contributes equally to the correlation functions. In order to perform this separation the assumption is made that  $\tau^{\text{MORI}}$  obtained from the model analysis of a very dilute solution (0.018mf) is equal to  $\tau_{1\text{R}}^{\text{S}}$  i.e. the cross terms in equation 1.23 are assumed to be negligible<sup>10,49</sup>. A similar assumption allows us to write  $\tau_{\text{D}}$  (Fouss-Kirkwood)  $\equiv \tau_{1\text{R}}^{\text{S}}$ , for dilute solutions.

Assuming that the bands are pure Lorentzian we can write

$$\Delta\bar{\nu}_{1/2} = \left( \pi c \tau_{1\text{R}}^{\text{S}} \right)^{-1} \quad \dots\dots\dots 6.5$$

and hence obtain the far infrared/microwave rotational band width from the  $\tau$  value. The half widths obtained are then subtracted from the infrared (total) band width<sup>1</sup> for comparison with the isotropic Raman<sup>4</sup> values. The results of this analysis are given in Table 6.9.

Band	IR (TOTAL)	FIR (MORI) (318K) (0.018mf)	Calculated IR <sub>vib</sub>	FIR/Microwave (Fouss-Kirkwood) (298K)(0.016mf)	Calculated IR <sub>vib</sub>	Raman (ISO) (318K) (0.03mf)
$\nu_1$	12.0	4.8	7.2	3.7	8.3	4.5
$\nu_3$	8.0	4.8	3.2	3.7	4.3	4.8

TABLE 6.9  
CALCULATED AND OBSERVED VIBRATIONAL HALF WIDTHS  
FOR ACETONITRILE IN CARBON TETRACHLORIDE

It is evident from these results that the vibrational contribution to the infrared and Raman spectral bands  $\nu_1$  and  $\nu_3$  are not equal. In an attempt to understand this discrepancy it is necessary to examine more closely the processes from which the 'vibrational' contribution (s) might arise. These are more accurately described as the 'non-reorientational' processes and can be divided in to



that dipole-dipole forces are predominant.<sup>30,31</sup> It has been shown<sup>4,5,7</sup> that this cannot be the case since for this mode the relaxation rate  $(\tau_v^{ISO})^{-1}$  increases with temperature (at constant density) the opposite of the  $\rho\eta/T$  dependence expected if dipole-dipole interactions were predominant. The cross term for the  $\nu_3$  mode a symmetric bend is positive which indicates the presence of dispersive interactions.<sup>30,31</sup> This hypothesis is not supported by the non linear variation in band width of these bands with concentration which has been observed for this mode. In the light of these results it would appear that resonance energy transfer effects do not account for the invalidity of equation 1.20.

Another possible explanation is that collision induced contributions are significant as indicated by previous studies<sup>4,5,7</sup> of the temperature density and concentration dependence of these bands. If this is the case then the transition moment  $\partial\bar{\mu}/\partial Q$  and the polarisability derivatives  $\partial\alpha/\partial Q$  and  $\partial\beta/\partial Q$  might be affected differently by such processes and then there would be no reason to assume that the contributions to the vibrational bands would be the same.

Finally attention is returned to the assumptions made in Chapter 1 which allow the separation of the vibrational contributions to these bands via equations 1.5, 1.6, 1.13, 1.14. It was assumed that the vibrational and reorientational motions of the molecules are statistically uncorrelated, which may not be true particularly for the complex highly polar acetonitrile molecule.<sup>7,14</sup> In addition the possibility of the coupling of the vibrational relaxational mechanisms has been neglected in the expression for the phase relaxation correlation function given by 1.21. This should be constructed in full as the ensemble average of the correlation functions of the  $j$  mechanisms by which  $\langle Q^i v(0) \cdot Q v^i(t) \rangle$  may decay<sup>1</sup> i.e.

$$\phi_{pp}(t) = \langle \phi_1(t) \cdot \phi_2(t) \dots \phi_j(t) \rangle \dots \dots \dots 6.7$$

The relative effects of the cross terms between these mechanisms on the infrared and Raman spectra are not known.

The conclusion of this analysis is that the non reorientational contributions to the infrared and Raman spectra correlation functions are not fully understood and therefore the results obtained by subtraction procedures commonly employed must be treated with caution.

**C. A FURTHER DISCUSSION OF THE INTERNAL FIELD CORRECTION FACTORS APPLIED IN CHAPTER 5**

The internal field expressions which relate the macroscopic relaxation time  $\tau_D$  to the single particle (molecular) relaxation time  $\tau^S$  provide an indication of the local order which exists in the system via the Kirkwood<sup>87</sup> g factors. The correlation function for the far-infrared/microwave region can be expressed,

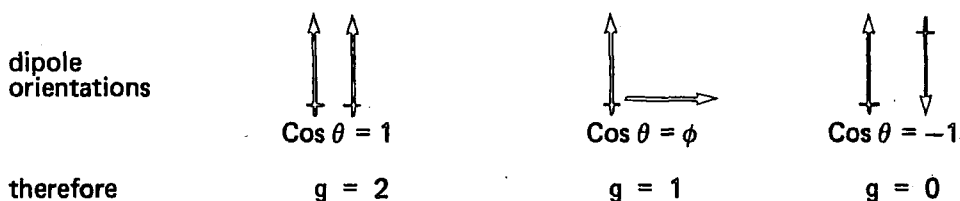
$$g(t) = \langle \cos \theta_{ij}(t) \rangle + \sum_{i \neq j} \langle \cos \theta_{ij}(t) \rangle \quad \dots\dots\dots 6.8$$

which at zero time is equivalent to the Kirkwood g factor and becomes,

$$g(0) = 1 + \sum_{i \neq j} \langle \cos \theta_{ij}(0) \rangle \quad \dots\dots\dots 6.9$$

where  $\theta$  = the angle of rotation of the dipole.

Inspection of this relationship enables the construction of a crude physical picture of the static dipole orientations as shown below.



The results given in Chapter 5 (Table 5.10) show clearly that in all cases the  $\tau^S$  factors are greater than the  $\tau^{mic}$  or  $\tau_D$  values from which they are derived i.e. the g factors are less than 1. The g factors derived from the internal field expression given by Kluk (denoted K in Table 5.10) have an average value of approximately 0.75 which in terms of the crude physical model described previously indicates that the dipoles have a preferred orientation between orthogonal and in line opposed at 105°. In addition the overall decrease in the g value indicates that there may be further alignment on average (opposed) as the concentration is increased. The alignment of the dipoles in this way seems to be very plausible in light of the highly polar nature of CH<sub>3</sub>CN, in fact it is difficult to imagine that the dipoles would exist in the average configuration of 90° orientation which would be expected if the molecules were randomly aligned. However, it is often assumed that the single particle rotational correlation time  $\tau^S$  will be shorter than the observed correlation time  $\tau_D$ . This condition dictates that g is greater than 1 and hence infers that the dipoles have some preferred alignment between 0° and 90°, a situation which is even more difficult to envisage for molecules with a dipole moment of 3.9 Debyes.

The results of this analysis reveal an interesting paradox by the following argument. Order in the system i.e. the alignment of dipoles appears to be reasonable but it must lead to a greater cross term contribution to  $\tau_D$  and hence  $\tau_D$  would be greater than  $\tau^S$ . This is in contradiction to the results found where  $\tau_D < \tau^{SP}$  but it is order, in this case with the dipoles aligned between 0° and 90°. The answer to this enigma probably lies in the neglect of the dynamic effects in these relations.

Finally, attention is returned to Hildebrand's comments<sup>125</sup> referred to in Chapter 2. He has shown from vapour pressure studies, that 'simple' liquids are in a state of maximum disorder i.e. their entropy is complete. If this is also the case for these solutions then it obviously disallows the possibility of structure (order) existing over any timescale. Assuming that this is the case, then models pertaining to the molecular dynamics of these solutions, which refer to such structure eg. holes, cells, clusters, lattices must be regarded as suspect.

**CHAPTER 7**  
**ION-ION AND ION-SOLVENT INTERACTION IN NON-POLAR SOLVENTS**

## CHAPTER 7

### ION-ION AND ION-SOLVENT INTERACTION IN NON-POLAR SOLVENTS

#### INTRODUCTION

Far-infrared spectroscopy is well-suited for the study of liquid phase interaction as it corresponds to the time scale 0.1 - 10 pico seconds. It is on this time scale that the intermolecular vibrations of such systems as tetra-n-alkyl ammonium halide solutions in non-polar solvents occur. The study of these quaternary salts has been considered to be worth while since the elucidation of their complex interactions in solution may enable a better understanding of biologically important systems such as those concerned with cell membrane ion transport phenomena<sup>206-210</sup> which cannot easily be studied directly due to the intense absorption by water in this region.<sup>211</sup> A programme of work carried out in this laboratory<sup>212-215</sup> has extended our knowledge of ion-ion and ion-molecule interactions by systematic study of the spectra of a range of the salts  $R_4N^+X^-$  (where R = an alkyl group and X = a halide) at different concentrations, temperatures and in various solvents. The hypothesis has been proposed that these spectra comprise at least three main features each of which may arise from more than one process. In this work further studies of these systems<sup>214,215</sup> have been made using the more advanced instrumentation and techniques described in Chapter 3 and reference 132. The research carried out has been divided into three main areas as follows:

- i. Extended studies of the concentration effect.
- ii. Possible ion or solvent penetration effects.
- iii. The role of water in these systems.

Throughout this work the solutions were freshly prepared using spectrosol solvents (previously dried over 4A molecular sieves for 2-3 days) and analar grade salts supplied by Eastman-Kodak Ltd. The solutions thus prepared were transferred with all glass syringes to Beckman-R11C FH03 demountable cells fitted with 2.5mm white polyethylene windows for mounting in the interferometer. The double sided interferograms were recorded at a sampling interval of 16 microns over a path difference of 0.8cm (from z.p.d.). After apodisation and transformation the resolution of the spectra was approximately  $2.4\text{cm}^{-1}$ .

- i. Extended studies of the concentration effect.

The low concentration limit to which these systems have been studied previously<sup>212,213</sup> has been limited to approximately 0.1 molar (0.3m in some cases<sup>212</sup>). Below this concentration the path lengths required have been too long to achieve sufficient energy throughput (due to solvent absorption) to record the solution spectra. Figure 7.1 shows an example of a spectrum of a 0.0133 molar solution of tetra-n-butyl ammonium chloride ( $n\text{.Bu}_4\text{N}^+\text{Cl}^-$ ) in benzene recorded with a path length of 7.5mm using the conventional optics and a Golay detector. Figure 7.2 shows the spectrum of the same solution recorded with the more sensitive germanium bolometer detector (also with conventional optics). In addition to the improvement in signal-to-noise ratio over the frequency range studied previously ( $20 - 250\text{cm}^{-1}$ ), it has also become possible to extend the

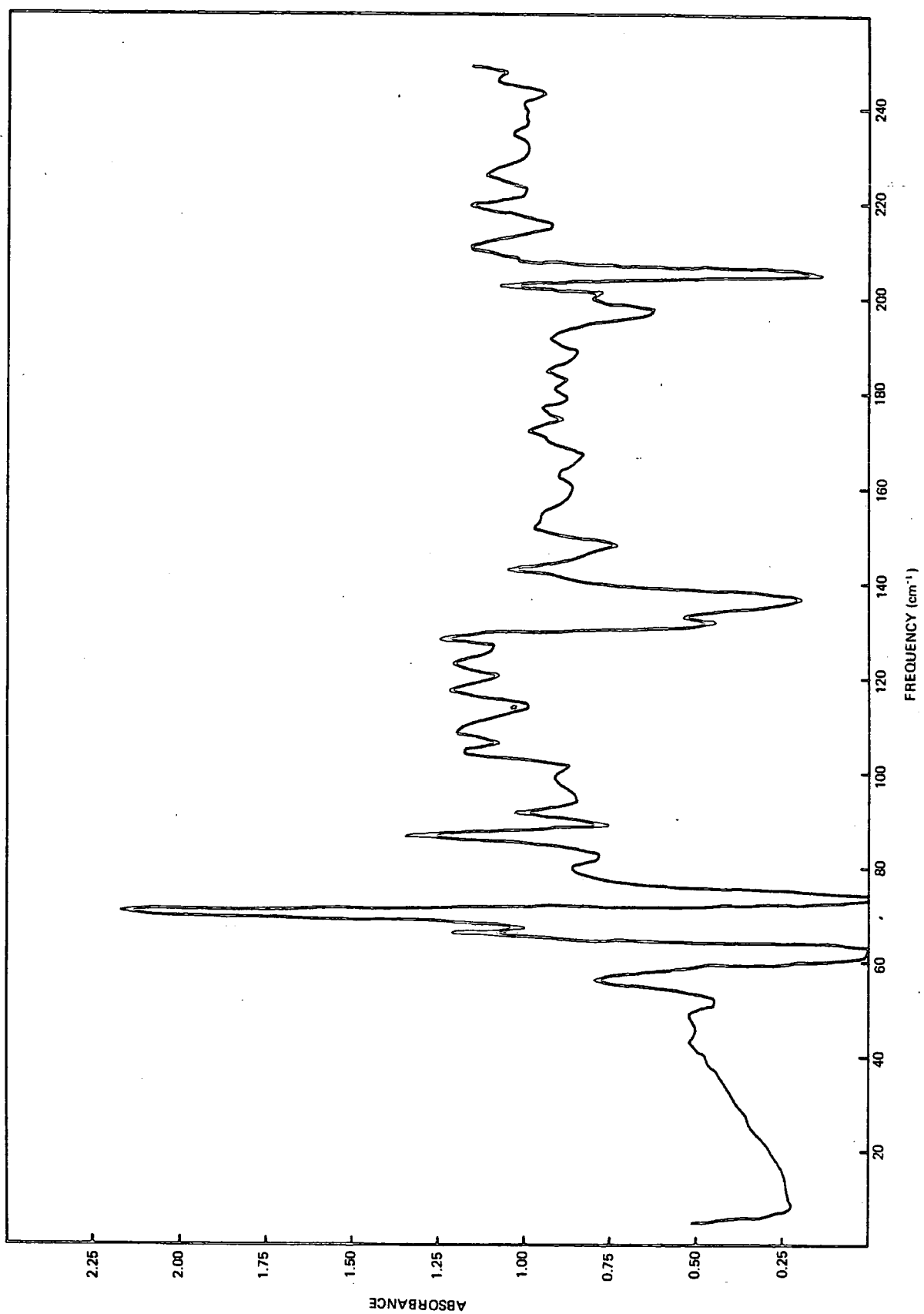
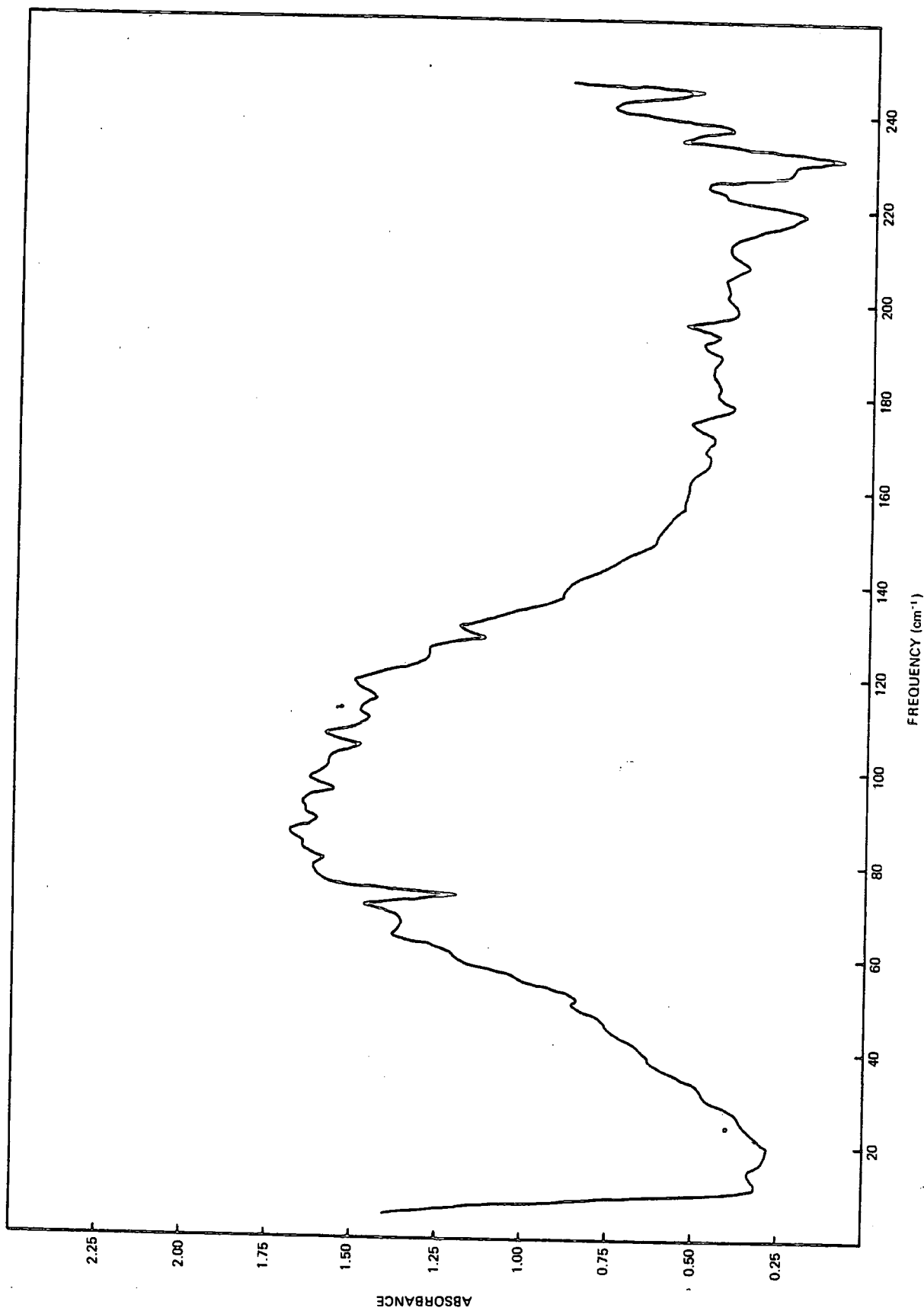


FIGURE 7.1

ABSORPTION SPECTRA OF  $\text{Bu}_4\text{N}^+\text{Cl}^-$  in BENZENE SOLUTION (0.0133 mol l<sup>-1</sup>)  
RECORDED WITH THE GOLAY DETECTOR (PATH LENGTH 7.5mm)



FREQUENCY (cm<sup>-1</sup>)

FIGURE 7.2

ABSORPTION SPECTRUM OF  $\text{Bu}_4\text{N}^+\text{Cl}^-$  IN BENZENE SOLUTION ( $0.0133 \text{ mol l}^{-1}$ ) RECORDED WITH THE COOLED DETECTOR (PATH LENGTH 7.5mm)

measurements to the low frequency 'tails' of the spectra with the use of the polarising optics in conjunction with the germanium bolometer detector. Figure 7.3 shows an example of such a spectra which illustrates that it is now possible to obtain real information down to below  $5\text{cm}^{-1}$  (and possibly<sup>132</sup> as low as  $2\text{cm}^{-1}$ ), which should help in the separation of spectral features which give rise to the overall band shape.

During previous work<sup>212, 213</sup> the band profile of  $n.\text{BU}_4\text{N}^+\text{Cl}^-$  in benzene has been assumed to be the sum of at least three main absorption bands. Figure 7.4 shows a typical band fit to a  $n.\text{BU}_4\text{N}^+\text{Cl}^-$  solution spectra which has been obtained by computer fitting three gaussian bands to the most obvious features of the spectra. Table 7.1 summarises the peak frequencies of the fitted band B for a range of salts in benzene and chloroform solution. These results clearly show that  $\bar{\nu}_{\text{max}}$  of band B is both cation and anion dependent and it is therefore thought to arise from some kind of vibration of the ion pair.

Salt	Solvent <sup>a</sup>	Band Centre ( $\text{cm}^{-1}$ )
$n.\text{Bu}_4\text{N}^+\text{Cl}^-$	$\text{C}_6\text{H}_6$	$121 \pm 1$
$n.\text{Bu}_4\text{N}^+\text{Br}^-$	$\text{C}_6\text{H}_6$	$79 \pm 1$
$\text{Pe}_4\text{N}^+\text{Cl}^-$	$\text{C}_6\text{H}_6$	$115 \pm 3$
$\text{Hp}_4\text{N}^+\text{Cl}^-$	$\text{C}_6\text{H}_6$	$112 \pm 3$
$n.\text{Bu}_4\text{N}^+\text{I}^-$	$\text{CHCl}_3$	$61 \pm 3$
$n.\text{Bu}_4\text{N}^+\text{NO}_3^-$	$\text{CHCl}_3$	$100 \pm 3$
$n.\text{Bu}_4\text{N}^+\text{ClO}_4^-$	$\text{CHCl}_3$	$85 \pm 3$

a - Concentration 0.5M

TABLE 7.1  
BAND CENTRE OF B WITH RESPECT TO CATION AND ANION

Some support for this hypothesis has been obtained by assuming that the band arises from a normal mode in which the vibration of the ion pair occurs along the axis joining their centres. For this case the frequency of vibration,  $\nu_{\text{obs}}$  is given in the (harmonic) diatomic approximation by

$$\bar{\nu}_{\text{obs}} = \frac{1}{2\pi c} (K_{\text{obs}}/\mu^1)^{1/2} \quad \dots\dots\dots 7.1$$

where  $K_{\text{obs}}$  is the force constant of the bond between cation and anion

$$\mu^1 = M_{\text{C}}M_{\text{A}} / (M_{\text{C}} + M_{\text{A}}) \text{ the reduced mass}$$

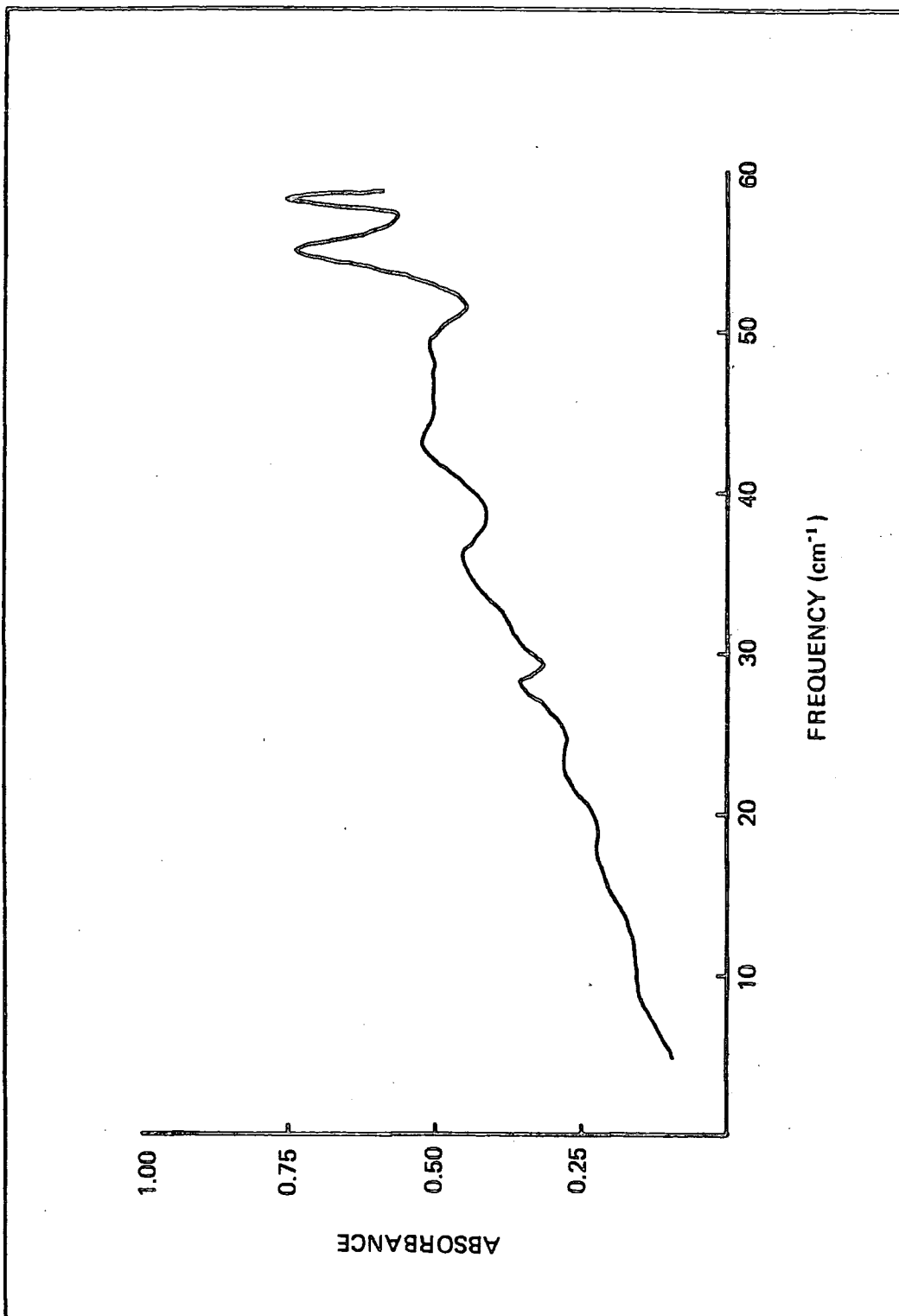


FIGURE 7.3  
LOW FREQUENCY SPECTRUM OF Bu<sub>4</sub>N<sup>+</sup>Cl<sup>-</sup> IN BENZENE SOLUTION (0.0133 mol l<sup>-1</sup>)  
RECORDED WITH COOLED DETECTOR AND POLARISING OPTICS

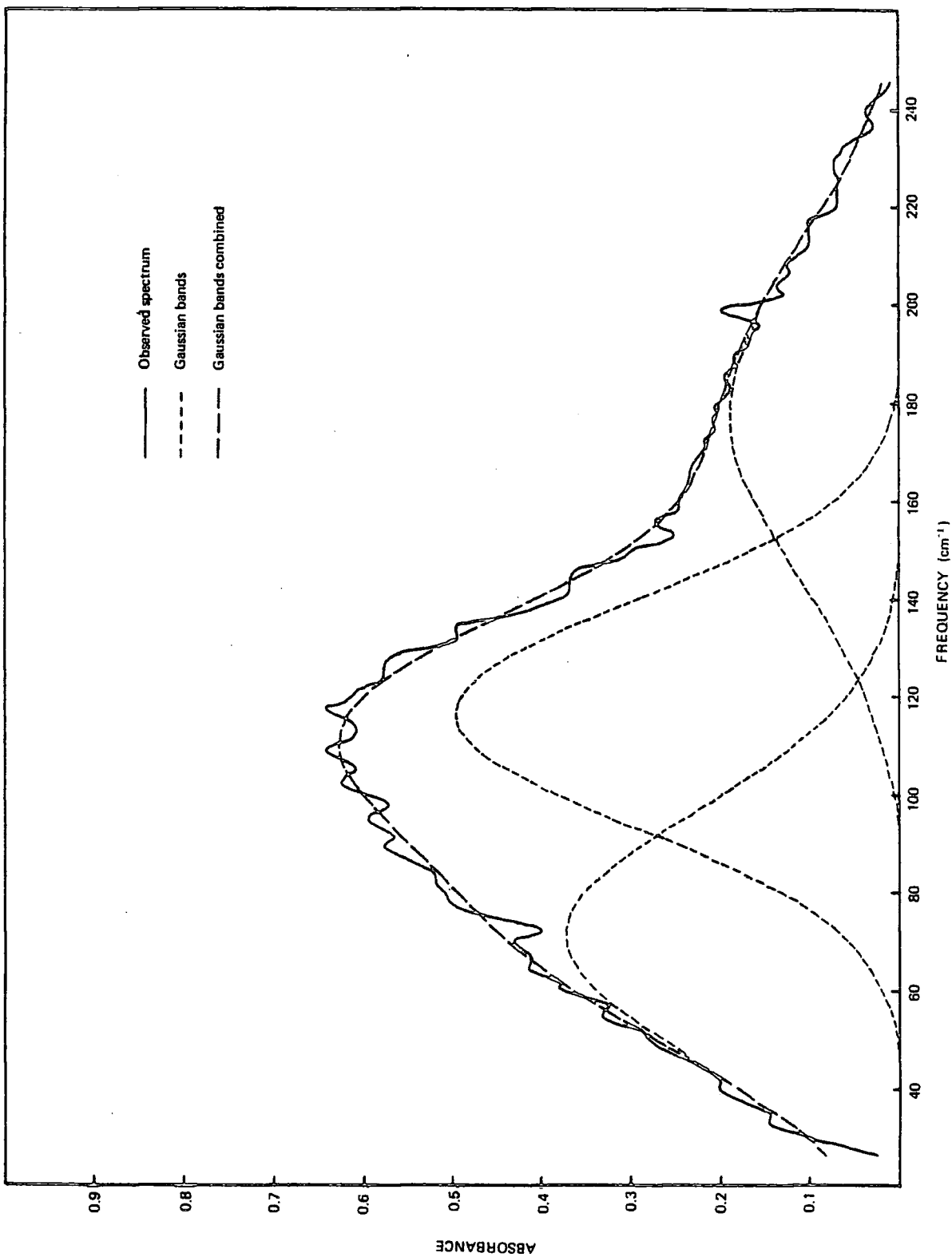


FIGURE 7.4

COMPUTED BAND FIT OF 3 GAUSSIAN BANDS TO THE SPECTRUM OF  $\text{Bu}_4\text{N}^+\text{Cl}^-$  IN BENZENE SOLUTION (0.4980 mol l<sup>-1</sup>)

By assuming that the restoring force between the ions is purely coulombic (i.e. a purely electrostatic ion pair model) the force constant can be calculated from the expression<sup>122</sup>

$$K_{\text{CALC}} = \frac{-2e^2}{4\pi\epsilon_0\epsilon r_{\text{CA}}^2} \quad \dots\dots\dots 7.2$$

- where  $e$  = electronic charge
- $\epsilon_0$  = permittivity of a vacuum
- $\epsilon$  = relative permittivity of medium
- $r_{\text{CA}}$  = sum of ionic radii

If it is now assumed that, to a first approximation,  $r_{\text{CA}}$  is constant then a linear relationship between  $\bar{\nu}_{\text{Obs}}$  and  $(1/\mu)^{1/2}$  would be expected. Calculations<sup>214</sup> using equations 7.1 and 7.2 have indicated that this is so however there is much evidence to suggest that the cation-anion vibrations may be occurring in large aggregates rather than free ion pairs. For example cryoscopic measurements,<sup>216</sup> which suggest aggregates of about 20-30 ion pairs, and measurements of the concentration dependence of the ion pair dipole moment.<sup>217</sup> Therefore it is concluded that the electrostatic ion pair model proposed is far too simple (although quite plausible) to fully describe these systems.

Early concentration studies<sup>212</sup> revealed that there are severe deviations from Beer's law in these systems. If there is a contribution to the absorption from some kind of aggregate vibration then these non-linear effects might be accounted for by these aggregates breaking up at lower concentration (since, potentially there are less  $\nu_{\text{CA}}$  vibrations as the aggregation number goes down). Figure 7.5 shows the spectra of a range of concentrations of  $n\text{-Bu}_4\text{N}^+\text{Cl}^-$  in benzene plotted on a  $\text{neper cm}^{-1} \text{ mole}^{-1}$  scale for direct comparison. Despite the overall increase in intensity, band fitting procedures<sup>214</sup> have shown that band b is becoming relatively less intense with the decrease in concentration, which indicates that the aggregates are breaking up as predicted.

It has also been shown<sup>214</sup> that there are variations in the calculated force constant and interionic distances with the decrease in concentration. In all cases the calculated interionic distances ( $r_{\text{CA}}$ ) are shorter, by a factor of 2, than the values obtained from estimates of the effective charge separation<sup>218-220</sup> which in itself supports the cluster hypothesis. Furthermore, the force constant reaches a maximum at a concentration of about  $0.5 \text{ mol l}^{-1}$  which is in agreement with cryoscopic studies<sup>216</sup> of similar systems. Unfortunately the signal-to-noise in the spectra of the very dilute solution ( $0.013 \text{ mol l}^{-1}$ ) is still insufficient for a computer band fitting for inclusion in these calculations. However an approximate calculation of the values of  $K_{\text{Obs}}$  and  $r_{\text{CA}}$  show very little difference from the values for higher concentrations which implies that there is still extensive aggregation. This is in agreement with conductivity measurements which indicate that there is some degree of aggregation down to concentrations as low as  $10^{-5} \text{ mol l}^{-1}$ .

Although the band fittings and calculations seem to fit the theories of the interactions in these systems very well, the interpretations of the spectra are by no means unique. In order to study band B alone it has been necessary to assume the presence of two other bands (A and C)

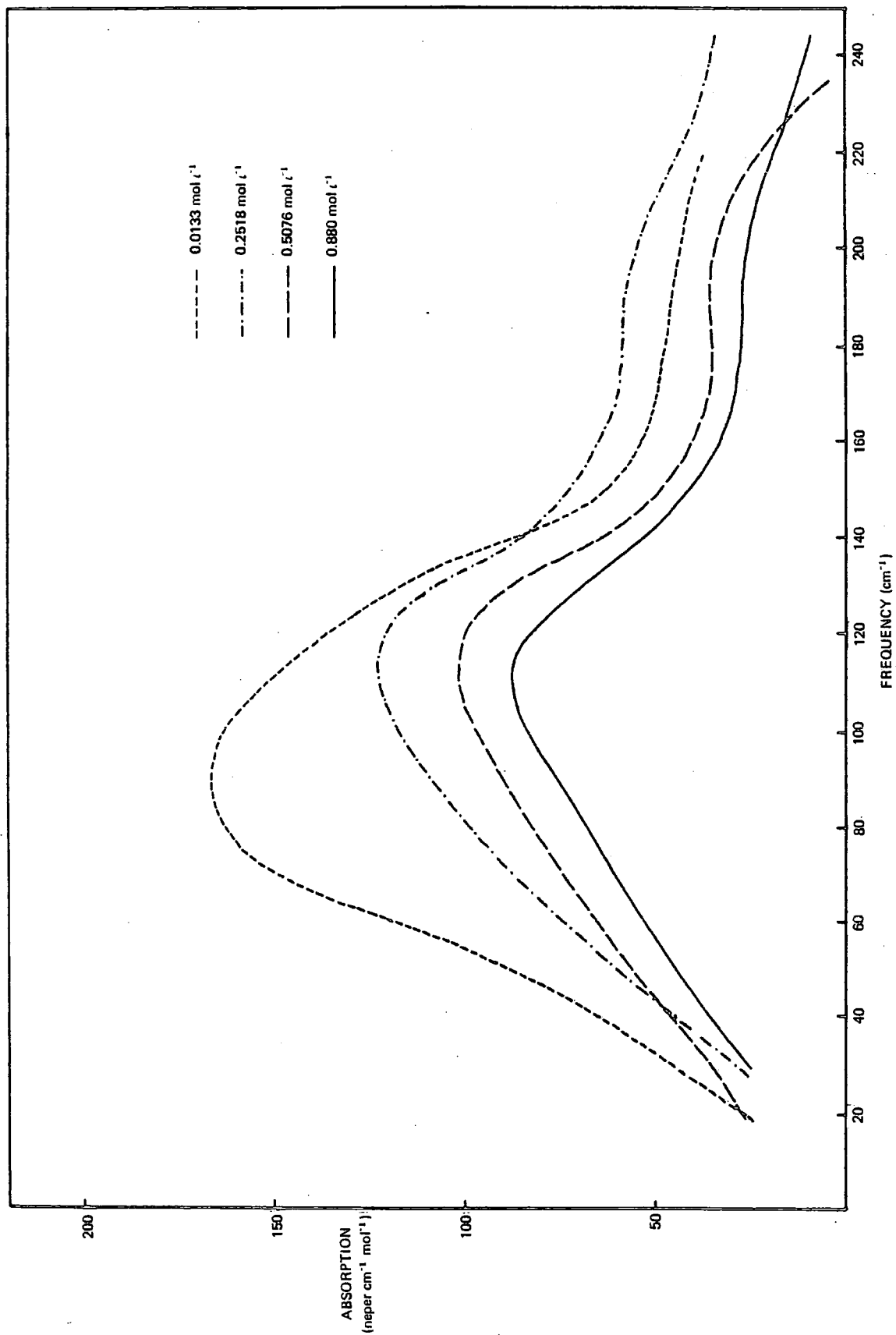


FIGURE 7.5  
ABSORPTION SPECTRA OF A RANGE OF CONCENTRATIONS OF  $\text{Bu}_4\text{N}^+\text{Cl}^-$  IN BENZENE

contributing to the overall band profile. The low frequency asymmetry has been fitted with one band although it is thought to arise from two main processes:<sup>214, 215</sup> (see Chapters 2 and 6).

- (a) The low frequency part arising from the Debye rotation or reorientation of the rigid ion aggregate dipoles.
- (b) The absorption due to fluctuations of induced dipoles caused by ion solvent interactions (collision-induced dipole effects).

It has been shown<sup>214</sup> with calculations using the Gordon intensity sum rule<sup>192</sup> that the intensity arising from the rotation of a rigid ion pair can account for about one half of the total intensity of band A. This calculation was based on the assumption that the effective dipole moment for an ion pair in an aggregate is  $33 \times 10^{-30} \text{Cm}$  and the average interionic distance is 0.3nm. (Note that this implies penetration of the anion into the alkyl chain). Further evidence for the contribution of these two processes to band A is the lack of temperature dependence of the peak frequency.<sup>214</sup> This might be due to a cancellation effect where the absorption arising from the Poley-Hill mechanism decreases in frequency<sup>45, 222</sup> and the absorption arising from the dipole-collision induced dipole effect increases when the temperature is raised. (See Chapter 6).

In the light of this information, where the relative intensities and positions of these features are unknown (and therefore cannot be fitted with separate bands), we cannot be sure that the determination of the intensities and positions of band B are accurate because we cannot be certain how much of band(s) A contributes to the overall spectra. Because of this and evidence for further complexity in the nature of these solutions (see Parts ii and iii for discussion of band C) the systematic study and assignment of band B to vibration of ion aggregates, and in general of the spectra tetra n-alkyl halides in non-polar solvents, have to be made very carefully indeed.

#### ii. Attempts to study solvent and/or ion penetration effects

In the previous section it was indicated that band A probably arises from at least two absorption processes: (a) Debye rotation of rigid ion aggregates and (b) induced dipole, ion-solvent interactions. The first of these two processes was used to account for approximately half the intensity of band A by using the Gordon intensity sum rule which assumed some degree of anion penetration into the alkyl chain. The other half of the intensity of band A has been predicted with the equation given below<sup>215</sup>

$$B = \frac{N\pi}{3c^2 m_{CS}} \left[ \frac{-6\mu_{CA} a_s}{4\pi\epsilon_0 \epsilon R^4} \right]^2 \quad \dots\dots\dots 7.3$$

where R = ion pair-solvent distance

$a_s$  = solvent polarisability

$m_{CS}$  = ion pair-solvent reduced mass

Calculations have shown that to satisfy equation 7.3 and account for the remaining intensity in the observed band the ion pair-solvent distance (R) must be 0.25nm, which implies that there is penetration of the solvent molecules between the alkyl chains. A study of molecular models of

these systems indicates that this is quite feasible since the tetra-alkyl ammonium groups have a very open structure which would allow the close approach of the solvent molecules. Dielectric permittivity measurements<sup>217, 218, 223, 224</sup> on similar systems have indicated that an average value of 0.25nm for the ion pair-solvent distance is reasonable, and so have led to a consideration of the possibility that the solvent molecules are trapped in the large alkyl chain (cation) clusters (or aggregates). If this is the case then the relative size of the solvent molecule to alkyl chain should be important. In order to check this, an investigation was carried out using bulkier solvents such as methylated benzenes and cations with different alkyl chain lengths.

When using p.xylene as a solvent for n.Bu<sub>4</sub>N<sup>+</sup>Cl<sup>-</sup> it was found that the solution (0.48mol l<sup>-1</sup>) immediately separated into two layers, both of which were stable. This phenomenon has been observed previously in several systems including, picrates of the type (C<sub>5</sub>H<sub>11</sub>)<sub>4</sub>N<sup>+</sup>Pic<sup>-</sup> in benzene<sup>225</sup> and tertiary alkyl-ammonium salts of organo metallic anions in various aromatic solvents.<sup>226</sup>

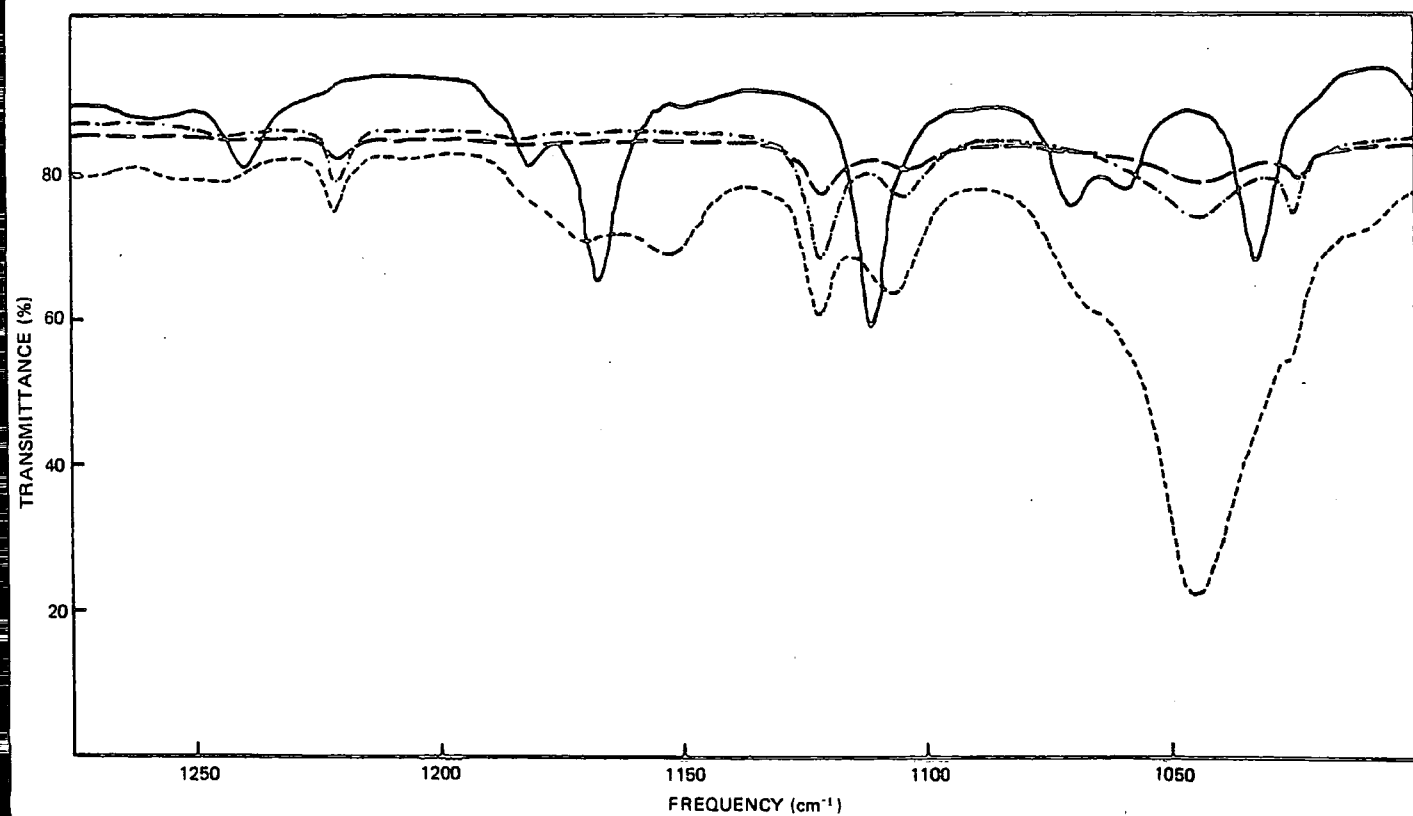
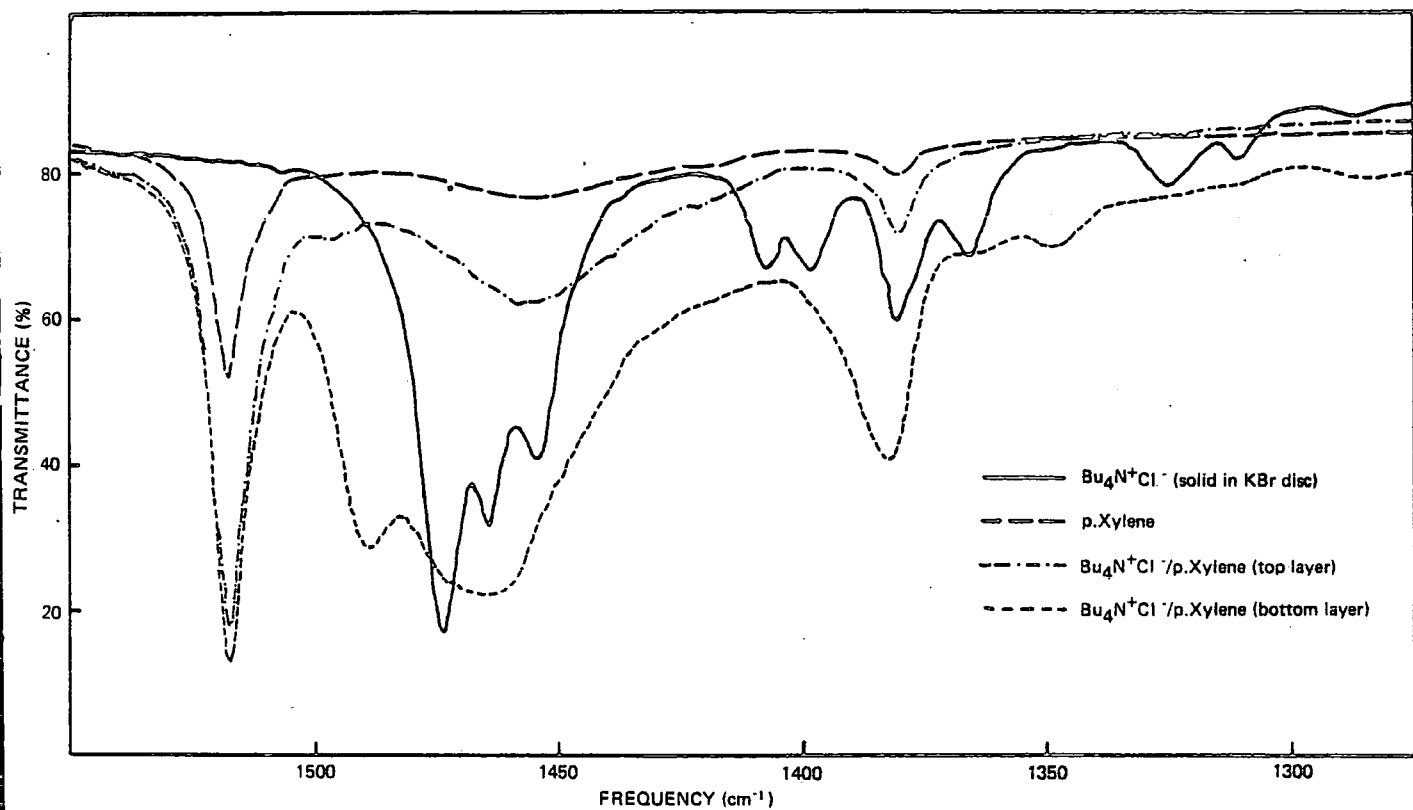
Further experiments with different solvents and solutes indicated that there was a series of these solutions which separated into two layers. Table 7.2 summarises the results obtained.

Solute	Solvent		
	benzene C <sub>6</sub> H <sub>6</sub>	p.xylene C <sub>6</sub> H <sub>4</sub> (CH <sub>3</sub> ) <sub>2</sub>	mesitylene C <sub>6</sub> H <sub>3</sub> (CH <sub>3</sub> ) <sub>3</sub>
n.Bu <sub>4</sub> N <sup>+</sup> Cl <sup>-</sup>		X	X
n.Pe <sub>4</sub> N <sup>+</sup> Cl <sup>-</sup>			X
n.Hex <sub>4</sub> N <sup>+</sup> Cl <sup>-</sup>			

X = two phase system formed

TABLE 7.2  
A SUMMARY OF THE SOLUTE/SOLVENT SYSTEMS OBSERVED

An investigation of the n.Bu<sub>4</sub>N<sup>+</sup>Cl<sup>-</sup>/xylene system was carried out. Initial analysis for the chloride indicated that all of the salt was in the bottom layer, and the concentration of this layer was constant at 2.7 mol l<sup>-1</sup>. Chloride analysis of the top layer proved negative and so it was concluded that the concentration was less than 0.5%. Evidence in support of this was obtained from the near-infrared spectrum of the top layer which did not exhibit any bands other than those attributed to pure p.xylene. The near-infrared spectrum of the bottom layer clearly showed the p.xylene and solute bands expected. In addition the expansion of the 1000cm<sup>-1</sup> to 1500cm<sup>-1</sup> region (Figure 7.6) revealed several features not present in either the solvent or solute spectra and two strongly perturbed p.xylene bands at approximately 1050cm<sup>-1</sup> and 1380<sup>-1</sup>.



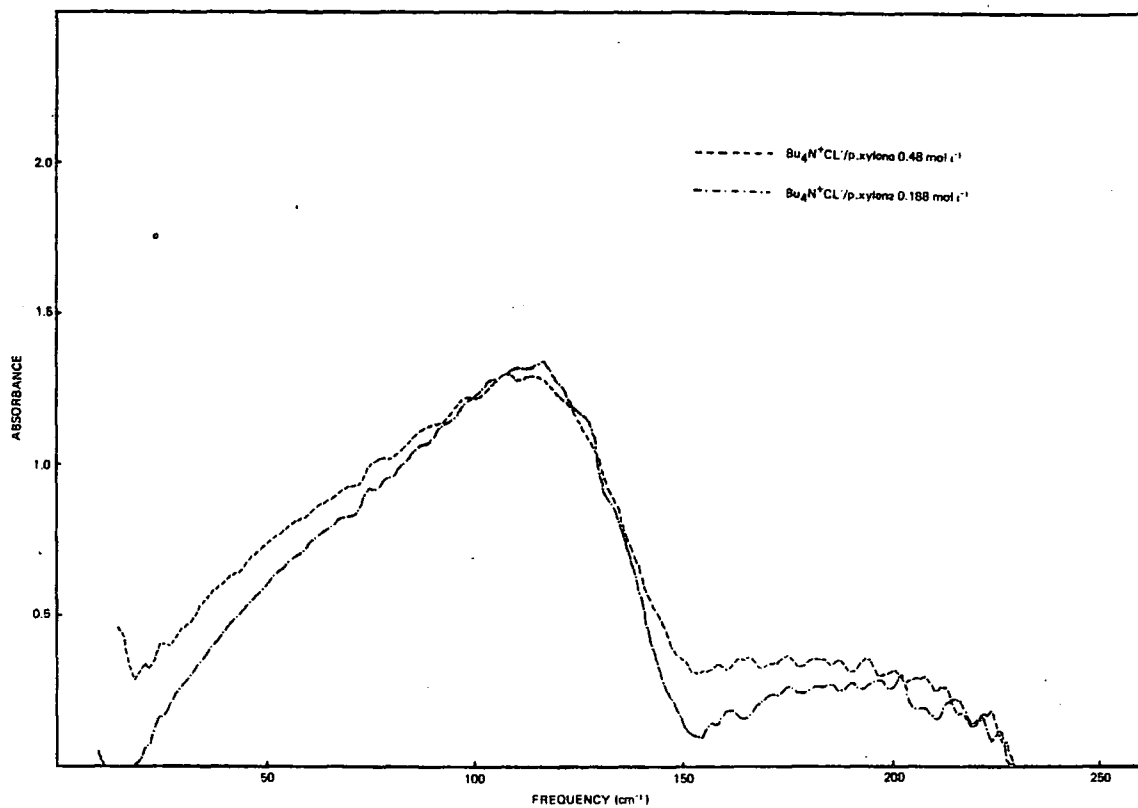
**FIGURE 7.6**  
**NEAR-INFRARED SPECTRA OF  $\text{Bu}_4\text{N}^+\text{Cl}^-$  (SOLID), P.XYLENE AND SOLUTION LAYERS**

Figure 7.7 shows the far-infrared spectra of the bottom layer extracted from two different (bulk) concentration solutions. These spectra exhibit the same general features as the homogenous benzene solutions described previously however they appear to be more clearly defined particularly in the case of band C. Comparing these two concentrations it can be seen that the spectra have the same shape and maximum intensity, but that of the more concentrated solution shows a larger band A and band C contribution. Figure 7.8 shows the far-infrared spectra of the top layer from the same two solutions for comparison with the pure p.xylene spectrum (obtained by ratioing two thicknesses of p.xylene 0.1/0.2mm). It is clear from these spectra that there is evidence for the presence of a small amount of the salt in the top layer which is leading to the perturbation of a p.xylene band. It should be noted that the perturbation appears to be stronger in the more concentrated solution.

In an attempt to understand the phase separation phenomenon a systematic study was embarked upon to check again for the differences in solute concentrations in top and bottom layers derived from a range of (bulk) concentrations of  $n\text{-Bu}_4\text{N}^+\text{Cl}^-$  in p.xylene. Additional precautions were taken to eliminate water from the systems as follows (these had not been thought necessary for benzene solutions in previous work<sup>212</sup>). The p.xylene was dried as normal over a 4A molecular sieve and transferred to a dry nitrogen flushed glove box. The  $n\text{-Bu}_4\text{N}^+\text{Cl}^-$  was transferred to a flask and dried (with warming  $40^\circ\text{C}$ ) under vacuum for 7 hours. Samples of the dried salt were then weighed out in the glove box and made up with p.xylene to known concentrations. It was found that under these conditions the  $n\text{-Bu}_4\text{N}^+\text{Cl}^-$  appeared to be insoluble and no phase separation occurred. The far-infrared spectra (Figure 7.9) of the resulting 'solutions' showed little evidence of the features observed previously. The addition of small amounts of water to the 'solutions' (containing the undissolved salt) with a microsyringe brought about immediate solution and separation into two layers. The spectra of the bottom layers resulting from this process seem to be similar to the previous examples and analysis showed that all the salt was present in the bottom layer as observed previously. The near-infrared spectra recorded of the bottom layers of these systems show water in the bottom layer with the salt (Figure 7.10). Table 7.3 summarises the volumes of water added for complete solution over a range of concentrations of  $n\text{-Bu}_4\text{N}^+\text{Cl}^-$  in p.xylene.

concentration (bulk) of salt ( $\text{mol}^{-1}$ )	volume $\text{H}_2\text{O}$ (mls)	volume solution (mls)	% water	phases observed
$5.037 \times 10^{-4}$	0.0	25	0.0	Cloudy
$6.657 \times 10^{-3}$	0.002	10	0.02	Cloudy
$5.624 \times 10^{-2}$	0.008	10	0.08	2 layers
$1.844 \times 10^{-1}$	0.017	10	0.17	2 layers

TABLE 7.3



**FIGURE 7.7**  
**FAR-INFRARED SPECTRA OF  $\text{Bu}_4\text{N}^+\text{Cl}^-/\text{P.XYLENE}$  (BOTTOM LAYER)**

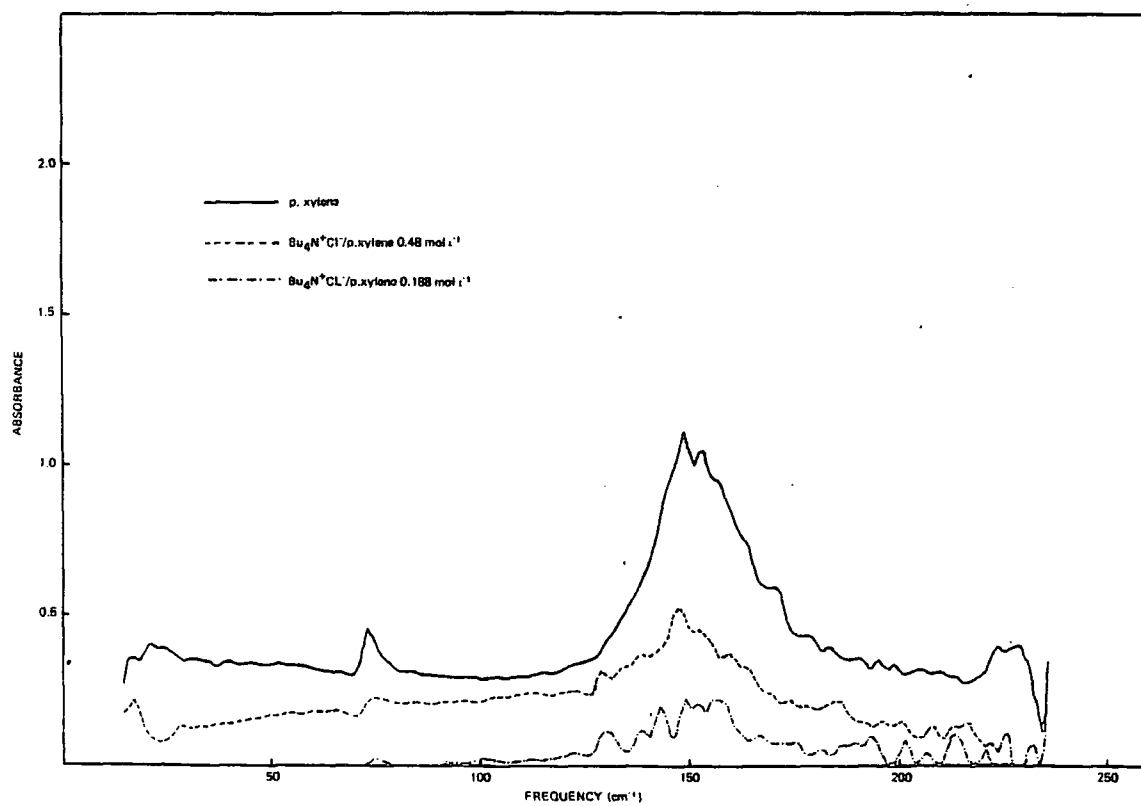


**FIGURE 7.8**  
**FAR-INFRARED SPECTRA OF  $\text{Bu}_4\text{N}^+\text{Cl}^-/\text{P.XYLENE}$  (TOP LAYER)**

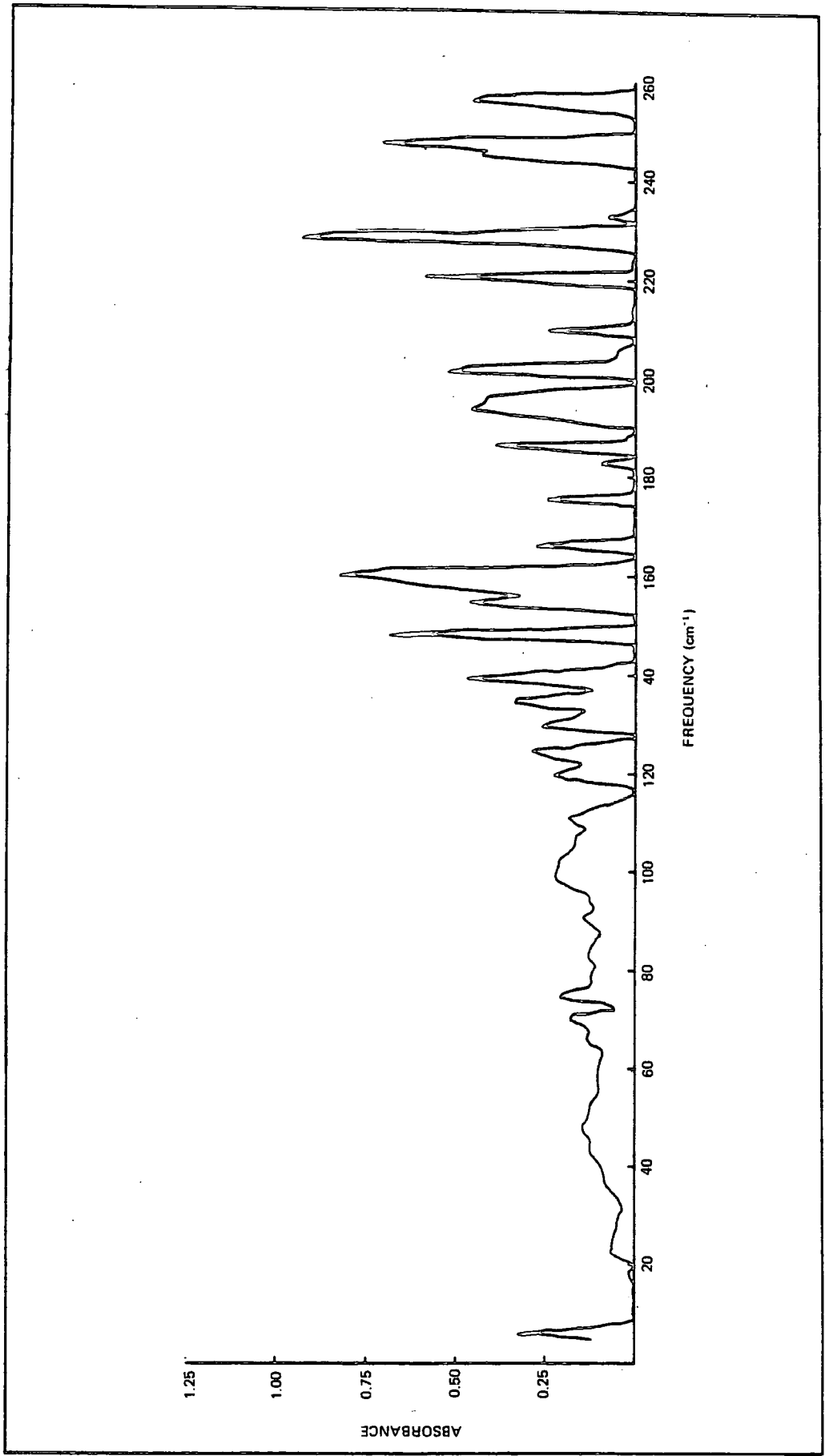
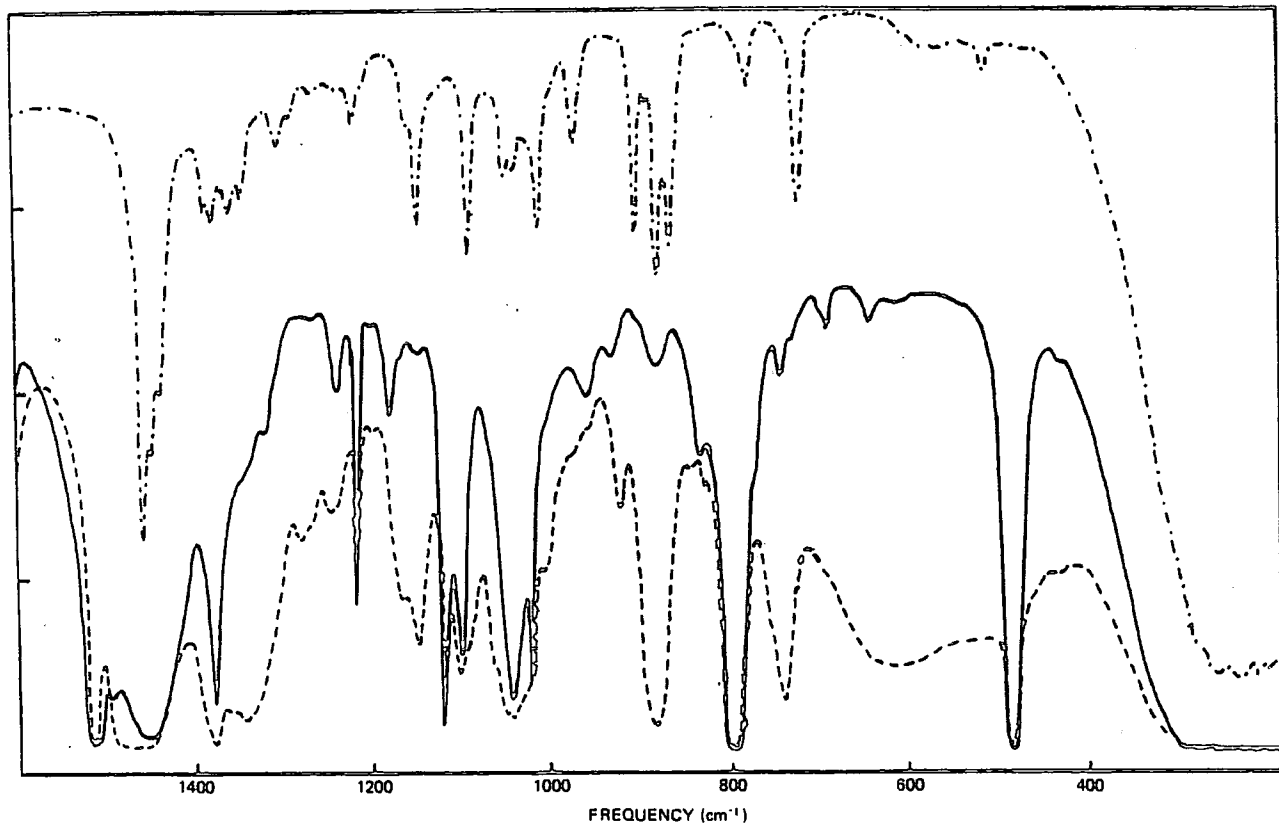
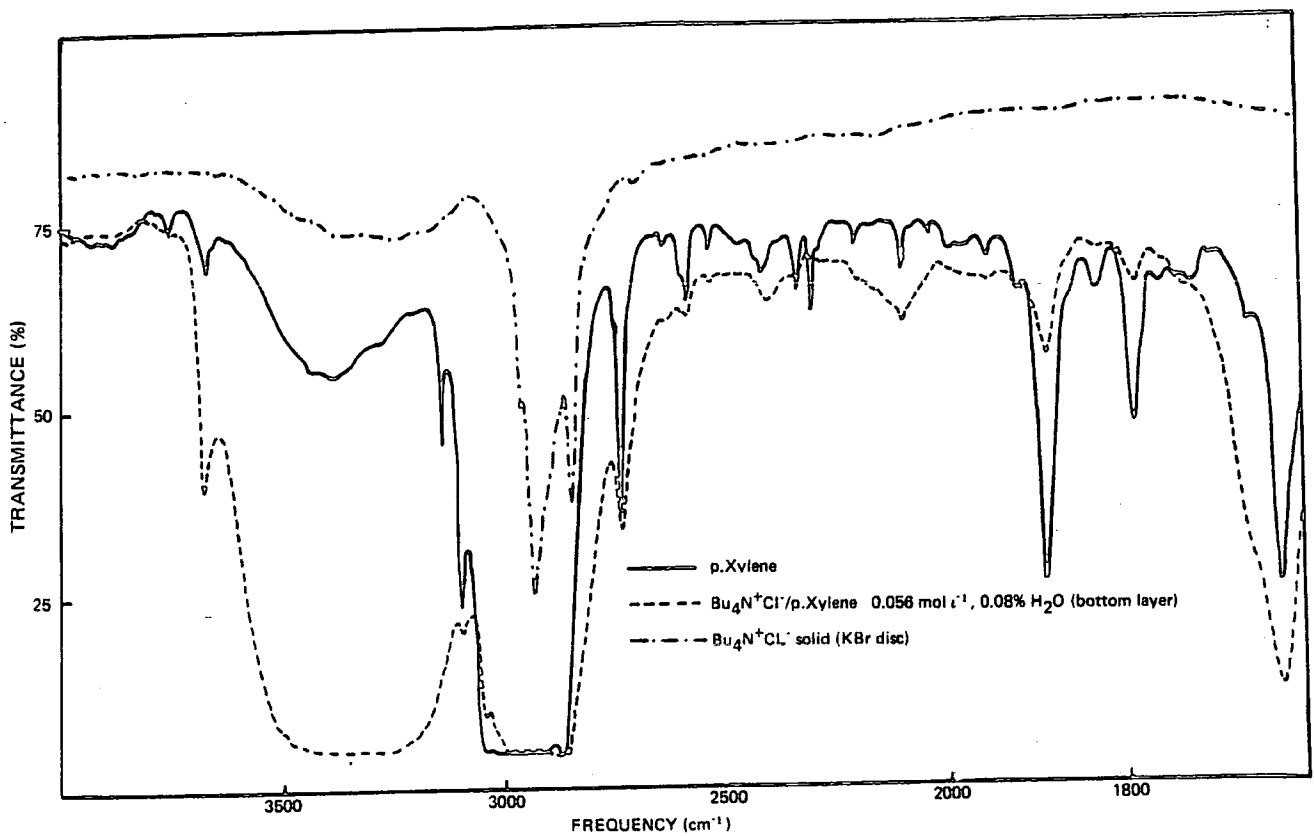


FIGURE 7.9  
ABSORPTION SPECTRUM OF DRIED  $\text{Bu}_4\text{N}^+\text{Cl}^-$  IN P.XYLENE (SATURATED SOLUTION)



**FIGURE 7.10**  
**NEAR-INFRARED SPECTRA OF Bu<sub>4</sub>N<sup>+</sup>Cl<sup>-</sup> (SOLID), P.XYLENE AND SOLUTION H<sub>2</sub>O (BOTTOM LAYER)**

The stoichiometry of the bottom layer of the  $1.844 \times 10^{-1} \text{ M}$  solution (Table 7.3) has been calculated based on the following assumptions:

- the only water present was that added for complete solution (separation)
- the density of the solid salt was used to calculate the volume in solution.

The stoichiometric ratio obtained was as follows:



The difficulties involved in adding very small amounts of water for solution and the uncertainties of the water content of the salt prohibited any further analysis.

### Discussion

The far-infrared spectra of the lower layer of the xylene solutions (Figure 7.7) show the same maximum intensity but the more concentrated solution exhibits a larger low and high frequency asymmetry. However the chloride analysis of these two solutions indicates that the solute concentration is the same ( $2.7 \text{ mol l}^{-1}$ ). Therefore the difference between these two might be due to their water content since these salts are considerably hygroscopic. Band C has been assigned previously<sup>215</sup> to a hydrogen bonded water interaction, possibly a stretching mode<sup>227, 228</sup> O—H...—Cl<sup>-</sup>. In Section iii the role of water in these systems is considered in more detail.

The far-infrared spectra of the top layers of these solutions show a strong absorption at  $150 \text{ cm}^{-1}$  which is thought to be due to a perturbed p.xylene internal mode. This band appears to be more intense in the more concentrated solution which would be expected for a feature which arises from a solute/water-xylene interaction. It might also be expected for this band to occur in the very much more concentrated lower layer. Indeed it is thought that it is present but is very weak, due to the small concentration of xylene. Alternatively the salt may be preferentially interacting with the water in the bottom layer.

The separation of a solution into two liquid phases, sometimes called 'unmixing'<sup>229</sup> has been found previously in many systems. For example, in 1922 Hill<sup>230</sup> observed a two-phase separation in a solution of  $\text{AgClO}_4$  in benzene (1% water) with both phases containing all three components. A system closely related to the ones observed in this work is the  $(i\text{-C}_5\text{H}_{11})_4\text{N}^+\text{Pic}^-$  in benzene studied by Fuoss.<sup>225</sup> More recently a series of two phase systems has been described for a tetra alkyl-ammonium salts of organo-metallic anions in a range of aromatic solvents.<sup>226</sup> Friedman<sup>229</sup> has explained 'unmixing' in terms of severe thermodynamic non-ideality as follows: if the dielectric constant of a solution increases strongly enough with increasing concentration, instability will occur. This is because the solute dipoles are stabilised (relative to their state in pure solvent) by increasing dielectric constant. This stabilisation may become so great that the activity of the solute no longer increases with increasing concentration. The single phase then becomes unstable with respect to two phases and so unmixing occurs.

The results obtained in this work do not follow the same trend as that observed by Atwood<sup>226</sup> for the tetra alkylammonium salts of the organo-metallic anions. In the systems described there is a clear relative size effect and hence the solutions are referred to as 'liquid clathrates'. If the size effect were predominant in the systems studied in this work, one might

expect  $n\text{-Bu}_4\text{N}^+\text{Cl}^-$  to take up more benzene than the other solvents and,  $n\text{-PeN}^+\text{Cl}^-$  more benzene and p.xylene than mesitylene. From Table 7.2 we can see that this is not the case since benzene does not form a two phase system with any of the salts at the concentrations employed here and the tertiary pentyl salt separated into two phases with mesitylene only.

It is apparent then that a further study of these unmixing systems and a search for different systems (in the same series) are necessary before any firm conclusions can be reached about the nature of the interactions involved. In particular, a careful study of the stoichiometries of the solutions with accurate water determination is needed for a systematic examination and correlation of molecular models with the near-infrared and far-infrared spectra.

### iii. The role of water in these systems.

Following the observation of insolubility of the tertiary alkyl ammonium salts in p.xylene (Section ii), an investigation was made into the effects of eliminating water from the systems described in Section i. It was found that these salts are almost completely insoluble in benzene when dried in the manner described in Section ii. The far-infrared spectra of these dry solutions, an example of which is shown in Figure 7.11, show very little absorption in the  $20\text{cm}^{-1}$  to  $140\text{cm}^{-1}$  region and, significantly, none at all to higher frequency where band C has been attributed to a water interaction. Adding small amounts of water to the dry systems (containing solid salt) brought about immediate solution. The spectra of these resulting solutions were found to be identical with the spectra obtained previously for the undried salt (as supplied) systems.

From the analysis<sup>215</sup> of previous studies<sup>212, 137</sup> of the role of water in these systems it is clear that band C increases with the addition of water and hence has been attributed to some kind of water (hydrogen bond) interaction. A comparable effect has been observed by Corset et al<sup>227</sup> where the band at  $170\text{cm}^{-1}$  is shown to increase when phenol ('H' bonding) is added to solutions of tetra alkyl ammonium salts in carbon tetrachloride. It is also significant that band C has never been observed<sup>215</sup> in the considerably less hygroscopic bromide salts, though these salts are still soluble possibly due to the large size of the anion.

Previous investigations<sup>137, 212</sup> of the presence and effect of water in these systems have concluded that the amounts of water present in the solution and measured with the Karl Fisher technique were too small to be significant and the effects of the water in the raw salt were negligible. Spectral intensities were compared of freshly-made (presumably wet due to water carried in salt) solutions and solutions 'dried' over molecular sieves for several days, and found to be identical within the limits of the experiment. However it is apparent that the interaction of the water in these systems is very complex and it may be too tightly bound to be either removed by the molecular sieves or detected accurately by the Karl Fischer techniques. Therefore in order to further clarify the intermolecular processes which give rise to the absorptions in this region it is necessary to prepare completely dry salts and solvents and add carefully known amounts of water whilst monitoring the relative spectral intensities of bands A, B and C.

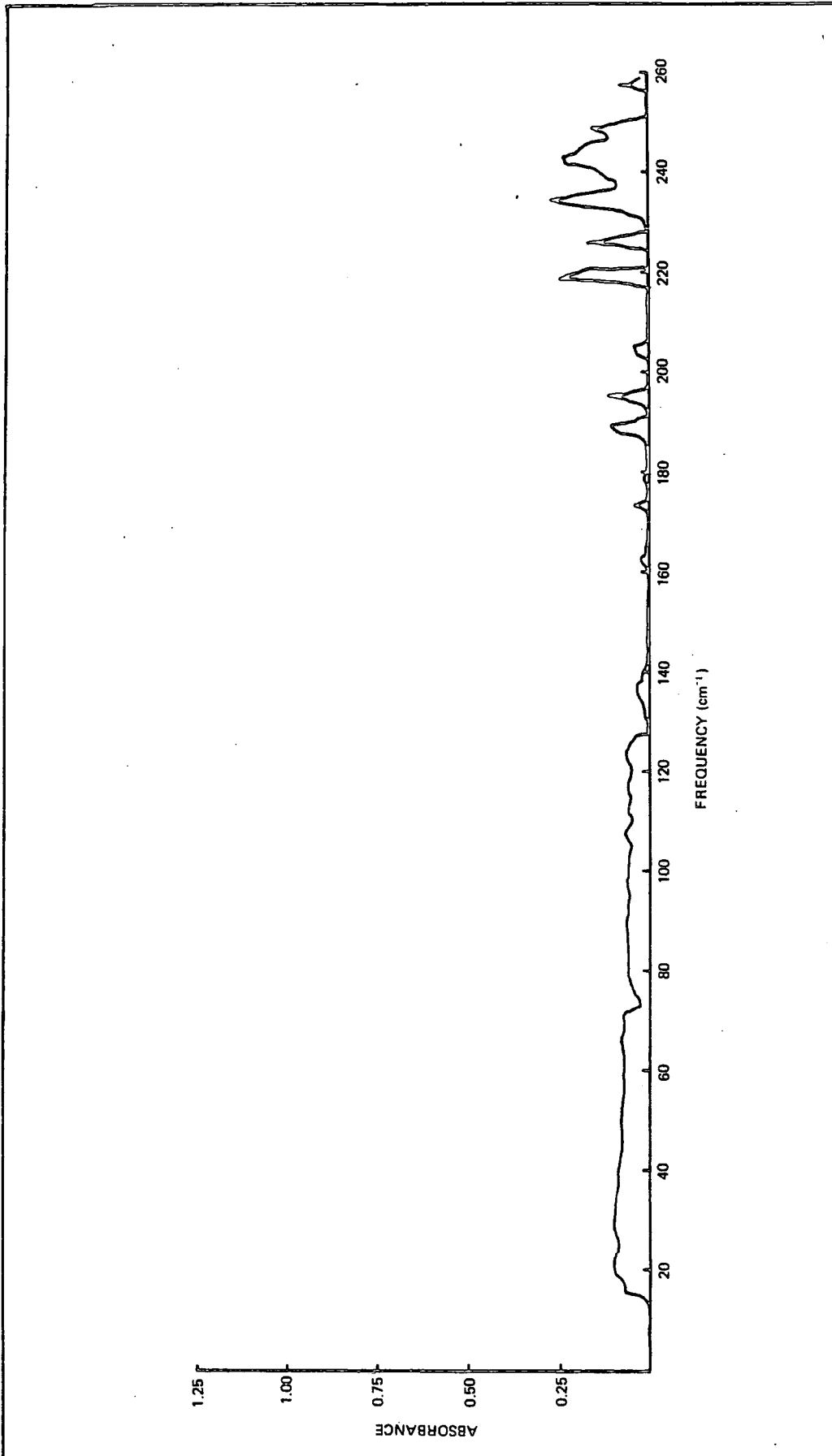


FIGURE 7.11  
ABSORPTION SPECTRUM OF DRIED  $\text{Bu}_4\text{N}^+\text{Cl}^-$  IN BENZENE (SATURATED SOLUTION)

**APPENDIX 1**  
**REFERENCES**

APPENDIX 1  
REFERENCES

1. J.Yarwood, P.L.James, G.Döge, R.Arndt. Faraday Discussions. Vol.66, p.252 (1978)  
[Appendix 2, this Thesis]
2. M.W.Evans, G.J.Evans, J.Yarwood, P.L.James, R.Arndt. Mol.Phys. Vol.38, No.3, p.699 (1979)  
[Appendix 3 this Thesis]
3. R.Arndt, J.Yarwood, Chem Phys Lett Vol.45 1, p.155 (1977)
4. J.Yarwood, R.Arndt, G.Döge, Chemical Physics Vol.25, p.387 (1977)
5. G.Döge, A.Khuen, J.Yarwood, Chem.Phys. Vol. 42, p.331 (1979)
6. J.Yarwood, Advances in Molecular Relaxation Processes Vol.5, p.375  
Elsevier Scientific, Amsterdam. (1973)
7. J.Yarwood, R.Arndt, 'Molecular Association', ed.R.Foster Academic Press, London (1979)
8. R.T.Bailey 'Molecular Spectroscopy' Vol.2 ed.R.F.Barrow, D.A.Long, D.J.Millen  
The Chemical Society, London (1974)
9. W.G.Rothschild, G.J.Rosasco, R.C.Livingston J.Chem.Phys Vol.62, p.1253 (1975)
10. J.E.Griffiths, Vibrational Spectra and Structure, ed.J.R.Durig (Elsevier, Amsterdam 1966)  
Vol.6 J.Chem.Phys Vol.75, p.751 (1973)
11. F.J.Bartoli, T.A.Litovitz J.Chem Phys. Vol.56, ps.404,413 (1972)
12. S.L.Wittenburg, C.H.Wang J.Chem.Phys. Vol.66, p.4255 (1977)
13. J.Schroeder, V.H.Schiemann, P.T.Sharko, J.Jones J.Chem Phys.Vol.66, p.3215 (1977)
14. A.M.Amorim da Costa, M.A.Norman, J.H.R.Clarke Mol Phys.Vol.29, p.191 (1975)
15. P.Debye 'Polar Molecules' The Chemical Catalogue Co. New York (1929)
16. P.S.Hubbard, Phys.Rev. Vol.131, p.1155 (1963)
17. J.S.Rowlinson, M.Evans An. Rep. Chem. Soc. A. Vol.5 (1975)
18. R.G.Gordon J. Chem Phys Vol.42, p.3658 (1965; Vol.43 p.1307 (1965)  
Adv. Mag.Res. Vol.3 p.1 (1968)
19. a R.E.D. McClung J. Chem Phys Vol.51, p.3842 (1969);  
b Vol.54 p.3248 (1971);  
c Vol.55 p.3459 (1971);  
d Vol.57 p.5478 (1972).
20. T.E.Eagles, R.E.D.McClung, Chem.Phys.Lett.Vol.22, p.414 (1973);  
J. Chem. Phys. Vol.59, p.435 (1973)
21. R.Arndt, R.E.D.McClung J. Chem. Phys. Vol. 69, p. 4280 (1978)
22. G.J.Evans, M.Evans J. Chem. Soc. Faraday II Vol.72, p.1169 (1976)
23. G.J.Davies, G.J.Evans, M.Evans J. Chem. Soc. Faraday II Vol.72 p.1901 (1976)
24. W.T.Coffey, G.J.Evans, M.Evans, G.H.Wegdam J. Chem Soc Faraday II Vol.74 p.310 (1978)
25. M.W.Evans, Chem Phys Lett Vol.48 p.385 (1977)

26. M.W.Evans, *Adv.Mol Relaxation Processes* Vol.10 p.203 (1977)
27. M.Evans, 'Dielectric and Related Molecular Processes' ed. M.Davies  
*Specialist Periodical Reports Chem Soc London* Vol.3 p.1 (1977)
28. W.G.Rothschild *J. Chem Phys* Vol.65, p.455 (1976)
29. G.Döge, *Z.Naturforsche* Vol. 28a, p.919 (1973)
30. R.M.Lynden-Bell, *Mol Phys* Vol.33, p.907 (1977)
31. R.M.Lynden-Bell, *Faraday Symp, Chem Soc* Vol.11 (1977) (General Discussion)
32. A.V. Rakov *Opt Spectros* Vol.7, p.128 (1959)
33. A.V. Rakov *Opt Spectros* Vol.13 p.203 (1962)
34. J.Sousseu-Jacob, E.Dervil, J.Vincent-Geisse, *Mol Phys* Vol.28 p.935 (1974)
35. J.E.Griffiths *Chem Phys Lett* Vol.21 p.354 (1973)
36. M. Constant, R.Fauquembergue, *J. Chem Phys* Vol.58 p.4030 (1973)
37. C. Breuillard-Alliot, J.Soussen-Jacob *Mol. Phys* Vol.28 p.905 (1974)
38. S. Bratos, J.Rios, Y. Guissani *J. Chem Phys* Vol.52 p.439 (1970)
39. A.Allerhand, *J. Chem Phys* Vol.52 p.3596 (1970)
40. W.G. Rothschild, *J Chem Phys* Vol.53 p.3265 (1970)
41. L.C. Rosenthal, H.L.Straus, *J Chem Phys* Vol.64 p.282 (1976)
42. C.Brot, *Dielectric and Related Molecular Processes*  
*The Chemical Society (London)* Vol.2 Chap.1 (1975)
43. T.W. Nee, R.Zwanzig, *J. Chem Phys* Vol.52 p.6353 (1970)
44. T.Keyes, D.Kivelson, *J. Chem Phys* Vol.56 p.1057 (1972)
45. H. Dardy, V. Volterra, T.A. Litovitz *Faraday Symp. Che. Soc.* Vol.6 p.71 (1972)
46. R.M.Van Aalst, J. van der Elsken, D. Frenkel, G.H. Wegdam *Faraday Symp. Chem. Soc.*  
Vol.6 p.94 (1972)
47. G. Wyllie *Dielectric and Related Molecular Processes* *The Chemical Society (London)*  
Vol.1 p.21 (1972)
48. G.W. Beer, R. Pecora *Faraday Symp. Chem. Soc.* Vol.11 p.78 (1977)
49. B. Quantrec, P. Bezot. *Mol. Phys.* Vol.27 p.879 (1974)
50. B.J. Berne, G.D.Harp. *Adv. Chem. Phys.* Vol.17 p.100 (1970)
51. H. Mori, *Prog. Theor. Phys.* Vol.33 p.423 (1965)
52. R. Zwanzig, *Ann. Rev. Phys. Chem.* Vol.16 p.67 (1965)
53. C. P. Smyth, 'Molecular Relaxation Processes' *The Chemical Society* (1966)
54. G.W. Chantry, 'Submillimetre Spectroscopy' *Academic Press LONDON and NEW YORK*  
(1971)
55. G.W.Chantry, H.A.Gebbie, *Nature* Vol.208 p.378 (1965)
56. N.E.Hill, *Proc.Physical Soc.* Vol.82 p.723 (1963)
57. G.Wyllie, *J.Physics C* Vol.4 p.564 (1971)
58. N.E.Hill, W.E.Vaughan, A.H.Price, M.M.Davies, 'Dielectric Properties and Molecular  
Behaviour'. *Van Nostrand, LONDON* (1969)

59. H.A.Gebbie, N.W.B.Stone, F.D.Findlay, E.C.Pyatt. *Nature* Vol.205 p.377 (1965)
60. Bradley, H.A.Gebbie, Gilby, Kechin, King. *Nature* Vol.211 p.839 (1966)
61. J.Ph Poley *J.Chem Phys* Vol.23 p.405 1955
62. G. Wyllie. *Specialist Periodical Report, The Chemical Society* Vol.1 p.21 (1972)
63. J. Ph Poley *J.Appl. Sci. B.* Vol.4 p.337 (1955)
64. G.W.Chantry, H.A.Gebbie, B.Lassier, G.Wyllie. *Nature* Vol.214 p.163 (1967)
65. M.Davies, G.Pardoe, J.Chamberlain, H.A.Geddie. *Transactions of Faraday Soc* Vol.64 p.847 (1968)
66. J.Chamberlain, Werner, H.A.Geddie, Slough. *Trans Faraday Soc.* Vol.63 p.2605 (1967)
67. Y. Leroy, E.Constant *Compt.Rend.* Vol.262 p.1391 (1966)
68. D.H.Whiffen, *Trans Faraday Soc* Vol.45 p.124 (1949)
69. M.Davies, G.W.F.Pardoe, J.Chamberlain, H.A.Geddie, *Chem Phys Lett* Vol.2 p.411 (1968)  
*Trans Faraday Soc* Vol.66 p.273 (1970)
70. H.R.Wyss, R.D.Werder, Hs.H.Günthard *Spec Acta* Vol.20 p.573 (1964)
71. Kroon S.G, J. Van der Elksen *Chem Phys Lett* Vol.1 p.285 (1967)
72. J. Chamberlain *Chem.Phys.Lett* Vol.2 p.464 (1968)
73. N.E.Hill, *Chem.Phys.Lett* Vol.2 p.5 (1968)
74. B.Lassier, C.Brot. *Disc. Faraday Soc* Vol.48 p.39 (1969)
75. I.Darmon, A.Gerschel, C.Brot. *Chem Phys Lett* Vol.8 p.454 (1971)
76. I.Darmon, A.Gerschel, C.Brot. *Mol. Phys.* Vol.23 p.317 (1972)
77. Y. Rocard *J. Physique Radium* Vol.4 p.247 (1933)
78. J.G.Powles *Trans Faraday Soc* Vol.44 p.802 (1948)
79. R.A.Sack *Proc.Phys Soc* Vol.B70 ps.402,414 (1957)
80. R.Kubo *J.Phys.Soc. (Japan)* Vol.12 p.570 (1957)  
*Lectures in Theoretical Physics* Vol.1 Chap.4 Interscience, N.York
81. R.G.Gordon *J.Chem.Phys.* Vol.44 p.5 1830 (1966)
82. P.Langevin *J.Phys* Vol.4(4) p.678 (1905) *Ann.Chim.Phys.* Vol.5(8) p.70 (1905)
83. H.A.Lorentz 'Theory of Electrons', Leipzig (1909)
84. A.Einstein *Ann Physik* Vol.17 p.549 (1905); Vol.19 p.371 (1906)
85. L. Onsager *J.Am.Chem.Soc.* Vol.58 p.1486 (1936)
86. C.H.Collie, J.B.Hasted, D.M.Ritson *Proc.Phys.Soc.* Vol.60 p.145 (1948)
87. J.G.Kirkwood *J.Chem.Phys.* Vol.7 p.911 (1939)
88. H. Frohlich 'Theory of Dielectrics'. Oxford University Press LONDON (1949)
89. W.F.Brown : *Handbuch der Physik* Vol.XVII, Dielectrics, Springer BERLIN (1956)
90. R.H.Cole *J.Chem Phys* Vol.27 p.33 (1957)
91. J.H.Van Vleck *J.Chem.Phys.* Vol.5 p.556 (1937)
92. R.H.Cole *J.Chem Phys* Vol.42 p.637 (1965)
93. S.H.Glarum *J.Chem.Phys* Vol.33 p.1371 (1960)
94. J.G.Powles *J.Chem.Phys* Vol.21 p.633 (1953)

95. G.Williams, D.C.Watts, M.Cook *Trans.Faraday Soc* Vol.66 p.2503 (1970)
96. D.D.Klug, D.E.Kranbnell, W.E.Vaughn *J.Chem.Phys.* Vol.50 p.3904 (1969)
- 97a. E.Fatuzzo, P.R.Mason *Proc.Phys.Soc.* Vol.90 p.729 (1967)
- 97b. E.Fatuzzo, P.R.Mason *Proc. Phys. Soc.* Vol.90 p.741 (1967)
98. B.K.P. Scaife *Proc. Phys. Soc.* Vol.84 p.616 (1964)
99. N.E.Hill *J.Phys C* Vol.5 p.415 (1972)
100. U.M.Titulaer, J.M.Deutch *J.Chem.Phys.* Vol.60 p.1502 (1974)
101. D. Kivelson, P.A.Madden *Mol.Phys.* Vol.30 p.1749 (1975)
102. R.Lobo, J.E.Johnson, S.Rodriquez; *J.Chem.Phys.* Vol.59 p.5992 (1973)
- 103a. J.B.Hubbard, P.G.Wolynes, *J.Chem.Phys.* Vol.69 p.998 (1978)
- 103b. J.B.Hubbard *J.Chem.Phys.* Vol.69 p.1007 (1978)
104. C.Brot *Mol.Phys.* Vol.40 p.1053 (1980)
105. H.B.Quantrec, C.Brot *Mol.Phys.* Vol.39 p.1233 (1980)
106. G.Bossis; *Mol.Phys* Vol.38 p.2023 (1979)
107. P.Bordewijk *Chem.Phys.* Vol.33 p.451 (1978)
- 108a. E. Kluk *Acta. Phys. Polonica* Vol.A58 p.51 (1980)
- 108b. A. Kocot, S.Gandor, E.Kluk; *Acta.Phys.Polonica* Vol.A58 p.149 (1980)
109. T.D.Kierke *J.Chem.Phys.* Vol.65 p.3873 (1976)
110. P.Brito, P.Bordewijk *Mol Phys* Vol.39 p.217 (1980)
111. J.M.Schurr *Mol Phys* Vol.40 p.1025 (1980)
112. J.L.Rivail *J.Chem Phys* Vol.66 p.981 (1969)
- 113a. G.J.Davies, M.Davies *J.Chem.Soc. Faraday II* Vol.71 p.1275 (1975)
- 113b. G.J.Davies, M.Davies *J.Chem.Soc. Faraday II* Vol.72 p.40 (1976)
114. A.I.Baise, *J.Chem.Soc. Faraday II* Vol.68 p.1904 (1972)
115. G.Williams, *Chem.Rev.* Vol.71 p.55 (1972)
116. F. Perrin *J.Phys. Radium* Vol.5 p.497 (1934)
117. B.K.P. Scaife 'Complex Permittivity' *English Universities LONDON* (1971)
118. G.W.Chantry, J.R.Birch, J.H.Calderwood, J.McConnell  
Unpublished - Private Communication
119. C.Brot, *J.Phys. Radium* Vol.28 p.789 (1967)
120. J.McConnell *Physica* Vol.105A p.593 (1981)
121. J.H.Calderwood, W.T.Coffey, *Proc.R.Soc* Vol.A356 p.269 (1977)
122. C.F.Botcher, 'Theory of Electric Polarisation', Elsevier, Amsterdam (1952)
123. K.S.Cole, R.H.Cole *J.Chem.Phys* Vol.9 p.341 (1941)
124. S.G.Lipson, H.Lipson 'Optical Physics', Cambridge University Press (2nd edition) (1981)
125. J.H.Hildebrand 'Faraday Discussion' 66/10 (1978)
126. K.E.Arnold, Ph.D.Thesis, University of Durham, (1981)
127. C.J.Reid, M.W.Evans, 'Molecular Interactions' Vol.3 John Wiley & Sons (1982)

128. R.Kubo Reports on Progress in Physics Vol.29, Inst. of Physics LONDON (1966)
129. G.Stephenson, 'Mathematical Methods for Science Students' LONGMAM (1961)
130. M.R.Spiegel, 'Advanced Mathematics' Schaum's Outline Series, McGraw-Hill (1971)
- 131a. R.J.Bell 'Introductory Fourier Transform Spectroscopy' Academic Press. London and New York, (1972)
- 131b. J.Chamberlain 'Principles of Interferometric Spectroscopy', Wiley-Interscience, New York (1970)
132. P.L.James, M.Sc Thesis, University of Durham (1976)
- 133a. P.Fellgett, P.hD Thesis, University of Cambridge (1951)
- 133b. P.Fellgett, J.Phys.Radium Vol.19 p.187 (1958)
134. H.A.Gebbie, R.Q.Twiss, Rep.Prog.Phys. Vol.29 p.729 (1966)
- 135a. P.Jacquinet, C.J.Dufor. J.Rech. CNRS Vol.6 p.91 (1948)
- 135b. P.Jacquinet, J.Opt.Soc. Am. Vol.44 p.761 (1954)
136. G.P. O'Neill, PhD Thesis, University of Durham (1982)
137. C.Barker, Ph.D.Thesis, University of Durham (1977)
138. M.L.Forman, W.H.Steele, G.A.Vanasse, J.Opt.Soc.Am. Vol.56 p.59 (1966)
139. D.H.Martin, E.Puplett, Infrared Physics Vol.10 p.105 (1969)
140. J.W.Cooley, J.W.Tukey, Math Comput. Vol.19 p.297 (1965)
141. J.E.Chamberlain, J.E.Gibbs, H.A.Gebbie, Nature Vol.198 p.874 (1963)
142. J.E.Chamberlain, F.D.Findlay, H.A.Gebbie, App Optics Vol.4 p.1382 (1965)
143. J.E.Chamberlain, H.A.Gebbie, Nature Vol.280 p.480 (1965)
144. J.E.Chamberlain, H.A.Gebbie, App Optics Vol.5 p.393 (1966)
145. J.E.Chamberlain, J.E.Gibbs, H.A.Gebbie IR Physics Vol.9 p.185 (1969)
146. E.E.Bell, Japan J. appl. Phys Vol.4 Suppl.1 p.412 (1965)
147. E.E.Bell IR Physics Vol.6 p.57 (1966)
148. E.E.Russell, E.E.Bell J.Opt.Soc.Am Vol.57 ps.341,543 (1967)
149. R. Sanderson, Appl.Optics Vol.6 p.1527 (1967)
150. J.R.Birch, M.N.Afsar, J.Yarwood, P.L.James, IR Physics Vol.21 p.9 (1981)  
[Appendix 4 this Thesis]
151. D.D.Honijk, W.F.Passchier, M.Mandel, M.N.Afsar, IR Physics Vol.17 p.9 (1977)
152. D.D.Honijk, W.F.Passchier, M.Mandel, M.B.Afsar, IR Physics Vol.16 p.257 (1976)
153. W.F.Passchier, D.D.Honijk, M.Mandel, IR Physics Vol.15 p.95 (1975)
154. W.F.Passchier, W.F.Honijk, D.D.Mandel, M.N.Afsar, IR Physics Vol.17 p.381 (1977)
155. J.E.Chamberlain, A.E.Costley, H.A.Gebbie, Spec Acta Vol.23A p.2255 (1967)
156. M.N.Afsar, J.B.Hasted, J.Chamberlain, IR Physics Vol.16 p.301 (1976)
157. J.Yarwood, C.Barker, P.L.James, G.P.O'Neill, W.A.Scott, R.N.McKenzie,  
J.Phys.E: Sci Instrum. Vol.14 p.161 (1981) [Appendix 5 this Thesis]
158. J.R.Birch, G.P.O'Neill, J.Yarwood, M.Bennouna  
J.Phys. E: Sci Instrum Vol.15 p.684 (1982)
159. M.N.Afsar, D.D.Honijk, W.F.Passchier, J.Goubn  
IEEE Trans MTT25 No.6 505 (1977)

- 160a. D.D.Honijk, W.F.Passchier, M.Mandel, *Physica* Vol.64 p.171 (1973)
- 160b. D.D.Honijk, W.F.Passchier, M.Mandel, *Physica* Vol.68 p.457 (1973)
- 160c. W.F.Passchier, D.D.Honijk, M.Mandel *IR Physics* Vol.15 p.95 (1975)
- 160d. W.F.Passchier, D.D.Honijk, M.Mandel *IR Physics* Vol.16 p.389 (1976)
161. J.R.Birch, T.J.Parker 'Infrared and Millimetre Waves' ed K.J.Bulton, Academic Press, LONDON (1979)
162. J.A.Birch, T.J.Parker *IR Physics* Vol.19 p.201 (1979)
163. M.M.Davies, 'Molecular Motions in Liquids' 615, Dordrecht, Reidel (1974)
164. M.N.Afsar. National Physical Laboratory Report DES 42 June (1977)
165. M.N.Afsar, J.Chamberlain, J.B.Hasted *IR Physics* Vol.16 p.587 (1976)
166. Kramer, *Zeit Phys* Vol.157 p.134 (1959)
167. G.P.O'Neill Private Communication. University of Durham (1982)
168. M.Davies, J.Chamberlain, G.J.Davies *J.Chem.Faraday II* Vol.69 p.1223 (1973)
169. M.Born, E.Wolf 'Principles of Optics', Pergamon Press, Oxford (1959)
170. M.Davies, J.Chamberlain *J.Chem.Soc. Faraday II* Vol.69 p.1739 (1973)
171. D.Lentloff, E.Knozinger. *Spectroscopy Lett* Vol.12 p.815 (1979)
172. K.E.Arnold, J.Yarwood, A.W.Price. *Mol Phys* (1982)
173. P.Desplanques. These d'Etat University of Lille, France (1974)
174. J.H.R.Clark, 'Advances in Infrared and Raman Spectroscopy' Vol.4 Henden, LONDON (1978)
175. M.N.Evans, G.J.Evans. *Chem Phys Lett* Vol.45 p.454 (1977)
176. G.J.Evans. *J.Chem Soc. Faraday II* Vol.73 p.729 (1977)
177. M.W.Evans. Personal Communication.
178. M.Drawid, J.W.Halley. *J.Chem.Phys. Solids* Vol.38 p.1269 (1977)
179. M.J.D.Powell. *Comp.J.* Vol.7 p.155 (1964)
180. A.H.Price, G.H.Wegdam. *J.Phys.E.* Vol.10 p.478 (1977)
181. D.Frenkel, G.H.Wegdam, J.Van der Elsken. *J.Chem.Phys.* Vol.57 p.2691 (1972)
182. D.Frenkel, G.H.Wegdam. *J.Chem.Phys.* Vol.61 p.4671 (1974)
183. J.O'Dell, B.J.Berne. *J.Chem.Phys.* Vol.63 p.2376 (1975)
184. C.J.Reid, R.A.Yadav, G.J.Evans, M.W.Evans. *J.Chem.Soc. Faraday II* Vol.74 p.2143 (1978)
185. G.J.Evans, M.W.Evans. *J.Chim.Phys.* Vol.75 p.21 (1978)
186. S.R.Polo, M.K.Wilson. *J.Chem.Phys.* Vol.23 p.2576 (1955)
187. J.Timmermans, 'Physico-Chemical Constants' Elsevier LONDON (1950)
188. J.Eloranta, P.K.Kadaba. *Mat Sci Eng* Vol.8 p.203 (1971)
189. D.H.Whiffen. *Trans.Faraday Soc.* Vol.46 p.124 (1950)
190. P.A.Madden. Unpublished Paper. (1982)
191. G.P.O'Neill, A.Khuen, J.Yarwood, J.R.Birch, A.H.Price. *J. Mol. Struct.* Vol.80 p.383 (1982)
192. R.G.Gordon. *J.Chem.Phys.* Vol.38 p.1724 (1963)

193. K.Sato, Y.Ohkubo, T.Moritsu, S.Ikawa, M.Kimura  
Bull. Chem. Soc. Japan. Vol.51 p.2493 (1978)
194. E.Knozinger, M.E.Jacox. Ber.Bunsenges Phys.Chem. Vol.82 p.57 (1978)
195. C.Ried. Ph.D.Thesis U.C.W. Aberystwyth (1979)
196. T.Tokuhiro, W.G.Rothschild. J.Chem.Phys. Vol.62 p.2150 (1975)
197. G.Döge, R.Arndt, A.Khuen. Chem.Phys. Vol.21 p.53 (1977)
198. J.E.Griffiths, M.Cherc, P.M.Rentzepis. J.Chem.Phys. Vol.60 p.3824 (1974)
199. K.Spanner, A.Lambereau, W.Kaiser. Chem.Phys.Lett Vol.44 p.88 (1976)
200. A.Lanbureau, W.Kaiser. Ann.Rev.Phys.Chem. Vol.26 p.83 (1975)
201. S.Bratos. J.Chem.Phys. Vol.63 p.3499 (1975)
202. P.A.Madden, R.M.Lynden-Bell. Chem.Phys.Lett. Vol.38 p.163 (1976)
203. M.Kakimoto, T.Fujiyama. Bull.Chem.Soc. Japan Vol.47 p.1883 (1974)
204. K.A.Valiev. Opt.Spectroscopy. Vol.II p.253 (1951)
205. S.F.Fischer, A.Laubereau. Chem.Phys.Lett. Vol.35 p.6 (1975)
206. 'Biological Membranes'. ed.D.Chapman. Academic Press Vol.4 (1964)
207. 'Transport phenomena in Bio Membranes'. N.Lakshminarayanaiah Academic Press (1969)
208. Proceedings of 'Symposium on Calcium and Cellular Function'.  
ed. A.W.Cuthbert, McMillan (1970)
209. P.A.Lambert, I.C.Hancock, J.Baddiley. Biochem J. Vol.149 p.519 (1975)
210. J.Baddiley 'Essays in Biochem. Vol.8 p.35 (1972)
211. 'Water, A comprehensive Treatise' ed. F.Franks Plenum Press, LONDON Vol.3 p.1 (1973)
212. C.Barker, J.Yarwood. J.Chem.Soc. Faraday II Vol.71 p.1322 (1975)
213. C.Barker, J.Yarwood. Chem.Soc. Faraday Symp.II (1977)
214. C.Barker, P.L.James, J.Yarwood. Chem.Soc.Faraday Disc. 64 (1978)  
[Appendix 6 to this Thesis]
215. C.Barker, P.L.James, J.Yarwood. 'Protons and Ions Involved in Fast Dynamic Phenomena'.  
Elsevier, Amsterdam (1978) [Appendix 7 this Thesis]
216. D.T.Copenhafer, C.A.Kraus. J.Am.Chem.Soc. Vol.73 p.4557 (1951)
217. H.Cachet, F.F.Hanna, J.Pouget. J.Chim.phy. Vol.71 p.285 (1974)
218. M.Davies, G.Williams. Trans.Faraday Soc. Vol.56 p.1619 (1960)
219. K.Bange, J.W.Smith. J.Chem.Soc. 4244 (1964)
220. M.J.Wooton, Specialist Periodical Report, Vol.3 Chemical Society London (1973)
221. L.E.Strong, C.A.Kraus. J.Am.Chem.Soc. Vol.72 p.166 (1950)
222. G.W.F.Pardoe. Trans Faraday Soc. Vol.66 p.2599 (1970)
223. L.Aimone, J.P.Badiali. H.Cachet. J.Chem.Soc. Faraday II (1977)
224. M.K.Wong, W.J.McKinney, A.I.Popov, J.Phys.Chem. Vol.75 p.56 (1971)
225. R.M.Fuoss, C.A.Kraus. J.Am.Chem.Soc. Vol.55 p.3617 (1933)
226. J.L.Atwood. 'Recent Developments in Separation Science Vol.III

- 227. P.Bacelon, J.Corset, C. de Loze. Chem.Phys.Lett. Vol.32 p.458 (1975)
- 228. J.L.Wood 'Spectroscopy and Structure of Molecular Complexes' ed.J.Yarwood  
Plenum Ltd. London (1973)
- 229. H.L.Friedman, J.Phys.Chem. Vol.66 p.1595 (1962)
- 230. A.E.Hill J.Am.Chem.Soc. Vol.44 p.1163 (1922)

**APPENDIX 2**

**COMPARISON OF INFRARED AND RAMAN  
VIBRATIONAL RELAXATION FUNCTIONS OF  
THE  $\nu_1$  AND  $\nu_3$  MODES OF ACETONITRILE**

**J. YARWOOD, P.L. JAMES, G. DÖGE, R. ARNDT**

**FARADAY DISCUSSIONS OF THE CHEMICAL SOCIETY  
No. 66, 1978**

Comparison of Infrared and Raman Vibrational Relaxation  
Functions of the  $\nu_1$  and  $\nu_3$  Modes of Acetonitrile †

BY JACK YARWOOD AND PETER L. JAMES

Department of Chemistry, University of Durham, Durham

AND GOTTFRIED DÖGE AND REINER ARNDT

Institut für Physikalische Chemie, Techn. Universität,  
Braunschweig, West Germany

Reprinted from

FARADAY DISCUSSIONS  
OF  
THE CHEMICAL SOCIETY

No. 66

STRUCTURE AND MOTION  
IN MOLECULAR LIQUIDS

1978

## Comparison of Infrared and Raman Vibrational Relaxation Functions of the $\nu_1$ and $\nu_3$ Modes of Acetonitrile †

BY JACK YARWOOD AND PETER L. JAMES

Department of Chemistry, University of Durham, Durham

AND GOTTFRIED DÖGE AND REINER ARNDT

Institut für Physikalische Chemie, Techn. Universität,  
Braunschweig, West Germany

*Received 9th May, 1978*

Measurements of the  $\tau_{1a}$  single particle correlation time for acetonitrile (in dilute solution in carbon tetrachloride) using far-infrared measurements have enabled us to compare the vibrational correlation times obtained using infrared and Raman bands arising from the same ( $A_1$ ) modes. The results of this comparison show, for the first time, that quantitative differences do occur, especially for  $\nu_1$  of acetonitrile, even in dilute solution. Possible reasons for this difference are discussed. It is emphasized that derivation of  $\tau_{1a}$  or  $\tau_{1b}$  correlation times from infrared or Raman spectra using  $\tau$ , from isotropic Raman band profiles may therefore give erroneous results.

### INTRODUCTION AND THEORETICAL BACKGROUND

The analysis<sup>3-10</sup> of infrared and Raman spectral band shapes in order to derive the reorientational correlation functions  $\langle P_l[\mu(0) \cdot \bar{u}(t)] \rangle$  (where  $\bar{u}$  is a unit vector along the direction of the transition moment of the normal mode) has usually been made<sup>3-5,7,11</sup> using the following assumptions:

- (i) that the reorientation and vibrational motions are statistically uncorrelated, enabling one to write,<sup>7</sup> for example, for Raman spectra,

$$\langle [Q_v(0) \cdot Q_v(t)] \cdot [\beta'(0) \cdot \beta'(t)] \rangle \equiv \langle Q_v(0) \cdot Q_v(t) \rangle \langle \beta'(0) \cdot \beta'(t) \rangle \quad (1a)$$

$$= \varphi_v^2(t) \varphi_{2k}(t) \quad (1b)$$

where  $Q_v$  is the normal coordinate of the  $\nu$ th mode and where  $\beta'$  is the polarisability derivative tensor,  $\partial\beta/\partial Q$ . The correlation function  $\langle \beta'(0) \cdot \beta'(t) \rangle$  then gives a measure of reorientational motions for  $l = 2$ , where  $P_2$  (the 2nd order Legendre polynomial) is  $\frac{1}{2}[3 \cos^2 \theta(t) - 1]$ ;

- (ii) that the vibrational (in general non-reorientational) parts of the  $I_{VV}(\omega)$ ,  $I_{VH}(\omega)$  and  $I_{IR}(\omega)$  band profile are all identical for a given mode of vibration.

Thus in the separation of the reorientational and vibrational parts of a given Raman band profile<sup>3-9</sup> it has been standard practice to use,

$$\varphi_v^{1so}(t) \varphi_{2R}^2(t) \propto \int_{\text{band}} I_{niso}(\omega) \exp(-i\omega t) d\omega \quad (2)$$

and 
$$\varphi_v^{1so}(t) \propto \int_{\text{band}} I_{iso}(\omega) \exp(-i\omega t) d\omega \quad (3)$$

† Part 3 of the series "Studies of molecular motions and vibrational relaxation in acetonitrile".<sup>1,2</sup>

$$\text{where } I_{\text{aniso}}(\omega) = I_{\text{VH}}(\omega) \tag{4a}$$

$$\text{and } I_{\text{iso}}(\omega) = I_{\text{VV}}(\omega) - \frac{4}{3} I_{\text{VH}}(\omega) \tag{4b}$$

(for plane polarised incident laser light<sup>11</sup> and where the observed band profiles  $I_{\text{iso}}(\omega)$  and  $I_{\text{aniso}}(\omega)$  have been suitably<sup>1,3-6,11</sup> corrected for the effects of finite instrument resolution).

For the corresponding infrared band<sup>3-5,10</sup> one uses the assumption that

$$\begin{aligned} \langle [Q_i(0) \cdot Q_i(t)] \cdot [\bar{u}(0) \cdot \bar{u}(t)] \rangle &= \langle Q_i(0) \cdot Q_i(t) \rangle \langle \bar{u}(0) \cdot \bar{u}(t) \rangle \\ &= \varphi_{\text{V}}^{\text{IR}}(t) \varphi_{\text{IR}}^{\text{R}}(t) \end{aligned} \tag{5a}$$

where  $\bar{u}$  is a unit vector along the direction of the transition moment,  $\partial\mu/\partial Q_i$ ; the function  $\langle \bar{u}(0) \cdot \bar{u}(t) \rangle$  then giving a measure of reorientational motion for  $l = 1$ , where  $P_1 = \cos \theta_1(t)$ . One may then use,

$$\varphi_{\text{V}}^{\text{IR}}(t) \varphi_{\text{IR}}^{\text{R}}(t) \propto \int_{\text{band}} I_{\text{IR}}(\omega) \exp(-i\omega t) d\omega. \tag{6}$$

[Note that in eqn (2) and (6) the superscript ' refers to the single particle correlation function,<sup>4,10-13</sup> see below]. Using these relationships and making the usual assumption that for a given mode

$$\varphi_{\text{V}}^{\text{IR}}(t) = \varphi_{\text{V}}^{\text{iso}}(t) = \varphi_{\text{V}}^{\text{aniso}}(t) \tag{7}$$

we then get

$$\varphi_{\text{IR}}^{\text{R}}(t) = \frac{\int I_{\text{IR}}(\omega) \exp(-i\omega t) d\omega}{\int I_{\text{iso}}(\omega) \exp(-i\omega t) d\omega} \tag{8a}$$

and

$$\varphi_{\text{IR}}^{\text{A}}(t) = \frac{\int I_{\text{aniso}}(\omega) \exp(-i\omega t) d\omega}{\int I_{\text{iso}}(\omega) \exp(-i\omega t) d\omega} \tag{8b}$$

Such a process has been desirable in the past since, from the relative values of the reorientational correlation times,  $\tau_{\text{IR}}^{\text{R}}$  [for first ( $l = 1$ ) and second ( $l = 2$ ) rank tensor relaxations], one can derive important information about the validity (or otherwise) of models<sup>3,4,7,16-24</sup> for reorientational motions in liquids. However, it has recently been shown<sup>4</sup> that for acetonitrile eqn (7) is invalid for at least one of the normal modes, in particular that  $\tau_{\text{V}}^{\text{IR}} \neq \tau_{\text{V}}^{\text{iso}}$  for either  $v_1$  or  $v_3$  or both (see table 1 and further discussion below). Attention has recently been focused by Lynden-Bell<sup>25</sup> on the possible theoretical reason(s) for the invalidity of eqn (7) [and therefore, of course, the invalidity of using eqn (8) to calculate  $\tau_{\text{IR}}^{\text{R}}$ ]. She has made the point that the vibrational (phase) relaxation function of the  $v$ th normal mode may be written<sup>1,4</sup> as

$$\varphi_{\text{vp}}(t) = \sum_i \langle Q_{vi}(0) \cdot Q_{vi}(t) \rangle_{\text{'self'}} + \sum_{i \neq j} \langle Q_{vi}(0) \cdot Q_{vj}(t) \rangle_{\text{'exchange'}} \tag{9}$$

where the total non-reorientation relaxation function is

$$\varphi_{\text{v}}(t) = \varphi_{\text{vp}}(t) \varphi_{\text{R}}(t)$$

and  $\varphi_{\text{R}}(t)$  is a function measuring the rate (assumed<sup>1,4,25</sup> to be relatively "slow") of "population" or "energy" relaxation. It has then been shown<sup>25</sup> (for an effective

potential of "dipolar" or "dispersive" forces) that the cross terms between the "self" and "exchange" parts of  $\phi_{pp}(t)$  in eqn (9) contribute strongly to the  $l = 0$  (isotropic Raman) relaxation function but only very weakly to the  $l = 2$  (anisotropic Raman) function and not at all to the  $l = 1$  (infrared) function. Thus, in the presence of an "exchange" term [in eqn (9)], there is no reason to expect that eqn (7) should be valid. Indeed, it has been known for some time,<sup>26,28</sup> that strong mode-mode coupling via resonant transfer of vibrational energy together with a non-random distribution of molecules in the liquid leads to a difference between the vibrational parts of the isotropic and anisotropic Raman band profiles.

The standard experimental test<sup>26,28</sup> for the importance of an "exchange" term in the effective intermolecular potential is an isotropic dilution experiment in which one might reasonably expect to eliminate the effects of resonance energy transfer between molecules  $i$  and  $j$ . We have clearly shown<sup>1</sup> that neither the  $\nu_1$  nor  $\nu_3$  bands of acetonitrile have more than a minor contribution from such resonance energy transfer effects. In the light of current theories<sup>25-28</sup> it is thus rather surprising that discrepancies  $\tau_v^{iso}$  and  $\tau_v^R$  do occur even in dilute solution (see below) when any exchange term in eqn (9) would (in any event) have been removed. Since such a discrepancy has never been established nor investigated in a quantitative fashion we decided to attempt to measure  $\tau_v^{iso}$  and  $\tau_v^R$  separately so that direct comparison may be made and so that the reasons for discrepancies in this case may be further investigated.

Although  $\phi_v^{iso}(t)$  (and hence  $\tau_v^{iso}$ ) may be easily obtained from eqn (2) it is clear from eqn (6) that, in order to determine  $\phi_v^R(t)$ , one must first determine  $\phi_{1R}(t)$  [or  $\tau_{1R}(t)$ , and hence make a reasonable assumption about the analytical form of  $\phi_{1R}$ , see below]. In principle,<sup>10,13,29-32</sup> one may determine the reorientational correlation time  $\tau_{1R}$  from the microwave spectrum remembering,<sup>13</sup> however, that such spectra give the reorientational autocorrelation function,<sup>4,16,29</sup>

$$C_m(t) = \sum_i \langle P_1[\mu_i(0) \cdot \mu_i(t)] \rangle + \sum_{i \neq j} \langle P_1[\mu_i(0) \cdot \mu_j(t)] \rangle \quad (10)$$

"self" correlations                      "cross" correlations

( $\mu_i$  is a unit vector along the direction of the permanent electric dipole moment). This shows that multiparticle "cross" correlations between the rotating molecules are again important. Madden and Kivelson<sup>13</sup> have shown that the relation between the multiparticle and single particle correlation times is given by,

$$\tau_{1R}^m = \tau_{1R} \frac{(1 + Nf)}{(1 + Nf)} \quad (11)$$

where  $Nf$  and  $Nf$  are measures of the "static" and "dynamic" orientation correlation factors<sup>13-15</sup> respectively. It is expected,<sup>14,15</sup> however, that in dilute solution of the probe molecule in a non-interacting solvent the second term in eqn (10), or equivalently, the  $Nf$  and  $Nf$  factors of eqn (11), may be effectively ignored and that one may then put  $\tau_{1R}^m = \tau_{1R}$ . It is on this basis that we have sought to analyse our data.

#### EXPERIMENTAL

Raman isotropic band profiles for the  $\nu_1$  and  $\nu_3$  bands (as a function of temperature and concentration in carbon tetrachloride) were obtained<sup>1</sup> using a CODERG LRT 800 spectrometer equipped with a Spectra Physics model 171-06 argon ion laser. The details of these measurements have been published previously<sup>1</sup> and the profiles observed in the liquid and at 0.03 m<sup>3</sup> in carbon tetrachloride are shown in fig. 1. It should be noticed<sup>1</sup> that the  $\nu_3$  band has a depolarisation ratio  $\rho \cong 0.3$  and so the use of eqn (4b) is necessary to calculate  $I_{1R}(\omega)$ . For  $\nu_1$ ,  $\rho$  is so small that  $I_{1R}(\omega) = I_{VV}(\omega)$  to a very good approximation. Correlation functions  $\phi_{1R}^{iso}(t)$  for both the  $\nu_1$  and  $\nu_3$  modes were obtained from the low frequency half of each band because of disturbance in the high frequency wing by the  $\nu_2$  and  $\nu_6(E)$  bands (respectively).

The infrared spectra shown at the same concentration and 318 K in fig. 2 clearly demonstrate the interference by the *E* bands. These spectra, obtained using a Perkin-Elmer model 577 spectrometer with Beckman-R.I.I.C. (variable temperature) potassium bromide cells, have been fitted to an overlapping combination of *n* lorentzian-gaussian "sum" bands<sup>33</sup>

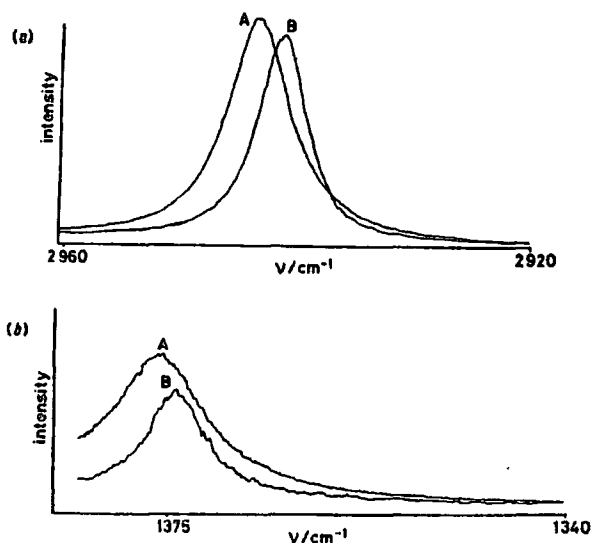


FIG. 1. Isotropic Raman spectra of (a)  $\nu_1$  and (b)  $\nu_3$  of acetonitrile in (A) the liquid phase, (B) in dilute solution in carbon tetrachloride (288 K).

( $n = 5$  for the  $\nu_1/\nu_3$  region and  $n = 4$  for the  $\nu_3/\nu_3$  region) using the band fitting program of Jones and co-workers.<sup>34</sup> The quality of the least squares fit is shown in fig. 3 and the band half-widths of the  $\nu_1$  and  $\nu_3$  fitted bands are collected in table 1 for both liquid and dilute solutions. Also in table 1 are the band half-widths obtained by visual (graphical separation)

TABLE 1.—COMPARISON OF HALF-WIDTHS OF  $\nu_1$  AND  $\nu_3$  BANDS OF  $\text{CH}_3\text{CN}$  IN THE LIQUID AND IN 0.02 M CARBON TETRACHLORIDE SOLUTION. (ALL VALUES ARE FULL-WIDTH AT HALF HEIGHT IN  $\text{cm}^{-1}$ )

	Raman <sup>1</sup> (isotropic)	infrared <sup>a</sup>	infrared <sup>b</sup>
liquid			
$\nu_1$	6.5	~15	—
$\nu_3$	8.0	15.0	13.8
$\text{CCl}_4$ solution (0.02 M)			
$\nu_1$	4.5	12.0	14.0
$\nu_3$	4.8	8.0	7.8

<sup>a</sup> Values measured directly from spectra. <sup>b</sup> Values from fitted band profiles, see text.

of the  $\nu_1$  and  $\nu_3$  bands (in dilute solution). It can be seen that agreement of these measured widths is reasonably good considering the complexity of the observed spectra.

The far-infrared/microwave spectra (fig. 4) were obtained using our Beckman-R.I.I.C.

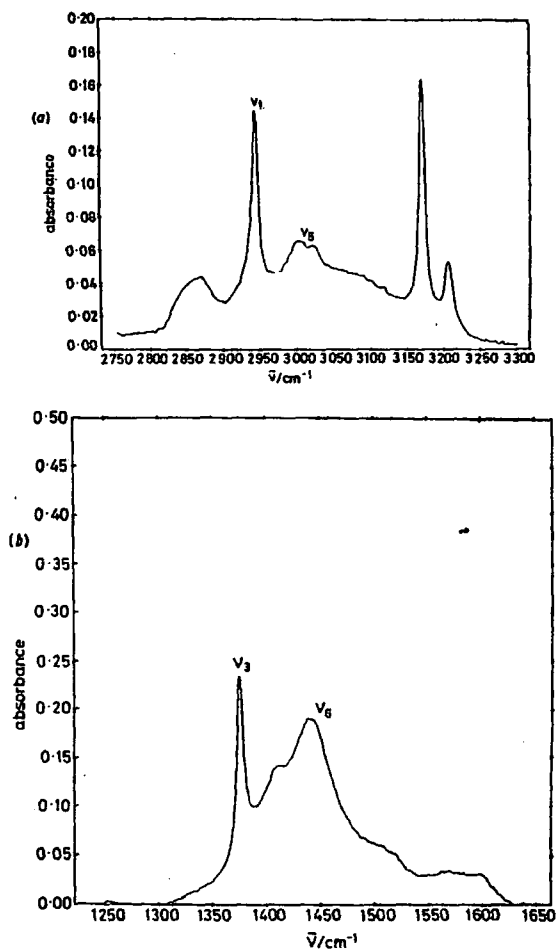


FIG. 2. Infrared spectrum of a dilute solution of acetonitrile in carbon tetrachloride (318 K; 0.02 mf), (a) the region of  $\nu_1$  and  $\nu_5$ , (b) the region of  $\nu_3$  and  $\nu_6$ . (Other bands in the spectrum are identified as far as possible.)

model FS720 interferometer with Beckman variable temperature polyethylene cells. Between 20 and 250  $\text{cm}^{-1}$  the instrument was used in the conventional mode with a 50 gauge Mylar beam splitter and Golay detector. In the 2–40  $\text{cm}^{-1}$  region the interferometer was used in the polarising mode<sup>23</sup> and a Q.M.C. Industrial Research, liquid helium cooled germanium

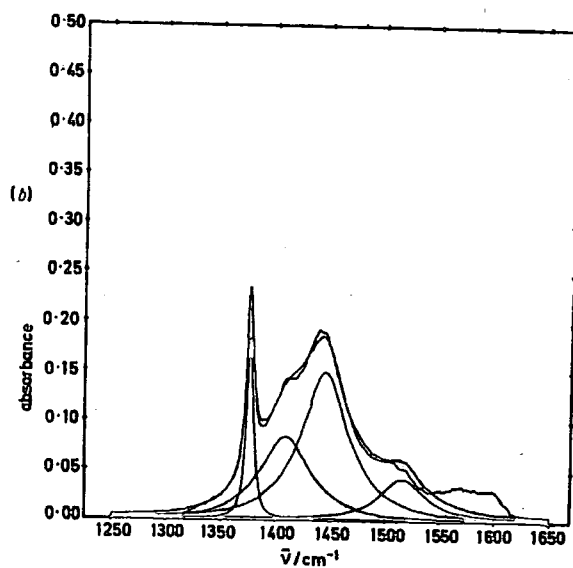
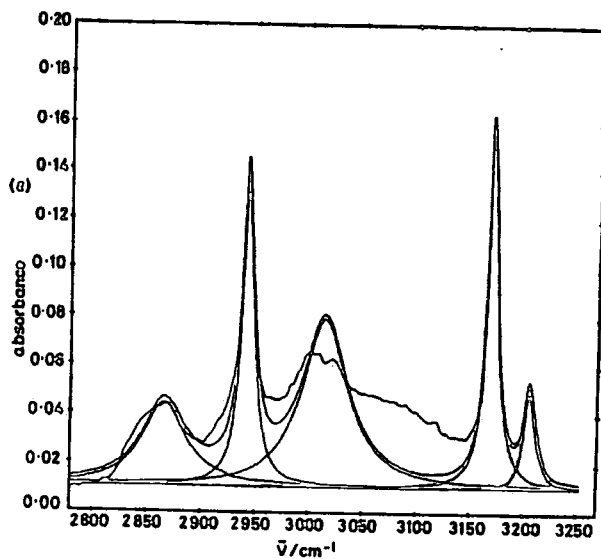


FIG. 3.—Results of fitting total band profiles to a sum of overlapping lorentzian/gaussian bands, (a)  $\nu_1$  and  $\nu_2$  region, (b)  $\nu_3$  and  $\nu_4$  region. Data at 318 K and 0.02 mf.

bolometer was employed as the detector. It is estimated that spectra are reproducible to within  $\pm 2\%$  in the  $30\text{-}250\text{ cm}^{-1}$  region and within  $\pm 1\%$  at frequencies between 2 and  $30\text{ cm}^{-1}$ .

#### DATA ANALYSIS AND COMPUTATION OF CORRELATION TIMES

In order to derive  $\tau_{1a}$  values from our far-infrared data it is necessary to employ a model for reorientational motion since one does not actually measure the relaxation time of the rotating dipoles directly. The model which we have used is based on the "memory function" approach<sup>36,37</sup> developed by Evans and co-workers.<sup>21-24,38,39</sup> Using this approach the Mori<sup>40</sup> formalism is employed to provide a solution of the generalised rotational Langevin equation.<sup>21</sup>

$$\ddot{u}(t) + \int_0^t K_u(t-\tau)u(\tau) d\tau = \Gamma_u(t) \quad (12)$$

where  $u$  is a unit dipole vector and  $K_u(t)$  is a time dependent friction tensor, the memory function, which can in turn be shown to be the correlation function of the random torque,  $\Gamma(t)$ . Using the definition<sup>41,42</sup> of the time autocorrelation functions associated with the far-infrared and microwave spectrum, *viz*:

$$C_u(t) \propto \int_0^\infty \frac{\alpha(\omega)}{\omega^2} \cdot \exp(-i\omega t) d\omega \quad (13)$$

$$\text{and } -\tilde{C}_u(t) \propto \int_0^\infty \alpha(\omega) \exp(-i\omega t) d\omega \quad (14)$$

[where  $\alpha(\omega)$  is the absorption coefficient, as measured directly from the far-infrared spectrum] one may proceed<sup>21,38,39</sup> to expand  $C_u(t)$  in a set of memory functions  $K_0(t)$  ...  $K_n(t)$  which obey the relationship,

$$\frac{\partial}{\partial t} [K_{n-1}(t)] = - \int_0^t K_n(t-\tau)K_{n-1}(\tau) d\tau \quad (15)$$

such that, for example,

$$\frac{\partial [C_u(t)]}{\partial t} = - \int_0^t K_0(t-\tau)C_u(\tau) d\tau \quad (16a)$$

$$\text{and } \frac{\partial [K_0(t)]}{\partial t} = - \int_0^t K_1(t-\tau)K_0(\tau) d\tau \quad (16b)$$

*etc.*

Hence taking Laplace transforms one gets a continued fraction<sup>43</sup> expression for the spectral density

$$\tilde{C}_u(t) = C_u(-i\omega) = \frac{C_u(0)}{i\omega + K_0(\omega)} = \frac{C_u(0)}{i\omega + \{K_0(0)/[i\omega + K_1(\omega)]\}} = \dots \quad (17)$$

which may be truncated at any desired point.

In our analysis we have followed Evans<sup>21-24,38,39</sup> and used eqn (17) with truncation at first order. Such a truncation leads to finite<sup>21</sup> intermolecular torques if,

$$K_1(t) = K_1(0) \exp(-\gamma t) \quad (18)$$

and the model is then characterised by three parameters;  $K_0(0)$ ,  $K_1(0)$  and  $\gamma$ . The memory functions are related<sup>21</sup> to the spectral moments [*i.e.* to the even time expansion

of  $C_v(t)$ ). For a symmetric top molecule  $K_0(0)$  is the rotational second moment given by  $2kT/I_B$ , where  $I_B$  is the moment of inertia about a direction perpendicular to the symmetry axis.  $K_1(0)$  is related to the intermolecular mean square torque<sup>43</sup> (via the

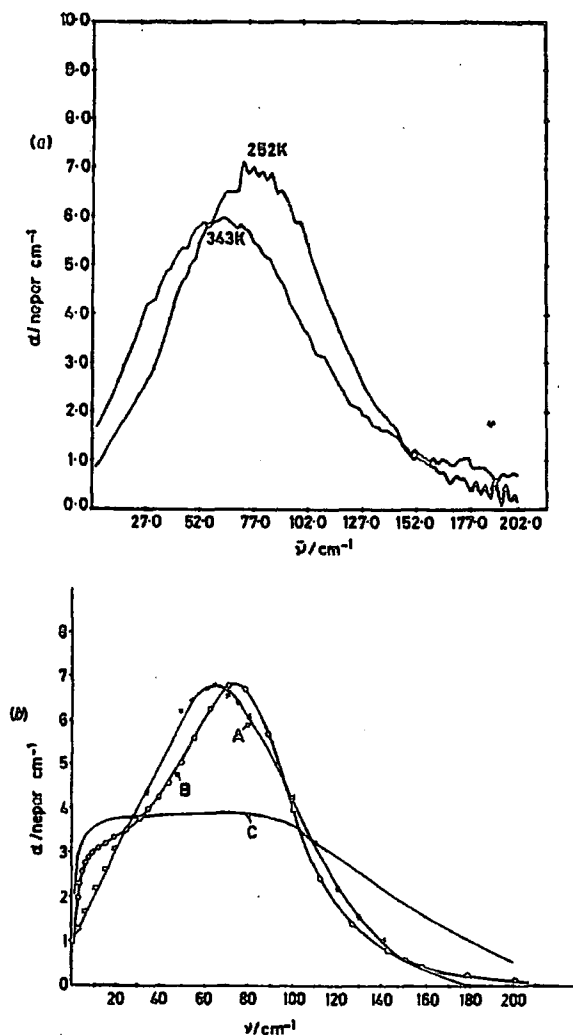


FIG. 4.—(a) Far-infrared and microwave spectra of a 0.02 M solution of acetonitrile in carbon tetrachloride at two different temperatures. (b) Far-infrared and microwave spectra of a 0.02 M solution at 318 K (A) as compared with spectra calculated using the parameters shown in table 2; (B) using eqn (26); (C) using eqn (21) and (22).

fourth moment). The form of eqn (18) then shows that  $\gamma^{-1}$  is a correlation time, this time is related to the duration of intermolecular torques.<sup>21</sup> Clearly, all three parameters are temperature dependent. Using first order truncation in eqn (17) it may be shown<sup>21-24</sup> that the absorption coefficient is given by,

$$\alpha(\omega) = \frac{A\omega^2 K_0(0)K_1(0)\gamma}{\gamma^2[K_0(0) - \omega^2]^2 + \omega^2[\omega^2 - [K_0(0) + K_1(0)]]^2} \quad (19)$$

with

$$A = \frac{\epsilon_0 - \epsilon_\infty}{n(\omega)c}$$

where  $\epsilon_0 - \epsilon_\infty$  is the total dispersion and  $n(\omega)$  the frequency dependent refractive index. In principle, the parameters  $K_1(0)$  and  $\gamma$  can be obtained by fitting to eqn (19) provided that both  $(\epsilon_0 - \epsilon_\infty)$  and  $n(\omega)$  are known. The Debye relaxation time,<sup>21</sup> which in the limit of infinite dilution<sup>14,15</sup> should be equivalent to  $\tau_{1R}$  is given<sup>46</sup> by,

$$\tau_D^2 = \frac{[K_0(0) + K_1(0)]^2 - 2K_0(0)\gamma^2}{K_0^2(0)\gamma^2} \quad (20)$$

In the absence of a knowledge of  $(\epsilon_0 - \epsilon_\infty)$  and/or  $n(\omega)$ , measurements on both these quantities are currently in progress, one may differentiate<sup>46</sup> eqn (19) giving the frequency of  $\alpha_{max}$  as a function of  $K_1(0)$ ,

$$K_1(0) = \frac{4\omega_m^4[\omega_m^2 - K_0(0)]}{\pi[K_0(0) - \omega_m^2][K_0(0) + \omega_m^2] + 4\omega_m^4} \quad (21)$$

Since<sup>45</sup> then

$$\gamma = \left[ \frac{K_1(0)\pi}{2} \right]^{\frac{1}{2}} \quad (22)$$

one may calculate  $K_1(0)$  and  $\gamma$  without recourse to fitting procedures. Further, by differentiating<sup>45</sup> the dielectric loss curve one can calculate  $\tau_D$  using the approximation that

$$K_1(0) \cong \frac{\pi}{2} \left[ \frac{2kT\tau_D}{T_D} \right]^2 \quad (23)$$

Alternatively, it is possible<sup>39</sup> through the definition of dielectric loss

$$\epsilon''(\omega) = \frac{\alpha(\omega)n(\omega)c}{\omega} \quad (24)$$

and refractive index

$$n(\omega) = \left\{ \frac{[\{\epsilon''(\omega)\}^2 + \{\epsilon'(\omega)\}^2]^{\frac{1}{2}} + \epsilon'(\omega)}{2} \right\}^{\frac{1}{2}} \quad (25)$$

to obtain an expression for  $\alpha(\omega)$  which does not depend on  $n(\omega)$ , viz,

$$\alpha(\omega) = 2\sqrt{2}\epsilon''(\omega)\omega / \{[\epsilon'(\omega)^2 + \epsilon''(\omega)^2]^{\frac{1}{2}} + \epsilon'(\omega)\} \quad (26)$$

where 
$$\epsilon''(\omega) = \frac{(\epsilon_0 - \epsilon_\infty)K_0(0)K_1(0)\gamma\omega}{\gamma^2[K_0(0) - \omega^2]^2 + \omega^2[\omega^2 - [K_0(0) + K_1(0)]]^2} \quad (27)$$

and

$$\epsilon'(\omega) = \epsilon_0 - \frac{(\epsilon_0 - \epsilon_\infty)\omega^2\{[\omega^2 - K_1(0)][\omega^2 - [K_0(0) + K_1(0)]] + \gamma^2[\omega^2 - K_0(0)]\}}{\gamma^2[K_0(0) - \omega^2]^2 + \omega^2[\omega^2 - [K_0(0) + K_1(0)]]^2} \quad (28)$$

Thus one is able to fit eqn (26) to the observed  $\alpha(\omega)$  data without a knowledge of  $n(\omega)$  [the dispersion  $(\epsilon_0 - \epsilon_\infty)$  is, however, still needed or must be used as a fitted parameter].

We have analysed our far-infrared data on two dilute solutions in carbon tetrachloride (fig. 4) using three different approaches [see ref. (47) for more details and consideration of other models]:

- fitting to eqn (26) with  $\epsilon_0 - \epsilon_\infty = 0.5$  ( $\epsilon_\infty \approx n_{IR}^2 = 2.20$ ) and also using  $(\epsilon_0 - \epsilon_\infty)$  as a fitted parameter.
- using eqn (21) and (22) to calculate the parameters  $K_1(0)$  and  $\gamma$ .
- fitting our data to eqn (19) with the aid of recently determined refractive index data<sup>48</sup> and  $\epsilon_0 - \epsilon_\infty = 0.5$ . These fittings are still in progress and will be ready for a future publication.<sup>47</sup>

In each case  $\tau_D \equiv \tau_{IR}^*$  values have been obtained from eqn (20) and (23) (the agreement between these two values of  $\tau_D$  at the same concentration and temperature being very good). The data are summarised in table 2 and the quality of the fitting

TABLE 2.—MODEL PARAMETERS<sup>a</sup> AND RESULTING  $\tau_D \equiv \tau_{IR}^*$  VALUES FOR CH<sub>3</sub>CN IN DILUTE CCl<sub>4</sub> SOLUTIONS

temp./K	concentration/mf	$\bar{\nu}_{max}$	$\gamma^b$	$K_1(0)^b$	$\tau_D^b$ /ps	$\gamma^c$	$K_1(0)^c$	$\tau_D^c$ /ps
343	0.018	61 ± 2	29.5	554.4	1.8	14.2	274.8	1.9
318	0.018	66 ± 2	32.3	666.0	2.1	12.1	264.4	2.3
288	0.018	72 ± 2	35.7	809.9	2.6	11.8	281.3	2.8
252	0.018	76 ± 2	37.9	914.9	3.2	11.1	313.2	3.8
318	0.061	70 ± 2	34.5	757.4	2.3	12.9	265.4	2.2
288	0.061	73 ± 2	36.2	834.6	2.7	12.9	291.7	2.6
252	0.061	82 ± 3	41.1	1072.9	3.4	12.5	329.9	3.5

<sup>a</sup> Units are  $10^{21} \text{ s}^{-1}$  for  $K_1(0)$  and  $10^{12} \text{ s}^{-1}$  for  $\gamma$ ; <sup>b</sup> values obtained using eqn (21) and (22); <sup>c</sup> values obtained by fitting to eqn (26) with  $\epsilon_0 - \epsilon_\infty$  as a variable parameter and  $\epsilon_\infty = 2.20$  (see text).

procedures are shown in fig. 4. (In comparing observed and calculated  $\alpha(\bar{\nu})$  curves it is worthwhile remembering that the far-infrared spectrum will contain contributions from the variation of induced dipoles during collision and not only from permanent dipole reorientations. Further, that the equations fitted contain no "internal field"<sup>21,38,39</sup> factor.)

Having obtained a value for the correlation time  $\tau_{IR}^*$  by measuring  $\tau_D$  at extremely low concentration we are able to obtain the correlation function  $\phi_{IR}^*(t)$  (but only by assuming a particular analytical form of this particular function). We have made the usual assumption that,

$$\phi_{IR}^*(t) = \exp(-t/\tau_{IR}^*) \quad (29)$$

and we have then computed  $\phi_{IR}^{IR}(t) = \phi_{IR}(t)/\phi_{IR}^*(t)$  [eqn (6)] at each particular time using the fitted band profiles for  $\nu_1$  and  $\nu_3$  shown in fig. 3.  $\phi_{IR}^{IR}(t)$  may then be compared with  $\phi_{IR}^{IR}(t)$  obtained directly from our previous<sup>1</sup> Raman measurements. The results of these comparisons are shown in fig. 5 (a) and (b) and the correlation times derived are given in table 3.

TABLE 3.—SUMMARY OF CORRELATION TIMES FOR A 0.02 mf SOLUTION OF CH<sub>3</sub>CN IN CARBON TETRACHLORIDE (ALL VALUES IN ps)

	$\tau_{IR}$	$\tau_{IR}^*$	$\tau_{IR}^{IR}$	$\tau_{IR}^{IR \sigma}$
$\nu_1$ band	0.9	2.3	1.3	2.4
$\nu_3$ band	1.6	2.3	3.5	1.7

<sup>a</sup> Measured at 288 K; other data at 318 K.

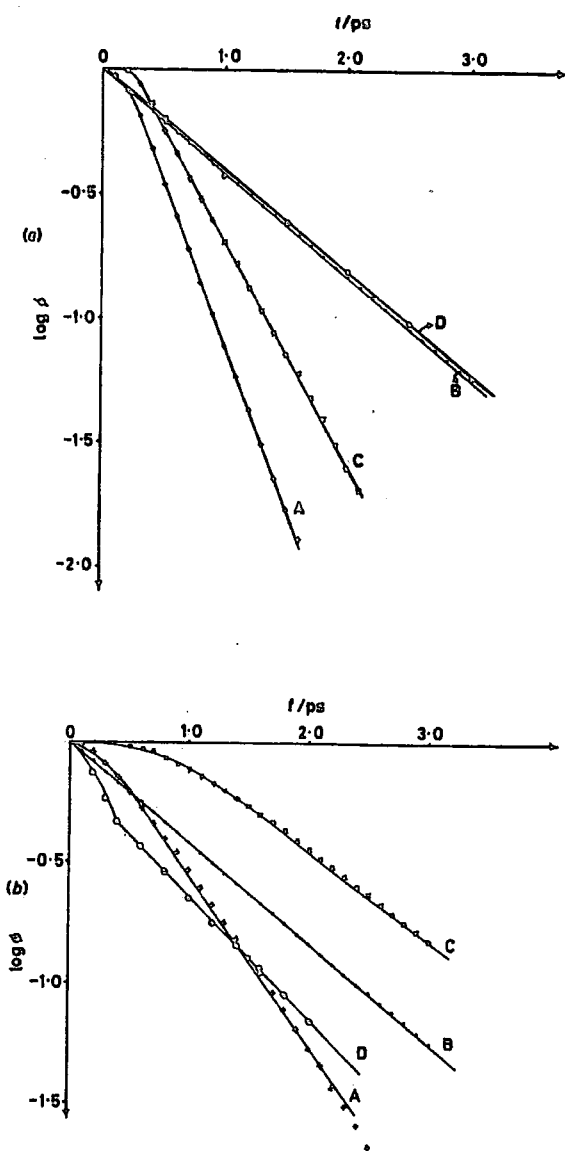


FIG. 5.—(a) (Logarithmic) reorientational correlation functions calculated using Raman, infrared and far-infrared band profiles for  $\nu_1$  of acetonitrile (dilute solution in  $\text{CCl}_4$ ). (A)  $\log \phi_{\text{R}}(t)$ , (B)  $\log \phi_{\text{IR}}(t)$  using eqn (29), (C)  $\log \phi_{\text{IR}}^{\text{R}}(t)$ , (D)  $\log \phi_{\text{R}}^{\text{IR}}(t)$ . (b) The same correlation functions for the  $\nu_2$  mode.

## RESULTS AND DISCUSSION

From table 2 it is clearly seen that the value of  $\tau_{12}^R$  obtained from our far-infrared/microwave data at 318 K (the temperature of our infrared measurements) is about 2.2 ps at the lowest concentrations we have investigated. This compares well with the value found in "dilute" solution in benzene by Krishnaji and Masingh.<sup>50</sup> The values found by Eloranta and Kadaba,<sup>49</sup> on the other hand, are considerably longer (about 5.8 ps at 318 K) reflecting a much higher concentration of 0.25 mf, and hence a much greater contribution from the "cross" correlation term of eqn (10). The value of  $\tau_D$  in liquid acetonitrile<sup>50</sup> is also considerably higher at 3.8 ps. It appears that on dilution the  $\tau_D$  value first increases as would be expected from viscosity arguments<sup>6,13</sup> and then decreases<sup>10</sup> as cross correlations are successively removed. We are now in the process of making measurements at higher concentrations so that the effects of viscosity and increasing cross correlations (mainly through changes in band shape)<sup>13</sup> may be investigated. There are good physical grounds for believing that  $\tau_{12}^R \geq \tau_{12}^I$  for any molecule (simply because the first Legendre polynomial,  $\cos \theta_i(t)$ , varies with time more slowly than the 2nd order function,  $\frac{1}{2}[3 \cos^2 \theta_i(t) - 1]$ ). It is, therefore, important to consider the values of  $\tau_{12}^R$  obtained here in comparison with the  $\tau_{12}^I$  values quoted in the literature.<sup>1,6,7</sup> These appear to range from 1.3 ps for the liquid (318 K) to 2.0 ps for a 0.03 mf solution in  $\text{CCl}_4$  (288 K). It thus seems likely that our  $\tau_{12}^R$  value of  $\sim 2.2$  ps (318 K) should be compared with a value near 1.7 ps at the same concentration and temperature. Notice, however, that the Raman values quoted<sup>1,6,7</sup> have been obtained using  $\phi_v^{120}(t) = \phi_v^{210}(t)$ , an approximation which we have shown may not always be valid. The  $\tau_{12}^R$  data show therefore that the reorientational motion in  $\text{CCl}_4$  is distinctly non-diffusive<sup>4,18,19</sup> (for which  $\tau_{12}^R/\tau_{12}^I = 3$ ). This situation is different from that indicated by n.m.r. data<sup>31</sup> in the liquid phase and may well reflect the extreme thermodynamic non-ideality<sup>32</sup> of the solution.

We now turn our attention to the discrepancies between  $\phi_v^{120}(t)$  and  $\phi_v^{210}(t)$  (or  $\tau_v^{120}$  and  $\tau_v^{210}$ ) clearly shown in fig. 5, and in table 3. There are several reasons why this situation might arise.

First Lynden-Bell<sup>25</sup> has shown very clearly that in the presence of a sizeable exchange term in eqn (9) the infrared and isotropic Raman band profiles are expected to be different. However, as mentioned above, the amount of resonance energy transfer (R.E.T.) is small for these two modes even in the liquid phase. Further, any small amount of R.E.T. operative should be removed on going to a dilute solution  $\text{CCl}_4$ . It should also be noticed that our Raman measurements on the  $\nu_1$  and  $\nu_2$  bands showed that  $\nu_{\text{max}}^{120} = \nu_{\text{max}}^{210}$ , in contradiction to what is expected<sup>26-28</sup> if mode-mode coupling is the result of liquid phase "order" caused by a non-random distribution of "probe" molecules. Further evidence that our data do not follow the predictions of Lynden-Bell is provided by the fact that any "cross" term (assuming one exists) between self and exchange processes appears to be negative for our  $\nu_1$  data ( $\tau_v^{120} > \tau_v^{210}$ , see table 3) indicating<sup>25</sup> (for a stretching mode) dipole-dipole forces to be predominant. This we know<sup>1,2,4</sup> not to be the case (see below). A positive cross term ( $\tau_v^{120} > \tau_v^{210}$ ) occurs, on the other hand, for the  $\nu_2$  (symmetric bending) mode which would indicate the presence of dispersive interactions, in a situation where the band profile is sensitive to dilution in a non-polar solvent. It thus appears certain that we can eliminate R.E.T. as a source of the observed discrepancy between  $\phi_v^{120}(t)$  and  $\phi_v^{210}(t)$ .

Secondly, it is possible that collision-induced processes make a significant contribution to the profiles of these bands. This would imply that the intermolecular potential in dilute solution may be dominated by short range repulsive forces. There is already a certain amount of evidence<sup>1,4,8</sup> from temperature,<sup>1,8</sup> density<sup>8</sup> and concentra-

tion<sup>6</sup> studies that this may indeed be the case, especially for the  $\nu_1$  (symmetric CH<sub>3</sub> stretching) mode. In particular, the  $(\tau_v^{\text{iso}})^{-1}$  relaxation rate increases on increasing the temperature at constant density (in contravention of the  $\rho\eta/T$  dependence expected<sup>4,25</sup> for the dephasing rate controlled by longer range, dipole-dipole interactions). Furthermore, the behaviour on dilution is unusual in that the  $\tau_v^{-1}$  relaxation rate (obtained using the Kubo<sup>25</sup> model to separate correlation time and second moment contributions to  $\tau_v^{-1}$ ) shows an increase as the amount of CCl<sub>4</sub> is increased. (Notice that the change in band-width and  $\tau_v^{-1}$  is non-linear,<sup>1</sup> also in disagreement with the prediction<sup>25</sup> based on dipolar or dispersive interactions.) If indeed collision induced interactions are important then it is possible that such processes affect the transition moment,  $\partial\mu/\partial Q$ , differently from how they affect the polarisability derivatives,  $\partial\alpha/\partial Q$  or  $\partial\beta/\partial Q$ . In that case there is no reason why the various vibrational band profiles should be the same.

Finally, it may well be that at least part of the discrepancy between  $\phi_v^{\text{iso}}(t)$  and  $\phi_v^{\text{R}}(t)$  is a result of our neglect of one or more of several factors involved in making the original separation *via* eqn (2) and (6). It may be, for example, that for a complex highly polar molecule such as acetonitrile the approximation made in eqn (1) and (5) are simply not valid and that statistical correlation of reorientational and vibrational motions are important.<sup>9</sup> Furthermore, the necessarily simplified treatments neglect possible coupling of vibrational relaxation mechanisms. Eqn (9) should, of course, be constructed such that,

$$\phi_{\text{vvp}}(t) = \langle \phi_1(t) \cdot \phi_2(t) \dots \phi_j(t) \rangle$$

where there are supposed to be  $j$  mechanisms by which  $\langle Q_i^!(0) \cdot Q_i^!(t) \rangle$  may decay. How large the cross terms between such mechanisms are expected to be and how differently they would affect infrared and Raman spectra is not yet established. It is clear that there has so far not emerged a well-established reason for the disagreement between the vibrational relaxation functions obtained from isotropic Raman and infrared spectra. More theoretical and experimental work is obviously needed. The type of work we have described here does, however, show how theoretical predictions may be checked, at the same time demonstrating clearly the dangers of transferring correlation times or half widths between data from different techniques.

Valuable discussions with Dr. Myron Evans, Dr. Ruth M. Lynden-Bell and Dr. Paul A. Madden are gratefully acknowledged. Thanks are also due to NATO, the S.R.C., the Royal Society and the D.F.G. for research and equipment grants.

<sup>1</sup> Part 1, J. Yarwood, R. Arndt and G. Döge, *Chem. Phys.*, 1977, **25**, 387.

<sup>2</sup> Part 2, G. Döge, A. Khuen and J. Yarwood, *Chem. Phys.*, 1979, in press.

<sup>3</sup> R. T. Bailey, in *Molecular Spectroscopy*, ed. R. F. Barrow, D. A. Long and D. J. Millen (The Chemical Society, London, 1974), vol. 2 and references therein.

<sup>4</sup> J. Yarwood and R. Arndt, *Molecular Association*, ed. R. Foster (Wiley-Interscience, London, 1978), vol. 2 and references therein.

<sup>5</sup> W. G. Rothschild, G. J. Rosasco and R. C. Livingston, *J. Chem. Phys.*, 1975, **62**, 1253 and references therein.

<sup>6</sup> S. L. Whittenberg and C. H. Wang, *J. Chem. Phys.*, 1977, **66**, 4255, and references therein.

<sup>7</sup> J. E. Griffiths, in *Vibrational Spectra and Structure*, ed. J. R. Durig (Elsevier, Amsterdam, 1966), vol. 6; *J. Chem. Phys.*, 1973, **75**, 751.

<sup>8</sup> J. Schroeder, V. H. Schiemann, P. T. Sharko and J. Jonas, *J. Chem. Phys.*, 1977, **66**, 3215; J. Hyde-Campbell, J. F. Fisher and J. Jonas, *J. Chem. Phys.*, 1974, **61**, 346.

<sup>9</sup> A. M. Amorim da Costa, M. A. Norman and J. H. R. Clarke, *Mol. Phys.*, 1975, **29**, 191.

<sup>10</sup> L. C. Rosenthal and H. L. Strauss, *J. Chem. Phys.*, 1976, **64**, 282.

<sup>11</sup> F. J. Bartoli and T. A. Litovitz, *J. Chem. Phys.*, 1972, **56**, 404.

<sup>12</sup> T. Keyes and D. Kivelson, *J. Chem. Phys.*, 1972, **56**, 1057.

- <sup>13</sup> D. Kivelson and P. A. Madden, *Mol. Phys.*, 1975, 30, 1749.
- <sup>14</sup> G. R. Alms, D. R. Bauer, J. I. Brauman and R. Pecora, *J. Chem. Phys.*, 1973, 59, 5310, 5321; 1973, 58, 5570; 1974, 61, 2255.
- <sup>15</sup> C. W. Beer and R. Pecora, *Faraday Symp. Chem. Soc.*, 1977, 11, 78.
- <sup>16</sup> J. S. Rowlinson and M. Evans, *Ann. Rep. Chem. Soc. A*, 1975, 5.
- <sup>17</sup> R. G. Gordon, *J. Chem. Phys.*, 1965, 42, 3658; 1965, 43, 1307; *Adv. Magnetic Resonance*, 1968, 3, 1.
- <sup>18</sup> R. E. D. McClung, *J. Chem. Phys.*, 1969, 51, 3842; 1971, 54, 3248; 1971, 55, 3459; 1972, 57, 5478.
- <sup>19</sup> T. E. Eagles and R. E. D. McClung, *Chem. Phys. Letters*, 1973, 22, 414; *J. Chem. Phys.*, 1973, 59, 435.
- <sup>20</sup> R. Arndt and R. E. D. McClung, *J. Chem. Phys.*, 1978, 69, 4280.
- <sup>21</sup> G. J. Evans and M. Evans, *J.C.S. Faraday II*, 1976, 72, 1169; G. J. Davies, G. J. Evans and M. Evans, *J.C.S. Faraday II*, 1976, 72, 1901.
- <sup>22</sup> W. T. Coffey, G. J. Evans, M. Evans and G. H. Wegdam, *J.C.S. Faraday II*, 1978, 74, 310; M. W. Evans, *Chem. Phys. Letters*, 1977, 48, 385.
- <sup>23</sup> M. W. Evans, *Adv. Mol. Relaxation Processes*, 1977, 10, 203.
- <sup>24</sup> M. Evans, *Dielectric and Related Molecular Processes*, ed. Mansel Davies (Specialist Periodical Reports, Chem. Soc., London, 1977), vol. 3, p. 1.
- <sup>25</sup> R. M. Lynden-Bell, *Mol. Phys.*, 1977, 33, 907; *Faraday Symp. Chem. Soc.*, 1977, 11, 167.
- <sup>26</sup> G. Döge, *Z. Naturforsch.*, 1973, 28a, 919.
- <sup>27</sup> T. Tokuhiko and W. G. Rothschild, *J. Chem. Phys.*, 1975, 62, 2150.
- <sup>28</sup> D. C. M. van Woerkom, J. de Beyser, M. de Zwart, P. J. H. Burgers and J. C. Leyte, *Ber. Bunsenges. phys. Chem.*, 1974, 78, 1303.
- <sup>29</sup> H. Dardy, V. Volterra and T. A. Litovitz, *Faraday Symp. Chem. Soc.*, 1972, 6, 71.
- <sup>30</sup> R. M. van Aalst, J. van der Elsken, D. Frenkel and G. H. Wegdam, *Faraday Symp. Chem. Soc.*, 1972, 6, 94.
- <sup>31</sup> G. Wylie, *Dielectric and Related Molecular Processes*, ed. Mansel Davies (Specialist Periodical Report, Chem. Soc., London, 1972), vol. 1, p. 21.
- <sup>32</sup> C. Brot, *Dielectric and Related Molecular Processes*, ed. Mansel Davies (Specialist Periodical Report, Chem. Soc., London, 1975), vol. 2, p. 1.
- <sup>33</sup> R. N. Jones and J. Pitha, *Canad. J. Spectr.*, 1966, 44, 3031; 1967, 45, 2347.
- <sup>34</sup> R. N. Jones and J. Pitha, N. R. C. Bulletin No. 12 (National Research Council of Canada, Ottawa, 1968).
- <sup>35</sup> D. H. Martin and E. Puplett, *Infrared Phys.*, 1969, 10, 105.
- <sup>36</sup> B. J. Berne and G. D. Harp, *Adv. Chem. Phys.*, 1970, 17, 100; B. J. Berne, *Physical Chemistry—An Advanced Treatise*, ed. H. Eyring, D. Henderson and W. Jost (Academic Press, N.Y., 1971), vol. 8B, chap. 9.
- <sup>37</sup> B. Quentrec and P. Bezot, *Mol. Phys.*, 1974, 27, 879.
- <sup>38</sup> G. J. Davies, G. J. Evans and M. Evans, *J.C.S. Faraday II*, 1977, 73, 1071.
- <sup>39</sup> G. J. Evans and M. W. Evans, *Chem. Phys. Letters*, 1977, 45, 454; G. J. Evans, *J.C.S.-Faraday II*, 1977, 73, 729.
- <sup>40</sup> H. Mori, *Prog. Theor. Phys.*, 1965, 33, 423.
- <sup>41</sup> M. Evans, *J.C.S. Faraday II*, 1975, 71, 843, 2051; A. Gerschel, I. Darmon and C. Brot, *Mol. Phys.*, 1972, 23, 317.
- <sup>42</sup> G. Williams, *Chem. Soc. Rev.*, 1978, 7, 89.
- <sup>43</sup> R. G. Gordon, *Adv. Magnetic Resonance*, 1968, 3, 1; *J. Chem. Phys.*, 1966, 44, 1830.
- <sup>44</sup> M. W. Evans, personal communication.
- <sup>45</sup> M. Drawid and J. W. Halley, *J. Chem. Phys. Solids*, 1977, 38, 1269.
- <sup>46</sup> G. W. Chantry, *Submillimetre Waves* (Academic Press, London, 1971).
- <sup>47</sup> J. Yarwood, P. L. James, R. Arndt and M. Evans, *J.C.S. Faraday II*, to be published.
- <sup>48</sup> P. L. James, M. N. Afsar, J. R. Birch and J. Yarwood, *Mol. Phys.*, submitted.
- <sup>49</sup> J. K. Elooranta and P. K. Kadaba, *Mat. Sci. Eng.*, 1971, 8, 203.
- <sup>50</sup> Krishnaji and A. Mansingh, *J. Chem. Phys.*, 1964, 41, 827.
- <sup>51</sup> T. E. Bull, *J. Chem. Phys.*, 1975, 62, 222.
- <sup>52</sup> K. J. Czworniak, H. C. Andersen and R. Pecora, *Chem. Phys.*, 1975, 11, 451.
- <sup>53</sup> R. Kubo in *Fluctuation, Relaxation and Resonance in Magnetic Systems*, ed. D. Ter Haar (Oliver and Boyd, London, 1962), p. 23.

**APPENDIX 3**

**STUDIES OF MOLECULAR MOTIONS AND VIBRATIONAL  
RELAXATION IN ACETONITRILE  
IV. FAR-INFRARED AND MOLECULAR DYNAMICS  
IN CARBON TETRACHLORIDE SOLUTION**

**M.W. EVANS, G.J. EVANS, J. YARWOOD,  
P.L. JAMES, R. ARNDT**

**MOLECULAR PHYSICS, 1979, VOL.38 No.3**

**Studies of molecular motions and vibrational relaxation  
in acetonitrile**

**IV. Far-infra-red and molecular dynamics in carbon  
tetrachloride solution**

by M. W. EVANS and G. J. EVANS

Edward Davies Chemical Laboratory, U.C.W. Aberystwyth, Dyfed, Wales

J. YARWOOD and P. L. JAMES

Department of Chemistry, University of Durham, Durham City, England

and R. ARNDT

Institut für Physikalische Chemie,  
Techn. Universität, Braunschweig, W. Germany

(Received 17 November 1978)

Far-infra-red spectra in the 2-200  $\text{cm}^{-1}$  region of dilute solutions of  $\text{CH}_3\text{CN}$  in  $\text{CCl}_4$  solution have been employed to test the various analytical models available for the description of rotational motions of a symmetric top dipole in the liquid phase. It is found that none of the various approximations of the Mori continued fraction description of reorientational correlation function fit the experimental data satisfactorily. This implies that, although the data (from this and other techniques) may appear to be properly described by a simple rotational diffusion model at long times, the short time dynamics are too complicated to be reproduced even by much more sophisticated models. The data are able to clearly discriminate between the various models tried and, in addition, give valuable information about the nature and extent of the mean square torques acting on the probe molecule.

---

I. INTRODUCTION

The problem of describing analytically the molecular dynamics and interactions in a dense fluid of dipolar molecules may be approached using a wide range of spectroscopic methods [1-3]. These include infra-red, far-infra-red and microwave absorption, Raman and Rayleigh light scattering, neutron scattering, and nuclear magnetic resonance techniques. (There have recently been several excellent reviews of the subject [1-4].) A viable model of the dynamical evolution of the  $N$  molecules from an arbitrary initial time,  $t=0$ , must then be capable of describing the various spectroscopic features in a consistent manner. In other words, it must be consistent with *all* the data and must allow such data to be expressed in physical terms which are suitable for intercomparison. It has become clear recently [2, 5] that models described in terms of inverse frequencies (such as the Debye relaxation time [6] or the time between collisions of extended diffusion theory [7]) lead to disparate and contradictory results for extensively studied [5, 8] liquids such as  $\text{CH}_2\text{Cl}_2$ . The fundamental reason for this is that

the models involved approximate the Liouville equation [3, 8] of motion too roughly. Most, if not all, these models are early approximants (or truncations) of the Mori continued fraction [8-10] expansion of the Liouville equation and, as such, define the potential energy of the total hamiltonian using only one or two terms, in the effective Taylor expansion [3, 4 (b)]. For example, in the *J*-diffusion model [3, 7, 11] even the mean square torque, the first derivative of the potential energy with respect to orientation, is not defined. Furthermore, this is true for any model which relies on the concept of an elastic collision regardless of the type of underlying statistics employed [12].

This situation will remain unless a realistic intermolecular potential is employed, either by direct numerical integration of the equations of motion [13] (molecular dynamics simulation) or by taking a fundamentalist line in employing later approximants of various continued fractions. We describe here a method for the evaluation of the mean square torque acting on a dipolar molecule and its derivative using the truncated Mori expansion of the orientational auto-correlation function  $C_u(t) = \langle \mathbf{u}(0) \cdot \mathbf{u}(t) \rangle$  ( $\mathbf{u}$  is a dipole unit vector) without recourse to least mean squares fitting [10 (a)] to the observed far-infra-red spectra. This technique is applied to the analysis of data on dilute solutions of acetonitrile in a range of solvents by observing the peak frequencies of both the dielectric loss,  $\epsilon''(\omega)$ , and the power absorption,  $\alpha(\omega)$ , spectra. We express some currently popular models in terms of Mori approximants and evaluate them using the 0-THz frequency spectra for the same solutions. In this way we are able to discriminate, in a very powerful manner, the relative validities of the assumed models. In order to counteract the complexity of the overall dynamics in an isotropic fluid we have also studied the far-infra-red spectrum of  $\text{CH}_3\text{CN}$  in a solvent which forms a cholesteric phase (and which therefore restricts, to some extent, the freedom of molecular motion).

## 2. GENERAL THEORETICAL BACKGROUND

The starting point is the model-independent Mori equation of motion [15-17] of a dynamical array of  $N$  interacting molecules, viz.

$$\dot{\mathbf{A}}(t) = i\Omega_{\mathbf{A}}\mathbf{A}(t) - \int_0^t K_{\mathbf{A}}(t-\tau)\mathbf{A}(\tau) d\tau + \mathbf{F}_{\mathbf{A}}(t), \quad (1)$$

where  $\mathbf{A}_i(t)$  are the  $n$  linearly independent variables and  $\Omega_{\mathbf{A}}$  is a resonance frequency operator. The matrix  $K_{\mathbf{A}}$  is a memory function and  $\mathbf{F}_{\mathbf{A}}(t)$  is a random force or torque which is Mori-propagated from  $\mathbf{A}(0)$  and is a generalized stochastic variable [16]. Physical realization of equation (1) may be expressed through the following models which have often been used in the interpretation [1-4] of infra-red, Raman, N.M.R., (spin-spin, nuclear quadrupole and spin-lattice relaxation) and neutron scattering data.

(1) When the memory kernel  $K_{\mathbf{A}}$  has delta function components (i.e.  $K_0(t) = D\delta(t)$ ) equation (1) reduces to the Langevin equation [15 (b)] for an asymmetric top, solved very recently by Morita [18]. This represents the inertia-corrected asymmetric top analogue of the Debye model of rotational diffusion (infinitely small reorientations taking place infinitely rapidly). The solution leads to friction coefficients [17 (d)]  $\beta_{xx}$ ,  $\beta_{yy}$  and  $\beta_{zz}$  along the principal inertial axes and they may be found using the shape factor analysis of Budo *et al.* [19].

For a symmetric top molecule  $\beta_{xx} = \beta_{yy}$  and, since the friction coefficients are obtained from the maximum in the dielectric loss curve, the two  $\beta$  values can be obtained without the use of adjustable parameters (see equation (7)).

(2) The next simplest model is characterized [20 (a)] by writing

$$K_0(t) = {}^{FR}K_0(t) \exp(-|t|/\tau_\omega), \quad (2)$$

where  $\tau_\omega$  is the correlation time of the dynamical system and  ${}^{FR}K_0(0)$  the memory kernel for a maxwellian ensemble of non-interacting rotors. This model corresponds to the Gordon  $J$ -diffusion model [7] for instantaneous, elastic collision-interrupted free rotations or to the Chandler binary collision model [20 (b)]. The resulting spectrum (the Fourier transform of  $\langle \omega(0) \cdot \omega(t) \rangle$ , where  $\omega$  is the angular velocity about the dipole axis) is therefore analytically identical [21] with that obtained using the  $J$ -diffusion model. Equation (2) represents a first order approximant of the Mori continued fraction [9, 10].

(3) More complicated, but tractable, expressions for the dipole orientational correlation [8 (b)] function  $C_u(t)$  may be obtained [10] using other approximants of the Mori continued fraction expansion. The rate of convergence of successive terms to the Liouville equation

$$\dot{u} = i\mathcal{L}u \quad (3)$$

is, however, (at present) unknown.

Truncations at second- and third-order respectively [8, 10, 22] lead to the approximants defined by,

$$K_u^{(1)}(t) = K_u^{(1)}(0) \exp(-[\pi K_u^{(1)}(0)/2]^{1/2} t) \equiv K_u^{(1)}(0) \exp(-\gamma_1 t) \quad (4)$$

and

$$K_u^{(2)}(t) = K_u^{(2)}(0) \exp(-[\pi K_u^{(2)}(0)/2]^{1/2} t) \equiv K_u^{(2)}(0) \exp(-\gamma_2 t), \quad (5)$$

where  $K_u^{(1)}(t)$  and  $K_u^{(2)}(t)$  are the second and third memory functions of  $C_u(t)$ . In previous publications [10, 14 (a)] the  $\gamma_1$  and  $\gamma_2$  factors in (4) and (5) have been treated as adjustable parameters but, as is made clear later (and elsewhere [8]) the equilibrium averages ( $K_u^{(0)}(0)$ ,  $K_u^{(1)}(0)$ ) and ( $K_u^{(0)}(0)$ ,  $K_u^{(1)}(0)$ ,  $K_u^{(2)}(0)$ ) (depending on the approximant used) may be calculated (without need for least squares fitting) from the maxima of the dielectric loss ( $\epsilon''(\omega)$ ) and power absorption ( $\alpha(\omega)$ ) curves in the 0-THz frequency region. Furthermore, only one set of experimental data is needed (provided refractive index data are available [14 (c)]) since the relationship

$$\alpha(\bar{\nu}) = 2\pi\epsilon''(\bar{\nu})\bar{\nu}/n(\bar{\nu}) \quad (6)$$

can be used. The memory functions mentioned here are, of course, closely related to the dynamics and interactions of the molecules in the fluid [10, 23, 24] and their determination can throw considerable light on these molecular properties.  $K_u^{(0)}(0)$  is proportional to the orientational second moment ( $2kT/I_D$  for a symmetric top molecule),  $K_u^{(1)}(0)$  is related [24] to the mean square torque,  $\langle O(V)^2 \rangle$ , while  $K_u^{(2)}(0)$  is related to the torque and to its mean squared time derivative.

(4) Finally one may use an itinerant libration model as developed by Coffey *et al.* [17]; details of which are presented fully elsewhere [17]. This is a zeroth approximant of the *matrix* Mori series considered by Damle *et al.* [25] for a translational itinerant oscillator in the context of neutron scattering. In particular, [8 (a)] the memory function  $K_A$  of equation (1) is given by

$$K_A = \begin{bmatrix} \beta_2 \delta(t) + \omega_0^2 & -\omega_0^2 \\ -\Omega_0^2 & \beta_1 \delta(t) + \Omega_0^2 \end{bmatrix}, \quad (7)$$

where  $\omega_0^2 = K_u^{(0)}(0)$  and  $\Omega_0^2 = K_u^{(1)}(0) = (I_2/I_1)K_u^{(0)}(0)$  in this notation,  $\beta_1$  and  $\beta_2$  are friction coefficients. The librating disc-like molecule is situated [17 (b)] in a rigid annulus (cage) of neighbouring molecules, both disc and annulus being free to rotate about a central axis perpendicular to their plane.  $I_1$  and  $I_2$  are the moments of inertia of the disc and annulus respectively. The parameters of this model [17], with one exception, may be identified with measurable frequencies such as those of the dielectric loss and power absorption. The adjustable parameter,  $\beta_2$ , is defined as the hydrodynamic friction between the librating/diffusing molecule and the annulus of surrounding molecules. Analytical tractability is only achieved for planar reorientations of the symmetric top dipolar axis. In general, however, this restriction may be lifted by using numerical methods (computer simulations) [26] or by noticing that the stochastic equations of motion governing the system may be identified with those developed by Budó [19] for the brownian motion of a molecule carrying a pair of interacting dipoles. However, this dipole-dipole coupling mechanism, whilst surely being important for pure dipolar liquids, should be much reduced or even negligible at the very low concentrations used in this work (in order to attempt to avoid the problem of ignoring the internal field [27 (a)] and to eliminate cross correlation effects on  $C_u(t)$ ). We investigate here the effect of  $\beta_2$  on the low frequency (theoretical) power absorption profile.

### 3. DEFINITION OF THE VARIABLES OF MODEL 3

The analytical expression [10 (a)] for the power absorption coefficient of the two variable approximant (equation (4)) is

$$\alpha(\omega) = \frac{A\omega^2 K_u^{(0)}(0)K_u^{(1)}(0)\gamma}{\gamma^2 [K_u^{(0)}(0) - \omega^2]^2 + \omega^2 [\omega^2 - (K_u^{(0)}(0) + K_u^{(1)}(0))]^2}. \quad (8)$$

If this expression is differentiated we obtain  $K_u^{(1)}(0)$  in terms of the maximum frequency,  $\omega_1$ , of the  $\alpha(\omega)$  curve, viz.

$$K_u^{(1)}(0) = \frac{4\omega_1^4(\omega_1^2 - K_u^{(0)}(0))}{\pi(K_u^{(0)}(0) - \omega_1^2)(K_u^{(0)}(0) + \omega_1^2) + 4\omega_1^4}. \quad (9)$$

Thus the mean square torque can be measured directly from the infra-red peak frequency, this band shifting to higher frequency as the torque increases.

By differentiating the corresponding expression for the dielectric loss  $\epsilon''(\omega)$  we arrive at the useful approximation

$$K_u^{(1)}(0) = \frac{\pi}{2} \left[ \frac{2kT\tau_D}{I_B} \right]^2, \quad (10)$$

where  $\tau_D$  is the inverse of the dielectric loss peak frequency,  $\omega_0$ .  $\tau_D$  may therefore be directly calculated through equation (10). In the next approximant the two equations,

$$\left[ \frac{\partial \epsilon''(\omega)}{\partial \omega} \right]_{\omega=\omega_0} = 0 \quad (11)$$

and

$$\left[ \frac{\partial \alpha(\omega)}{\partial \omega} \right]_{\omega=\omega_1} = 0, \quad (12)$$

are solved simultaneously to give  $K_u^{(1)}(0)$  and  $K_u^{(2)}(0)$ . (The details of this solution are given in the Appendix.)

Needless to say, the  $K_u^{(1)}(0)$  value estimated from equation (10) or from the pair of following equations should be the same were the truncated (continued) fraction already a reasonable approximant to  $\hat{u} = i\mathcal{L}u$ . By noticing that the far wing of the Rayleigh depolarized band decays [29] approximately as  $\epsilon''(\omega)/\omega$ , this method may be extended one step further to evaluate the set ( $K_u^{(0)}(0)$ ,  $K_u^{(1)}(0)$ ,  $K_u^{(2)}(0)$  and  $K_u^{(3)}(0)$ ) given the interrelations between the coefficients of time in the Maclaurin expansions of  $C_u(t)$  [3, p. 18] and the correlation function appropriate to Rayleigh scattering, i.e. for simplest geometries  $\frac{1}{2} \langle 3(u(0) \cdot u(t))^2 - 1 \rangle$ . By this method we can move towards experimental consistency without recourse to modelling at too early a stage. It may also be possible to extend the set of  $K_u^{(n)}(0)$  further in the future with aid of recent mathematical developments [27 (b)] in the ill-posed problem theory as a method of estimating the statistical information lost by using approximants.

#### 4. EXPERIMENTAL

The far-infra-red measurements reported here for acetonitrile in solution in  $\text{CCl}_4$  were made using a Beckman-R.I.I.C. Ltd. FS720 (20–250  $\text{cm}^{-1}$ ), Michelson interferometer equipped with a Golay (IR50) detector and a QMC Industrial Research Ltd. liquid helium cooled germanium bolometer (2–30  $\text{cm}^{-1}$ ). In the low frequency region the interferometer was converted to the Martin-Puplett [31] mode. The variable temperature cell unit was equipped with polyethylene windows and temperature control was via a Beckman R.I.I.C. Ltd. controller. It is estimated that spectra are reproducible to within  $\pm 2$  per cent in the 30–250  $\text{cm}^{-1}$  region and within  $\pm 1$  per cent at frequencies between 2 and 30  $\text{cm}^{-1}$ . Static permittivities were made with a W.T.W., Model DM01 dipolemeter while the refractive indices were obtained at the National Physics Laboratory using a special dispersive cell [32] developed there (these measurements will be described in detail elsewhere). Spectroscopic grade  $\text{CH}_3\text{CN}$  and  $\text{CCl}_4$  were used throughout after drying over molecular sieves. Solutions were made up by volume immediately prior to measurement. Measurements on  $\text{CH}_3\text{CN}$  in cholesteryl oleyl carbonate were made using a Grubb Parsons/NPL Michelson interferometer equipped with Golay and helium cooled Indium/Antimonide detectors in order to cover the region between 1 and 250  $\text{cm}^{-1}$ . A saturated solution of  $\text{CH}_3\text{CN}$  in this solvent was prepared by refluxing for 48 hours and separating layers. This yielded a solution with a mole fraction for  $\text{CH}_3\text{CN}$  of about 0.04.

## 5. RESULTS

Measurements of  $\text{CH}_3\text{CN}$  in  $\text{CCl}_4$  have been made over a mole fraction range of 0.018–0.37 and at temperatures between 252 K and 343 K. Some typical power absorption spectra are shown in figure 1. We concentrate here on model fitting spectra at the lowest concentrations (mole fractions of 0.018 and 0.06) for the reasons outlined previously. Figures 2 and 3 show the refractive index data,  $n(\bar{\nu})$ , and a comparison of the  $\alpha(\bar{\nu})$  and  $\epsilon''(\bar{\nu})$  curves at these two concentrations and 318 K. The static ( $\epsilon_0$ ) and long wavelength ( $\epsilon_\infty$ ) (i.e.  $> 50 \text{ cm}^{-1}$ ) permittivities are summarized in table 1.

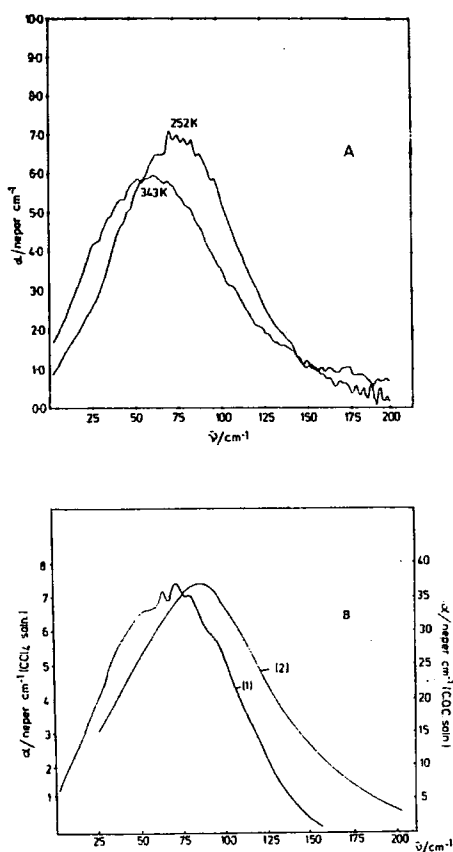


Figure 1. (A) Comparison of observed data for a mole fraction for  $\text{CH}_3\text{CN}$  in  $\text{CCl}_4$  of 0.02 at two temperatures. (B) Comparison of observed data for  $\text{CH}_3\text{CN}$  in an isotropic phase ( $\text{CCl}_4$ ) (1) and a mesomeric phase (cholesteryl oleyl carbonate, c.o.c.) (2) at comparable concentration and the same temperature.

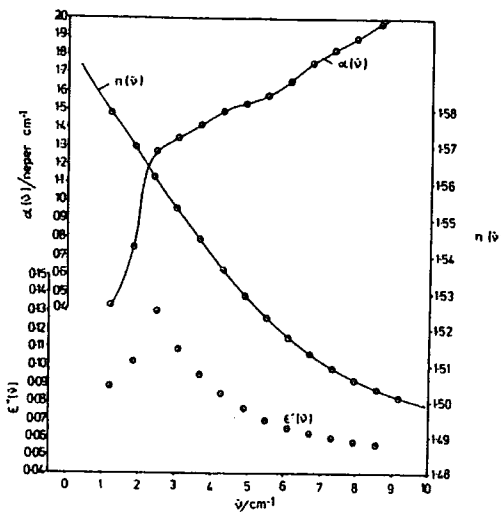


Figure 2. Low frequency observed  $\alpha(\nu)$ ,  $n(\nu)$  and  $\epsilon''(\nu)$  data for a mole fraction for  $\text{CH}_3\text{CN}$  in  $\text{CCl}_4$  of 0.02 at 318 K.

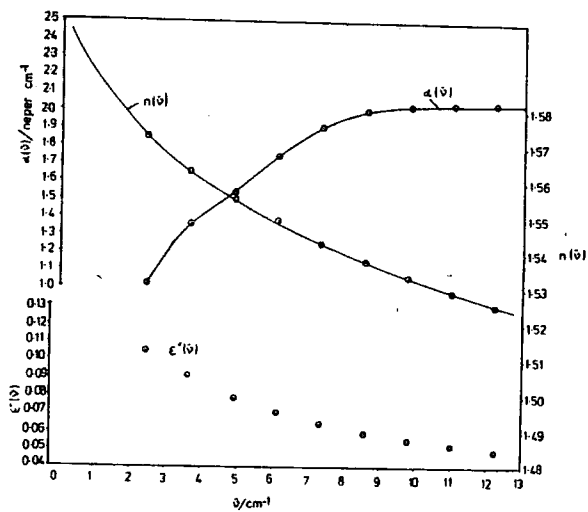


Figure 3. Low frequency observed  $\alpha(\nu)$ ,  $n(\nu)$  and  $\epsilon''(\nu)$  data for a mole fraction for  $\text{CH}_3\text{CN}$  in  $\text{CCl}_4$  of 0.06 at 318 K.

Table 1. Permittivities and refractive index† of solutions of CH<sub>3</sub>CN in CCl<sub>4</sub> (temperature‡ in K given as a superscript).

Mole fraction CH <sub>3</sub> CN	$\epsilon_0^{318}$	$\epsilon_0^{288}$	$\epsilon_0^{252}$	$n_{\infty}^{318}$	$n_{\infty}^{288}$	$\epsilon_{\infty}^{318}$	$\epsilon_{\infty}^{288}$	$\epsilon_{\infty}^{252}$
0.018	2.38	2.42	2.51	1.474	1.488	2.17	2.21	2.30
0.061	2.79	2.83	2.92	1.480	1.490	2.19	2.23	2.32

† At frequencies beyond 3 THz (100 cm<sup>-1</sup>).

‡ Values of  $\epsilon_0$  and  $\epsilon_{\infty}$  at 288 and 252 obtained from those measured at 318 K with  $\partial\epsilon/\partial T = -0.002$ .

## 6. EVALUATION OF MODELS AND DISCUSSION

Before comparing our spectra with the models considered it is worth making the point that these models are applied in such a way that the microwave dielectric loss curve is reproduced accurately. This implies that, at long times, we assume in each case that the orientational correlation function,  $\langle \mathbf{u}(0) \cdot \mathbf{u}(t) \rangle$ , decays exponentially. This in turn ensures that the short time characteristics of each model (corresponding in the spectral domain to the high frequency, far-infra-red, region) may be individually compared with each other and with the experimental data. It has been emphasized [4, 8] that the great importance of far-infra-red data is that they provide a means of discriminating between different models all of which predict an exponential decay of the relevant correlation function at long-times (and therefore all of which appear to fit the observed low frequency data equally well).

The models were fitted to the solutions of CH<sub>3</sub>CN in CCl<sub>4</sub> which are respectively 1.8 and 6.1 per cent mole fraction in solute. We have assumed that the effects of collision induced dipoles and of cross correlations of the type,  $\langle \mathbf{u}_i(0) \cdot \sum_{i \neq j} \mathbf{u}_j(t) \rangle$  ( $i$  and  $j$  referring to different molecules) are negligible at these very low concentrations. (Notice, however, evidence from Raman data [14 (a)] that dipole-dipole coupling [27] may be operative even at 2 per cent mole fraction.)

The delta function memory of model (1) is not able to produce a far-infra-red Poley absorption since the mean intermolecular potential energy is inaccurately defined (for example, its first derivative with respect to reorientation, the r.m.s. torque is undefined). This model therefore simply predicts a Debye plateau, [3, 4, 8] even when inertial corrections have been made [18] and this is the maximum value  $\alpha(\bar{\nu})$  reaches.

Figure 4 shows the observed spectrum at lowest concentration compared with those predicted by the  $J$ -diffusion or Chandler binary collision model (model 2) and with the planar itinerant oscillator (model 4). It is seen that the former is totally inadequate in that it peaks at the position predicted by the average rotational energy and makes no allowance for torques which shift the far-infra-red spectrum to higher frequency [3, 4, 8]. In other words, the  $J$  diffusion model merely broadens the  $J+1 \leftarrow J$  pure rotational contour and again no evaluation of the mean square torque is possible. This is true even where the analytical statistics underlying this process of collision interrupted, free rotation

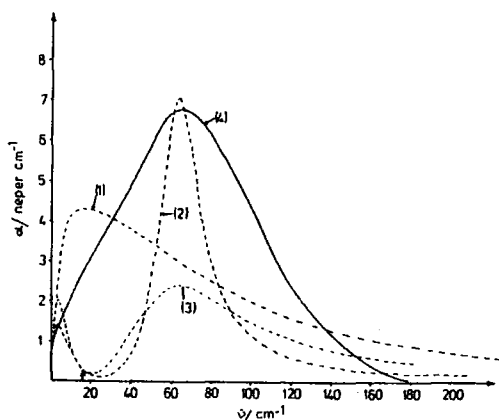


Figure 4. Comparison of observed and predicted data for  $\text{CH}_3\text{CN}$  in  $\text{CCl}_4$  (0.02 mole fraction, 318 K). Curve (1), Binary collision ( $J$  diffusion) model first-order truncation;  $\beta_1=20$  THz; Curve (2), Symmetric top itinerant oscillator model  $I_1=10I_2$ ,  $\beta_2=5$  THz; Curve (3), same with  $\beta_1=15$  THz; Curve (4), observed data.

are generalized since the collisions are elastic and infinitely short. The r.m.s. torque is again undefined.

As in previous studies on highly polar molecules [8 (b), 17 (b, d)] the itinerant oscillator model produces a far-infrared spectral distribution (figure 4) which is too narrow even for large values of the molecule-annulus friction parameter  $\beta_2$  (figure 4). It is clear that fixing  $\beta_1$  at  $kT\tau_D/I_2$  (where  $\tau_D$  is the inverse frequency of the loss peak) and varying  $\beta_2$  does little to improve the situation (using  $I_1=10I_2$  as one would expect [17 (b)]). Furthermore, the dipole-dipole coupling interpretation of equation (7) is not considered to be realistic for dilute solutions since such coupling should have been largely removed.

Figure 5 shows the results of comparing our observed data at 318 K with the higher order approximants of the Mori continued fraction (for example, equations (4) and (5)). It is seen that second- and successive-order continued fraction approximants of the orientational autocorrelation function,  $C_u(t)$ , first used by Barojas *et al.* [32] seem a little more realistic than models (1) and (2) which are respectively the zeroth- and first-order approximants to the continued fraction representation of the angular momentum autocorrelation function. Since we have approached these model calculations in several ways, it is worth outlining the methods used.

At first we had some difficulty in fitting our data to equation (8) since complete refractive index data were not available [14 (a)]. Initially we therefore fitted our  $\alpha(\omega)$  data to an expression [23 (c, f), 14 (a)] which is independent of  $n(\omega)$ , viz.

$$\alpha(\omega) = \sqrt{2}\epsilon''(\omega)\omega/c[(\epsilon'(\omega)^2 + \epsilon''(\omega)^2)^{1/2} + \epsilon'(\omega)]^{1/2}, \quad (13)$$

where  $(\epsilon_0 - \epsilon_\infty)$  was fixed at the observed value (table 1). This equation gives

Table 2. Summary of parameters† obtained using second-order truncation of the Mori contained fraction.

Temperature/K	Mole fraction CH <sub>3</sub> CN	$\bar{\nu}_1/\text{cm}^{-1}$	$\gamma$ ‡	$K_{\infty}^{(1)}(0)$ §	$\bar{\nu}_{\text{max}}$ §	$\tau_D/\text{ps}$ §	$\tau_D/\text{ps}$ †	$\tau_D$ (obs)‖
343	0.018	61 ± 2	4.4‡	26.5‡	72 ± 2‡	1.9‡	1.8	—
318	0.018	66 ± 2	3.0	21.0	68 ± 2	2.3	2.1	2.1
288	0.018	72 ± 2	2.7	24.1	73 ± 2	3.0	2.6	—
252	0.018	76 ± 2	2.6	32.9	82 ± 2	4.6	3.2	—
318	0.061	70 ± 2	7.9	59.2	88 ± 4	2.5	2.3	> 2.6
288	0.061	73 ± 2	7.4	58.6	88 ± 4	2.8	2.7	—
252	0.061	80 ± 2	5.23	50.1	90 ± 4	3.6	3.4	—

† Given in terms of  $x^{1/2}$ ,  $\gamma$  and  $xK_{\infty}^{(1)}(0)$  where  $x = I_B/2kT$ .

‡ Calculated using equations (9) and (14)—see text.

§ Values obtained by fitting to equation (13) with  $\epsilon_0 - \epsilon_{\infty}$  fixed at observed value (see table 1).‖  $\tau_D$  measured off the  $\epsilon''(\bar{\nu})$  versus  $\bar{\nu}$  plots of figures 2 and 3—calculated using equation (6).¶ Values obtained by fitting to equation (13) with (variable)  $\epsilon_0 - \epsilon_{\infty} = 0.29$ ; observed ( $\epsilon_0 - \epsilon_{\infty}$ ) not available at this temperature.

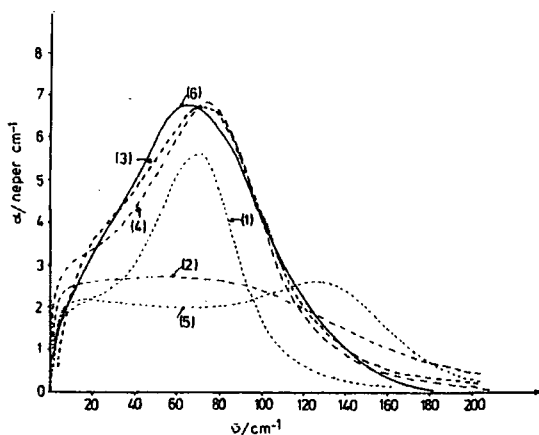


Figure 5. Comparison of observed (curve (6)) and predicted data for  $\text{CH}_3\text{CN}$  in  $\text{CCl}_4$  (0.02 mole fraction, 318 K). Curve (1), second-order Mori truncation; best fit to equation (13) with observed  $\epsilon_0 - \epsilon_\infty = 0.21$ . Curve (2), second-order Mori truncation—values calculated using equations (9) and (14). Curve (3), second-order Mori truncation, best fit to equation (8) with variable  $K_u^{(0)}(0)$  and  $\epsilon_0 - \epsilon_\infty$ ; see text for details. Curve (4) best fit to equation (13) with variable  $\epsilon_0 - \epsilon_\infty$ ;  $K_u^{(0)}(0) = 27.5$ ,  $\gamma = 3.9$ ,  $\epsilon_0 - \epsilon_\infty = 0.33$ . Curve 5, third-order Mori truncation, equations (A 1) and (A 2) with observed  $\epsilon_0 - \epsilon_\infty$ .

reasonably good fit (curve 1) with a maximum frequency somewhat higher than that observed (table 2). This result may be compared with that (curve 2) obtained when expressions (9) and (14) (see [22]) are used to calculate the two parameters  $K_u^{(0)}(0)$  and  $\gamma$  without recourse to least squares fitting,

$$\gamma = \left[ \frac{\pi}{2} K_u^{(0)}(0) \right]^{1/2}. \quad (14)$$

Clearly the fitting procedure is more satisfactory, at least, for this molecule. We then attempted to check the internal consistency of equations (8) and (13). Using the  $\epsilon'(\omega)$  and  $\epsilon''(\omega)$  data calculated by fitting to equation (14) we were able to recalculate the refractive index curve since

$$n(\omega) = \left\{ \frac{(\epsilon''(\omega))^2 + \epsilon'(\omega)^2}{2} + \epsilon'(\omega) \right\}^{1/2}. \quad (15)$$

This dispersion curve is shown in figure 6 (together with the experimental refractive index data obtained so far). As expected the curve shows a shallow minimum at  $\sim 90 \text{ cm}^{-1}$  to high frequency of  $\alpha_{\text{max}}$  at  $\sim 66 \text{ cm}^{-1}$  (for a mole fraction of 0.018 at 318 K). The  $n(\omega)$  data of figure 6 was then used to obtain a best fit to equation (8). Curve (3) of figure 5 shows the result of this fit allowing both  $\epsilon_0 - \epsilon_\infty$  and  $K_u^{(0)}(0)$  to vary. Although this fitted curve is in good agreement with the observed data it can only be achieved with a  $K_u^{(0)}(0)$  value of 2.9 and  $\epsilon_0 - \epsilon_\infty = 0.55$ . We then get a value of  $\tau_D = 0.66 \text{ ps}$  and the

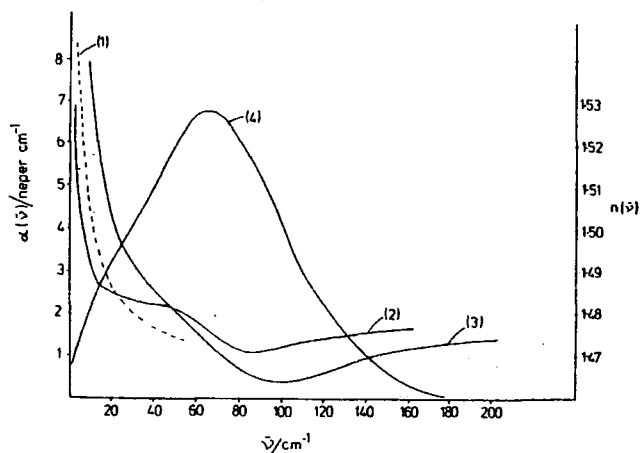


Figure 6. Refractive index and absorption data for a mole fraction for  $\text{CH}_3\text{CN}$  in  $\text{CCl}_4$  of 0.02 (318 K). Curve (1), experimental data. Curve (2), calculated data using equation (15) with parameters calculated by a best fit to equation (13) (see table 5). Curve (3), calculated data using parameters calculated by a best fit to equation (8). Curve (4), experimental absorption spectrum.

calculated  $\epsilon''(\omega)$  curve peaks at  $\sim 8 \text{ cm}^{-1}$ . Any attempt to fix  $K_u^{(0)}(0)$  and/or  $\epsilon_0 - \epsilon_\infty$  results in totally unreasonable low values of  $\gamma$  (leading to an extremely narrow band profile). The observed value of  $\epsilon_0 - \epsilon_\infty$  is 0.21 (based on  $\epsilon_\infty = n_\infty^2$ ; see table 1) and since  $K_u^{(0)}(0)$  is already normalized to  $I/2kT$  it should be fixed at a value of 1.0. The lack of consistency is thus a measure of the inadequacy of the model based on second-order truncation of the Mori continued fraction.

The next higher order approximant (equation 5) was then used to obtain  $K_u^{(1)}(0)$ ,  $K_u^{(2)}(0)$  and  $\gamma_2$  (table 3) as outlined in the Appendix. Again there is significant deviation between observed and calculated data (curve (5)) and, clearly, convergence has still not been reached. This is reflected by the fact that  $K_u^{(1)}(0) = 21.0 K_u^{(0)}(0)$  for the second approximant and  $K_u^{(1)}(0) = 43.2 K_u^{(0)}(0)$  for the third approximant (tables 2 and 3). If this kind of continued fraction is to be physically meaningful (as opposed to useful) a means of extending it to infinity without introducing more adjustable variables must be found. One way in which this may be achieved is mentioned in § 3.

Table 3. Summary of parameters† obtained using third-order truncation to Mori continued fraction.

Temperature/ K	Mole fraction $\text{CH}_3\text{CN}$	$\gamma$	$K_u^{(1)}(0)$	$K_u^{(2)}(0)$	$\epsilon_0 - \epsilon_\infty$
318	0.018	10.0	43.2	64.1	0.21
318	0.061	10.6	48.7	72.4	0.60

† Units as in table 2.

Meanwhile, we have to make the point that the 0-THz absorption band of dipolar liquids eludes satisfactory analysis by the currently available analytical methods. The statistical mechanics of the autocorrelation function are too complicated even *without* taking into account the electrostatics giving rise to the internal field problem. Attempts to reproduce the band shapes by varying phenomenological parameters for best fit are often unhelpful in that the underlying theoretical differences are obscured. However these empirical methods may be useful as the *only* available yardsticks when comparing data from different sources (see later).

In view of the significant discrepancies shown in figures 4 and 5 it is clear that inter-experimental comparisons will be meaningless if models such as these are used without great care. On the other hand, it is only by studying the high frequency (short time) regime of the orientational spectrum (correlation function) that we are able to discriminate *at all* between the various models. As mentioned previously (and as may be *seen* from figures 4 and 5) all the models considered here give excellent fits to the dielectric loss curve below  $\sim 4 \text{ cm}^{-1}$  (i.e. in the low frequency, long time regime) but the physical meaning attributed to the relaxation times ( $\tau_D = 1/\omega_{\text{max}}$  of the  $\epsilon''(\omega)$  curve) will all be different. Each of the other techniques available for the measurement of  $\tau_{IR}$  has associated with it significant drawbacks in this respect. The N.M.R. spin-spin relaxation technique, for example, gives information only about the area under the appropriate autocorrelation function and not the details of its decay. It is therefore usual to use the rotational diffusion model for calculating N.M.R. correlation times, the results being apparently reasonable only because the details of the ensemble molecular dynamics (embodied in figures 4 and 5) are obscured (and models which give the same overall relaxation times cannot, in any case be distinguished). In principle, infra-red and Raman studies of vibrational-rotational band broadening can be used to obtain information about the short time regime. In practice, however the bands have to be carefully chosen to avoid overlap in the wings with other (including hot band) transitions. Isotope effects and vibration-rotation coupling are also complicating features and it is rarely possible to achieve high enough signal/noise ratios in the high frequency regime. Likewise, since the far wings of the depolarized Rayleigh scattering [29] measures approximately the factor  $\epsilon''(\omega)/\omega$ , the short time details are clearly seen only with careful intensity control.

In view of the fact that most of the  $\tau_{IR}$  data in the literature were obtained using information from the long time regime it is rather surprising that agreement between data from different techniques is difficult to find (tables 2 and 4). However, in comparing data from different techniques it is important to remember the following points (1) data obtained from depolarized Rayleigh scattering [35] or from dielectric relaxation measurements [36] in the *liquid* phase include contributions from cross correlations (i.e. correlation between the motions of neighbouring molecules); (2) that some of the data obtained from Raman and infra-red measurements are erroneous [33], either because the vibrational part of the band was not properly accounted for [43] or because the band profiles used [38, 39, 41] were disturbed by hot bands (this is particularly true [33] of the  $\nu_2$  and  $\nu_4$  bands). In his review of the extensive data for this molecule Griffiths [33] came to the conclusion that the best values for  $\tau_{1R}(\perp)$  and  $\tau_{2R}(\perp)$  were 3.3 and 1.1 ps respectively (at 298 K) which is (conveniently) exactly the

Table 4. Summary of reorientational correlation times† obtained for CH<sub>3</sub>CN.

Liquid phase		Reference		Technique		Temperature/K		τ <sub>b</sub> /ps		Reference	
τ <sub>1R</sub> /ps	Temperature/K	Technique	Reference	τ <sub>2R</sub> /ps	Technique	τ <sub>2R</sub> /ps	Temperature/K	τ <sub>b</sub> /ps	Temperature/K	Technique	Reference
3-2, 3-3	298	IR(ν <sub>4</sub> )	[42, 43]	2.0 ± 0.2	R(ν <sub>2</sub> , ν <sub>3</sub> )	252					[37]
				1.5 ± 0.2	R(ν <sub>2</sub> , ν <sub>3</sub> )	286					[37]
1-1, 1-5	308	IR(ν <sub>2</sub> , ν <sub>4</sub> )	[41]	1.2-1.4	R(ν <sub>1</sub> , ν <sub>2</sub> , ν <sub>4</sub> )	293					[38]
				1-1, 1-4	R(ν <sub>2</sub> ), N.M.R.	294					[39]
				1.5 ± 0.3, 1-2	R(ν <sub>2</sub> ), N.M.R.	296					[35, 40]
				0.9, 1.8	R(ν <sub>1</sub> ), Rayleigh	298					[34, 35]
				1-4	R(ν <sub>1</sub> )	309					[41]
				1.2 ± 0.1	R(ν <sub>2</sub> , ν <sub>3</sub> )	318					[37]
				0.7 ± 0.1	R(ν <sub>2</sub> )	343					[37]
								3-8	303		[36]
								(microwave)			
								3-1	323		[36]
Solutions											
τ <sub>1R</sub> /ps	Solvent†	Temperature/K	Technique	Reference	τ <sub>2R</sub> /ps	Solvent†	Temperature/K	Technique	Reference		
2-3 ± 0-1	CCl <sub>4</sub> (1-8)	318	Far I.R.	[14 (a)]	2.0 ± 0.2	CCl <sub>4</sub> (3)	288	R(ν <sub>2</sub> )	[37]		
2-2 ± 0-1	CCl <sub>4</sub> (6-0)	318	Far I.R.	[14 (a)]	2.1 ± 0.2	CCl <sub>4</sub> (6)	288	R(ν <sub>2</sub> )	[37]		
					1.9 ± 0.2	CCl <sub>4</sub> (16)	288	R(ν <sub>2</sub> )	[37]		
2-8 ± 0-1	CCl <sub>4</sub> (1-8)	288	Far I.R.	[14 (a)]	2.6 ± 0.2	CCl <sub>4</sub> (37)	288	R(ν <sub>2</sub> )	[37]		
2-6 ± 0-1	CCl <sub>4</sub> (6-0)	288	Far I.R.	[14 (a)]							
7-6 ± 0-5	CCl <sub>4</sub> (25)	297	Microwave	[48]							
6-3 ± 0-5	CCl <sub>4</sub> (25)	313	Microwave	[48]							
4-5 ± 0-5	CCl <sub>4</sub> (25)	333	Microwave	[48]							
6-7 ± 0-5	Bz (25)	297	Microwave	[48]							
4-5 ± 0-5	Bz (25)	313	Microwave	[48]							
3-1 ± 0-5	Bz (25)	333	Microwave	[48]							

† Values are those obtained for rotation of the principal axis (i.e. τ<sub>1</sub>).

‡ Concentration in mole per cent given in brackets.

ratio expected theoretically [44] for rotational diffusion. There is evidence, however, that both of these values may be incorrect. The  $\tau_{1R}$  value is obtained from microwave data on the liquid and includes the effects of cross correlations. Data on  $\tau_{2R}$  obtained from more recent measurements on  $\nu_2$  and  $\nu_3$  of acetonitrile suggest a value nearer 1.4 ps at 298 K (see table 4). Thus our  $\tau_{1R}/\tau_{2R}$  ratios which, for dilute solutions, lie in the 1.2–2.0 region (assuming that the temperature dependence of  $\tau_{2R}$  is the same in  $\text{CCl}_4$  as it is in the pure liquid) are probably not at variance with previous data. In any case, our far-infrared data demonstrate conclusively that such a model is hopelessly inadequate to explain the details of molecular motion in the short time regime (a regime which cannot be studied properly using any of the other techniques currently employed). One possible way of making further progress in comparing the dynamics in the two time regimes would be to undertake an extensive molecular dynamics simulation of  $\text{CH}_3\text{CN}$  using a suitable empirical intermolecular potential. At the same time we should attempt to proceed analytically by approximating more realistically, using advanced statistical techniques, the Liouville equation for  $\mathbf{u}$  or  $\omega$ .

Table 5. Far-infrared peak frequencies for  $\text{CH}_3\text{CN}$  solutions.

Solvent	Temperature/K	Mole fraction $\text{CH}_3\text{CN}$	$\nu_{\text{max}}/\text{cm}^{-1}$	Reference
$\text{CCl}_4$	343	0.018	$61 \pm 2$	This work
$\text{CCl}_4$	318	0.018	$66 \pm 2$	This work
$\text{CCl}_4$	252	0.018	$76 \pm 2$	This work
$\text{CCl}_4$	338	0.061	$65 \pm 2$	This work
$\text{CCl}_4$	318	0.061	$70 \pm 2$	This work
$\text{CCl}_4$	252	0.061	$82 \pm 3$	This work
Cyclohexane	296	dilute soln.	$\sim 50$	[45]
Carbon disulphide	314	2 per cent volume	$\sim 60$	[46]
<i>n</i> -heptane	314	2 per cent volume	$\sim 38$	[46]
$\text{CH}_3\text{CN}$	314	1.0	$75 \pm 5, 90 \pm 2$	[46, 49]
Cholesteryl oleyl carbonate	298	0.04	$83 \pm 2$	This work

Finally, as mentioned previously, the far-infrared data give, in principle, information about the intermolecular mean square torque. The simplest way to obtain a feeling for such torques is to notice that equation (9) gives an increased torque parameter  $K_2^{(1)}(0)$  as the maximum frequency of the  $\alpha(\omega)$  curve increases. Table 5 summarizes the  $\omega_{\text{max}}$  data which have been obtained so far including data (see figure 1 (b)) in cholesteryl oleyl carbonate (which when pure, forms a cholesteric mesophase). It is rather obvious that the short time torsional oscillation of the  $\text{CH}_3\text{CN}$  even in isotropic phases is significantly environment sensitive. The mean square torques appear to increase on decreasing the temperature (large shifts occur, for example, when  $\text{CH}_2\text{Cl}_2$  is frozen to the glassy state [47]) and also to increase when the number of acetonitrile molecules in the mixture increases. This provides direct evidence that molecular interactions

(presumably dipolar in origin) have a significant influence on the molecular distribution even in dilute solutions. Furthermore, it appears likely that such torques are smaller in hydrocarbon solvents (such as *n*-heptane) and much larger in mesomeric phases.

Thanks are due to Beckman-R.I.I.C. Ltd. and S.R.C. for equipment grants, for a C.A.S.E. studentship (to P.L.J.) and a research Fellowship (to G.J.E.). This work was also supported by a research grant from N.A.T.O. M.W.E. thanks the Ramsay Memorial Trust for the 1976-78 Fellowship.

## APPENDIX

For third-order truncation of the Mori continued fraction,

$$\epsilon''(\omega) = (\epsilon_0 - \epsilon_\infty)\omega K_u^{(0)}(0)K_u^{(1)}(0)K_u^{(2)}(0)[\pi K_u^{(2)}(0)/2]^{1/2}/D, \quad (\text{A } 1)$$

where

$$D = \pi/2 K_u^{(2)}(0)\omega^2[\omega^2 - (K_u^{(0)}(0) + K_u^{(1)}(0))]^2 + [\omega^4 - \omega^2(K_u^{(0)}(0) + K_u^{(1)}(0) + K_u^{(2)}(0)) + K_u^{(0)}(0)K_u^{(2)}(0)]^2$$

and

$$\alpha(\omega) = \frac{\omega\epsilon''(\omega)}{n(\omega)c}. \quad (\text{A } 2)$$

In the region where  $\alpha(\omega)$  reaches a maximum, the refractive index  $n(\omega)$  is constant to within a few per cent (figures 2 and 3) so that differentiation of (A 1) and (A 2) according to equations (11) and (12) yields the expressions

$$K_u^{(2)}(0) = \frac{\pi/2\omega_0^2[(K_u^{(0)}(0) + K_u^{(1)}(0))^2 - 2\omega_0^2 K_u^{(0)}(0)(K_u^{(0)}(0) + K_u^{(1)}(0))]}{K_u^{(0)}(0)(K_u^{(0)}(0) + 2\omega_0^2)} \quad (\text{A } 3)$$

and

$$[K_u^{(2)}(0)]^2[(K_u^{(0)}(0))^2 - \omega_1^4] + \omega_1^4 K_u^{(2)}(0)[\omega_1^2(4 - \pi) + K_u^{(0)}(0)(\pi - 4) + K_u^{(1)}(0)(\pi - 2)] + [\omega_1^4 - \omega_1^2(K_u^{(0)}(0) + K_u^{(1)}(0))][\omega_1^2(K_u^{(0)}(0) + K_u^{(1)}(0)) - 3\omega_1^4] = 0. \quad (\text{A } 4)$$

By solving these equations simultaneously a quartic is developed in  $K_u^{(1)}(0)$  which may be solved numerically. The quartic is

$$A[K_u^{(1)}(0)]^4 + B[K_u^{(1)}(0)]^3 + C[K_u^{(1)}(0)]^2 + DK_u^{(1)}(0) + E = 0, \quad (\text{A } 5)$$

where

$$A = a^2[(K_u^{(0)}(0))^2 - \omega_1^4],$$

$$B = a[2b[K_u^{(0)}(0)]^2 + \omega_1^4[\pi - 2(1 + b)]],$$

$$C = [K_u^{(0)}(0)]^2(b^2 + 2ac) + \omega_1^4[a(4 - \pi)(\omega_1^2 - K_u^{(0)}(0)) + b(\pi - 2) - b(b^2 + 2ac + 1)],$$

$$D = 2bc[K_u^{(0)}(0)]^2 + \omega_1^4\{b(4-\pi)(\omega_1^2 - K_u^{(0)}(0)) + c[\pi - 2(1+b)] + 4\omega_1^3 - 2K_u^{(0)}(0)\},$$

$$E = c^2[K_u^{(0)}(0)]^2 + \omega_1^4\{(4-\pi)(\omega_1^2 - K_u^{(0)}(0))c - c^2 - (3\omega_1^4 - 4\omega_1^3 K_u^{(0)}(0) + [K_u^{(0)}(0)]^2)\}$$

and

$$a = \frac{\omega_0^2 \pi}{2K_u^{(0)}(0)(K_u^{(0)}(0) + 2\omega_0^2)},$$

$$b = \frac{(\pi - 2)\omega_0^2}{K_u^{(0)}(0) + 2\omega_0^2},$$

$$c = \frac{K_u^{(0)}(0)\omega_0^2}{K_u^{(0)}(0) + 2\omega_0^2} \left[ \frac{\pi}{2} - 2 \right].$$

The quartic equation (A 5) is solved numerically and the appropriate real root of the equation then gives  $K_u^{(1)}(0)$ , and hence  $K_u^{(2)}(0)$ .

## REFERENCES

- [1] WILLIAMS, G., 1978, *Chem. Soc. Rev.*, **7**, 89.
- [2] STERLE, W. A., 1976, *Adv. chem. Phys.*, **34**, 1.
- [3] EVANS, M. W., 1977, *Dielectric and Related Molecular Processes*, Vol. 3 (Senior reporter: M. Davies) (The Chemical Society), pp. 1-44.
- [4] (a) EVANS, M. W., 1977, *Adv. Molec. Rel. Int. Processes*, **10**, 203. (b) ROWLINSON, J. S., and EVANS, M. W., 1975, *A. Rep. chem. Soc. A*, p. 5.
- [5] BRIER, P. N., and PERRY, A., 1978, *Adv. Molec. Rel. Int. Processes*, **13**, 1.
- [6] DAVIES, M., 1970, *A. Rep. A*, **67**, 65.
- [7] (a) GORDON, R. G., 1966, *J. chem. Phys.*, **44**, 1830. (b) GORDON, R. G., 1968, *Adv. magn. Reson.*, **3**, 1. (c) MCCLUNG, R. E. D., 1972, *J. chem. Phys.*, **57**, 5478.
- [8] (a) EVANS, G. J., EVANS, M. W., and REID, C. J., 1978, *J. chem. Soc., Faraday II*, **74**, 343. (b) REID, C. J., YADAV, R. A., EVANS, G. J., and EVANS, M. W., 1978, *J. chem. Soc., Faraday II*, **74**, 2143.
- [9] MORI, H., 1965, *Prog. theor. Phys.*, **33**, 423.
- [10] (a) EVANS, G. J., and EVANS, M., 1976, *J. chem. Soc., Faraday II*, **72**, 1169. (b) EVANS, G. J., and EVANS, M., 1976, *J. chem. Soc., Faraday Trans.*, **72**, 1901. (c) DAVIES, G. J., EVANS, G. J., and EVANS, M., 1977, *J. chem. Soc., Faraday II*, **73**, 1071. (d) EVANS, G. J., and EVANS, M., 1977, *Chem. Phys. Lett.*, **45**, 454.
- [11] BROU, C., 1975, *Dielectric and Related Molecular Processes*, Vol. 2 (Senior reporter: M. Davies) (The Chemical Society), pp. 1-47.
- [12] (a) LINDENBERG, K., and CUKIER, R. I., 1975, *J. chem. Phys.*, **62**, 3271. (b) FRENKEL, D., WEGDAM, G. H., and VAN DER ELSKEN, J., 1972, *J. chem. Phys.*, **57**, 2691.
- [13] STRETT, W. B., and TILDESLEY, D. J., 1978, *J. chem. Phys.*, **68**, 1275.
- [14] (a) YARWOOD, J., JAMES, P. L., DÖGE, G., and ARNDT, R., 1979, *Faraday Discussion* No. 66 (The Chemical Society), paper No. 19. (b) EVANS, M. W., and EVANS, G. J. (unpublished data). (c) YARWOOD, J., JAMES, P. L., BIRCH, J. R., and AFSAR, M. N. (in preparation).
- [15] (a) BERNE, B. J., and HARP, G. D., 1971, *Physical Chemistry—An Advanced Treatise*, Vol. VIII B, edited by H. Eyring, D. Henderson and W. Jost (Academic Press), pp. 540-713. (b) BERNE, B. J., and HARP, G. D., 1970, *Adv. chem. Phys.*, **17**, 63.
- [16] DAVIES, A. R., and EVANS, M. W., 1978, *Molec. Phys.*, **35**, 857.
- [17] (a) CALDERWOOD, J. H., and COFFEY, W. T., 1977, *Proc. R. Soc. A*, **356**, 269. (b) COFFEY, W. T., EVANS, G. J., EVANS, M. W., and WEGDAM, G. H., 1978, *J. chem. Soc., Faraday II*, **74**, 310. (c) COFFEY, W. T., and EVANS, M. W., 1978, *Molec. Phys.*, **35**, 975. (d) EVANS, G. J., and EVANS, M. W., 1978, *J. Chim. phys.*, **75**, 21.
- [18] MORITA, A., 1978, *J. Phys. D*, **11**, L9, L1.

- [19] BUDÓ, A., FISCHER, E., and MIYAMOTO, S., 1939, *Phys. Z.*, **40**, 337.
- [20] (a) BERNE, B. J., and MONTGOMERY, J. A., 1976, *Molec. Phys.*, **32**, 363. (b) CHANDLER, D., 1974, *J. chem. Phys.*, **60**, 3508.
- [21] BLIOT, F., ABBAR, C., and CONSTANT, E., 1972, *Molec. Phys.*, **24**, 241.
- [22] DRAWID, M., and HALLEY, J. W., 1977, *J. Phys. Chem. Solids*, **38**, 1269.
- [23] (a) BLIOT, F., and CONSTANT, E., 1973, *Chem. Phys. Lett.*, **18**, 253; 1974, *Ibid.*, **29**, 618. (b) EVANS, G. J., 1977, *J. chem. Soc., Faraday II*, **73**, 729. (c) EVANS, M. W., 1976, *Spectrochim. Acta A*, **32**, 1259. (d) DAVIES, G. J., and EVANS, M. W., 1976, *J. chem. Soc., Faraday II*, **72**, 1206. (e) EVANS, G. J., and EVANS, M. W., 1977, *Chem. Phys. Lett.*, **45**, 454.
- [24] DESPLANQUES, P., 1974, Thèse d'Etat, Univ. Lille.
- [25] DAMLE, P. S., SJÖLANDER, A., and SINGWI, K. S., 1968, *Phys. Rev.*, **165**, 277.
- [26] HERMANS, F., KESTERMONT, E., VAN LOON, R., and FINSY, R., 3rd International Conference on Submillimetre Waves and their Applications, Abstracts, p. 1026.
- [27] (a) COFFEY, W. T., 1979, *Molec. Phys.*, **37**, 473. (b) DAVIES, A. R. (personal communication).
- [28] GERSCHEL, A., DARMON, I., and BROT, C., 1972, *Molec. Phys.*, **23**, 317.
- [29] DILL, J. F., LITOVITZ, T. A., and BUCARO, J. A., 1975, *J. chem. Phys.*, **62**, 3839.
- [30] CHAMBERLAIN, J., 1968, *Chem. Phys. Lett.*, **7**, 464.
- [31] MARTIN, D. H., and PUPLETT, E., 1969, *Infrared Physics*, **10**, 105.
- [32] BAROJAS, J., LEVESQUE, D., and QUENTREC, B., 1973, *Phys. Rev. A*, **7**, 1092.
- [33] GRIFFITHS, J. E., 1977, *Vibrational Spectra and Structure*, Vol. 6, edited by J. R. Durig (Elsevier).
- [34] GRIFFITHS, J. E., 1973, *J. chem. Phys.*, **75**, 751.
- [35] BARTOLI, F. J., and LITOVITZ, T. A., 1972, *J. chem. Phys.*, **56**, 413.
- [36] MANSINGH, K., and A., 1964, *J. chem. Phys.*, **41**, 827.
- [37] YARWOOD, J., DÖGE, G., and ARNDT, R., 1977, *Chem. Phys.*, **25**, 387.
- [38] AMAN DA COSTA, A. M., NORMAN, M. A., and CLARKE, J. H. R., 1975, *Molec. Phys.*, **29**, 191.
- [39] WHITTENBURG, S. L., and WANG, C. H., 1977, *J. chem. Phys.*, **66**, 4255. LYERLA, J. R., GRANT, D. M., and WANG, C. H., 1971, *J. chem. Phys.*, **55**, 4676.
- [40] BULL, T. E., 1975, *J. chem. Phys.*, **62**, 222.
- [41] JONES, D. R., ANDERSON, H. C., and PECORA, R., 1975, *Chem. Phys.*, **9**, 339.
- [42] BREUILLARD-ALLIOT, C., and SOUSSEN-JACOB, J., 1974, *Molec. Phys.*, **28**, 905.
- [43] ROTHSCHILD, W. G., 1972, *J. chem. Phys.*, **57**, 991 and references therein.
- [44] McCLUNG, R. E. D., 1969, *J. chem. Phys.*, **51**, 3842; 1971, *Ibid.*, **54**, 3248; 1971, *Ibid.*, **55**, 359; 1972, *Ibid.*, **57**, 5478.
- [45] PARDOE, G. W. F., 1969, Ph.D. Thesis, Univ. Wales.
- [46] VAN AALST, R. M., VAN DER ELSKEN, J., FRENKEL, D., and WEGDAM, G. H., 1972, *Faraday Symposium Chem. Soc.*, No. 6, p. 94. KROON, S. G., and VAN DER ELSKEN, J., 1967, *Chem. Phys. Lett.*, **1**, 285.
- [47] EVANS, M. W. (unpublished data).
- [48] ELORANTA, J., and KADABA, P. K., 1971, *Mater. Sci. Engng*, **8**, 203.
- [49] BULKIN, B. J., 1969, *Helv. chim. Acta*, **52**, 1348.

**APPENDIX 4**

**THE FAR-INFRARED DISPERSION OF  
ACETONITRILE IN DILUTE SOLUTION IN  
CARBON TETRACHLORIDE**

**J.R.BIRCH, M.N.AFSAR, J. YARWOOD, P.L.JAMES**

**INFRARED PHYSICS, 1981, VOL.21**

## THE FAR-INFRARED DISPERSION OF ACETONITRILE IN DILUTE SOLUTION IN CARBON TETRACHLORIDE\*

J. R. BIRCH, M. N. AFSAR†

Division of Electrical Science, National Physical Laboratory, Teddington,  
Middlesex TW11 0LW, U.K.

J. YARWOOD and P. L. JAMES

Department of Chemistry, University of Durham, Durham DH1 3LE, U.K.

(Received 28 May 1980)

**Abstract**—The results of refraction and absorption measurements using dispersive Fourier transform techniques are reported for dilute solutions of acetonitrile in carbon tetrachloride in the spectral region 2–200  $\text{cm}^{-1}$ . The results are used to help to interpret the power absorption spectra in this region in terms of a model for dipole rotation in liquids developed by Evans *et al.*<sup>(1,2)</sup>

### INTRODUCTION

Refractive index data in the region 2–200  $\text{cm}^{-1}$  are important in a number of ways when attempting to derive information about the dynamics<sup>(1–5)</sup> of polyatomic molecules from their liquid phase 'pure' rotational spectra. The quantity measured in this region (for example, by far-infrared absorption spectroscopy<sup>(4,5)</sup>) is the power absorption coefficient  $\alpha(\tilde{\nu})$ —proportional to the imaginary part  $k(\tilde{\nu})$  of the complex refractive index  $\hat{n}$

$$\hat{n}(\tilde{\nu}) = n(\tilde{\nu}) + ik(\tilde{\nu}) \quad (1)$$

where

$$\alpha(\tilde{\nu}) = 4\pi\tilde{\nu}k(\tilde{\nu}) \quad (2)$$

and  $\tilde{\nu} = \omega/2\pi c$  is wavenumber, with  $\omega$  angular frequency and  $c$  the speed of light.

In order to get information about the reorientational motion, however, the principal quantity of interest<sup>(1–3)</sup> is the imaginary part of the complex permittivity,  $\hat{\epsilon}$ ,

$$\hat{\epsilon}(\tilde{\nu}) = \epsilon'(\tilde{\nu}) + i\epsilon''(\tilde{\nu}) \quad (3)$$

where  $\epsilon''(\tilde{\nu})$ , the dielectric loss factor, is given by

$$\epsilon''(\tilde{\nu}) = \frac{n(\tilde{\nu})\alpha(\tilde{\nu})}{2\pi\tilde{\nu}} \quad (4)$$

Indeed, it is the frequency of maximum dielectric loss which measures the rotational correlation time,  $\tau_{1R}$ , given by

$$\tau_{1R} = \int \phi_{1R}(t) dt \quad (5)$$

where

$$\phi_{1R}(t) = C \int_{\text{band}} \frac{\epsilon''(\tilde{\nu})}{2\pi c \tilde{\nu} [1 - \exp(-h\tilde{\nu}c/kT)]} \exp(2\pi i c \tilde{\nu} t) d\tilde{\nu} \quad (6)$$

In order to make a direct measurement of the rotational relaxation time one therefore needs to determine both  $n(\tilde{\nu})$  and  $\alpha(\tilde{\nu})$  so that  $\epsilon''(\tilde{\nu})$  can be obtained from equation (4).

\*Part VI of a series on 'Molecular Motions and Vibrational Relaxation of Acetonitrile'.

† Present address: National Magnet Laboratory, Massachusetts Institute of Technology, Cambridge, MA 02139, U.S.A.

Furthermore, in order to calculate  $\tau_{1R}$  from  $\phi_{1R}$  one needs to be able to make an 'internal field' correction which is included in the 'constant'  $C$  in equation (6). This factor might typically be,<sup>(2a,d)</sup>

$$C = \frac{4\pi N \mu^2}{3kTcV} \left[ \frac{9n_\infty}{(n_\infty^2 + 2)^2} \right] = \frac{(\epsilon_0 - \epsilon_\infty)}{n(\tilde{\nu})c} \left[ \frac{9n_\infty}{(n_\infty^2 + 2)^2} \right] \quad (7)$$

and so depends on a measurement of  $n(\tilde{\nu})$  over the region of interest and on the value ( $n_\infty$ ) of the refractive index at frequencies high compared with that of  $\epsilon''_{\max}$  (say in the 100–150  $\text{cm}^{-1}$  region). If the  $\tau_{1R}$  values obtained from the far-infrared spectrum are to be compared<sup>(4)</sup> with those obtained from vibration/rotational spectroscopy then it is necessary to make measurements of the (polar) molecules diluted in a non-polar solvent in order to eliminate,<sup>(4,5)</sup> as far as possible, contributions to the correlation function  $\phi_{1R}(t)$  from the 'distinct' terms caused by interaction induced intermolecular correlations

$$\phi_{1R}(t) = \underbrace{\langle P_1[\cos \theta_{AA}(t)] \rangle}_{\text{'self' term}} + \underbrace{\langle \sum_{A \neq B} P_1[\cos \theta_{AB}(t)] \rangle}_{\text{'distinct' term}} \quad (8)$$

where  $P_1$  is the first order Legendre polynomial and where  $A$  and  $B$  refer to *different* molecules.  $\theta$  is the angle between the molecular dipole at times  $t = 0$  and  $t = t$ .

Measurements of the refractive indices of liquids in this region are relatively scarce (as a recent bibliography<sup>(6)</sup> demonstrates) and measurements in dilute solution are virtually non-existent.<sup>(7)</sup> We have undertaken these measurements to demonstrate that one *need* not make assumptions<sup>(1–3)</sup> about the variations of  $n(\tilde{\nu})$  in making rotational dynamics measurements on polar molecules.

#### EXPERIMENTAL

The refraction and absorption spectra of two dilute solutions of acetonitrile in carbon tetrachloride (0.018 and 0.061 mole fractions) were determined at 288 and 318 K in the spectral range between 2 and 50  $\text{cm}^{-1}$  and between 5 and 180  $\text{cm}^{-1}$  using the techniques of dispersive Fourier transform spectrometry<sup>(8)</sup> in which the amplitude attenuation and phase shift caused by a specimen are measured by placing it in one arm of a two beam interferometer. The measurements were made in transmission with the liquid specimen contained in a variable path length, variable temperature cell<sup>(9,10)</sup> which terminated the fixed mirror arm of a two beam interferometer of modular design.<sup>(11)</sup> The active elements of the cell consisted of a 2.5 mm thick plane parallel silicon window ( $n$ -type, 0.355  $\Omega\text{m}$ ) with a gold plated stainless steel plane mirror behind it and aligned to give a plane parallel space between them. The distance between the window and the mirror could be varied between 10  $\mu\text{m}$  and 5 mm, allowing the cell to be used to study liquids ranging from the near opaque to the near transparent by transmission methods. The volume between the window and the mirror was completely filled by the liquid specimen, thereby avoiding the possibility of systematic errors due to the presence of any liquid vapour in the optical path.<sup>(12)</sup> The measurements were made using two detectors, a liquid helium cooled indium antimonide hot electron bolometer for the region below 30  $\text{cm}^{-1}$ , and a quartz-windowed Golay cell for the higher wavenumbers.

The optical constants of the two solutions were calculated from the measured complex insertion loss,  $\hat{L}(\tilde{\nu})$ , of each specimen. This is the ratio

$$\hat{L}(\tilde{\nu}) = \hat{S}_L(\tilde{\nu})/\hat{S}_O(\tilde{\nu}) \quad (9)$$

of the complex spectra,  $\hat{S}_L(\tilde{\nu})$  and  $\hat{S}_O(\tilde{\nu})$ , obtained from the Fourier transformation of the interferograms recorded with (subscript  $L$ ) and without (subscript  $O$ ) the liquid present in the cell. The full interferogram detected from this interferometer is the superposition of many individual interference signatures, each corresponding to one of the many rays multiply reflected between the three interfaces of the cell (interferometer–window, window–cell, cell–mirror) and the derivation of optical constants from such interferograms

can be difficult due to the necessary use of procedures which are sensitive to experimental error.<sup>(13)</sup> However, the pattern of these interference signatures is very dependent on the specimen thickness and in the present measurements this was such that only the signature due to the ray making a direct pass through the cell fell in the recorded range of path difference values used in the transformations. Under this condition the optical constants can be calculated from the measured insertion loss by an iterative solution of the equation

$$\hat{L}(\tilde{\nu}) = \frac{(1 - \hat{r}_{WL}^2)}{(1 - \hat{r}_{WO}^2)} \cdot \exp[-\alpha(\tilde{\nu})d] \cdot \exp[i4\pi\tilde{\nu}(n(\tilde{\nu}) - 1)d] \quad (10)$$

where  $\hat{r}_{WL}$  is the complex reflection coefficient of the window-liquid interface and  $\hat{r}_{WO}$  that of the window-vacuum interface, provided that the complex refractive index of the window material and  $d$ , the liquid thickness, are known. The thicknesses of the liquid specimens were determined from the path difference positions at which certain interference signatures were observed in the empty cell measurement,<sup>(9,14)</sup> while the complex refractive index of the silicon window was directly determined from measurements taken with it *in situ* in the cell.<sup>(15)</sup>

#### RESULTS AND DISCUSSION

The refractive index (dispersion) spectra are shown in Figs 1 and 2 at two different temperatures and concentrations. In the 2-50  $\text{cm}^{-1}$  region these curves show the expected decrease corresponding to the loss of orientational polarisation.<sup>(16)</sup> The refractive index is also expected<sup>(17)</sup> to show a shallow minimum in the region of  $\alpha_{\text{max}}$  corresponding to the maximum power absorption coefficient of the relaxation process involved and Fig. 3 demonstrates the presence of this minimum.

The r.i. data have been used to help interpret the far-infrared absorption spectra in terms of a model of molecular reorientation used by Evans and co-workers.<sup>(1,2)</sup> The model has been developed by solving the generalised Langevin equation<sup>(18)</sup> for molecular rotation of a dynamical array of interacting molecules. This so-called Mori equation of motion<sup>(19)</sup> gives a solution in terms of a set of memory functions  $K_{\mu}^{(n)}(t)$  in terms of which the correlation function  $\phi_{\mu}(t)$  can be expanded. Laplace transformation gives a continued fraction<sup>(1,2,4,5)</sup> expression for the spectral density

$$\phi_{\mu}(-i\omega) = \frac{\phi_{\mu}(0)}{i\omega + K_{\mu}^{(0)}(\omega)} = \frac{\phi_{\mu}(0)}{i\omega + \{K_{\mu}^{(0)}(0)/[i\omega + K_{\mu}^{(1)}(\omega)]\}} = \dots$$

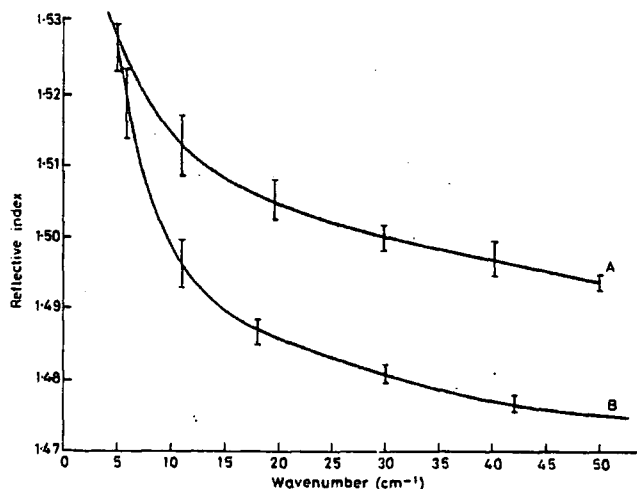


Fig. 1. The measured refractive index spectrum for a 0.018 m/l solution of acetonitrile in carbon tetrachloride between 5 and 50  $\text{cm}^{-1}$ . (A) 288 K (B) 318 K.

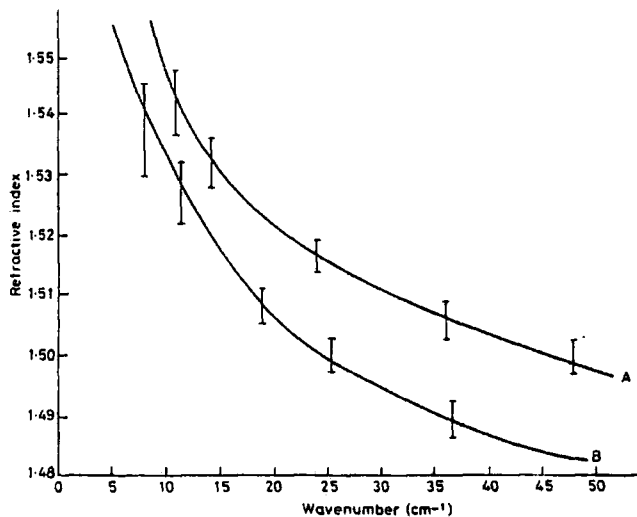


Fig. 2. The measured refractive index spectrum for a 0.061 M solution of acetonitrile in carbon tetrachloride between 5 and 50  $\text{cm}^{-1}$ . (A) 288 K (B) 318 K.

which may be truncated at any convenient point. With truncation at 2nd order, Evans *et al.*<sup>(1,2,4)</sup> have used an exponential memory function with

$$K_u^{(1)}(t) = K_u^{(1)}(0) \exp(-\gamma t) \quad (11)$$

and the resulting absorption coefficient is given by,<sup>(1,2,4,5)</sup>

$$\alpha(\omega) = \frac{A\omega^2 K_u^{(0)}(0) K_u^{(1)}(0) \gamma}{\gamma^2 [K_u^{(0)}(0) - \omega^2]^2 + \omega^2 [\omega^2 - [K_u^{(0)}(0) + K_u^{(1)}(0)]]^2} \quad (12)$$

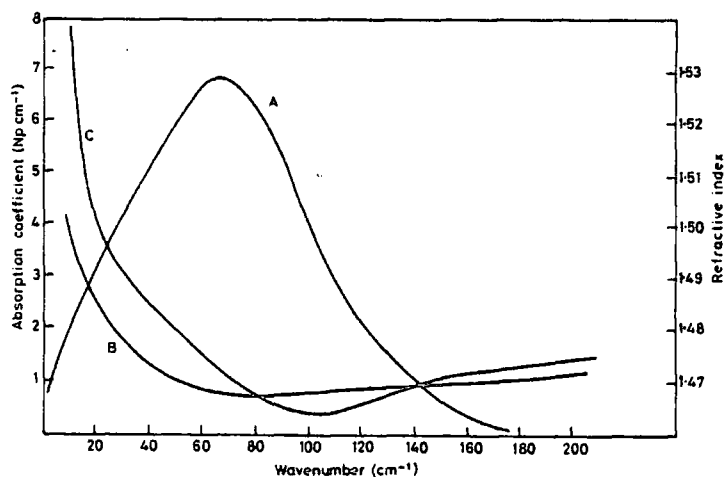


Fig. 3. The measured power absorption spectrum (A) and refractive index spectrum (B) for the 0.018 M solution of acetonitrile in carbon tetrachloride at 318 K. Curve C shows the recalculated refraction spectrum derived from the parameters obtained by the best fit of the absorption spectrum to equation (12).

Table 1. Summary of model parameters\* and rotational correlation times

Temp/K	Mole fraction CH <sub>3</sub> CN	$\nu_1$ (for $\alpha_{\max}$ )	$\gamma$	$K_u^{(1)}(0)$	$\tau_{1R}/\text{psec}^\dagger$	$\tau_{1R}(\text{obs})/\text{psec}$	$\tau_0^\ddagger(\text{microwave})$
318	0.018	$66 \pm 2$	3.0	21.0	2.3	2.1	—
288	0.018	$72 \pm 2$	2.7	24.1	3.0	—	$4.2 \pm 0.5$
318	0.061	$70 \pm 2$	7.9	59.2	2.6	> 2.6	—
288	0.061	$73 \pm 2$	7.4	58.6	2.8	—	$4.6 \pm 0.5$

\* Given in terms of  $x^{1/2}\gamma$  and  $xK_u^{(1)}(0)$  where  $x = I_B/2kT$ .

† Values obtained by fitting to equation (12) with variable  $\epsilon_0 - \epsilon_\infty = 0.29$ .

‡ Ref. (21).

where

$$A = \frac{\epsilon_0 - \epsilon_\infty}{n(\omega)c} \quad (13)$$

The measured absorption spectrum between 2 and 250  $\text{cm}^{-1}$  has been fitted (using non-linear least squares criteria) to equation (12) with  $K_u^{(0)}(0)$  fixed at the value of the rotational 2nd moment ( $2kT/I_B$  where  $I_B$  is the moment of inertia about an axis perpendicular to the symmetry axis). This leaves two variable parameters  $K_u^{(1)}(0)$  and  $\gamma$  related (respectively) to the intermolecular mean square torque and its correlation time. The values of these two parameters obtained by fitting to equation (12) are given in Table 1 along with the values of  $\tau_{1R}$  obtained from the frequency of the maximum in the loss spectrum (see Fig. 4) calculated from the measured refraction and absorption spectra via equation (4). Since  $K_u^{(1)}(0)$  is related to the correlation time<sup>(20)</sup> by

$$K_u^{(1)}(0) = \frac{\pi}{2} \left[ \frac{2kT\tau_{1R}}{I_B} \right]^2 \quad (14)$$

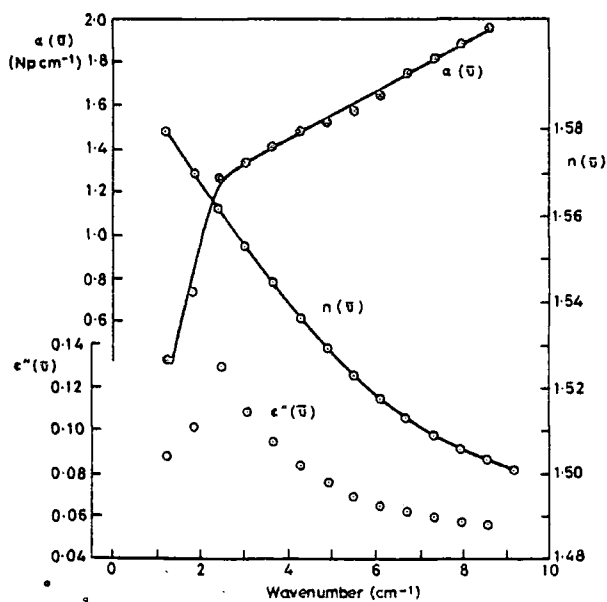


Fig. 4. The measured absorption,  $\alpha(\bar{\nu})$ , and refraction,  $n(\bar{\nu})$ , spectra of the 0.018 m solution of acetonitrile in carbon tetrachloride at 318 K and millimetre wavelengths. The imaginary part of the complex relative permittivity,  $\epsilon''(\bar{\nu})$ , calculated from these spectra is also shown. The maximum in this indicates a value of 2.1 psec for the rotational correlation time.

one is able to compare 'fitted' and directly measured  $\tau_{1R}$  values provided that the refractive index is known. Since, furthermore, the refractive index is related to the quantities of equations (3) by

$$n(\tilde{\nu}) = \left\{ \frac{[\epsilon''(\tilde{\nu})^2 + \epsilon'(\tilde{\nu})^2]^{1/2} + \epsilon'(\tilde{\nu})}{2} \right\}^{1/2} \quad (15)$$

[\(\epsilon''(\tilde{\nu})\) and \(\epsilon'(\tilde{\nu})\) being written<sup>(4)</sup> in terms of the  $K_{ij}^{(1)}(0)$  and  $\gamma$  parameters] one can recalculate the refractive index implied by fitting to equation (12). In Fig. 3 we also show this recalculated  $n(\tilde{\nu})$  which compares (qualitatively) reasonably well with the observed data. The measured refractive index thus helps to assess the validity of the assumed model in a definitive fashion. The model is by no means perfect but it does represent the short time part of the molecular reorientational process and it gives a value of  $\tau_{1R}$  through equation (14) which is in reasonable agreement with that obtained directly from the measured  $\epsilon''(\tilde{\nu})$  distribution.

#### SUMMARY

The importance of refractive index determinations described here is threefold.

- (i) one is able to fit the experimental  $\alpha(\tilde{\nu})$  data for a model for molecular reorientation which includes the frequency dependent refractive index [equation (12)]. Otherwise the factor  $A$  of this equation must be treated as a constant.
- (ii) the  $n(\tilde{\nu})$  data enable one to calculate  $\epsilon''(\tilde{\nu})$  directly [by equation (4)] and directly measure the relaxation time  $\tau_{1R}$ . These values have been found to agree well with values obtained directly by microwave methods<sup>(2,11)</sup> (Table 1).
- (iii) by recalculating the refractive index [equation (15)] using parameters fitted to the experimental  $\alpha(\tilde{\nu})$  data one is able to make an additional definitive test of the assumed model.

It is clear that dispersive Fourier transform spectroscopy (DFTS) is to be preferred in this region since it results in the determination of both the real and imaginary parts of  $\hat{n}$ .

*Acknowledgements*—One of us (P.L.J.) is grateful for the opportunity to use the special refractive index cell and for hospitality while working at the N.P.L. Thanks are also due to Beckman-R.I.I.C. Ltd and the S.R.C. for support via the CASE studentship scheme.

#### REFERENCES

1. (a) EVANS M. W., *Dielectric and Related Molecular Processes* (edited by DAVIES M. M.), Vol. 3. The Chemical Society (1977). (b) EVANS M. W., *Adv. Molec. Rel. Int. Processes* 10, 203 (1977).
2. (a) EVANS G. J. & M. EVANS, *J. chem. Soc. Faraday Trans. II* 72, 1169 (1976). (b) DAVIES G. J., G. J. EVANS & M. EVANS, *J. chem. Soc. Faraday Trans. II* 73, 1071 (1977). (c) EVANS G. J., M. W. EVANS & C. J. REID, *J. chem. Soc. Faraday Trans. II* 74, 343 (1978). (d) GERSCHEL A., I. DARMON & C. BROT, *Molec. Phys.* 23, 317 (1972).
3. BROT C., *Dielectric and Related Molecular Processes* (edited by DAVIES M. M.), Vol. 2. The Chemical Society (1975).
4. YARWOOD J., P. L. JAMES, G. DOGE & R. ARNDT, *Discus. Faraday Soc.* 66, 252 (1978).
5. EVANS M. W., G. J. EVANS, J. YARWOOD, P. L. JAMES & R. ARNDT, *Molec. Phys.* 38, 699 (1979, Part 4).
6. BIRCH J. R. & T. J. PARKER, *Infrared Phys.* 19, 201 (1979).
7. DAVIES G. J. & J. CHAMBERLAIN, *J. Phys.* A5, 767 (1972).
8. BIRCH J. R. & T. J. PARKER, *Infrared and Millimeter Waves* (edited by BUTTON K. J.), Vol. 2. Academic Press, New York (1979).
9. HONUJ D. D., W. F. PASSCHIER, M. MANDEL & M. N. AFSAR, *Infrared Phys.* 17, 9 (1977).
10. AFSAR M. N., D. D. HONUJ, W. F. PASSCHIER & J. GOULON, *IEEE Trans. Microwave theor. Techniques MTT-25*, 505 (1977).
11. CHANTRY G. W., H. M. EVANS, J. CHAMBERLAIN & H. A. GEBBIE, *Infrared Phys.* 9, 85 (1969).
12. PASSCHIER W. F., D. D. HONUJ & M. MANDEL, *Infrared Phys.* 16, 389 (1976).
13. PASSCHIER W. F., D. D. HONUJ, M. MANDEL & M. N. AFSAR, *Infrared Phys.* 17, 381 (1977).
14. AFSAR M. N., PH.D. THESIS, UNIVERSITY OF LONDON, (1978).
15. PASSCHIER W. F., D. D. HONUJ, M. MANDEL & M. N. AFSAR, *J. Phys.* D10, 509, 1977.
16. HILL, N. E., W. E. VAUGHAN, A. H. PRICE & M. M. DAVIES, *Dielectric Properties and Molecular Behaviour*. Van Nostrand, London (1969).
17. CHAMBERLAIN J., *Chem. Phys. Lett.* 2, 464 (1968).

18. (a) DAVIES A. R. & M. W. EVANS, *Molec. Phys.* **35**, 857 (1978). (b) QUENTREC B. & P. BEZOT, *Molec. Phys.* **27**, 879 (1974). (c) CALDERWOOD J. H. & W. T. COFFEY, *Proc. R. Soc.* **356A**, 269 (1977). (d) COFFEY W. T. & M. W. EVANS, *Molec. Phys.* **35**, 975 (1978).
19. (a) MORI H., *Prog. theor. Phys.* **33**, 423 (1965). (b) BERNE J. & G. D. HARP, *Adv. chem. Phys.* **17**, 100 (1970).
20. DRAWID M. & J. W. HALLEY, *J. Phys. Chem. Solids* **38**, 1269 (1977).
21. PRICE A. H., K. E. ARNOLD & J. YARWOOD, unpublished data.

**APPENDIX 5**

**A NEW CELL FOR LIQUID PHASE REFRACTIVE  
INDEX DETERMINATIONS IN THE  
SUBMILLIMETRE SPECTRAL REGION**

**J. YARWOOD, C. BARKER, P.L. JAMES, G.P. O'NEILL,  
W.A. SCOTT, R.N. MCKENZIE**

**JOURNAL OF PHYSICS E: SCIENTIFIC INSTRUMENTS, 1981, VOL.14**

# A new cell for liquid phase refractive index determinations in the submillimetre spectral region

J Yarwood†, C Barker†, P L James†, G P O'Neill†, W A Scott‡ and R N McKenzie‡

† Chemistry Department, University of Durham, Durham City, UK

‡ Beckman-RIIC Ltd, Glenrothes, Fife, Scotland, UK

Received 8 May 1980

**Abstract** A simple refractive index cell for use in the spectral range between  $0.2\text{--}20\text{ mm}^{-1}$  is described. The module is designed to be compatible with a Beckman-FS720 interferometer and it is extremely easy to align and use. The cell has the advantage of high energy throughput and low reflection losses from the thin polymer front window. The results obtained for liquid tetrabromoethane and *p*-difluorobenzene agree within 1–2% of the published data, the random error in our measurements being about  $\pm 1\%$ .

## 1 Introduction

There are a number of spectroscopic problems of physical, chemical and biochemical importance for which a knowledge of the dispersion of the refractive index in the far infrared region is important. For example, Chamberlain (1968) has shown that one might be able to establish more easily whether an absorption band is due to a relaxation process or a resonance phenomenon. There are many spectral features which occur in the submillimetre region whose exact origin is still obscure. These include (i) bands associated with ion-ion and ion-molecule interactions in alkyl salt (Yarwood and Barker 1975, 1977, Yarwood *et al* 1978a) or metal salt solutions (Popov *et al* 1971, Popov and Handy 1972, Edgell 1972) in solvating or (supposedly) non-solvating media, (ii) absorption associated with hindered rotational and translational motions of both polar (Evans 1975b, Evans *et al* 1977, 1978a, b, 1979, Yarwood *et al* 1978b, 1979) and non-polar (Evans 1975a, Evans and Davies 1976) liquids, (iii) bands (probably of a composite nature) arising due to the formation of electron donor-acceptor complexes (Yarwood 1973).

In addition, refractive index data are of use in the study of band integrated intensities (Chamberlain 1965, Chamberlain and Gebbie 1966) and are essential (Yarwood *et al* 1979) if one is to make comparison of infrared and microwave data in the interesting overlap region at submillimetre wavelengths (since the relationship between the absorption coefficient  $\alpha(\nu)$  and the dielectric loss  $\epsilon''(\nu)$  depends on the refractive index).

The problem of making accurate refractive index measurements on condensed phases in the  $60\text{--}6000\text{ GHz}$  ( $0.2\text{--}20\text{ mm}^{-1}$ ) region has been solved, in principle, by the use of a dispersive Michelson interferometer (Chamberlain *et al* 1969, Chantry 1971, Chamberlain 1979) with the specimen placed in one of the active arms. This allows the attenuation and phase shift caused by the specimen to be determined and the optical constants can then be calculated (Birch and Parker 1979a, b). The earliest work was performed with the liquid forming a gravity held layer over one of the interferometer mirrors but more recently it has been shown how a closed cell leads to certain advantages. In particular, the gravity held arrangement leads to liquid pathlength variations due to losses by evaporation from volatile liquids. Furthermore, for highly absorbing samples, it is often not possible to make layers thin enough (due to surface tension and viscosity effects). The one closed cell which has been described (Honijk *et al* 1976, 1977) is quite sophisticated in design but is complicated to use in practice and has the disadvantage of a thick front window (silicon) which leads to high energy losses. Our aim was to design and test a cell which is simple to align and use with a commercially available interferometer (a Beckman-RIIC Ltd model FS720) and which produces refractive index data with an overall accuracy of about  $\pm 1\%$  for a wide range of highly absorbing liquids and solutions.

## 2 Cell design and construction

In order to achieve these aims we designed a system with the following features:

- (i) The liquid sample is enclosed by a thin, inert (plastic) window which is easily removable without removing the cell or disturbing the optical alignment. Energy loss through the window is very small.

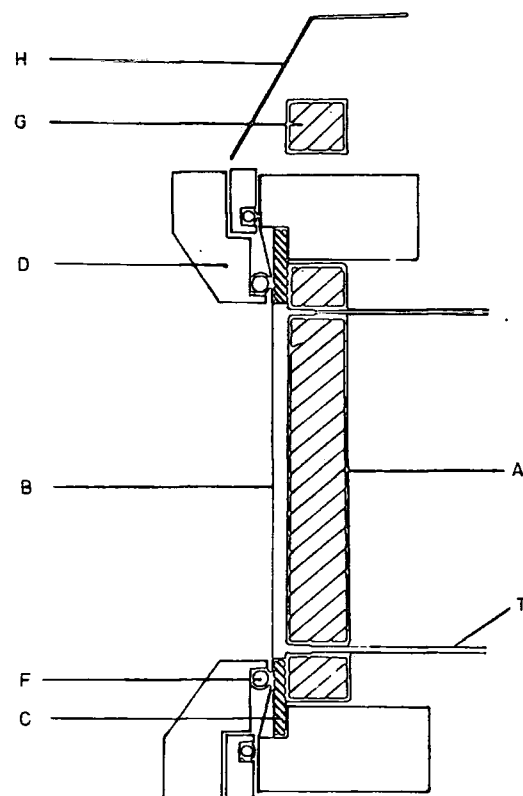


Figure 1 Diagrammatic through section of refractive index cell.

- (ii) There is provision for variable sample thickness down to and below the thickness which may be achieved using a gravity held liquid.
- (iii) Accurate measurement of the dispersive interferogram maximum displacement (on introduction of the sample) is achieved by simply leaving part of the cell mirror uncovered.
- (iv) The cell mirror has as large an area as possible and is capable of sensitive adjustment to ensure that the sample is perpendicular to the interferometer beam.
- (v) The instrument is easily converted between dispersive and non-dispersive modes with only minor optical adjustments.

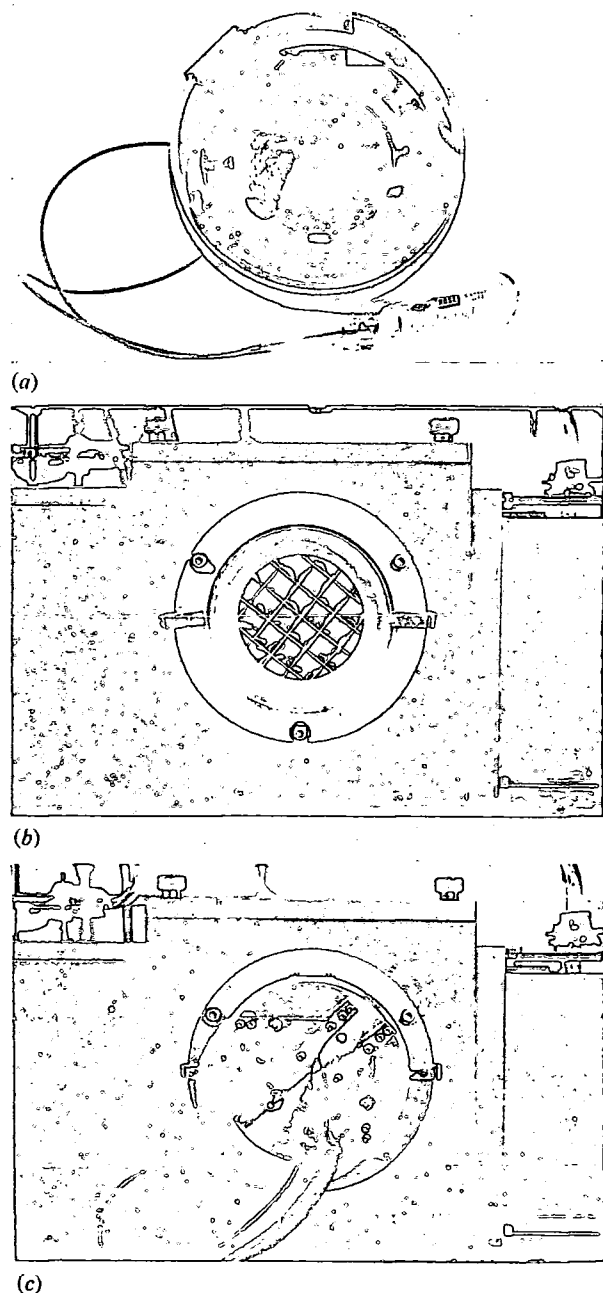


Figure 2 The completed refractive index cell: (a) the whole cell showing the reference mirror and cell window holder; (b) the vacuum membrane and supporting grid; (c) the whole module mounted in the FS720 interferometer.

Figure 1 shows a diagrammatic representation of the cell module which we have designed. The rear wall of the cell consists of a circular, gold covered plane mirror (A) which forms the 'fixed' mirror of the interferometer system. This mirror is covered by a thin plastic (mylar or polyethylene) window (B) which is mounted in a stretched configuration, on a frame (D) with aid of the O ring (F). This frame is then screwed down over the mirror, in such a way that the spacer gasket (C) is sealed between the window and the mirror A. Both the window and spacer thicknesses are variable. After optical alignment using a standard Beckman fixed mirror three-point adjustable mounting, the sample is introduced through the Teflon tubes (T) which are bonded directly into the back of the glass mirror (A). By mounting the mirror (A) slightly off centre on the main mounting plate we have been able to include in the beam, a small rectangular reference mirror (G) which, if not covered by the diaphragm (H), provides a small reference 'marker' on the dispersive interferogram (see §3). The two mirrors are produced from separate pieces of material but are lapped and polished together to ensure that they are coincident in the beam direction. The constructed cell is shown in figure 2(a).

The cell described above is isolated from the main part of the interferometer by a plastic vacuum membrane (see figure 2(b)) which is held over a wire grid and sealed against the mounting flange with an O ring device. This supported membrane (usually of 25 gauge mylar beam splitter material) is used to enable the rest of the interferometer to be evacuated without significantly reducing the energy throughput. The space between the vacuum membrane and the cell window (about 10 mm) is flushed with dry nitrogen.

### 3 Operation and calculations

Cell operation is straightforward in every way. One has only to be sure that the cell is aligned properly and that the window holding the liquid sample against the mirror is not 'bowing' in such a way that the sample is of variable thickness. This

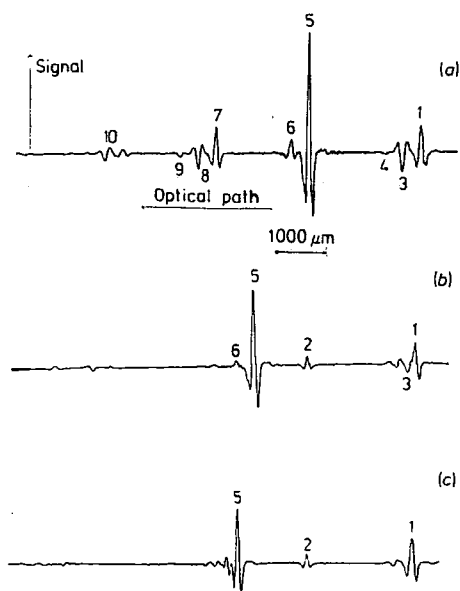


Figure 3 Interferograms produced by FS720 with dispersive cell (of 1 mm thickness) using a 100 gauge mylar beam splitter and a liquid helium cooled germanium bolometer. (a) Empty cell; (b) liquid p-difluorobenzene; (c) liquid tetrabromoethane.

**Table 1** Optical path differences of observed fringes relative to reflection from top surface of cell window (fringe 1).

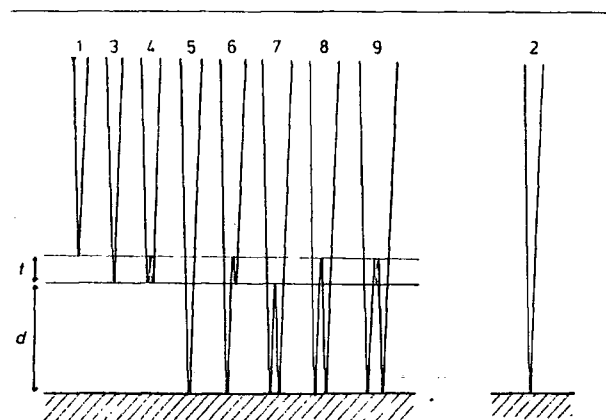
Fringe	Phase change	Optical path difference	Recorded† path difference ( $\mu\text{m}$ )	Predicted‡ PD ( $\mu\text{m}$ )	% error
2	$\pi$	$2d + 2t$	$2052 \pm 4$	2036	0.8
3	0	$2t + \bar{x}_w$	$354 \pm 6$	357	0.6
4	0	$4t + 2\bar{x}_w$	$682 \pm 10$	713	4.3
5	$\pi$	$2t + 2d + \bar{x}_w + \bar{x}_s$	$2170 \pm 6$	2189	0.9
6	$\pi$	$4t + 2d + 2\bar{x}_w + \bar{x}_s$	$2522 \pm 6$	2545	0.9
7	$3\pi$	$2t + 4d + \bar{x}_w + 2\bar{x}_s$	$4010 \pm 6$	4021	0.3
8	$2\pi$	$4t + 4d + 2\bar{x}_w + 2\bar{x}_s$	$4366 \pm 10$	4378	0.3
9	$2\pi$	$6t + 4d + 3\bar{x}_w + 2\bar{x}_s$	$4721 \pm 7$	4734	0.3

† Obtained from 'sample' interferogram.

 ‡ Using  $t = 102 \mu\text{m}$ ,  $\bar{n}_w = 1.748 \pm 0.015$  and  $d$  value of  $916 \pm 12 \mu\text{m}$ .

problem can be overcome, if it arises (and it is easily recognised, see below) by adjusting the height of an external liquid reservoir. Some chemicals (notably acetone and tetrabromoethane) tend to etch off the gold covering from the mirror but this is easily replaced using a standard gold evaporator.†

Typical interferograms produced using the cell with a standard FS720 interferometer and liquid helium cooled bolometer are shown in figure 3. The numbered fringes on each trace may be correlated with the expected optical path differences shown in table 1 and with the ray diagrams shown in figure 4. The average refractive indices are referred to as


**Figure 4** Ray diagram showing origin of fringes observed in the interferogram.

$\bar{n}_w$  and  $\bar{n}_s$  for window and sample materials respectively while the thicknesses of the optical layers are  $t$  and  $d$  respectively. The refractive index of the liquid at wavenumber  $\bar{\nu}$  is determined (Chamberlain *et al* 1969) by the relation.

$$n(\bar{\nu}) = 1 + \frac{\bar{x}_s}{2d} + \frac{1}{4\pi\bar{\nu}d} [\phi_s(\bar{\nu}) - \phi_0(\bar{\nu}) + 2m\pi] \quad (1)$$

where  $\phi_s(\bar{\nu})$  and  $\phi_0(\bar{\nu})$  are the phase functions of the sample and background spectra. If  $\Delta(\bar{\nu}) (= 2d[\bar{n}(\bar{\nu}) - 1])$  and  $\delta_0(\bar{\nu})$  are the phase differences introduced by sample and instrumental imperfections (respectively) then the true phase

difference is given by,

$$\Phi_s(\bar{\nu}) = 2\pi\bar{\nu}[\Delta(\bar{\nu}) + \delta_0(\bar{\nu})] \quad (2)$$

The integer  $m$  is introduced in equation (1) because the phase difference  $\phi_s(\bar{\nu})$  is the *principal* value of the true phase difference given in equation (2). It is expected that  $m=0$  except in regions of very high absorption where the optical thickness  $n(\bar{\nu})d$  may deviate by more than  $\frac{1}{2}\pi$  from the mean optical thickness  $\bar{n}d$  (Chamberlain *et al* 1969). Since the phase functions  $\phi_s(\bar{\nu})$  and  $\phi_0(\bar{\nu})$  are easily determined from the respective spectra, the calculation of  $n(\bar{\nu})$  from equation (1) requires only the determination of the average optical path difference ( $\bar{x}_s$ ) caused by the introduction of the sample into the second beam of the interferometer. The procedure is as follows (referring to figure 4 and table 1):

- (i) the cell pathlength,  $d$ , is first determined from the fringe spacing (3)–(5), given by  $2d + \bar{x}_s$  (but with  $\bar{x}_s = 0$  for an empty cell interferogram);
- (ii) the window thickness  $t$  is then calculated from the distance (1)–(2) ( $= 2d + 2t$ ) on a full cell interferogram;
- (iii) the average optical path difference of the window material,  $\bar{x}_w$ , is then easily calculated using the distance (1)–(3) ( $= 2t + \bar{x}_w$ );
- (iv) finally, since the fringe spacing (2)–(5) (for a full cell interferogram) is simply  $\bar{x}_w + \bar{x}_s$ , the value of  $\bar{x}_s$  (and if necessary  $\bar{n}_s$  since  $\bar{x}_s = 2d(\bar{n}_s - 1)$ ) can be easily computed.

The other fringes, given in table 1 and shown in figure 3 may then be employed to perform an internal consistency check on the fringe assignments and associated calculations.

#### 4 Results and discussion

Table 1 shows that there is very good agreement between calculated and observed fringe positions and this serves to confirm the fringe assignments shown in figure 4. At least some part of the errors given in table 1 are probably due to the effects of phase changes on reflection at the various boundaries. These will affect the distances measured in order to calculate  $\bar{x}_s$  and  $d$  and lead to discrepancies between observed and calculated fringe positions. It should be noted that equation (1) gives a refractive index which is also uncorrected for these effects. The only way of avoiding such effects is to use the 'full interferogram' methods (Honijik 1976, 1977, Birch and Parker 1979a) of computation but large shifts in refractive index are not expected. In this work it was considered undesirable to use this technique because we wish to check our data against previous measurements which also employed equation (1). It is worth noting, however,

† We are grateful to Dr M J Morant and Mr J Gibson of our Applied Physics Department for helping us with this and various related optical measurements.

that the full-interferogram method also has the advantage of automatically eliminating problems associated with the reflection fringes (1), (3) and (6) – which, for example, in this work limit the phase resolution obtainable since such fringes have to be either 'edited' out or omitted from the calculation of  $\phi_s(\bar{\nu})$  and  $\phi_o(\bar{\nu})$ .

Figure 3 demonstrates that we have encountered no major problems with 'bowing' of the front window. This is expected to give rise to loss of optical alignment and subsequent loss of fringe modulation and definition. There is *some* loss of modulation depth for the extremely dense tetrabromoethane ( $\rho^{20} = 2.96 \times 10^3 \text{ kg m}^{-3}$ ) (figure 3(c)) but for liquids with more 'normal' densities this is not a problem (figure 3(b)).

The refractive index dispersion curves shown in figure 5 indicate that our results for the two 'test' liquids are within ~1–2% of the previously published data at approximately the same temperature (Davies 1974, Chamberlain *et al* 1967). The overall 'level' of refractive index is some 2% higher than that fixed (using a laser operating at  $2.97 \text{ mm}^{-1}$ ) at the National Physical Laboratory. There are several sources of possible systematic error between our data and those published previously. These include differences in temperature between the two sets of measurements. However since this could not have been more than 5°C and since the variation of  $n$  with temperature is only about 0.0005 per degree (Int. Critical

Tables, Vol. VII) this could not lead to more than about 0.2% error. Another possible source of error is the determination of the thickness of liquid ( $d$ ) and the central fringe displacement,  $\bar{x}$ . These determinations have been checked using the techniques employed by Chamberlain and those advocated more recently (Birch and Parker 1979b) and found to give results within about 1% of each other. We are therefore convinced that our results are not subject to any obvious systematic error (in comparison with the techniques used to obtain the published data). The shapes of the dispersion curves are virtually identical. Since no error bars are given on the NPL curves it is difficult to say, however, whether the two sets are within the experimental random error. From the errors given in table 1, however, it seems likely that this is the case. Certainly Chantry (1971) regards a  $\pm 1\%$  error as being entirely acceptable using this technique. The results are therefore regarded as being satisfactory when one considers the simplicity of our hardware. We now propose to make some minor modifications (such as installing variable temperature control) before using the cell to make measurements on more chemically useful systems.

#### Acknowledgments

We are grateful for valuable discussions with Dr J R Birch and the late Dr J. Chamberlain. Professor D H Martin and Dr P Ade helped us to put our cooled detector into operation and thanks are also due to the SRC and Beckman RIIC Ltd for their continued support of this project with equipment grants and CASE studentship awards.

#### References

- Birch J R and Parker T J 1979a Dispersive Fourier transform spectroscopy  
*Infrared and Millimetre Waves* Vol. 2 ed K J Button (New York: Academic) Chapter 3
- Birch J R and Parker T J 1979b The role of the origin of computation in the determination of phase spectra by dispersive Fourier transform spectroscopy  
*Infrared Phys.* **19** 103
- Chamberlain J 1968 On the submillimetre wave refraction of liquids  
*Chem. Phys. Lett.* **2** 464
- Chamberlain J, Gibbs J E and Gebbie H A 1969 The determination of refractive index spectra by Fourier spectrometry  
*Infrared Phys.* **9** 185
- Chamberlain J E 1965 On a relation between absorption strength and refractive index  
*Infrared Phys.* **5** 175
- Chamberlain J E 1979 *Principles of Interferometric Spectroscopy* (New York: Wiley) Chapter 7
- Chamberlain J E and Gebbie H A 1966 Dispersion measurements on polytetrafluoro-ethylene in the far infrared  
*Appl. Optics* **5** 393
- Chamberlain J E, Gibbs J E and Gebbie H A 1967 Submillimetre dispersion of liquid tetrabromoethane  
*Spectrochimica Acta* **23A** 2255
- Chantry G W 1971, *Submillimetre Spectroscopy* (New York: Academic) Chapter 4 and Appendix 4
- Davies M M 1974 Infrared absorptions in non-dipolar liquids  
*Molecular Motions in Liquids* (Dordrecht: Reidel) pp 615–35

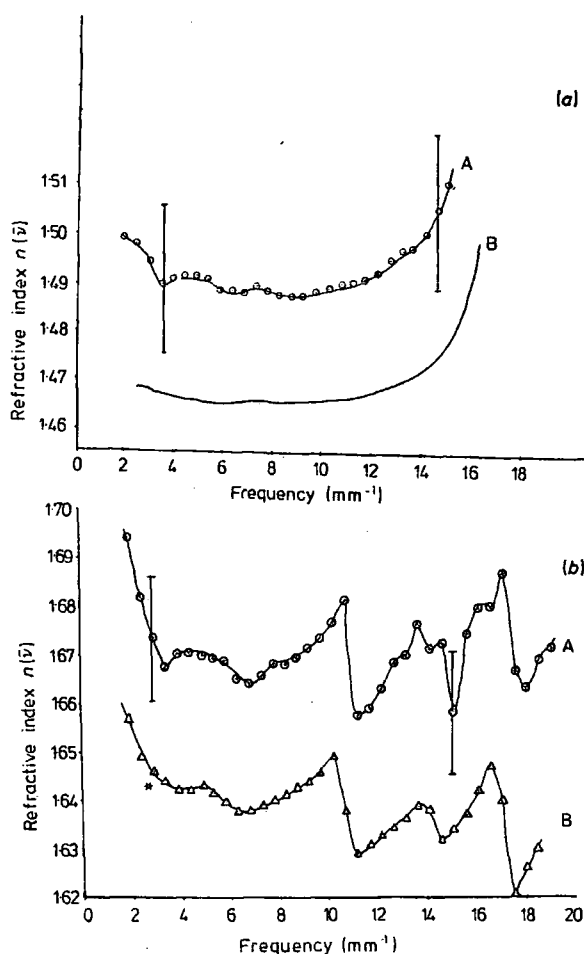


Figure 5 Dispersion curves obtained using the refractive index cell. (a) p-difluorobenzene; (b) tetrabromoethane. The temperature is  $23 \pm 1^\circ\text{C}$  in each case. Our data is labelled A and the NPL data is labelled B.

*Far infrared liquid phase refractive indices*

- Edgell W F 1972 Infrared and Raman studies of ions and ion pairs  
*Ions and Ion Pairs in Organic Reactions* Vol. I ed M Szwarc (New York: Wiley-Interscience) Chapter 4 and references therein
- Evans G J, Reid C J and Evans M W 1978a Far-infrared absorption of  $\text{CH}_2\text{Cl}_2$  in isotropic and cholesteric solvents  
*J. Chem. Soc., Faraday Trans. II* **74** 343
- Evans M W 1975a Investigation of the intermolecular dynamics of non-polar molecules using the rotational velocity correlation function  
*J. Chem. Soc., Faraday Trans. II* **71** 71
- Evans M W 1975b Comparison in the time region 0–1.2 ps of model and experimental absorptions of liquid and rotator phases in the far-infrared  
*J. Chem. Soc., Faraday Trans. II* **71** 2051
- Evans M W and Davies G J 1976 Use of generalised Langevin theory to describe far infrared absorptions in non-dipolar liquids. Effect of pressure and temperature on the intermolecular mean square torques in liquid  $\text{CS}_2$  and  $\text{CCl}_4$   
*J. Chem. Soc., Faraday Trans. II* **72** 1194 1206
- Evans M W, Evans G J and Davies G J 1977 Absorption of dipolar liquids in the far infrared—a sensitive measure of the Mori continued fraction  
*J. Chem. Soc. Faraday Trans. II* **73** 1071
- Evans M W, Evans G J and Davies G J 1979 Zero-THz absorptions and the rotational Langevin equation  
*J. Chem. Soc. Faraday Trans. II* **75** 1428
- Evans M W, Reid C J, Yadav R A, Evans G J and Davies G J 1978b Liquid state dynamics of  $\text{CH}_2\text{Cl}_2$   
*J. Chem. Soc. Faraday Trans. II* **74** 2143
- Honijk D D, Passchier W F, Mandel M and Afsar M N 1976 Determination of complex refractive index spectra of liquids in the far-infrared region ( $5\text{--}500\text{ cm}^{-1}$ ) with dispersive Fourier transform spectrometry  
*Infrared Phys.* **16** 257
- Honijk D D, Passchier W F, Mandell M and Afsar M N 1977 Determination of complex refractive indices with Fourier transform interferometry. V Methods for determination of complex refractive index spectra of liquids in the  $5\text{--}500\text{ cm}^{-1}$  region using a variable pathlength, variable temperature cell  
*Infrared Phys.* **17** 9
- Popov A I and Handy P R 1972 Spectroscopic studies of ionic solvation, XII Ionic solvation in pyridine and substituted pyridine solutions  
*Spectrochimica Acta* **28A** 1545
- Popov A I, Wong M K and McKinney W J 1971 Spectroscopic studies of ionic solvation, VIII Alkali metal salts in acetone solutions  
*J. Phys. Chem.* **75** 56
- Yarwood J 1973 Measurement and interpretation of vibrational spectra of molecular complexes  
*Spectroscopy and Structure of Molecular Complexes* ed J Yarwood (London: Plenum) Chapter 2
- Yarwood J and Barker C 1975 Vibrational spectroscopic studies on ion–molecule interactions in non-aqueous solutions Part I. Far-infrared studies on tetra-n-butyl ammonium chloride in benzene  
*J. Chem. Soc. Faraday Trans. II* **71** 1322
- Yarwood J and Barker C 1977 Studies of ion–ion and ion–molecule interactions using far infrared interferometry  
*Faraday Symp., Chem. Soc.* **11** 136
- Yarwood J, James P L, Arndt R, Evans M W and Evans G J 1979 Studies of molecular motions and vibrational relaxation in acetonitrile IV Far-infrared and molecular dynamics in carbon tetrachloride solution  
*Mol. Phys.* **38** 699
- Yarwood J, James P L and Barker C 1978a Studies of ion–ion and ion–solvent interactions using far-infrared spectroscopy Part 3. Comparison of observed spectra with results of simple model calculations  
*Faraday Diss. Chem. Soc.* **64** 188
- Yarwood J, James P L, Döge G and Arndt R 1978b Comparison of infrared and Raman vibrational relaxation functions of the  $\nu_1$  and  $\nu_3$  modes of acetonitrile  
*Faraday Diss. Chem. Soc.* **66** 252

**APPENDIX 6**

**STUDIES OF ION-ION AND ION-SOLVENT  
INTERACTIONS USING FAR-INFRARED  
SPECTROSCOPY**

**C. BARKER, P.L. JAMES, J. YARWOOD**

**FARADAY DISCUSSIONS OF THE CHEMICAL SOCIETY No. 64, 1978**

**Studies of Ion-Ion and Ion-Solvent Interactions  
using Far-infrared Spectroscopy**

**Part 3.<sup>1,2</sup> Comparison of Observed Spectra with Results of  
Simple Model Calculations**

**BY COLIN BARKER, P. L. JAMES AND JACK YARWOOD<sup>o</sup>**

**Department of Chemistry, University of Durham, Durham City, DH1 3LE**

Reprinted from

**FARADAY DISCUSSIONS  
OF  
THE CHEMICAL SOCIETY**

No. 64

**ION-ION AND ION-SOLVENT  
INTERACTIONS**

1978

## Studies of Ion-Ion and Ion-Solvent Interactions using Far-infrared Spectroscopy

### Part 3.<sup>1,2</sup> Comparison of Observed Spectra with Results of Simple Model Calculations

BY COLIN BARKER, P. L. JAMES AND JACK YARWOOD<sup>3</sup>

Department of Chemistry, University of Durham, Durham City, DH1 3LE

Received 16th May, 1977

The principal features of the far-infrared spectra of tetra-n-alkylammonium salts in non-polar solvents have been compared with the results of some simple model calculations for the motions of, and interactions between, ion-ion and ion-solvent "aggregates." It has been shown that the spectral features, and their variation with solute, solvent, temperature and concentration, are consistent with the absorptions arising from ion-ion vibrations, ion aggregate "librational" motions and fluctuating electrical fields due to "effective" dipole-induced interactions. The observed intensities are reproduced for model geometries and effective aggregate dipoles which agree very well with those obtained using dielectric relaxation measurements, and it is concluded that the high degree of ion "clustering" in the solutions leads to severe restrictions on the movement of solute and solvent species. It is also thought likely that some solvent molecules may be trapped within the ion "cluster". Extension of previous measurements down to concentrations of  $0.01 \text{ mol dm}^{-3}$  show no obvious changes in band shape or structure and it seems clear that extensive aggregation occurs even in relatively dilute solutions.

The far-infrared region is in many ways an ideal one for the study of molecular interactions. This frequency region corresponds to observation times of the order of 0.1 to 10 ps and it is well known that the dynamic properties of molecules in the liquid phase have "characteristic" (more strictly "correlation")<sup>2,3</sup> times of this order. Thus one is able to "observe" *directly*, using this technique, the effects of reorientational and translational (collisional) motions and their variation due to molecular interactions.

In the particular case of solutions containing dissociated or partly dissociated salts we<sup>1,2</sup> and others<sup>4-7</sup> have been able to look specifically at the effects of (a) ion pair (or ion cluster) vibrations; (b) solvent band perturbations<sup>1</sup> and (c) reorientation or "rattling" of ionic species in a dynamic "cage" of surrounding solvent molecules. Considerable amounts of work have been published<sup>8-12</sup> in relatively high solvating media such as acetone, dimethylsulphoxide, pyridine, nitromethane and tetrahydrofuran. Relatively little work has been reported in so-called "poorly" solvating media such as benzene and carbon tetrachloride where the effect of the solvent on salt dissociation and the effect of ion-solvent interactions on the observed spectra is much less clearly understood.<sup>1,2,6</sup> We have recently embarked on a more complete study of some quaternary ammonium salts in non-polar solvents in an attempt to improve our understanding of the dynamic phenomena which occur in such solutions. This paper considers the answers to three questions which arise when one tries to interpret the type of spectra shown in fig. 1-4. First, how is one to assign these bands to the various dynamic phenomena which can occur and how well do the observed spectral variations (with solvent, concentration and temperature) support these assignments?

Secondly, is it possible to devise models for the dynamic phenomena involved which will reasonably reproduce the observed spectra? If so, what are the implications of such models? Finally, what light do such spectra throw on the way in which molecule-ion interactions occur and on the ways in which clustering phenomena are concentration and temperature dependent? The answers to these questions are not only important to structural chemists but also to a wide range of other physical chemists<sup>13-15</sup> and to biologists<sup>16,17</sup> interested in membrane and associated phenomena.

#### EXPERIMENTAL AND DATA TREATMENT

Most of the experimental details have been published previously.<sup>1-3</sup> Considerable improvement in the quality of the spectra obtained especially at low frequency has been recently achieved using a Beckman-R.I.I.C. Ltd. FS720 interferometer converted to the polarizing mode<sup>19-20</sup> and employing a liquid helium cooled germanium bolometer.<sup>21,22</sup> These systems have enabled us to reach a frequency of  $5\text{ cm}^{-1}$  and to considerably improve our signal/noise ratio in the  $5\text{--}120\text{ cm}^{-1}$  region. This is illustrated by the spectra of fig. 2. Further, since the sensitivity of the germanium bolometer is considerably greater than that of a Golay detector we are able to study much lower concentrations of salt than was the case previously. Path lengths approaching 1 cm may be employed; fig. 3 shows a spectrum obtained at a concentration of  $0.01\text{ mol dm}^{-3}$ . In all cases the solution spectrum has been ratioed against that of the pure solvent, so that only "excess" absorption due to the solution is reported.

A band fitting procedure<sup>23,24</sup> was employed to separate the three bands which are clearly visible on all spectra obtained using tetrabutylammonium chloride as solute (fig. 1). We have tried both pure Gaussian and pure Cauchy band profiles, and also a series of sum functions (*i.e.*, Gaussian/Cauchy mixtures). In all cases the relevant statistics (table 1) show

TABLE 1.—COMPARISON OF R.M.S. RESIDUAL TRANSMITTANCE PARAMETERS FOR BAND FITTING OF OBSERVED SPECTRA (AS SHOWN IN FIG. 1)

type of fit	r.m.s. discrepancy (transmittance differences)
single band, pure Gaussian	0.174
single band, pure Cauchy	0.320
two component bands, pure Gaussian	0.019
two component bands, pure Cauchy	0.033
three component bands, pure Gaussian	0.013
three component bands, pure Cauchy	0.047

that pure Gaussian profiles give the best fit (discrepancies for sum functions are larger and in any case lead to  $>90\%$  Gaussian components). It should be noted that this is possible partly due to baseline problems, but the Gaussian profile is in fact predicted<sup>2,3</sup> if, for these highly viscous solutions, the environmental modulation is slow compared with the rate of decay of the observed dipole correlation function. We, therefore, believe there is good evidence that there are, as is shown for example in the spectra of fig. 1, *three* bands (although we cannot completely rule out the possibility of *more* than three bands).

#### RESULTS

Typical spectra of  $\text{Bu}_4\text{N}^+\text{X}^-$  salts in non-polar solvents are shown in fig. 1-3 together, in fig. 1, with the decomposition into their separate components. In all cases which we have studied there are two bands [denoted by "A" and "B" in fig. 1(a) and (b)]. When  $\text{X}^- = \text{Cl}^-$  there is also a third band (denoted "C"). The principal features of these spectra have been pointed out previously.<sup>1,2</sup> We wish here only to

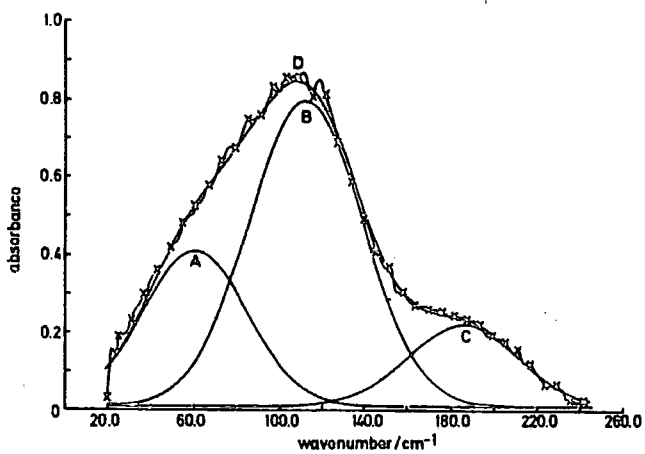


FIG. 1(a).—Far-infrared spectrum of  $\text{Bu}_4\text{N}^+\text{Cl}^-$  in benzene.  $\times$ , observed spectrum; A,  $\nu$ , band at  $\sim 65\text{ cm}^{-1}$ ; B,  $\nu_{\text{CA}}$  band at  $\sim 115\text{ cm}^{-1}$ ; C, band at  $\sim 185\text{ cm}^{-1}$ ; D, total computed band envelope.

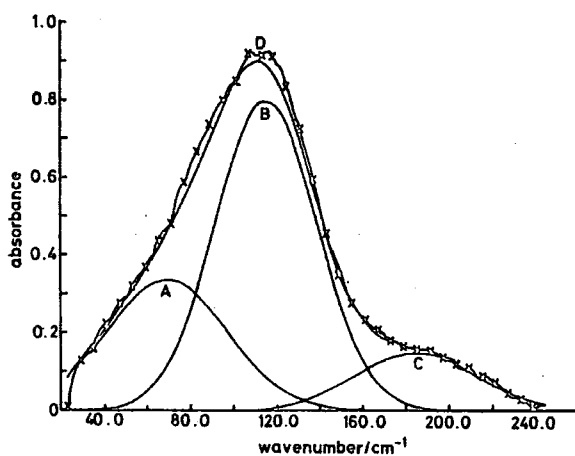


FIG. 1(b).—Far-infrared spectrum of  $\text{Bu}_4\text{N}^+\text{Cl}^-$  in carbon tetrachloride.  $\times$ , observed spectrum; A,  $\nu$ , band at  $\sim 70\text{ cm}^{-1}$ ; B,  $\nu_{\text{CA}}$  band at  $\sim 120\text{ cm}^{-1}$ ; C, combination band at  $\sim 185\text{ cm}^{-1}$ ; D, total computed band envelope.

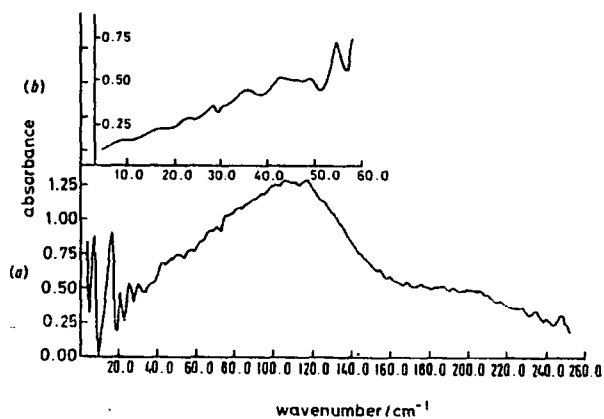


FIG. 2.—Far infrared spectra of  $\text{Bu}_4\text{N}^+\text{Cl}^-$  in benzene, ( $0.5 \text{ mol dm}^{-3}$  solution at  $0.2 \text{ mm}$  path length). (a), with conventional optics and Golay detector; (b) with polarising optics and cooled germanium bolometer.

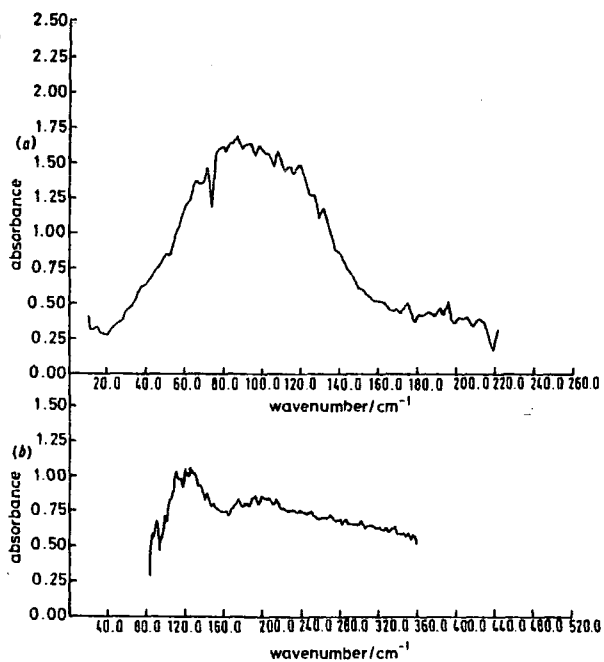


FIG. 3.—Far-infrared spectra of  $\text{Bu}_4\text{N}^+\text{Cl}^-$  in benzene ( $0.01 \text{ mol dm}^{-3}$  solution at  $7.5 \text{ mm}$  path length); (a) with cooled germanium bolometer; (b) with Golay detector.

emphasise certain key points relevant to our interpretations given in the next section. (In this paper we shall consider only bands A and B since the band designated C is still of somewhat obscure origin and is not universally present.)

(i) While the observed frequency and intensity of band "B" is sensitive to both anion and cation, the band "A" features remain remarkably constant (table 2) with changes of anion, cation or solvent.

TABLE 2.—SUMMARY OF SOME TYPICAL SPECTRAL DATA FOR TETRA-N-ALKYLAMMONIUM SALTS IN VARIOUS SOLVENTS

salt	solvent	concentra- tion/mol dm <sup>-3</sup>	temp/K	band "A"			band "B"		
				$\nu_{\max}/\text{cm}^{-1}$	$\Delta\nu_{1/2}/\text{cm}^{-1}$	intensity <sup>a</sup>	$\nu_{\max}/\text{cm}^{-1}$	$\Delta\nu_{1/2}/\text{cm}^{-1}$	intensity <sup>a</sup>
Bu <sub>4</sub> N <sup>+</sup> Cl <sup>-</sup>	C <sub>6</sub> H <sub>6</sub>	0.25	293	71 ± 3	69 ± 3	4.6 ± 2.4	117 ± 3	45 ± 3	4.0 ± 2.3
		0.40	293	78 ± 3	70 ± 3	6.1 ± 1.6	119 ± 3	48 ± 4	4.2 ± 1.6
		0.66	293	73 ± 4	70 ± 4	6.1 ± 0.9	119 ± 2	56 ± 3	6.3 ± 0.9
		0.86	293	70 ± 4	75 ± 4	6.8 ± 0.7	121 ± 2	63 ± 3	7.9 ± 0.7
		1.04	293	72 ± 4	79 ± 3	8.4 ± 0.6	117 ± 2	53 ± 3	5.2 ± 0.6
Bu <sub>4</sub> N <sup>+</sup> Cl <sup>-</sup>	CCl <sub>4</sub>	0.10	293	72 ± 4	62 ± 3	4.4 ± 0.4	117 ± 2	48 ± 2	4.3 ± 0.4
		0.39	293	84 ± 3	68 ± 3	~6.3	120 ± 2	49 ± 2	~6.0
		0.69	293	72 ± 3	64 ± 3	5.3 ± 1.6	115 ± 2	53 ± 2	9.0 ± 1.6
		0.69	293	70 ± 3	63 ± 3	4.0 ± 0.9	115 ± 2	54 ± 2	7.0 ± 0.9
		0.10	293	82 ± 2	57 ± 4	~2.0	116 ± 2	47 ± 2	~6.0
Bu <sub>4</sub> N <sup>+</sup> Cl <sup>-</sup>	CHCl <sub>3</sub>	0.60	293	64 ± 2	64 ± 5	2.1 ± 1.2	113 ± 2	51 ± 2	6.6 ± 1.0
		0.25	294	76	59	2.6	119	53	3.5
		0.25	314	70	60	2.9	117	56	4.2
		0.25	334	67	63	3.5	114	55	4.2
		0.25	349	81	71	4.1	118	60	5.9
Bu <sub>4</sub> N <sup>+</sup> Br <sup>-</sup>	C <sub>6</sub> H <sub>6</sub>	0.30	293	69 ± 3	81 ± 3	3.5 ± 0.8	77 ± 2	59 ± 3	1.9 ± 0.8
		0.40	293	61 ± 3	73 ± 3	3.0 ± 0.6	81 ± 2	54 ± 3	2.1 ± 0.6
Bu <sub>4</sub> N <sup>+</sup> Br <sup>-</sup>	CCl <sub>4</sub>	0.27	293	71 ± 3 <sup>b</sup>	50 ± 3 <sup>b</sup>	6.0 ± 1.7 <sup>b</sup>	—	—	—
Bu <sub>4</sub> N <sup>+</sup> I <sup>-</sup>	-CHCl <sub>3</sub>	0.51	293	61 ± 3 <sup>b</sup>	50 ± 3 <sup>b</sup>	1.2 ± 0.3 <sup>b</sup>	—	—	—
Bu <sub>4</sub> N <sup>+</sup> NO <sub>3</sub> <sup>-</sup>	CHCl <sub>3</sub>	0.32	293	100 ± 3 <sup>b</sup>	65 ± 3 <sup>b</sup>	7.2 ± 2.6 <sup>b</sup>	—	—	—

<sup>a</sup> 10<sup>-4</sup>m mol<sup>-1</sup>, <sup>b</sup> parameters for total band profile.

(ii) The overall appearance of the spectrum remains constant for a given salt regardless of the solvent or concentration used (*cf.* fig. 2 and 3) (although it has been shown<sup>1</sup> that in some cases there are severe deviations from Beer's Law—see below).

(iii) The type of spectrum in this frequency range (with two bands of the general

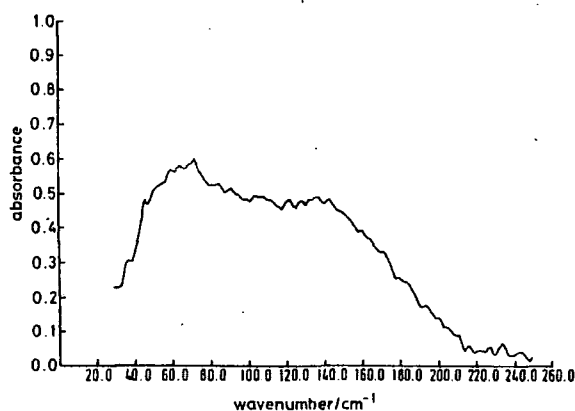


FIG. 4.—Far-infrared spectrum of Ag<sup>+</sup>ClO<sub>4</sub><sup>-</sup> in benzene (0.12 mol dm<sup>-3</sup> solution at 1.0 mm path length). Conventional optics and Golay detector.

kind described here) has been observed for other types of salt solution in relatively poorly solvating media. For example, McDonald and co-workers<sup>6,7</sup> have shown the presence of two bands for trialkylammonium salts in cyclohexane, carbon tetrachloride and chloroform, while we have shown (fig. 4) that a very similar spectrum is obtained on dissolving  $\text{Ag}^+\text{ClO}_4^-$  in benzene. Any interpretation or "model" for ion-solvent or ion-ion interactions must, of course, account for such spectral features and be at least consistent with the observed variations with ion, solvent, concentration and temperature.

#### INTERPRETATION AND DISCUSSION

It is appropriate first to consider the nature of phenomena which may contribute to the absorption in this spectral region in the light of previous work on other types of molecular system. These phenomena are as follows;

(1) Low frequency, vibrational modes.<sup>25,26</sup> These may arise in the case of tetraalkylammonium salts from either internal vibrations of the cation (or anion in the case of polyatomic species)—including difference modes—or from cation-anion stretching modes of the ion pairs or ion clusters.<sup>4,5</sup>

(2) The high frequency component of the (permanent) dipole "reorientational" spectrum.<sup>27,28</sup> Rotational and diffusional motions give rise to a low frequency (Debye)<sup>29</sup> absorption (observed principally in the microwave spectrum but with a Debye "plateau"<sup>28,30</sup> extending into the  $100\text{ cm}^{-1}$  region) and to a high frequency absorption, showing, as distinct from the Debye plateau, an absorption maximum somewhere between 10 and  $100\text{ cm}^{-1}$ . This latter absorption may be thought of as arising from the comparatively rapid librational motion (torsional oscillation) of the dipoles in a potential arising from interactions with neighbouring molecules (the so-called "Poley-Hill" absorption).<sup>31</sup>

(3) Collision induced interaction<sup>27,32</sup> which leads to transient dipoles and hence to radiation absorption at frequencies corresponding roughly to collision rates in liquids (*i.e.*, to absorption in the  $2\text{--}250\text{ cm}^{-1}$  region with a characteristic frequency of maximum absorption in the same region as that expected for the Poley-Hill process). Such absorption is well known for simple non-polar liquids.<sup>25,33-35</sup> In the case of salts such as those studied in this work, the interactions are expected to be of the dipole-induced dipole type, which are modulated at the collision frequency. It should be noted that there will be ion-pair (or cluster)-solvent and solvent-solvent collisions giving rise to this process, although to some extent at least effects due to the latter will have been removed (see Experimental section).

It is expected that all three processes will contribute to the observed spectra shown in fig. 1-4. However, since the "B" band has been clearly shown to be both cation and anion dependent it seems reasonable to conclude that the band arises from some sort of ion-pair or ion cluster "vibration" involving motion of both anion and cation. This conclusion has been reached before, of course, but we present in this work the supporting evidence of some simple force constant and intensity considerations. If we make the assumption that this band arises from a normal mode in which the movement of anion and cation is along a line joining their centres, then the frequency of vibration is given in the (harmonic) diatomic approximation by

$$\bar{\nu}_{\text{obs}} = \frac{1}{2\pi c} (k_{\text{obs}}/\mu')^{\frac{1}{2}} \quad (1)$$

where  $k_{\text{obs}}$  is the force constant of the bond between cation and anion and  $\mu'$  is the reduced mass of the vibrating system [ $\mu' = m_c m_a / (m_c + m_a)$ ] using "whole" cation

and anion masses  $m_C$  and  $m_A$ . Provided that the restoring force between the anion and cation is Coulombic (*i.e.*, electrostatic) then the force constant for univalent ions is given<sup>36</sup> by

$$k_{\text{calc}} \equiv \frac{\partial F}{\partial r} = \frac{-2e^2}{4\pi\epsilon_0\epsilon r_{\text{CA}}^3} \quad (2)$$

where  $e$  is the electronic charge,  $\epsilon_0$  is the permittivity of a vacuum ( $8.854 \times 10^{-12}$  C V<sup>-1</sup>m<sup>-2</sup>) and  $\epsilon$  is the relative permittivity of the medium ( $\epsilon = 2.28$  for pure benzene).  $r_{\text{CA}}$  (which may be estimated from the sum of the effective ionic radii or from dipole moment measurements - see below) is expected to remain, to a first approximation, constant for the salts studied here. Thus from eqn (2) and (1), for the purely electrostatic ion pair model,  $\nu_{\text{obs}}$  should be proportional to  $1/(\mu)^{1/2}$ ; fig. 5 shows that this is

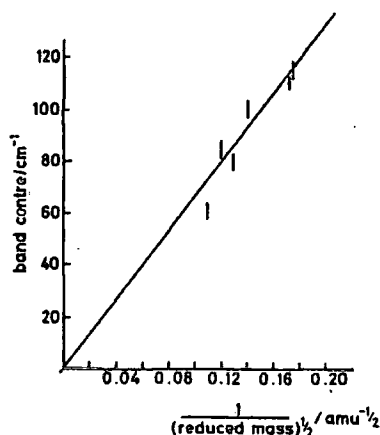


FIG. 5.—Illustration of linear frequency against reduced mass relationship for the ion aggregate vibrational band at  $\sim 115$  cm<sup>-1</sup>.

indeed the case (to within the experimental error). This would tend to indicate that the model is a reasonably good one despite the evidence<sup>37-40</sup> that, for solutions of the concentrations used here, the average size of ionic aggregate is of the order of 20-30 ion pairs. A further test of the model could be made by comparing the values of  $k_{\text{obs}}$  and  $k_{\text{calc}}$  from eqn (1) and (2). Since the "correct" value of  $r_{\text{CA}}$  is not really known<sup>41-43</sup> for salts of this type, it is preferable to calculate the value of  $r_{\text{CA}}$  from eqn (2) using the experimental  $k_{\text{obs}}$  values. The result of such a calculation for a range of salts and solvents are collected in table 3. There are several points of interest which emerge from this table, the most significant of which is that the calculated values of  $r_{\text{CA}}$  seem to be very much smaller than the values obtained for estimates<sup>41-43</sup> of the effective charge separation—these being in the region of 0.4-0.5 nm for a series of tetra-alkylammonium salts. It is significant that microwave (dielectric) data<sup>44-46</sup> on similar complexes also lead to an "expected"  $r_{\text{CA}}$  which is also very much lower than that obtained using dipole moment measurements.<sup>41-43</sup> It has been postulated<sup>46</sup> that such disagreement is due to the formation of large aggregates which lead to a reduction in the "effective" charge separation. In this connection it is interesting to examine the changes which occur in the calculated  $r_{\text{CA}}$  values as a function of con-

TABLE 3.—FORCE CONSTANTS AND EFFECTIVE INTERIONIC SEPARATIONS FOR THE ELECTROSTATIC ION PAIR MODEL

salt	solvent	concentration /mol dm <sup>-3</sup>	band centre <sup>a</sup> /cm <sup>-1</sup>	$k_{obs}/N\ m^{-1}$	$r_{CA}$ [from eqn (2)]/nm
Bu <sub>4</sub> N <sup>+</sup> Cl <sup>-</sup>	C <sub>6</sub> H <sub>6</sub>	0.01	115 ± 5 <sup>b</sup>	24.1 ± 2.0	0.204 ± 0.002
		0.21	112 ± 1	22.9 ± 0.4	0.206 ± 0.001
		0.50	121 ± 1	26.7 ± 0.4	0.196 ± 0.001
		0.80	119 ± 1	25.8 ± 0.4	0.198 ± 0.001
		1.40	117 ± 1	25.0 ± 0.4	0.200 ± 0.001
Bu <sub>2</sub> N <sup>+</sup> Cl <sup>-</sup>	C <sub>6</sub> H <sub>6</sub>	0.50	121 ± 1	26.7 ± 0.4	0.196 ± 0.001
	CCl <sub>4</sub>	0.50	115 ± 1	24.1 ± 0.4	0.204 ± 0.001
	CHCl <sub>3</sub>	0.50	114 ± 1	23.7 ± 0.4	0.185 ± 0.001
	T.H.F.	0.50	110 ± 5 <sup>b</sup>	22.1 ± 2.0	0.141 ± 0.002
Bu <sub>4</sub> N <sup>+</sup> Br <sup>-</sup>	C <sub>6</sub> H <sub>6</sub>	0.50	79 ± 1	22.1 ± 0.6	0.209 ± 0.001
	CHCl <sub>3</sub>	0.50	79 ± 3 <sup>b</sup>	22.1 ± 1.7	0.161 ± 0.004
Bu <sub>4</sub> N <sup>+</sup> I <sup>-</sup>	CHCl <sub>3</sub>	0.50	61 ± 3 <sup>b</sup>	18.3 ± 1.8	0.172 ± 0.017
Bu <sub>4</sub> N <sup>+</sup> NO <sub>3</sub> <sup>-</sup>	CHCl <sub>3</sub>	0.50	100 ± 3 <sup>b</sup>	29.1 ± 1.7	0.147 ± 0.003
Bu <sub>4</sub> N <sup>+</sup> ClO <sub>4</sub> <sup>-</sup>	CHCl <sub>3</sub>	0.50	85 ± 3 <sup>b</sup>	30.1 ± 2.1	0.146 ± 0.004
Pe <sub>4</sub> N <sup>+</sup> Cl <sup>-</sup>	C <sub>6</sub> H <sub>6</sub>	0.50	115 ± 3 <sup>b</sup>	24.7 ± 1.3	0.201 ± 0.004
Hp <sub>3</sub> N <sup>+</sup> Cl <sup>-</sup>	C <sub>6</sub> H <sub>6</sub>	0.50	112 ± 3 <sup>b</sup>	24.2 ± 1.3	0.203 ± 0.003

<sup>a</sup> Errors are standard deviations obtained from band fitting statistics. <sup>b</sup> Error estimated by eye.

centration. Since the degree of aggregation ought to change as the concentration is lowered, one might expect this to be reflected in the effective force constant or calculated  $r_{CA}$ . From table 3 it may be seen that there are small but real changes in  $k_{obs}$  and  $r_{CA}$  as the concentration changes. It appears that the effective force constant reaches a maximum (for Bu<sub>4</sub>N<sup>+</sup>Cl<sup>-</sup> in benzene) at about 0.5 mol dm<sup>-3</sup> and then decreases again at higher concentrations. This is entirely in line with the conclusions drawn previously from permittivity,<sup>37</sup> conductivity<sup>40</sup> and freezing point<sup>38,39</sup> measurements. It is also clear that in the 0.01 mol dm<sup>-3</sup> solutions (the lowest we have reached so far) the degree of aggregation is still quite high since the  $k_{obs}$  (and therefore,  $r_{CA}$ ) shows little change. Table 3 also shows that the effective force constant also decreases on going (for Bu<sub>4</sub>N<sup>+</sup>X<sup>-</sup>) from Cl<sup>-</sup> to Br<sup>-</sup> to I<sup>-</sup> (all in chloroform solution). This is, of course, expected from the frequency and reduced mass changes and probably reflects an increasing effective separation as the anion increases in size. It should be noted that comparison of  $r_{CA}$  calculated from eqn (2) for different solvents is complicated by the unknown relative permittivity  $\epsilon$  of these solutions in the far-infrared region. Bauge and Smith<sup>42</sup> have used  $\epsilon = 1$  for non-polar solvents since it was felt that the solvent molecules do not penetrate between the cation and anion. We have used the pure liquid values (at 298 K) for our solvents bearing in mind the small variations of  $\epsilon_{\infty}$  for solutions of trialkylammonium salts in benzene and *p*-xylene,<sup>43</sup> and the comments of Grunwald *et al.*<sup>47</sup> concerning the almost total lack of medium effects on the measured dipole moments of this type of salt in non-polar solvents. The values of  $r_{CA}$  seem to be smaller in chloroform than they are in benzene, which seems strange unless this weakly polar solvent somehow stabilises the ionic aggregates.

A more promising, although experimentally more difficult, approach to the problem of ion clustering in these solutions is to use intensity measurements since it is well known that vibrational intensities are extremely sensitive even to weak molecular interactions.<sup>48</sup> We have already shown<sup>1,18</sup> that, at least for Bu<sub>2</sub>N<sup>+</sup>Cl<sup>-</sup>, the  $r_{CA}$

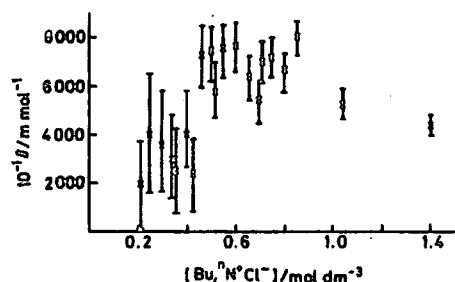


FIG. 6.—Variation of intensity with concentration for the  $\sim 115 \text{ cm}^{-1}$  band of  $\text{Bu}_4\text{N}^+\text{Cl}^-$  in benzene (293 K).

band intensity is concentration dependent (see fig. 6). Using the simplest possible approximation of non-polarisable point charges, the variation of ion-pair dipole as a function of vibrational coordinate ( $\partial\mu/\partial Q$ ), which controls the vibrational intensity,<sup>49</sup> is given by,

$$\partial\mu/\partial Q = e/m^{\ddagger} \quad (3)$$

where,

$$\mu = er_{\text{CA}} \quad (4)$$

and  $m^{\ddagger}$  is the reduced mass of the ion pair. The intensity<sup>49</sup> value is

$$B = \frac{N\pi}{3c^2} \left( \frac{\partial\mu}{\partial Q} \right)^2 = \frac{N\pi e^2}{3c^2 m^{\ddagger}} \quad (5)$$

This gives  $B = 31\,400 \text{ m mol}^{-1}$  in reasonably good agreement with the experimental values of  $B$  given in table 2. Several authors<sup>41,42,47</sup> have pointed out, of course, that for polarisable ions the dipole moment of the ion pair is considerably lower [ref. (47), p. 453] than that calculated using eqn (4) and that more complicated expressions, including the effects<sup>36</sup> of mutual polarisation of the ions, should be employed. Davies and Williams,<sup>41</sup> for example, have used

$$\mu = er_{\text{CA}}(1 - a_{\text{eff}}/4\pi\epsilon_0\epsilon r_{\text{CA}}^3) \quad (6)$$

(where  $a_{\text{eff}}$  is an effective ion polarisability)—whence

$$\partial\mu/\partial Q = \left( e + \frac{2ea_{\text{eff}}}{4\pi\epsilon_0\epsilon r_{\text{CA}}^2} \right) \frac{1}{m^{\ddagger}} \quad (7)$$

while Grünwald *et al.*<sup>47</sup> obtain

$$\mu = er_{\text{CA}} \left\{ 1 - \frac{r_{\text{CA}}^2(a_{\text{C}} + a_{\text{A}}) + 4a_{\text{C}}a_{\text{A}}}{\epsilon[r_{\text{CA}}^3 - 4a_{\text{C}}a_{\text{A}}]} \right\} \quad (8)$$

for isolated alkali halide ion pairs, where  $a_{\text{C}}$  and  $a_{\text{A}}$  are the polarisabilities of the cation and anion [ref. (47), p. 455]. The values of  $B$  obtained using a range of  $r_{\text{CA}}$  values and the expression for  $\partial\mu/\partial Q$  obtained from eqn (7) are given in table 4. It is seen that the value of  $r_{\text{CA}}$  necessary to give agreement with the observed data is about 0.35 nm, again lower than one would expect on the basis of an individual ion pair, the sum of  $r_{\text{C}}$  and  $r_{\text{A}}$  being 0.49 nm<sup>42,40</sup>—however considerably greater than that required to pro-

TABLE 4.—INTENSITY VALUES CALCULATED<sup>a</sup> FROM EQN (7)<sup>b,c</sup> FOR THE ION AGGREGATE VIBRATIONAL BAND 'B' AT  $\sim 118 \text{ cm}^{-1}$  AS A FUNCTION OF  $r_{CA}$ .

$r_{CA}/\text{nm}$	$10^{30}\mu_{eff}[\text{eqn (6)}]/\text{C m}$	$B/\text{m mol}^{-1}$
0.20	4.13	333 100
0.25	8.40	127 600
0.30	10.70	67 600
0.35	12.13	44 300
0.40	13.04	33 400
0.50	14.11	24 100

<sup>a</sup> The average observed intensity over the concentration range studied is  $57\,600 \text{ m mol}^{-1}$ . <sup>b</sup> The polarizability  $\alpha_{eff}$  is taken as that of the tetrabutylammonium cation [ref. (47)] which is much higher than that of the halide anion. <sup>c</sup> The medium permittivity used is that of pure benzene ( $\epsilon = 2.28$ ).

duce the observed force constant using eqn (2). Thus, the intensity data presented here lead to  $r_{CA}$  values which are semi-quantitatively correct for the vibration of a polarisable ion-pair or "cluster" especially when one bears in mind the following points, (a) we have used  $\epsilon = 2.28$  for the medium—if this value were to be reduced to 1 (assuming contact ion pairs) then the observed intensity value would be produced for  $r_{CA} > 0.45 \text{ nm}$ ; (b) that dipole moment data for relatively concentrated solutions<sup>42,46</sup> lead, with allowance for the presence of weakly polar ion-pair dimers and more complex units, to values of  $r_{CA}$  which are lower than the  $(r_C + r_A)$  values and (c) that the approximation in eqn (6) is known<sup>47</sup> to lead to calculated values of  $r_{CA}$  which are lower than that obtained using the Böttcher model [eqn (8)].

We now turn our attention to bands "A" in the spectra (fig. 1) which lie to lower frequency and which, as we have pointed out, show little variation in band position or half-width on changing either the salt or the solvent (table 2). Although we have previously attributed<sup>1,2</sup> this band to the collision of perturbed solvent molecules, it has become clear more recently that, in principle at least, both librational motions of the ion-pair (or aggregate) dipole and collision induced effects may contribute to the low frequency absorption. We consider here attempts to separate the intensities of the two contributions and the implications, for the structure of these solutions, of calculated and observed collision induced intensities.

A number of authors<sup>20,50-53</sup> have used the Gordon intensity sum rule<sup>54</sup> to calculate the intensity arising from the rotation of a rigid linear dipolar molecule (in any phase). The intensity (per molecule) is

$$\frac{9n_\infty}{(n_\infty^2 + 2)^2} \int_0^\infty \alpha_p(\nu) d\nu = \frac{\pi\mu_z^2}{3c^2} \left( \frac{1}{I_x} + \frac{1}{I_y} \right) = A_p \quad (9)$$

where  $\alpha_p(\nu)$  is the absorption coefficient as a function of wave number  $\nu$  arising from this mechanism,  $n_\infty$  is the (infrared) refractive index, and  $I_x$  and  $I_y$  are the moments of inertia perpendicular to the direction of the molecular dipole moment  $\mu_z$ . The factor  $9n_\infty/(n_\infty^2 + 2)^2$  is an internal field correction,<sup>27</sup> which is difficult to apply in this case since the refractive index is unknown. The dipole moment of the ion pair is known to be about 10 D ( $33.35 \times 10^{-30} \text{ C m}$ ) but may be less, of course, for large aggregates.<sup>42,46</sup> Table 5 shows the values obtained for the integrated intensities,  $\int \alpha(\nu) d\nu$ , from eqn (9) using a range of  $\mu_{CA}$ . The  $I_x (=I_y)$  value used is based on the diatomic approximation. The average intensity of the band over a wide range of concentrations (table 2) is  $1060 \times 10^{-22} \text{ m}$  so that this contribution may account for a maximum of

TABLE 5.—PREDICTED INTENSITY<sup>a</sup> CONTRIBUTION TO BAND 'A' FROM EQN (9) FOR THE POLEY-HILL MECHANISM OF ION-PAIR LIBRATION

effective cation-anion distance, $r_{CA}/\text{nm}$	0.30	0.4	0.5	0.3	0.4	0.5	0.3	0.4	0.5
ion pair moment of inertia, $10^{41}/\text{kg m}^2$	462.6	822.4	1285.1	462.6	822.4	1285.1	462.6	822.4	1285.1
effective ion pair dipole, $10^{18}\mu_{CA}/\text{C m}$	33.0	33.0	33.0	20.0	20.0	20.0	10.0	10.0	10.0
$10^{19}A_p/m$	504.1	283.0	181.5	181.5	102.3	65.3	45.4	25.5	16.3
$A/m \text{ mol}^{-1}$	30 362	17 045	10 931	10 931	6149	3933	2734	1536	981

<sup>a</sup> The average observed intensity over the concentration range studied is  $1060 \times 10^{-22} \text{ m}$  (or  $63 900 \text{ m mol}^{-1}$ ).

about half the total intensity assuming an effective dipole moment of  $33 \times 10^{-30} \text{ C m}$  and an average  $r_{CA}$  of 0.3 nm. It has been shown<sup>50,55</sup> that the Poley-Hill mechanism ought to lead to a decrease in band frequency when the temperature is increased, whereas one would expect that any absorption arising from electrical fields modulated by collisions would have the opposite frequency dependence. Our temperature variation studies (fig. 7) show that the observed band shows no obvious frequency

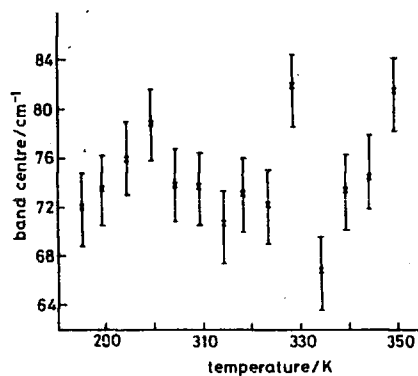


FIG. 7.—Variation of band centre with temperature for the  $\sim 75 \text{ cm}^{-1}$  band of  $\text{Bu}_4^+\text{N}^+ \text{Cl}^-$  in benzene.

dependence (over the range studied); it, therefore, seems likely that both mechanisms *do* contribute to the observed spectra in this region. It is not easy to estimate the contribution from collision induced effects because of the large cluster sizes and our lack of knowledge of the dynamic properties of the solvent molecules in relation to those of the solute particles. For simple dipolar molecules<sup>53</sup> the collision induced contribution observed over and above that due to librational motions has been used (using a binary collision<sup>58</sup> approximation) to estimate the relevant multiple moment of the colliding molecules. If one writes,

$$\int_{\text{band}} a_{\tau}(\bar{\nu}) d\bar{\nu} = A_p N + B_c N^2 \quad (10)$$

$a_{\tau}(\bar{\nu})$  being the total observed absorption coefficient,  $N$  the number density and  $B_c$  the intensity contribution due to collision induced effects] then by measuring the

left hand side of eqn (10) as a function of concentration one may calculate  $B_c$  and compare this with various possible theoretical values. In this work the intensity data as a function of concentration (fig. 9) were not accurate enough for us to carry out such an analysis (see below). We have, therefore, attempted only to estimate  $B_c$

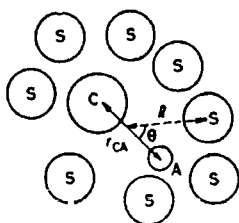


FIG. 8.—The "idealised" ion-pair and surrounding solvent molecules. Parameters needed to estimate the dipole-induced dipole interactions between solute and solvent.

using a simple dipole-induced dipole expression which assumes that the interaction energy between ion-pair and solvent is a maximum. When the dipole-solvent distance,  $R$  (see fig. 8) is large compared with  $r_{CA}$  the potential at the solvent molecule due to the dipole  $\mu_{CA}$  is given<sup>36,56</sup> by,

$$V(R, \theta) = \frac{\mu_{CA} \cos \theta}{4\pi\epsilon_0\epsilon R^2}. \quad (11)$$

The electric field at the solvent molecule is  $-\text{grad}[V(R, \theta)]$  or,

$$E = \frac{2\mu_{CA} \cos \theta}{4\pi\epsilon_0\epsilon R^3}. \quad (12)$$

Thus for  $\cos \theta = 1$  (maximum interaction) the dipole induced in the solvent molecule is simply,

$$\mu_{\text{ind}} = a_s E = \frac{2\mu_{CA} a_s}{4\pi\epsilon_0\epsilon R^3} \quad (13)$$

where  $a_s$  is the average solvent polarizability and  $\mu_{CA}$  is given by eqn (6). The intensity expected using this simple model is then obtained by taking,

$$\partial\mu/\partial Q = \frac{-6\mu_{CA} a_s}{4\pi\epsilon_0\epsilon R^4 m_{cs}^2} \quad (14)$$

whence

$$B_c = \frac{N\pi}{3c^2 m_{cs}} \left\{ \frac{-6\mu_{CA} a_s}{4\pi\epsilon_0\epsilon R^4} \right\}^2 \quad (15)$$

In table 6 we show the  $B$  values calculated for a range of  $\mu_{CA}$  and  $R$  values and it is seen that the excess intensity values

$$\left[ \int_{\text{band}} a_T(\bar{\nu}) d\bar{\nu} \right] - A_p \left[ \text{from right hand side of eqn. (9)} \right]$$

are reproduced for values of  $R$  between 0.20 and 0.25 nm (depending on the value of  $\mu_{CA}$  taken). Again, these values appear to be smaller than one might expect using,

TABLE 6.—PREDICTED INTENSITY<sup>a,b</sup> CONTRIBUTION TO BAND 'A' FROM EQN (15) FROM AGGREGATE DIPOLE-INDUCED DIPOLE INTERACTION

effective aggregate-solvent distance, $R/\text{nm}$	effective ion aggregate dipole, $10^{30}\mu_{\text{CA}}/\text{C m}$		
	33.0	20.0	10.0
0.20	190 000	71 700	18 000
0.25	33 400	12 100	3 000
0.30	7 800	2 800	700
0.35	2 270	810	200
0.40	780	280	70

<sup>a</sup> Values are in  $\text{m mol}^{-1}$ . (The experimental value attributable to this type of interaction is of the order of  $30\,000\text{ m mol}^{-1}$ —see text.) <sup>b</sup> The permittivity used is that of pure benzene ( $\epsilon = 2.28$ ). The polarisability  $\alpha$ , is also that of benzene ( $11.48 \times 10^{-40}\text{ C m}^2\text{ V}^{-1}$ ). The reduced mass  $m_{\text{ca}}$  is that of an ion-pair dipole/solvent molecule system.

for example, the sum of the van der Waals and ionic radii for the solvent and  $\text{Bu}_4\text{N}^+$  ion (*i.e.*,  $\sim 0.45\text{--}0.50\text{ nm}$ ). It is also interesting (table 6) that reducing the value of  $\mu_{\text{CA}}$  below the "ion-pair" value of  $33 \times 10^{-30}\text{ C m}$  gives an even smaller estimate of the  $R$  value.

It is important to notice that values of average aggregate distance  $R$  deduced using the observed intensities of both bands agree very well with values of the average distance between all the particles in solution obtained by Lestrade<sup>44,46</sup> and his co-workers using complex dielectric permittivity measurements of tetra-*n*-alkylammonium salts.

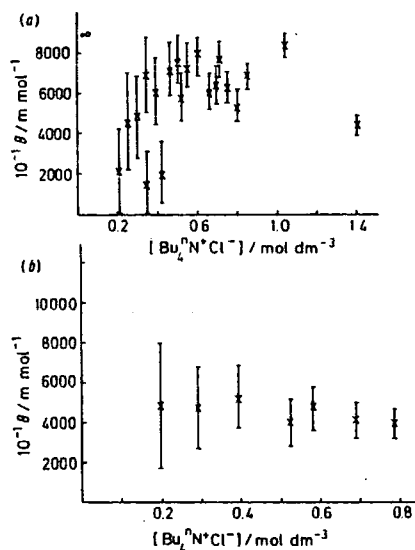


FIG. 9.—Comparison of intensity variations for  $\sim 75\text{ cm}^{-1}$  band of  $\text{Bu}_4\text{N}^+\text{Cl}^-$  in (a) benzene and (b) carbon tetrachloride (293 K).

(The agreement is remarkable when one considers the approximations inherent in the relatively simple models used to describe what must be extremely complicated processes.) These authors have interpreted these results to indicate that the ions move in a restricted region in space—that space being the interior of the aggregate or clusters. It appears likely, therefore, that the benzene molecules involved in dipole-induced dipole interactions (this number will be relatively small compared with the total present—the mole fraction of solute even at the highest concentration being only 0.1) are “compressed” by the cluster formation. It is tempting to speculate that *maybe* some benzene molecules are even trapped within “cages” formed by the rather open structure of the alkyl chains. This would at least be consistent with the assertion made by some authors<sup>59</sup> that concentrated benzene solutions should be regarded as solutions of benzene in the fused salt. There is also some evidence from solutions in different solvents that the properties of the benzene solvent in these solutions are somewhat anomalous. Fig. 9 compares the (intensity, concentration) graphs for the low frequency band in benzene and carbon tetrachloride. As expected, neither band obeys Beers Law [eqn (10)] but the data for benzene show much wider variations than do those for carbon tetrachloride. This may be related to the less isotropic polarizability of benzene<sup>60</sup> (or to very small amounts of water, although this is doubtful)<sup>1</sup> but we suspect it is due to severe and inhomogeneous ion cluster-solvent interactions. It is observed from fig. 9 that, in fact, the intensity of band A does not vary a great deal from benzene to carbon tetrachloride. This is in accord with their comparable polarizabilities<sup>60</sup> and provides further support for the proposed mechanism.

#### SUMMARY AND CONCLUSIONS

It is clear from the lack of temperature and solvent dependence, and from the force constant and approximate intensity calculations given in the previous section that band “B” in the spectra of these salts must be assigned to some kind of ion-aggregate vibrational mode which involves both anion and cation. We have previously shown<sup>2</sup> that the width and shape of this band are consistent with the vibrating aggregate being (relatively slowly) modulated by the stochastic solvent environment—this we believe to be due to the presence of large (relatively long lived) ionic clusters and the observed high solution viscosity. The large half width (and associated short correlation time) may be a reflection of the large number of species of slightly different geometries which result from the stochastic nature of the surrounding medium.

Band “A” in the spectra is almost certainly of hybrid character (as noted before<sup>48</sup> for bands in this region arising in solutions containing polar complexes). The two most likely phenomena which may contribute intensity consist essentially of a restricted orientational motion of the aggregate “effective” dipole and effective dipole-induced dipole interactions which lead to fluctuating electric fields in the vicinity of the ionic clusters and the first solvation shell of solvent molecules. The relative lack of dependence of the frequency and intensity of this band on the solvent and on temperature supports the assertion that more than one phenomenon is involved, and that collisions of the perturbed solvent molecules (although probably involved) do not control the frequency maximum. In attempting to establish the relevance of either or both of these processes (via our intensity calculations) we have assumed that the clusters present in solution *do* have finite effective dipoles of the order of  $10\text{--}20 \times 10^{-30}$  C m. If the aggregates were non-polar only the effects of higher multipoles would be observed. These may, in fact, be important<sup>53</sup> but with the present accuracy of our data we could not estimate how large these effects may be. However, the values of our mean  $r_{CA}$  and  $R$  distances (obtained using the effective dipoles mentioned above)

agree well with those derived using dielectric relaxation measurements<sup>44,46</sup> and it seems likely that in these solutions dipole-induced dipole effects predominate.

Valuable discussions with Prof. M. Davies and Dr. G. Williams are gratefully acknowledged. Thanks are also due to the S.R.C. and the Royal Society for equipment grants. C. B. and P. L. J. also thank the S.R.C. and Beckman-R.I.I.C. Ltd. for support via C.A.S.E. studentships.

- <sup>1</sup> Part 1, C. Barker and J. Yarwood, *J.C.S. Faraday II*, 1975, 71, 1322.
- <sup>2</sup> Part 2, C. Barker and J. Yarwood, *Faraday Symp. Chem. Soc.*, 1977, 11, 136.
- <sup>3</sup> R. Kubo, *Fluctuation, Relaxation and Resonance in Magnetic Systems*, ed. D. Ter Haar (Oliver and Boyd, London, 1962), pp. 23-68.
- <sup>4</sup> J. C. Evans and G. Y. S-Lo, *J. Phys. Chem.*, 1965, 69, 3223.
- <sup>5</sup> M. J. French and J. L. Wood, *J. Chem. Phys.*, 1968, 49, 2358.
- <sup>6</sup> J. R. Kludt, G. Y. W. Kwong and R. L. McDonald, *J. Phys. Chem.*, 1972, 76, 339.
- <sup>7</sup> R. A. Work and R. L. McDonald, *J. Phys. Chem.*, 1973, 77, 1148.
- <sup>8</sup> W. F. Edgell, J. Lyford, R. Wright, W. Risen and A. Watts, *J. Amer. Chem. Soc.*, 1970, 92, 2240.
- <sup>9</sup> W. F. Edgell, *Ions and Ion Pairs in Organic Reactions*, ed. M. Szwarc (Wiley-Interscience, New York, 1972), vol. 1, chap. 4.
- <sup>10</sup> M. K. Wong, W. J. McKinney and A. I. Popov, *J. Phys. Chem.*, 1971, 75, 56.
- <sup>11</sup> W. J. McKinney and A. I. Popov, *J. Phys. Chem.*, 1970, 74, 535.
- <sup>12</sup> P. R. Handy and A. I. Popov, *Spectrochim. Acta*, 1972, 28A, 1545.
- <sup>13</sup> P. P. Schmidt, *J.C.S. Faraday II*, 1976, 72, 1125.
- <sup>14</sup> T. S. Chow and J. J. Hermans, *J. Colloid Interface Sci.*, 1973, 45, 566.
- <sup>15</sup> M. Szwarc, *Ions and Ion Pairs in Organic Reactions*, ed. M. Szwarc (Wiley-Interscience, New York, 1972), vol. 1, chap. 1.
- <sup>16</sup> M. R. J. Salton, *Biomembranes*, ed. L. A. Manson (Plenum, New York, 1971), vol. 1, chap. 1.
- <sup>17</sup> H. R. Kaback, *Bacterial Membranes and Walls*, ed. L. Leive (Marcel Dekker, New York, 1973), chap. 5.
- <sup>18</sup> C. Barker, *Ph.D. Thesis* (University of Durham, 1977).
- <sup>19</sup> D. H. Martin and E. Puplett, *Infrared Phys.*, 1969, 10, 105.
- <sup>20</sup> P. L. James, *M.Sc. Thesis* (University of Durham, 1976).
- <sup>21</sup> *Spectroscopic Techniques*, ed. D. H. Martin (North Holland, Amsterdam, 1967), chap. 4.
- <sup>22</sup> F. J. Low, *J. Opt. Soc. Amer.*, 1961, 51, 1300; S. Zwerdling, R. A. Smith and J. P. Theriault, *Infrared Phys.*, 1968, 8, 271.
- <sup>23</sup> J. Pitha and R. N. Jones, *Canad. J. Chem.*, 1966, 44, 3031; 1967, 45, 2347.
- <sup>24</sup> J. Pitha, R. N. Jones and R. P. Young, *N.R.C. Bulletins 12 and 13*, (N.R.C. Ottawa, 1968-69).
- <sup>25</sup> K. D. Möller and W. G. Rothschild, *Far-infrared Spectroscopy* (Wiley-Interscience, New York, 1971).
- <sup>26</sup> A. Finch, P. N. Gates, K. Radcliffe, F. N. Dickson and F. F. Bentley, *Chemical Applications of Far-infrared Spectroscopy* (Academic Press, New York, 1970).
- <sup>27</sup> M. Evans, *J.C.S. Faraday II*, 1975, 71, 2051 and references contained therein; 1976, 72, 727.
- <sup>28</sup> A. Gerschel, I. Darmon and C. Brot, *Mol. Phys.*, 1972, 23, 317.
- <sup>29</sup> P. Debye, *Polar Molecules* (Dover, New York, 1929).
- <sup>30</sup> G. J. Davies, G. W. F. Pardoe, J. Chamberlain and H. A. Gebbie, *Trans. Faraday Soc.*, 1968, 64, 847.
- <sup>31</sup> I. Larkin and M. Evans, *J.C.S. Faraday II*, 1974, 70, 477.
- <sup>32</sup> M. Evans, *Spectrochim. Acta*, 1976, 32A, 1253, 1259; *Mol. Phys.*, 1975, 29, 1345.
- <sup>33</sup> G. J. Davies, J. Chamberlain and M. Davies, *J.C.S. Faraday II*, 1973, 69, 1223.
- <sup>34</sup> G. J. Davies and J. Chamberlain, *J.C.S. Faraday II*, 1973, 69, 1739.
- <sup>35</sup> M. Evans and G. J. Davies, *J.C.S. Faraday II*, 1976, 72, 1206; M. Evans, *J.C.S. Faraday II*, 1973, 69, 763; 1975, 71, 71.
- <sup>36</sup> C. F. J. Böttcher, *The Theory of Electrical Polarisation* (Elsevier, London, 1952).
- <sup>37</sup> G. S. Hooper and C. A. Kraus, *J. Amer. Chem. Soc.*, 1934, 56, 2265.
- <sup>38</sup> F. M. Batson and C. A. Kraus, *J. Amer. Chem. Soc.*, 1934, 56, 2017.
- <sup>39</sup> C. A. Kraus and R. A. Vingee, *J. Amer. Chem. Soc.*, 1934, 56, 511.
- <sup>40</sup> D. T. Copenhaver and C. A. Kraus, *J. Amer. Chem. Soc.*, 1951, 73, 4557.
- <sup>41</sup> M. Davies and G. Williams, *Trans. Faraday Soc.*, 1960, 56, 1619.

- <sup>42</sup> K. Bauge and J. W. Smith, *J. Chem. Soc.*, 1964, 4244.
- <sup>43</sup> M. J. Wootten, *Electrochemistry*, ed. G. J. Hills (Specialist Periodical Report, The Chemical Society, London, 1973), vol. 3, chap. 2 and references therein.
- <sup>44</sup> J. C. Lestrade, J. P. Badiali and H. Cachet, *Dielectric and Related Processes*, ed. M. Davies (Specialist Periodical Reports, Chemical Society, London, 1975), vol. 2, pp. 6-50.
- <sup>45</sup> E. A. S. Cavell and M. A. Sheikh, *J.C.S. Faraday II*, 1973, 69, 315; 1975, 71, 474.
- <sup>46</sup> H. Cachet, F. F. Hanna and J. Pouget, *J. Chim. phys.*, 1974, 71, 285, 1546; H. Cachet and J. C. Lestrade, *Bull. Soc. Chim. belg.*, 1976, 85, 481.
- <sup>47</sup> E. Grunwald, S. Highsmith and T-P. I., *Ions and Ion Pairs in Organic Reactions*, ed. M. Szwarc (J. Wiley, New York, 1974), vol. 2, chap. 5.
- <sup>48</sup> *Spectroscopy and Structure of Molecular Complexes*, ed. J. Yarwood (Plenum, London, 1973), chap. 2.
- <sup>49</sup> J. Overend, *Infrared Spectroscopy and Molecular Structure*, ed. M. Davies (Elsevier, London, 1963), chap. 10.
- <sup>50</sup> H. Dardy, V. Volterra and T. A. Litovitz, *Faraday Symp. Chem. Soc.*, 1972, 6, 71.
- <sup>51</sup> M. Davies, G. F. Pardoe, J. Chamberlain and H. A. Gebbie, *Trans. Faraday Soc.*, 1970, 66, 273.
- <sup>52</sup> I. Darmon, A. Gerschel and C. Brot, *Chem. Phys. Letters*, 1971, 8, 454.
- <sup>53</sup> A. I. Baise, *Chem. Phys. Letters*, 1971, 9, 627.
- <sup>54</sup> R. G. Gordon, *J. Chem. Phys.*, 1963, 38, 1724.
- <sup>55</sup> G. W. F. Pardoe, *Trans. Faraday Soc.*, 1970, 66, 2699.
- <sup>56</sup> E. A. Moelwyn-Hughes, *Physical Chemistry* (Pergamon, London, 1961), pp. 303-4.
- <sup>57</sup> R. A. Stuckart, C. J. Montrose and T. A. Litovitz, *Faraday Symp. Chem. Soc.*, 1976, 11, 94.
- <sup>58</sup> J. van der Elsken and D. Frenkel, *Faraday Symp. Chem. Soc.*, 1976, 11, 125.
- <sup>59</sup> L. E. Strong and C. A. Kraus, *J. Amer. Chem. Soc.*, 1950, 72, 166.
- <sup>60</sup> H. A. Stuart, *Molekülstruktur* (Springer, Berlin, 1967), pp. 416-20.

**APPENDIX 7**

**FAR-INFRARED SPECTROSCOPIC STUDIES OF  
MOTIONS AND INTERACTIONS IN SOLUTIONS OF  
TETRA-N-ALKYLAMMONIUM HALIDES**

**C. BARKER, P.L. JAMES, J. YARWOOD**

**PROTONS AND IONS INVOLVED IN FAST DYNAMIC PHENOMENA, 1978**

FAR-INFRARED SPECTROSCOPIC STUDIES OF MOTIONS AND INTERACTIONS IN SOLUTIONS OF  
TETRA-N-ALKYLAMMONIUM HALIDES. (PART 4 OF 'VIBRATIONAL SPECTROSCOPIC STUDIES  
ON ION-MOLECULE INTERACTIONS IN NON-AQUEOUS SOLVENTS')

C. BARKER, P.L. JAMES and J. YARWOOD

Department of Chemistry, University of Durham, DURHAM CITY, DH1 3LE, England

ABSTRACT

A summary of the most up-to-date interpretation of the far-infrared spectra of  $R_4N^+X^-$  salts in non-polar and weakly polar solvents is presented. Consideration is given to the role of cation-anion vibration, dipole-dipole interactions (and the evidence for dipole aggregation) dipole-induced field fluctuations at the solvent molecule and rigid dipole (or aggregate) reorientation. The separation of the spectral intensity contributions of these phenomena is attempted and it is shown that the inter-particle distances are considerably smaller than those expected from estimates of the ionic radii. The importance of water in the solutions is discussed with special regard to the observation of a band due to  $X^-/H_2O$  hydrogen bonding and the formation of double layers using certain solvents.

---

INTRODUCTION

A few years ago we embarked (refs. 1-3) upon a programme of far-infrared spectroscopic work aimed at a more detailed study of the molecular processes occurring in solutions of tetra-n-butylammonium salts in solvents such as benzene, carbon tetrachloride and chloroform. We have very recently begun to extend this work to other salts and other solvents with some extremely interesting and unexpected results. In this short paper we present a summary of the results obtained so far (mainly for the tetrabutylammonium salts) and examine the implications of the new results. At the same time we give a critical appraisal of the importance (or otherwise) of the presence of water in these solutions.

The far-infrared region ( $5-400\text{ cm.}^{-1}$ ) is an extremely useful part of the electromagnetic spectrum for the examination of liquid phase molecular interactions because it is this frequency region which corresponds to the time scale (0.1 - 10 ps) of molecular (reorientational and translational) motions and where one is able to characterise intermolecular vibrations. We (refs. 1-3) and others (refs. 4-7) have used this region to look specifically at the following phenomena for tetra-n-alkylammonium salts (1) ion pair or ion 'aggregate' vibrations (2) absorption due to

presence of fluctuating induced dipoles (3) reorientation or 'oscillation' of the ionic species within a dynamic 'cage' of surrounding molecules. We have been able to account for most of the observed features in the spectrum (refs. 1-3) and have shown how calculations using simple models of ion-ion and ion-solvent interactions lead to conclusions which are in good agreement with microwave data (refs. 8-10) for the same systems.

#### EXPERIMENTAL

All the far-infrared spectra reported here were obtained using a Beckman-R.I.I.C. Ltd. FS720 interferometer with either a Golay detector or a liquid helium cooled germanium bolometer. Using a resolution of  $\sim 2 \text{ cm.}^{-1}$  and path lengths of up to 1 cm. we were able to get good S/N ratios down to  $5 \text{ cm.}^{-1}$  (refs. 3, 12). In each case the solution spectrum was ratioed against that of the pure solvent. The salts used were all as purchased (mainly from Eastman-Kodak Ltd.). All the solvents were 'Analar' or 'Spectro' grade dried by standing over molecular sieves.

The three bands in the spectrum (Figs. 1 and 2) have been separated using a band fitting procedure based on the computer fitting programmes of R.N. Jones and co-workers (ref. 11). Analysis of the statistics (refs. 3, 12) resulting from a 'best fit' procedure shows that Gaussian band profiles are the most realistic ones to use. Although this may be partly due to base line problems, it is relevant to point out that, in a highly viscous medium (ref. 9) the vibrating system may be subjected to environmental changes in the slow modulation limit whence Gaussian band shapes are, in fact, expected (ref. 14).

#### RESULTS AND DISCUSSION

From Figures 1 and 2 it is clear that the far-infrared spectrum of  $n\text{-Bu}_4\text{N}^+\text{Cl}^-$  dissolved in either a non-polar or polar solvent is composed of at least three bands labelled A, B and C. Bands A and B are present for all the tetraalkylammonium salts which we have examined but band C is only present with any appreciable intensity for chlorides (refs. 1-3).

Considering band B first, it is fairly clear that this feature may be assigned to a vibration involving both anion and cation since (as one may see from Table 1) the frequency depends on both cation and anion (in a way (ref. 3) which shows that the mass effect is predominant). It is not clear to what extent ion aggregation occurs in such solutions beyond the production of ion pairs. Friedman (ref. 15) has pointed out that cryoscopic measurements (ref. 16) (previously taken (refs. 1-3) to indicate the presence of long lived ionic aggregates) may give erroneously high 'association' numbers due to very strong dipole-dipole interactions. In fact there seems to be conflicting evidence about the formation of ion-pair aggregates in these systems. Most of the dipole moment measurements (refs. 8-10) have shown that  $\vec{\mu}_{CA}$  is, in fact,

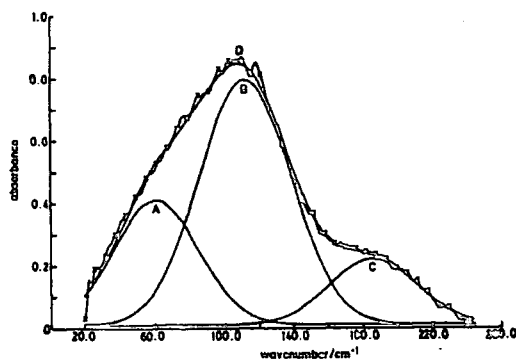


Fig. 1. Far-infrared spectrum of  $\text{Bu}_4\text{N}^+\text{Cl}^-$  in benzene. X, observed spectrum; A,  $\nu_{\text{S}}$  band at  $\sim 65 \text{ cm}^{-1}$ ; B,  $\nu_{\text{CA}}$  band at  $\sim 115 \text{ cm}^{-1}$ ; C, band at  $\sim 185 \text{ cm}^{-1}$ ; D, total computed band envelope.

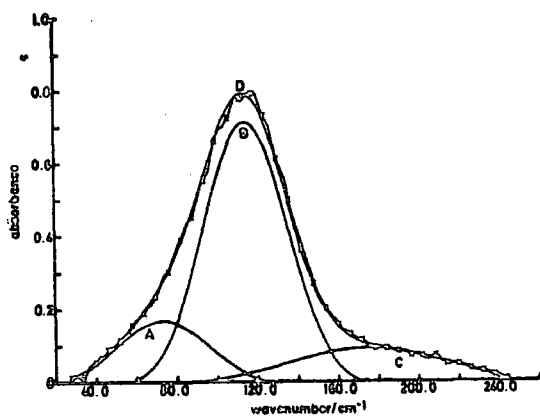


Fig. 2. Far-infrared spectrum of  $\text{Bu}_4\text{N}^+\text{Cl}^-$  in chloroform. X, observed spectrum; A,  $\nu_{\text{S}}$  band at  $\sim 70 \text{ cm}^{-1}$ ; B,  $\nu_{\text{CA}}$  band at  $\sim 120 \text{ cm}^{-1}$ ; C, band at  $\sim 180 \text{ cm}^{-1}$ ; D, total computed band envelope.

concentration dependent—indicating that aggregation does occur. Furthermore, our infrared intensity measurements (refs. 2, 3) which enable us to get an estimate of the average interionic distance  $r_{\text{CA}}$  using,

$$\delta\vec{\mu}_{CA}/\delta Q = \left[ e + \frac{2e\alpha_{\text{eff}}}{4\pi\epsilon_0\epsilon r_{CA}^2} \right] \frac{1}{M_{CA}^{\ddagger}} \quad (1)$$

(where  $\alpha_{\text{eff}}$  and  $M_{CA}$  are the polarisability and reduced mass of the ion pair) show (Table 2) that, for  $r_{CA} \approx 0.30$  nm, the values of  $\vec{\mu}_{CA}$  from (ref. 10),

$$\vec{\mu}_{CA} = er_{CA} \left[ 1 - \frac{\alpha_{\text{eff}}}{4\pi\epsilon_0\epsilon r_{CA}^3} \right] \quad (2)$$

TABLE 1

Force constants and effective interionic separations for the electrostatic ion pair model

salt	Solvent	Concentration /mol dm <sup>-3</sup>	Band centre <sup>a</sup> /cm <sup>-1</sup>	$k_{\text{obs}}/N \text{ m}^{-1}$	$r_{CA}$ (from eqn. (3)) /nm
Bu <sub>4</sub> N <sup>+</sup> Cl <sup>-</sup>	C <sub>6</sub> H <sub>6</sub>	0.01	115 ± 5 <sup>b</sup>	24.1 ± 2.0	0.204 ± 0.002
		0.21	112 ± 1	22.9 ± 0.4	0.206 ± 0.001
		0.50	121 ± 1	26.7 ± 0.4	0.196 ± 0.001
		0.80	119 ± 1	25.8 ± 0.4	0.198 ± 0.001
		1.40	117 ± 1	25.0 ± 0.4	0.200 ± 0.001
Bu <sub>4</sub> N <sup>+</sup> Cl <sup>-</sup>	C <sub>6</sub> H <sub>6</sub>	0.50	121 ± 1	26.7 ± 0.4	0.196 ± 0.001
	CCl <sub>4</sub>	0.50	115 ± 1	24.1 ± 0.4	0.204 ± 0.001
	CHCl <sub>3</sub>	0.50	114 ± 1	23.7 ± 0.4	0.185 ± 0.001
	T.H.F.	0.50	110 ± 5 <sup>b</sup>	22.1 ± 2.0	0.141 ± 0.002
Bu <sub>4</sub> N <sup>+</sup> Br <sup>-</sup>	C <sub>6</sub> H <sub>6</sub>	0.50	79 ± 1	22.1 ± 0.6	0.209 ± 0.001
	CHCl <sub>3</sub>	0.50	79 ± 3 <sup>b</sup>	22.1 ± 1.7	0.161 ± 0.004
Bu <sub>4</sub> N <sup>+</sup> I <sup>-</sup>	CHCl <sub>3</sub>	0.50	61 ± 3 <sup>b</sup>	18.3 ± 1.8	0.172 ± 0.017
Bu <sub>4</sub> N <sup>+</sup> NO <sub>3</sub> <sup>-</sup>	CHCl <sub>3</sub>	0.50	100 ± 3 <sup>b</sup>	29.1 ± 1.7	0.147 ± 0.003
Bu <sub>4</sub> N <sup>+</sup> ClO <sub>4</sub> <sup>-</sup>	CHCl <sub>3</sub>	0.50	85 ± 3 <sup>b</sup>	30.1 ± 2.1	0.146 ± 0.004
Pe <sub>4</sub> N <sup>+</sup> Cl <sup>-</sup>	C <sub>6</sub> H <sub>6</sub>	0.50	115 ± 3 <sup>b</sup>	24.7 ± 1.3	0.201 ± 0.004
Hp <sub>4</sub> N <sup>+</sup> Cl <sup>-</sup>	C <sub>6</sub> H <sub>6</sub>	0.50	112 ± 3 <sup>b</sup>	24.2 ± 1.3	0.203 ± 0.003

<sup>a</sup> Errors are standard deviations obtained from band fitting statistics.

<sup>b</sup> Error estimated by eye.

agree very well with the measured values (ref. 10) of  $\vec{\mu}_{CA}$  for a series of tetra-butylammonium salts (i.e. in the 20 - 25 × 10<sup>-30</sup> Cm. range). Our spectra also show some variation on diluting from 1.0M to 0.01M. Figure 3 shows that there is some

TABLE 2  
 Calculated<sup>a</sup> effective dipole moments (eqn. 2)<sup>b,c</sup> and band B intensities (eqn. 1) for  
 a range of  $r_{CA}$  values

$r_{CA}/\text{nm}$	$10^{30} \frac{\mu_{CA}^2}{Cm}$	B/m.mol
0.25	4.3	127,600
0.30	23.0	67,600
0.35	37.7	44,300
0.40	50.0	33,400
0.45	61.0	27,500
0.50	71.0	24,100

<sup>a</sup> The average observed intensity over the concentration range studied is 57,600 m.mol.<sup>-1</sup>

<sup>b</sup> The polarisability  $\alpha_{\text{eff}}$  is taken as that of the tetrabutylammonium cation (ref. 17) which is much bigger than that of the halide ion.

<sup>c</sup> The medium permittivity used was that of pure benzene ( $\epsilon = 2.31$ ).

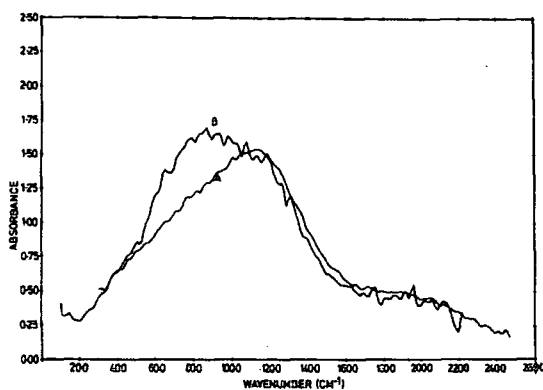


Fig. 3. Spectra of  $\text{Bu}_4\text{N}^+\text{Cl}^-$  in benzene at (A) 0.88M (B) 0.01M at 298K  
 (The path lengths are 0.2 and 7.5 mm. respectively.)

change of relative intensity of the A and B bands on dilution. It seems that the B band may decrease in relative intensity and this may indeed be due to some effect connected with aggregate size. However, since the signal/noise ratio achieved so far for 0.01M solutions (Fig.3(B)) is insufficient to justify separation of bands A and B (as shown on Figures 1 and 2) we cannot be sure of the absolute intensities of

the two bands. In previous publications (refs. 1-3) we also regarded the deviation from Beers Law for  $\text{Bu}_4^{\text{n}}\text{N}^+\text{Cl}^-$  in benzene (ref. 3, Figure 6) to be evidence in favour of ion pair association since it was felt that the aggregates were breaking up on dilution. However, Barker (ref. 12) has found that for  $\text{Bu}_4^{\text{n}}\text{N}^+\text{Br}^-$  the intensity data do obey Beers Law (Fig. 4). These effects may still be real since the bromide ought

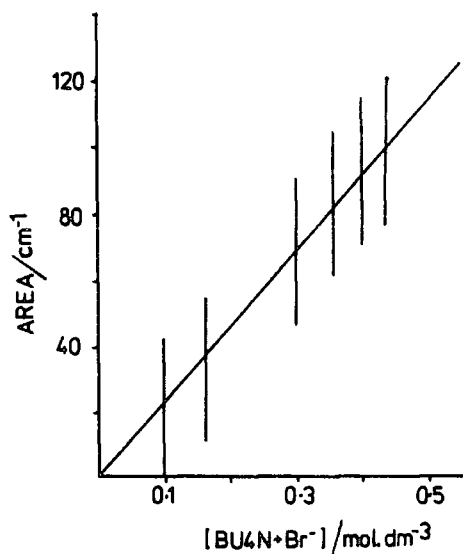


Fig. 4. Beers Law plot for  $\text{Bu}_4^{\text{n}}\text{N}^+\text{Br}^-$  in benzene at 298K.

to be less likely to form aggregates (ref. 19). Nevertheless, the presence of small amounts of water may affect the intensity data more than we at first thought (see below for further discussion). Despite this 'regular' intensity behaviour for the bromide and the apparently sensible force constant results obtained with a simple  $\text{C}^+ - \text{A}^-$  model most of the evidence seems to indicate that these salts (and especially the chlorides) do form ion pair aggregates in non-polar solvents.

One of the most interesting features of these salt solutions is that (as mentioned above) the calculated  $r_{\text{CA}}$  values obtained from both, the force constant data (Table 1) using

$$k_{\text{calc}} = \frac{-2e^2}{4\pi\epsilon_0\epsilon r_{\text{CA}}^3} \quad (3)$$

and the intensity data using equation 2 (Table 2) are considerably shorter (0.2 - 0.3 nm) than one might expect (0.5 nm) using the sum of ionic radii (ref. 17). These measurements seem to indicate that penetration on effects (refs. 18-20) may be

operative and that in a non-polar, low permittivity solvent the anion approaches the 'centre' of positive charge on the cation (presumably on or near the nitrogen atom) as indicated by osmotic coefficient (ref. 18) and conductivity (ref. 19,20) measurements. We might therefore expect that this  $r_{CA}$  distance might increase on using a polar solvent such as chloroform. From Table 1 it may be seen that such an effect is not observed and so there is little evidence for strong anion solvation by solvents such as chloroform (ref. 13). Studies in strongly protic solvents such as methanol would be necessary in order to get further information on this phenomenon.

Turning attention now to band A in the spectrum, we have presented good evidence (ref. 3) that this band is composite in nature. The two major components are (i) the high frequency part of the spectrum caused by Debye rotation of the rigid ion-pair dipoles, (ii) absorption due to the fluctuation of induced dipoles caused by ion pair - solvent interactions (these are expected to be mainly dipole-induced dipole interactions). From Fig. 5 it may be seen that the intensity of this

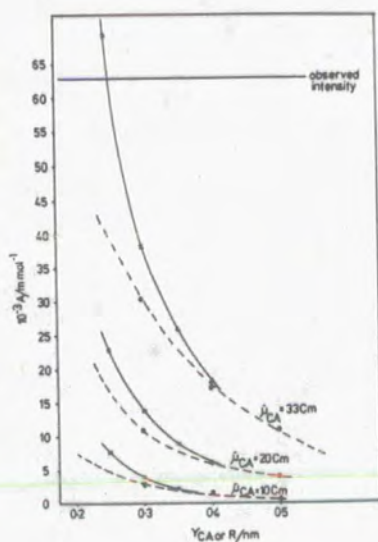


Fig. 5. Band intensities calculated for band A of the spectra shown in Figs. 1 and 2 as a function of cation-anion or ion-pair - solvent distance. Broken lines represent the 'Poley' band intensity of equation (4). Solid lines represent the total intensity of equations (4) and (5).

band using the Gordon intensity sum rule

$$A_p = \frac{\pi \vec{u}_{CA}^2}{3c^2} \left( \frac{1}{I_x} + \frac{1}{I_y} \right) \quad (4)$$

( $I_x = I_y$  for a 'diatomic' ion-pair dipole) represents about half the total intensity for reasonable values of  $r_{CA} = 0.3$  nm and  $\vec{u}_{CA} = 33$  Cm (ref. 17) (assuming that ion pairs are the predominant species in solution). The other half of the total spectral intensity may be then be predicted by an equation of the form,

$$B = \frac{N\pi}{3c^2 m_{cs}} \left[ - \frac{6\vec{u}_{CA} \alpha_s}{4\pi\epsilon_0 \epsilon R^4} \right]^2 \quad (5)$$

where  $R$  is the ion pair - solvent distance,  $\alpha_s$  the solvent polarisability and  $m_{cs}$  the ion-pair/solvent reduced mass. Fig. 5 shows that, in order to make up the other half of the band A intensity, one has to employ a value of  $R = 0.25$  nm for a  $\vec{u}_{CA}$  of 33 Cm. This implies that not only is there anion penetration of the bulky alkyl cation but that solvent molecules may also 'penetrate' between the alkyl chains (this can be shown to be feasible using molecular models). This interesting result for the average value of  $R$  - which agrees very well with the results of dielectric permittivity measurements (refs. 8-10) on very similar systems - leads one to speculate that the ionic 'aggregates' in solution include solvent molecules which are 'trapped' within the alkyl chains. If this is the case then the process ought to be at least partly dependent upon the relative dimensions of the solvent molecule and the alkyl chain 'cavities'. We have recently tried to get further information on possible effects of this kind using methylated benzene solvents and different cation alkyl chain lengths. We immediately noticed that using *p*-xylene as a solvent at concentrations  $> 0.05M$  of  $n\text{-Bu}_4\text{N}^+\text{Cl}^-$  separation into two layers occurred as may have been expected from previous work (ref. 21) on  $(i\text{-C}_5\text{H}_{11})_4\text{N}^+\text{Pic}^-$  in benzene and on tetraalkylammonium salts of organo-metallic anions (ref. 22). This phenomenon known as 'unmixing' is believed (ref. 23) to result from severe thermodynamic non-ideality caused by very large dipole-medium interactions. From Table 3 (and from data presented in ref. 22) it is clear that the relative solvent/cation sizes have an important influence as would be expected if dipole-solvent interactions are important.

TABLE 3

Dependence of double layer formation on the cation and solvent.

Salt	$\text{C}_6\text{H}_6$	$p\text{-C}_6\text{H}_4(\text{CH}_3)_2$	$\text{C}_6\text{H}_3(\text{CH}_3)_3$
$(i\text{C}_5\text{H}_{11})_4\text{N}^+\text{Pic}^-$	X	?	?
$n\text{Bu}_4\text{N}^+\text{Cl}^-$	-	X	X
$n\text{Pe}_4\text{N}^+\text{Cl}^-$	-	-	X
$n\text{Hex}_4\text{N}^+\text{Cl}^-$	-	-	-

We are now trying to spectroscopically characterise the two layers in terms of cation chain or solvent perturbations and monitoring changes in the far-infrared spectra with concentration and solvent. From one of the initial spectra (shown in Fig. 6) it is clear that almost all the salt and all the water present is concentrated

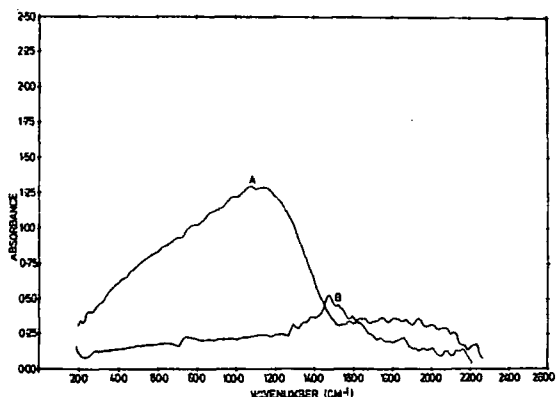


Fig. 6. Spectra of the two layers formed by  $\text{Bu}_4\text{N}^+\text{Cl}^-$  and p-xylene at room temperature (A). Spectrum of the 'salt-rich' layer at a path length of 0.06 mm. (B) Spectrum of 'salt-poor' layer at a path length of 0.2 mm.

in the bottom layer. Figure 6 also demonstrates the perturbing effect of the salt on the p-xylene internal vibrational mode at about  $150\text{ cm}^{-1}$ .

Until very recently the band C in the spectrum had been assigned (ref. 2) to some kind of combination band due to strong coupling of the ion-ion and ion-solvent interactions. Indeed there may still be some absorption in the  $180\text{ cm}^{-1}$  region (for  $n\text{-Bu}_4\text{N}^+\text{Cl}^-$ ) due to such coupling. However, it is now felt that this band is at least partly due to the presence of water (albeit in very small amounts). Fig. 7 shows that on adding small amounts of water to benzene solutions this band increases in intensity relative to the other bands. Furthermore, Corset et al. (ref. 7) have shown that a band arises in this region when phenol is added to solutions of tetra-alkyl ammonium salts in carbon tetrachloride. This band, which significantly does not appear in solutions of the (much less hygroscopic) bromide salts (Fig. 8), is due to some sort of  $\text{O-H}\cdots\text{X}^-$  interaction and may well be the  $\nu_{\text{O}}$  stretching mode (refs. 7, 24) of such a hydrogen-bonded complex. The presence of this band has led us to consider more closely the effects of water on solutions of these salts in non-polar solvents. The solubility is, of course, very sensitive to the amount of water

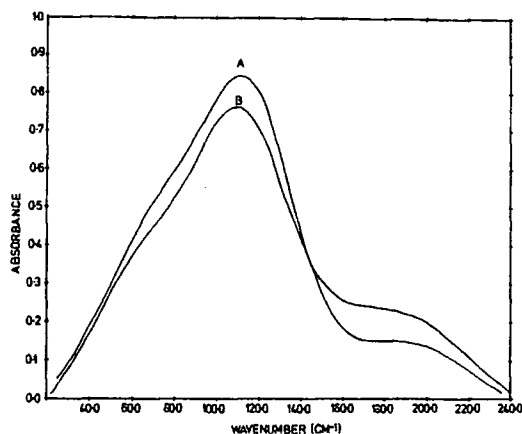


Fig. 7. Effect of adding water to a 0.8M solution of  $\text{Bu}_4\text{N}^+\text{Cl}^-$  in benzene at 0.2 mm. path length. (A) 0.1%  $\text{H}_2\text{O}$  (B) 1%  $\text{H}_2\text{O}$ .

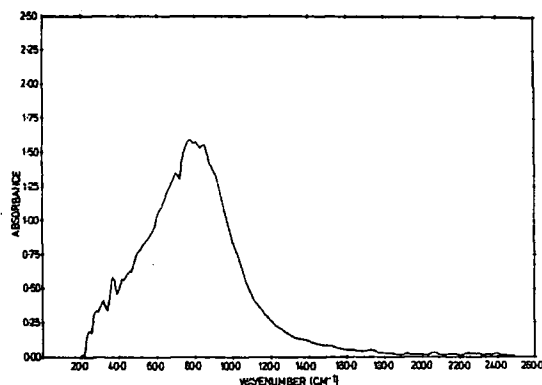


Fig. 8. Spectrum of a 0.35M solution of  $\text{Bu}_4\text{N}^+\text{Br}^-$  in chloroform showing complete absence of a band attributable to  $\text{Br}^-/\text{H}_2\text{O}$  interactions.

present and one may consider that the water molecule may, in fact, be involved in the 'aggregate' or 'cluster' formed in solution. Fig. 6 shows that any water present remains in the salt rich layer and further small addition of water leads to further concentration of water in the bottom layer. It appears that a certain proportion of water is essential for the formation of such double layers and this implies a definite 'role' for the water molecule presumably at a site where anion-water

hydrogen bonding is facilitated.

#### ACKNOWLEDGEMENTS

Valuable discussions with Prof. H.L. Friedman are gratefully acknowledged. Our thanks are also due to the S.R.C. and Beckman R.I.I.C. Ltd. for equipment grants and C.A.S.E. awards (to C.B. and P.L.J.).

#### REFERENCES

- 1 Part 1, C. Barker and J. Yarwood, *J.C.S., Faraday II*, 71 (1975) 1322.
- 2 Part 2, C. Barker and J. Yarwood, *Faraday Symp. Chem. Soc.*, 11 (1977) 136.
- 3 Part 3, C. Barker, P.L. James and J. Yarwood, *Faraday Discussion Chem. Soc.*, 64 (1978) 000.
- 4 J.C. Evans and G.Y. S-Lo, *J. Phys. Chem.*, 69 (1965) 3223.
- 5 M.J. French and J.L. Wood, *J. Chem. Phys.*, 49 (1968) 2358.
- 6 J.R. Kludt, G.Y.W. Kwong and R.L. McDonald, *J. Phys. Chem.*, 76 (1972) 339.
- 7 P. Bachelon, J. Corset and C. de Loze, *Chem. Phys. Lett.*, 32 (1975) 458.
- 8 J.C. Lestrade, J.P. Badiali and H. Cachet, *Dielectric and Related Processes* (Ed. M. Davies) The Chemical Society, London 1975, Vol. 2, pp. 6-50.
- 9 H. Cachet, F.F. Hanna and J. Pouget, *J. Chim. Phys.*, 71 (1974) 285, 1546; H. Cachet and J.C. Lestrade, *Bull. Soc. Chim. Belg.*, 85 (1976) 481.
- 10 G. Williams and M. Davies, *Trans. Faraday Soc.*, 56 (1960), 1619.
- 11 J. Pitha, R.P. Young and R.N. Jones, *Canad. J. Chem.*, 44 (1966) 3031; 45 (1967) 2347; *N.R.C. Bulletins* 12 and 13, N.R.C., Ottawa, 1968-69.
- 12 C. Barker, Ph.D. Thesis, University of Durham, 1977; P.L. James, M.Sc. Thesis University of Durham, 1976.
- 13 D.E. Irish in A.K. Covington and T. Dickinson (Eds.), *Physical Chemistry of Organic Solvent Systems*, Plenum Press, London, 1973, Chapter 4.
- 14 R. Kubo in D. Ter Haar (Ed.) *Fluctuation, Relaxation and Resonance in Magnetic Systems*, Oliver and Boyd, London, 1962, pp. 23-68.
- 15 H.L. Friedman, *Faraday Discussion Chem. Soc.*, 64 (1978) 000.
- 16 F.M. Batson and C.A. Kraus, *J. Amer. Chem. Soc.*, 56 (1934) 2017; C.A. Kraus and R.A. Vingee, *J. Amer. Chem. Soc.*, 56 (1934) 511.
- 17 E. Grunwald, S. Highsmith and T.P.I. in M. Szwarc (Ed.), *Ions and Ion Pairs in Organic Reactions*, J. Wiley, New York, 1974, Vol. 2, Ch. 5 (and references therein).
- 18 R.W. Kreis and R.H. Wood, *J. Phys. Chem.*, 75 (1971) 2319.
- 19 D.F. Evans and P. Gardam, *J. Phys. Chem.*, 72 (1968) 3281; *ibid.*, 73 (1969) 158.
- 20 S.R.C. Hughes and S.H. White, *J. Chem. Soc., A* (1966) 1216; S.R.C. Hughes and D.H. Price, *J. Chem. Soc. A* (1967) 1093.
- 21 R.M. Fuoss and C.A. Kraus, *J. Amer. Chem. Soc.*, 55 (1933) 3617.
- 22 J.L. Atwood in *Recent Developments in Separation Science*, Vol. III.
- 23 H.L. Friedman, *J. Phys. Chem.*, 66 (1962) 1595.
- 24 J.L. Wood in J. Yarwood (Ed.) *Spectroscopy and Structure of Molecular Complexes*, Plenum Pub. Ltd., London, 1973, Chapter 4.

## DISCUSSION

### M. YARWOOD

M. Szwarc - The proposed interpenetration of anions or benzene molecules into quaternary ammonium ions implies that the alkylhydrocarbon chains are not folded, as apparently they are in aqueous solutions, but extended, giving a straw-shape form to cations. Even then it is difficult to see how could the centers of N nucleus and Cl nucleus be brought together to a distance of 3 to 3.5 Å.

J. Yarwood - Our intensity data are subject, of course, to some error (see fig. 4 of our paper) so a range of  $r_{CA}$  values can be obtained. However, using the simplest model (as we have done) one cannot easily explain the intensity of this band using  $r_{CA} < 4$  Å. This means that there may possibly be an extra contribution to the observed spectrum which we have not considered. This could, for example, be the "internal" librational mode mentioned by Dr. White. On the other hand it is possible that a more sophisticated model may be necessary to explain the intensity data.

J.F. Coetzee - Is there any simple quantitative correlation between the solubility of  $Bu_4N^+Cl^-$  in benzene and the activity of water present?

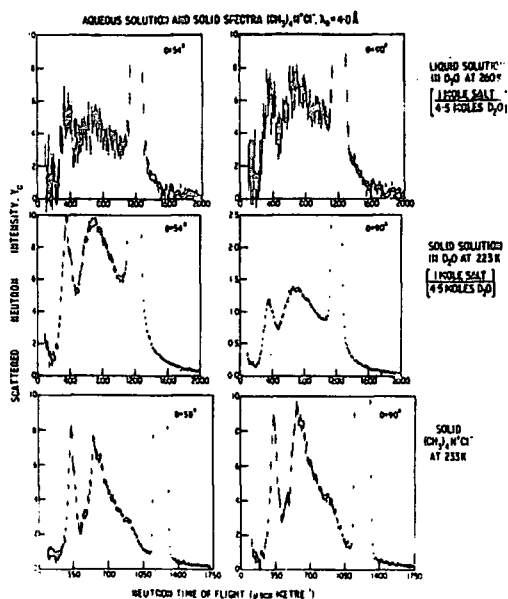
J. Yarwood - We have no quantitative measure of the relation between solubility and water concentration but I do not know that if the water level is reduced beyond about 0.1 % (by volume) then the solubility is less than 0.01 M (the lowest concentration we can detect using far infrared methods). Better methods of concentration determination are obviously necessary before one could say more than this.

H.L. Friedman - a/ Since  $Bu_4N^+Cl^-$  dissolves in benzene only to the degree that water is present (which implies that in solution we have only  $Cl^-$  with  $H_2O$  hydrogen-bonded to it), it seems paradoxical that the intensity of band 3 is so sensitive to still more water.  
b/ In some other solvents the solvation enthalpy data show clearly that in  $R_4N^+$  the alkyl chains are stretched out, as you also find necessary to assume.

J. Yarwood - a/ Without quantitative solubility/water concentration data it is difficult to be sure that this apparent paradox is "neat". If, however, the molar concentration of water is lower than that of the salt (which I believe it is from our Karl-Fischer titration data) then it may be that the water molecule is important in "aggregate" formation. One may then only need one water molecule per aggregate but addition of more water would, of course, lead to a higher concentration of H-O-H...X species.  
b/ This would provide extra evidence that our idea of solvent molecules being "trapped" (on our time scale) within the alkyl chains (or chain aggregates) is not totally unreasonable.

J.W. White - I have a few comments which I hope may help to understand some of the points raised in this and the preceding paper. Firstly it is known that a small amount of water (0.1 %) stabilises an abnormal crystalline phase of tetramethylammonium chloride compared to the phase for the dry crystal. Perhaps the same is true for other alkyl ammonium salts and the lack of solubility of the dry form in benzene results. Secondly I would like to suggest that there are two different classes of librations possible for alkylammonium species in solution i/ libration of the whole ion pair or cluster in the crystal field provided by the solvent and ionic neighbours and ii/ librations of the tetraalkylammonium ions themselves. Because high

vibrational amplitude proton scattering dominates neutron spectra librations, particularly of the type (ii), appear strongly. The neutron spectra are thus complementary to the infrared and effects due to solvent scattering can be significantly attenuated using deuterated (low scattering) solvents. The figure is an example of this (Brown and White, unpublished work) and shows the persistence of both molecular modes (A) and the whole tetramethylammonium in libration, B, (though with changed frequency), through out the series 1/ tetramethylammonium chloride solid, 2/ glassy supercooled eutectic of  $(\text{CH}_3)_4\text{N}^+\text{Cl}^- \cdot 4\text{H}_2\text{O}$  and 3/ the same solution at 25°C.



H. Cachet - The anion-cation distance  $r_{CA}$ , deduced from experiment strongly depends on the model, as shown by the differences between your values ( $\sim 3 \text{ \AA}$ ) and our values ( $\sim 5 - 6 \text{ \AA}$ ). In relation with this point, can you explain why, in the restoring force governing the ion-pair vibration, you neglect all forces other than the Coulombic one? The  $\phi(r)$  potential of mean force we use yields both  $r_{CA}$  and the force constant; in the latter, the main term does not arise from the Coulomb attraction, but from the repulsive force.

J. Yarwood - Our force constants (table I of our paper) are "observed" values and the data are fitted to a diatomic molecule model using equation 3. I agree that this equation uses an electrostatic model and that for a meaningful force constant one needs a certain degree of "covalent" bonding. However, the intensity data also give a value of  $r_{CA} \approx 3.5 - 4.0 \text{ \AA}$  and it seems likely, in view of the interpretation of conductivity data, that penetration of the cation alkyl chain by the anion produces an effective  $r_{CA}$  lower than the sum of ionic radii. Nevertheless, I agree that the precise value of  $r_{CA}$  obtained is model dependent and that this parameter probably also depends on the degree of "clustering" in concentrated solutions.

## APPENDIX 8

The Board of Studies in Chemistry requires that each postgraduate research thesis contain an Appendix listing:

- (a) all research colloquia, research seminars and lectures (by external speakers) arranged by the Department of Chemistry since 1 October 1976; and
- (b) all research conferences attended and papers read out by the writer of the thesis, during the period when the research for the thesis was carried out.

## APPENDIX 8

### a) Research Colloquia, Seminars and Lectures by External Speakers

Arranged by the Department of Chemistry of the University of Durham between  
1 October 1976 and 31 December 1978.

- 20 October 1976 Professor J. B. Hyne (University of Calgary), "New Research on an Old Element - Sulphur".
- 10 November 1976 Dr J.S. Ogden (Southampton University), "The Characterization of High Temperature Species by Matrix Isolation".
- 17 November 1976 Dr B.E.F. Fender (University of Oxford), "Familiar but Remarkable Inorganic Solids".
- 24 November 1976 Dr M.I. Page (Huddersfield Polytechnic), "Large and Small Rate Enhancements of Intramolecular Catalysed Reactions".
- 8 December 1976 Professor A.J. Leadbetter (University of Exeter), "Liquid Crystals".
- 26 January 1977 Dr A. Davis (E.R.D.R.), "The Weathering of Polymeric Materials".
- 2 February 1977 Dr M. Falk, (N.R.C. Canada), "Structural Deductions from the Vibrational Spectrum of Water in Condensed Phases".
- 9 February 1977 Professor R.O.C. Norman (University of York), "Radical Cations; Intermediates in Organic Reactions".
- 23 February 1977 Dr G. Harris (University of St Andrews), "Halogen Adducts of Phosphines and Arsines".
- 25 February 1977 Professor H.T. Dieck (Frankfurt University), "Diazadienes - New Powerful Low-Valent Metal Ligands".
- 2 March 1977 Dr F. Hibbert (Birkbeck College, London), "Fast Reaction Studies of Slow Proton Transfers Involving Nitrogen and Oxygen Acids".
- 4 March 1977 Dr G. Brink (Rhodes University, South Africa), "Dielectric Studies of Hydrogen Bonding in Alcohols".
- 9 March 1977 Dr I.O. Sutherland (Sheffield University), "The Stevens' Rearrangement: Orbital Symmetry and Radical Pairs".
- 18 March 1977 Professor H. Bock (Frankfurt University), "Photoelectron Spectra and Molecular Properties: A Vademecum for the Chemist".
- 30 March 1977 Dr J.R. MacCallum (University of St Andrews), "Photooxidation of Polymers".
- 20 April 1977 Dr D.M.J. Lilley (Research Division, G.D. Searle), "Tails of Chromatin Structure - Progress towards a Working Model".
- 27 April 1977 Dr M.P. Stevens (University of Hartford), "Photocycloaddition Polymerisation".
- 4 May 1977 Dr G.C. Tabisz (University of Manitoba), "Collision Induced Light Scattering by Compressed Molecular Gases".

- 11 May 1977 Dr R.E.Banks (U.M.I.S.T.), "The Reaction of Hexafluoropropene with Heterocyclic N-Oxides".
- 18 May 1977 Dr J. Atwood (University of Alabama), "Novel Solution Behaviour of Anionic Organoaluminium Compounds: the Formation of Liquid Clathrates".
- 25 May 1977 Professor M.M.Kreevov (University of Minnesota), "The Dynamics of Proton Transfer in Solution".
- 1 June 1977 Dr J. McCleverty (University of Sheffield), "Consequences of Deprivation and Overcrowding on the Chemistry of Molybdenum and Tungsten".
- 6 July 1977 Professor J. Passmore (University of Brunswick), "Adducts Between Group V Pentahalides and a Postscript on  $S_7I^+$ ".
- 27 September 1977 Dr T.J.Broxton (La Trobe University, Australia), "Interaction of Aryldiazonium Salts and Arylazoalkyl Ethers in Basic Alcoholic Solvents".
- 19 October 1977 Dr B. Heyn (University of Jena, D.D.R.), " $\sigma$ -Organo-Molybdenum Complexes as Alkene Polymerisation Catalysts".
- 27 October 1977 Professor R.A.Filler (Illinois Institute of Technology), "Reactions of Organic Compounds with Xenon Fluorides".
- 2 November 1977 Dr N. Boden (University of Leeds), "NMR Spin-Echo Experiments for Studying Structure and Dynamical Properties of Materials Containing Interacting Spin -  $\frac{1}{2}$  Pairs".
- 9 November 1977 Dr A.R. Butler (University of St Andrews), "Why I lost Faith in Linear Free Energy Relationships".
- 7 December 1977 Dr P.A.Madden (University of Cambridge), "Raman Studies of Molecular Motions in Liquids".
- 14 December 1977 Dr R.O.Gould (University of Edinburgh), "Crystallography to the Rescue in Ruthenium Chemistry".
- 25 January 1978 Dr G. Richards (University of Oxford), "Quantum Pharmacology".
- 1 February 1978 Professor K.J.Ivin (Queens University, Belfast), "The olefin metathesis reaction: mechanism of ring-opening polymerisation of cycloalkenes".
- 3 February 1978 Dr A. Hartog (Free University, Amsterdam), "Surprising recent Studies in Organo-magnesium Chemistry".
- 22 February 1978 Professor J.D.Birchall (Mond Division, I.C.I. Ltd.), "Silicon in the Biosphere".
- 1 March 1978 Dr A. Williams (University of Kent), "Acyl Group Transfer Reactions".
- 3 March 1978 Dr G. van Koten (University of Amsterdam), "Structure and Reactivity of Arylcopper Cluster Compounds".
- 15 March 1978 Professor G. Scott (University of Aston), "Fashioning Plastics to match the Environment".
- 22 March 1978 Professor H. Vahrenkamp (University of Freiburg), "Metal-Metal Bonds in Organometallic Complexes".

- 19 April 1978** Dr M. Barber (U.M.I.S.T.), "Secondary Ion Mass Spectra of Surfaces and Absorbed Species".
- 16 May 1978** Dr P. Ferguson (C.N.R.S., Grenoble), "Surface Plasma Waves and Absorbed Species on Metals".
- 18 May 1978** Professor M. Gordon (University of Essex), "Three Critical Points in Polymer Science".
- 22 May 1978** Professor D. Tuck (University of Windsor, Ontario), "Electro-chemical Synthesis of Inorganic and Organometallic Compounds".
- 24 and 25 May 1978** Professor P. von R. Schleyer (University of Erlangen, Nurnberg),
- I. "Planar Tetra-co-ordinate Methanes, Perpendicular Ethylenes, and Planar Allenes".
  - II. "Aromaticity in Three Dimensions".
  - III. "Non-classical Carbocations".
- 21 June 1978** Dr S.K.Tyrlik (Academy of Science, Warsaw), "Dimethylgloximecobalt Complexes - Catalytic Black Boxes".
- 23 June 1978** Professor W.B. Person (University of Florida), "Diode Laser Spectroscopy at 16 $\mu$ m".
- 27 June 1978** Professor R.B. King (University of Georgia, Athens, Georgia, U.S.A.), "The Use of Carbonyl Anions in the synthesis of Organometallic Compounds".
- 30 June 1978** Professor G. Mateescu (Cape Western Reserve University), "A Concerted Spectroscopy Approach to the Characterisation of Ions and Ion Pairs: Facts, Plans and Dreams".
- 15 September 1978** Professor W. Siebert (University of Marburg, West Germany), "Boron heterocycles as ligands in transition metal chemistry".
- 22 September 1978** Professor T. Fehlner (Notre Dame, U.S.A.), "Ferraboranes: syntheses and photochemistry".
- 12 December 1978** Professor C.J.M. Stirling (University of Bangor). "Parting is such sweet sorrow' - the leaving group in Organic Reactions".

**b) Conferences Attended During the Period October 1976 to December 1978**

- 13 and 14 December 1976** The Chemical Society, Faraday Division, Symposium No.11, "Newer Aspects of Molecular Relaxation Processes". The Royal Institution, London.
- 13, 14 and 15 September 1977** The Chemical Society, Faraday Division, General Discussion No.64, "Ion-Ion and Ion-Solvent Interactions". St.Catherine's College, Oxford.
- 29 March – 1 April 1978** The Institute of Physics, '3rd International Conference on Submillimetre Waves and their Applications'. University of Surrey, Guildford.
- July 1978** 'Synchrotron Users Meeting', Daresbury Laboratory.
- 13 September – 15 September 1978** The Chemical Society, Faraday Division. General Discussion No.66 'Structure and Motion in Molecular Liquids'. The University of Kent, Canterbury.  
Paper presented by the author 'Comparison of Infrared and Raman Vibrational Relaxation Functions of the  $\nu_1$  and  $\nu_3$  Modes of Acetonitrile'.  
J.Yarwood, P.L.James, G.Döge, R.Arndt. [Appendix 2]
- 6 December 1978** The Institute of Physics, Spectroscopy Group.  
'Aspects of Submillimetre Spectroscopy'.  
Westfield College, London.